MINERALOGY AND PROVENANCE OF THE NAMAKWA SANDS HEAVY MINERAL SATELLITE DEPOSITS.

by

Candice Carelse

Thesis presented in partial fulfilment

of the requirements for the degree of

Master of Science

in the Department of Earth Sciences

University of Stellenbosch

Supervisor: Prof. Abraham Rozendaal

Faculty of Science

Stellenbosch

December 2012

DECLARATION

I, the undersigned, hereby declare that the work contained in this thesis is my own original work and has not been previously, in its entirety or in part, been submitted at any university for a degree. Where use was made of the work of other authors, it has been duly acknowledged in the text.

_____ 28 November 2012

C.B Carelse Date

_____

Student number

ABSTRACT

Five areas proximal to the world class Namakwa Sands heavy mineral deposit have been studied and include the farms Houtkraal Remainder Portion 2, Houtkraal Remainder, Geelwal Karoo, Graauwduinen and Rietfontein. These are locally referred to as the satellite deposits and are sub-economic occurrences. The primary objective of the study was to quantify the mineralogy and mineral chemistry, determine the provenance of the heavy mineral suite and draw a comparison between the satellite deposits and the Namakwa Sands deposit from an exploratory point of view. Methodology used to achieve the above objectives included optical microscopy, Scanning Electron Microscope (SEM), Laser Ablation Inductively Coupled Plasma Mass Spectrometry (LA-ICP-MS), Quantitative Evaluation of Minerals by Scanning Electron Microscopy (QEMSCAN), X- Ray Fluorescence (XRF) and Zr-geothermometry of rutile.

The five satellite areas contain the same heavy mineral suite but mineral proportions differ. The total heavy mineral population (THM) are diverse and consist of ilmenite and its alteration products (hydrated ilmenite, pseudorutile and leucoxene), magnetite, hematite, spinel, rutile, tourmaline, pyroxene, amphibole, garnet, aluminosilicates, staurolite, corundum, epidote, zircon, monazite and sphene. Ilmenite and garnet are the two most dominant heavy minerals present. The valuable heavy minerals (VHM) suite consists of ilmenite, zircon, rutile and leucoxene.

The mineralogy of the satellite areas and chemistry of the ore minerals (rutile, zircon, ilmenite and leucoxene) are similar to the Namakwa Sands deposit.

The whole spectrum of ilmenite alteration products (hydrated ilmenite, pseudorutile, and leucoxene) is present and allowed the quantitative use of the alteration index. The indices is low (22-24%) and indicates that the surficial deposits have formed under arid to semi-arid climatological conditions which preserved the pristine character of most of the minerals.

This allowed reliable provenance studies using the characteristics of most of the heavy mineral suite, which showed that the minerals were derived from a diversity of source rocks. These included mainly medium to high-grade metamorphites and felsic intrusives of the underlying Mesoproterozoic Namaqualand Metamorphic Complex and a minor contribution

from the Neoproterozoic Gariep Supergroup. This relationship indicates a limited transport distance from source to depositional basin.

Mineral ratios in particular the THM-VHM relationship showed that the deposits located close to the shoreline such as Geelwal Karoo, Graauwduinen and Rietfontein have a relatively low proportion of valuable heavy minerals whereas those more inland such as Houtkraal Remainder Portion 2 and Houtkraal Remainder are close to unity.

Heavy mineral concentration as such is low in the satellite areas and the mechanism to increase the concentration is clearly not only a function of distance from the present shoreline but is also topographically controlled. Steep sided linear depressions channelled the unconsolidated sediments and heavy minerals were upgraded into economic concentrations by aeolian processes. The quality of the valuable heavy minerals in the satellite areas however is similar to those of the adjacent Namakwa Sands deposit. This study has demonstrated that Houtkraal Remainder is the northeasterly continuation of the red aeolian sand (RAS) associated East Mine orebody and offers the best exploration potential.

UITTREKSEL

Vyf areas proksimaal aan die Namakwa Sands swaar mineral afsetting is bestudeer en sluit in Houtkraal Remainder, Houtkraal Remainder Portion 2, Geelwal Karoo, Graauwduinen en Rietfontein. Hierdie areas word plaaslik na verwys as satelliet afsettings en is subekonomies. Die hoofdoel van hierdie studie was om die mineralogie en mineral chemie te kwantifiseer, die oorsprong van die swaar mineraal suite te bepaal asook n vergelyking te tref tussen die satelliet areas en die Namakwa Sands afsetting vanuit n verkennende eksplorasie oogpunt. Optiese mikroskopie, SEM, LA-ICP-MS, QEMSCAN, XRF en die Zr-geotermometer van rutiel is gebruik om bostaande doele te bereik.

Die vyf satellite areas bestaan uit dieselfde swaar minerale maar mineral proporsies verskil. Die totale swaar mineraal populasie is divers en bestaan uit ilmeniet en ilmeniet se veranderingsprodukte (gehidreerde ilmeniet, pseudorutiel en leukokseen), magnetiet, hematiet, spinel, rutiel, toermalyn, pirokseen, amfibool, granaat, aluminiumsilikate, stauroliet, korund, epidoot, sirkoon, monasiet and sfeen. Ilmenite en granaat is die twee mees dominante swaar minerale teenwoordig. Die waardevolle swaar mineraal populasie bestaan uit ilmeniet, rutiel, sirkoon en leukokseen.

Die mineralogie van die satelliet areas en die chemie van die erts minerale (rutiel, sirkoon, ilmeniet en leukokseen) is dieselfde as die van die Namakwa Sands afsetting.

Die hele spektrum ilmeniet veranderingsprodukte is teenwoordig en het die kwantitatiewe gebruik van die alterasie indeks toegelaat. Die alterasie indekse is laag (22-24%) en dui aan dat die oppervak afsettings gevorm het tydens droë tot semi droë toestande wat die eertydse karakter van meeste minerale bewaar het.

Deurdat die karakter van meeste minerale behoue gebly het, kon provenans studies toegepas word op die swaar mineraal suite. Provenans studies het aangedui dat die swaar minerale afkomstig is van n verskeidenheid van bron gesteentes. Dit sluit in medium tot hoë graad metamorfe gesteentes en felsiese intrusies van die Mesoproterosoïese Namakwaland Metamorfiese Kompleks met n geringe bydrae van die Neo Proterosoïese Gariep Supergroep. Hierdie verhouding dui n beperkte vervoer afstand aan vanaf die bron tot by die afsettings omgewing.

Mineraal vehoudings spesifiek die totale swaar mineraal-waardevolle swaar mineraal verhoudings dui aan dat afsettings na aan die kus soos Geelwal Karoo, Graauwduinen en Rietfontien n lae inhoud van waardevolle swaar minerale het teenoor afsettings soos Houtkraal Remainder Portion 2 en Houtkraal Remainder wat meer land in is met verhoudings na aan eenheid.

Swaar mineral konsentrasie is laag in die satellite areas en die meganisme verantwoordelik vir die toename in konsentrasie is nie net n funksie van die afstand van die bestaande kuslyn nie maar word ook deur topografie beheer. Steil sydige lineêre depressies kanaliseer die ongekonsolideerde sediment en swaar minerale en word opgradeer tot ekonomiese konsentrasies deur wind prossese. Die kwaliteit van die waardevolle swaar minerale in die satelliet areas is egter dieselfde as die van die aangrensende Namakwa Sands afsetting. Hierdie studie het gewys dat Houtkraal Remainder is die noordelike voortsetting van die Rooi Aeoliese Sand geassosieerde Oos Myn ertsliggam en bied die beste eksplorasie potensiaal.

.

ACKNOWLEDGEMENTS

First of all I give thanks to the Lord for giving me the strength, wisdom and determination during the course of this study.

I want to thank my supervisor professor Rozendaal for his guidance, positive criticism and encouragement during the course and upon completion of my Masters degree. His guidance has benefited me throughout my graduate studies.

I express my gratitude to Carlo Philander for being a great mentor, for providing me with data and his willingness to always help me and answering many questions.

Thanks must also be given to the department staff at Stellenbosch University whose direct assistance helped this project. These include Mrs Madeleine Frazenburg who helped me with my SEM analysis and Mr Dirk Frei for providing me with good LA-ICP-MS data.

I must also recognize Namakwa Sands Ltd for funding this project.

I want to thank my parents, my brother and sister for their love, for believing in me and for supporting me in more ways that I can list.

My gratitude goes to my friends Runique, Byron, Theo, Enid, Avina, Monica and Nohlanhla for their support and encouragement during the course of this thesis.

TABLE OF CONTENTS

LIST OF ABBREVIATIONS

Alt-Ilm -	Altered ilmenite (presented per THM)
Alt-IDX -	Alteration Index
a.p.f.u -	atoms per formula unit
HKRP -	Houtkraal Remainder Portion 2 (satellite area)
HKR -	Houtkraal Remainder (satellite area)
Grt -	Garnet
GW -	Geelwal Karoo (satellite area)
GRW -	Graauwduinen (satellite area)
Hem -	Hematite
Ilm -	Ilmenite
LA-ICP-MS -	Laser Ablation Inductively Coupled Plasma Mass Spectrometry
Lcx -	Leucoxene
LMT -	Lower Middle Terrace
Mn-Ilm -	Manganese ilmenite (pyrophanite)
MT -	Million tons
NMC -	Namaqualand Metamorphic Complex
NS -	Namakwa Sands
OFS -	Orange feldspathic sand
Px -	Pyroxene
QEMSCAN -	Quantitative evaluation of minerals by scanning electron microscopy
RAS -	Red aeolian sand
RF -	Rietfontein
Rt -	Rutile
SEM -	Scanning Electron Microscopy
THM (%) -	Total Heavy Mineral content as a percentage of total

TC -	Transgression Complex
Unalt-Ilm -	Unaltered ilmenite
UMT -	Upper Middle Terrace
VHM -	Valuable heavy minerals
XRF -	X-Ray Fluorescence
XRD -	X-Ray Diffraction
Zrn -	Zircon
∑-Ilm -	Sum of altered and unaltered ilmenite including Mn-ilmenite end-member (pyrophanite)
%	always represents wt% unless otherwise indicated

Abbreviations as used in figures 5.1-5.51

C -	Colourless
G -	Garnet
H -	Hematite
I -	Ilmenite
L -	Leucoxene
M -	Magnetite
O -	Oxides
P -	Pink
Si -	Silica
Q -	Quartz
R -	Rutile
T -	Tourmaline
Y -	Yellow

Abbreviations as used in figures 6.1-6.12

H - Hydrated ilmenite

I - Ilmenite

L - Leucoxene

P - Pseudorutile

R - Rutile

Si - Silica

LIST OF FIGURES

LIST OF TABLES

CHAPTER 1 INTRODUCTION

1.1 Location

The Namakwa Sands deposit is surrounded by five satellite areas north and south of it (Figure 1.2). Graauwduinen, Rietfontein and Geelwal Karoo form the southern anomaly (Janse van Vuuren et al, 2008) and Houtkraal Remainder and Houtkraal Remainder Portion 2 form the Houtkraal anomaly (Figure 1.2). The location of the five satellite areas as well as the rivers draining these and surrounding areas are illustrated in Figure 1.2. A satellite area is an area surrounding the main orebody that also contains mineralization. It usually has a lower concentration of heavy minerals and the satellite deposits are smaller in size than the main orebody. An increase in demand and record commodity prices of heavy minerals drew interest to these satellite deposits. These satellite deposits can increase the life-of-mine of the Namakwa Sands deposit if it proves to be economic. The latter depends on factors such as ore mineral composition and high VHM grades. This thesis presents the first data on the Namakwa Sands heavy mineral satellite Cenozoic deposits on above -mentioned five farms.

The Namaqualand coast is known for its onshore and offshore diamond occurrences. These occurs on beach terraces, in fluvial placer deposits along rivers such as the Swartlintjies River and Groen River and in marine deposits (beach and near shore sands and gravels) such as near the towns of Kleinzee, Alexander Bay and Hondeklip Bay along the Namaqualand coast and further north in to Namibia (Figure 1.1). The west coast is also well known for its archaeological and paleontological remains at Langebaanweg phosphate quarry and lignite occurrences at Koekenaap and further south. Salt with a NaCl content of between 92 and 99% is mined at the Rietfontein salt pan in the estuary of the Sout River (De Beer, 2010, Figure 1.2). Other mineral resources of the area include gypsum, limestone, dolomite, kaolin, iron, marble, kyanite, granite, sandstone, phosphate and graphite. Emphasis shifted in recent decades to include the exploration for and successful mining of heavy mineral deposits. Haughton (1931) was the first to report the occurrence of heavy mineral placer deposits along the west coast of South Africa.

The Namakwa Sands mine is one of the largest of its kind in the world and produces rutile, zircon and ilmenite of top quality. It includes two zircon products (prime zircon and zirkwa) and two rutile products (prime rutile and tiokwa). The average total heavy mineral content

(THM) of the deposit is 10% with an ilmenite grade of ± 3.3%, zircon grade of ± 0.85% and a rutile grade of ± 0.2% (Macdonald et al, 1997; Rozendaal and Philander, 2007, Rozendaal et al, 2009). The operation mines 17 MT of ore per annum and produces 350 000 tons of ilmenite, 110 000 tons of zircon and 25 000 tons of rutile (Rozendaal et al, 2009). It has a resource base of 800 million tons with a life- of- mine of 35 years (Palmer, 1994; Rozendaal et al, 2009).

The mine site is located at Brand-se-Baai, 385km north of Cape Town, together with two primary and secondary concentrator plants where dry mining (conveyers and loaders) is utilized (Rozendaal et al, 2009).

Heavy mineral concentrates are transported via a tarred road from the concentrator plants by truck to a mineral separation plant located 7km west of Koekenaap. The products are then transported via the Sishen-Saldanha railway line to the smelter close to Saldanha Bay. From here it is shipped via the Saldanha harbour to overseas markets (Gous, 2006).

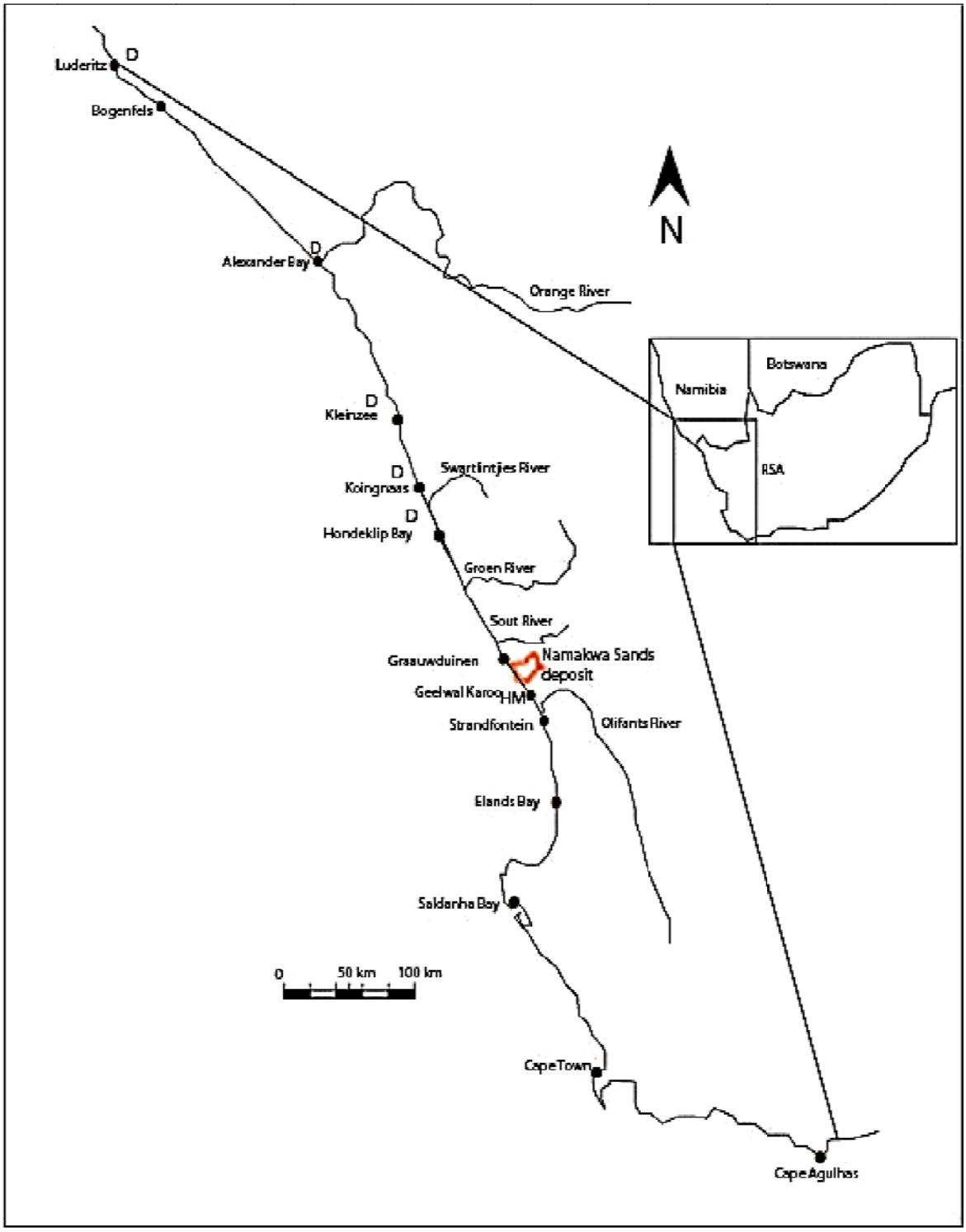

Figure 1.1. Map showing location of mining areas of diamonds and heavy mineral deposits. D indicates diamonds and HM indicates heavy mineral deposits.

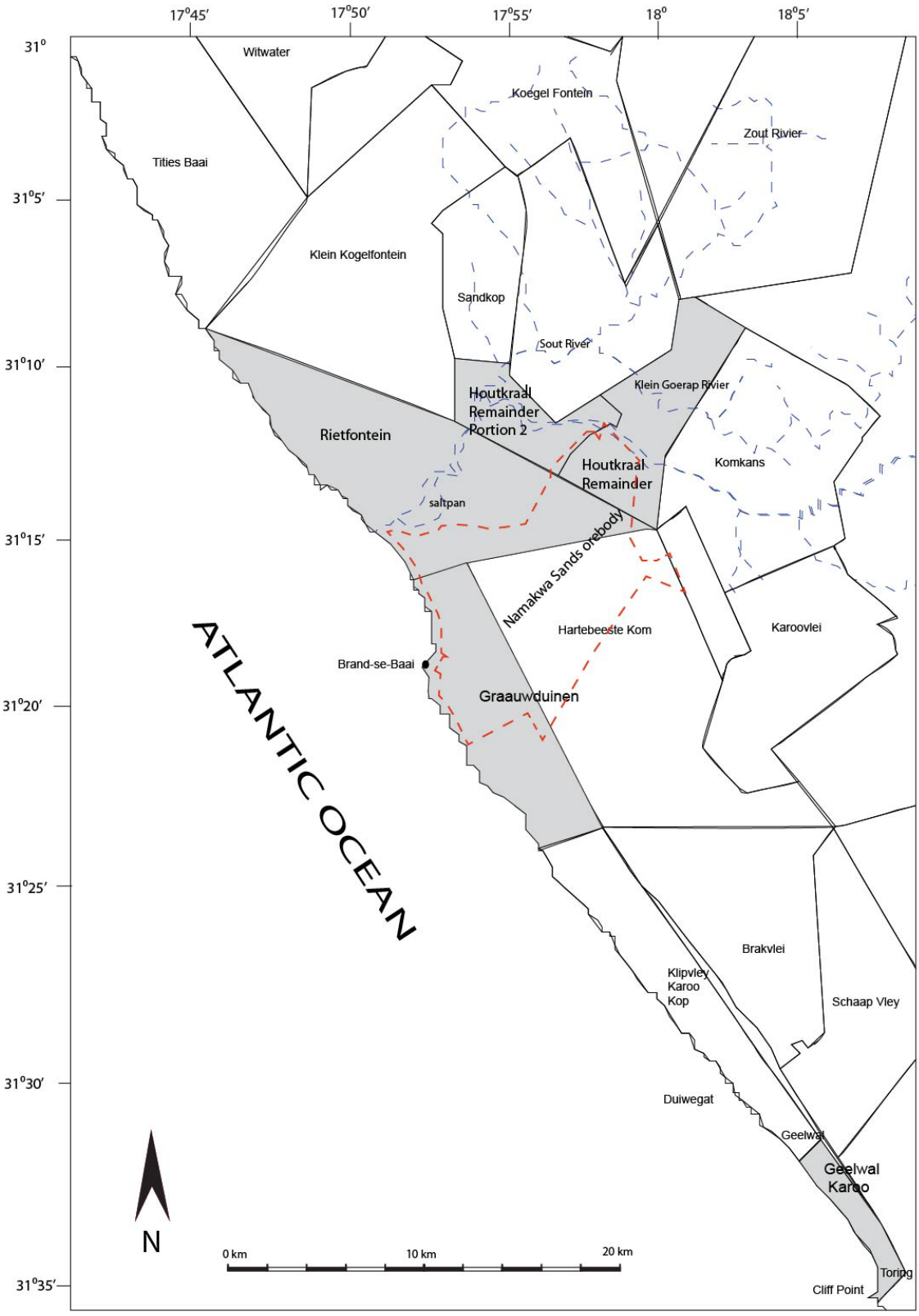

Figure 1.2. Locality map of the five satellite areas. Satellite areas are shaded in grey.

1.2 Previous work

Diamond discoveries in 1908 at Kolmanskop east of Lüderitz in Namibia and near Port Nolloth in 1925 and Alexander Bay in 1926 (Merensky, 1927) generated and directed significant interest to the west coast. It subsequently developed into the world's largest alluvial and marine diamond placer resource.

Haughton (1931) studied the heavy mineral placer deposits on the west coast of South Africa, in particular, in the vicinity of Geelwal Karoo where he identified the presence of raised beaches.

Toerien and Groeneveld (1957) did the first comprehensive study on the mineralogy and distribution of heavy mineral sands and deposits along the west coast between Strandfontein in the south to the Sout River in the north (Figure 1.1).

In the 1960's, the Geological Survey undertook an airborne radiometric/magnetic survey between the Olifants River and Hondeklip Bay area. Herzberg (1969, 1970) described follow-up prospecting and sampling results performed by the Geological Survey and identified three anomalous areas including Wallekraal, Soutfontein/Roodeheuwel and Graauwduinen (Palmer, 1994).

Anglo American Geophysical Services initiated a heavy mineral sampling programme along the Namaqualand coast to follow up on aeromagnetic and radiometric anomalies in 1986.

In 1987 they found Tertiary heavy mineral-bearing sands of up to 35m thick on the farm Graauwduinen. These positive findings led to the establishment of the Namakwa Sands Ltd heavy mineral mine in 2002. The Namakwa Sands deposit is currently operated by Exxaro Resources. Geelwal Karoo, a small beach placer deposit was discovered during the same time, and is owned by the Trans Hex Group (MacDonald 1996).

Rogers (1980) described the Cenozoic sediments on the coastal plain between Cape Town and Saldanha. He subdivided these sediments into five formations namely the Elandsfontyn Formation, the Saldanha Formation, the Varswater Formation, Rietvlei Formation and the Bredasdorp Formation.

Pether (1986, 1994) and Pether et al (2000) described the Neogene marine packages present along the Namaqualand coast. They identified three packages namely the 90m package, a 50m package and a 30m package with the latter being the youngest.

Cilliers (1995) completed his M.Sc. thesis on the Graauwduinen deposit, later to become the Namakwa Sands deposit, investigating its mineralogy, stratigraphy and provenance. Apart from establishing the first detailed stratigraphy for the sediments he also proposed the Namaqualand Metamorphic Complex (NMC) as the main provenance terrain for the heavy minerals of the Namakwa Sands deposit.

A year later MacDonald (1996) also completed his M.Sc. thesis studying the Geelwal Karoo modern day beach placer or strandline deposit. Heavy minerals accumulate along a 10km long beach in an active beach environment (Figure 1.3). He studied the mineralogy, geometry and internal structure of the Geelwal Karoo beach placer as well as the active processes that led to the development of such a modern day marine/beach placer. Macdonald (1996) following Force (1991) came to the conclusion that the morphology of the coast, together with wave action, formed this modern day strandline deposit.

Lignite deposits occur along the west coast of South Africa particularly near Koekenaap. Cole and Roberts (1996) studied these deposits concentrating on its characteristics and resources. They found that these deposits are of Miocene age and has in-situ exploitable resources of 29.7 MT which may be considered as physically and legally exploitable, now or in the near future (Bredell, 1987, Cole and Roberts, 1996). Due to its high ash and sulphur content these lignite deposits are of low rank making them uneconomic and only suitable for agricultural purposes.

Various scientific papers have been published on the Geelwal Karoo and Namakwa Sands deposits. Macdonald and Rozendaal (1995) investigated the mineralogy, stratigraphy and provenance of the Geelwal Karoo strandline and Macdonald et al (1997) studied the radiometric characteristics of heavy mineral deposits along the west coast. Zircon characteristics along the west coast were studied by Philander et al (1999) in the Kleinzee area.

A 125:000 geological map and explanation sheet of the Calvinia area was compiled by De Beer et al (2002) and included the regional and local geology of the Geelwal Karoo and Houtkraal areas.

Elferink (2005) studied the Cenozoic raised beaches on Geelwal Karoo, in particular the sedimentology, mineralogy and stratigraphy. The latter was then compared to the regional west coast stratigraphy to propose a regional geological model. She identified a fluvial clay unit that correlates with the channel clay formation at Kleinzee, two aeolian units that correlate with the Prospect Hill and Springfontyn Formations respectively, marine units that correlate with the 30m and 50m marine packages of Pether (1986) and a Recent aeolian unit which is equated with the Recent Witzand Formation.

The west coast region is characterized by a later superimposed duricrust also described as dorbank. Rozendaal and Philander (2007) studied this dorbank layer by means of 13 vertical profiles in the mine area and documented its influence on the recovery of heavy minerals at Namakwa sands. Several mineralogical studies of the Namakwa Sands deposit have been completed and most of them by Rozendaal et al (2009) and Philander and Rozendaal (2009).

De Beer (2010) produced a 125:000 geological map of the Garies area showing the geology of and around the Graauwduinen, Houtkraal and Rietfontein areas. An explanation sheet accompanying the map describes the nature of the rocks, its mineralogy, ages, deformation and metamorphism.

No detailed work on the satellite areas has been undertaken thus far in particular from a heavy mineral potential perspective. Namakwa Sands Ltd has completed a shallow drilling program to ascertain their heavy mineral potential because of their proximity to the present mining lease area. This study forms part of the Namakwa Sands exploration program and the specific areas of focus are listed under the aims and objectives heading (1.3).

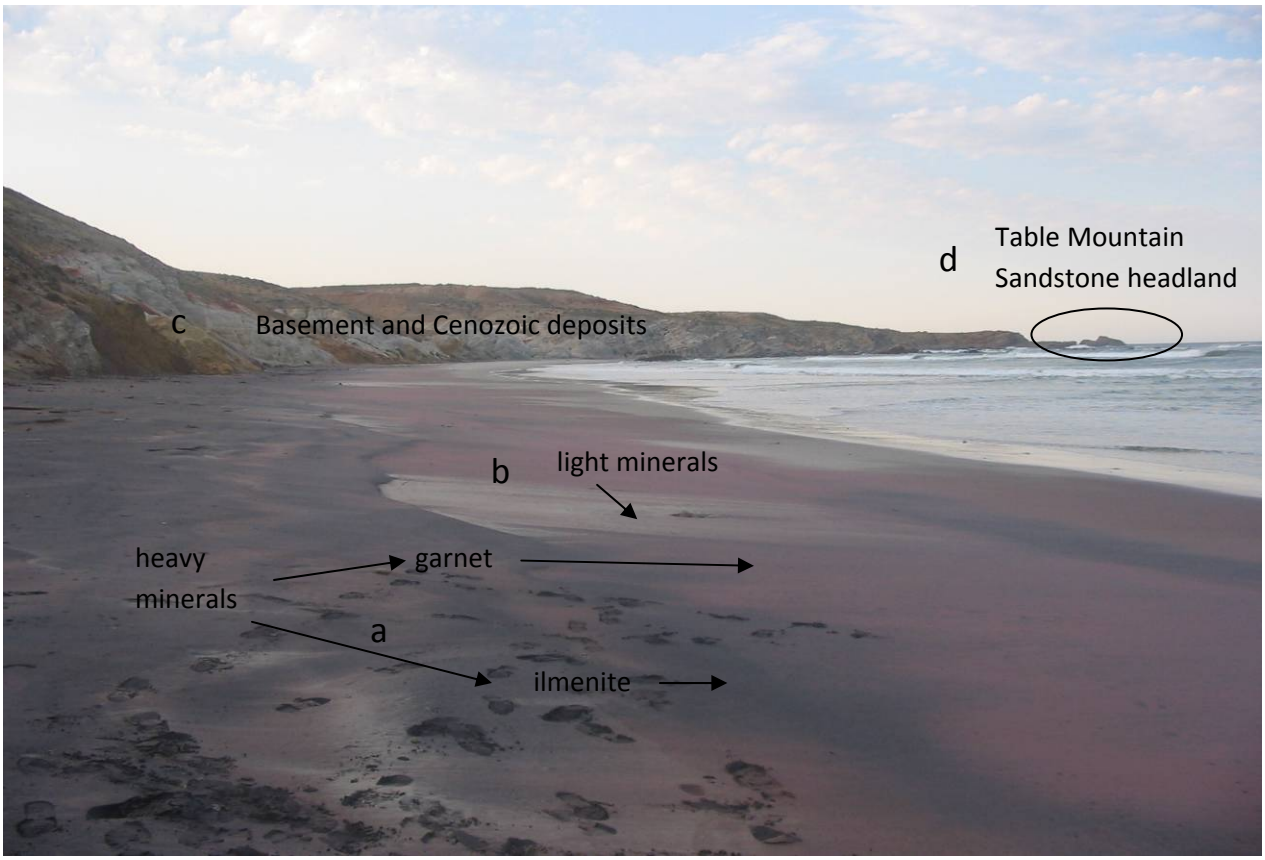

Figure 1.3. Geelwal Karoo, a modern day beach placer deposit along a section of the J-Bay shaped beach. a) Heavy minerals on back shore include ilmenite (dark) and garnet (red). b) Light minerals in swash zone/ foreshore. c) Embankment of basement and Cenozoic deposits (Photo looking southeast). d) Table Mountain Sandstone headland.

1.3 Aims and objectives

The satellite deposits surrounding the world class Namakwa Sands heavy mineral deposit are sub-economic occurrences that are peripheral and spatially distal to the main orebody. Revival of the heavy mineral market, indicated by high demand and record commodity prices, has generated new interest in these deposits. Previous studies on these peripheral areas were related to the determination of total heavy mineral (THM) content of borehole intersections and X-Ray Fluorescence (XRF) analysis for Zr and Ti content and with limited regard for the local and regional stratigraphic relationships. That situation has now changed and it has become imperative to understand the THM potential of these areas particularly with respect to Cenozoic stratigraphy, its lateral continuity and influence of surface features such as the development of duricrust. Previous mineralogical studies by Namakwa Sands were limited and simplistic and excluded modern analytical techniques such as Scanning

Electron Microscopy (SEM), Laser Ablation Inductively Coupled Plasma Mass Spectrometry (LA-ICP-MS) and QEMSCAN. Mineral surface features (i.e. coatings) and trace element content (Mn, Cr, Th, U) of individual mineral phases are important from an economic point of view and may also serve as diagnostic indicators of mineral provenance and deposit genesis.

The aims of this research are to:

- Determine mineralogy of the THM fraction of 54 composite samples representing 375 borehole intersections with special reference to the grain coatings and mineral chemistry. These results will contribute to assessing the economic importance of the suite and provide indicators of provenance.
- Compare the mineralogy of the satellite deposits to that of the presently mined Namakwa Sands deposit.
- Study ilmenite alteration and chemistry.
- Determine the provenance of the heavy mineral populations from the mineral chemistry and mineral petrography.
- Deduce the economic potential of the five satellite areas from the THM-VHM and mineral chemistry relationships.
- Explain the genetic relationships between the peripheral satellite and Namakwa Sands deposit.
- Is the Namakwa Sands deposit unique, if so, why?

CHAPTER 2 METHODOLOGY

To be able to achieve above listed objectives a diversity of methods have been used. These include optical microscopy, SEM, LA-ICP-MS, QEMSCAN, point-counting, XRF and hand-picking. The details of the various methods are discussed below.

2.1 Sampling

2.1.1 Sampling locality

Samples were collected by Namakwa Sands using hotline auger drilling on all five satellite areas. The locality of the holes is shown in Figure 2.1. The five satellite areas include:

- Houtkraal Remainder
- Houtkraal Remainder Portion 2

Houtkraal

- Geelwal Karoo
- Graauwduinen
- Rietfontein

In total 381 holes were drilled: 60 on the Houtkraal Remainder Portion 2 area, 44 on Houtkraal Remainder, 86 on the Geelwal Karoo area, 121 on Graauwduinen and 70 on Rietfontein. Borehole identification, grid used, XYZ co-ordinates and the total depth for all 381 holes are listed in Table A.1, (Appendix A). Borehole depth ranges from 0.03 to 4.68 m. The entire borehole depth is represented by one sample. Borehole depth was constrained by the first encounter of impenetrable dorbank or silcrete a function of the drilling technique used. This indicates that only the upper part of the Cenozoic stratigraphy was sampled. Boreholes were planned on a widely spaced (500m x 125m and 125m x 125m) grid system and surveyed following the LO17 survey system using Clarke 1880 as the projection.

2.1.2 Sampling method

Drilling was done in three phases starting with a wide grid and narrowing it down up to 50m x 50m to increase confidence levels of the data base. Phase 1 involved a 500m x 125m spaced

grid, sampling the surface unconsolidated sand on the farms of Geelwal Karoo, Graauwduinen and Rietfontein. A 125m spaced grid program was used for Houtkraal Remainder and Houtkraal Remainder Portion 2. As a protocol Namakwa Sands usually samples the surface sands first and if these sands do not prove to be economic, deeper sampling is not considered.

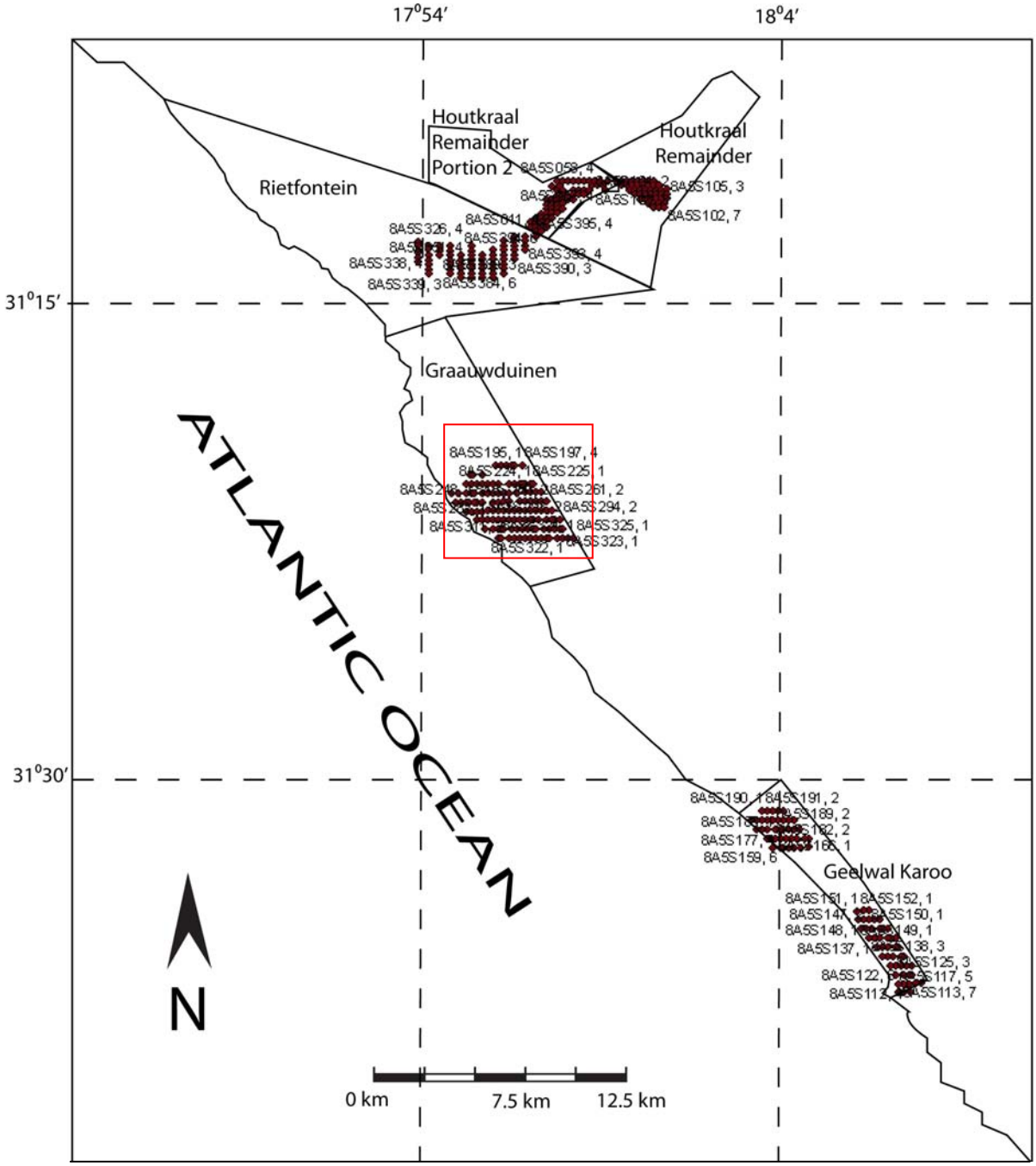

Figure 2.1. Map showing the locality of boreholes for the five satellite areas. The number adjacent to each borehole represents the borehole number (first digit) followed by the THM content.

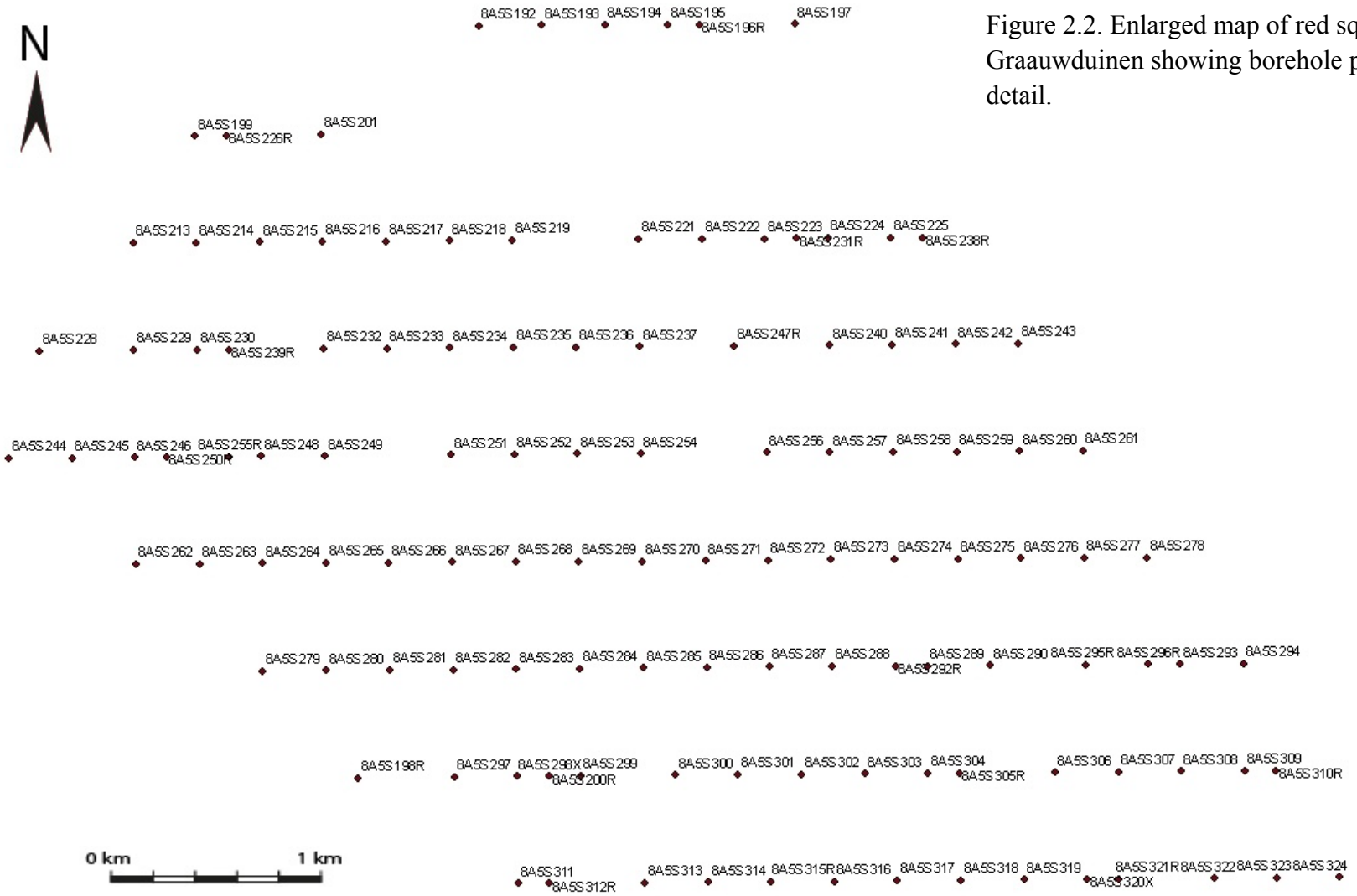

Figure 2.2. Enlarged map of red square area of Graauwduinen showing borehole positions in detail.

This is because historically THM content decreases with depth. Strandlines are the exception and have high concentrations of heavy minerals. A second drilling program was started in 2008 and was completed the same year (Janse van Vuuren et al, 2008).

Hotline auger drilling involves a light, pneumatic drill mounted onto a vehicle driven by a 50 cc diesel engine. The surface sand was sampled up to a maximum depth of 4.68m or until it reaches the dorbank/silcrete layer. This dorbank layer restricts further sampling since the upper part is silica-rich and is hard to drill through. It is also more lucrative to drill down to the dorbank layer. Therefore only the Red aeolian sand (RAS), upper part of sedimentary sequence, and probably part of the Orange Feldspathic Sand (OFS) was sampled (Cilliers, 1995). Each sampling site is indicated by wooden pegs in the field along an even spaced grid (Janse van Vuuren et al, 2008).

After sampling, the auger samples were put into a large plastic sample bag and then split by a riffle splitter repeatedly to obtain a mass of 1kg. 500g is kept by the mine as a back-up for future splits and reference. The 381 satellite samples of this study are splits of the back-up samples. As per definition total heavy minerals (THM) as indicated in the diagram below (Figure 2.3) are all minerals with a density of more than 2.9g/cm^3 and are represented as the float portion of a sample in a heavy liquid such as bromoform with a specific gravity of 2.85 to 2.89 (Janse van Vuuren et al, 2008). The procedure followed from sample collection to analysis is summarised below. XRF, QEMSCAN and point-counting were done on the 381mounts shown in Fig 2.3.

The 381 samples were also composited into a representative and homogeneous total of 54 samples based on the THM content, Al/ (Al+Fe) and Fe/ (Fe+Ti) ratios as prescribed by Namakwa Sands (Appendix A). The 54 composite samples with its THM content, Al/ (Al+Fe) and Fe/ (Fe+Ti) ratios are listed in Table A.2, (Appendix A). Al, Fe and Ti were used since they are the most diagnostic elements present in the heavy mineral fraction.

A detailed description of the procedure and rational to composite the samples is explained in Appendix B. Each of the 54 composite samples was split into two equal parts with a mini-splitter. One split was kept by Namakwa Sands. The other split was further split with a micro-splitter to obtain a representative amount of sample for the making of 54 polished sections by the Council of GeoScience in Pretoria. Methods listed below were employed to determine the heavy mineral suite, their chemical characteristics and end-members.

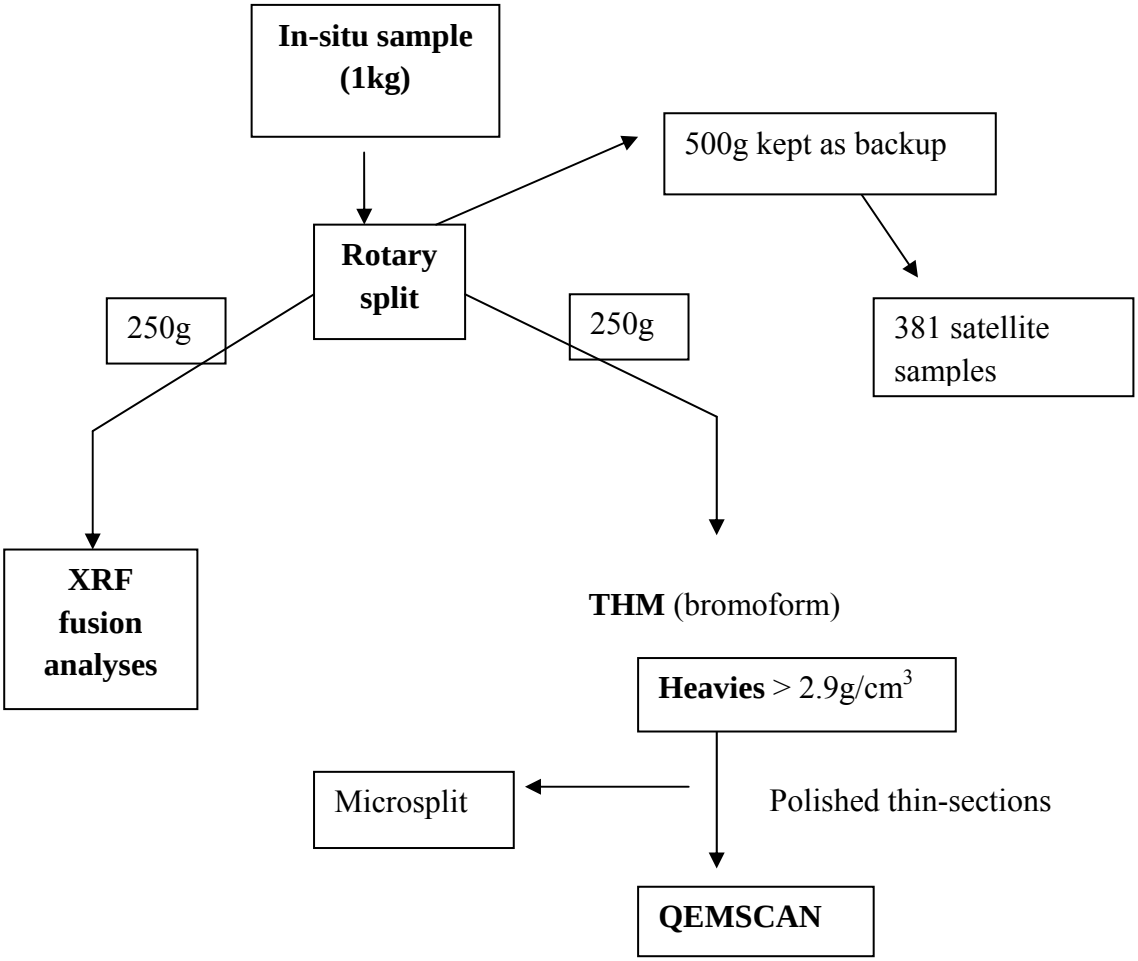

Figure 2.3. Schematic diagram illustrating the procedure for sample splitting before the QEMSCAN and XRF analytical methods used.

2.2 Analytical Techniques

2.2.1 Optical Microscopy

A Leitz polarizing microscope was used to identify minerals, alteration, textures and to describe the grain morphology (e.g. shape, coatings, mineral inclusions and possible mineral exsolutions) of the heavy minerals of all 54 samples. Transparent phases were studied using transmitted light and reflected light was used for opaque phases.

2.2.2 Handpicking

Some 200 rutile grains, 200 zircon grains and 200 ilmenite grains were randomly handpicked using a binocular microscope. The handpicked grains were mounted and polished and were used for SEM and LA-ICP-MS mineral chemistry studies.

2.2.3 Point-counting

Mineral point-counting for each of the 381 samples was done with the aid of QEMSCAN. Mineral proportions determined with the point-counting method are listed in Appendix D and were determined for ilmenite, rutile, zircon, leucoxene, garnet, pyroxene and other minerals. The latter includes the rest of the minerals in the heavy mineral suite present in minor to subordinate amounts such as tourmaline, staurolite, aluminosilicates, sphene, amphibole, corundum, epidote and monazite.

2.2.4 X-Ray fluorescence (XRF)

X-ray fluorescence analyses were done at the Mineral Separation plant facility at Namakwa Sands mine. Pressed pellets of the pulverized sand samples were prepared and used for analysis. XRF results obtained for all 381 samples are presented in Appendix E. Operating conditions are given in Appendix C.

2.2.5 Quantitative Evaluation of Minerals by Scanning Electron Microscopy (QEMSCAN)

QEMSCAN is a scanning electron microscope system that provides quantitative data on minerals, rocks and materials. It is an abbreviation for Quantitative Evaluation of Minerals by Scanning Electron Microscopy. It consists of a Scanning Electron Microscope (SEM), up to four light element Energy-dispersive X-ray spectroscopy (EDS) detectors and a software program that controls automated data acquisition. iDiscover is one such software package used for data processing. The dispersive spectrometers can identify minerals in just a few milliseconds. The surface of a specimen is scanned by a high energy acceleration electron beam along a predefined scan pattern creating a mineral compositional map (http://en.wikipedia.org/wiki/QEMSCAN). Elemental composition at each measurement

point of the scan pattern is provided by the generated energy dispersive X-ray spectra (EDX). Back-scattered electron (BSE) brightness and X-ray count information together with the elemental composition are converted into mineral phases. QEMSCAN in this study was used to do point-counting and to determine the percentage of altered ilmenite grains present in each sample. The latter allowed the calculation of an alteration index. The operation conditions are listed in Appendix C.

2.2.6 Laser Ablation Inductively Coupled Mass Plasma Spectrometry (LA-ICP-MS)

Approximately 200 rutile grains and 200 zircon grains were analyzed for its trace element and rare earth element (REE) chemistry with the aid of the LA-ICP-MS. Between 40 and 60 single grains were analyzed per satellite area and were considered statistically feasible for this study. Operating conditions are listed in Appendix C.

2.2.7 Scanning Electron Microscopy (SEM)

Seven representative (HKRP 001, HKRP 002, HKRP 004, HKR 001, GW 001, GRW 001 and RF 006) polished thin-sections were chosen to be studied under the SEM. The 54 polished sections showed similar mineralogy, textures and alteration. As a result the seven polished thin-sections were considered representative to reflect the salient features of the heavy mineral suite. The SEM provided a means of studying textural relationships within a single grain and between grains that could not be detected with the microscope as well to assist with the identification of unknown phases and mineral end-members. Operating conditions of the SEM are given in Appendix C. Approximately 200 ilmenite grains, between 40 and 60 grains per satellite area, were also analyzed with the SEM for its major element chemistry.

CHAPTER 3 GEOLOGICAL SETTING

3.1 Regional Geology

The regional geology of the west coast has been described by numerous authors (De Villiers and Söhnge, 1959; Carrington and Kensley, 1969; Tankard, 1976; Corvinus and Hendey, 1978; Rogers, 1980; de Decker, 1986 and Pether, 1986, 1994, Pether et al 2000; De Beer et al, 2002 and De Beer, 2010). It consists mostly of Precambrian crystalline basement rocks and Cenozoic mostly unconsolidated sediments. The basement rocks form part of the mid-Proterozoic Namaqualand Metamorphic Complex (NMC), which is unconformably overlain by the late Proterozoic Gariep Supergroup. The Vanrhynsdorp Group in turn unconformably overlies the Gariep Supergroup which is also overlain by Ordovician to Devonian sediments of the Cape Supergroup (De Beer et al, 2002). A brief description of each of the units follows below.

3.1.1 Basement rocks

Namaqualand Metamorphic Complex

The oldest rocks along the west coast include the Meso-Proterozoic Namaqualand Metamorphic Complex which is highly deformed and metamorphosed and was intruded by several pre-, syn- and late tectonic granitoids. Stratigraphically it consists of the Bushmanland (Kamiesberg) Group, (supracrustals – aluminous rocks, metapelites, quartzites, quartzofeldspathic gneisses, calc-silicates, mafic gneisses, metaconglomerates, amphibolites), Little Namaqualand Suite (metagranitoids – granite gneisses), Oorkraal Suite (mafic dykes and sills, amphibolites, two pyroxene granulites), Spektakel Suite (granites) and the Koperberg Suite (intermediate to mafic intrusive rocks). The latter four suites intruded the Kamiesberg Group between 1200 and 1030 Ma ago. The pelitic gneisses of the Sout River area have mineral assemblages indicative of granulite facies metamorphism with maximum temperatures of 850ºC and pressures of 5-7kbar (Waters et al, 1983; De Beer et al, 2002). Metapelitic rocks near Koekenaap (Figure 3.1) contain assemblages indicative of amphibolite facies (Moore, 1989). The various metamorphic facies zones have an east-west strike (Waters et al, 1983).

Gariep Supergroup

Table 3.1. Stratigraphy of the Gariep Supergroup (after De Beer et al, 2002).

		Formation	**Lithologies**
Gariep Supergroup	**Gifberg Group**	Bloupoort	Limestone, Sandstone, diamictite
		Aties	Shale, marble/dolomite/limestone
		Widouw	Marble/limestone/dolomite
		Karoetjies Kop	Quartzite/sandstone

The 883-717 Ma Gariep Supergroup rocks are exposed along the west coast and overlie gneiss of the Namaqualand Metamorphic Complex (Figure 3.1).

Vanrhynsdorp Group

The Neoproterozoic to Cambrian Vanrhynsdorp Group is correlated with the Nama Group in Namibia (De Beer, 2010). In the Sout River area there is an unconformity between the quartzite and schist of the NMC rocks and quartzite of the Vanrhynsdorp Group rocks. The age of this group of rocks is between 600 and 530 Ma (Gresse and Germs, 1993).

Table 3.2 Stratigraphy of the Varhynsdorp Group (after De Beer et al, 2002).

	Subgroup	Formation	Lithology
Vanrhynsdorp Group	**Brandkop**	Klipbak	Sandstone, shale
		Stofkraal	Mudstone, sandstone
		Van Zylkop	Shale, sandstone
	Knersvlakte	Astynskloof	Sandstone
		Dolkraals	Siltstone
		Kalk Gat	Mudstone
		Besonderheid	Shale, sandstone, conglomerate
		Gannabos	Shale, sandstone
		Arondegas	Sandstone
	Kwanous	Hoedberg	Shale, limestone/marble/dolomite
		Grootriet	Limestone/marble/dolomite
		Flaminkberg	Shale, sandstone

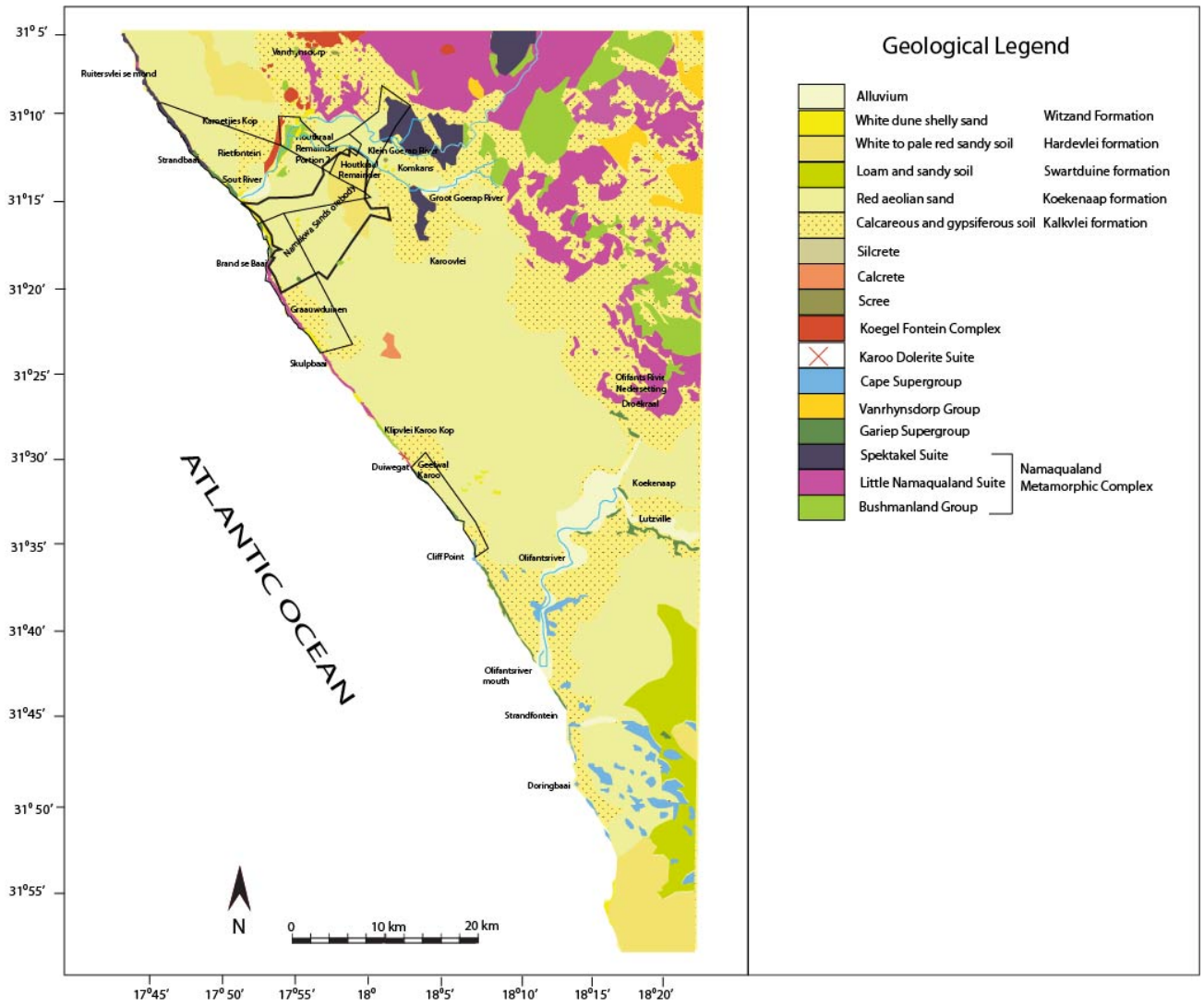

Figure 3.1. Geological map of the Namakwa Sands heavy mineral satellite deposits and surrounding areas. All geological information compiled and modified after maps 3017 Garies and 3118 Calvinia. (Scale 1: 250000, Council of Geoscience; De Beer (2010) and De Beer et al, 2002).

The Gariep Supergroup and the Vanrhynsdorp Group were metamorphosed and deformed during the Pan-African Orogeny which took place between 650 and 480 Ma years ago. The Pan-African Orogeny along the west coast involves two events: an early Gariep event and a younger Vanrhynsdorp event (De Beer et al, 2002). The Gariep Supergroup and Vanrhynsdorp Group rocks were subjected to greenschist facies conditions during the Pan-African orogeny with temperature and pressures around 400-450ºC and 4-5kbars respectively (De Beer et al, 2002).

Cape Supergroup

The Cape Supergroup along the west coast consists of the arenitic Table Mountain Group (arenites, diamictite, shale and conglomerate) and the alternating sandstone, shale and siltstone units of the Bokkeveld Group.

Koegel Fontein Complex and Biesjes Fontein Suite

The Namaqualand west coast was subjected to rifting in the Early Cretaceous period during which the basement rocks were intruded by the igneous Koegel Fontein Complex. It includes alkali and tholeitic basalt dykes, bostonite dykes, syenites, quartz porphyry dykes and a large pluton of alkali-feldspar granite. A large number of olivine melilite, olivine nephelinite and kimberlites of Upper Cretaceous age are also present along the Namaqualand coast (Dingle et al, 1983). These intrusive rocks are grouped as the Biesjes Fontein Suite. Alkaline mafic rocks of the Sandkopsdrift Complex (glimmerite, breccias, carbonatite) were emplaced after the Biesjes Fontein Suite. At Cliff Point on Geelwal Karoo evidence of Tertiary volcanic activity was found (Elferink, 2005).

3.1.2 Cenozoic deposits

Quaternary and Tertiary deposits cover large areas along the west coast and inland (Figure 3.1). Tertiary deposits occur both as shelf and continental slope deposits where it forms a vast but thin (up to 1.5km thick), coastal parallel lens along the margin from the Walvis Ridge to the Agulhas Fracture Zone (Dingle et al, 1983).

The Cenozoic deposits can be subdivided into two lithostratigraphic units based on age namely the Paleogene and Neogene units which in turn contains a variety of marine, fluvial

and aeolian deposits. Also present in the stratigraphy is a duricrust layer also referred to as silcrete, calcrete or ferricrete, as described by authors such as Pether et al (2000) and Roberts (2003). It consists of calcium and magnesium silicates, minor carbonates and clays from the smectite group and sepiolite. The rest of the stratigraphy consist of the Quagga's Kop Formation and various soils (loam and sandy soil, calcareous and gypsiferous soil, white to pale red sandy soil), red aeolian sand, white dune sands and alluvium of Neogene to Quaternary age that covers large areas along the coast and further inland.

Cenozoic deposits occur in three geographical areas: (1) deposits between Cape Town and the mouth of the Olifants River on the southwestern Cape coast (2) those on the Namaqualand coast between the mouth of the Olifants River and Orange River (3) those on the Namibian coast and further north (Pether et al, 2000). For this study the heavy mineral satellite areas occur along the Namaqualand coast. A brief description of the Cenozoic deposits along the Namaqualand coast is given below. Roberts et al (2006) termed the Cenozoic sediments along the west coast between Alexander Bay and Elands Bay the "West Coast Group".

Namaqualand coast

The most recent studies on the Neogene marine deposits especially along the Namaqualand coast are by Pether (1986, 1994), Pether et al (2000), Corbett (1996), De Beer et al (2002) and De Beer (2010). Late Cenozoic near shore marine deposits along the Namaqualand coast is important because of their diamond-placer and heavy mineral placer deposits.

Hondeklip Bay: The coastal plain of Namaqualand is mainly composed of three Neogene marine packages that were described by Pether (1986, 1994 and 2000). He identified three marine packages namely the younger 30m package, the 50m package and the oldest which is the 90m package. Roberts et al (2006) proposed the names Hondeklip Bay Member, Avontuur Member and the Kleinzee Member for these three units respectively and together forms the Alexander Bay Formation. The 30m package is transgressed by a 12m package, 4-6m package and a 2-3m package.

Carrington and Kensley (1969) did the first initial stratigraphic framework of the west coast and identified 75-90m, 45-50m and 17-2m transgression complexes (TC), 29-34m, 7-8m, 5m and 2m beaches. They ascribed the term transgression complex (TC) to the stratigraphic units

and perceived them to be all Pleistocene in age because of the bivalve shells and gastropod found in the deposits. They found distinct zone fossils in the 45-50m (*Donax haughtoni*) and 17-21m (*Donax Rogersi*) transgression complexes. The 29-34m beach contains the mollusc *Fissurella glarea*. Pether (1986) revised the work of Carrington and Kensley (1969), reclassified their nomenclature and improved the ages of the Cenozoic marine packages. He correlated the 30m package with the 29-34m beach and 17-21m TC of Carrington and Kensley (1969) since it also contains the zone fossil *Donax Rogersi* and *Fissurella glarea*. He referred to the 45-50m TC as the 50m package since it contains the zone fossil *Donax haughtoni* and the 75-90m TC as the 90m package (Table 3.3)

The 90m, 50m and 30m packages have their equivalents at Kleinzee termed the "Upper and Upper Middle Terrace, Lower Middle and Lower Terraces" respectively (Rogers et al, 1990). The Alexander Bay equivalents are the "Grobler, Upper and Middle Terraces" (Rogers et al, 1990).

Kleinzee: The Early Pliocene Upper Terrace at Kleinzee occurs at an elevation of 75-90m above mean sea level (amsl) (Figure 3.3 A). The Middle Terrace is divided into the Upper Middle Terrace (UMT) and the Lower Middle Terrace (LMT) (Rogers et al, 1990). The former are situated between 45-65m amsl and the LMT between 30-45m amsl. The Early Pleistocene Lower Terrace was deposited at an elevation between 10-30m amsl. Late Quaternary Terraces transgress the older Lower Terrace sediments in the Koingnaas area (Rogers et al, 1990). These terraces occur at an elevation between 10m and present sea level (8m, 5m and 2m) and are widely developed along the Namaqualand coast. The ages of these latter three terraces range from middle Miocene to Late Pleistocene with the 2m terrace being Holocene in age (Rogers et al, 1990).

Alexander Bay: In the vicinity of Alexander Bay further north from Kleinzee, well preserved marine terraces are present (Figure 3.3. B). The marine deposits are grouped into four terraces. The oldest Early Pliocene terrace is the Grobler Terrace at an elevation between 75-90m amsl. The Upper Terrace, the Middle and Lower Terraces occur between 35-60m amsl, 15-35m amsl and 0-15m amsl respectively. The Lower Terrace corresponds to Kleinzee's late Quaternary Terraces.

Table 3.3. A summary of previous work on the stratigraphic units of the west coast. Column 1: Succession after Carrington and Kensley (1969); TC, transgressive Complex; B, beach; FPS, fossiliferous phosphatic siltstone. Column 2: succession after Pether (1986); R, regression; T, transgression; 30m P, 30 metre Complex; 50m P, 50 metre Complex; 90m P, 90 metre Complex; FS, foreshore facies; USH, upper shoreface; LSH, lower shoreface; NSb, 50m Complex nearshore shelf; NSa, 90m Complex nearshore shelf. Column 3. Correlation between Carrington and Kensley (1969; Col 1) and Pether (1986; Col 2). Column 4: Neogene and Quaternary sea level cycles modified from Vail and Hardenbol (1979).

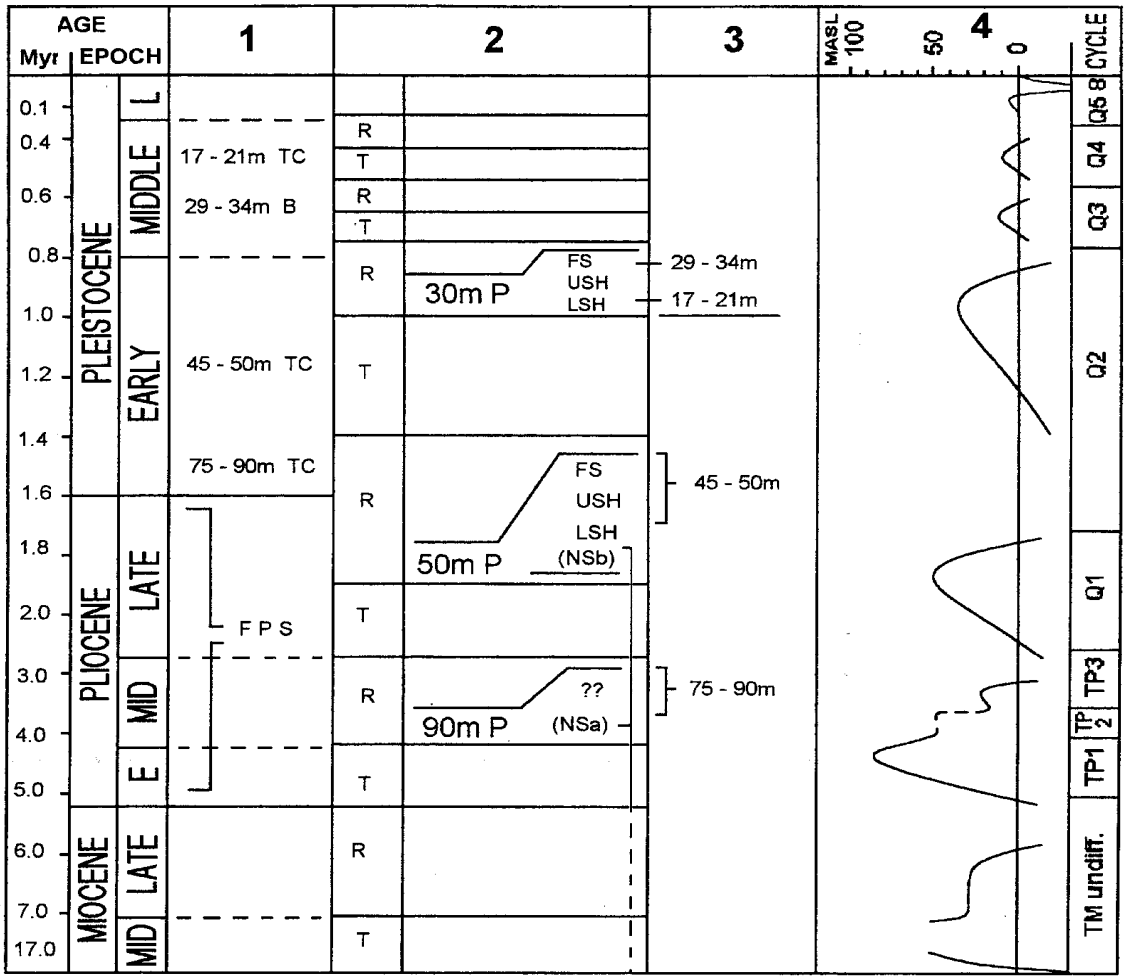

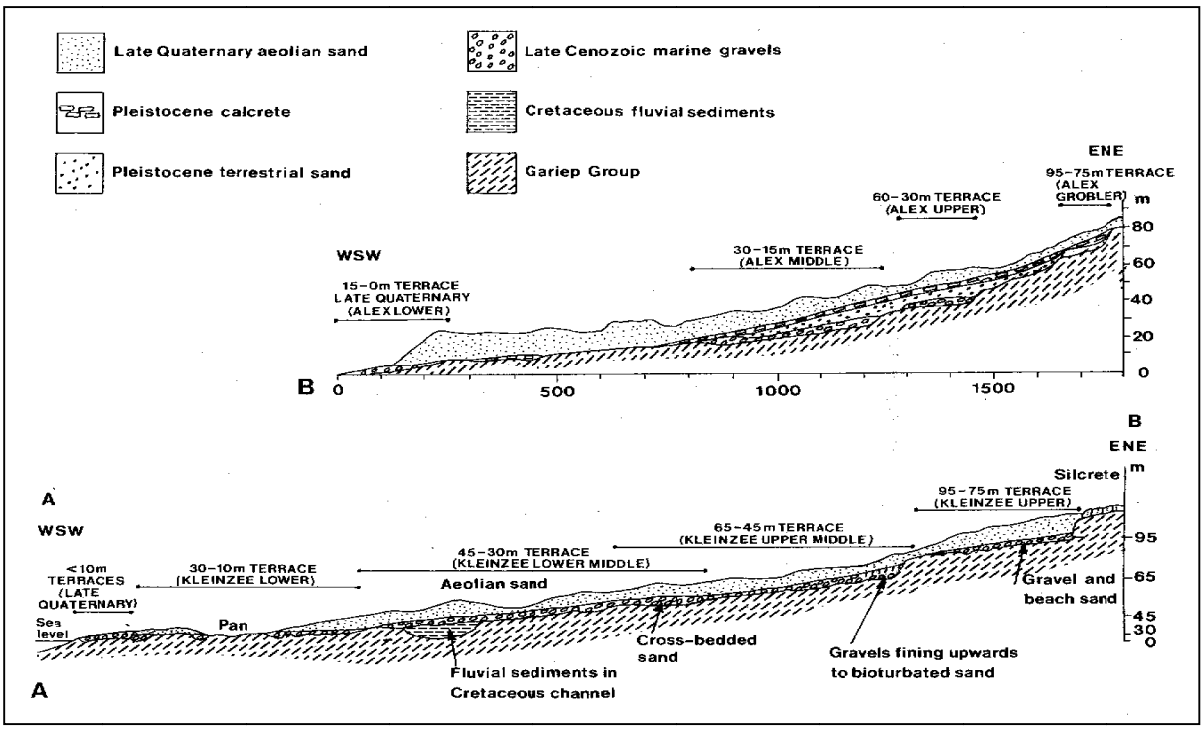

Figure 3.2. A) Geological southwest-northeast profile of the marine terraces at Kleinzee. B) Geological west-east profile of the marine terraces at Alexander bay (Rogers et al, 1990).

3.2 Local Geology of the Namakwa Sands satellite deposits and surroundings

The local geology surrounding the Namakwa Sands deposit and the satellite areas consist mostly of Cenozoic (Tertiary to Quaternary) sediments with outcrops of the Cretaceous Koegel Fontein Complex and basement of the Table Mountain Group, Vanrhynsdorp Group, Gariep Supergroup and the Namaqualand Metamorphic Complex (NMC; Figure 3.1).

Two east-west trending dolerite dykes of the Karoo Dolerite Suite occur on Geelwal Karoo near Duiwegat (Elferink, 2005; Figure 3.1). To the north of the study area large granitic and syenitic outcrops of the Koegel Fontein Complex intruded the Namaqualand Metamorphic Complex. Gneissic outcrops of the Little Namaqualand Suite cover large areas from Olifants River Nedersetting to the far north of the study area (Figure 3.1). The Little Namaqualand Suite is also present on Brand-se- Baai and further south on Geelwal Karoo where it parallels the coast. Large areas of the Sout River and its tributaries are underlain by pelitic gneisses of the Bushmanland Group. Granitic outcrops of the Spektakel Suite intruded around Houtkraal and Komkans southward to the farm Karoovlei and are present along the coast from south of

Strandbaai to north of Ruitersvlei se mond. NMC outcrops are also present along the Sout River, Groot Goerap and Klein Goerap rivers.

Quartzite and conglomerate of the Karoetjies Kop Formation of the Neoproterozoic Gariep Supergroup overlie NMC rocks on Karoetjies Kop along the coast. Limestone, marble, dolomite, quartzite and phyllite of the Widouw Formation are present along the Olifants River between Lützville and Koekenaap and on Geelwal Karoo along the coast to south of Cliff Point. North of Geelwal Karoo, along the coast, Gariep Supergroup rocks have rarely been preserved. A few small outcrops of the Aties and Widouw Formations are present north of Brand-se-Baai up to Karoetjies Kop in the north. Table Mountain sandstones unconformably overlie the Gariep Supergroup on Cliff Point. The latter unconformably overlies the NMC on Duiwegat (Macdonald and Rozendaal, 1995; Macdonald, 1996; De Beer et al, 2002).

Houtkraal Remainder Portion 2 consists of calcareous and gypsiferous soil, red aeolian sand, pale red to red dune sand and shelly white sand (Figure 3.1). De Beer (2010) grouped these sands under the Kalkvlei, Koekenaap and Hardevlei formations and Witzand Formation of the Sandveld Group (Theron et al, 1992) respectively. The latter are present surrounding the confluence of the Sout River with the Groot Goerap River. The shelly white sand overlies the pale red sand which in turn overlies the red aeolian sand. The red aeolian sand overlies the granitic and gypsiferous soil. According to De Beer (2010) the Kalkvlei formation consists of brown conglomerate, sand, silt, grit and clay with calcareous cement and grade into calcrete in places. The Koekenaap formation consists of unconsolidated red quartzose sands (De Beer, 2010). The red colour of the sand is due to prolonged oxidation of magnetite, ilmenite and maghemite grains in a hot and arid climate. The pale red to red dune sand consists of a mixture of dune plumes that were generated landward of sandy beaches and at river mouths during Pleistocene highstands (De Beer, 2010). These four sands were sampled by Namakwa Sands and used in this study.

Houtkraal Remainder consist mainly of the Hardevlei formation and also of the Koekenaap and Kalkvlei formations. These three sands were sampled by Namakwa Sands and used in this study.

The Cenozoic sediments on Geelwal Karoo consist of calcareous and gypsiferous soil (Kalkvlei formation), red aeolian sand (Koekenaap formation) and shelly white sand

(Witzand Formation; Figure 3.1). The latter three sands were sampled on Geelwal Karoo by Namakwa Sands and used in this study. The shelly white sand is present as narrow beach strips at the foot of the sea cliff on Geelwal Karoo and north of Cliff Point where it contains various heavy minerals such as rutile, ilmenite, zircon and garnet (De Beer 2010).

The satellite area Graauwduinen also consists of calcareous and gypsiferous soil and red aeolian sand as well as shelly white dune sand. Shelly white dune sand of the Witzand Formation are present along the coast as thin strips where it forms beach ridges and pocket beaches up the coast to north of Brand-se-Baai. On Graauwduinen the above three sands were sampled by Namakwa Sands and used in this study.

Rietfontein consists of calcareous and gypsiferous soil, red aeolian sand, pale red dune sand, shelly white sand and alluvium. The shelly white sand is present along the Sout River. Alluvium consists of unconsolidated coarse sand, gravel and silt and are present along all the rivers draining the Namakwa Sands deposit and satellite areas. The first two sands were sampled by Namakwa sands and used in this study.

The satellite areas according to De Beer (2010), with respect to the regional stratigraphy of the west coast, therefore fit into the Kalkvlei, Koekenaap and Hardevlei formations and Witzand Formation.

The satellite deposit areas in this study surround the Namakwa Sands and Geelwal Karoo heavy mineral deposits which form part of the local geology. De Beer (2010) applied a new stratigraphic name to the unusual heavy mineral enriched sediments of the Namakwa Sands deposit and called it the Graauw Duinen formation. Lithological details are shown in Figure 3.4 after Cilliers (1995). Sediments of the Namakwa Sands heavy mineral deposit consists of basal marine units that are overlain by aeolian sediments.

These sedimentary units are poorly exposed and the whole area is blanketed by the red aeolian sand (Koekenaap formation). Dorbank is also present in the Namakwa Sands ore body stratigraphy and causes the mineral sands to be unsuitable for treatment and proposes difficulties with separation. The layer is up to 15m thick and forms part of the Panvlei formation of De Beer (2010). The Panvlei formation which was named after a homestead on Zandkops Drift (De Beer, 2010) consists of fluvial deposits, sands and soils derived from

reworking of Cenozoic sediments and soils derived from bedrock erosion. When these sands are silicified it produces dorbank layers.

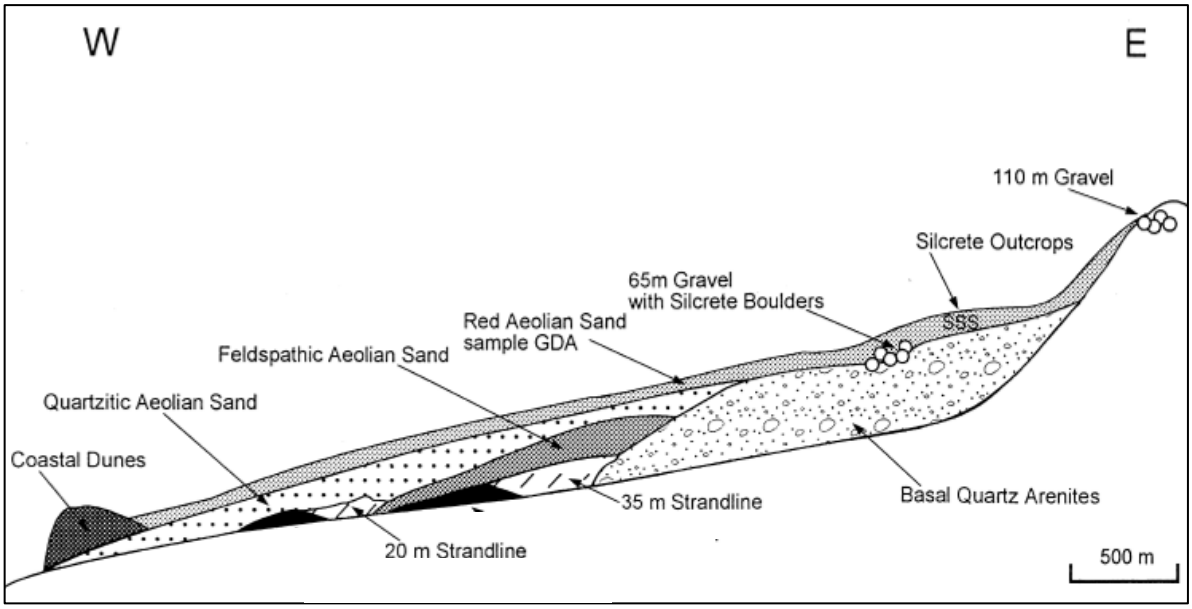

Figure 3.3. East-West geological cross section of the Namakwa Sands orebody.

Table 3.4. Comparison of the THM, mineralogy, TiO_2 content of ilmenite and resources of the Namakwa Sands and Geelwal Karoo heavy mineral deposits.

Deposit	**THM (%)**	**Resources (MT)**	**TiO_2 content of ilmenite (%)**	**Mineralogy**
Namakwa Sands	10	>800	48	ilmenite (60%), ilmenite alteration products (hydrated ilmenite, pseudo-rutile and leucoxene -11%), rutile, hematite, magnetite, chromite, garnet (40%), pyroxene, zircon, amphibole, tourmaline, staurolite, epidote, spinel, kyanite, monazite, collophane, corundum, cassiterite, marcasite, sphene, rhodonite, baddeleyite, Ce-florencite
Geelwal Karoo	67	10	51	ilmenite (65%), ilmenite alteration products (hydrated ilmenite, pseudo-rutile and leucoxene - 11%), rutile, hematite, magnetite, chromite, garnet (40%), pyroxene, zircon, amphibole, tourmaline, staurolite, glauconite, spinel

CHAPTER 4 GEOCHEMISTRY AND MINERAL DISTRIBUTION OF THE SATELLITE DEPOSITS

4.1 Introduction

This chapter discusses the chemical approach to determine the heavy mineral contents of the satellite deposits. This was done by means of XRF analysis. The conventional approach followed during exploration for heavy minerals is to determine the total heavy mineral content (THM) by means of heavy medium separation however this can also be done from XRF determined chemistry. Analyses were performed by Namakwa Sands (NS) at its Mineral Separation plant facility and chemical data is presented in Appendix E. Pressed pellets were made of each sand sample. QEMSCAN analyses were also performed on thin-section sand mounts by Namakwa Sands via Anglo American Research Laboratories to determine the mineral proportions and THM and were used to assist the XRF data in determining the heavy mineral content of the deposits. QEMSCAN data are presented in Appendix D. This XRF and QEMSCAN data were then used to construct chemistry and mineralogy correlation coefficient diagrams using GCDKit. Mineralogy correlation diagrams are presented in Appendix D (Figures D1-D5) and chemistry correlation diagrams in Appendix E (Figures E1-E5). These correlation coefficient diagrams indicate a relationship or trend between the matrix elements and minerals. This was done for each locality.

Maps were constructed of the THM concentration and of the thickness × THM, using Arcmap, which is a heavy mineral content parameter, of each satellite area,. The data was contoured to outline the mineral distribution and THM content. The thickness × THM maps were constructed since it gives a better idea of heavy mineral content in the deposits.

4.2 Rietfontein

Geochemistry

The southern part of the farm Rietfontein is located close to the coastline and borders on the northern periphery of the NS orebody and was sampled as previously discussed. Rietfontein does not show any correlations for the elements Al, Ca, Fe and Mg (Appendix E, Figure E1). This can be due to the diverse mineralogy of the area. Al for e.g. is concentrated in various minerals and not in one specific mineral. Rietfontein shows the same chemistry correlation

trends as the other satellite areas such as positive correlations between the matrix elements Fe and Mn (ρ=0.82), Fe and Ti (ρ=0.86) and Mn and Ti (ρ=0.77) (Appendix E, Figure E1). Fe, Mn and Ti show a positive correlation with Zr indicating the higher the zircon content, the higher the ilmenite, leucoxene and rutile content.

The mineralogy correlation diagram (Appendix D, Figure D1) shows that an increase in ilmenite, rutile, zircon and leucoxene content is accompanied by a garnet decrease. Leucoxene and unaltered ilmenite have a positive correlation. The THM and VHM have a positive correlation of (ρ=0.82) indicating that not all THM is VHM and a significant amount of non-economic minerals are present. Rietfontein has the lowest THM-VHM correlation coefficient of the satellite areas and from a sedimentological perspective is the least mature.

Mineral distribution

The THM content of Rietfontein (Figure 4.1) increases from a northwesterly direction towards the northeasterly striking outline of the Namakwa Sands orebody with a rapid increase in THM to reach a maximum of 6%. The thickness × THM map (Figure 4.2) shows that the THMm content remains low mainly because of the limited thickness of the intersection. As the Namakwa Sands orebody is approached the thickness increases significantly.

4.3 Houtkraal Remainder Portion 2

Geochemistry

The correlation coefficient matrix of the Houtkraal Remainder Portion 2 samples show a moderate positive correlation between Al and Ca (ρ=0.66) and Ca and Mg (ρ=0.74, Appendix E, Figure E2). Al and Ca indicate the presence of minerals such as garnet, amphibole and epidote and Ca and Mg the presence of garnet and pyroxene in the THM. The moderate correlation between Al and Ca indicate that these two elements are not concentrated in one Al -and Ca-bearing mineral but in more than one. The moderate correlation of Ca and Mg also indicates that the Ca and Mg are concentrated in garnet and pyroxene and not just garnet or just pyroxene. The moderate to good positive correlations between Fe and Mn (ρ=0.74), Fe and Ti (ρ=0.76) and Mn and Ti (ρ=0.97) indicate the presence of minerals such as ilmenite, rutile, leucoxene and garnet. The good correlation of Mn and Ti indicates that most of the Mn

and Ti are present in ilmenite (Fe, Mg, $MnTiO_3$). The good correlations between Ti and Zr (ρ=0.98), Fe and Zr (ρ=0.73), Mn and Zr (ρ=0.95) and Mn and Ti (ρ=0.97) indicate that as ilmenite, rutile and leucoxene, which are all titanium-, manganese- and iron-bearing, in the THM increases; the amount of zircon also increases. The THM and VHM data has also been included in the chemistry matrix and Fe, Mn, Ti and Zr show a positive, linear relationship with the VHM. This positive trend is expected since the latter elements make up or are concentrated in the VHM (ilmenite, rutile, zircon and leucoxene) fraction. Mn, Ti, Fe and Zr show a negative correlation with Si as expected.

Ilmenite has a positive relationship with the VHM (ρ=0.71) indicating that as ilmenite content increases, the VHM also increases as expected (Appendix D, Figure D2). Ilmenite shows a poor correlation with the THM (ρ=0.62). The latter is due to the presence of other heavy minerals in the THM such as rutile, garnet and staurolite that also plays a role in increasing the THM content. Ilmenite has a strong, negative correlation with garnet. The VHM and THM have a positive correlation of 0.99 indicating that as the VHM increases the THM also increases. It also indicates that 99% of the THM is VHM with few non-economic minerals present in the THM. From a sedimentological point of view this relationship indicates a high maturity based on the dominance of stable minerals in a marine-aeolian environment.

Mineral distribution

The THM content of Houtkraal Remainder Portion 2 does not exceed 6% (Figure 4.3) and is well below that of the average of the Namakwa Sands deposit. High grade areas are located to the southwest and northeastern side of the satellite area. Low THM areas are more extensive and occur in the southwest stretching towards the northeastern side of the satellite area.

The southwestern relatively high grade area borders on the edge of the Namakwa Sands deposit but rapidly decreases in concentration towards the northwest.

The thickness × THM map has THMm values as high as 15 (Figure 4.4). The best content of heavy minerals remains in the southwest and the sand thickness increases towards the Namakwa Sands orebody boundary.

4.4 Houtkraal Remainder

Geochemistry

Houtkraal Remainder located to the northeast has higher correlation coefficients than Houtkraal Remainder Portion 2 for Al and Ca (ρ=0.85), Al and Mg (ρ=0.83) and Ca and Mg (ρ=0.97) respectively (Appendix E, Figure E3). The higher correlation coefficient of Ca and Mg indicate that most of the Ca and Mg are concentrated in garnet or pyroxene with only a small amount in amphibole and epidote. The higher correlations between Al and Ca and Al and Mg also indicate that most Ca, Al and Mg are present in garnet and less in amphibole and epidote. Fe and Mn (ρ=0.93) and Fe and Ti (ρ=0.98) also show better correlations than Houtkraal Remainder Portion 2. These good correlations between the matrix elements indicate that almost all of the Fe, Ti and Mn occur in ilmenite with only a small amount in rutile, garnet and leucoxene.

Fe and Zr (ρ=0.96), Ti and Zr (ρ=0.99) and Mn and Zr (ρ=0.98) also have good correlations indicating the positive relationship between ilmenite and zircon in the heavy mineral suite. There is a negative, linear relationship between Al/Al+Fe and Zr, Fe, Ti and Mn, indicating the more Al/Al+Fe-rich minerals such as garnet and aluminosilicates are present in the THM, the less ilmenite, rutile, leucoxene and zircon are present. This further indicates that the higher the VHM the less non-economic minerals (garnet, aluminosilicates, and staurolite) are present. Houtkraal Remainder also has a positive, linear relationship between Fe, Mn, Ti and Zr and the VHM which is to be expected.

Mineral abundances and ratios as determined by QEMSCAN show that ilmenite increases with decreasing garnet (Appendix D, Figure D3). Unaltered ilmenite has a negative correlation with leucoxene and the alteration index (Chapter 6). Altered ilmenite has a positive correlation with the alteration index. This is to be expected as unaltered ilmenite alters to leucoxene (altered ilmenite). As the amount of leucoxene (altered ilmenite) increases, so the alteration index will also increase and the amount of unaltered ilmenite will decrease. The VHM and THM content of the sample suite have a correlation of ~1 indicating that effectively all heavy minerals present are of value. It also reflects a high maturity of these sediments with the most stable minerals being preserved.

Mineral distribution

Houtkraal Remainder has THM values as high as 11% (Figure 4.5). It has the highest THM values of all the satellite areas. It borders on the northeastern extension of the eastern Namakwa Sands orebody which consists mostly of RAS. From this information it can be deduced that the East Mine has the potential to be extended in an east-north-east direction. It is expected to rapidly terminate as is demonstrated by the northern and northeastern flank of the orebody. Low THM areas are restricted to the northeast of the satellite area and rapidly decrease away from the high grade areas.

The thickness × THM map (Figure 4.6) shows the same trend as the THM map. High grade areas are irregularly distributed and are present to the southeast of the satellite area with THMm values as high as 34 and rapidly tapers off to the north and northwest. The thickness of the sand also decreases in the same direction. The heavy mineral concentration is the highest of all satellite areas studied and marks the northern periphery and northeastern termination of the East Mine high grade RAS deposit. This sharp boundary between low and high THM or THMm values has important implications for the genesis of the deposit.

4.5 Geelwal Karoo

Geochemistry

Geelwal Karoo is the southernmost of all the satellite areas and is distal to the Namakwa Sands orebody and proximal to the coastline (Fig.1.2). The sample suite shows good, positive, linear relationships for Ca and Mg (ρ=0.88), Mg and Fe (ρ=0.8), Mg and Mn (ρ=0.81), Al and Fe (ρ=0.67) and Al and Ca (ρ=0.66) respectively (Appendix E, Figure E4). The two Houtkraal areas do not show these positive relationships for Mg and Fe, Mg and Mn and Al and Fe. These elements are present in garnet and the good correlations for Geelwal Karoo indicate that these elements occur mainly in garnet. The absence of above correlations in the two Houtkraal areas can be due to low concentration of garnet and the Mn, Fe and Mn being present in various other Mg-Fe-Al- and Mn-bearing minerals such as amphibole and pyroxene. Geelwal Karoo also has positive relationships between the matrix elements Fe and Mn (ρ=0.93), Mn and Ti (ρ=0.77) and Fe and Ti (ρ=0.76) indicating an ilmenite host. Characteristic of Geelwal Karoo is a positive correlation between Ca and P indicating the

presence of apatite. The high rho (ρ) value of 0.81 further indicates that most of the Ca and P are present in apatite. This is a common association for unconsolidated sediments proximal to the coast. Fe, Ti, Zr and Mn also show an increase with increasing VHM but has less good correlations (0.6, 0.72, 0.62 and 0.68 respectively) compared to the two Houtkraal areas.

The mineralogy correlation diagram indicates that ilmenite rutile, leucoxene and zircon, which makes up the VHM, increases with respect to each other (Appendix D, Figure D4). This trend is expected since Fe, Zr, Mn and Ti increases with the VHM. Garnet decreases with increasing ilmenite, rutile, leucoxene and zircon (Appendix D, Figure D4). The two Houtkraal areas only show a negative relationship between ilmenite and garnet. Ilmenite is the most abundant heavy mineral in the THM fraction and is therefore more likely to show relationships with other heavy minerals. As leucoxene increases, unaltered ilmenite increases as well. An explanation for the positive relationship is that these two minerals are not a product of one another. Leucoxene does not form from the alteration of unaltered ilmenite but is added to the heavy mineral fraction by e.g. the wind from the source area and therefore does not form in-situ (after deposition). The THM and VHM has a correlation of ρ=0.86 which indicates that a considerable amount of non-economic minerals are present in the THM fraction. This is a clear distinguishing factor and separates it from the two Houtkraal farms.

Mineral distribution

Geelwal Karoo consists of two sampled areas. It is referred to as Geelwal Karoo 1 and Geelwal Karoo 2. Geelwal Karoo 2 in Figure 4.9 is located southeast of Geelwal Karoo1 in Figure 4.7 (Figure 2.1, Chapter 2). The patches of high THM content of Geelwal Karoo 1 and 2 decreases away from the coastline towards the northeast (Figures 4.7 and 4.9). The patches of high THM (maximum of 17%) are related to the older proximal heavy mineral strandlines which acted as a source for the present deposits (Macdonald 1995 and Elferink, 2005). There was clearly no concentrating mechanism that facilitated the deposits to extend inland. The remaining extensive area has a very low THM content (Figures 4.7 and 4.9). The thickness × THM map of Geelwal Karoo 1 (Figure 4.8) does not show any significant concentration of heavy minerals indicating a thin surficial coverage only. The thickness × THM map of Geelwal Karoo 2 (Figure 4.10) show values as high as 21 THMm indicating a well mineralized thick strip that parallels and is proximal to the coastline. This association

indicates that the proximity of a high grade heavy mineral source is imperative to form aeolian deposits of significant grade.

4.6 Graauwduinen

Geochemistry

The Graauwduinen area sampled forms the southeastern periphery of the Namakwa Sands orebody and is located near the coastline. The sampling geochemical database shows positive, linear relationships similar to Geelwal Karoo for Al and Fe (ρ=0.76), Ca and Mg (ρ=0.73) and Al and Ca (ρ=0.73) respectively (Appendix E, Figure E5). Only Ti and Zr show a positive, linear relationship indicating as rutile, leucoxene and ilmenite increases, zirconium also increases. Mn and Fe do not show any trend with Zr as the other four areas do. Ti and Zr show a positive correlation with the VHM but there is no correlation between Fe, Mn and the VHM as for the other four areas. The latter conclusion indicates that the VHM increase is mainly due to an increase in rutile, leucoxene and zircon. Fe and Mn (ρ=0.76) show a good, positive correlation but there is no trend between Mn and Ti and Fe and Ti as for the other four areas indicating that the Mn, Fe and Ti are concentrated in a variety of Fe-, Mn- and Ti-bearing minerals such as ilmenite, rutile, garnet and leucoxene and not one specific mineral. The VHM and THM have a correlation of (ρ=0.83) and indicates that a considerable amount of non-economic minerals are present in the THM fraction.

The mineralogy correlation diagram of Graauwduinen show very similar correlation coefficients and mineral trends to that of Geelwal Karoo (Appendix D, Figure D5). Garnet also decreases with increasing ilmenite, rutile, leucoxene and zircon. This is expected because of their similar location along the coastline.

Mineral distribution

THM contents ranges from 1-7% (Figure 4.11) and increases from low concentrations in the southeast to grades of 7% THM in a fan shape towards the northwest. The thickness × THM map (Figure 4.12) indicates that towards the southwestern margin of the Namakwa Sands orebody the grade and thickness increases significantly over a very short distance. This has important implications with respect to orebody outline and genesis.

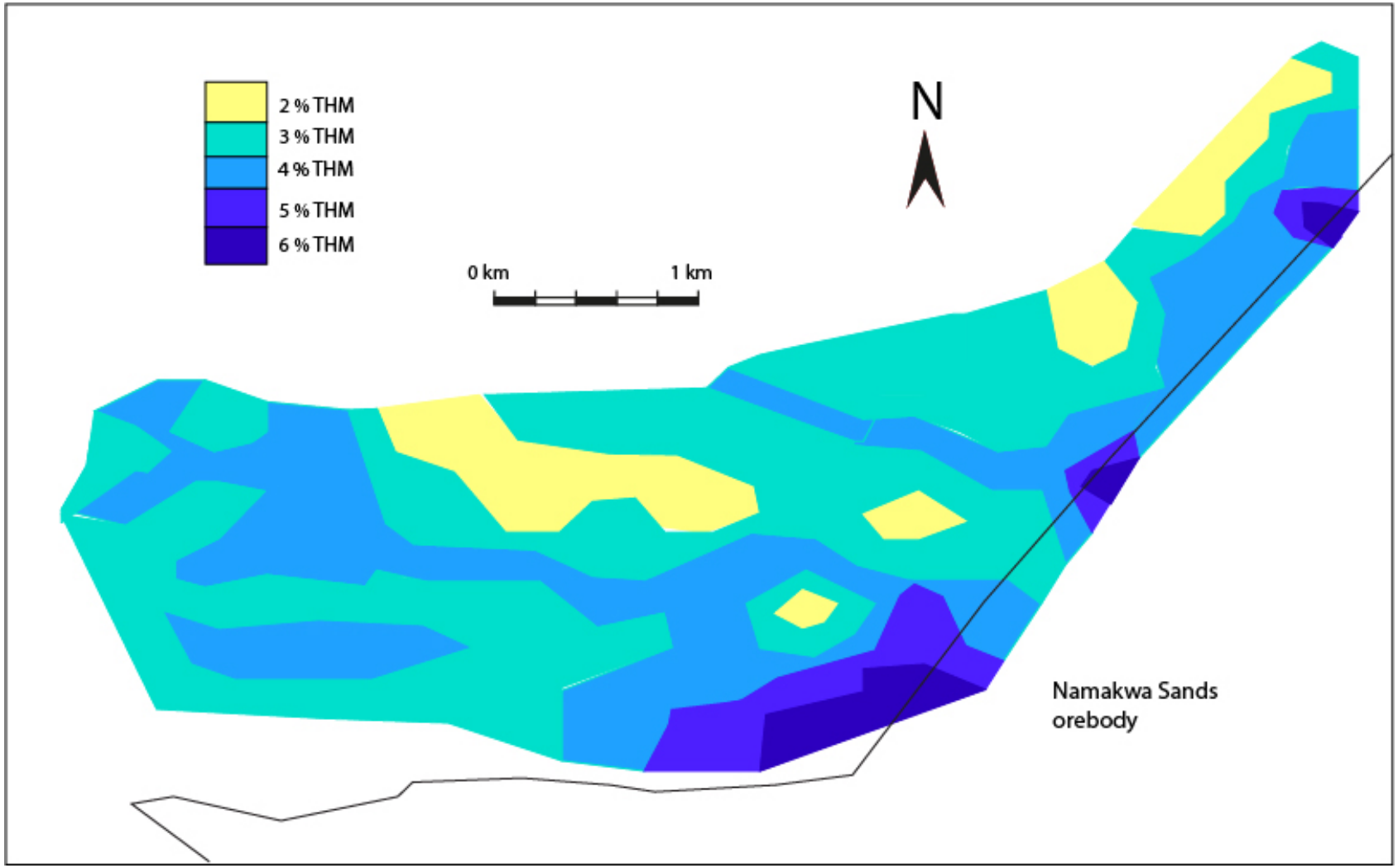

Figure 4.1. Map showing the THM distribution of Rietfontein.

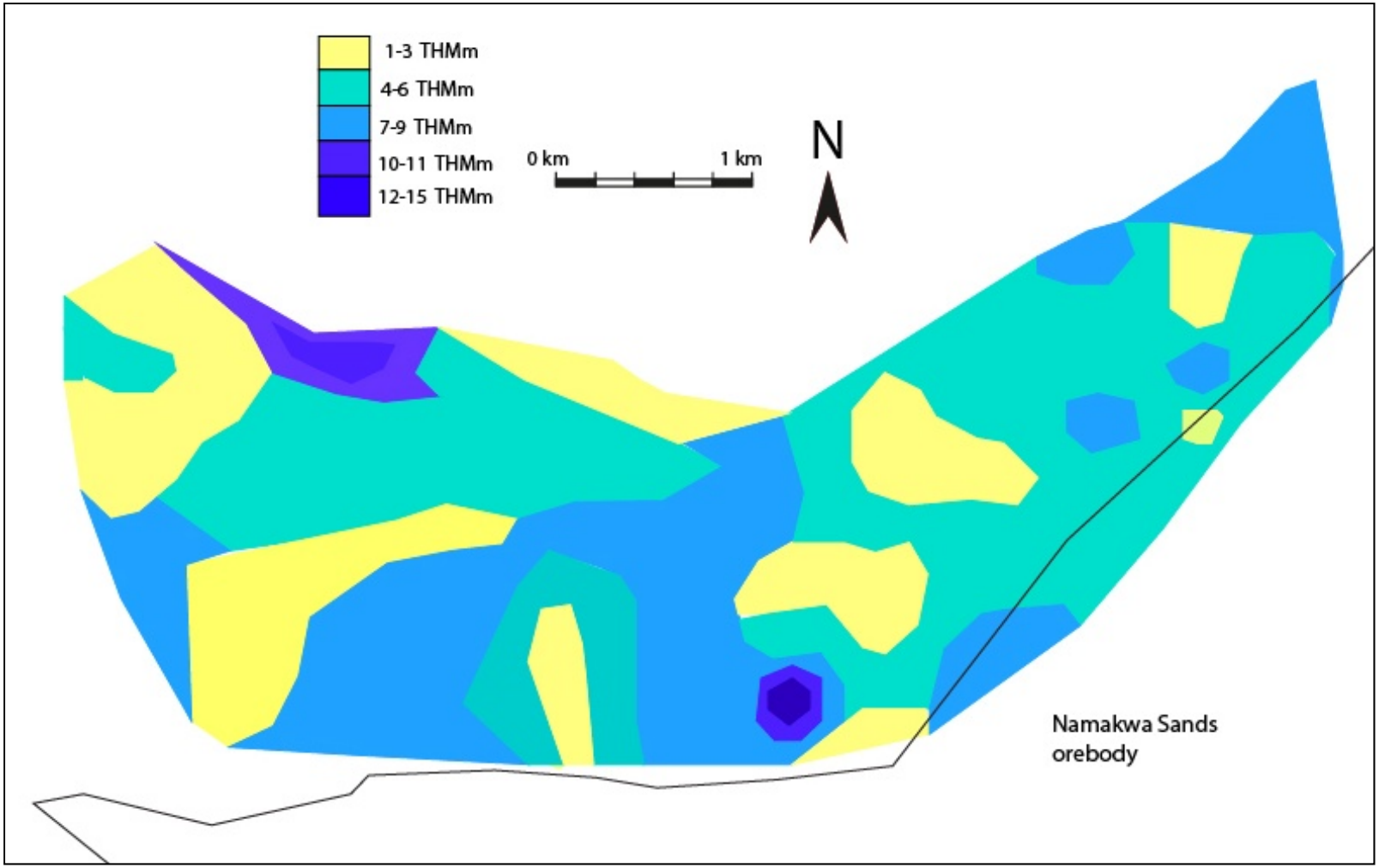

Figure 4.2. Thickness×THM map of Rietfontein.

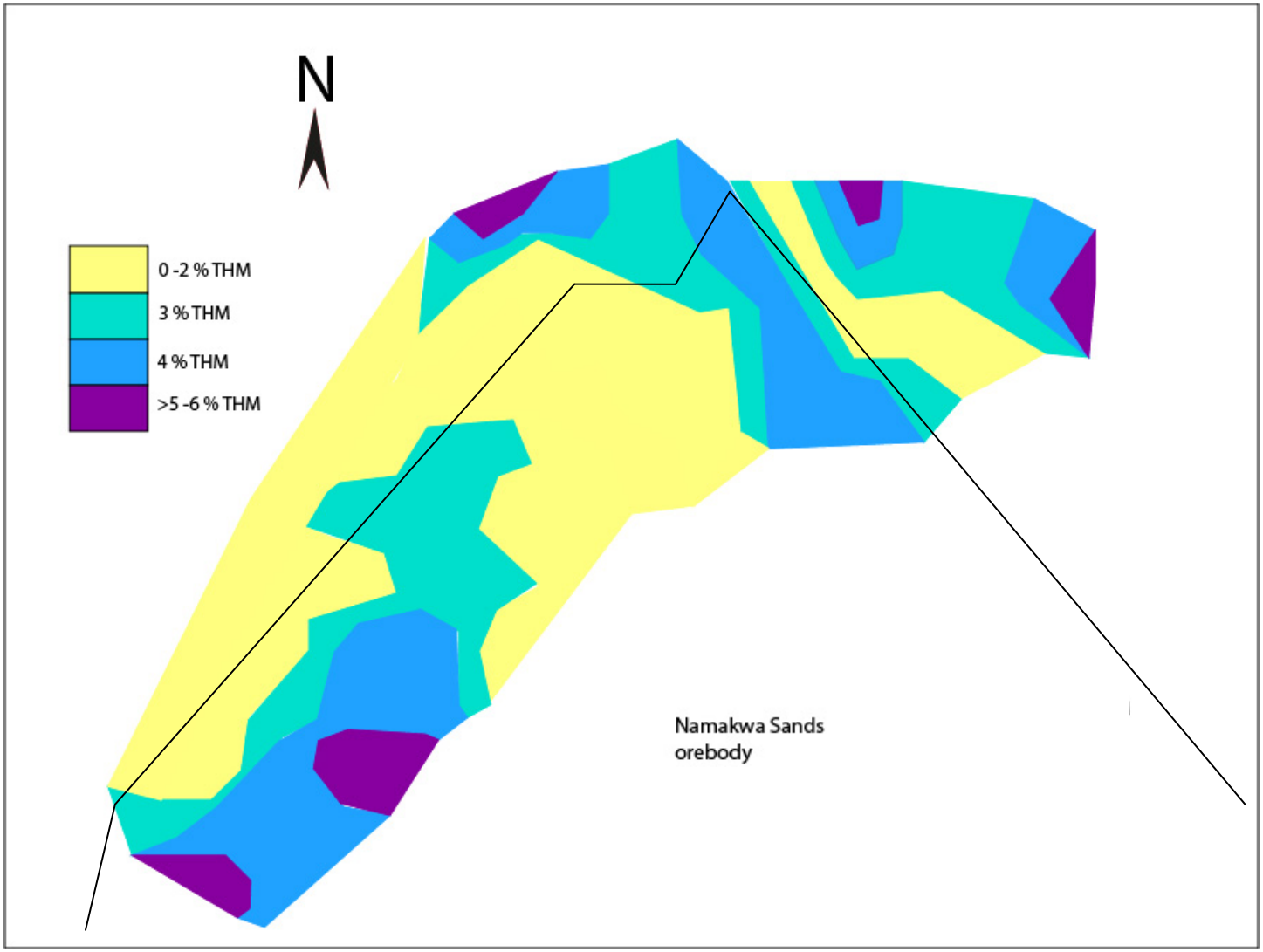

Figure 4.3. Map showing the THM distribution of Houtkraal Remainder Portion 2.

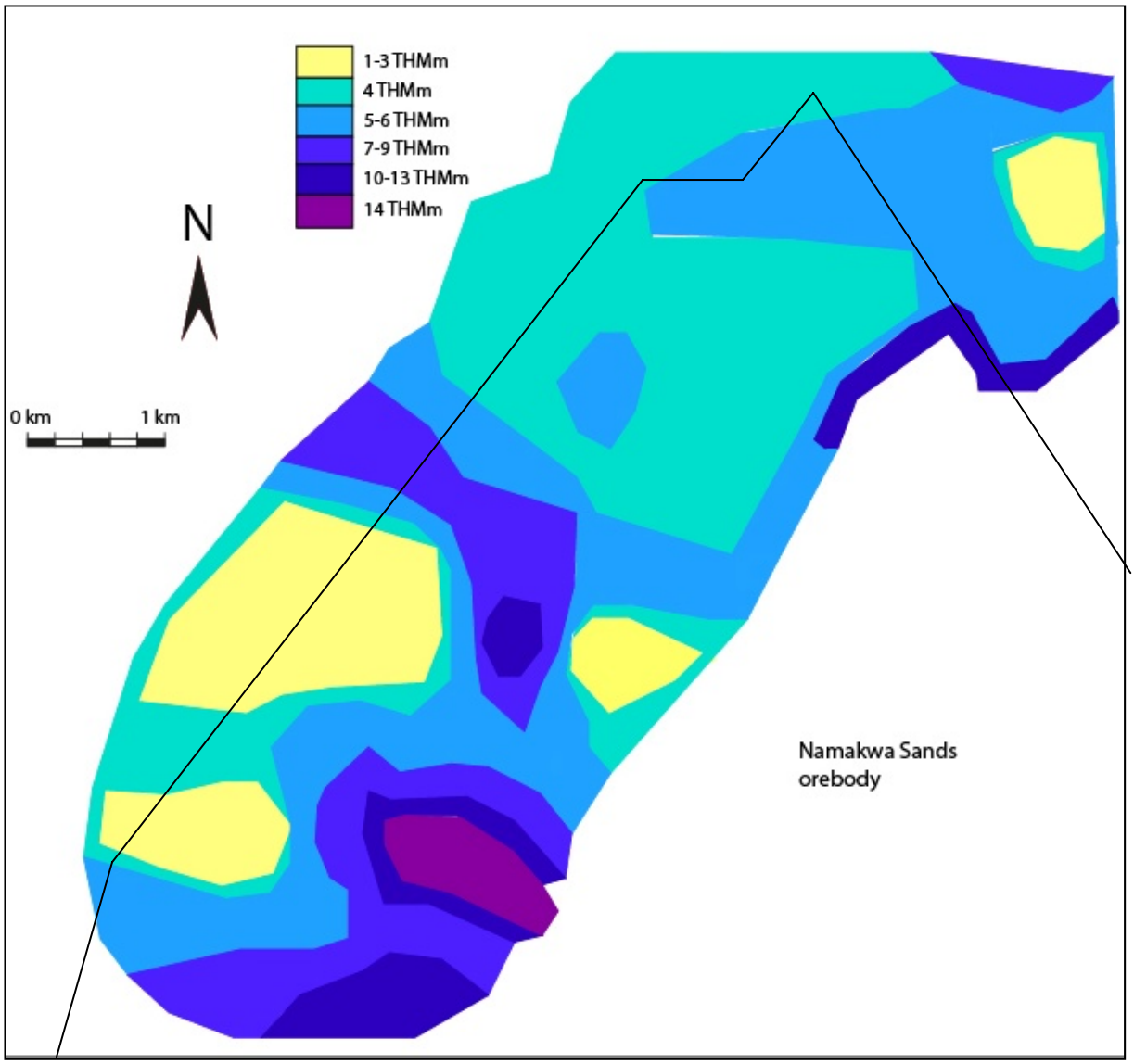

Figure 4.4.Thickness×THM map of Houtkraal Remainder Portion 2.

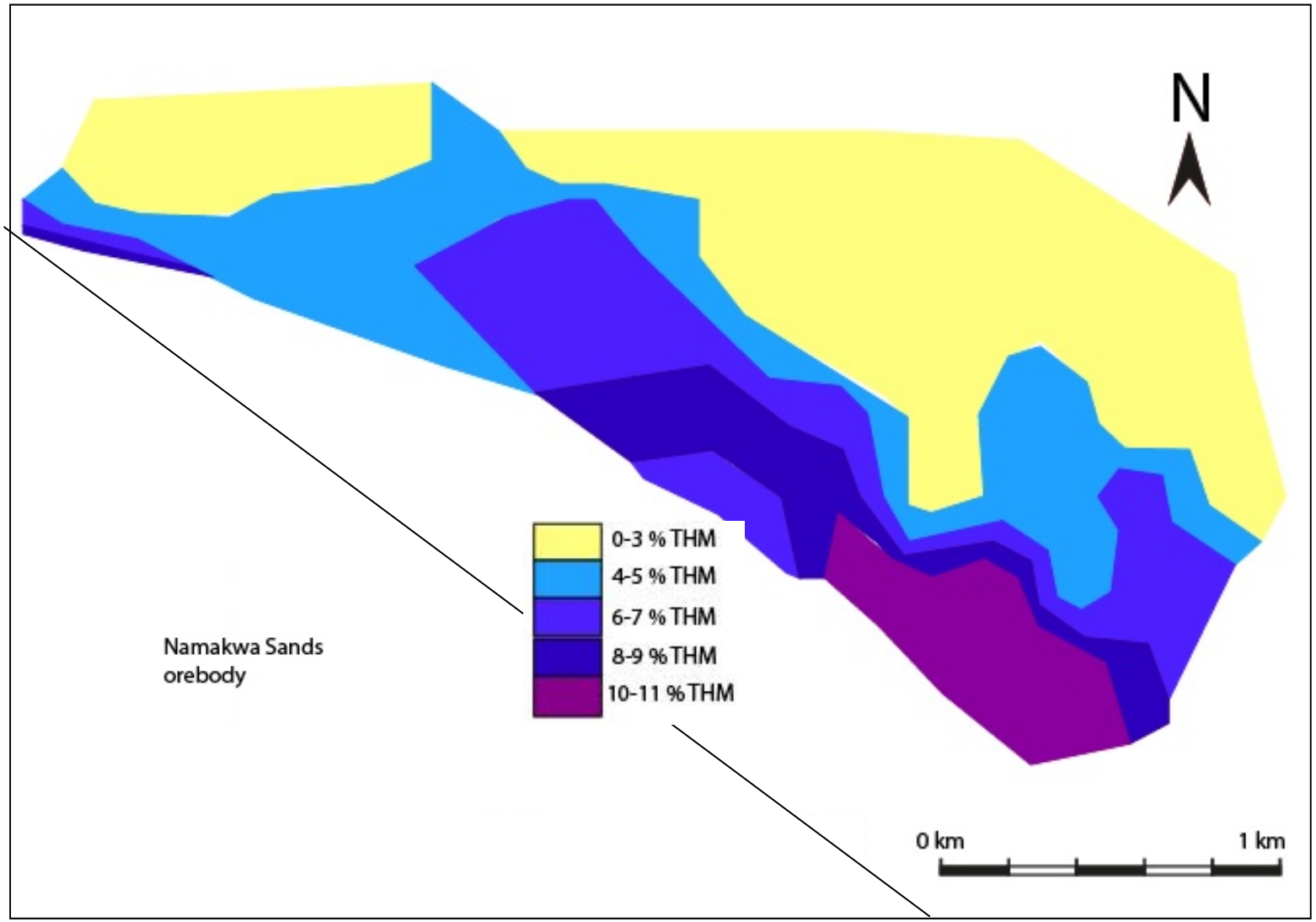

Figure 4.5. Map showing the THM distribution of Houtkraal Remainder.

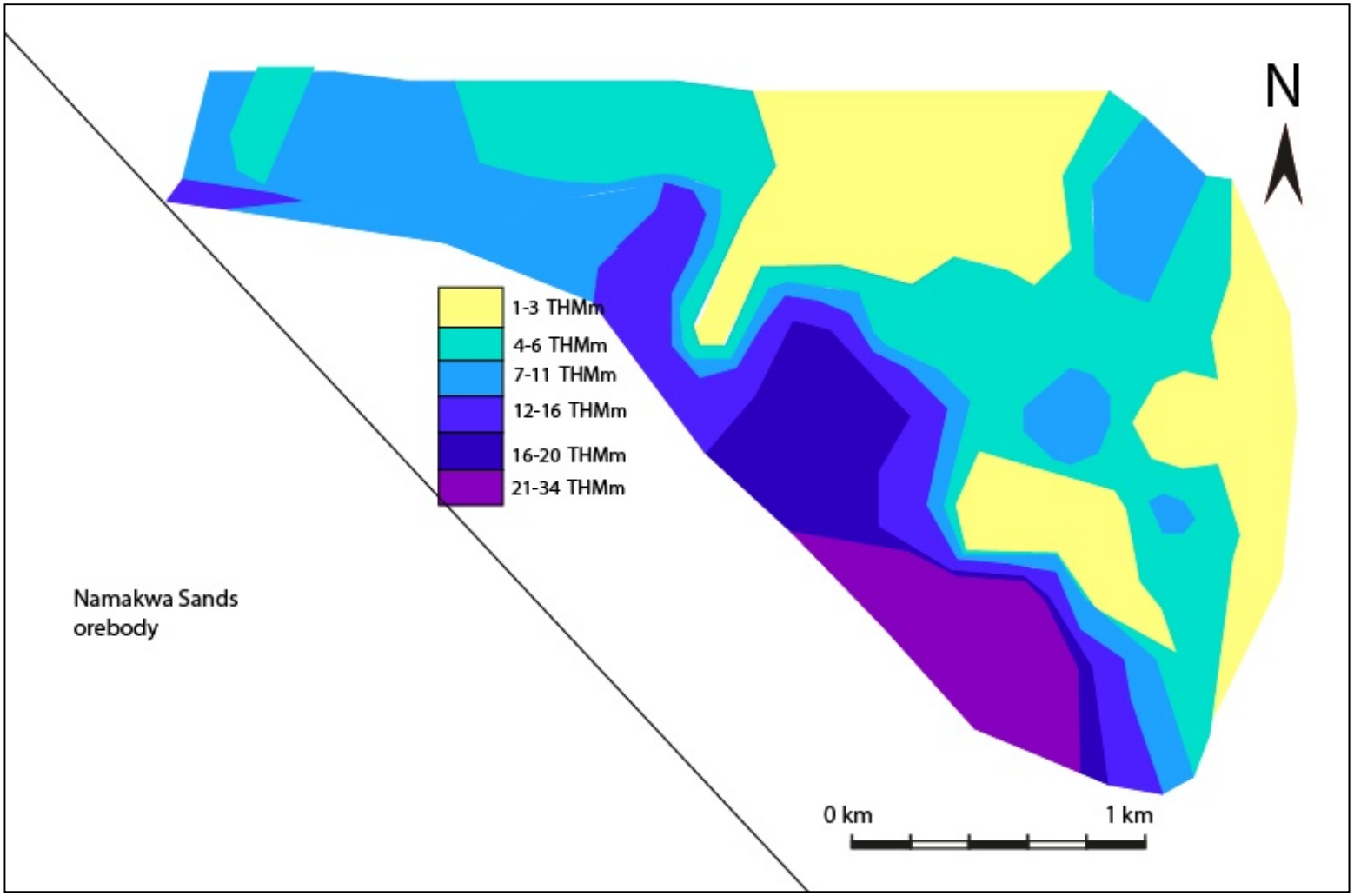

Figure 4.6. Thickness×THM map of Houtkraal Remainder.

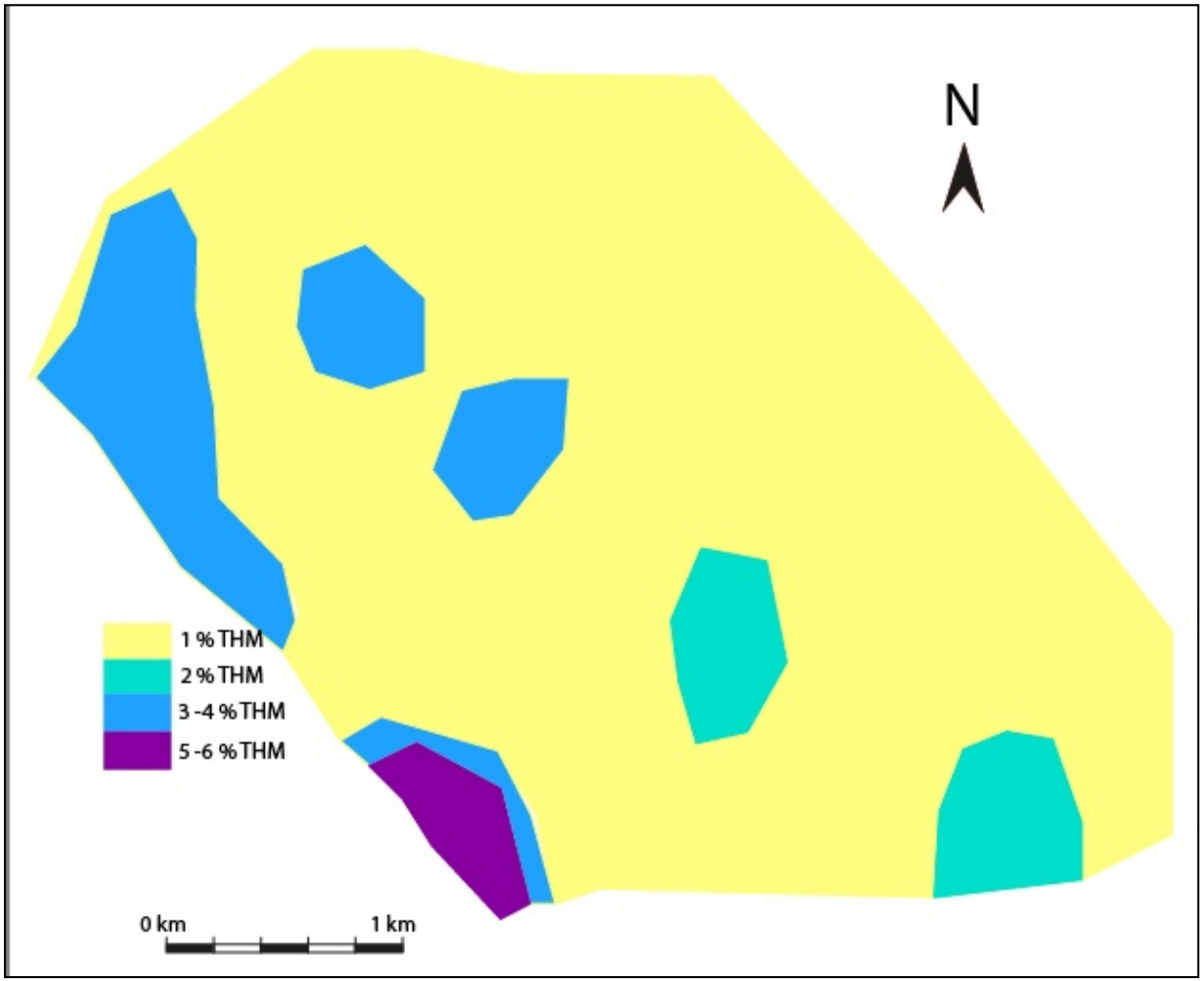

Figure 4.7. Map showing the THM distribution of Geelwal Karoo 1.

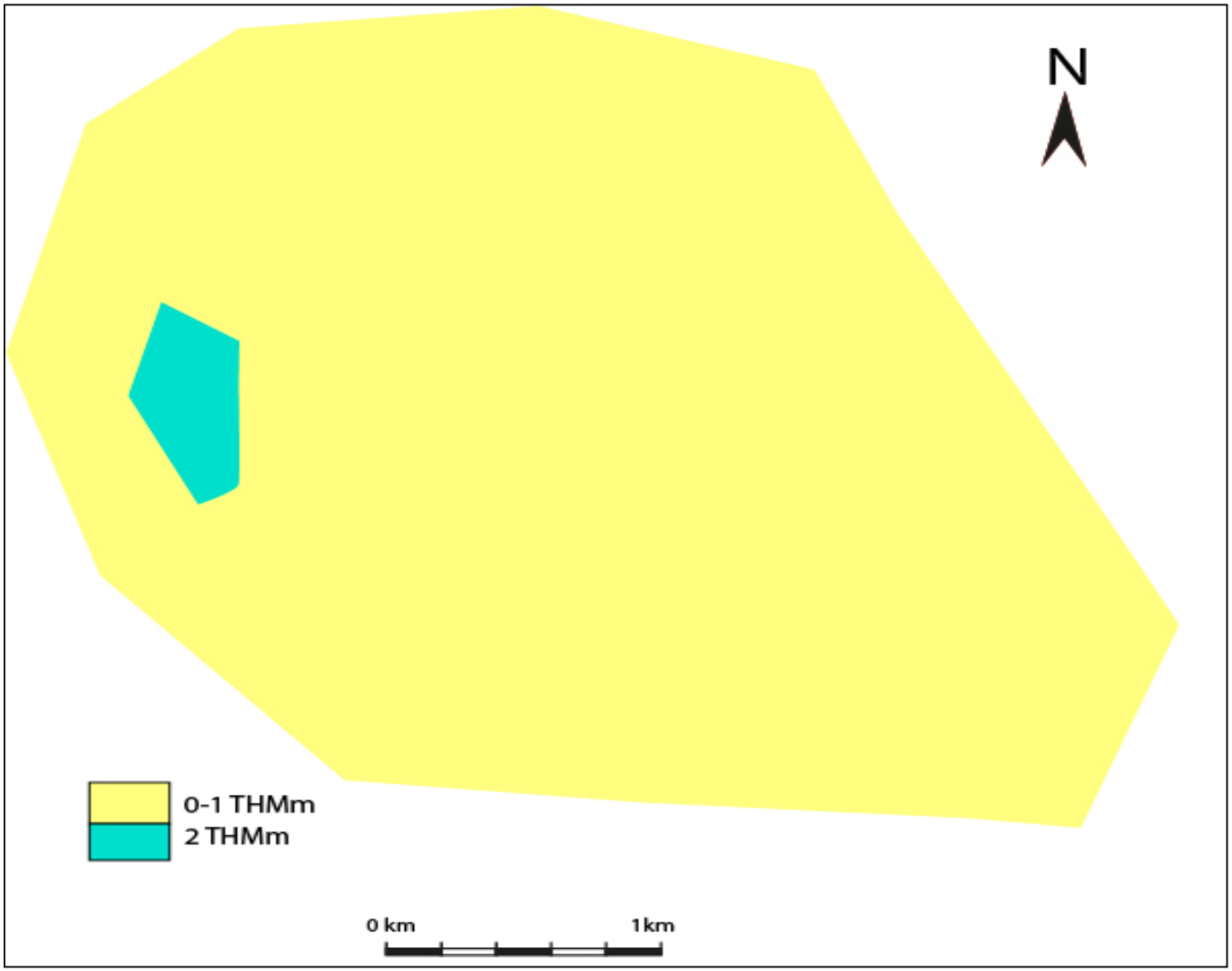

Figure 4.8. Thickness×THM map of Geelwal Karoo 1.

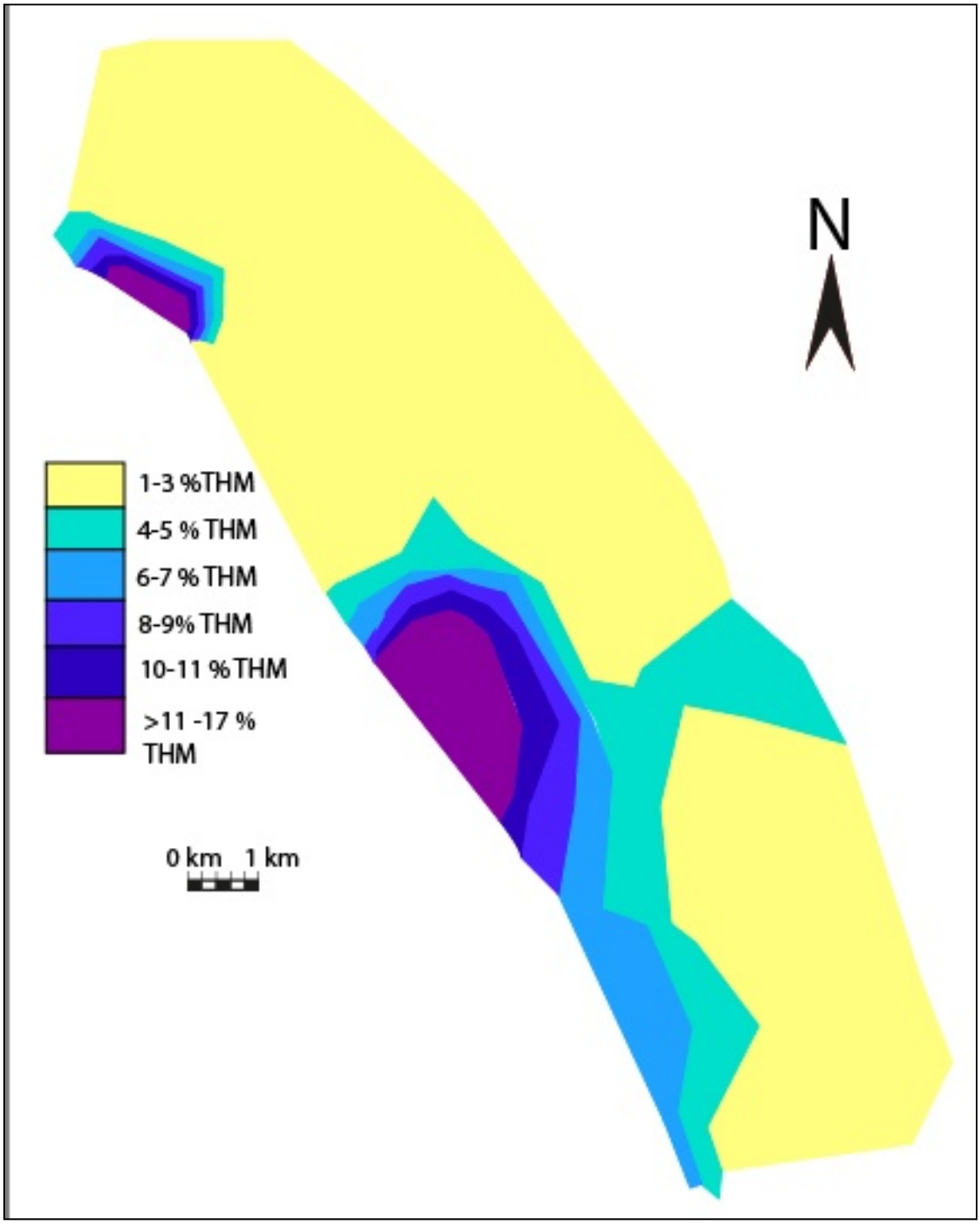

Figure 4.9. Map showing the THM distribution of Geelwal Karoo 2.

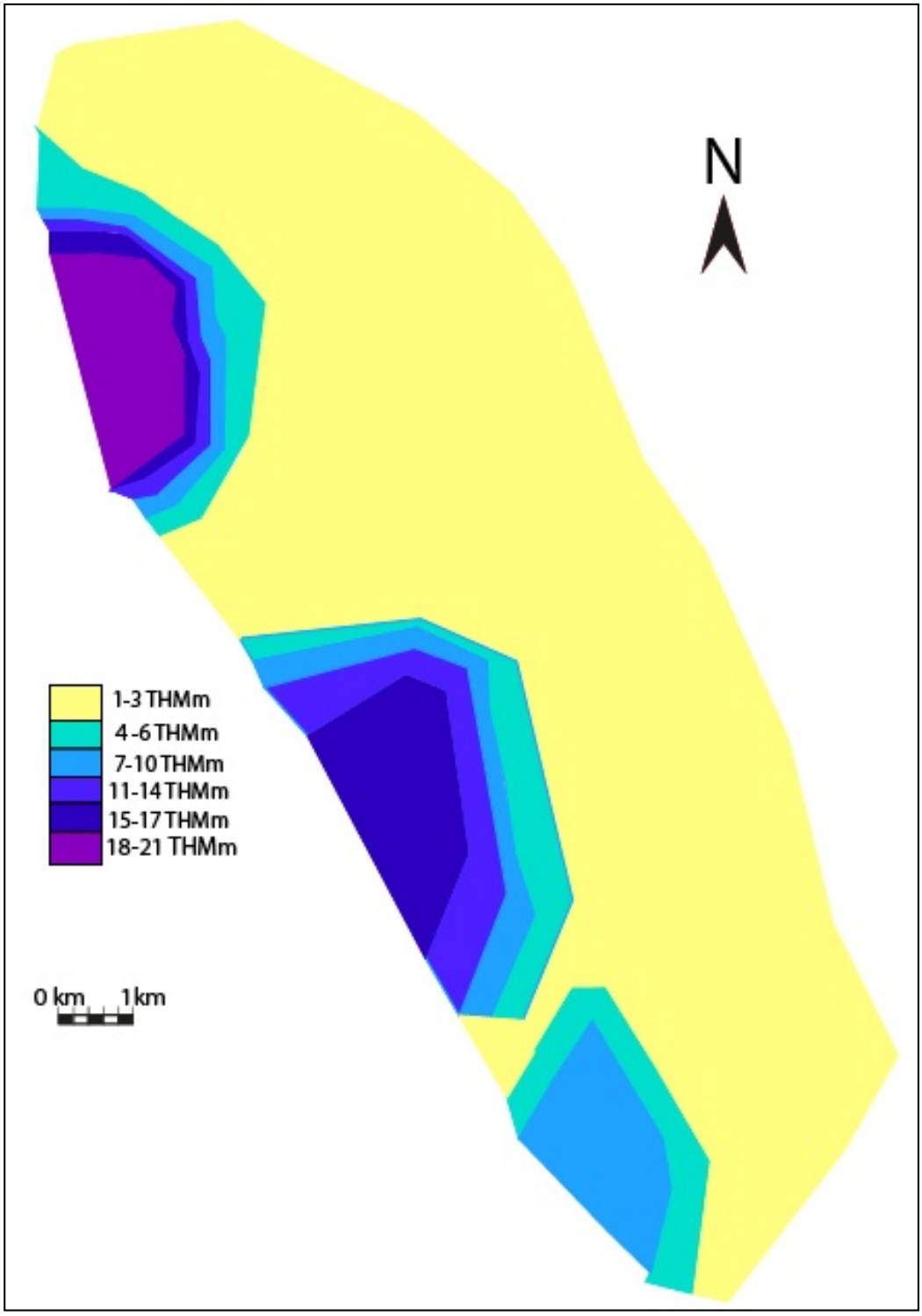

Figure 4.10. Thickness×THM map of Geelwal Karoo 2.

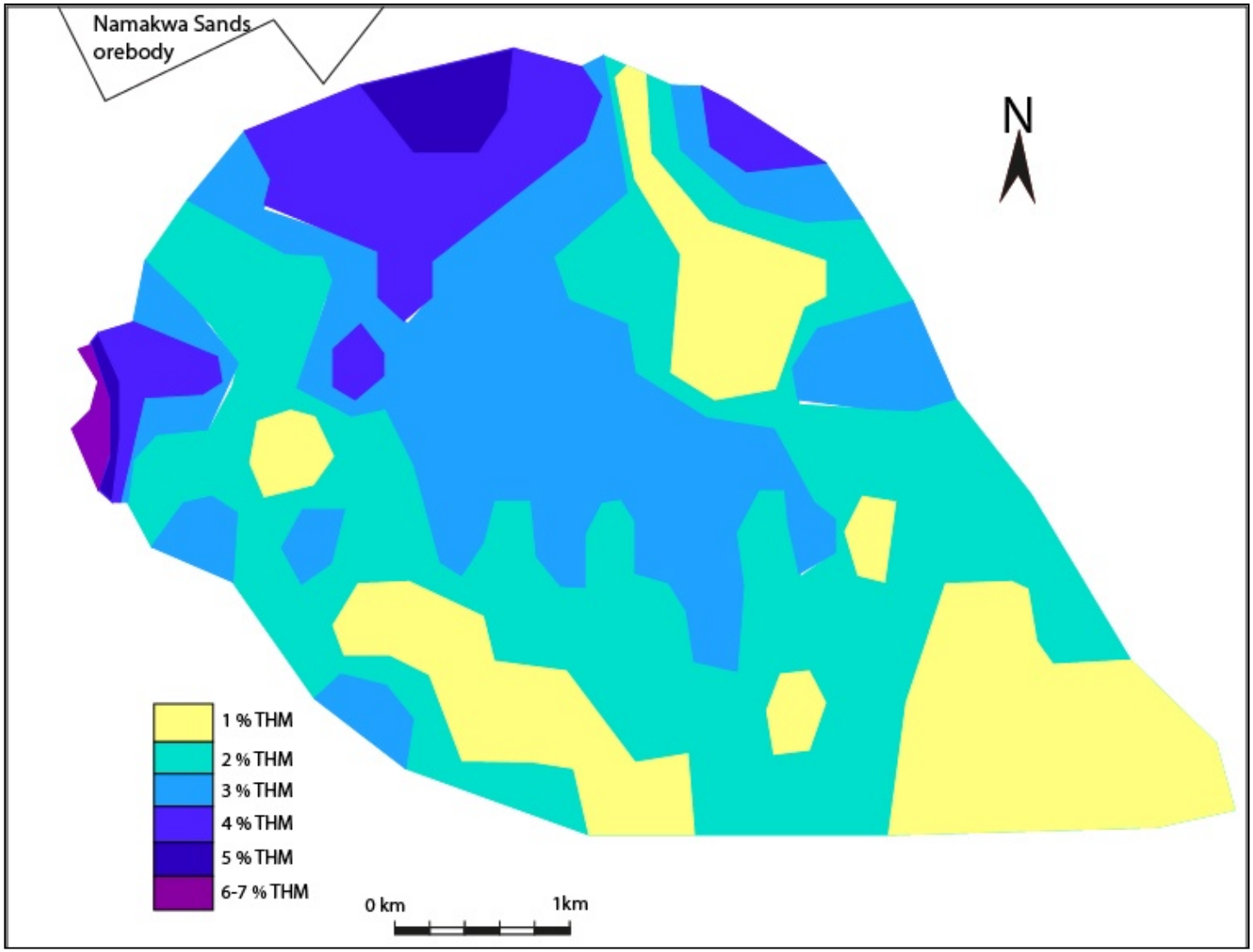

Figure 4.11. Map showing THM distribution of Graauwduinen.

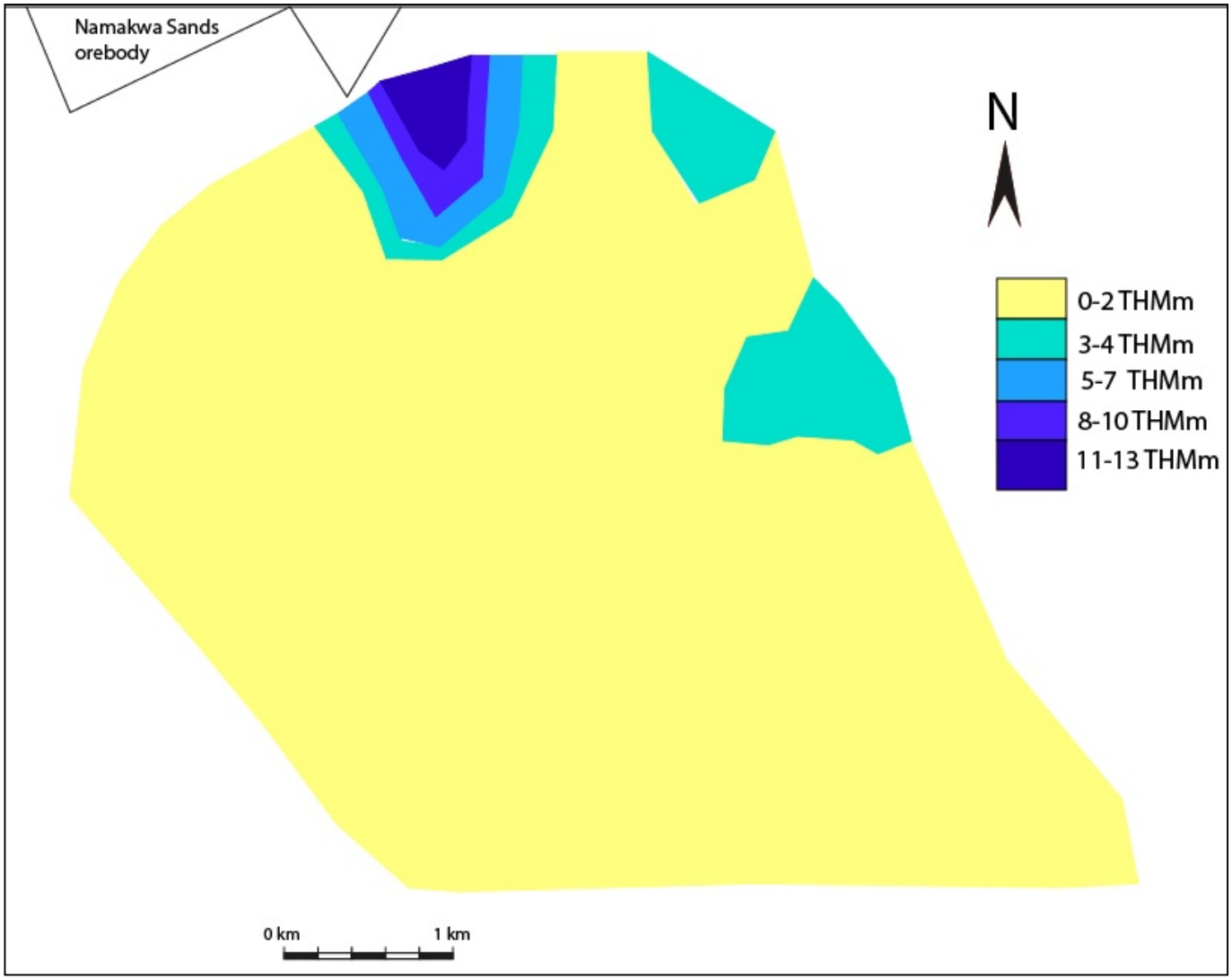

Figure 4.12. Thickness×THM map of Graauwduinen.

4.7 Discussion

The correlation diagrams indicate that the five satellite areas show contrasting mineral-and chemistry trends. Houtkraal Remainder has the highest correlation coefficients (Appendix E, Figure E1) for Fe and Ti, Fe and Mn and Ti and Mn than the other four satellite areas indicating that for Houtkraal Remainder these three elements occur mainly in ilmenite whereas in the other four areas significant amounts of these elements occur in rutile, leucoxene and garnet as well. Houtkraal Remainder also has the highest positive correlation between the VHM and THM (ρ=1) and therefore has the highest VHM content. Houtkraal Remainder Portion 2 has the 2nd highest VHM content. Rietfontein has the lowest VHM content indicated by the correlation coefficient of (ρ=0.82) between the VHM and THM. This indicates that as distance from the present coastline increases the THM:VHM ratio moves towards unity indicative of maximum maturity.

The negative correlation between Si and Mn, Ti, Zr and Fe is favourable and indicates that THM increases as low density silicate minerals are removed from the sand with distance from the coastline.

Graauwduinen, Geelwal Karoo and Rietfontein show a significant garnet concentration and decreases with increasing rutile, zircon, leucoxene and ilmenite (Appendix D, Figure D1, D4 and D5). The two Houtkraal areas do not show this negative relationship between garnet and rutile and garnet and leucoxene (Appendix D, Figure D2 and D3). Mineral correlation coefficient diagrams show a clear negative relationship between garnet and valuable heavy minerals such as ilmenite content (Fig. 4.13). As garnet decreases, ilmenite increases. Ilmenite is the most common heavy mineral present in the THM fraction and is therefore more likely to show a relationship with garnet than the other heavy mineral phases. This negative relationship is illustrated in Figure 4.13 and is a function of maturity where the less stable garnet gets winnowed and removed, concentrating the more stable ilmenite. The binary diagrams also indicate the concentration of garnet and ilmenite in the THM fraction. All five satellite areas except Rietfontein are low in garnet content indicated by the cluster of values at low concentrations (indicated by the circles). Houtkraal Remainder has less than 25% garnet in its THM, Geelwal Karoo less than 40%, Graauwduinen less than 30% and Houtkraal Remainder is

the least enriched in garnet with a garnet concentration of less than 10%. Rietfontein has a high garnet content indicated by the cluster of values between 25 and 50%.

Rietfontein has the lowest ilmenite content of between 30 and 40% followed by Geelwal Karoo with a content of between 30 and 50% (indicated by the circles). Houtkraal Remainder has the highest ilmenite content of between 58 and 70%.

The THM maps and thickness × THM maps indicate variable values of heavy mineral content for the five satellite areas. The THM relationship for the areas to the north of the Namakwa Sands orebody (Rietfontein, Houtkraal Remainder Portion 2 and Houtkraal Remainder) is indicated in Figure 4.14. All three the areas form the northern periphery of the West- and East Mine and show a very distinctive relationship. Gradation from the Namakwa Sands orebody in a northerly direction occurs over a very short distance from high concentrations of THM (8-10%) to concentrations as low as 1%. Sand thickness decreases in a similar fashion. Laterally along the strike of the NS orebody mineral composition as well as mineral ratios shows a significant change from the coastline inland. The Rietfontein heavy mineral suite has an immature composition dominated by garnets, however this changes as Houtkraal Remainder Portion 2 is approached and garnet content decreases. When the eastern part of Houtkraal Remainder is reached, garnet and other unstable mineral content is insignificant and the heavy mineral suite is dominated by minerals such as zircon, ilmenite, leucoxene and rutile. This relationship reflects an increase in maturity of the sediments away from the coastline. This is also seen from studies of the Namakwa Sands orebody (Philander pers comm). As a result Houtkraal Remainder is an eastern extension of the East Mine RAS orebody but it also terminates in that area.

The Graauwduinen area peripheral to the south of the Namakwa Sands orebody and located along the coast shows the same relationship. The sediments show a significant increase in heavy minerals as the Namakwa Sands orebody is approached and have an immature mineral composition similar to Rietfontein. Furthermore Geelwal Karoo also located on the coastline has a similar immature heavy mineral assemblage however its proximity to older heavy mineral-rich strandlines has resulted in local high grade patches that persist for short distances away from the coast.

THM-VHM binary diagrams (Figure 4.15) were plotted for the five satellite areas and are an indication of the maturity of the heavy mineral suite. Maturity refers to the texture and composition of the deposit. A deposit that has well rounded grains and is well-sorted (grains of equal grain size and homogenous) with stable minerals (zircon, ilmenite, tourmaline) is referred to as mature.

Figure 4.15 indicates a positive, linear relationship between the VHM and THM content for all five satellite areas indicating that as the THM increases the VHM also increases. The higher or steeper the gradient, the more enriched is the THM fraction in VHM up to unity where THM=VHM indicating maximum maturity. Houtkraal Remainder has the steepest slope (~45° slope) of the satellite areas, indicating that it is the most enriched in VHM. The ~45° slope further indicates that all the THM is VHM and very few to no non-economic minerals are present in the THM fraction. This ~45° slope is thus the ideal slope for any deposit. The East Mine of Namakwa Sands has this relationship.

Houtkraal Remainder Portion 2 has a roughly similar steep slope (~43°) to that of Houtkraal Remainder although it has lower VHM and THM contents. The lower VHM and THM contents are also due to less heavy minerals being supplied to Houtkraal Remainder Portion 2 by wind activity. This steep slope also indicates that almost all (99%) of the THM is VHM and very few non-economic minerals are present in the THM.

Graauwduinen has a mixed probably two THM-VHM populations. Population A has a less steep slope which is due to the presence of a considerable amount of non-economic minerals. Population B has a steeper slope which is due to the presence of more ore minerals in the THM fraction than non-economic minerals. The latter population has a similar slope to that of Houtkraal Remainder but has lower VHM and THM contents. The latter indicates that less heavy minerals were supplied to the area by the wind and as a population are less mature.

Geelwal Karoo also has a mixed probably two THM-VHM populations. Population A has a flat gradient indicating that the THM contains a considerable amount of non-economic minerals. Population B has a similar slope to that of Houtkraal Remainder Portion 2 but has lower VHM and THM contents.

Rietfontein also has a flat gradient which is due to the presence of a significant amount of non-economic minerals.

Elferink (2005) described the Cenozoic sedimentary successions on Geelwal Karoo and found immature dune sands and marine strandline type sands at the bottom of the stratigraphy which are overlain by a mature recent aeolian unit namely the RAS. The two THM-VHM populations of Geelwal Karoo and Graauwduinen may indicate a mixture of these two different sands. The low THM-VHM population may indicate dune and marine sands and the high THM-VHM population can be ascribed to the red aeolian sand. The latter sand was formed from the erosion of the older, underlying dune and marine sands units and were upgraded and matured by wind activity.

The relationships between the five satellite areas with respect to VHM, THM and maturity indicates that the surficial sands proximal to the coastline are normally immature and that the heavy mineral suite has been derived from the underlying enriched Cenozoic sediments. With increased distance from the shoreline the maturity increases and is a function of wind winnowing activity from the southwest. Sediments in areas that are peripheral to the Namakwa Sands orebody however may reach the high maturity but hardly ever the mineral concentration that typifies the NS deposit. To be able to achieve this it is concluded that topographical control i.e. linear depressions off the coast are required to channel, accumulate and concentrate the sediments. Such depressions can be steep-sided providing a relative thick accumulation of mature sediments that rapidly taper off along the margins. Termination of the body along strike is controlled by the flattening out of the depression against topographic highs allowing dispersal of the sediments over the adjacent plains.

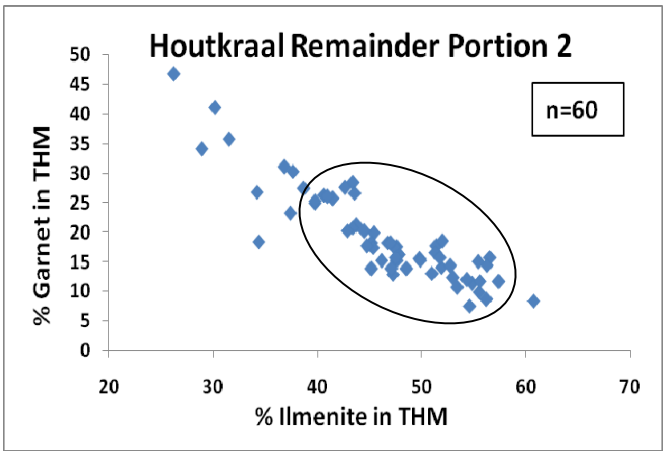

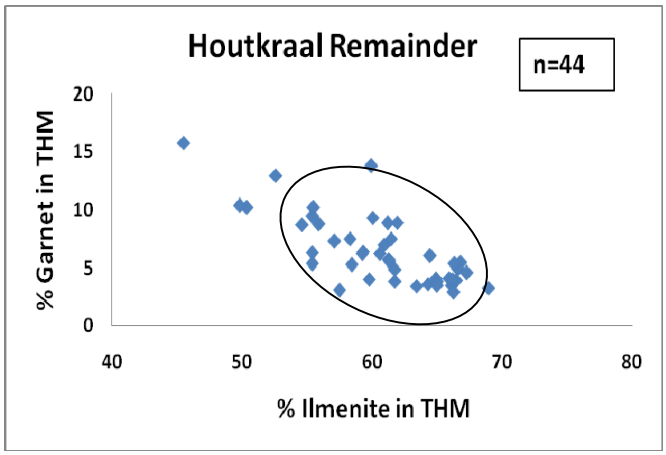

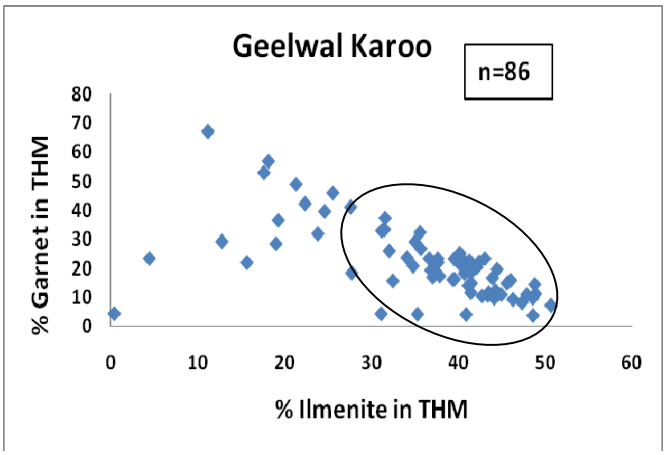

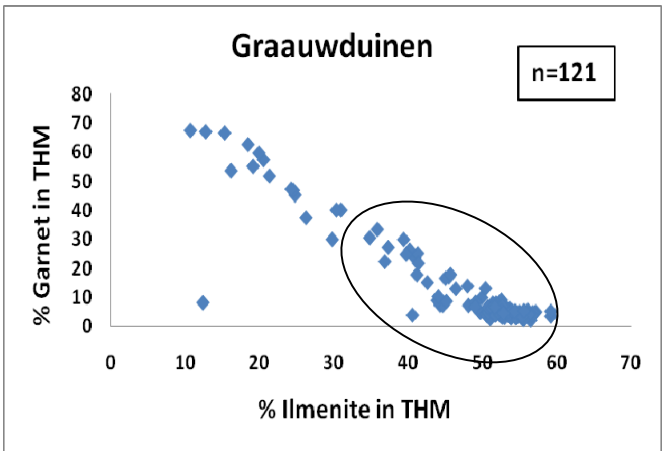

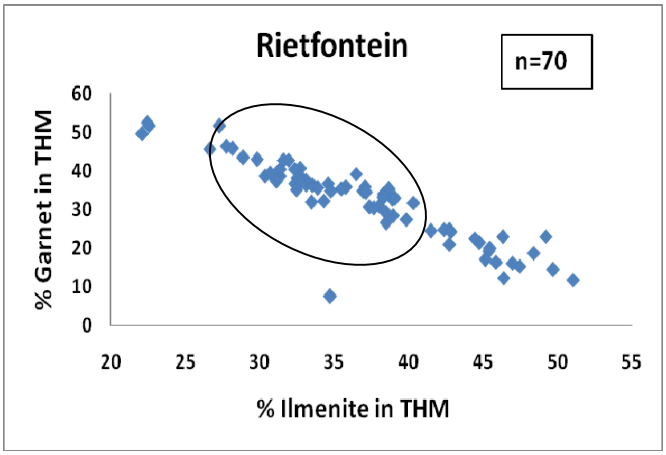

Figure 4.13. Ilmenite-garnet binary diagrams illustrating the negative relationship between ilmenite and garnet for the five satellite areas. Garnet decreases as ilmenite increases. Circles indicate cluster of values at specific concentrations.

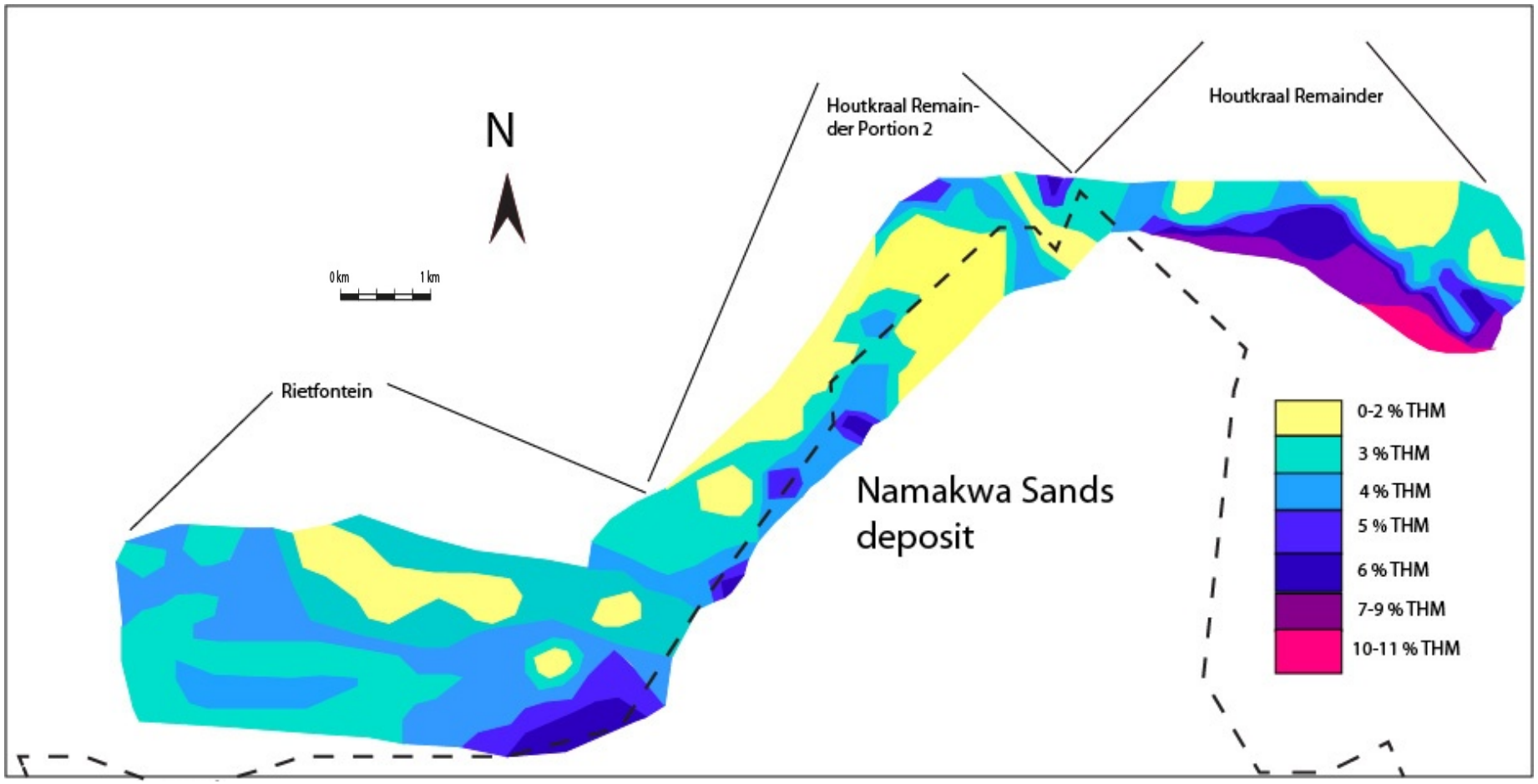
N
0 km
1 km
Houtkraal Remain-
der Portion 2
Houtkraal Remainder
Rietfontein
Namakwa Sands
deposit
0-2 % THM
3 % THM
4 % THM
5 % THM
6 % THM
7-9 % THM
10-11 % THM

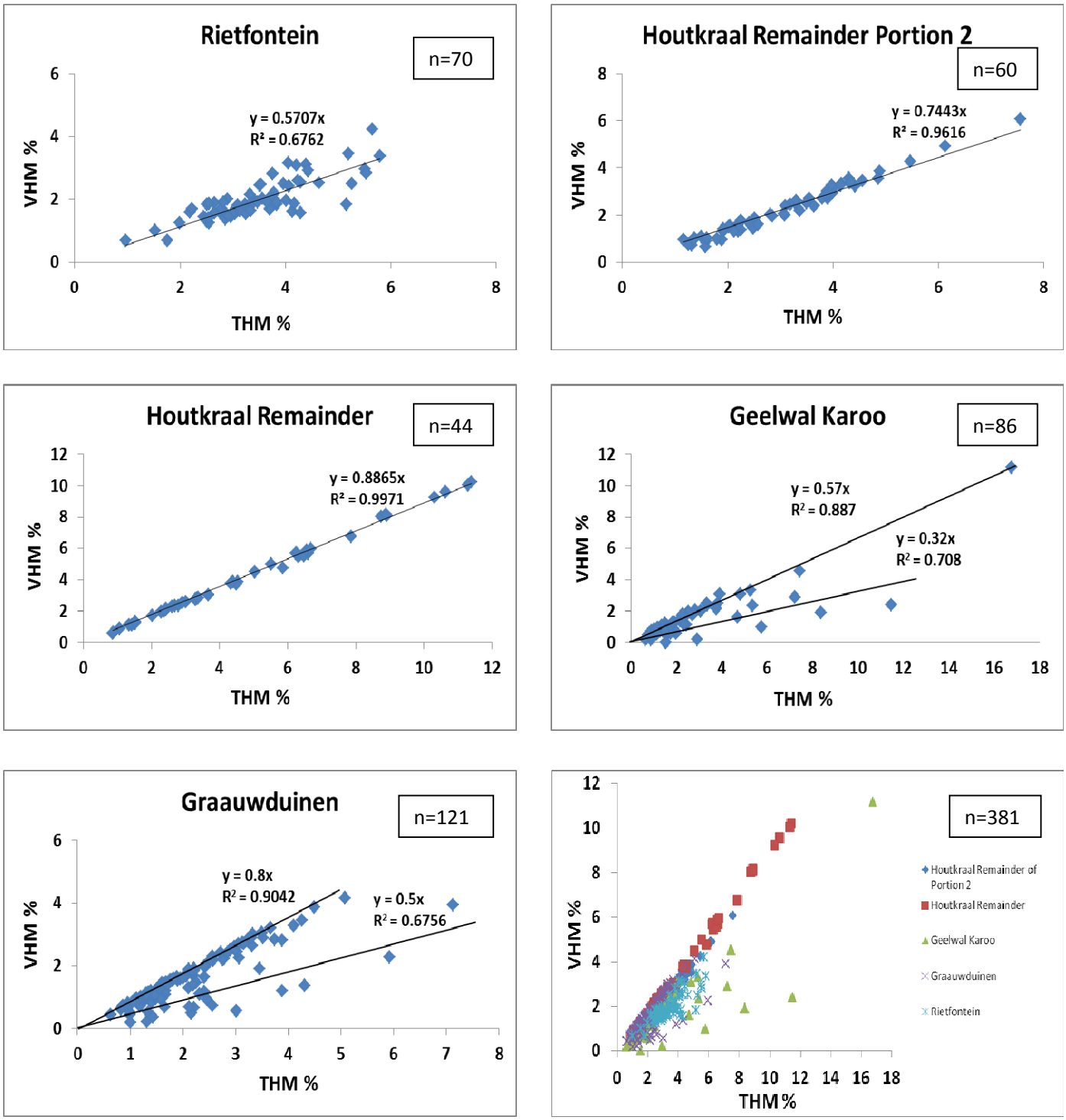

Figure 4.15. THM-VHM binary diagrams showing the positive relationship between THM and VHM for the five satellite areas. The strong, linear relationship for the two Houtkraal areas compared to the other three areas indicates better sorting and maturity.

CHAPTER 5 MINERALOGY

5.1 Introduction

The heavy mineral population of the five study areas are described in terms of their petrography and chemistry. Random heavy mineral grains were chosen from 54 polished sections and studied using an optical microscope. Heavy minerals were described as a group and not per satellite area. Exceptions were highlighted in the text. Heavy mineral assemblages of the five satellite areas are dominated by opaque oxides (ilmenite, hematite, rutile and magnetite) and transparent minerals such as spinel, sphene, epidote, pyroxene, aluminosilicates, garnet, zircon, tourmaline, amphibole, staurolite and corundum. Apatite is only present as an inclusion in zircon. The light mineral fraction comprises quartz and feldspar but was not studied. The grains, in most cases, are coated by a red to orange brown amorphous chemical precipitate. These coatings have variable chemistry and may consist of Si, Al, Fe ± K or Ti, Al and Mg or Si, Ti and Al (Table F19, Appendix F). The RAS (red aeolian sand) rutile of the Namakwa Sands orebody is generally coated with an amorphous precipitate of Si, Al, Fe and Ca (Rozendaal et al, 2009).

The five satellite areas contain the same suite of heavy minerals but in different proportions and are all dominated by ilmenite (Table 5.1). Mineral proportions were determined by QEMSCAN.

Table 5.1. Average mineral proportions of the five satellite areas. Other minerals include amphibole, tourmaline, sphene, epidote, monazite, apatite, aluminosilicates and staurolite.

Area	THM	Ilmenite	Leucoxene	Rutile	Zircon	Garnet	Pyroxene	Other minerals
HKRP2	3	46	6	6	13	19	3	7
HKR	5	61	6	6	13	7	2	6
GW	3	43	7	8	11	23	8	1
GRW	2	47	7	7	13	14	3	10
RF	3	37	5	6	10	32	4	6

5.2 Nomenclature of the iron-titanium oxide minerals

There is no general accepted terminology for the minerals of the FeO-TiO_2-Fe_2O_3 system. Most workers follow the classification systems of Buddington et al (1963) and Buddington and Lindsley (1964), although it is not universally accepted. The terminology used in this thesis is adopted from the above authors and Hugo (1993). Complex grains (grains showing intergrown mineral phases) are also present and a nomenclature is presented.

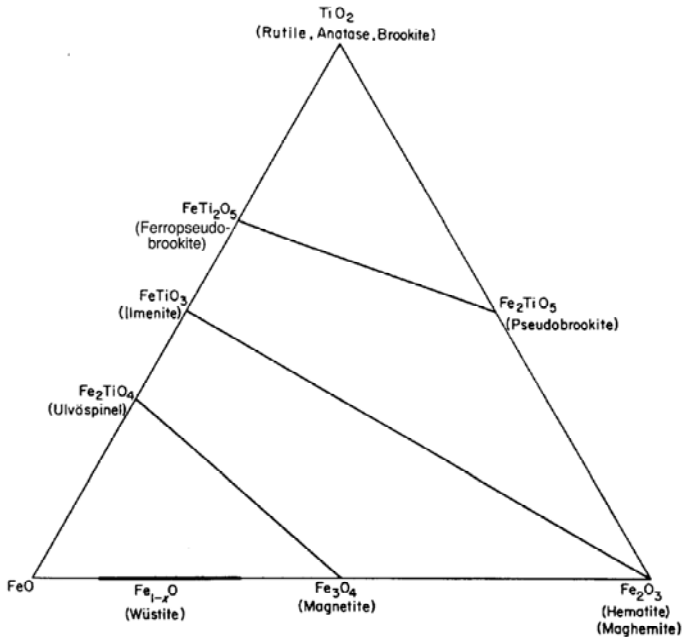

Figure 5.1. Ternary diagram showing the solid solution series in the FeO-TiO_2-Fe_2O_3 system (Buddington and Lindsley, 1968).

Ilmenite – unaltered ilmenite with a TiO_2 content ranging between 48% and 53% and a composition close to the theoretical formula ($FeTiO_3$) with up to 6% Fe_2O_3. It is strongly anisotropic with a purple grey colour under reflected light.

Ferrian-ilmenite – a homogeneous ilmenite phase with the formula $FeTiO_3$ with a Fe_2O_3 content between 6 and 13% and 3-4% excess TiO_2 in solid solution.

Hematite – a homogeneous, trigonal phase with an oxide stoichiometry approaching Fe_2O_3 and < 5 wt % TiO_2.

Titanohematite – an optically homogeneous Fe-Ti rhombohedral phase with a stoichiometry approaching Fe_2O_3 and with > 50 mol per cent hematite and > 5 wt % TiO_2 (Deer et al, 1992).

Rutile – a tetragonal phase consisting essentially of TiO_2 and forming part of the TiO_2 polymorphs together with brookite and anatase.

Magnetite – a spinel phase with a stoichiometry close to the theoretical end-member composition Fe_3O_4 and a TiO_2 content of less than 5% (Deer et al, 1992).

Titanomagnetite – a titanium-rich magnetite where Ti^{4+} replaces some of the Fe^{2+}.

Martite – magnetite that is being replaced by hematite through oxidation along octahedral planes.

Ilmenite and hematite form a complete solid solution series at temperatures more than 1050ºC (Deer et al, 1992). At 800ºC only a limited amount of TiO_2 can enter α –Fe_2O_3.

Complex grains:

The Fe-Ti oxides occur as both monomineralic and complex grains due to intergrowths or exsolution. The most common complex grains present are:

Hemo-ilmenite – ferrian-ilmenite with a mixture of ilmenite with exsolution lamellae of titanohematite and/or hematite.

Ilmo-hematite – a mixture of titanohematite and/or hematite with exsolution lamellae of ferrian-ilmenite and/or ilmenite

Other complex grains with the host mentioned first followed by the intergrown phase are:

Hematite-rutile – a hematite grain with rutile exsolution lamellae

Magnetite-rutile – rutile lamellae in magnetite

Ilmenite alteration products:

There is no standard nomenclature for the ilmenite alteration products. The nomenclature used in this text is taken from Hugo and Cornell (1991).

Hydrated ilmenite – altered ilmenite. These altered areas contain TiO_2 contents between 53 and 60%. It can be microscopically distinguished from unaltered ilmenite by its weaker anisotropism and grey blue colour under reflected light. Grey et al (1983) used the term to refer to mixtures of ilmenite and pseudorutile which contain crystalline water.

Pseudorutile – a deformed, hexagonal oxyhydroxide whose composition approximates $Fe_2Ti_3O_9$ (Deysel, 2007) and has a TiO_2 content of between 60% and 71%. It can be microscopically distinguished from unaltered ilmenite by its slightly higher reflectivity and blue grey colour (isotropic pseudorutile).

Leucoxene – a fine granular alteration product of Fe-Ti oxides consisting of mainly anatase or rutile with a TiO_2 content ranging between 70% and 93%. It can be optically distinguished by its sugary texture and white to yellow internal reflections. It can consist entirely of crypto- or microcrystalline rutile in the final stages of ilmenite alteration.

5.3 Ilmenite

5.3.1 Petrography

Ilmenite of this study has been grouped into three classes: (1) fresh or homogeneous ilmenite (no exsolution lamellae), (2) heterogeneous ilmenite (exsolution lamellae present) and (3) altered ilmenite. Boctor (1966) stated that the optical properties of ilmenite are affected by its chemical composition (Wassef, 1981). Reflectivity in air and specific gravity for example decreases towards geikelite ($MgTiO_3$) and pyrophanite ($MnTiO_3$). The latter two minerals are end-members of ilmenite.

Grain size ranges from 67-244 µm for Graauwduinen, 133-329 µm for Geelwal Karoo, 11-233 µm for Houtkraal Remainder, 78-244 µm for Houtkraal Remainder Portion 2 and 67-222 µm for

Rietfontein. The grain sizes are the same for all satellite areas except for Graauwduinen which is coarser grained. The long axis of the grains was measured.

Ilmenite is present as a black, opaque phase with yellow or red transparent edges under transmitted light. Under reflected light it has a distinct purplish grey colour with strong anisotropism and sub-metallic lustre (Figure 5.2 A). Rounded to sub-rounded ilmenite grains are the most abundant with only a few anhedral and euhedral ilmenite present. Ilmenite is coated with a redbrown amorphous precipitate which consists of Si, Ti, Al and Fe ± Mg. These coatings are described in detail in section 5.14. These coatings also exploit small fractures. A Si-rich amorphous phase is also present within cracks (Table F19, Appendix F). Most ilmenite contains only one generation of hematite and rutile exsolution lamellae (Figure 5.2 B, E and F).

Inclusions hosted by ilmenite include mostly randomly orientated transparent phases such as quartz, almandine garnet and biotite. A few grains contain hematite exsolution lamellae (hemo-ilmenite) and rutile lamellae (Figure 5.2 B, E). The majority of ilmenite is free from exsolution lamellae. Lamellae occurs as needle-like, thin lines and blebs (oval to convex in shape) and are randomly orientated forming a network of lamellae. Some have a particular pattern. Where hematite and rutile lamellae occur as fine, linear lines, the lamellae are orientated parallel to the 0001 plane of the ilmenite lattice (Figure 5.2 B, E). Where the lamellae are ragged, irregular and lens (convex) - shaped, it is orientated perpendicular to the (0001) plane (Figure 5.2 F).

Aggregates of ilmenite and quartz are also present and have anhedral shapes with thick, red oxide coatings. Some aggregates have baddeleyite (ZrO_2) as part of the cluster.

Some grains display a trellis-type lamellae texture (Figure 5.2 D) which is a distinctive intergrowth pattern that indicates the dissolution of ilmenite, leaving behind hematite (Mange and Wright, 2009).

Complex grains consisting of more than one oxide phase have also been identified (Figure 5.2 C) and consist of ilmenite and rutile. As a result it was difficult to distinguish between host and intergrown phase.

Philander (1999) and Macdonald (1996) found similar textures in ilmenite from Kleinzee and Geelwal Karoo along the west coast. They also reported the presence of hemo-ilmenite (hematite

lamellae in ilmenite) and ilmo-hematite (ilmenite lamellae in hematite). In addition complex grains, blitz textures and more than one generation of lamellae are typical for these areas. These similarities clearly suggest a common source, most probably, the nearby basement rocks.

5.3.2 Chemistry

Unaltered ilmenite

Some 200 ilmenite (< 6 wt % Fe_2O_3) grains were randomly picked and analysed with the aid of the SEM for each area to determine its chemical composition (Table F1 and F2, Appendix F). Table F2 represents ferrian-ilmenite (Fe_2O_3 > 6 wt % - 13 wt %). In this study, ferrian-ilmenite was included with the < 6 wt % Fe_2O_3 ilmenite since both represents unaltered ilmenite. The chemistry of the ilmenite is illustrated by means of frequency histograms of TiO_2, FeO, Fe_2O_3 and MnO and binary diagrams of TiO_2 versus selected elements (Figures 5.4-5.8). The Fe_2O_3 content was calculated using the Method of Droop (1987).

The TiO_2 content for the five satellite areas ranges from 45 wt % to 53 wt % (Figure 5.4). Houtkraal Remainder Portion 2, Graauwduinen and Rietfontein have an average TiO_2 content of 50 wt % and Houtkraal Remainder and Geelwal Karoo an average content of 49 wt %. Ilmenite generally has a TiO_2 content of between 48 and 53 wt %. Values below 48 wt % indicate that the Ti^{4+} has been replaced by elements such as Mg and Mn.

The Fe_2O_3 content ranges from 0-14 wt % and is skewed towards higher values of Fe (Figure 5.5). The majority of ilmenite from Houtkraal Remainder Portion 2 and Geelwal Karoo contain between 6-8 wt % Fe_2O_3 whereas the other three satellite areas contain between 8-10 wt % Fe_2O_3 and conforms to ferrian-ilmenite.

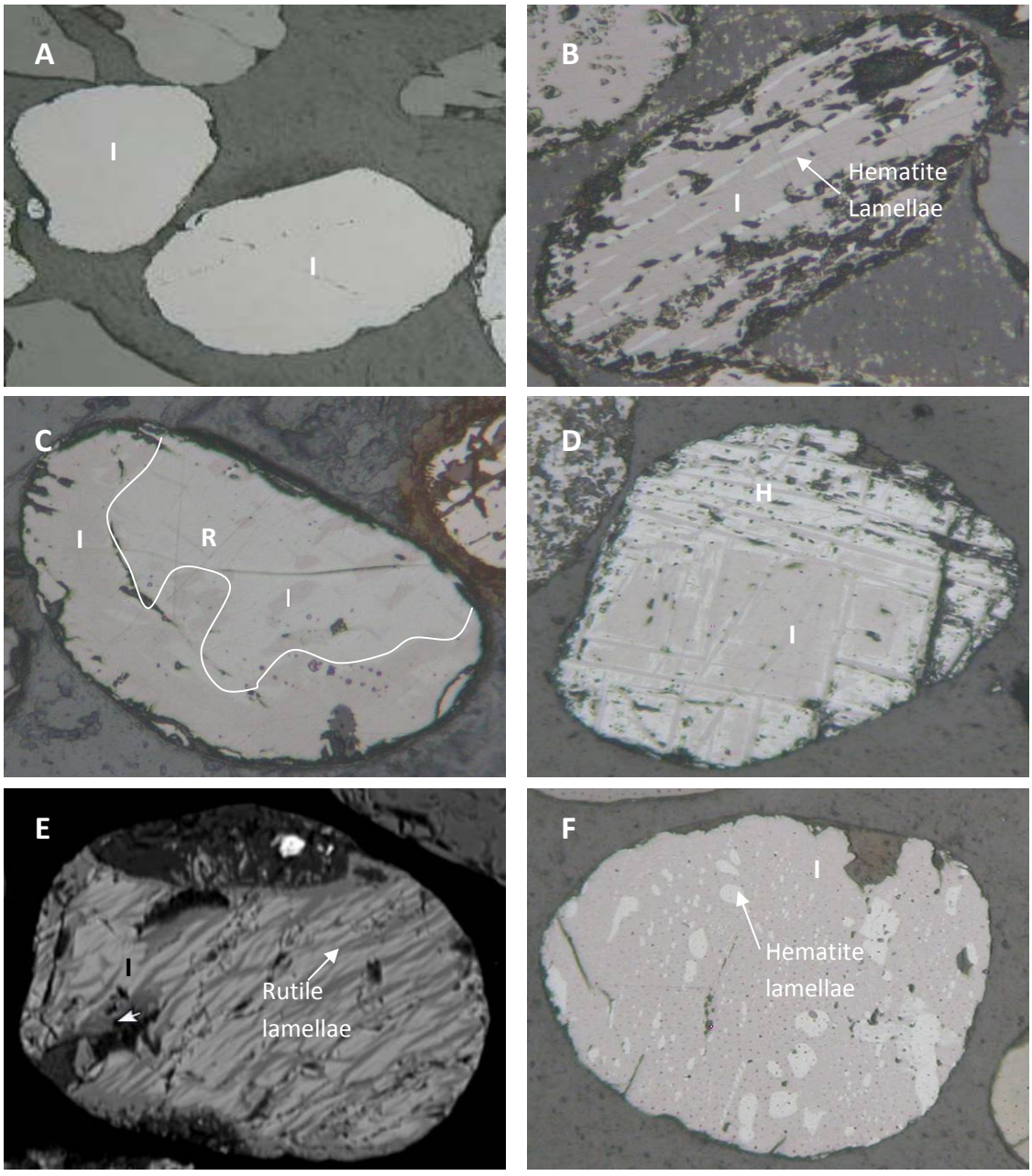

Figure 5.2. Microscope and SEM images of unaltered ilmenite. Microscope images were taken under reflected light. Scale: 20X. A) Unaltered ilmenite with its purplish grey colour. B) Hemo-ilmenite (ilmenite with hematite exsolution lamellae. C) Complex grain of ilmenite and rutile. Rutile is the light grey phase. D) Trellis-type texture. Trellis-type lamellae of hematite (light grey) in ilmenite (purplish grey). E) Ilmenite with rutile exsolution lamellae parallel to the (0001) plane of ilmenite). F) Ilmenite showing irregular shaped hematite exsolution lamellae with a linear orientation parallel to the (0001) plane of ilmenite.

Due to the lower Fe_2O_3 content of Houtkraal Remainder Portion 2 and Geelwal Karoo, it has higher FeO (Figure 5.6). The total amount of iron ($FeO+Fe_2O_3$) stays the same in the ilmenite crystal lattice and if Fe_2O_3 decreases, FeO will increase.

The MnO content for the five satellite areas range between 0 and 8 wt % and the majority of ilmenite throughout the study areas has 2 wt % MnO (Figure 5.7).

The Cr_2O_3 content is close to the detection limit of the SEM and range between 0 and 0.07 wt %. There are some outliers with values of up to 1.8 wt % Cr_2O_3.

Figure 5.8 indicates that a negative linear relationship is present between Fe_2O_3 and TiO_2 indicating the solid solution series that exists between hematite and ilmenite. The Fe_2O_3 content of the unaltered ilmenite is as high as 12 wt %. Unaltered ilmenite can contain up to 6 wt % Fe_2O_3 and ferrian- ilmenite up to 13 wt % Fe_2O_3.

FeO and TiO_2 show a positive linear relationship. The increase in FeO and decrease in Fe_2O_3 with TiO_2 indicates that the total amount of iron in the ilmenite lattice stays the same. No iron is lost only oxygen is gained.

The binary diagrams of TiO_2 versus SiO_2, Al_2O_3, Cr_2O_3, V_2O_5, MgO, ZnO, MnO and CaO show no characteristic trends (Figure 5.8). A few ilmenite grains have ZnO contents of up to 2 wt %. The V (< 0.27 wt %) contents of the majority of ilmenite are low. This is favourable for use in the pigment industry since high contents make it unsuitable for use as a pigment. Mn is also considered an impurity in ilmenite and can cause problems in the smelting process of the ilmenite production stage. A high Ti and low Mn-bearing ilmenite is needed for the final ilmenite product. The majority of ilmenite has MnO contents smaller than 2 wt % which makes it suitable for the heavy mineral industry.

Geelwal Karoo has ilmenite grains that show different shades of grey within one grain under the microscope and the SEM (Figure 5.3). SEM analysis indicated that the different phases of grey are all unaltered ilmenite but with a difference in the total iron content. (Table F1, Appendix F, analysis 20). As the titanium content increases, the ferrous iron increases and the ferric iron decreases. The latter indicates very early stages of oxidation where Fe^{2+} is oxidized to Fe^{3+}.

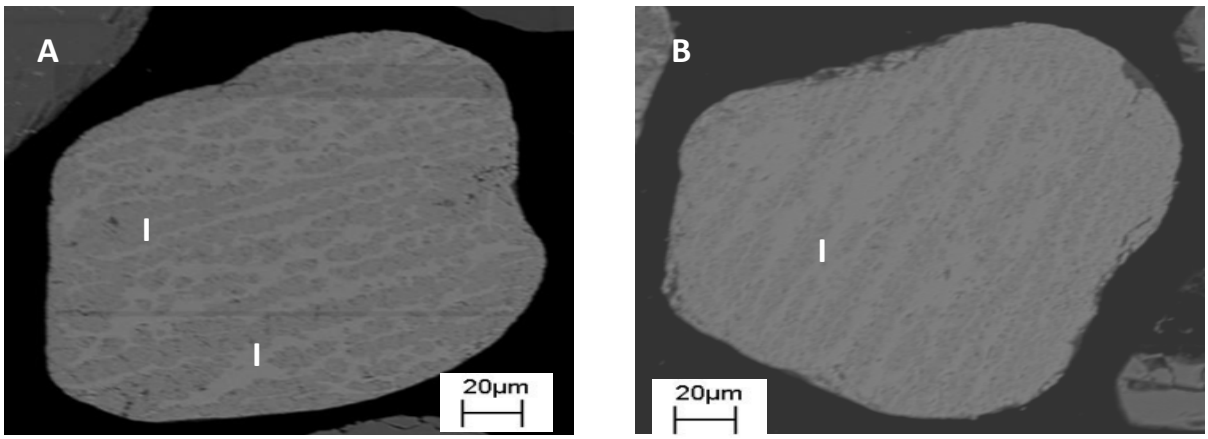

Figure 5.3. SEM images of unaltered ilmenite. A) and B) Unaltered ilmenite showing different shades of grey. The different shades of grey indicate differences in Fe content and the very start of alteration.

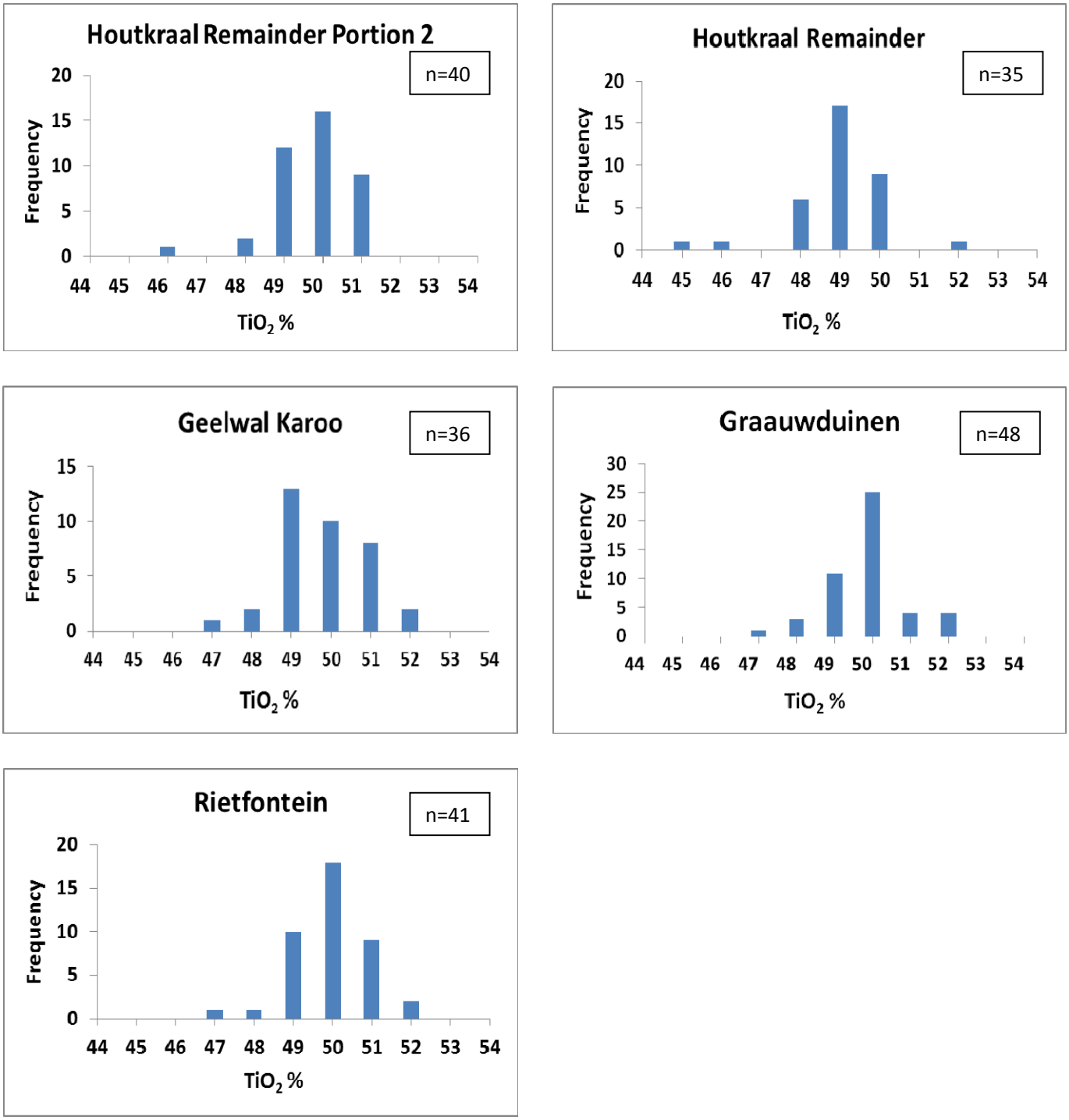

Figure 5.4. TiO_2 content frequency histograms of unaltered ilmenite from the five satellite areas. TiO_2 content for all five the satellite areas ranges between 45 wt % and 53 wt %.

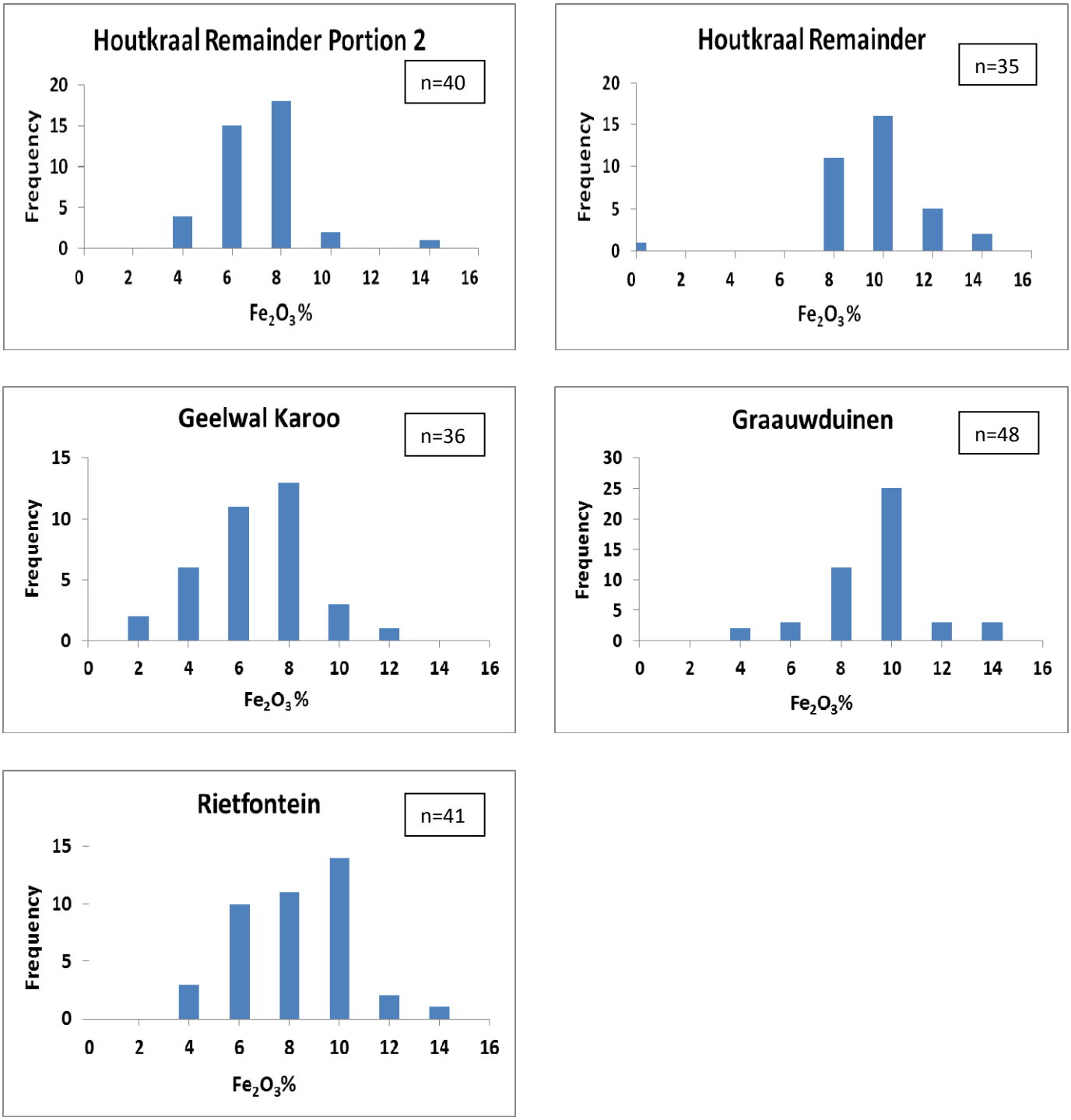

Figure 5.5. Fe_2O_3 content frequency histograms of unaltered ilmenite from the five satellite areas. The Fe_2O_3 content for all five the satellite areas range between 0 and 14 wt %. The majority of ilmenite from Houtkraal Remainder Portion 2 and Geelwal Karoo has 6-8 wt % Fe_2O_3 and Houtkraal Remainder, Graauwduinen and Rietfontein between 8-10 wt % Fe_2O_3.

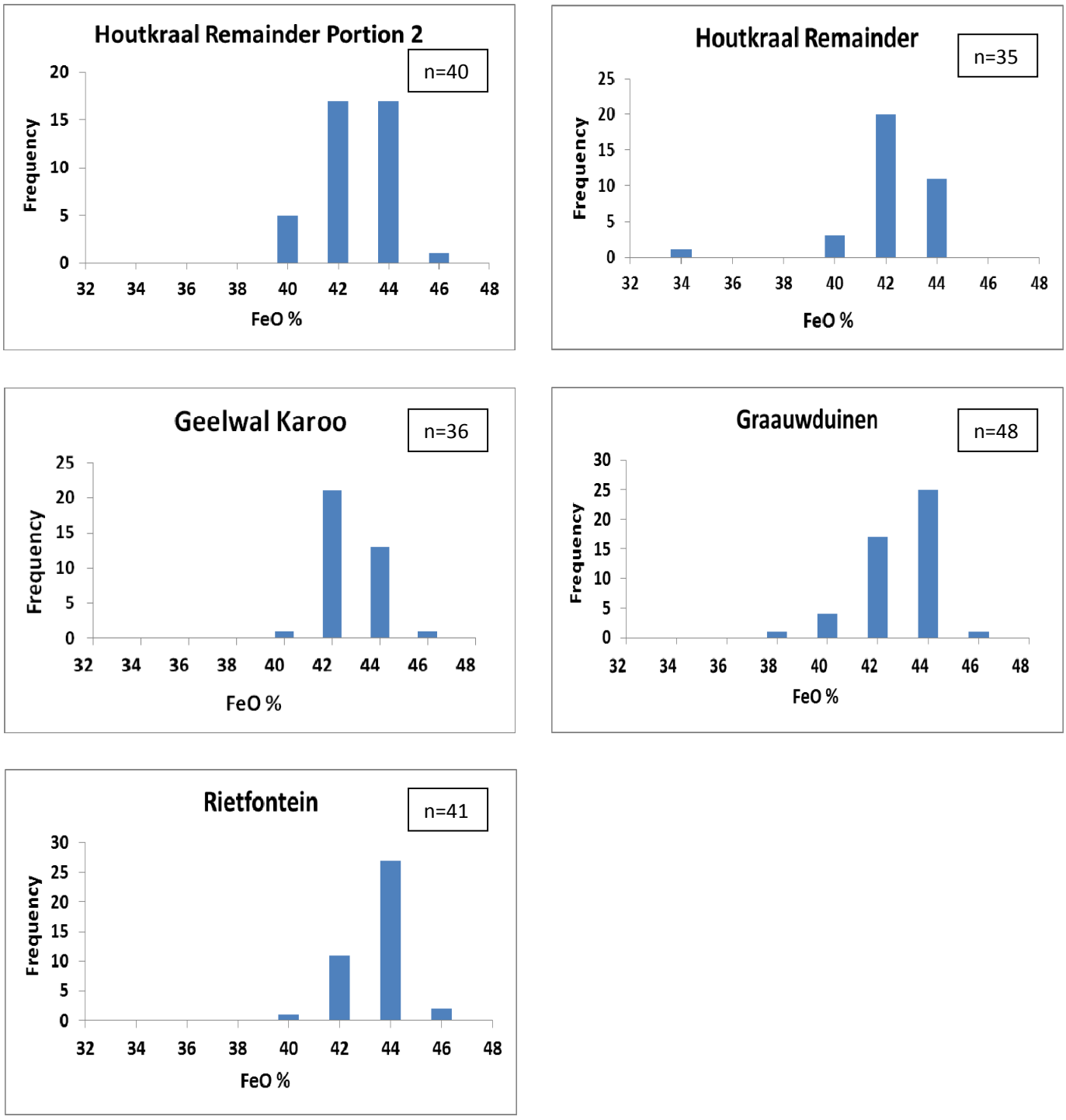

Figure 5.6. FeO content frequency histograms of unaltered ilmenite from the five satellite areas. The FeO content for all five the satellite areas range between 34 and 46 wt %. Houtkraal Remainder Portion 2 and Geelwal Karoo have the highest FeO content of the satellite areas.

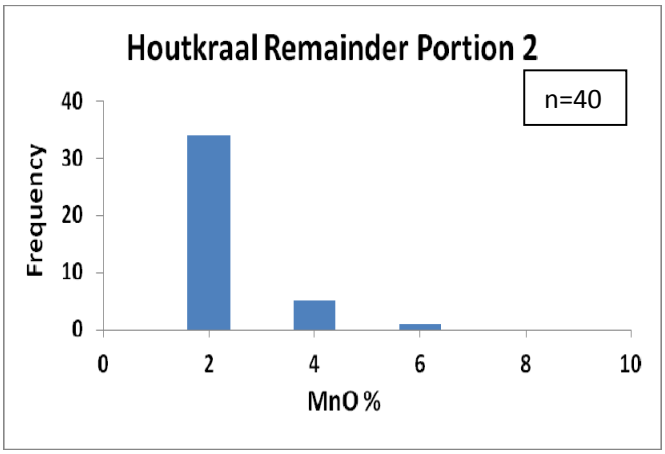

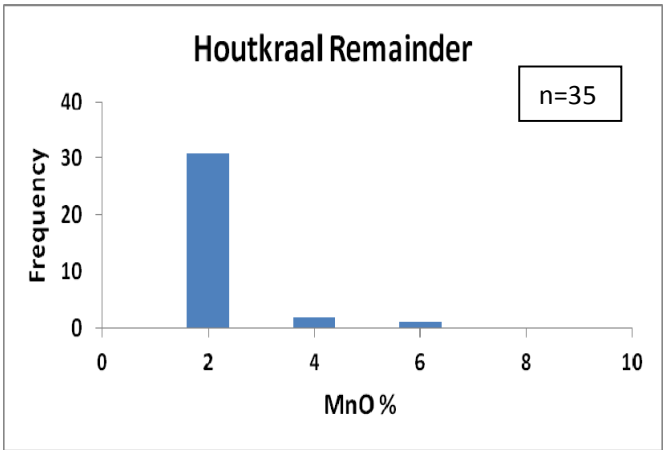

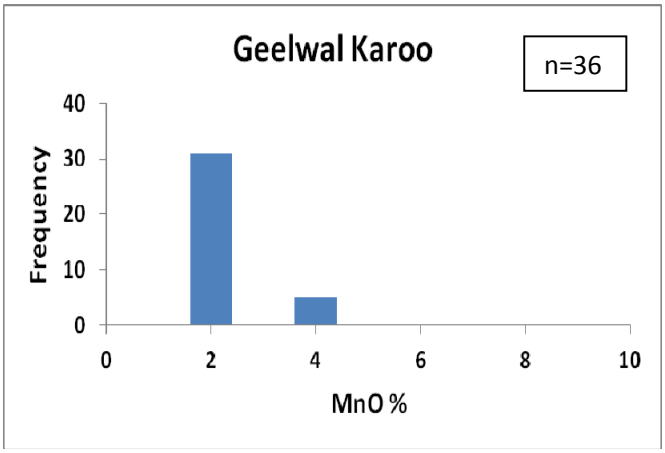

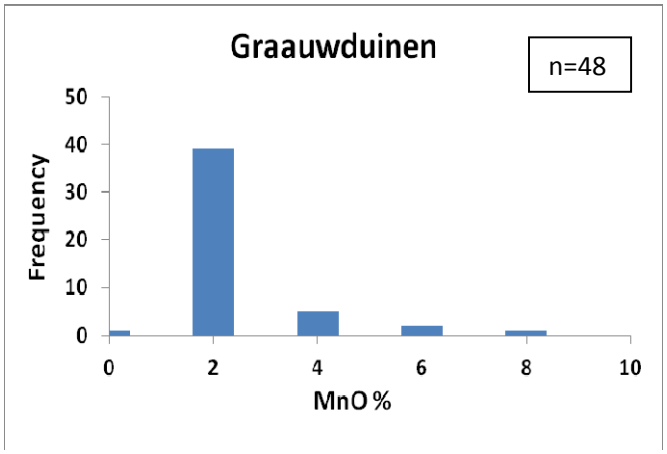

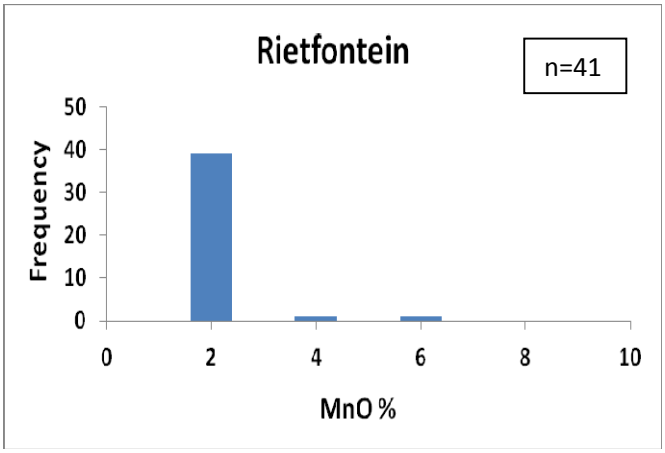

Figure 5.7. MnO content frequency histograms of unaltered ilmenite from the five satellite areas. The MnO content for all five the satellite areas range between 0 and 8 wt % with the majority of rutiles having 2 wt % MnO.

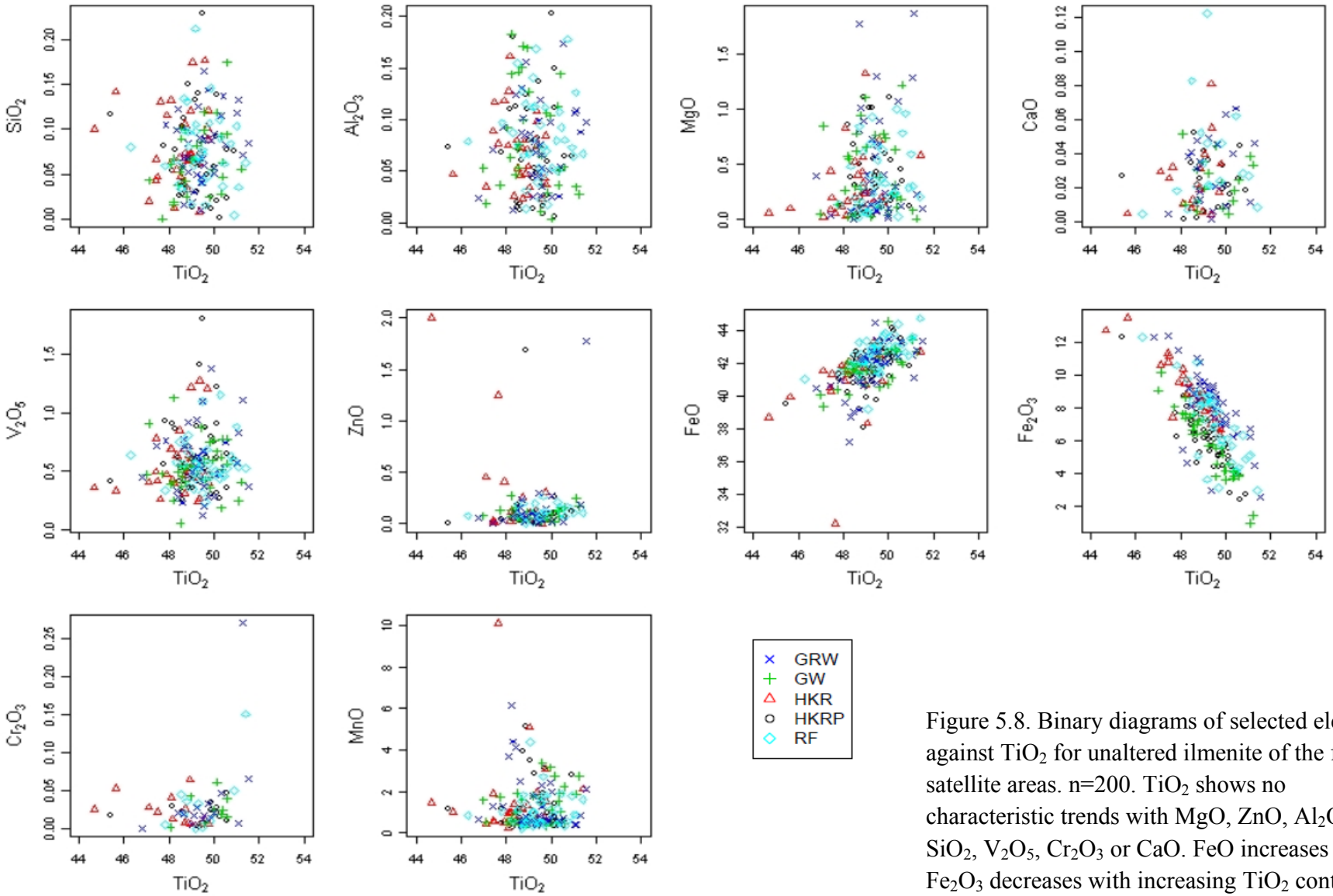

Figure 5.8. Binary diagrams of selected elements against TiO_2 for unaltered ilmenite of the five satellite areas. n=200. TiO_2 shows no characteristic trends with MgO, ZnO, Al_2O_3, SiO_2, V_2O_5, Cr_2O_3 or CaO. FeO increases and Fe_2O_3 decreases with increasing TiO_2 content.

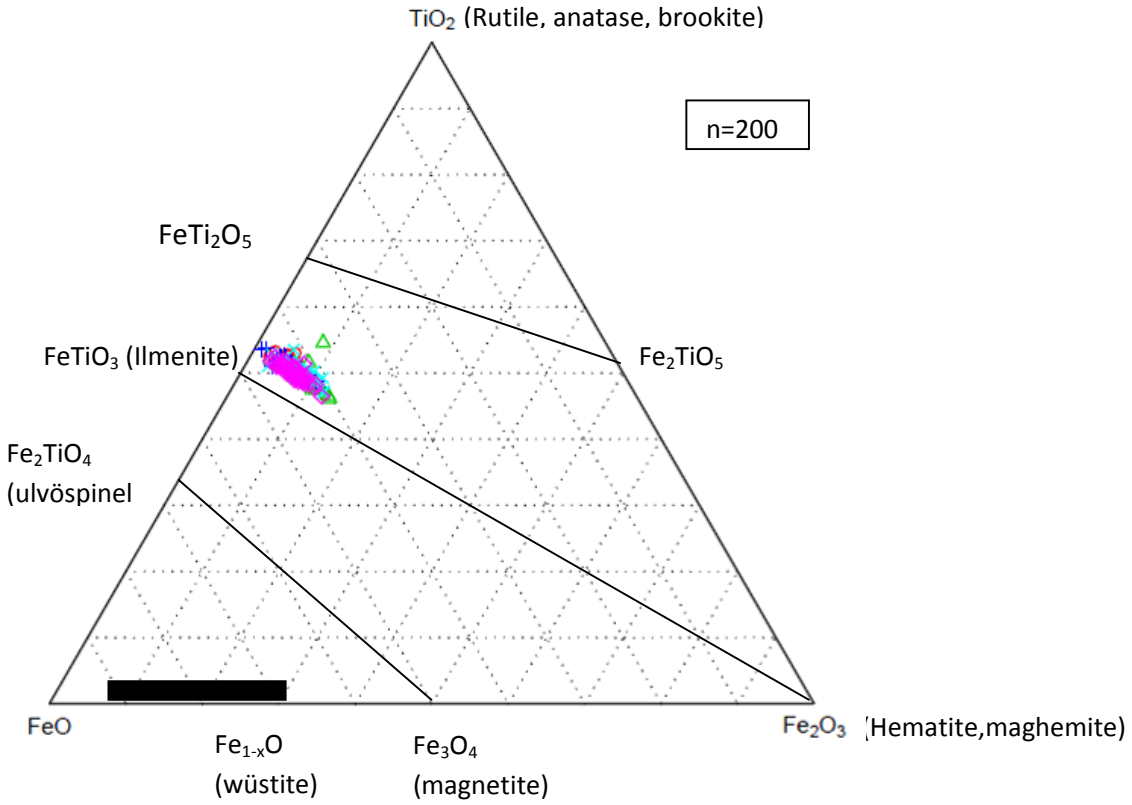

Figure 5.9. Ternary plot of unaltered ilmenite in the FeO-TiO_2-Fe_2O_3 system of the five satellite areas (diagram after Buddington and Lindsley, 1964).

The chemistry of the unaltered ilmenite from the five satellite areas are illustrated on the FeO-TiO_2-Fe_2O_3 ternary plot (Figure 5.9). Ilmenite of all five satellite areas plot near but not on the pure ilmenite end-member. It shows enrichment towards hematite indicated by the straight line of analysis parallel to the $FeTiO_3$-Fe_2O_3 line. This line indicates the solid solution series between ilmenite and hematite. The shift of the unaltered ilmenite from the pure ilmenite end-member is due to the presence of MnO where the FeO is replaced by MnO.

Altered Ilmenite

Some 47 randomly selected altered ilmenite grains were analysed by means of the SEM per study area locality. Five thin-sections (one from each satellite area) were chosen that are representative of the altered population of each area. Several analyses were done per grain to identify all the alteration products and their chemical variations. Analyses were done on clean

surfaces randomly chosen. Data are presented in Table F18, (Appendix F) as unaltered ilmenite relict chemistry and that of the alteration products. This table shows that the whole spectrum of ilmenite alteration products are present in the five satellite areas and include hydrated ilmenite (53-60% TiO_2), pseudorutile (60-71% TiO_2), leucoxene (70-93% TiO_2) and rutile* (> 93% TiO_2). The asterisk is used to distinguish rutile formed from the alteration of ilmenite from primary rutile, thus is a secondary rutile.

Chemistry also shows variations in the minor elements with increasing alteration. X-Y scatter plots of TiO_2 versus a range of substitution elements were plotted for each area (Figure 5.10).

For all five areas there is a marked decrease in total iron (FeO +Fe_2O_3) with increasing alteration. This is due to the ferrous iron that is converted to the ferric state and the latter is then leached. The Al_2O_3 content of altered ilmenite from the satellite areas increases up to a point of 76-86 wt % TiO_2 after which its abundance decreases.

SiO_2 does not show any reliable trend for Houtkraal Remainder and Rietfontein. Houtkraal Remainder Portion 2, Geelwal Karoo and Graauwduinen show a slight decrease after ± 90 wt % TiO_2 and are very similar to Al_2O_3 due to leaching.

The MgO content decreases after 82 wt % TiO_2 and thereafter occurs in trace amounts.

Cr_2O_3 shows no characteristic trend and remains low with increasing alteration. Houtkraal Remainder is an exception and shows a slight increase with increasing alteration.

CaO shows no trend with increasing alteration.

Nb_2O_5 shows a marked increase with increasing alteration and relates to the substitution of titanium in the rutile crystal structure.

MnO shows a significant decrease in its abundance with increasing alteration and is completely removed due to leaching.

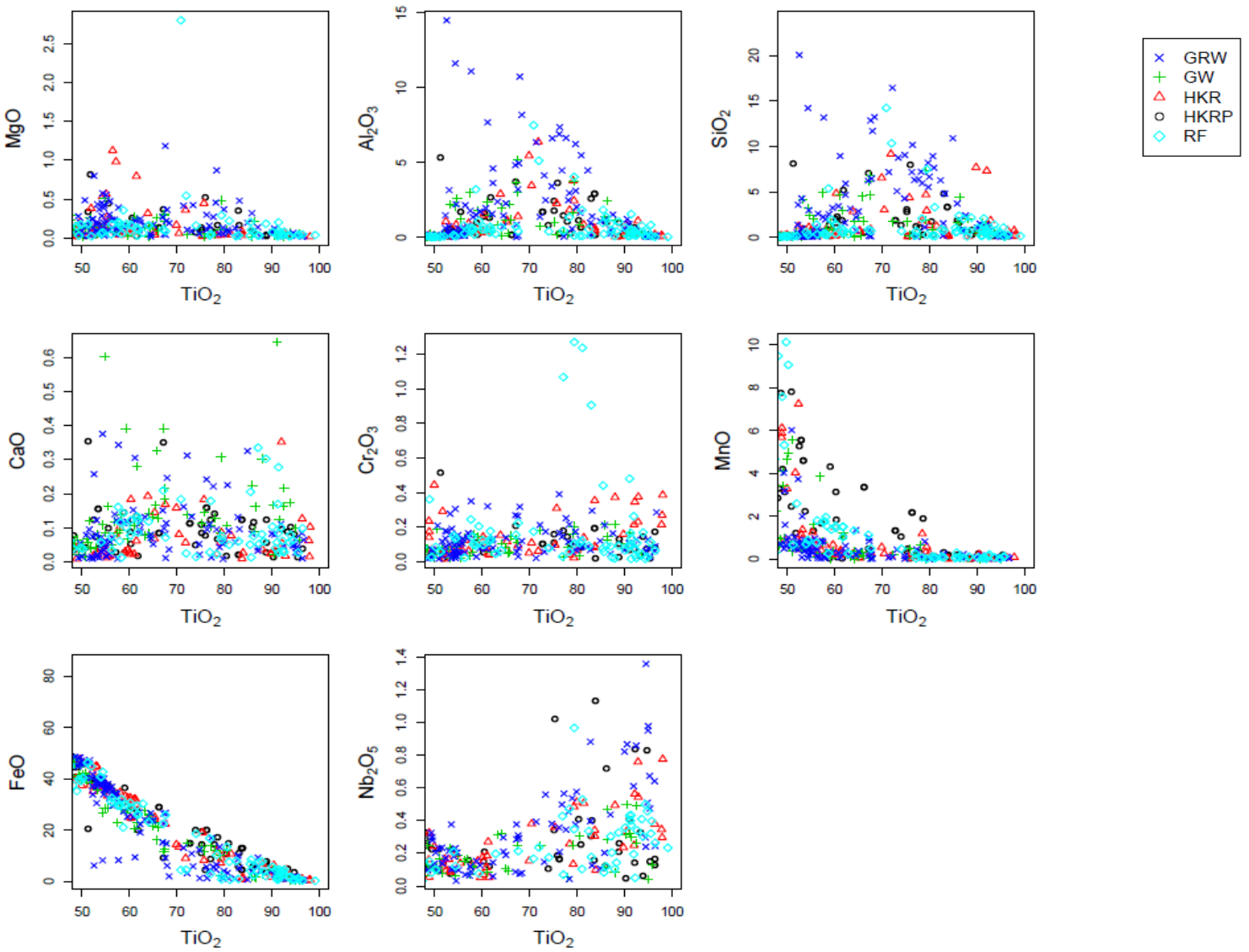

Figure 5.10. Binary diagrams of selected elements against TiO_2 for altered ilmenite of the five satellite areas. n=394. FeO represents total iron ($FeO+Fe_2O_3$). Total iron decreases and Nb_2O_5 increases with increasing alteration.

The increase in niobium content and the decrease in MgO, total Fe and MnO contents are in agreement with the findings of Grey et al (1983); Grey and Reid (1975); Anand and Gikes (1985) and Nair et al (2009). These authors found that MgO and MgO are leached along with iron and Nb_2O_5 increases with increasing alteration. The latter is favourable from an economic point of view since Mg and Mn are impurities that lower the grade or quality of ilmenite and its alteration products.

TiO_2 frequency histograms were plotted to determine what alteration product is the most common (Figures 5.11). This in turn is an indication of the degree of alteration experienced by the five satellite areas. Graauwduinen's alteration products have TiO_2 contents ranging from 54.04% - 96.74%, Geelwal Karoo: 54.37% - 95.84%, Houtkraal Remainder: 54.31% - 98.05%, Houtkraal Remainder Portion 2: 55.50% - 97.59% and 56.13% - 96.45% for Rietfontein in comparison with the 48% - 53% stoichiometric TiO_2 content of ilmenite. Houtkraal Remainder Portion 2 is dominated by leucoxene (45%). The rest of the altered ilmenite is made up of hydrated ilmenite (34%), pseudorutile (12%) and rutile* (9%). Houtkraal Remainder is dominated by hydrated ilmenite (44%). Leucoxene makes up 30%, pseudorutile 19% and rutile* 6% of the rest of the altered ilmenite. Geelwal Karoo is also dominated by hydrated ilmenite (49%). Leucoxene makes up 26% whereas pseudorutile and rutile* makes up 21% and 4% respectively. Graauwduinen is dominated by hydrated ilmenite (49%). Leucoxene, pseudorutile and rutile* make up 28%, 14% and 9% respectively of the rest of the altered ilmenite. Rietfontein's altered ilmenite fraction is dominated by leucoxene (45%). Hydrated ilmenite (33%), pseudorutile (12%) and rutile (11%) make up the rest of the altered ilmenite fraction.

It can be concluded from the TiO_2 frequency histograms that all five satellite area's altered ilmenite fraction contains the whole spectrum of ilmenite alteration products namely hydrated ilmenite, pseudorutile, leucoxene and rutile*. The dominance of leucoxene in the Houtkraal Remainder Portion 2 and in particular Rietfontein, shows that these two areas underwent a higher degree of alteration than the other three satellite areas and indicates that most ilmenite is altered up to the leucoxene stage. The dominance of hydrated ilmenite in Houtkraal Remainder, Geelwal Karoo and Graauwduinen indicate that most ilmenite grains in these three areas only experienced beginning stages of alteration.

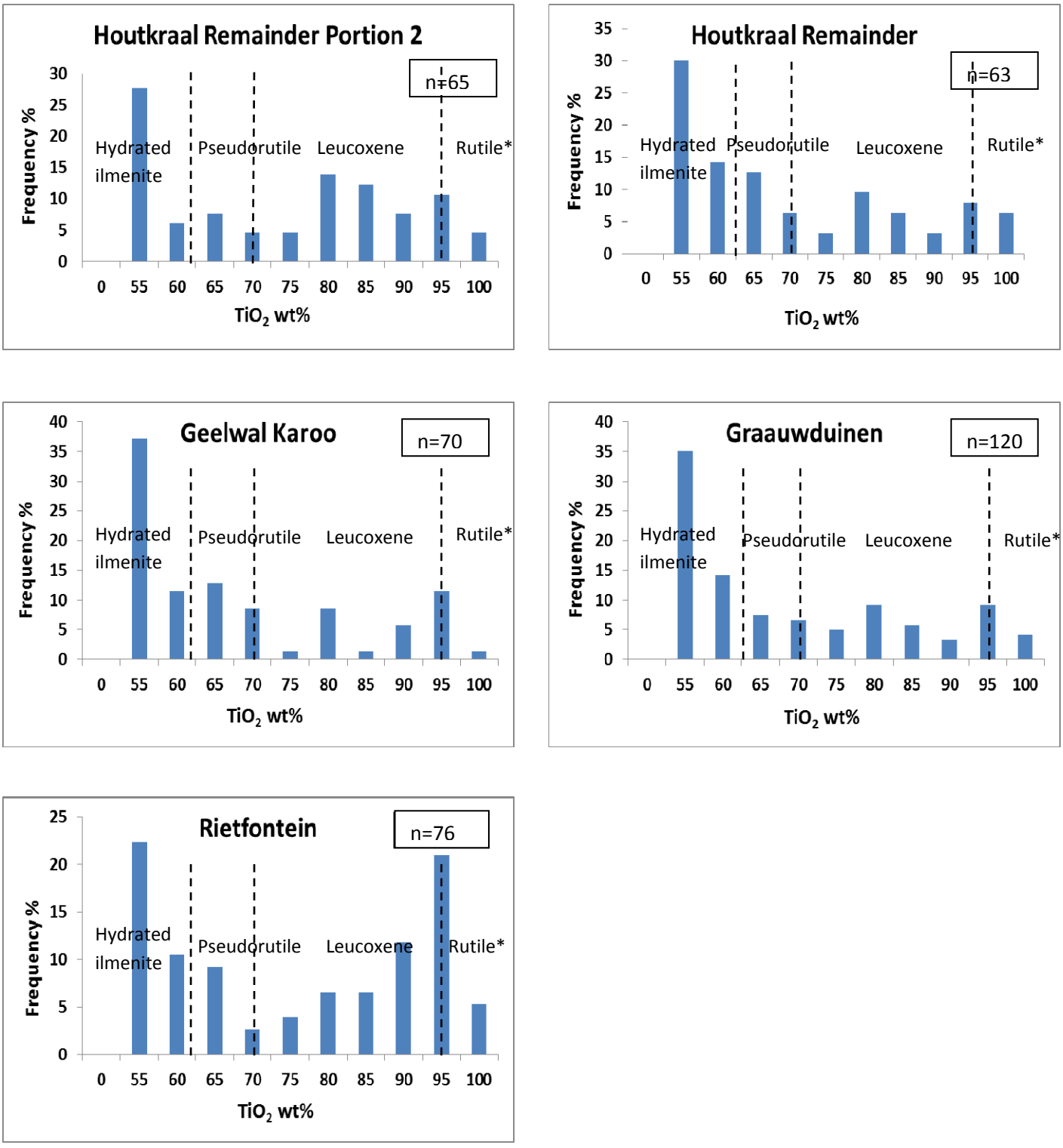

Figure 5.11. TiO_2 fequency histograms of altered ilmenite in the five satellite areas. Histograms indicate that the whole spectrum of ilmenite alteration products is present in the five satellite areas.

The above percentages indicate that the five satellite areas are very similar but have different ilmenite alteration product proportions. The latter can be due to factors such as in-situ alteration and transportation of alteration products. During these two processes ilmenite grains become fractured and can be broken down easily and removed from the heavy mineral fraction changing the mineral proportions. A third factor that could have played a role is the addition of altered ilmenite grains that are not a product of the unaltered ilmenite in the heavy mineral suite. These grains were formed in the source rocks and then added to the altered ilmenite suite by, example, wind activity. An alteration index, indicating the percentage of altered ilmenite grains, was quantified and explained in Chapter 6.

5.4 Zircon

5.4.1 Petrography

Zircon ($ZrSiO_4$) in this study has been classified according to colour and is shown in Figure 5.12: clear colourless zircon (Figure 5.12 A), yellow zircon (Figure 5.12 B) and a brown to dark brown metamict zircon (Figure 5.12 C). A metamict mineral refers to a mineral that underwent metamictization (destruction of the crystal structure by radiation). Metamictization of zircon results from the radiation damage to the crystal structure caused by the radioactive decay of U and Th that substitutes for Zr^{4+} (Woodhead et al, 1991). The crystalline zircon ultimately decomposes to zircon glass, microcrystalline zircon, crystalline and / or amorphous ZrO_2 and SiO_2.

Specific gravity and optical properties usually vary with the amount of Fe present and also with the degree of metamictization. For example non-metamict zircons have lower birefringence colours than metamict varieties. Colourless zircon is the most common in all five satellite areas followed by the metamict zircon. Yellow zircon is present in trace amounts only. Zircon can be easily identified by its high order interference colours and high relief. It is mostly rounded to sub-rounded (Figure 5.12) indicating advanced abrasion during transport. Elongated, anhedral forms are also present (Figure 5.12 D).

The euhedral form of zircon indicates short transport distances. A characteristic feature of zircon is oscillatory zoning (Figure 5.12 C) and is most abundant in the metamict variety. Grain size ranges between 92 and 462 µm for Houtkraal Remainder Portion 2, 123-236 µm

for Houtkraal Remainder, 92-400 µm for Geelwal Karoo, 62-431 µm for Graauwduinen although grains as large as 539 µm also occur throughout. Rietfontein has grains ranging in size between 92 and 323 µm. The long axis of the grains was measured.

Characteristic of most zircon grains are the presence of fractures that either cut across the grain, radiate outward from an inclusion in the middle or form concentric fractures. Present on most zircon grains is an amorphous redbrown coating. SEM analysis indicates that the coating consists of Si-Al-Fe and or K, Si-Al-Ca and Na, Ti-Al and Mg, Si-Ti-Al and Fe and Si-Al-Fe and Ti (Table F19, Appendix F). An Al-rich material is present in cracks and in dents (Table F19, Appendix F, analysis 25 and 30).

Zircon hosts a variety of inclusions of which apatite is the most abundant. Other phases include quartz, rutile, monazite, muscovite, barite and xenotime. These inclusions have tabular, needle-like, round, squarish and hourglass shapes (Figure 5.12 F) that range from transparent to opaque and show no preferred orientation.

In some samples complex zircon grains are present that are overgrown by a later stage zircon (Figure 5.12 E). This type of texture develops during crystallization in a terrain where possible multiple metamorphic events took place. Some zircons have complex internal structures and cores (Figure 5.13 A and B). Inclusions are also present within these cores.

5.4.2 Chemistry

LA-ICP-MS analyses were performed on 267 randomly selected zircon grains from the five satellite areas for the following elements: Mg, Al, P, K, Ca, Sc, Ti, Mn, Fe, Y, Hf, Pb, Th, U and REE. Due to coupled substitution in zircon, it can incorporate a wide range of trace elements. Only one analysis was done per grain and was considered representative for this study. Data are presented in Tables F3A and F3B, (Appendix F). Zircon usually contains about 1 wt % hafnium but always less than 3 wt %. Hf is the major substitute for Zr^{4+} in zircon. Geelwal Karoo, Houtkraal Remainder Portion 2 and Graauwduinen have Hf contents of up to 2 wt %. All other elements of the five satellite areas are present in concentrations of less than 1 wt %. These include U, Th, Al, Fe, P, Ti and Y. Concentrations range from 10 to 1000 ppm. Trace amounts of Mg, K, Mn, Pb and Ca are present and is close to or below the detection limit of the instrument.

Y has the second highest concentration in zircon after Hf and occurs in concentrations of up to 6300 ppm.

Comparing the mean values of the five satellite areas, significant differences are present for the major elements K, Mg, and Al and the trace element Fe (Table F3A, Appendix F). The other minor (Ca, Ti Mn) - and trace elements show a similar chemistry.

All five satellite area's zircons have TREE (total rare earth) contents of less than 1 wt % (Table F3B, Appendix F). The total REE content of zircons from Houtkraal Remainder Portion 2 range between 277 and 1689 ppm, 46-4704 ppm for Houtkraal Remainder, between 205-2081 ppm for Geelwal Karoo, 203-3173 ppm for Graauwduinen and 239-1925 ppm for Rietfontein. From above values it can be concluded that the satellite areas have the same REE chemistry.

REE profiles were constructed for each satellite area with GCDKit normalised to chondrite after Boynton (1984) (Figures 5.14-5.18). All five satellite areas have a uniform REE profile with a dominant and steep HREE profile and small to moderate LREE profile with prominent negative Eu anomalies and positive Ce anomalies. The HREE enrichment of the five satellite areas is similar (uniform HREE profiles) with small differences in the LREE profiles indicating a similar REE chemistry throughout the area.

For all five satellite areas, HREE dominate (Table F3B, Appendix F). This is due to the Zr^{4+}-cation that is closer in size to the HREE than to the LREE and therefore has a strong preference to fractionate the HREE (Philander, 1999).

Philander (1999) also found the HREE to dominate in the zircon from the Kleinzee area with respect to the LREE. The zircon had similar HREE enrichment with a variable LREE character. Philander (1999) related the variable LREE enrichment of the zircon to the primary trace element chemistry of the sample's respective zircon populations. Philander (1999) found no Ce anomaly but a negative Pr anomaly for zircon from the palaeochannels. He ascribed this Ce anomaly absence to suspect La values which are the result of La contamination in the flux. Rozendaal et al (1999) found that zircon from different geological environments and different colour zircon types (e.g. metamict) each have their own unique chemistry (different trace element and REE chemistries).

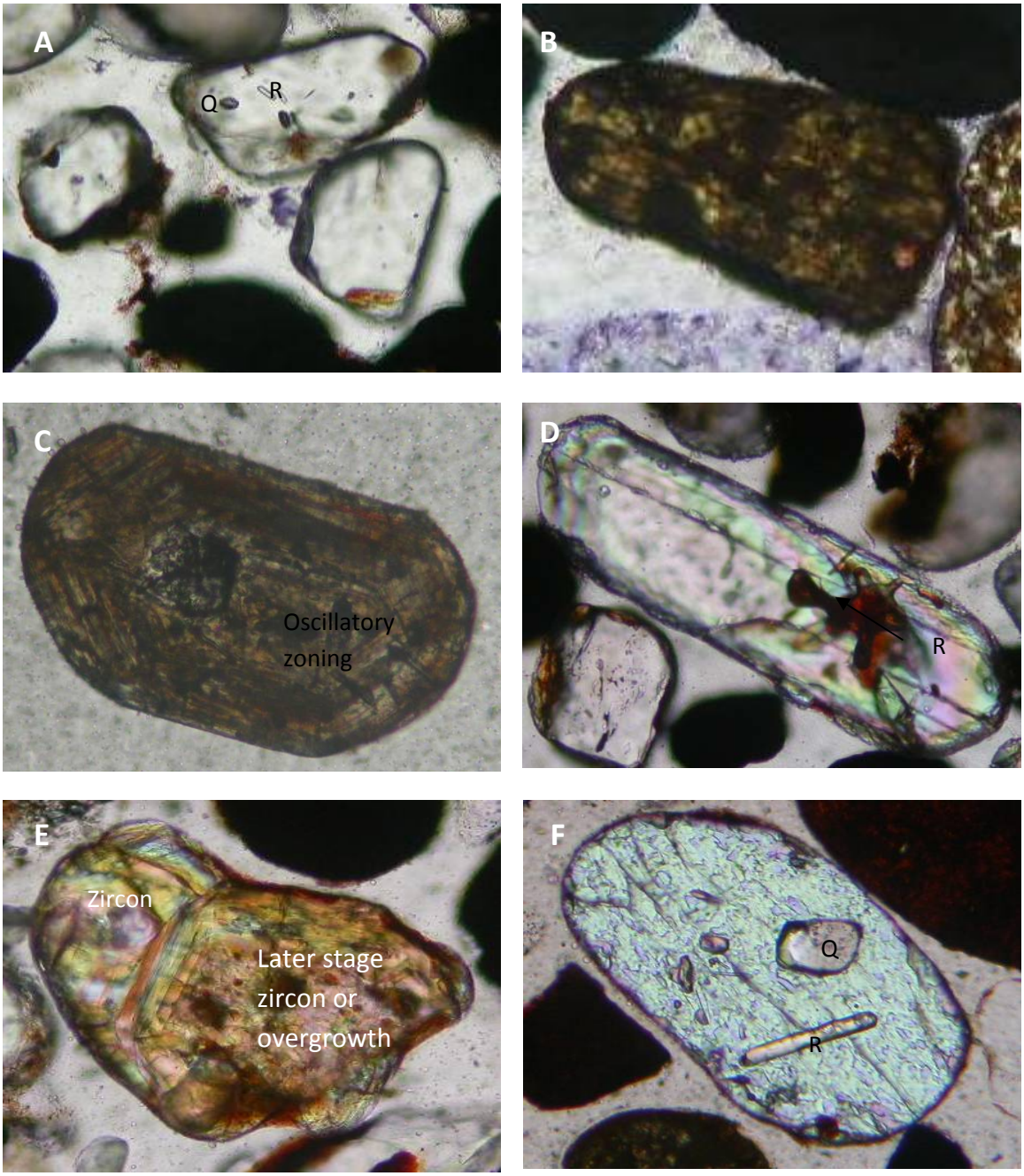

Figure 5.12. Microscope images showing the different types and colour of zircon present in the satellite areas. All pictures were taken under transmitted light. Scale: 20X. A) Colourless zircons with inclusions of rutile (R) and quartz (Q). B) Yellow metamict zircon. C) Brown metamict zircon with fine, oscillatory zoning. D) Colourless, elongated shape zircon with red rutile inclusions. E) Zircon overgrowth. Colourless zircon is overgrown by a later stage metamict zircon. F) Zircon showing needle (rutile) and square-shaped (quartz) inclusions.

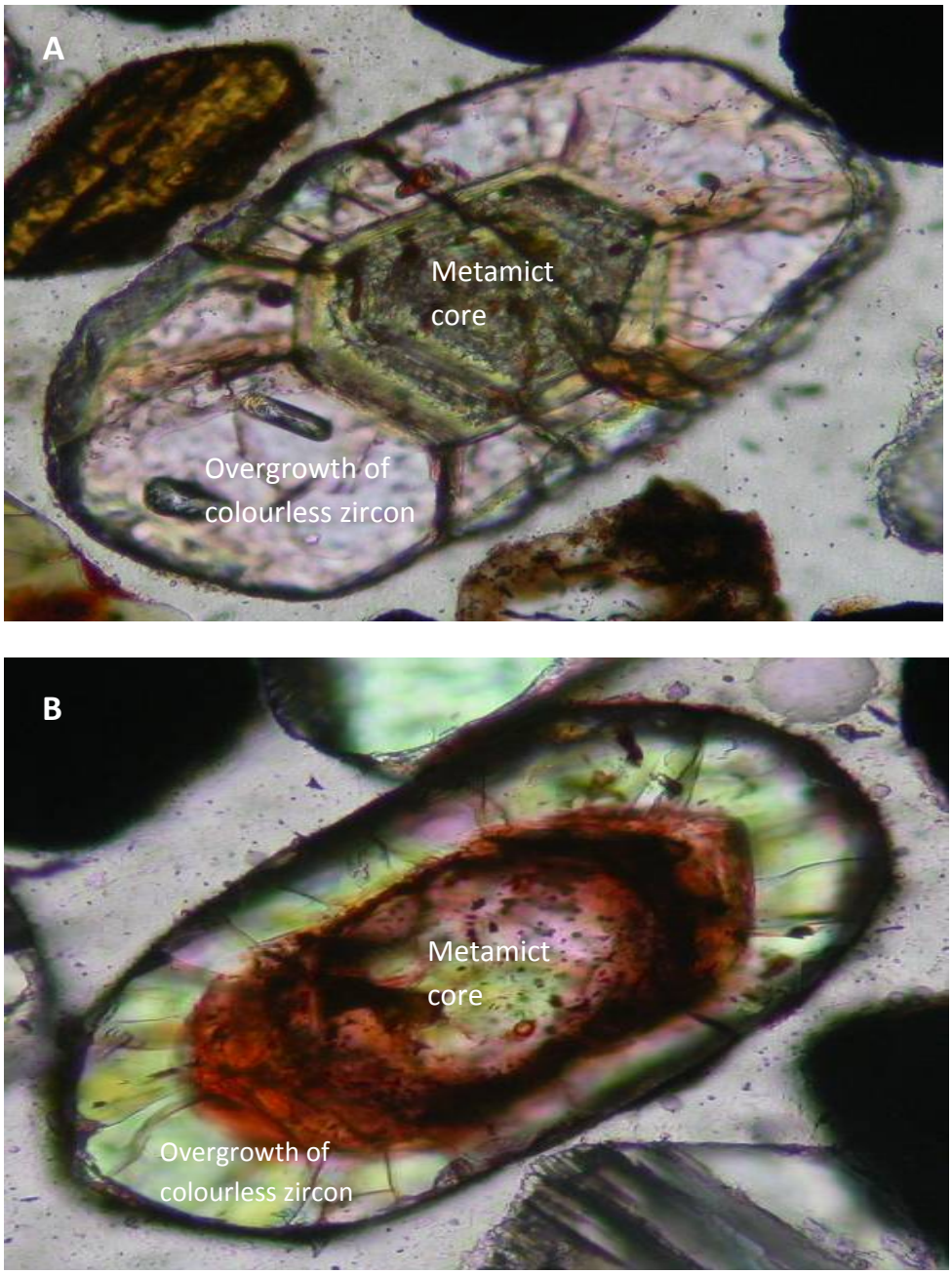

Figure 5.13 A and B. Pictures were taken under transmitted light. Scale 20X. Complex zircons. Metamict zircon core overgrown by later stage clear zircons with abundant inclusions. The latter is the result of multiple growth events (Hay et al, 2006).

It can therefore be concluded that the similar REE and trace element chemistry of the five satellite areas indicate that the zircons from the five satellite areas are from the same geological environment and are of the same type. All five satellite areas have an aeolian character and support the conclusion of a similar geological environment.

When comparing the zircon chemistry of the satellite areas with that of the Namakwa Sands deposit, it is evident that each satellite area consists of a mixture of colourless, yellow and brown zircon. The data was obtained from Namakwa Sands and zircons were analysed by means of the LA-ICP-MS method (Philander pers comm). The three colour zircon varieties of the Namakwa Sands deposit have differences in its U, Th, Cr, V, Fe, Ti, Mn, Pb, Ca, P and Mg contents. The latter elements are the least concentrated in the colourless zircon and the most enriched in the brown zircon. U+Th and Fe were used to determine what colour zircon varieties are present in each satellite area. This was done by constructing histograms of the Fe and U+Th contents (Figure 5.19 and 5.20) of the satellite areas and the colourless, yellow and brown zircons of the Namakwa Sands deposit.

The colourless and yellow zircons have Fe similar distribution patterns while the brown zircon has a wider distribution. The colourless, yellow and brown zircon histograms all peak at 200-400 ppm Fe. The colourless zircon is characterized by Fe contents < 400 ppm. The yellow zircon is characterized by < 600 ppm Fe and the brown zircon is characterized by zircon > 600 ppm.

Houtkraal Remainder's zircon population consists mainly of colourless zircon. Fe values > 400 ppm correlates with yellow and brown zircon and are present in accessory amounts. Geelwal Karoo has a similar distribution pattern to Houtkraal Remainder and so does Graauwduinen, Rietfontein and Houtkraal Remainder Portion 2.

The U+Th histogram of the colourless, yellow and brown zircon show distinct patterns. Colourless zircon has a narrow distribution peaking at 200-400 ppm. The yellow zircon has a wider distribution peaking at 200-600 ppm. The brown zircon has the widest distribution with most zircon having U+Th values of between 400 and 3000 ppm where after Fe's abundance decreases. From the U+Th histograms it is evident that all five satellite area's zircon populations are dominated by colourless zircon with trace amounts of yellow and brown zircon present. The low U+Th contents indicate that the zircons are of a high quality and are ideal for trading in the heavy mineral industry.

The different proportions of colourless, yellow and brown zircon in each satellite area's population are therefore responsible for the slight variation in the major and trace element chemistry between the satellite areas and with respect to the Namakwa Sands deposit. The

high quality of zircon from the satellite areas corresponds to the RAS's zircon of the Namakwa Sands deposit (Philander pers comm).

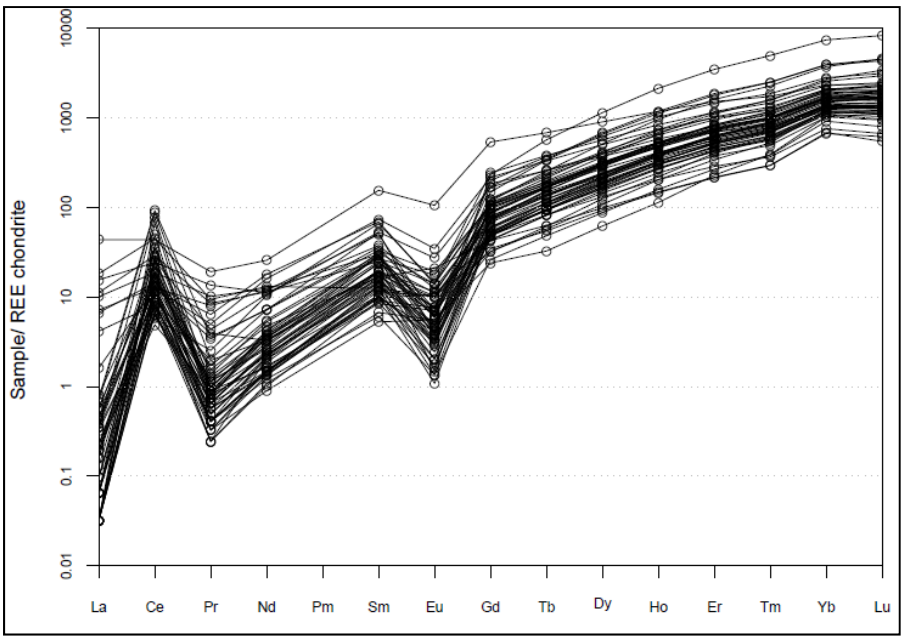

Figure 5.14. Chondrite normalized REE profile of the zircon grains of Houtkraal Remainder Portion 2. Zircon is enriched in HREE with a positive Ce anomaly and negative Eu anomaly.

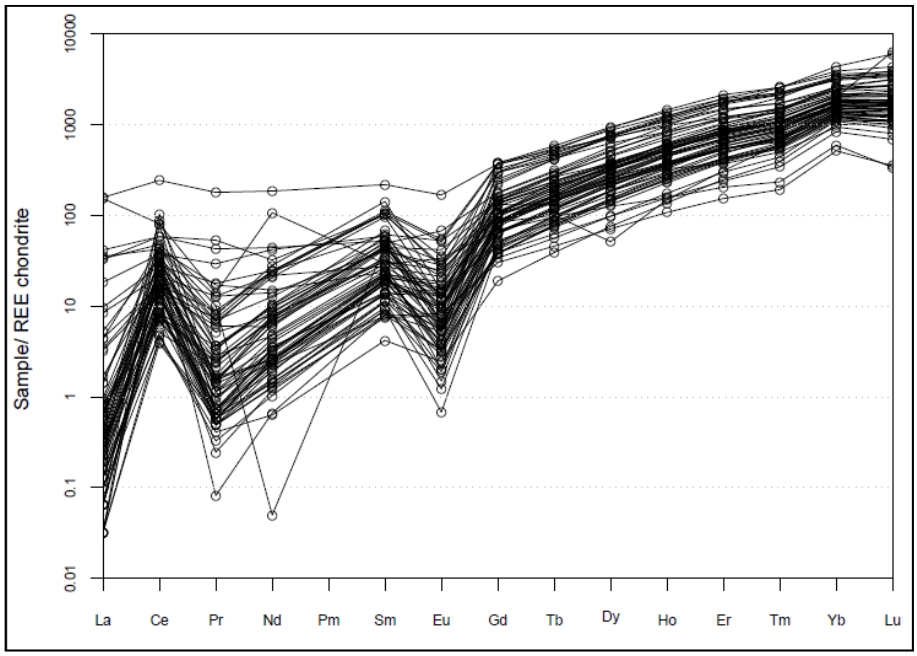

Figure 5.15. Chondrite normalized REE profile of the zircon grains of Houtkraal Remainder. Zircon is enriched in HREE with a positive Ce anomaly and negative Eu anomaly.

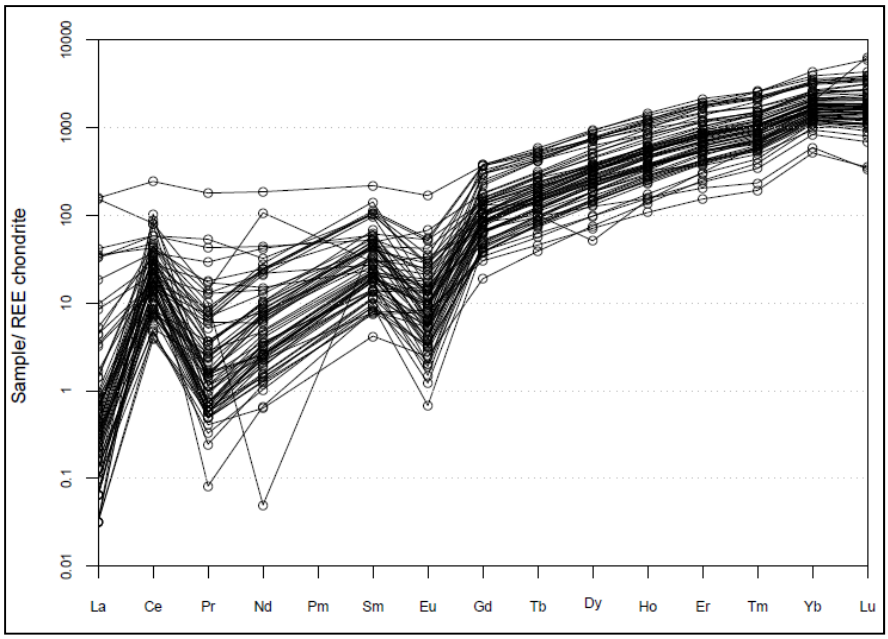

Figure 5.16. Chondrite normalized REE profile of the zircon grains of Geelwal Karoo. Zircon is enriched in HREE with a positive Ce anomaly and negative Eu anomaly.

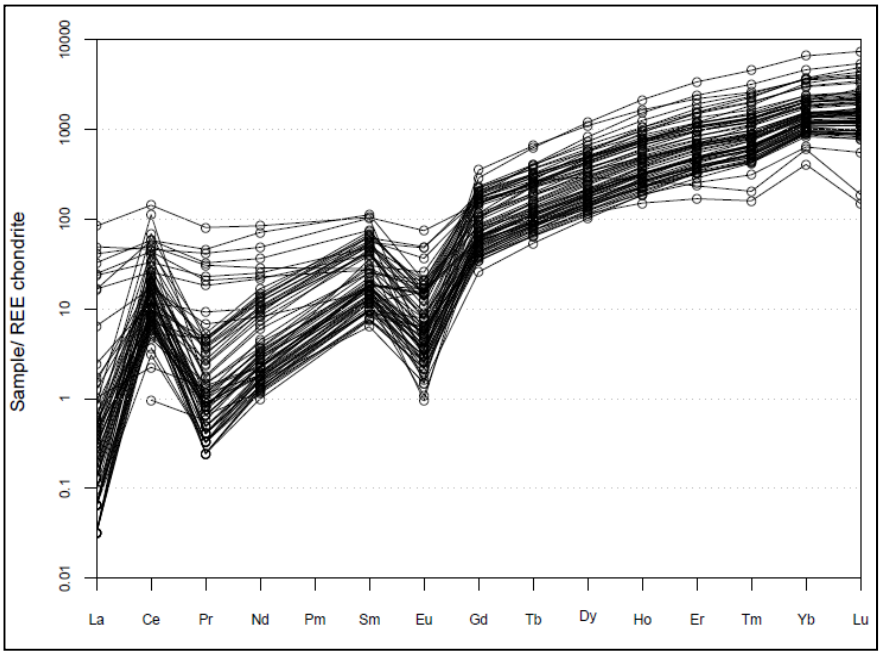

Figure 5.17. Chondrite normalized REE profile of the zircon grains of Graauwduinen. Zircon is enriched in HREE with a positive Ce anomaly and negative Eu anomaly.

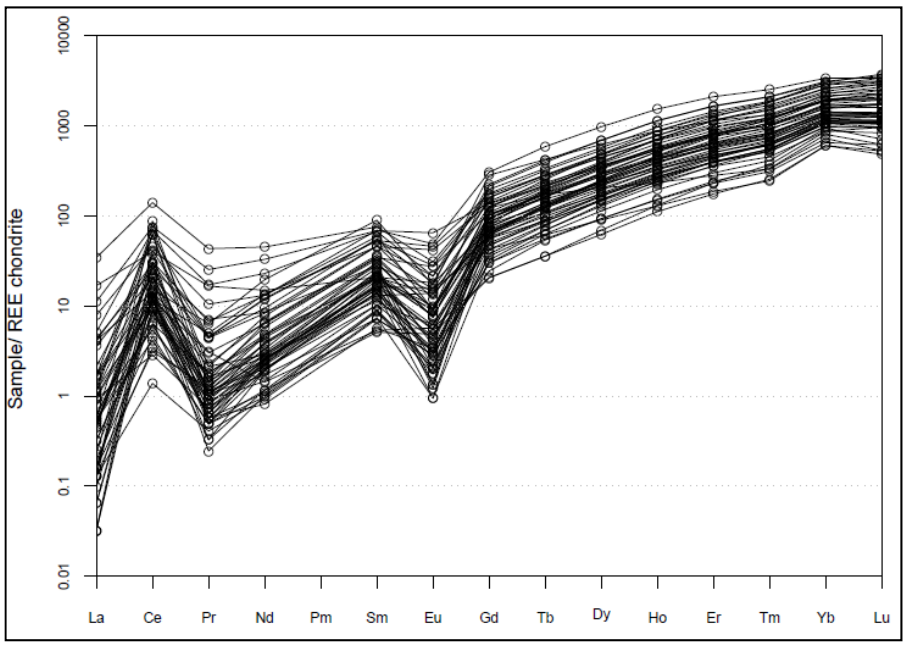

Figure 5.18. Chondrite normalized REE profile of the zircon grains of Rietfontein. Zircon is enriched in HREE with a positive Ce anomaly and negative Eu anomaly.

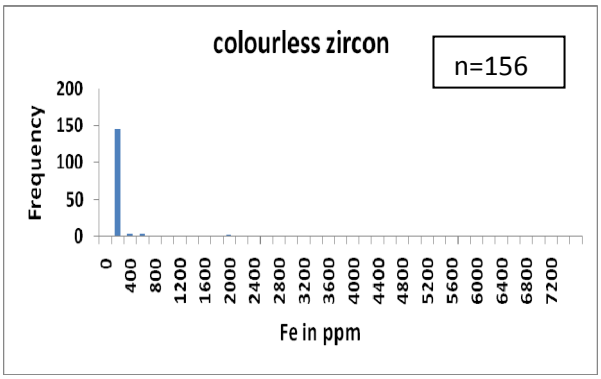

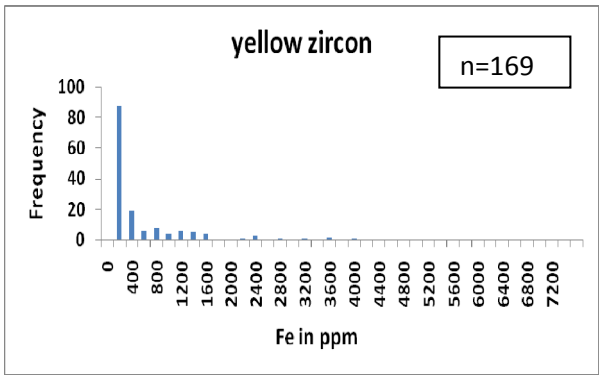

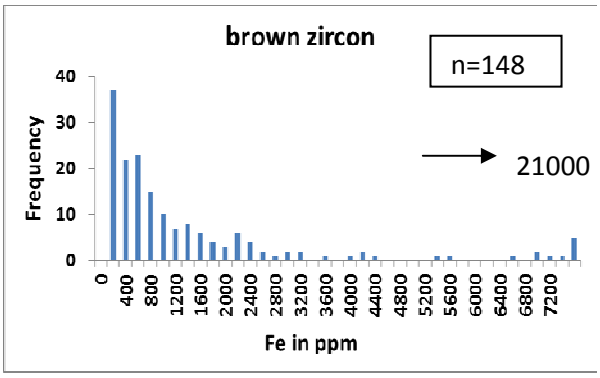

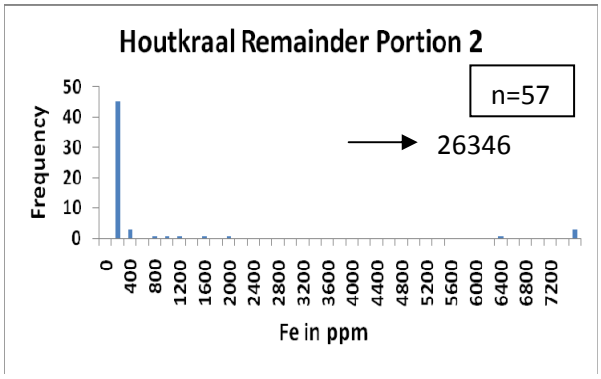

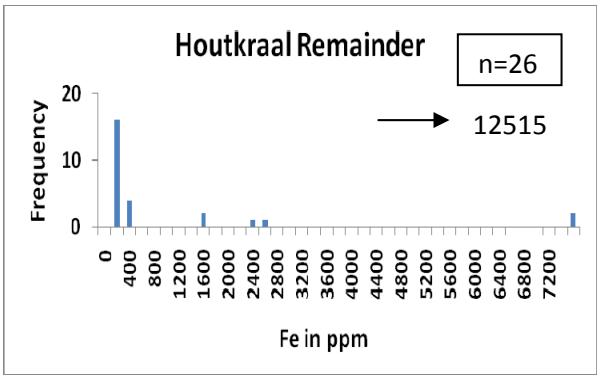

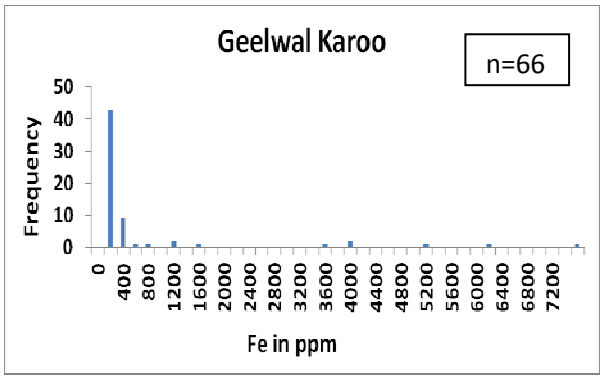

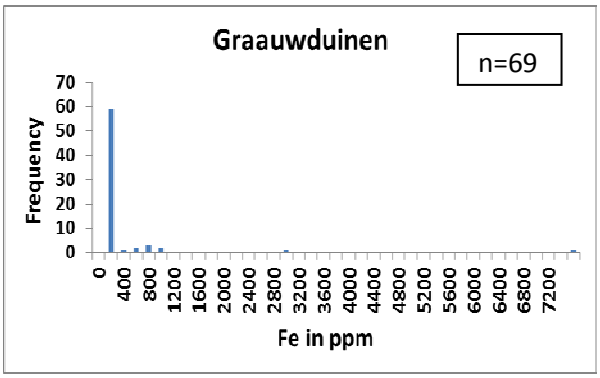

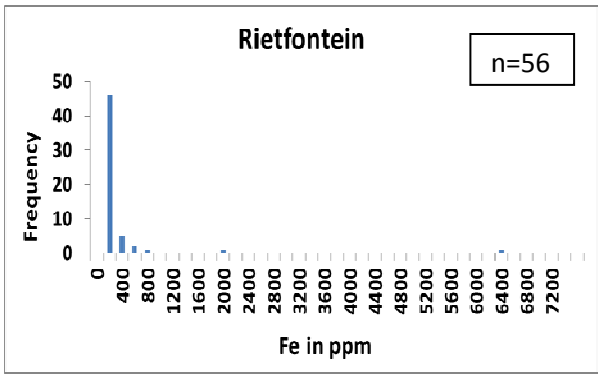

Figure 5.19. Histograms showing the Fe content of zircons from the five satellite areas and the colourless, yellow and brown zircons from the Namakwa Sands deposit. All five satellite area's zircon populations consist of mainly colourless zircon with trace amounts of yellow and brown zircon.

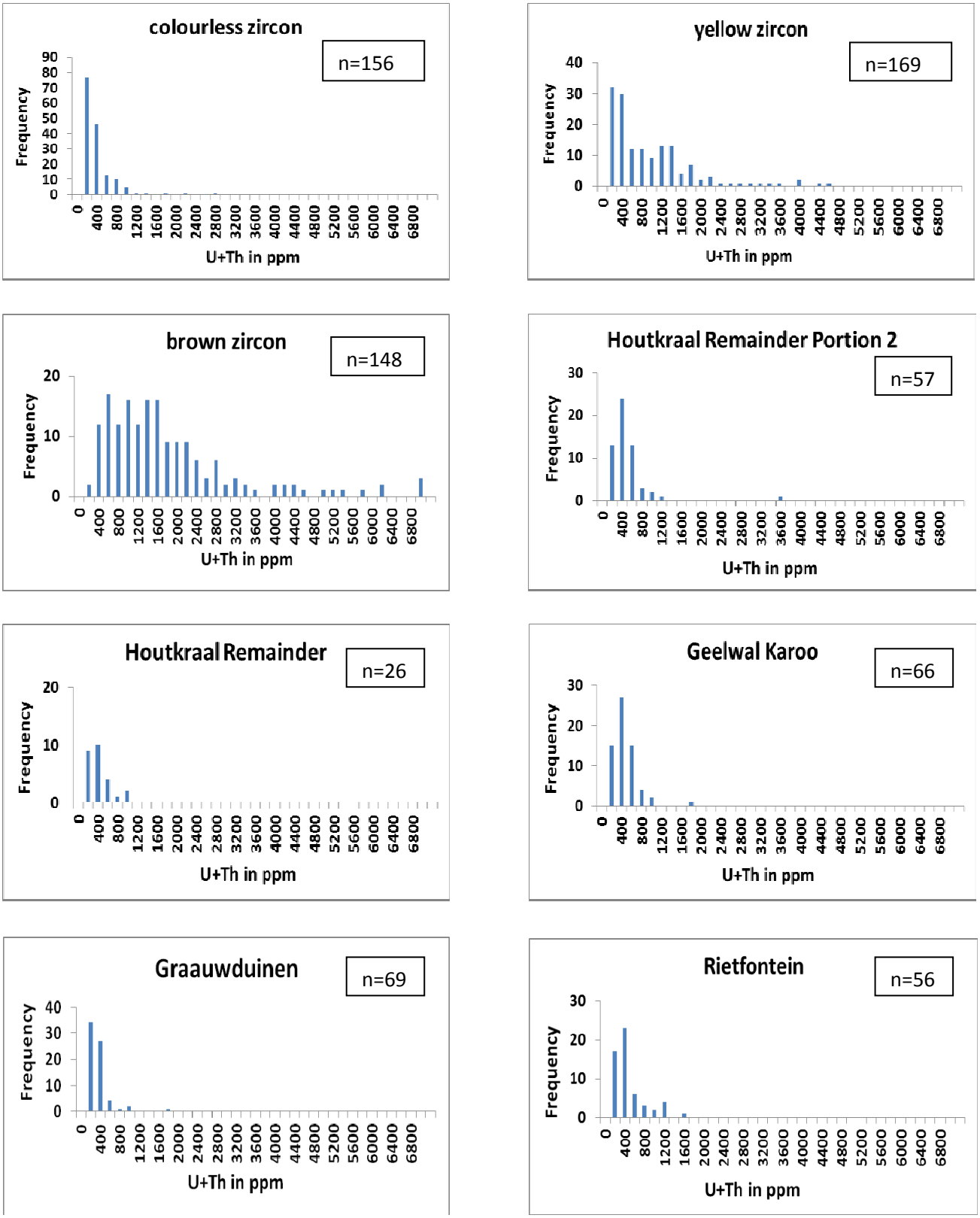

Figure 5.20. Histograms showing U+Th content of zircons from the five satellite areas and the colourless, yellow and brown zircons from the Namakwa Sands deposit. All five satellite area's zircon populations consist of mainly colourless zircon with trace amounts of yellow and brown zircon.

5.5 Rutile

5.5.1 Petrography

Rutile grains are yellow, red, orange to orange brown, violet, green brown and black (Figure 5.21 A-E). The violet variety is rare. Some of the Geelwal Karoo samples contain rutile that is bi-coloured (green and yellow, Figure 5.21 E). The depth of colour of rutile is related to the ferric iron, niobium and tantalum content as indicated by its mineral chemistry (section 5.5.2).

Grain size ranges between 100 and 286 µm for Houtkraal Remainder Portion 2, 88-288 µm for Houtkraal Remainder although grains as large as 375 µm also occur throughout. For Geelwal Karoo the grain size ranges between 75 and 225 µm, 74-222 µm for Graauwduinen and between 133 and 355 µm for Rietfontein although grains as large as 430 µm also occur throughout. All have very similar size.

Grain shapes range from dominantly sub-rounded and oval to anhedral and sub-elongated (Figure 5.21 A-E). Optically black rutile resembles ilmenite and can be distinguished by its strong yellow internal reflections under reflected light (Figure 5.22 B).

A characteristic feature of rutile is its oblique twinning, where the twin lamellae are present as oblique striations that intersect each other (Philander, 1999, Figure 5.21 A and Figure 5.22 B and D).

Also characteristic of most rutile grains is the presence of a redbrown, amorphous coating of Si, Al, Fe and K (Figure 5.22 C). The latter composition was determined with the SEM (Table F19, Appendix F).

Inclusions in rutile (as identified by SEM) include garnet (almandine), micas (biotite and muscovite), ilmenite, zircon, monazite and hematite. Quartz is the most common inclusion in rutile and is present in all the coloured rutile varieties. The unusual bi-colour rutile contains sphalerite as an inclusion. The inclusions are randomly orientated and have angular, anhedral, tabular, elongated and round shapes. Some rutile grains host up to four different inclusions in one single grain.

Also present are multi-colour aggregates or intergrowths of rutile and quartz. These aggregates have anhedral shapes with a SiO_2–rich amorphous coating (Figure 5.21 F).

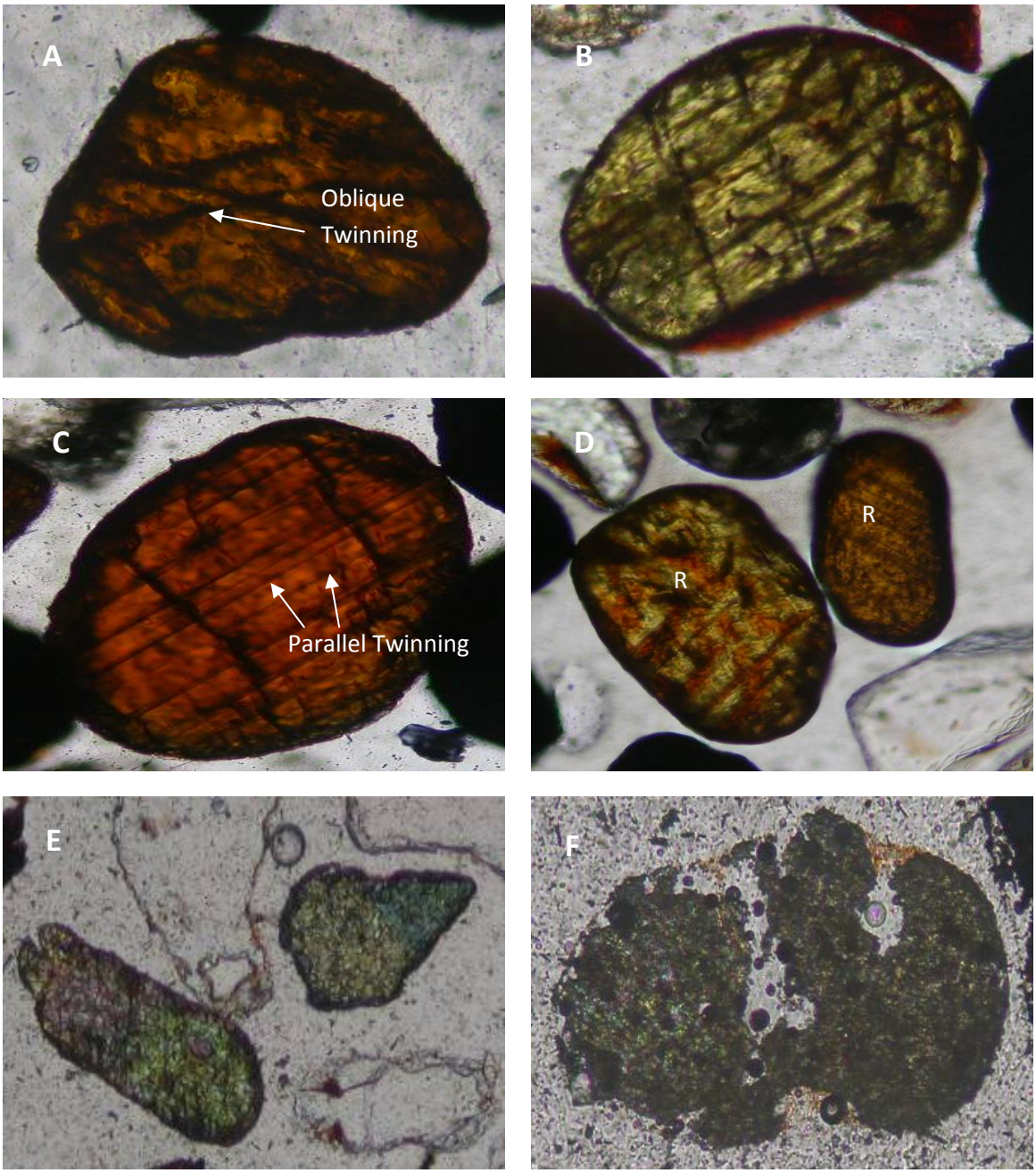

Figure 5.21. Microscope images showing different colour rutile present in the satellite areas. All photos were taken under transmitted light. Scale: 20X. A) An orange brown rutile showing oblique twinning. B) Yellow rutile showing twinning. C) Rounded red rutile with twinning parallel to length of grain. D) Rounded yellow rutile (R) with orange shades (due to amorphous coating) and orange rutile. E) Bi-colour rutile with euhedral and anhedral shapes. F) Rutile and quartz aggregate that is highly altered.

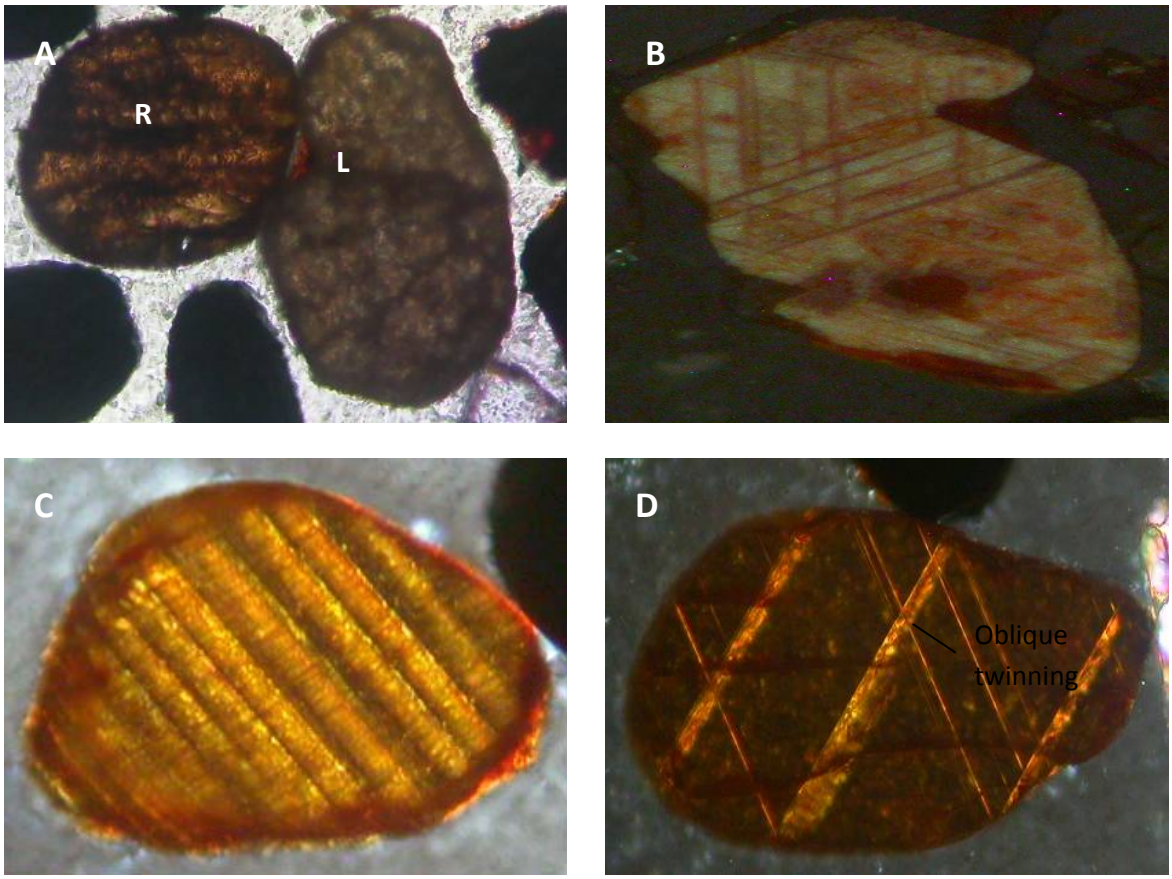

Figure 5.22. Microscope images showing rutile. All photos were taken under transmitted light except Figure 5.4 B that was taken in reflected light. Scale: 20X. A) Orange brown rounded rutile (R) on left of leucoxene (L). B) Rutile with yellow internal reflections under crossed nicols, reflected light. C) Orange rutile with red amorphous coating. Note the parallel twinning. D) Red rutile under crossed nicols showing oblique twinning.

5.5.2 Chemistry

228 Rutile grains were analysed with the LA-ICP-MS for a diversity of elements including the rare earth elements (REE). Results are presented in Table F4A and F4B, (Appendix F). There is a large variation in the trace element composition of rutile in each satellite area and between the five satellite areas. V, Cr, Zr, Fe and Nb are present in significant concentrations. These elements are responsible for the different colour of rutile varieties.

When comparing the chemistry of the rutile grains of the satellite areas with the yellow and red rutile of the Namakwa Sands deposit, a similar chemistry is evident except for elements such as Ba, Th, Y and the total rare earth elements (∑REE) which occurs in higher concentrations in the satellite areas (Table 5.2 and Table F4A, appendix F). The data of the Namakwa Sands deposit were obtained from the Namakwa Sands Mine and were analysed with the LA-ICP-MS method (Philander pers comm). The Ba content of Houtkraal Remainder, though, is similar to that of the Namakwa Sands deposit. Geelwal Karoo's Pb, Mn and ∑REE average contents are higher than that of the Namakwa Sands deposit and the other four satellite areas (Table 5.2). The U+Th, Pb and Hf average content of Rietfontein is also much higher than that of the Namakwa Sands deposit and the rest of the satellite areas. Some differences may be due to differences of the dataset.

Table 5.2. Average concentrations of specific elements analyzed with LA-ICP-MS.

Area	Ba	Th	Y	REE	Pb	Mn	Hf	U+Th
HKRP (n=40)	142	23	18	41	7	12	42	44
HKR (n=41)	2	14	4	52	1	6	38	40
GW (n=52)	264	59	22	125	61	42	43	95
GRW (n=50)	613	20	15	46	13	17	40	51
RF (n=45)	141	59	11	61	22	21	83	118
Yellow rutile East Mine (n=41)	7	5	16	37	5	11	52	65
Yellow rutile West Mine (n=140)	12	4	5	20	6	13	36	45
Red rutile East Mine (n=100)	4	7	5	16	3	8	73	45
Red rutile West Mine (n=261)	4	3	2	7	2	10	71	32

Rozendaal et al (2009) showed that red rutile is enriched in V, Hf, Cr and Zr and yellow rutile in Fe and Nb. V and Fe were used to determine which rutile colour varieties are present in each of the five satellite areas. This was done by constructing histograms of the V and Fe contents (Figure 5.23 and 5.24) and a Fe-V scatter diagram of the rutile of the satellite areas. The same diagrams were plotted for the red and yellow rutile of the Namakwa Sands deposit (Figure 5.25). The histograms and Fe-V diagram of the red and yellow rutile of the Namakwa Sands deposit were then compared with the histograms and Fe-V diagram of the five satellite areas.

The V histogram for the yellow rutile of the Namakwa Sands deposit has a narrow distribution with a peak at 1000-1500 ppm. The red rutile has a much wider spread of values with a peak at 3500-4000 ppm. Most red rutile has V contents of between 1500 and 5000 ppm. Rutile with > 2000 ppm V belong to the red rutile group since most of the red rutile has V contents > 2000 ppm while the yellow rutile is represented by V contents smaller than 2000 ppm.

For all five satellite areas a V content of < 2000 ppm has been selected to represent yellow rutile and V contents > 2000 ppm indicates red rutile.

From the V histograms (Figure 5.23), it is evident that Houtkraal Remainder Portion 2 has more yellow than red rutile. Houtkraal Remainder has slightly more red rutile than yellow rutile. Geelwal Karoo's rutile histogram has a similar distribution pattern as the yellow rutile of Namakwa Sands peaking at 1000-1500 ppm. It also contains more yellow rutile than red rutile. Graauwduinen also has a similar, narrow V distribution pattern with values ranging between 0 and 4000 ppm with a peak at 1000-1500 ppm. Graauwduinen is also dominated by yellow rutile. Rietfontein has a wide distribution ranging from 0 to 8000 ppm V. It has a peak at 3000-3500 ppm which represents red rutile. It has a moderate peak at 1000-1500 ppm representing yellow rutile. Rietfontein therefore has a similar distribution than the Namakwa Sands deposit (yellow and red rutile). The majority of Rietfontein's rutile is red in colour with only a small percentage being yellow.

The Fe histogram (Figure 5.24) of the red rutile has a narrow distribution (0-3500 ppm) with a peak at 500-1000 ppm. The yellow rutile has a wider distribution of between 0 and 19000 ppm peaking at 1000-1500 ppm. The red rutile is represented by Fe contents < 1000 ppm and the yellow rutile by Fe contents > 1000 ppm. From the satellite area's histograms it is evident that yellow rutile is the dominant rutile colour group for all five satellite areas. The V histograms of Houtkraal Remainder and Rietfontein shows red rutile to be the dominant rutile colour group. Philander and Rozendaal (2009) found that there is an overlap in the chemistry of the yellow and red rutile of the Namakwa Sands deposit. The difference shown by the V and Fe histograms of Houtkraal Remainder and Rietfontein can therefore be due to this overlap in chemistry of the yellow and red rutile. In conclusion all five the satellite areas have a mixed population of yellow and red rutile.

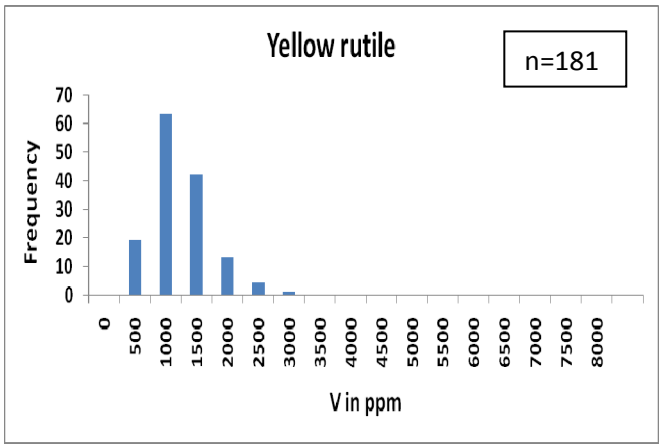

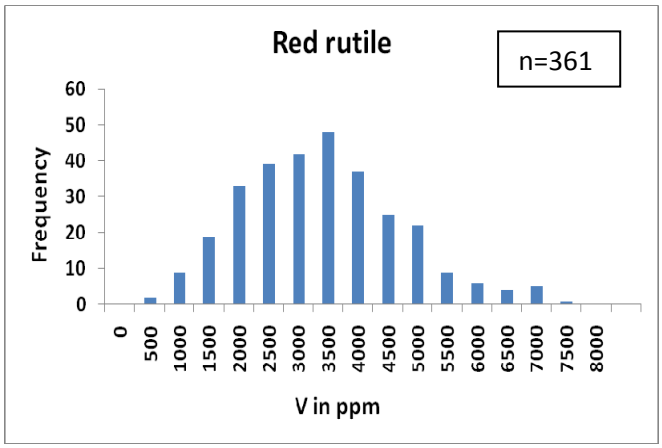

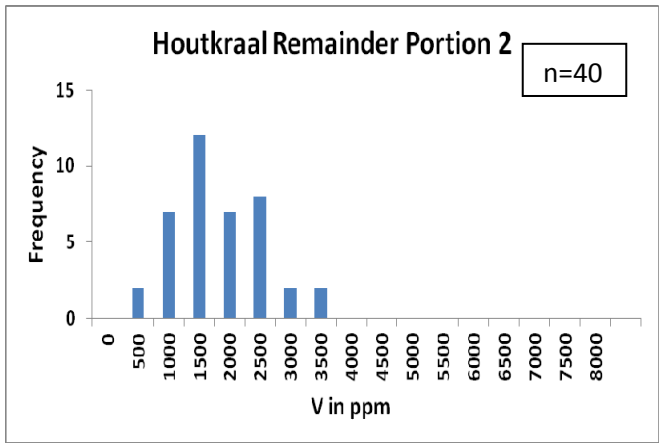

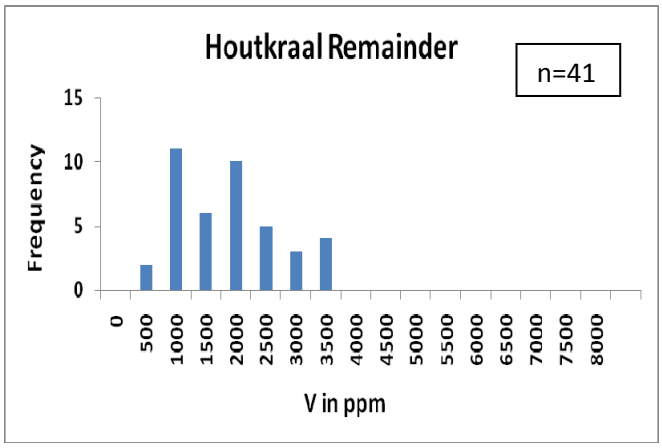

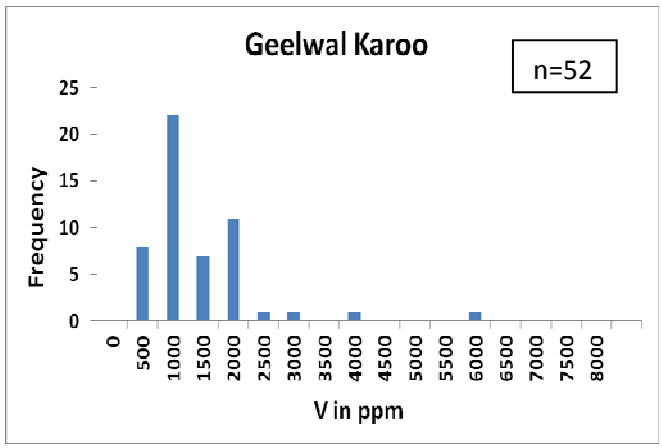

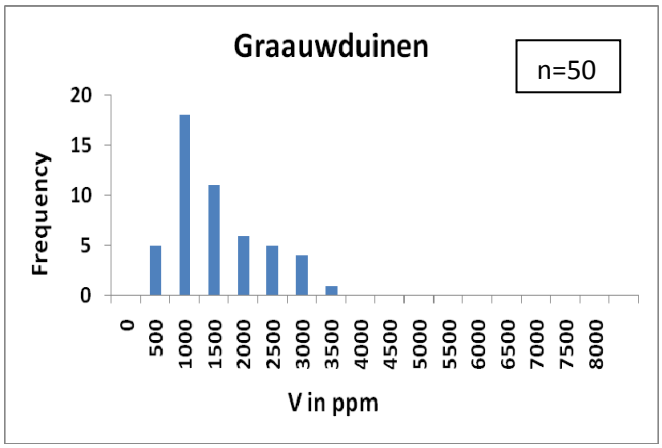

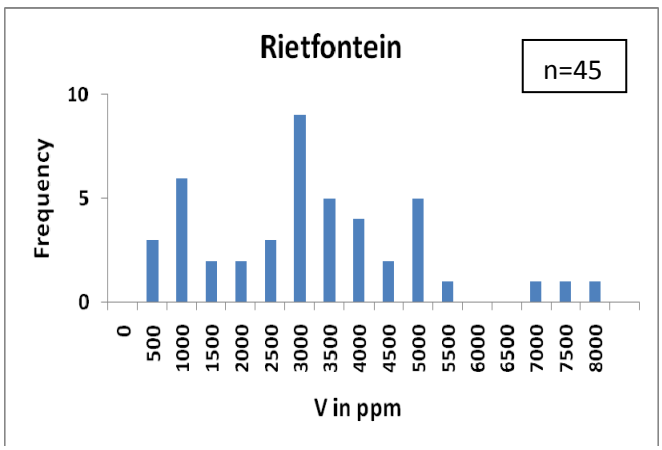

Figure 5.23. V histograms of rutile from the five satellite areas and of the red and yellow rutile of the Namakwa Sands deposit. Houtkraal Remainder and Rietfontein are dominated by red rutile and Houtkraal Remainder Portion 2, Geelwal Karoo and Graauwduinen by yellow rutile.

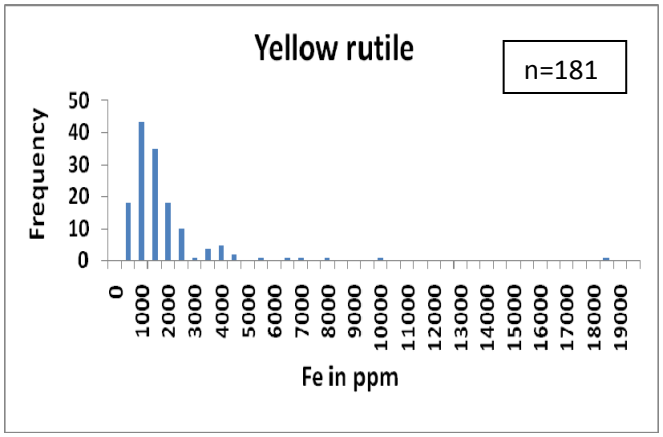

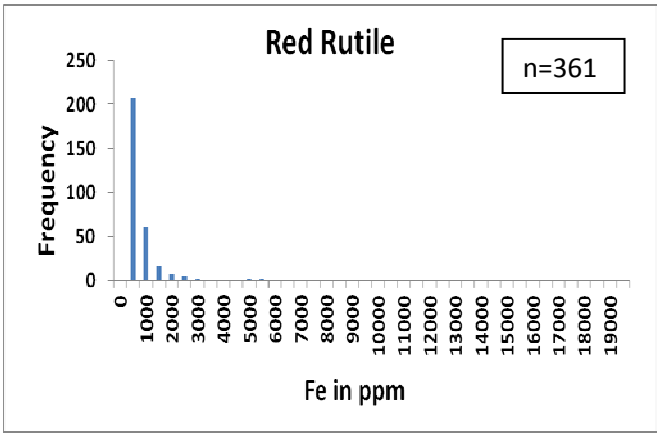

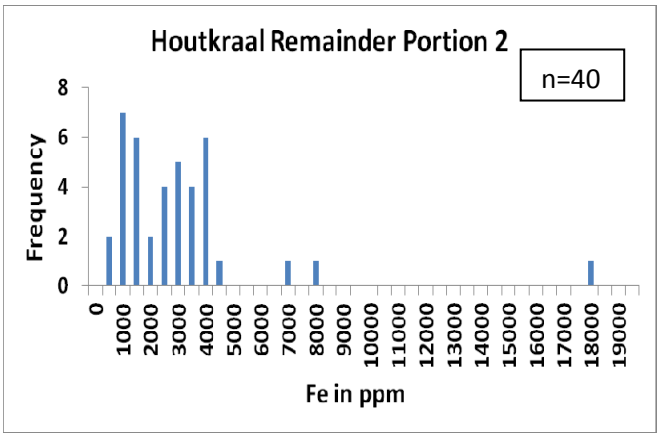

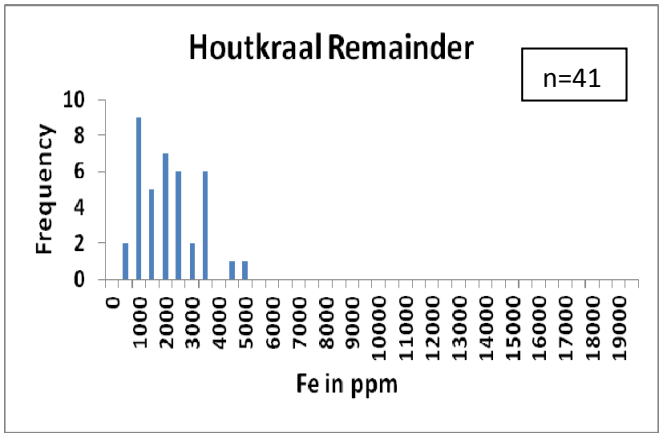

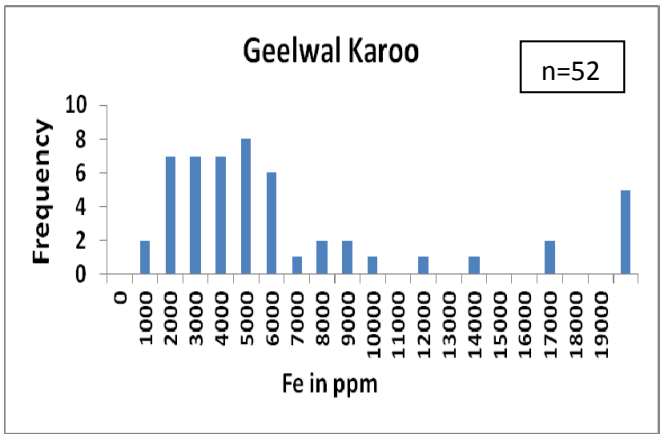

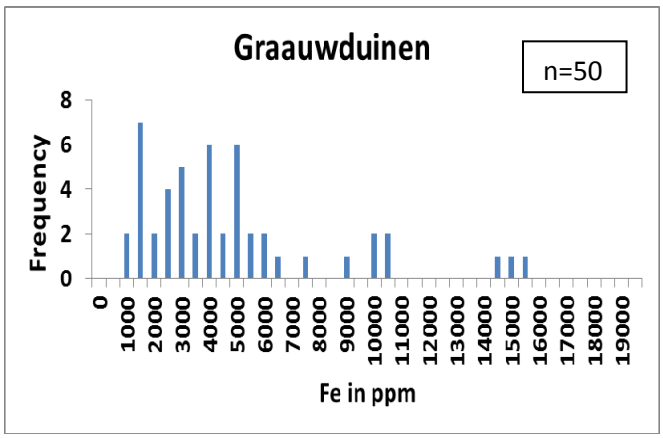

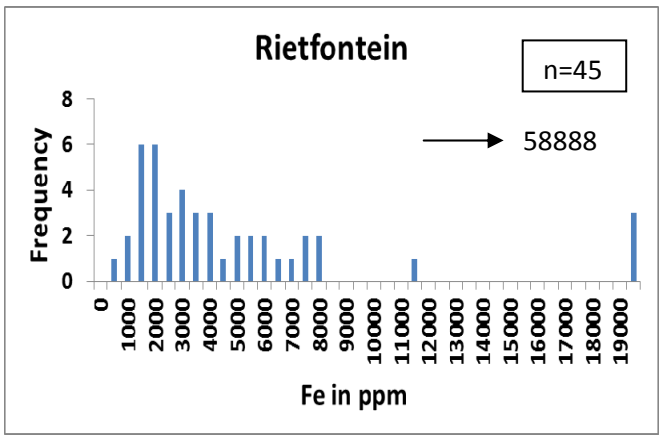

Figure 5.24. Fe histograms of rutile from the five satellite areas and the red and yellow rutile of the Namakwa Sands deposit. Al five satellite areas are dominated by yellow rutile.

The yellow rutile of the Namakwa Sands deposit has up to 18500 ppm of Fe. The satellite areas have up to 58000 ppm of Fe. These high Fe contents are usually present in the black rutile variety. The more Fe the rutile has in its structure, the darker the colour. The Fe and V contents of the satellite areas and of the Namakwa Sands deposit were plotted on the Fe-V scatter diagram of Philander and Rozendaal (2009) to discriminate between the red and yellow rutile varieties of the five satellite areas (Figure 5.25).

From Figure 5.25 it is evident that red rutile is enriched in V and yellow rutile in Fe. There is an overlap in chemistry of the yellow and red rutile since some of the red rutile grains show Fe enrichment and some yellow rutile show V enrichment. All five satellite areas are mostly enriched in Fe and therefore fall into the yellow rutile group. A few of the rutile falls into the red rutile group. Rietfontein is the exception and has a high V and high Fe population which is unique (enriched in both yellow and red rutile). This difference of Rietfontein's rutile population can be ascribed to maturity and specific gravity.

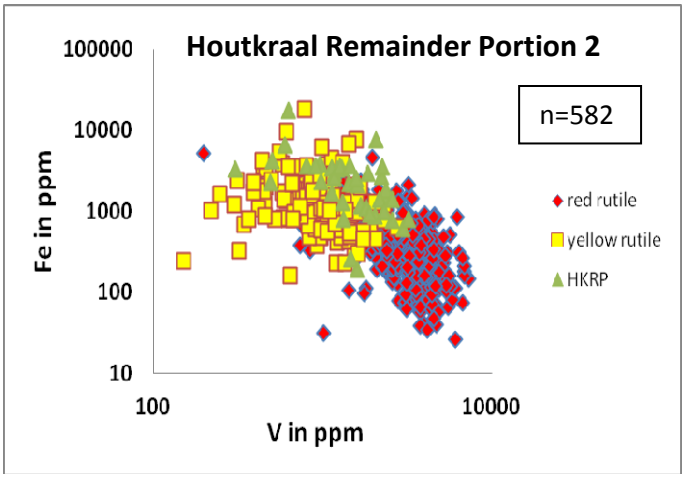

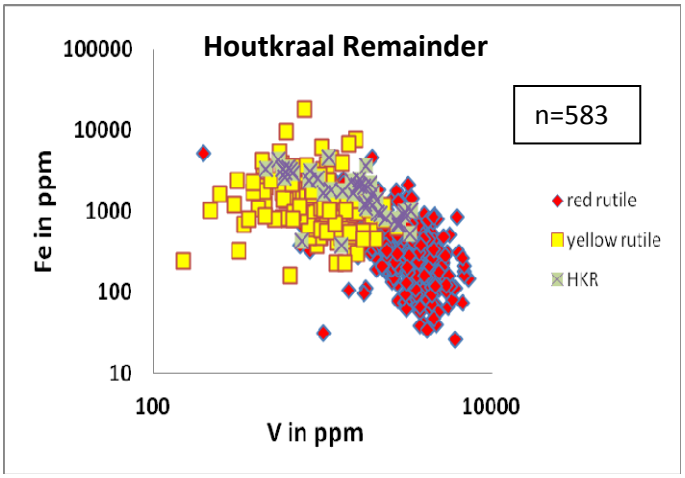

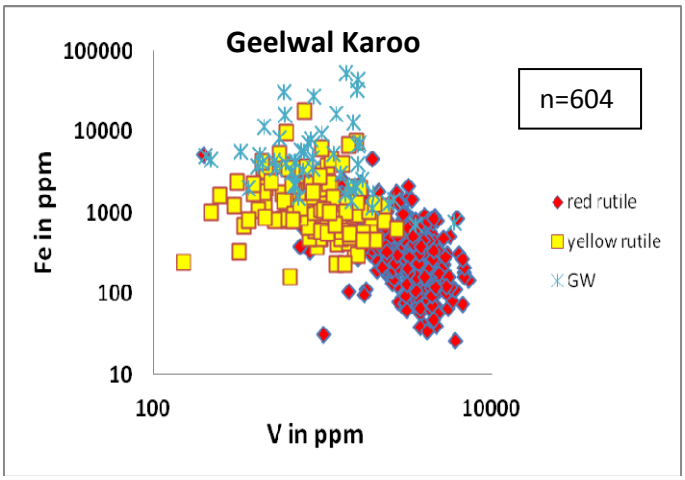

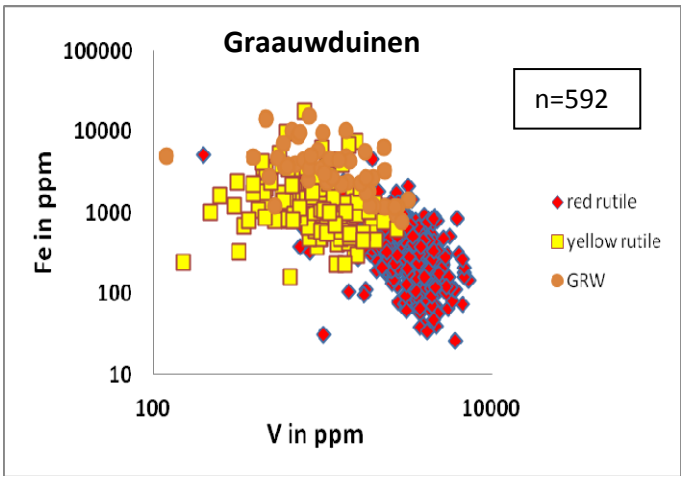

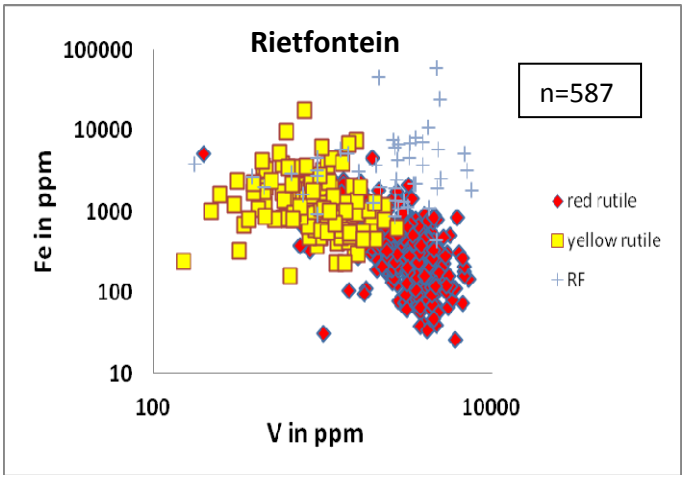

Figure 5.25. Fe-V histogram of the five satellite areas. Yellow and red rutile of the Namakwa Sands deposit is plotted for comparison (diagram after Philander and Rozendaal, 2009). Diagrams show that all five satellite areas consist of mainly yellow rutile except Rietfontein that is enriched in both yellow and red rutile.

5.6 Hematite

5.6.1 Petrography

Hematite has rounded to sub-rounded shapes with a few anhedral, and elongated grains. It is black and dark blood red in colour (Figure 5.26 A and B) with a bright white colour under reflected light (Figure 5.26 C-F). Hematite is present dominantly as the Ti-rich hematite variety titanohematite (Table F5, Appendix F). Titanohematite contains lamellae of ilmenite and rutile (Figure 5.26 C, E and F). The titanohematite grains of Rietfontein and Graauwduinen are generally lamellae free. Lamellae are orientated parallel (Figure 5.26 C, E and F) to each other. Hematite is also present as ilmo-hematite (hematite with ilmenite lamellae) (Figure 5.26 C).

Ilmenite and rutile are present as thin and thick lamellae and lensoid blebs (Figure 5.26 C). Some grains show cloth texture exsolution lamellae of ilmenite in hematite (Figure 5.27 A, Ramdohr, 1980). A few titanohematite grains also displays Ramdohr's (1980) "blitz"-texture where ilmenite or rutile lamellae forms z-shaped patterns (Figure 5.27 B). Figure 5.26 E and F show complex hematite grains with a hematite part with ilmenite lamellae and an ilmenite part with hematite lamellae. The different size populations of the exsolution lamellae in Figure 5.26 E indicate that at least two exsolution events occurred (Hugo, 1993). One forming the large, coarser exsolution lamellae and one event forming the small, finer exsolution lamellae. Figure 5.27 D shows another complex grain of hematite and ilmenite with hematite lamellae in the ilmenite part. Hematite lamellae in ilmenite and vice versa attest that the lamellae are exsolved from the $FeTiO_3$-Fe_2O_3 solid solution series. Figure 5.26 D indicates the mineral martite with ilmenite lamellae. Martite is hematite that was formed from magnetite through the process of martitization. The latter process is described in more detail in section 5.7.

Present in all samples but more abundant in the Geelwal Karoo samples are hematite and quartz aggregates (Figure 5.27 C). It has rounded to elongated shapes with thick, redbrown coatings with many quartz and some ilmenite inclusions and ilmenite-and rutile patches.

The most common inclusion in hematite is quartz, where the latter has round and hexagonal shapes (Figure 5.26 E and Figure 5.27 C). Other phases present as inclusions include monazite, sphene, garnet, mica, rutile, magnetite and aluminosilicates.

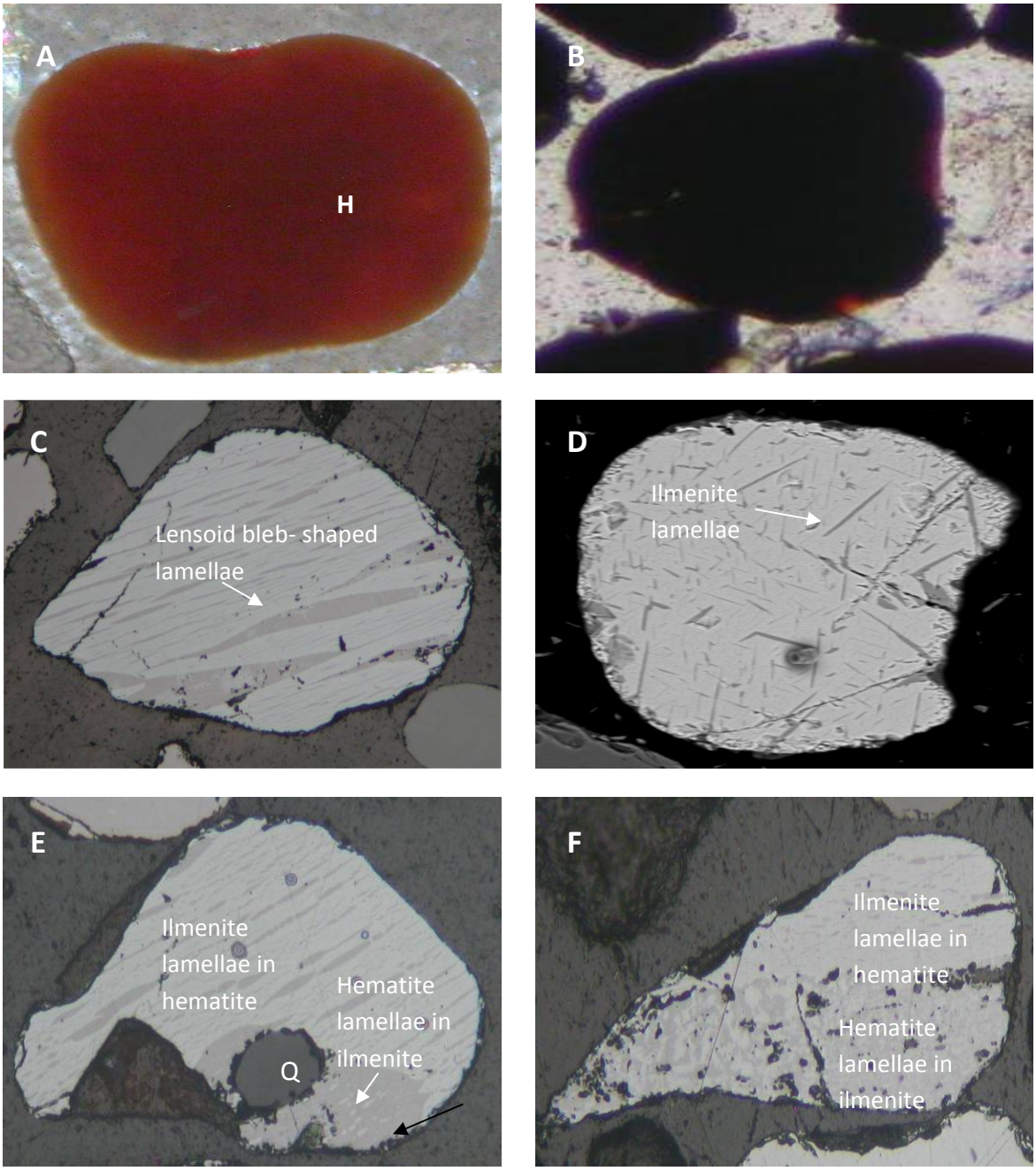

Figure 5.26. Microscope images of hematite showing different shapes of ilmenite lamellae. Figure 5.26 A-B was taken under transmitted light and C-F under reflected light. Scale: 20X. A) Red hematite (H) secondary. B) Black specular hematite with red transparent edges. C) Ilmo-hematite with fine. parallel and lense-shaped ilmenite lamellae. D) Martite grain with ilmenite lamellae. E) Complex hematite with quartz (Q) inclusion. F) Complex hematite consisting of ilmenite, with hematite lamellae, and hematite with ilmenite lamellae.

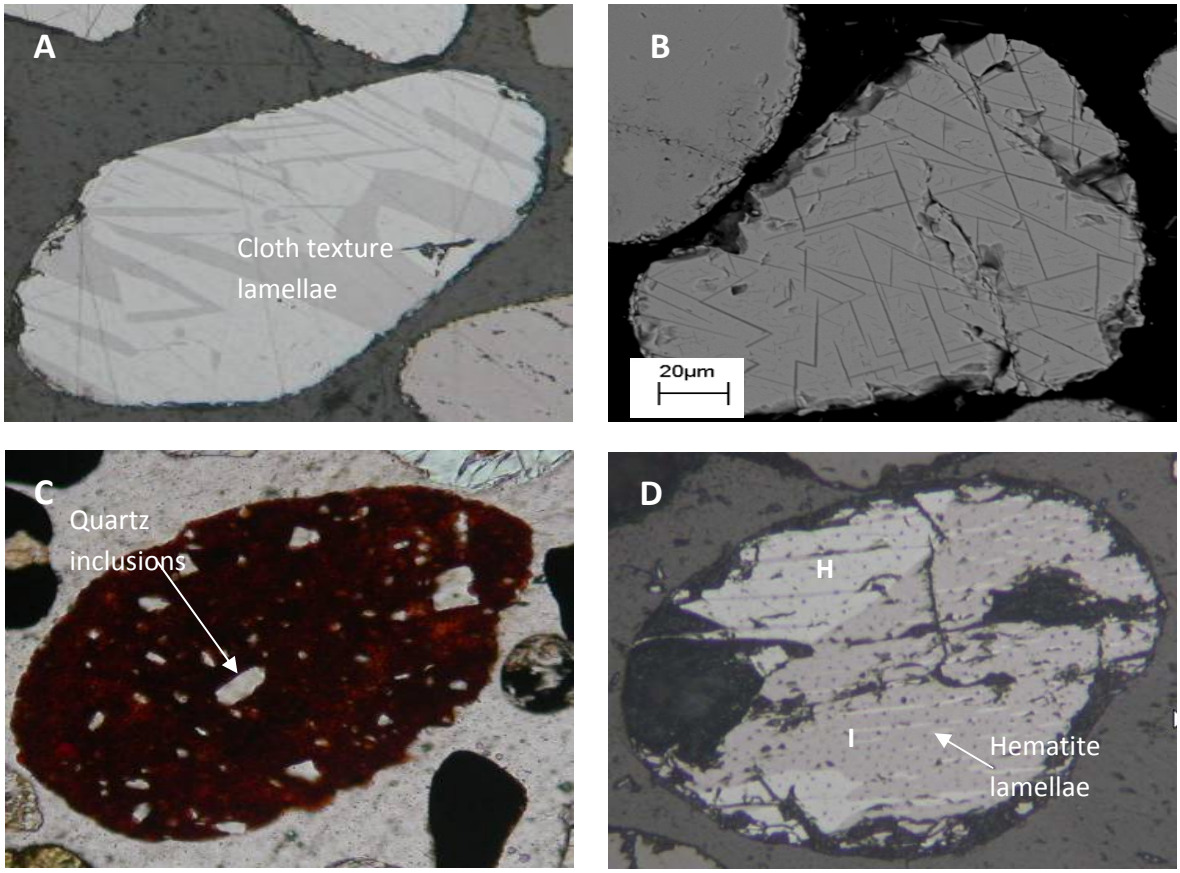

Figure 5.27 Microscope images of hematite showing ilmenite lamellae and inclusions. Figure 5.27 A, B and D was taken under reflected light and C under transmitted light. Scale: 20X. A) Cloth texture exsolution lamellae of ilmenite in hematite. B) SEM image of a hematite grain displaying the "blitz" texture of Ramdohr (1980). C) Hematite aggregate with quartz inclusions. D) Complex grain of hematite (H) and ilmenite (I) with hematite lamellae in ilmenite part.

5.6.2 Chemistry

Chemical data for hematite and titanohematite are presented in Tables F5 and F6, (Appendix F). Fe^{3+} was calculated with the Method of Droop (1987). Titanohematite for the five satellite areas has between 7 and 24 wt % TiO_2 and 50-61 wt % Fe_2O_3. The FeO content range between 21 and 28 wt %. Hematite has higher Fe_2O_3 content values that range between 62 and 70 wt %. The rest of the elements (CaO, MgO, Na_2O, Al_2O3, V_2O_3) are all below the detection limit of the SEM (0.5 wt %). Some hematite and titanohematite have MnO contents of up to 1 wt %. A few titanohematite grains have vanadium contents of up to 2 wt %.

The chemistry of hematite and titanohematite are illustrated on the FeO-TiO_2-Fe_2O_3 ternary diagram of Buddington and Lindsley (1964, Figure 5.28).

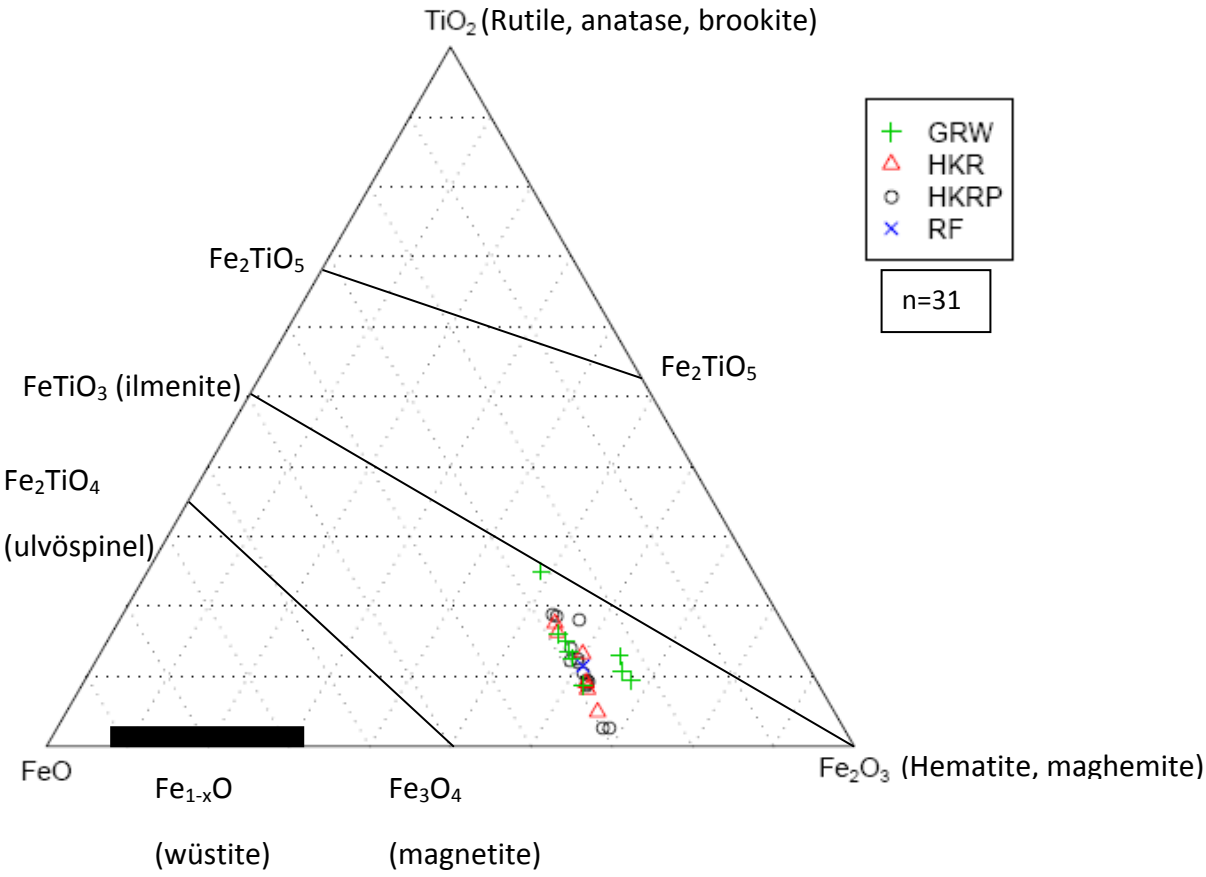

Figure 5.28. Ternary plot of hematite and titanohematite in the FeO-TiO_2-Fe_2O_3 system of the five satellite areas (diagram after Buddington and Lindsley, 1964). No pure hematite was analysed.

Hematite and titanohematite show a shift from the $FeTiO_3$- Fe_2O_3 line towards magnetite and enrichment towards TiO_2. Experimentally it has been found that at high temperatures there is complete solid solution between ilmenite and hematite (Deer et al, 1992). At lower temperatures however the solubility of hematite in ilmenite decreases due to a miscibility gap that develops. In natural ilmenite the amount of hematite in solid solution depends on factors such as the rate of cooling and the crystallization temperature (Deer et al, 1992). The shift from the $FeTiO_3$- Fe_2O_3 line can be due to low temperatures and slow cooling rates. The shift towards magnetite indicates hematite grains that were formed from the alteration of magnetite through the process of martitization.

5.7 Spinel-Magnetite series

5.7.1 Petrography

Magnetite

Magnetite grains have pitted textures with rounded, sub-rounded and anhedral shapes with a black colour and is opaque (Figure 5.29 A and B). Magnetite of all five satellite areas is mostly present as homogeneous grains with minor inclusions and internal features, such as ilmenite lamellae. Some magnetite grains have rutile inclusions. Lamellae are orientated parallel to the (111) crystallographic plane. Inclusions comprise mostly quartz with lesser baddeleyite, mica, rutile, barite and monazite.

Magnetite is a grey to brownish grey under reflected light and is characteristically isotropic (Figure 5.29 B).

Alteration of magnetite is present in the form of martitization where magnetite is replaced by hematite. Characteristic white grey, thin hematite lamellae, parallel to the (111) octahedral plane of the magnetite host, replaces the magnetite from the edges towards the core of the grain (Figure 5.29 C). When complete, the end-product is called martite. Grains display varying degrees of martitization. Martitization may occur in source rocks where magnetite and ilmeno-magnetite (ilmenite lamellae in magnetite) undergo oxidation to hematite at temperatures above 550°C (Lepp, 1957, Hugo, 1993) or in the sedimentary environment (Haggerty, 1976a, Riezebos, 1979; Hugo, 1993).

Spinel

Spinel has a dark green colour with characteristic prismatic and rounded shapes and comprises the hercynite ($FeAl_2O_4$) - spinel ($MgAl_2O_4$) series (Figure 5.29 D). It has thick, redbrown amorphous coatings. Spinel is present in trace amounts and is for the most part inclusion-free.

5.7.2 Chemistry

Chemical data for magnetite is presented in Table F7, (Appendix F). Fe_2O_3 content ranges between 39 wt % and 52 wt % and FeO content between 34 and 47 wt %. Typical substitution elements such as Cr_2O_3, MgO, V_2O_3, MnO, CaO, Nb_2O_5 and P_2O_5 are below the

detection limit of the SEM (0.5 wt %). Some magnetite grains have P_2O_5 contents of up to 2 wt %. A few magnetite grains have > 1 wt % (up to 8 wt % SiO_2 and 6 wt % Al_2O_3) SiO_2 and Al_2O_3. These magnetite grains have lower ferric and ferrous iron contents than the rest of the magnetite grains and possibly indicate magnetite aggregates. The chemistry of the magnetite grains is illustrated on the FeO-TiO_2-Fe_2O_3 ternary diagram (Figure 5.30). The magnetite of the five satellite areas are similar and plot on the pure magnetite end-member.

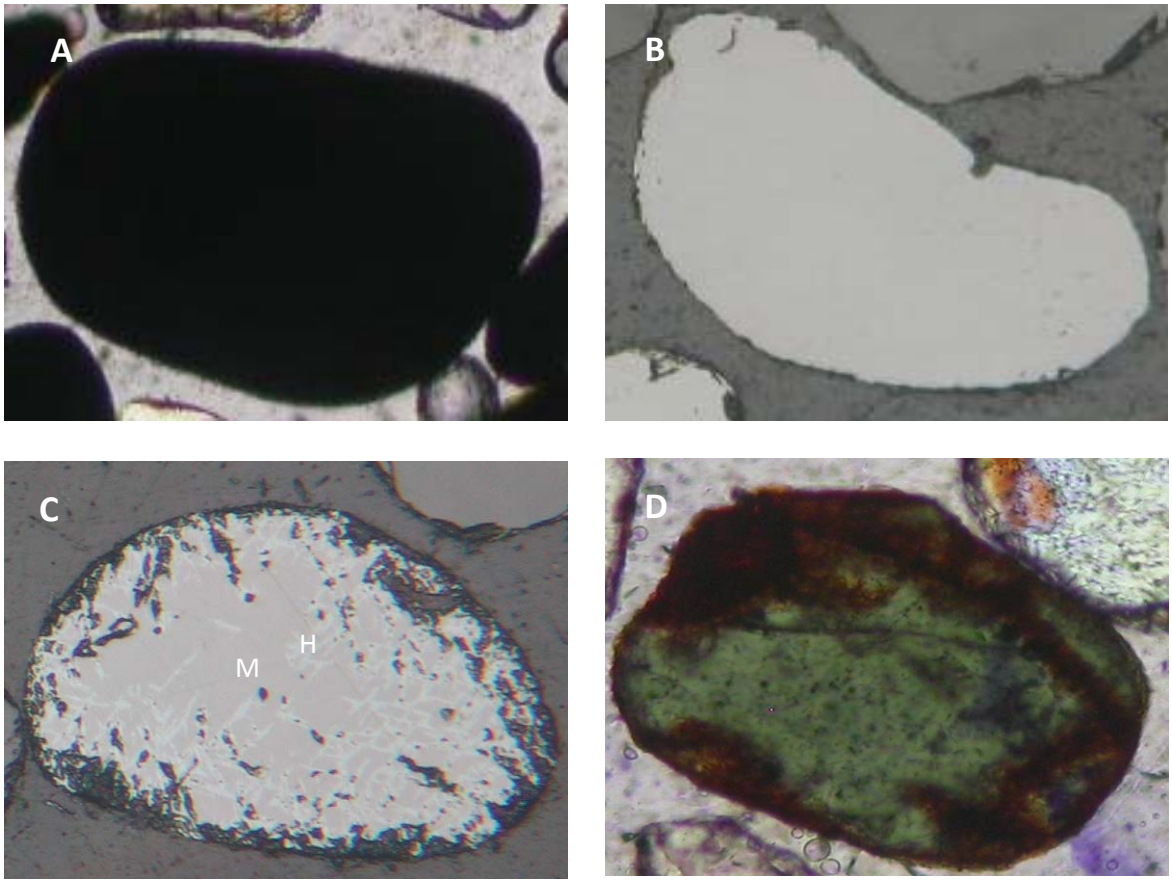

Figure 5.29. Microscope images of magnetite and spinel. Figure 5.25 B and C were taken under reflected light and A and D under transmitted light. Scale: 20X. A) Typical opaque magnetite grain. B) Unaltered magnetite grain showing pitted texture. C) Magnetite (M) grain showing martitization. Light grey is hematite (H) and dark grey is magnetite. Magnetite alters along crystallographic planes. D) Dark green hercynite spinel with red amorphous coating.

One grain from Houtkraal Remainder (analysis 3) shows enrichment towards ulvöspinel (Fe_2TiO_4). Titanium enters the magnetite crystal structure in the latter mineral and is also called titanomagnetite.

Spinel has considerable FeO and MgO with more iron than magnesium which indicates the hercynite (Fe-rich spinel) end-member also defined as Mg-rich hercynite spinel (Table F8, Appendix F). It forms part of the hercynite ($FeAl_2O_4$)-spinel ($MgAl_2O_4$) solid solution series where Fe^{2+} replaces Mg^{2+}. A considerable amount of Cr_2O_3 (2 wt %) is also present. Deer et al (1992) uses the term *picotite* for the chromium-rich hercynite variety. In the latter case Al^{3+} – Cr^{3+}substitution occurs, there being a solid solution series between hercynite ($FeAl_2O_4$) and chromite ($FeCr_2O_4$) spinels.

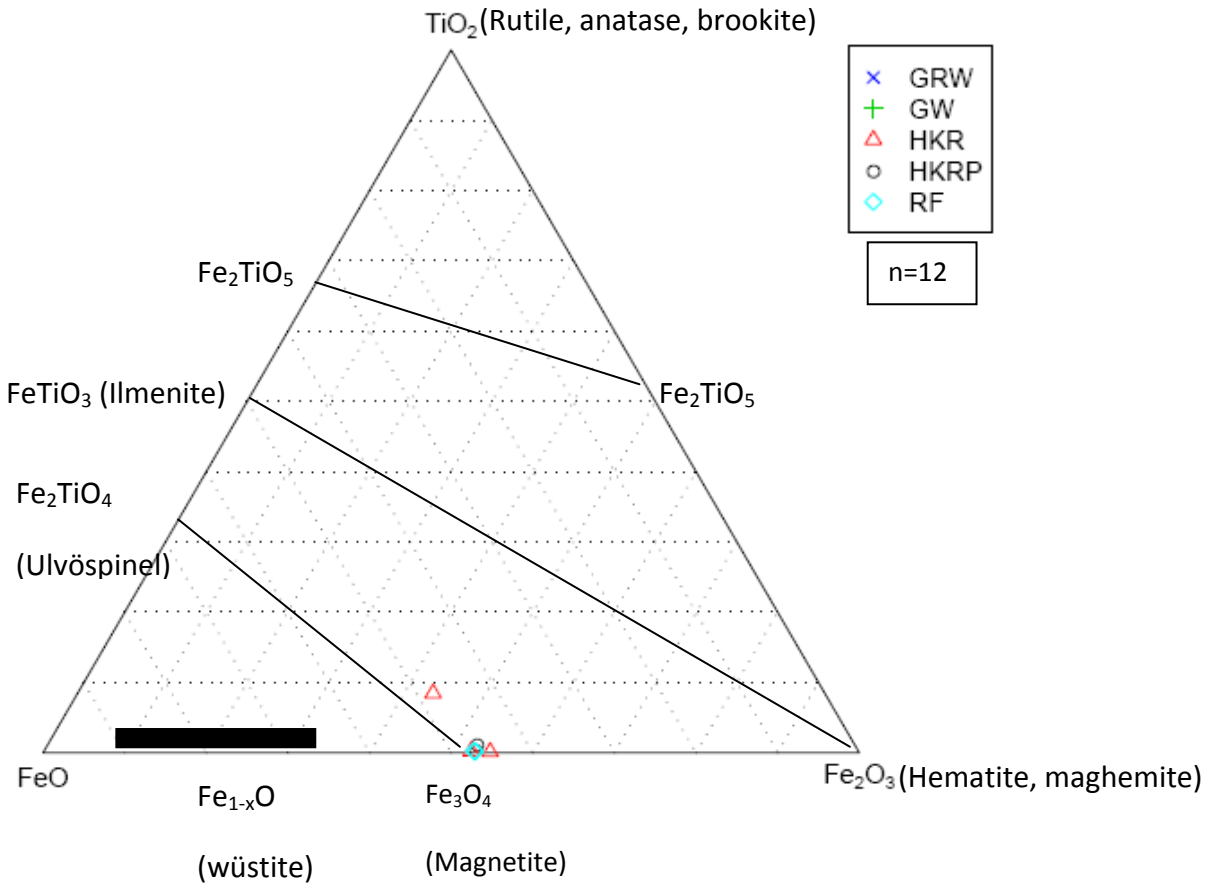

Figure 5.30. Ternary plot of magnetite in the FeO-TiO_2-Fe_2O_3 system of the five satellite areas (diagram after Buddington and Lindsley, 1964).

5.8 Garnet

5.8.1 Petrography

Garnets are dominantly present as sub-angular fragments with a few euhedral, isometric and round crystals and are marked by its isotropism and high relief. Graauwduinen, the two Houtkraal areas and Geelwal Karoo have a few spherical garnet grains. Garnets are present as colourless, yellow and pink varieties (Figure 5.31 A and B). The pink garnets are more abundant in the Rietfontein samples but the colourless garnets are more abundant in the other four satellite areas. Most grains are inclusion-free. Inclusions comprise transparent and opaque phases, needle-like (Figure 5.32 B), round, and anhedral and tabular inclusions (Figure 5.32 A) and have no preferred orientation. Phases identified with the SEM include quartz (Figure 5.31 C), zircon, magnetite, ilmenite, hematite, apatite, tourmaline, aluminosilicates, rutile and Na orthoclase.

Conchoidal fractures are common in the garnet grains because of no cleavage. Present on most garnets is the silica-aluminium-iron-potassium amorphous coating and is red to brown in colour (Figure 5.31 E and Figure 5.32 C). Garnets of Geelwal Karoo, Graauwduinen and the two Houtkraal areas have thick amorphous coatings and some grains appear altered (Figure 5.32 C). Alteration of a grain leads to destruction of the crystal structure, hence breaking up the grain thereby enhancing the infiltration of fluids. A network of fractures including concentric fractures marks certain garnets (Figure 5.31 F).

Aggregates of garnet and quartz are present. Hematite and rutile are common inclusions within the aggregates. Present in some garnets is internal structures which look like ‘fireworks’ (Figure 5.31 D). These structures are an indication that the garnets have a metamorphic origin and are characteristic of garnets from the Namaqualand region. It is mainly caused by rutile inclusions.

5.8.2 Chemistry

A total of 47 garnet grains were studied from the five satellite areas with the aid of the SEM (Table F9, Appendix F). Garnets lack any distinct chemical zonation and a single analysis per grain was considered representative. The dominant garnet end-members were calculated for each grain using the Locock (2008) Excel spreadsheet (Appendix G). One grain from

Geelwal Karoo show chemical zoning with a Ca-rich core with the edges enriched in Mn. This could be the result of decompression or changes in pressure and temperature during garnet growth (Hickmott and Spear, 1992). Such differing chemical compositions cause differential chemical weathering (Mange and Wright, 2009). Colour and chemical composition of garnet from this study cannot be correlated.

The dominant garnet end-members present in the five areas, are almandine (39 wt %), followed by grossular (26 wt %), spessartine (17 wt %), pyrope (13 wt %) and andradite (6 wt %). A few garnet grains contain small amounts, up to 2%, of the schorlomite-Al, morimotoite, goldmanite and blythite components (Appendix G). The composition of the garnets is graphically illustrated on ternary diagrams (Figures 5.33, 5.34, 5.35 and 5.36). Ternary diagrams were constructed using GCDKit version 2.3. From the ternary diagrams it is evident that the garnets of all five areas belong to two garnet end-member populations: almandine-spessartine and grossular–andradite (grandite) type garnets and is therefore enriched in Fe, Ca and Mn and depleted in Mg.

Houtkraal Remainder Portion 2 is mainly enriched in almandine (43%) and lesser in grossular (27%) (Table F9, Appendix F). Geelwal Karoo is dominated by the grossular (36%) and almandine end-members (35%). Graauwduinen is dominated by the almandine (34%) and spessartine (30%) end-members, Rietfontein by almandine (56%) and spessartine (15%) and Houtkraal Remainder by spessartine (56%) and grossular (26%). The different end-members present indicate a typical metamorphic provenance and will be discussed later in the text.

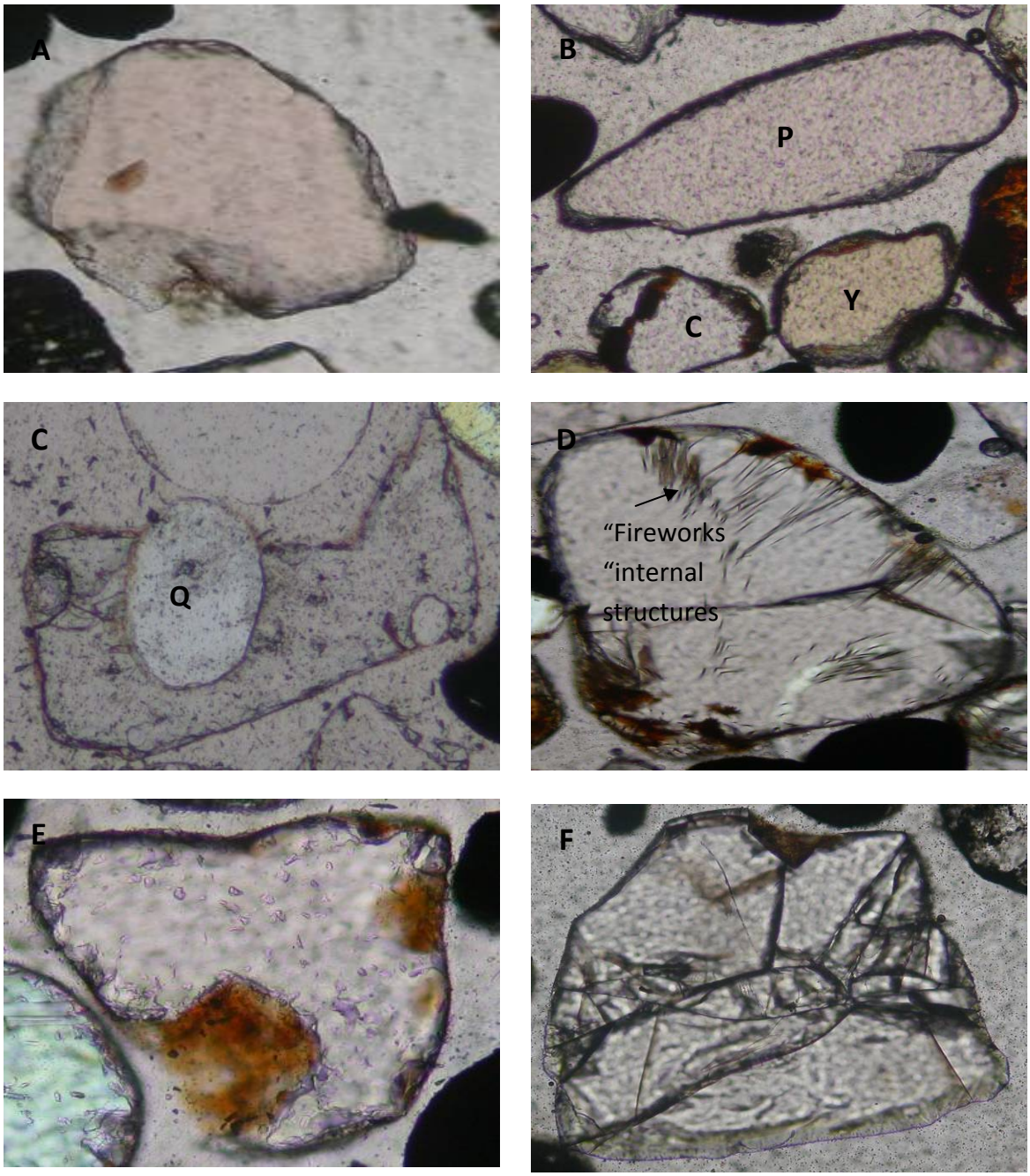

Figure 5.31. Microscope images showing different colour garnets present in the satellite areas. All pictures were taken under transmitted light. Scale: 20X. A) Pink garnet (almandine); the most abundant variety. B) Colourless (C), pink (P) and yellow (Y) garnets. C) Garnet with rounded quartz (Q) inclusion. D) Garnet with "fireworks" internal structures caused by rutile inclusions. E) Garnet with amorphous surficial coating. F) Fractured garnet indicating limited transport distance.

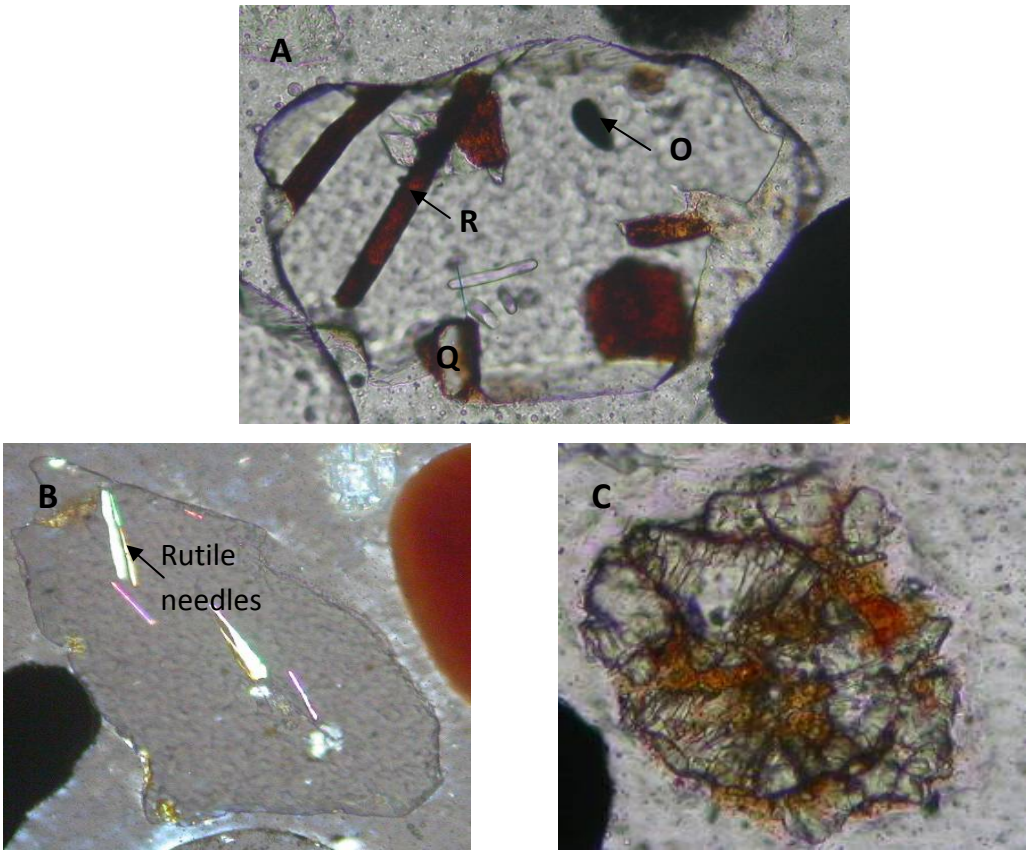

Figure 5.32. Microscope images of garnet. All pictures were taken under transmitted light. Scale: 20X. A) Garnet with rutile (R) needles and anhedral quartz (Q) and oxide (O) inclusions. B) Garnet with rutile needles as inclusions under partially crossed nicols. C) Garnet replaced by amorphous Si, Al, K and Fe precipitate along cracks.

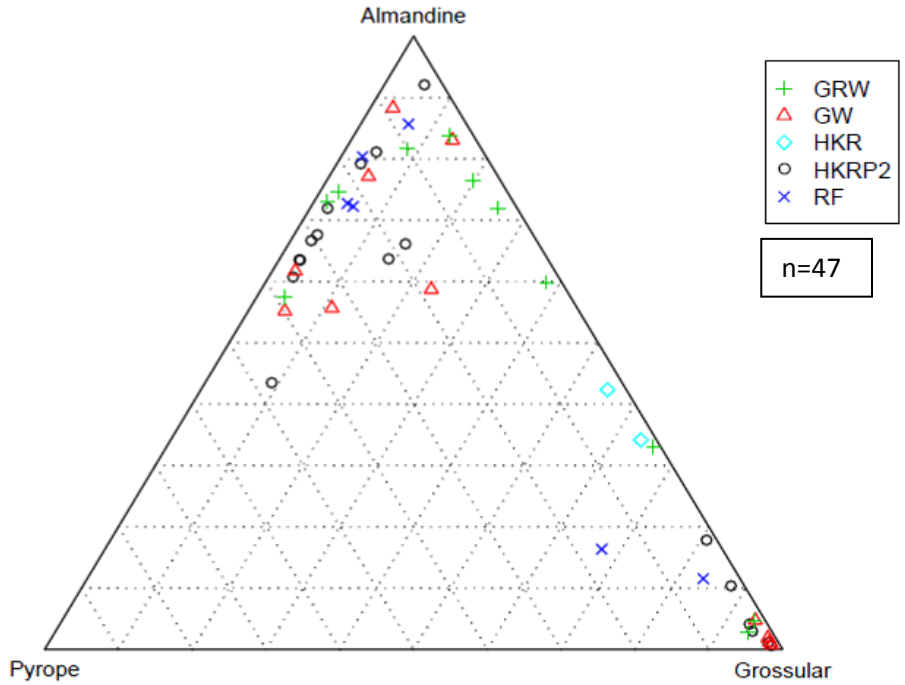

Figure 5.33. Pyrope-almandine-grossular ternary diagram showing the chemistry of garnet from the five satellite areas. Garnet suite is enriched in almandine and grossular.

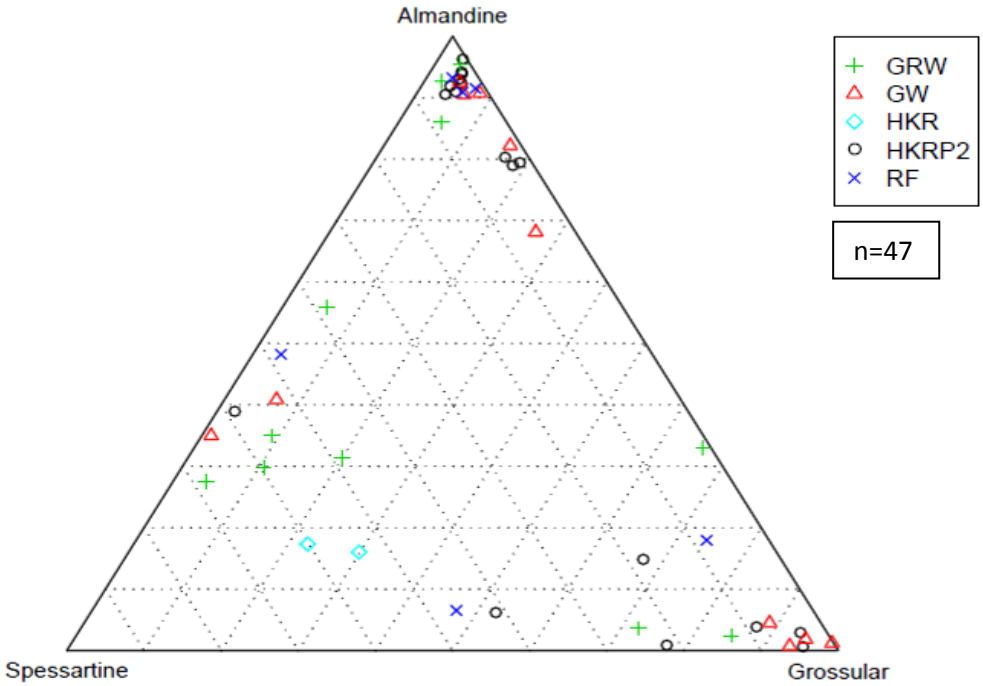

Figure 5.34. Spessartine-almandine-grossular ternary diagram showing the chemistry of garnet from the five satellite areas. Garnet suite is enriched in almandine and grossular.

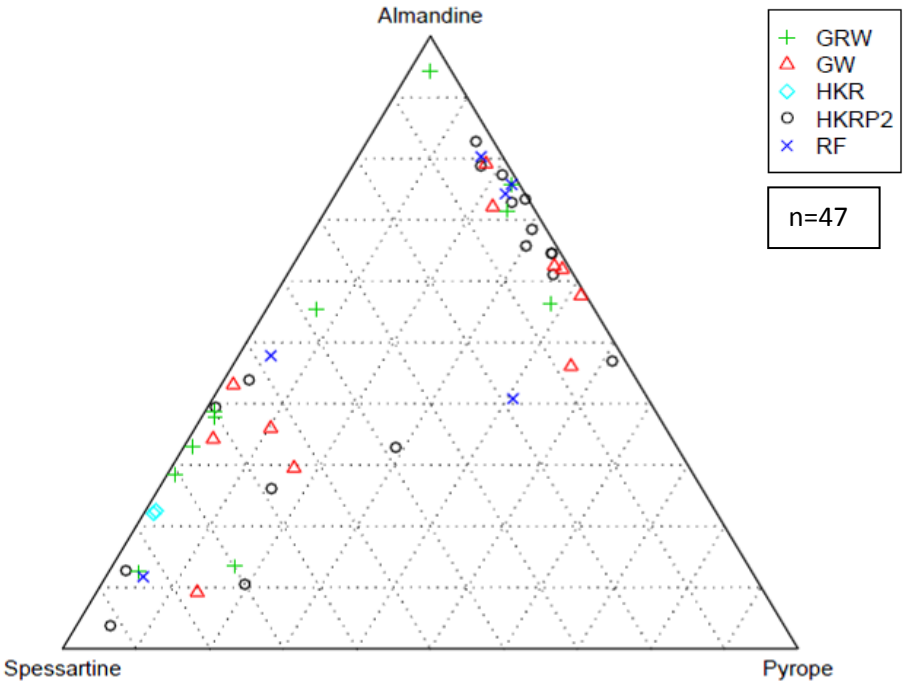

Figure 5.35. Spessartine-almandine-pyrope ternary diagram showing the chemistry of garnet from the five satellite areas. Garnet suite shows enrichment in spessartine.

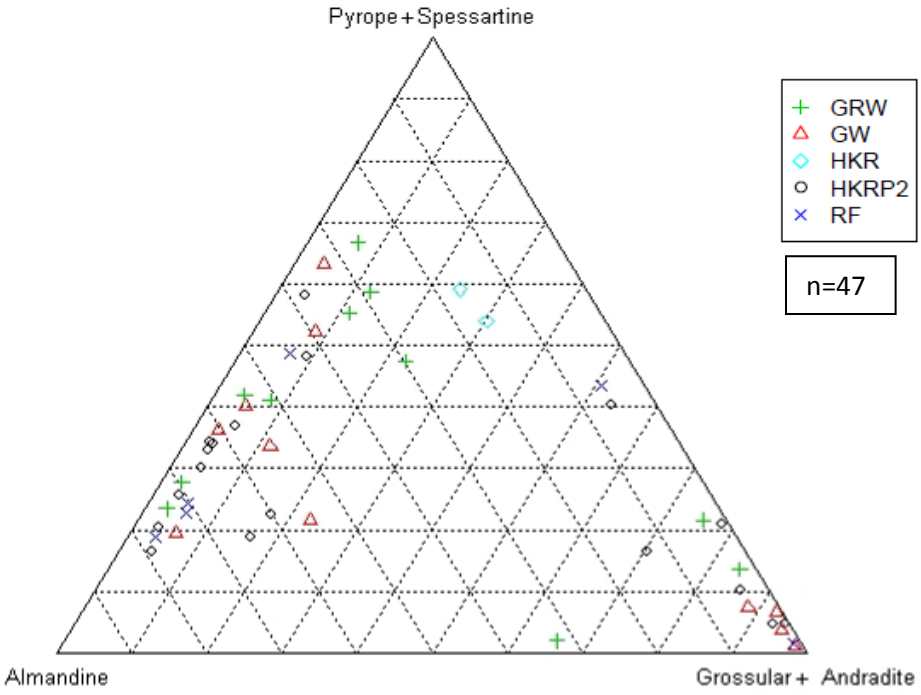

Figure 5.36. Almandine-pyrope+spessartine-grossular+andradite ternary diagram showing the chemistry of garnet from the five satellite areas. The garnet population for the five satellite areas consists of almandine-spessartine and grossular-andradite garnets.

5.9 Pyroxene

5.9.1 Petrography

Pyroxene is mostly present in the Rietfontein and Geelwal Karoo samples with only trace amounts in the other four satellite areas. Both orthopyroxene and clinopyroxene were identified, the latter being more abundant. Grains are sub-rounded, oval and prismatic in shape. Pyroxene has a moderate to high relief and can be easily identified by its 90º cleavage (Figure 5.37 A and C). A few brown green clinopyroxene (augite) are also present (Figure 5.37 D).

Grains are coated with the silica-aluminium-iron-potassium amorphous material which often masks the true colour of the grains. The latter occurs along and/or in cracks and cleavage planes also and has a brown and orange colour. Mineral inclusions include magnetite and quartz and other unidentified transparent phases (Figure 5.37 C). Inclusions are present along cleavage planes in some grains (Figure 5.37 C). One clinopyroxene has a black core with cracks radiating from it (Figure 5.37 B). The core could have formed as a result of radio-active emission which in turn caused the crystal structure to become weak and formed the cracks.

5.9.2 Chemistry

Pyroxenes were randomly analysed for in the Geelwal Karoo and Rietfontein samples. Colour and chemical composition failed to show any convincing correlation since two pyroxenes with different composition can have the same colour (colourless, brown green). No zoning was observed. The chemistry of the pyroxenes, as determined with the SEM, was used to calculate the end- members using PX-NOM (Appendix G).

The chemistry of the pyroxene grains is conveyed by two diagrams. The first is the Q-J diagram introduced by Morimoto et al (1988) where Q refers to $Ca+Mg+Fe^{2+}$ and J to 2Na. The further classification of the Ca–Mg–Fe pyroxenes (Quad) is executed in the Wo–En–Fs triangle (Strum, 2002).

Pyroxenes belong to one of four chemical groups namely Ca-Mg-Fe pyroxenes (Quad), Na pyroxenes (Na), Na-Ca pyroxenes (Na-Ca) and “Other” pyroxenes (Others) (Strum, 2002).

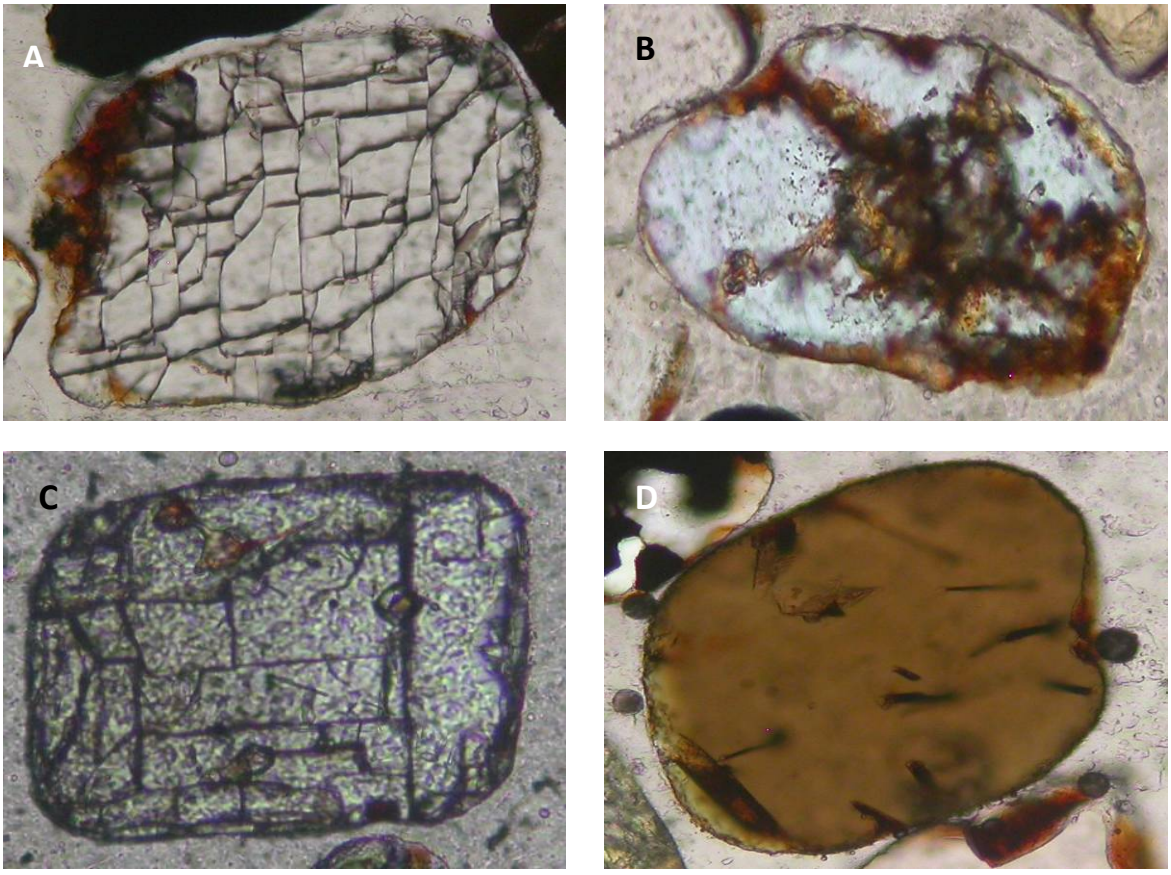

Figure 5.37. Microscope images showing different colour pyroxene. All pictures were taken under transmitted light. Scale: 20X. A) Augite showing characteristic 90º cleavage. B) Clinopyroxene with core and cracks radiating from it. C) Augite showing 90º cleavage and inclusions along cleavage planes. D) Rounded brown green augite.

"Other" refers to the mineral phases esseneite, kanoite and its dimorph donpeacorite, spodumene, johannsenite or petedunnite (Appendix G).

The two main pyroxene minerals present in the Geelwal Karoo area, are the clinopyroxenes augite and pigeonite (Table F10.1, Appendix F). On the Q-J diagram (Figure 5.38) all pyroxenes plot in the Quad group on the Q line indicating that the pyroxene suite is enriched in Ca, Mg and Fe and is depleted in Na.

Pike (1976) explained that the high Cr content (about 1% Cr_2O_3) in her low-Ca pyroxene study is responsible for the bottle green colour and unusual optical properties of the pyroxene. Some pyroxene grains also contain up to 1 wt % Cr_2O_3 and could be responsible for the brown green colour of the augitic pyroxene.

The Rietfontein pyroxenes also plot in the Quad field on the Q line indicating it is also enriched in Ca, Mg and Fe and depleted in Na (Figure 5.40). Three pyroxenes however show enrichment in Na. Figure 5.41 indicates that the dominant end-member species present for Rietfontein are also augite and pigeonite with lesser amounts of enstatite and wollastonite (Table F10.2, Appendix F).

From above four figures it is evident that the pyroxenes of Geelwal Karoo and Rietfontein have a similar chemistry. This uniform chemistry can indicate a similar provenance area and source rocks.

Three of the clinopyroxenes of the Rietfontein area have moderate Al_2O_3 contents (5-6.67 wt %). The rest of the ortho- and clinopyroxene have low Al_2O_3 (0.83-2.55 wt %). Al_2O_3 content is usually used as an indicator of changes in metamorphic grade (Wilson, 1976). Authors such as Dobretsov (1968) and Green and Ringwood (1967) pointed out that pyroxene with high Al contents are from high metamorphic grade areas. The Al contents of the pyroxene of this study are low (< 10 wt %) and reflect medium to high grade metamorphic source rocks.

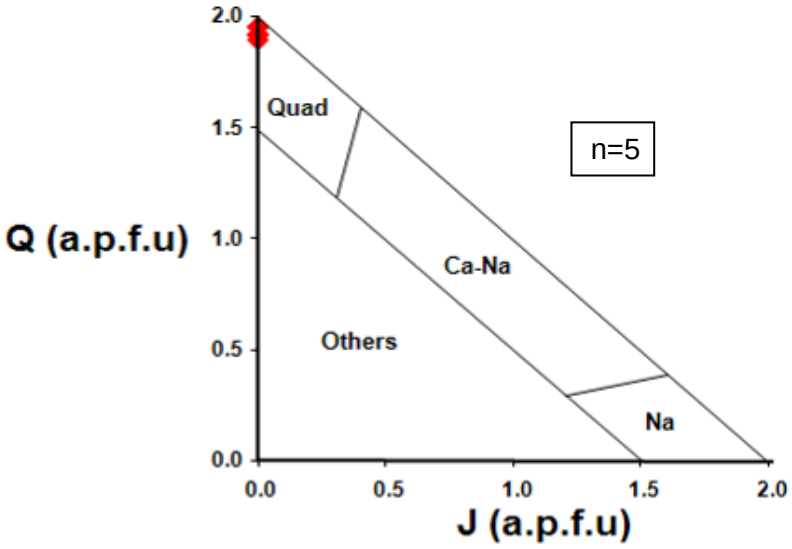

Figure 5.38. Q-J diagram of Geelwal Karoo pyroxenes (diagram after Morimoto et al, 1988). Pyroxenes are Ca, Mg and Fe–rich.

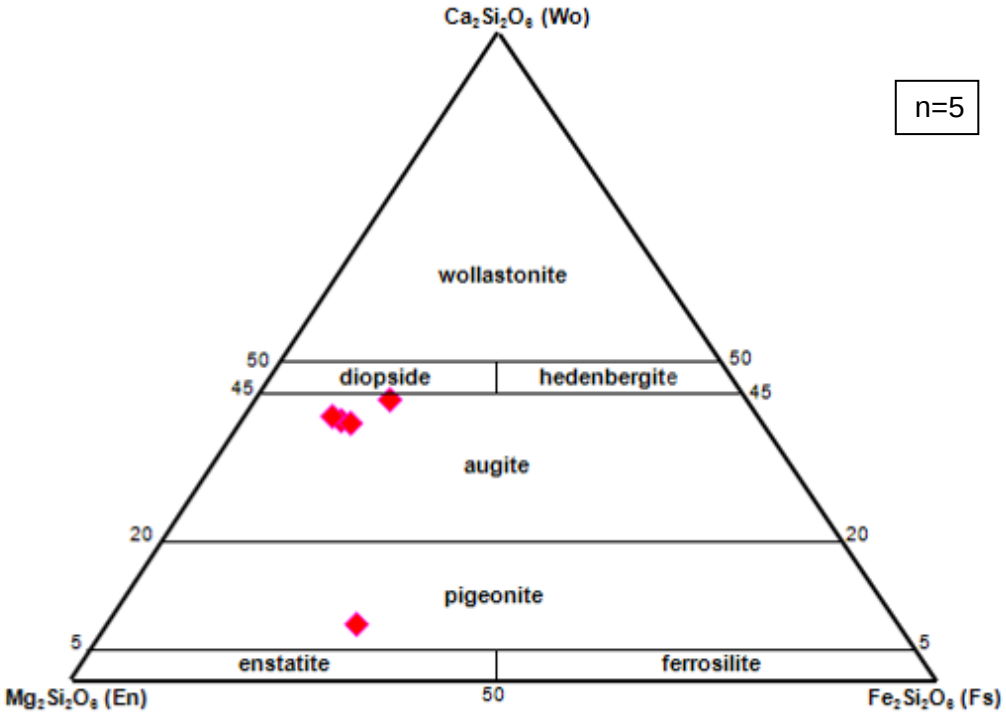

Figure 5.39. Wo-En-Fs triangle of Geelwal Karoo pyroxenes (diagram after Strum, 2002). Dominant pyroxene end-members are augite and pigeonite.

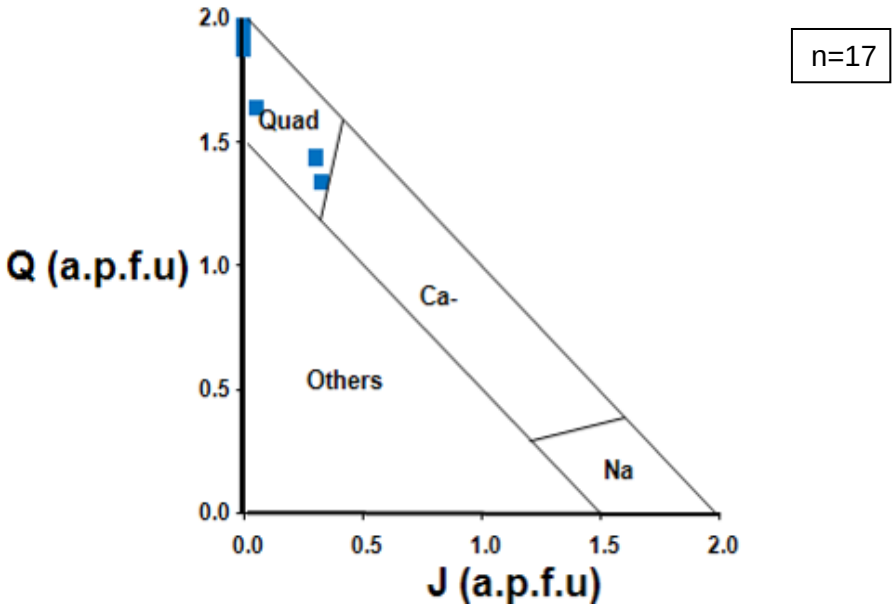

Figure 5.40. Q-J diagram of Rietfontein pyroxenes (diagram after Morimoto et al, 1988). Pyroxenes are Ca, Mg and Fe -rich.

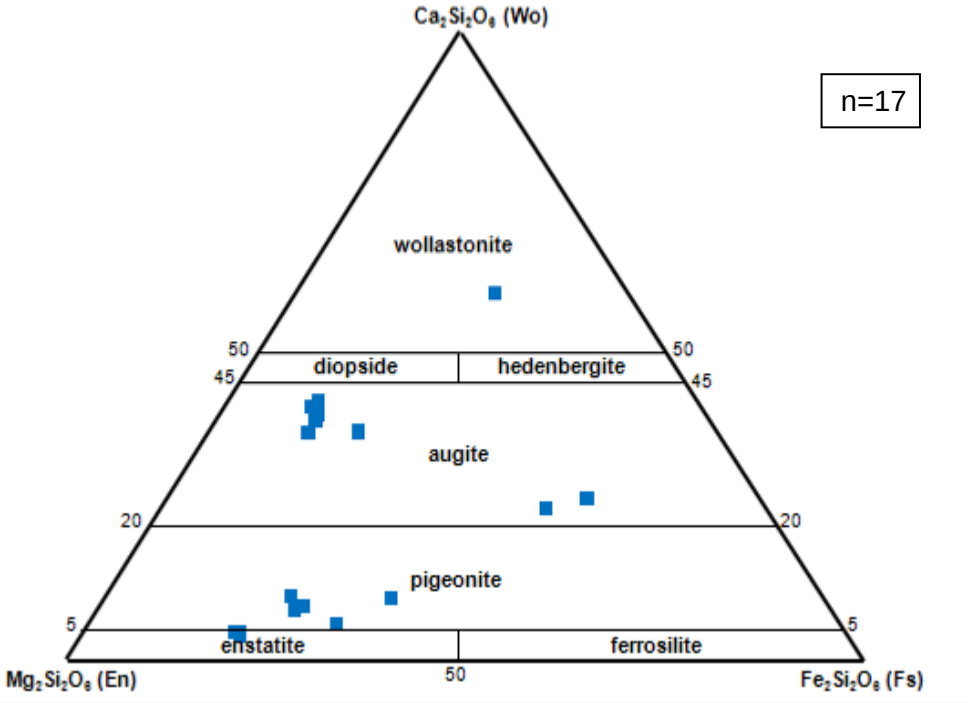

Figure 5.41. Wo-En-Fe triangle of Rietfontein pyroxenes (diagram after Strum, 2002). Dominant pyroxene end-members are augite and pigeonite with trace amounts of wollastonite and enstatite.

5.10 Tourmaline

5.10.1 Petrography

Tourmaline is present in significant amounts in all five satellite areas. It is easy identifiable by its characteristic green or yellow colour and moderate to strong relief. It is mostly structureless with only a few grains having inclusions. Grains display a high degree of roundness (Figure 5.42 A, C and D). Sub-rounded to bean shape (Figure 5.42 C), prismatic and oval shapes are present. The rounded nature of tourmaline can be an indication of high energy conditions during transport, considerable abrasion during the sedimentary cycle or multiple erosional, transportation and depositional cycles. Tourmaline colours range from different shades of green which include light olive green to a darker blue green and yellow green. Blue, pale and dark yellow, olive brown and colourless grains (Figure 5.42) are also present. Tourmaline colour is usually an indication of composition. No correlation was however found between colour and composition in this study. Characteristic of the tourmalines are its pleochrism form colourless to pink to a yellowish green or green to dark

green. The bean shape tourmalines have a characteristic yellow colour (Figure 5.42 C) and are pleochroic from yellow to a darker almost orange yellow.

Some tourmalines are black / isotropic under crossed nicols because it is viewed along/down the c-axis. Cleavage are present but occur mostly in the prismatic shape grains and are orientated parallel to the c-axis.

Inclusions hosted by tourmaline include transparent and opaque phases such as sphene, rutile, zircon, garnet, quartz, mica and ilmenite. Characteristic of the tourmalines from Geelwal Karoo is some minor barite inclusions.

5.10.2 Chemistry

A total of 38 tourmalines were randomly analysed for with the aid of the SEM (Table F11, Appendix F). FeO and MgO show an inverse relationship indicating that these two elements substitute for each other in the Y-site of the tourmaline crystal lattice in the schorl-dravite solid solution series (Figure 5.43). The five satellite areas have FeO values ranging from 4 wt % to over 18 wt % and MgO values ranging from 0-9 wt % (Table F11, Appendix F).

One tourmaline from the Graauwduinen area show chemical zoning (Figure 5.44). Backscatter imaging clearly shows the zoning lines. SEM analysis demonstrated differences in chemical composition between these different colour grey areas (Table F11, Appendix F). There is a difference in the FeO and MgO contents. The dark grey area is the least enriched in FeO and the most enriched in MgO and represents dravite. The dark grey zoning lines are also MgO enriched and represents dravite. The light grey area is low in MgO and high in FeO and belongs to the schorl end-member (Table F11, Appendix F). Blatt et al (1972) ascribed colour zoning in tourmaline to variations in the iron content within schorl and confirm this observation.

End-members were classified according to mineral chemistry following the classification scheme of Hawthorne and Henry (1999) and plotting the Al-Fe (tot)-Mg ternary diagram of Henry and Guidotti (1985, Figure 5.45). The procedure followed for classification of the end-members is explained in Appendix G.

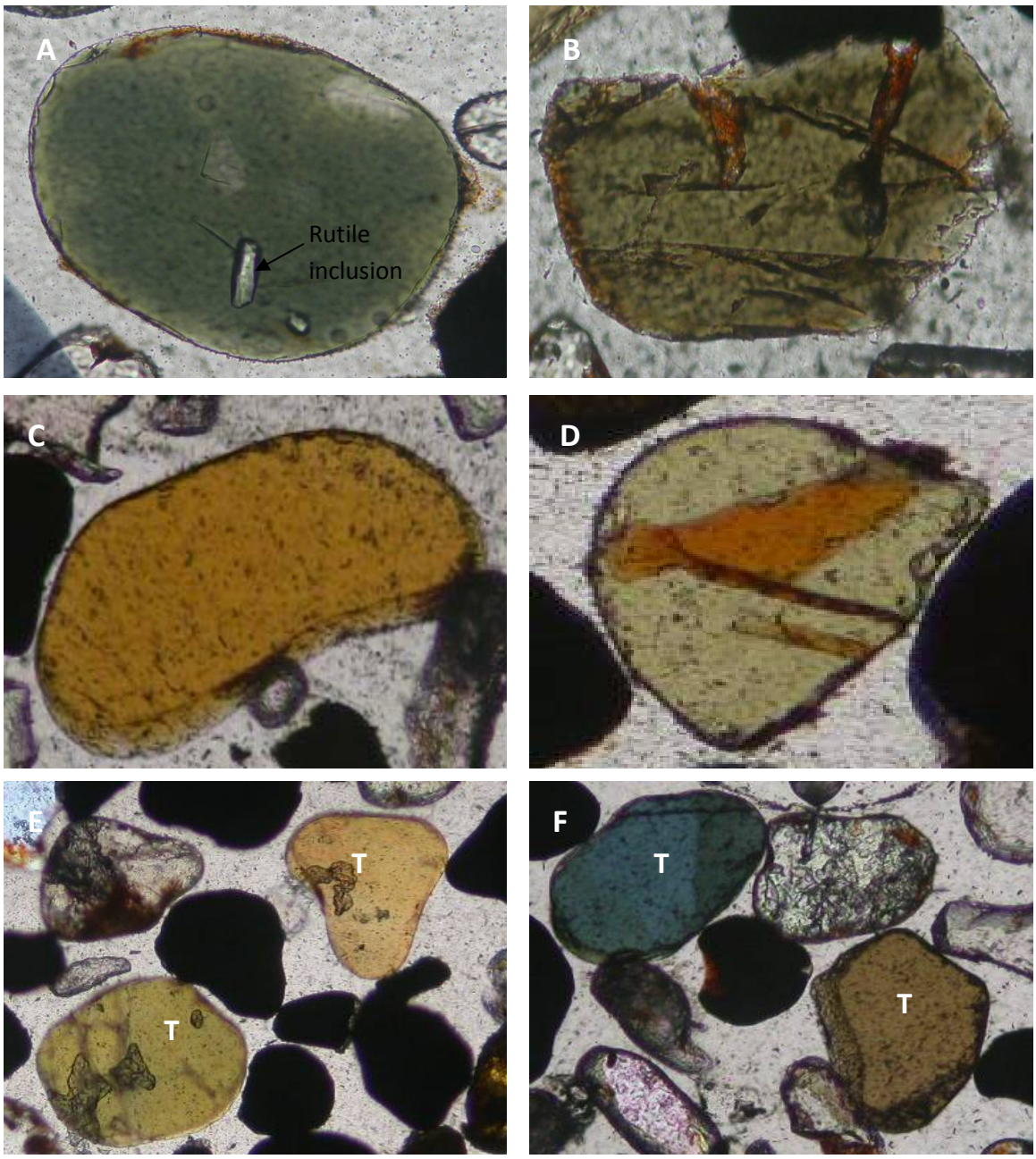

Figure 5.42. Microscope images showing different colour tourmaline present in the satellite areas. All pictures were taken under transmitted light. Scale: 20X. A) Olive green rounded tourmaline with rutile inclusions. B) Olive green tourmaline. C) Yellow bean shape tourmaline. D) Olive green tourmaline showing twinning. E) Yellow green and yellow tourmaline (T). F) Blue and olive brown tourmaline (T).

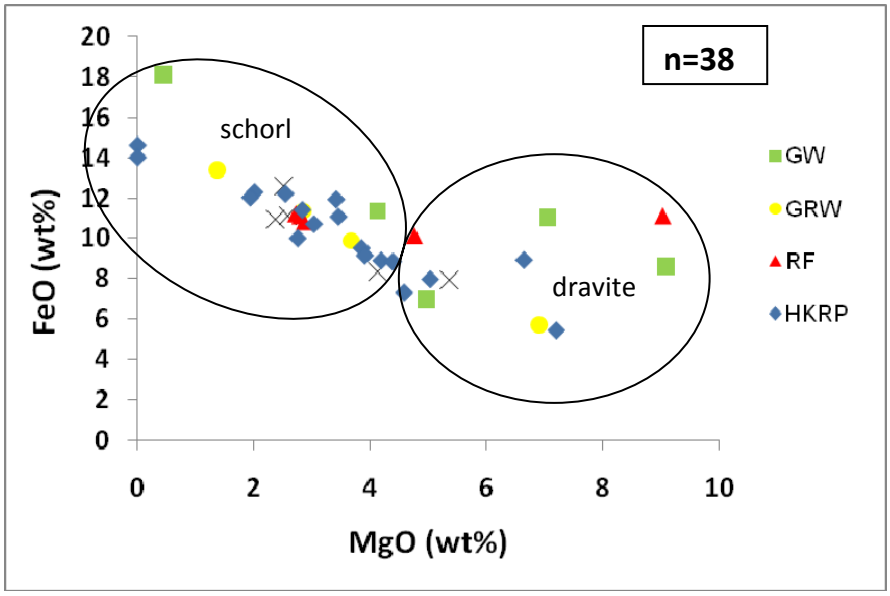

Figure 5.43. Binary diagram showing the linear relationship between MgO (dravite) and FeO (schorl). End-member distribution is random in the five satellite areas.

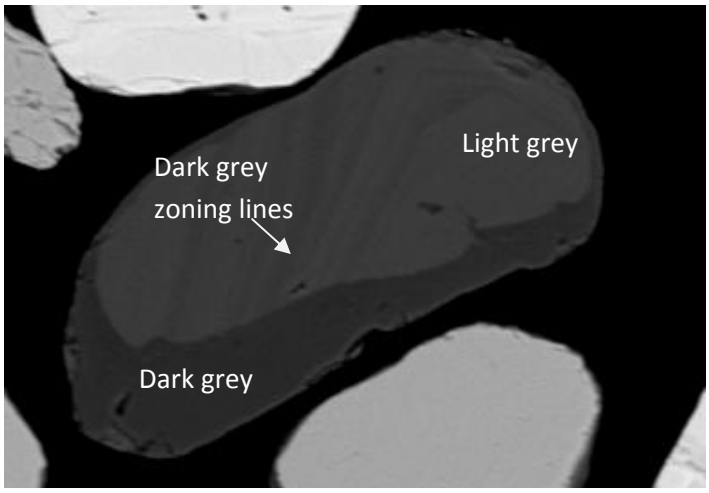

Figure 5.44. Bacskscatter (BSE) image of tourmaline showing zoning.

Tourmaline consists of mainly schorl with minor amounts of dravite. (Table F11, Appendix F, Figure 5.45 and 5.46). Figure 5.45 also indicates that there is an accessory amount of the buergerite tourmaline in the sample population. Buergerite is similar to schorl but has Fe^{3+} in the Y-site and F^- in the W-site.

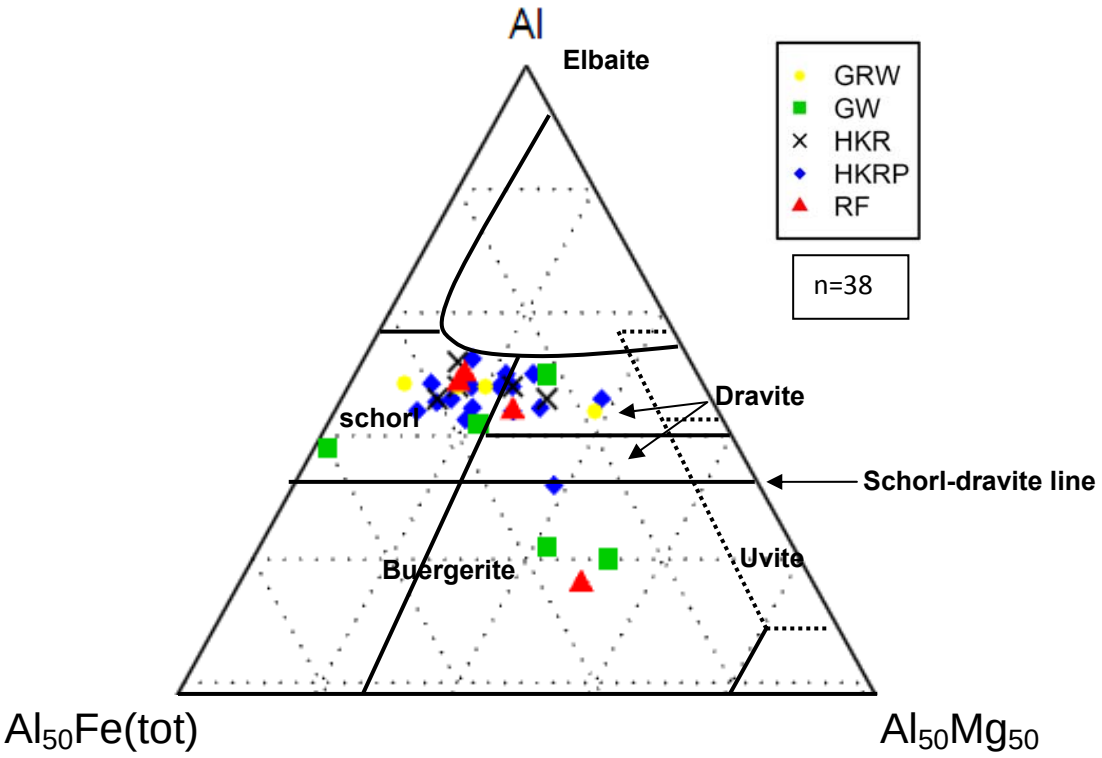

Figure 5.45 Al-Fe (tot)-Mg ternary diagram showing the composition of tourmaline from the five satellite areas (diagram after Henry and Guidotti, 1985). Tourmaline comprises schorl, dravite and buergerite.

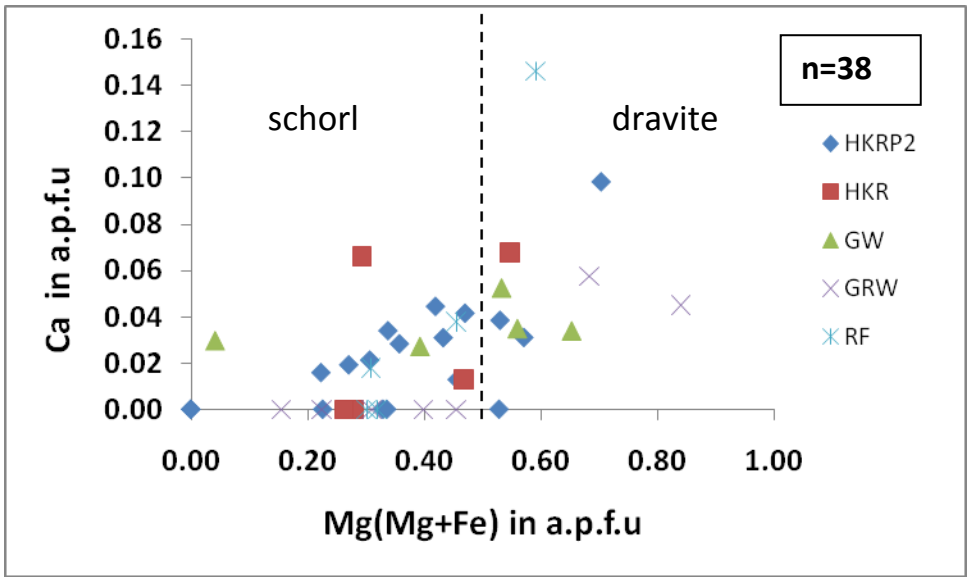

Figure 5.46. Binary diagram illustrating the chemistry of tourmaline and relationship between Mg/ (Mg+Fe) and Ca (diagram after Henry et al, 2002). Diagram indicates that dravite is more Ca-rich than schorl. A Mg/ (Mg+Fe) ratio > 0.5 a.p.f.u indicates dravite and a Mg/ (Mg+Fe) ratio < 0.5 a.p.f.u indicates schorl.

The Mg/ (Mg+Fe) ratios were calculated for all the tourmalines from the five satellite areas in atoms per formula unit (a.p.f.u). The Mg/ (Mg+Fe) ratios range from 0-0.9. Tourmalines with a Mg/ (Mg+Fe) ratio > 0.5 a.p.f.u indicate dravitic tourmaline and < 0.5 a.p.f.u schorl (Henry et al, 2002). Figure 5.46 show that dravite is more calcium-rich than schorl.

5.11 Aluminosilicates

5.11.1 Petrography

Aluminosilicates are common in all five satellite areas and include the varieties kyanite, sillimanite and andalusite with the former being the most abundant. Characteristic of the aluminosilicates is its grey white and creamy white colour under crossed nicols. Dissolution is prominent on many grains in the form of cracks. Inclusions hosted by the aluminosilicates include ilmenite, epidote, micas, tourmaline, apatite, rutile, quartz, monazite, zircon, barite, pyrite and magnetite. Some grains have aggregate inclusions consisting of barite, magnetite and quartz. Quartz inclusions are orientated parallel to the c-axis.

Andalusite

Andalusite has characteristic square shapes and is colourless and yellow in thin-section (Figure 5.47 B). Characteristic of some andalusite is its bow-tie intergrowths (Figure 5.47 C).

Sillimanite

Sillimanite is colourless and yellow in colour and has prismatic shapes (Figure 5.47 E). It has cleavage along the (010) plane.

Kyanite

Kyanite has elongated, squarish, rounded and prismatic shapes and is colourless to grey and yellow in colour (Figure 5.47 D, F) with blue pleochrism. Some of the kyanite grains of Houtkraal Remainder, Rietfontein and Graauwduinen show cleavage along the (010) and (100) plane (Figure 5.47 D and F respectively). Characteristic of kyanite is its transparent rutile needle-like inclusions that are orientated (Figure 5.47 D) along the (010) cleavage direction. Sub-angular grey kyanite grains show twinning oblique to the cleavage (Figure 5.47 A). The presence of all three aluminosilicates indicates three different metamorphic grades.

5.11.2 Chemistry

The chemistry of the aluminosilicates is given in Table F12, (Appendix F). Low totals were normalized to 100 wt %. Al_20_3 is present between 61 and 65 wt % and SiO_2 between 35 and 37 wt %. The rest of the elements are below the detection limit of the SEM (0.5 wt %). Aluminosilicates from the different localities have a similar chemistry.

5.12 Staurolite

5.12.1 Petrography

Staurolite is present as anhedral shaped grains. It has a characteristic yellow to pale or golden yellow colour in thin-section (Figure 5.48). It has a resinous lustre with lots of anhedral shape inclusions of which quartz is the most abundant (Figure 5.48 A and B). Inclusions have no specific orientation. Needle-like inclusions are also present but less abundant. The amorphous, secondary phase is present on most grains and within cracks.

5.12.2 Chemistry

Low totals were normalized to 98 wt % since staurolite can contain up to 2 wt % of water (Deer et al, 1992; Table F13, Appendix F). Staurolite from the different areas has similar chemistry. SiO_2 is present between 26 and 28 wt %, Al_2O_3 between 52 and 57 wt % and FeO between 11 and 15 wt %. Some staurolite may contain up to 2% MgO.

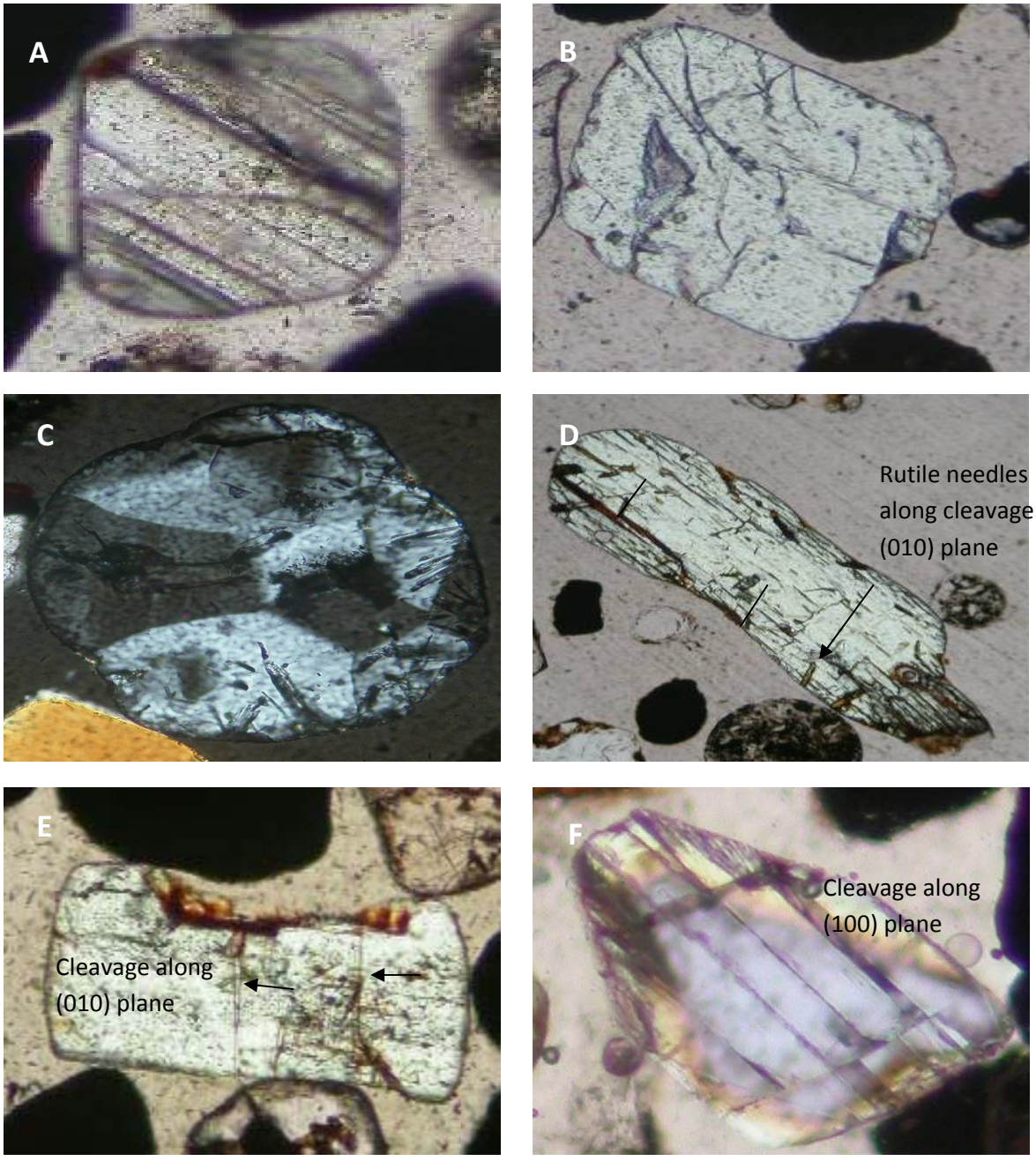

Figure 5.47. Microscope images of the different types of aluminosilicates present in the satellite areas. All pictures were taken under transmitted light. Scale: 20X. A) Colourless kyanite grain with oblique twinning. B) Andalusite. C) Bow-tie intergrowths in andalusite. D) Prismatic kyanite showing rutile needle-like inclusions orientated parallel to the (010) cleavage plane. E) Sillimanite with cleavage along the (010) plane. F) Kyanite showing cleavage along the (100) plane.

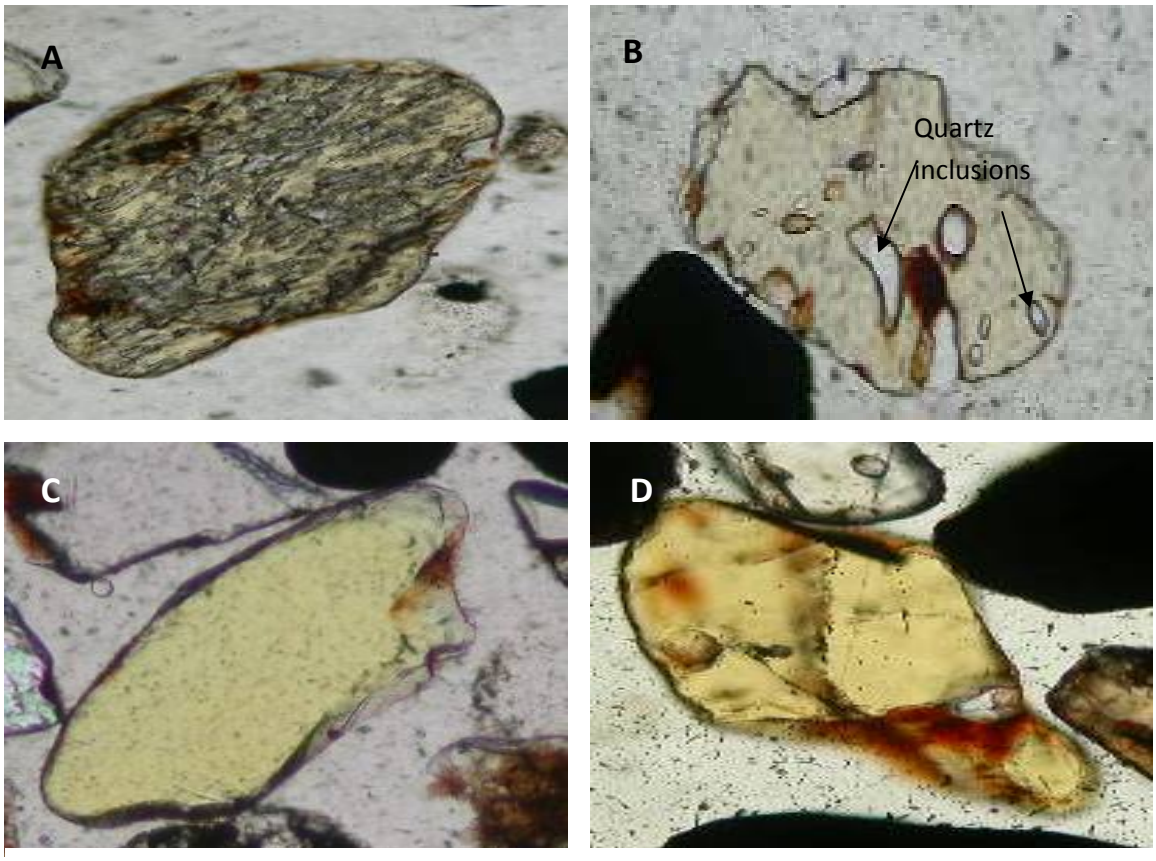

Figure 5.48. Microcsope images showing different colour staurolite present in the satellite areas. All pictures were taken under transmitted light. Scale: 20X). A) Golden yellow staurolite. B) Staurolite with poikiloblastic quartz inclusions. C) Pale yellow staurolite. D) Golden yellow staurolite with an amorphous secondary phase along cracks.

5.13 Epidote Group Minerals

5.13.1 Petrography

The epidote group of minerals was distinguished by making use of its optical properties. These minerals are abundant in the Rietfontein samples with only accessory amounts in the other four areas. It has mostly rounded shapes.

Epidote

Epidote has a characteristic lime green or lemon yellow colour, is colourless and is present as multi-colour (green, pink, blue and yellow) grains (Figure 5.49 A-C). The multi-coloured epidote has undulose extinction.

Epidote was distinguished from zoisite and clinozoisite by its characteristic yellow or green colour. Some epidote display colour zoning. The latter is the result of compositional differences. An amorphous coating is present on some grains and in or along cracks (Figure 5.49 A). Aggregates of epidote and quartz are also present (Figure 5.49 F). It has rounded shapes with many inclusions.

Zoisite and Clinozoisite

Zoisite and clinozoisite are usually colourless in thin-section with grey interference colours (Figure 5.49 D and E). The two minerals were distinguished by making use of its extinction angle. Zoisite has parallel extinction and clinozoisite has inclined extinction.

5.13.2 Chemistry

Chemistry reflects epidote. Epidote is more Fe-rich than zoisite and clinozoisite (Table F14, Appendix F). Low totals were normalized to 98 wt % since epidote can contain up to 2% of water. There is no major difference in chemistry between the five satellite areas but MgO is present in up to 4 wt %. SiO_2 range between 36 and 38 wt %, Al_2O_3 between 14 and 23 wt % and FeO are present in contents of between 6 and 15 wt %.

5.14 Other Non-opaque minerals

5.14.1 Sphene

Sphene is present in trace amounts and occurs as bended prismatic and oval shape grains. It is colourless to pale yellow and brown in thin-section with a pale yellow colour under crossed nicols (Figure 5.50 A). One specific rutile grain has irregular, black sphene bands. Albat (1983) also found partial rims of sphene around opaque grains in his research of the NMC near the West Coast.

The composition of sphene is generally close to stoichiometric proportions (Table F15, Appendix F). Some sphene grains contain up to 2 wt % vanadium.

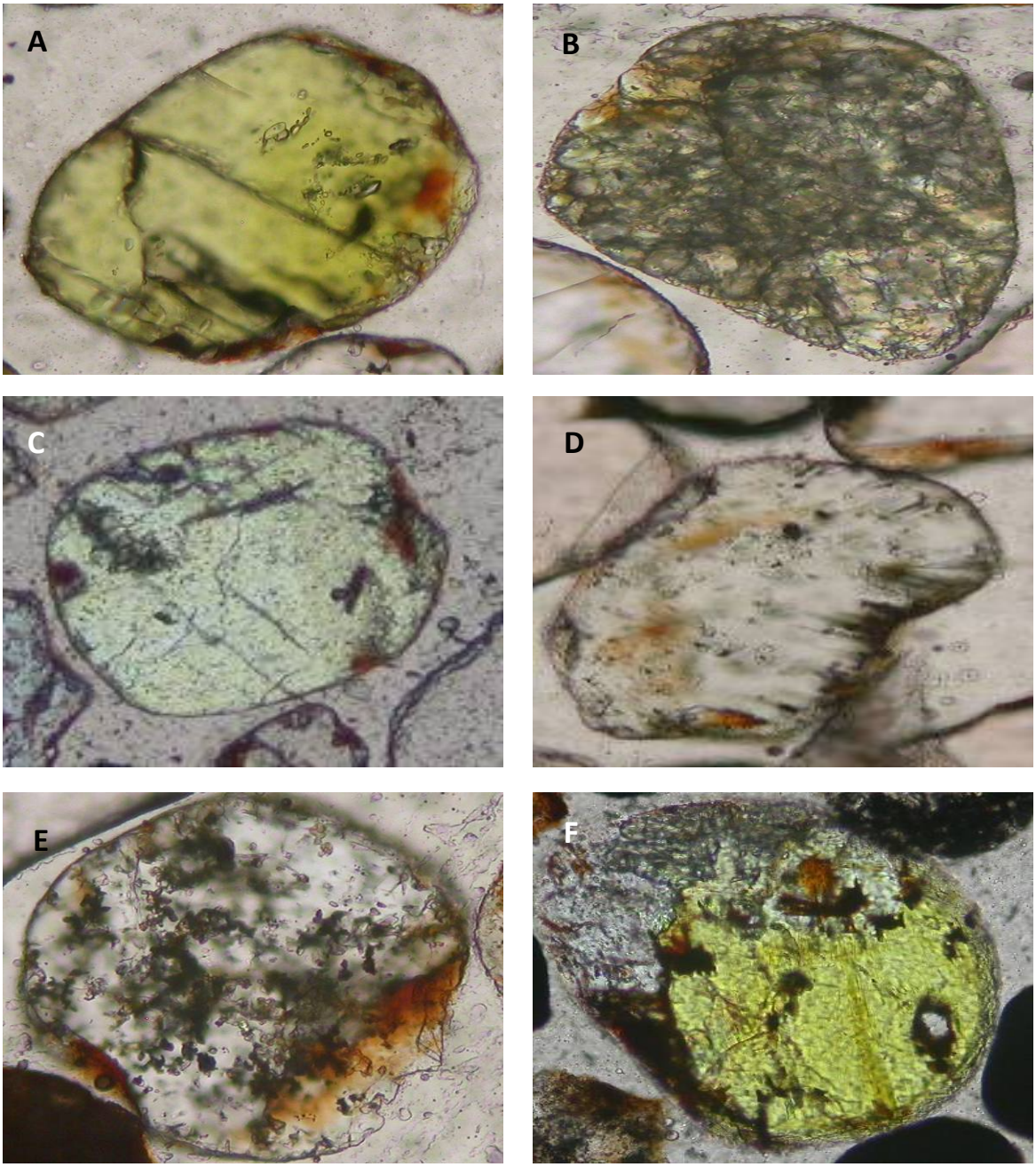

Figure 5.49. Microscope images showing the different types and colour of epidote group of minerals present in the satellite areas. All pictures were taken under transmitted light. Scale: 20X. A) Yellow to lime green epidote. B) Multi-coloured epidote. C) Pale yellow epidote. D) Colourless zoisite. E) Colourless clinozoisite with amorphous coating. F) Epidote-quartz aggregate.

5.14.2 Corundum

Corundum is rare in the satellite areas and only one corundum grain was identified in the Rietfontein samples. It is round in shape, colourless and white grey under crossed nicols (Figure 5.50 B).

The corundum grain consists essentially of pure Al_2O_3 with trace amounts of FeO (Table F16, Appendix F). The blue colour of sapphire and yellow and green colour of corundum is due to the presence of iron ($FeO + Fe_2O_3$).

5.14.3 Monazite

Monazite is present in trace amounts and can easily be mistaken for zircon. It has rounded shapes (Figure 5.50 C) and is colourless to a pale yellow. This pale yellow colour of the monazite was used to distinguish it from zircon.

Monazite in this study is complex and has variable concentrations of Th. Monazite generally has between 4 and 12 mol percent of ThO_2 (Deer et al, 1992). One monazite grain contains 17 wt % ThO_2 (Table F17, Appendix F). Other rare earth elements such as lanthanum, cerium and neodymium are present in contents of up to 9.15 wt %, 24.74 wt % and 9 wt % respectively. Sr and CaO are also present in considerable amounts of up to 5 and 2 wt % respectively. Two of the monazite grains contains high contents of Al_2O_3 and may be aluminosilicate inclusions.

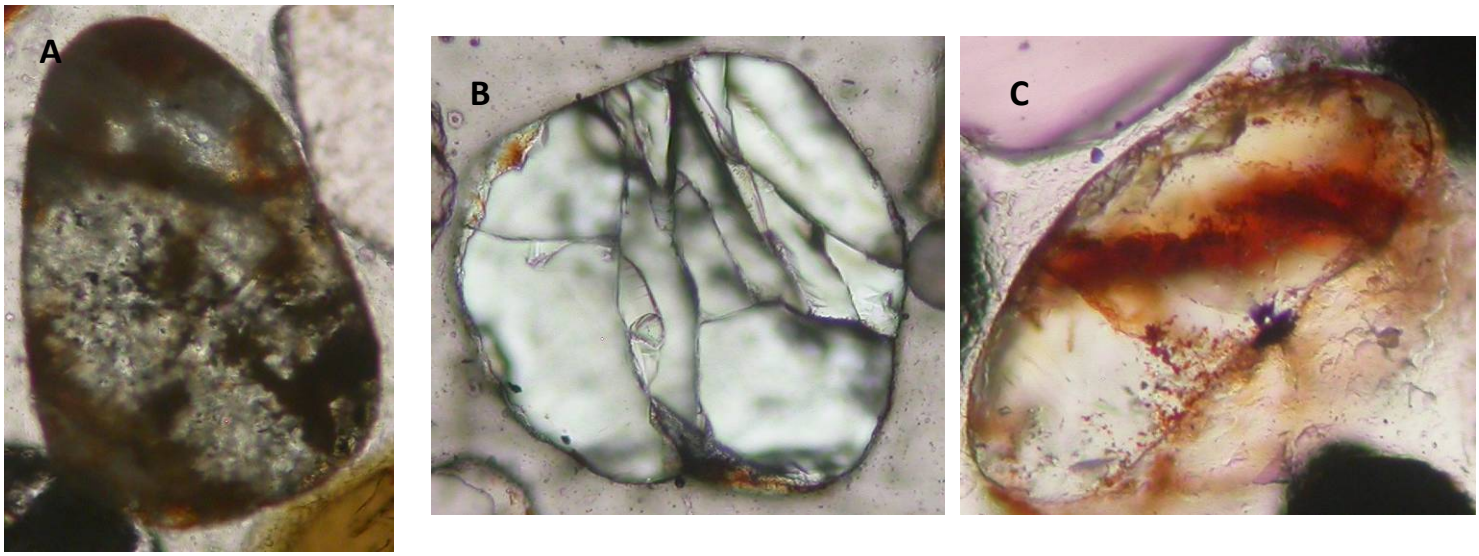

Figure 5.50. Microscope images of sphene, corundum and monazite. All pictures were taken under transmitted light. Scale: 20X. A) Sphene with thick amorphous coating. B) Rounded and cracked corundum C) Monazite with redbrown amorphous coating.

5.15 Amorphous coating

The chemistry of the amorphous coating, a common feature of almost all grains studied, was determined by means of the SEM. The coating consists mainly of SiO_2, Al_2O_3, and FeO with TiO_2, K_2O or MgO present in variable amounts (Table F19 and F20, Appendix F). The coating is brown to red to orange in colour (Figure 5.51 B). It occurs in cracks and dents of the various minerals (Figure 5.51 A and C). Some aggregate grains are" moulded" together by this amorphous material (Figure 5.51 D). It is common especially as thick coatings on the garnet and aluminosilicate grains of the Geelwal Karoo, Graauwduinen and Houtkraal samples.

The amorphous coating often masks the true colour of the heavy mineral grains. It also gives an isotropic appearance to anisotropic minerals. This amorphous material could be the result of (1) silica, alumina and potassium from silicate minerals such as aluminosilicates that broke down due to weathering and chemical alteration and / or (2) from the decomposition of clays (kaolinite) from the nearby environment that were adsorbed onto the surface of the various grains or (3) a water table above the heavy mineral-bearing layers that leached the top layers from silica, alumina, potassium and iron and these element enriched fluids then percolated

through the underlying heavy mineral layers and precipitated the elements onto the surface as well as in the fractures/ cracks and dents of the grains.

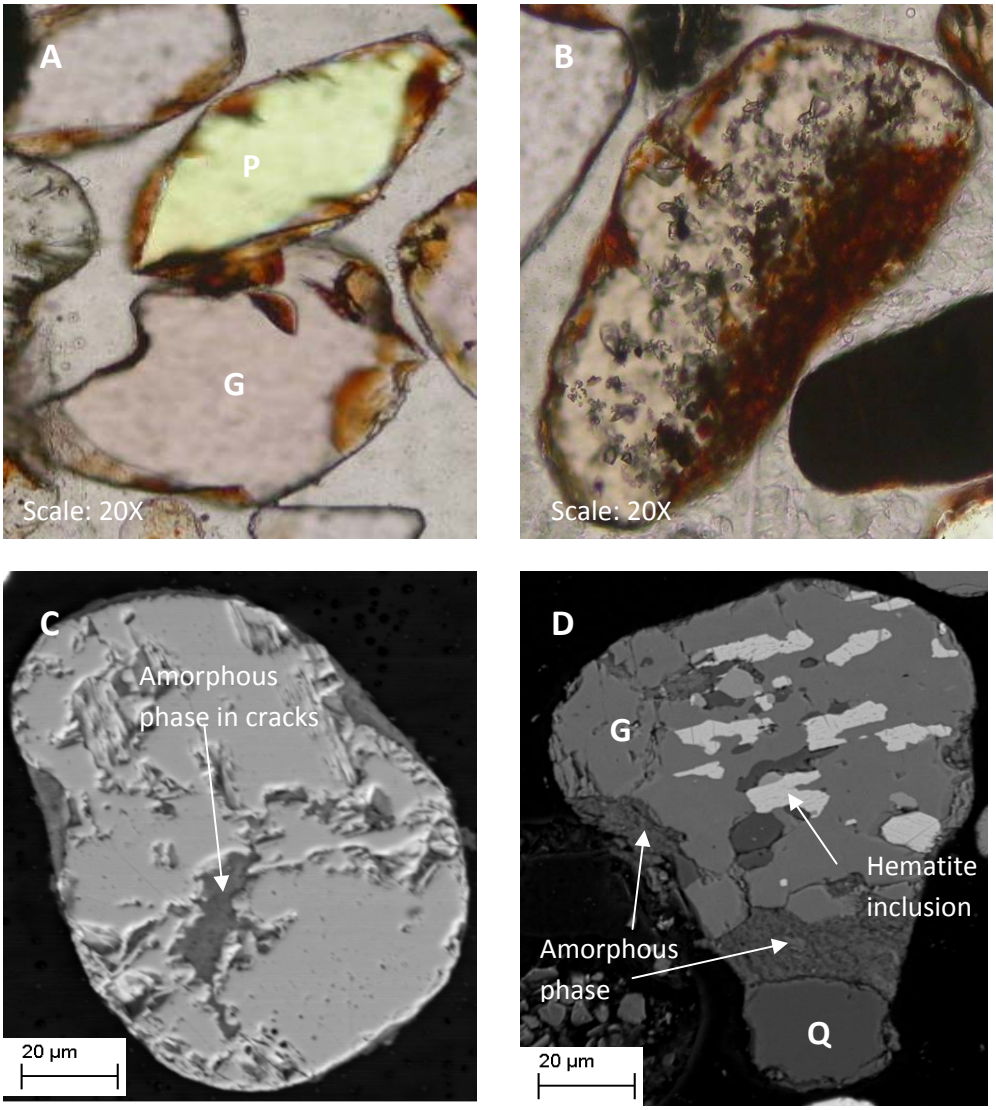

Figure 5.51. SEM and microscope images of amorphous coating on grains. Microscope images were taken under transmitted light A) Secondary amorphous coating on a garnet (G) and pyroxene (P) grain. The amorphous phase is present in dents also. B) Thick redbrown amorphous coating on a garnet grain. C) SEM image of a rutile grain with amorphous material in cracks. D) Garnet (G) and quartz (Q) aggregate being moulded together by amorphous material.

CHAPTER 6 ALTERATION OF ILMENITE

6.1 Literature review of alteration models

Ilmenite alteration is marked by the removal of iron and enrichment in titanium to eventually produce an end-product consisting essentially of TiO_2 with little or no iron and is termed cryptocrystalline rutile (leucoxene). Further removal of iron finally produces rutile*. The asterisk is used to distinguish rutile formed from the alteration of ilmenite from the primary rutile. Alteration starts along cleavage planes, fractures and surface of grains, i.e. structural discontinuities and grain boundaries. Physical and chemical characteristics are changed during alteration and involve different alteration indicators such as a change in the Fe/Ti and Fe^{2+}/Fe^{3+} ratios, change in density, composition, hardness and magnetic susceptibility (Rao et al, 2005). It is also marked by the depletion of Fe^{2+} and enrichment in Ti^{4+} and Fe^{3+}. Fe^{2+} decreases due to oxidation to Fe^{3+}. The latter are leached out at a later stage. The lower the ferrous iron and the higher the Ti^{4+} content the more advanced the alteration state. Elements such as Cr and V tend to increase during alteration whereas trace elements like Mn, Cu, Mg, Zn, Ni, Ca and Co tend to decrease (Grey et al, 1983; Grey and Reid, 1975; Anand and Gikes, 1985).

A simple ilmenite alteration mechanism is:

Ilmenite → Pseudorutile → Rutile* or Anatase + Hematite

$Fe^{2+}\ TiO_3 \longrightarrow Fe^{3+}Ti_3O_9 \longrightarrow TiO_2 + Fe_2O_3$ equation 1

The oxidation of Fe^{2+} to Fe^{3+} is given by:

$3Fe^{2+}TiO_3 \longrightarrow Fe_2^{3+}\ Ti_3O_9 + Fe$ (Grey and Reid, 1975) equation 2

Grey et al (1983) found that there is a marked increase in the impurities SiO_2 and Al_2O_3 within alteration phases with higher than 60 per cent TiO_2. Grey et al (1983) described the above observations to occur due to silica and aluminium being extracted from the ambient environment and adsorbed on to or co-precipitated with alteration products. Anand and Gikes (1985) suggested that the formation of clay minerals within pore spaces between alteration phases is also a possible explanation for the Si and Al increase. Incomplete alteration leads to the co-existence of more than one alteration phase (Suresh Babu et al, 1994).

Alteration takes place due to weathering during transportation or in the source rocks or after deposition. During alteration an ilmenite grain gets physically broken down, etched, pitted, grooved with cracks developing. As alteration progresses these cracks can become wider and can become filled by secondary minerals such as clays.

Grey et al (1983) performed single grain XRD studies on ilmenite grains from Eneabba and Capel mines in Western Australia. He recognized that the ratios of Ti/(Ti+Fe), Fe/Ti and Fe^{3+}/Fe^{2+} can be used as indicators of the extent or different stages of ilmenite alteration. These stages include ferrian- ilmenite, hydrated ilmenite, pseudorutile and leucoxene which corresponds to Ti/(Ti+Fe) values of < 50 wt %, 50-60 wt %, 60-70 wt % and > 70 wt % respectively.

Bailey et al (1956) suggested a three stage model for the alteration of ilmenite seen under the microscope. The first stage involves patchy ilmenite where unaltered and altered ilmenite is intergrown. Elongated stringers, rounded patches and rims usually mark the beginning of this stage of alteration. Stage two is marked by the formation of an isotropic amorphous iron-titanium oxide (pseudorutile). Stage three is marked by the formation of leucoxene.

Grey and Reid (1975) proposed a two stage mechanism for the natural alteration of ilmenite. This was done by performing single crystal X-ray structure analysis on pseudorutile. Pseudorutile has the chemical formula $Fe_2Ti_3O_9$ with a TiO_2 content of 60% -71%. The first stage involves the oxidation of the ferrous iron (Fe^{2+}) to ferric iron (Fe^{3+}) to form pseudorutile from ilmenite and the leaching of one third of the Fe^{3+} without any disturbance of the oxygen lattice. It takes place below the water table via an electrochemical corrosion process under mildly, acidic groundwater conditions (Grey and Reid, 1975). The volume of the crystal lattice is reduced by up to 6% from ilmenite to pseudorutile. An equation for this stage can be written as follows:

$$3Fe^{2+}TiO_3 + 2H^+ + 1/2O_2 \longrightarrow Fe_2^{3+}Ti_3O_9 + Fe^{2+} + H_2O \qquad \text{equation 3}$$

During the second stage of alteration both iron and oxygen are removed from the crystal structure with an enrichment in Ti^{4+} to form cryptocrystalline rutile (leucoxene) from pseudorutile and takes place above the water table via a leaching and reprecipitation process under acidic conditions (Grey and Reid, 1975). Pseudorutile is believed to be unstable under acidic conditions and is therefore transformed to leucoxene. The second stage reaction is:

$Fe_2^{3+}Ti_3O_9 + 4H^+ \longrightarrow 3TiO_2 + 2Fe^{2+} + ½\ O_2 + 2H_2O$ equation 4

Iron oxide and titanium oxide are removed (leached) from the structure but titanium oxide gets reprecipitated to form microcrystalline rutile (leucoxene). In the upper parts of a deposit, above the water table, the role of bacteria, presence of water, available atmospheric oxygen, to name a few, enhances the alteration process and dissolves the pseudorutile.

Hugo and Cornell (1991) proposed a multistage alteration mechanism consisting of three stages of alteration that forms in distinctly different physical environments.

Type I Alteration

This type of alteration is marked by the gradual weathering of ilmenite to pseudorutile via hydrated ilmenite and then finally to leucoxene. Hydrated ilmenite is an alteration product of ilmenite with TiO_2 contents between 53 and 60% and contains water (OH^-). Nair et al (2006) refers to it as leached ilmenite. It occurs as irregular patches along plane weaknesses within the grain and along grain boundaries in regions below the water table. Some grains are altered to consisting entirely of leucoxene. The latter can be described by the two stage model of Grey and Reid (1975).

Type II Alteration

Ilmenite is directly altered to leucoxene, rutile* or anatase by a single step dissolution-reprecipitation process without the formation of pseudorutile. It differs from the mechanism of Grey and Reid (1975) due to this direct alteration. Alteration usually occurs along weaknesses and from grain boundaries and above the water table in acidic soils and mildly reducing conditions (Hugo and Cornell, 1991). An equation for this type of alteration is:

$FeTiO_3 + 2H^+ \longrightarrow TiO_2 + Fe^{2+} + H_2O$ equation 5

Ilmenite $\longrightarrow$ rutile+ dissolved hematite

Type III alteration

In this type of alteration process, ilmenite is replaced by prismatic and or vermiform TiO_2 micro crystals. In the former, alteration is achieved through supergene or hydrothermal alteration. In the latter, grains are altered in the original igneous or metamorphic source rocks.

Pownceby (2010) proposed a Type I and Type II alteration models for the ilmenite of the Murray Basin, Australia. In Type I alteration ilmenite is altered to leucoxene via hydrated ilmenite and pseudorutile. Type II alteration is where ilmenite is altered directly to hydroxylian pseudorutile. The latter is believed to have a pseudorutile-like structure but a leucoxene-like composition. For this study the alteration model of Hugo and Cornell (1991) best describes alteration in the satellite areas and is therefore used for the ilmenite alteration interpretation.

6.2 Ilmenite alteration in the five satellite areas

Altered ilmenite in the satellite areas are described in terms of petrography and chemistry. Alteration has been studied by means of the optical microscope and the Scanning Electron Microscope. Both methods showed that ilmenite alteration was initiated along grain boundaries and structural weaknesses (cracks/fractures and cleavage planes) within the grain.

In general the ilmenite grains of all five satellite areas occur mostly as homogeneous, relatively unaltered grains with only a few grains showing moderate to extreme alteration. The altered ilmenite grains occur mostly as sub- rounded and elongated grains. Despite the relatively fresh nature of most ilmenite grains the whole spectrum of alteration phases (hydrated ilmenite, pseudorutile, leucoxene and rutile*) are present (Table F18, Appendix F). Most altered grains contain more than one alteration phase indicating incomplete alteration. Table F18, (Appendix F) presents the chemistry of the unaltered ilmenite plus its alteration products. Some 3 to 10 analysis were done per grain in this study.

Weathering can destroy primary textures (lamellae, inclusions) or modify them to such a degree that they are unrecognizable (Riezebos, 1979). In the grains of the five satellite areas, the textures have been well preserved. This in turn can be an indication that weathering was not sufficient to obliterate or modify the textural characteristics significantly.

In this study, alteration took place by dissolution and replacement by secondary minerals. Secondary minerals refer to minerals that form from the breakdown or alteration of other or parent minerals such as leucoxene, clays, hematite and rutile*. Alteration also occurred via the proposed alteration models of Grey and Reid (1975) and Hugo and Cornell (1991). So far

the latter two models are the generally accepted alteration models together with the model of Mücke and Chaudhuri (1991).

Evidence of alteration occurring due to dissolution is Figure 6.1 A where rutile* or hematite lamellae were dissolved out of the ilmenite grain leaving parallel voids (Darby, 1984; Morad and Aldahan, 1986). Dissolution can also result in etching and cracking of ilmenite grains. An example of alteration due to replacement is Plate 6.1 B where leucoxene replaces ilmenite along cracks. Some ilmenite grains have a Si and Al and Ti-rich material and or a Si and Ti and Fe-rich material present in the cracks or along cleavage planes and in dents. This amorphous material is derived from the dissolution of Fe-Ti oxide grains during alteration and infiltrates along cracks and voids or can indicate the presence of clays.

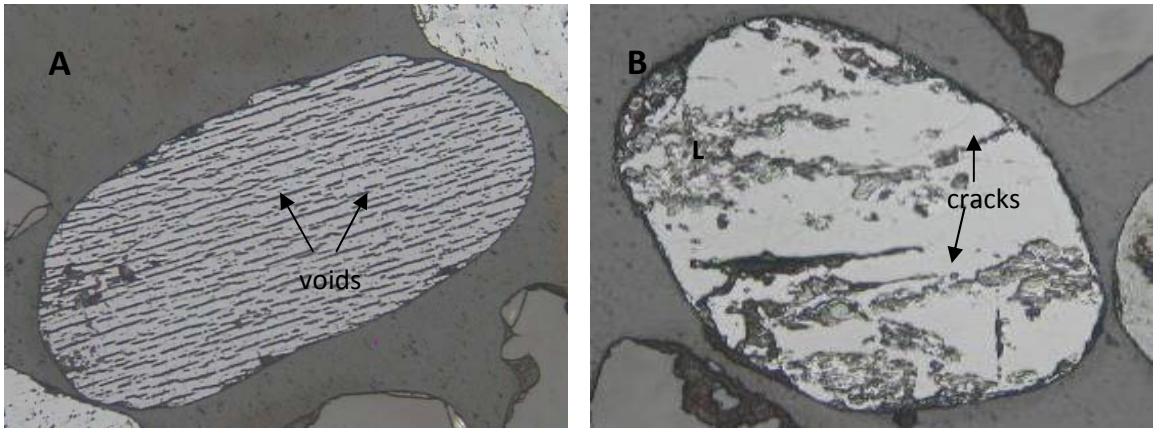

Figure 6.1. Grains, from Houtkraal Remainder Portion 2, showing ilmenite alteration achieved through dissolution and replacement by secondary phases. Pictures were taken under reflected light. Scale: 20X. A) Parallel voids on an ilmenite grain resulting from the dissolution of rutile*- and or hematite exsolution lamellae. B) Leucoxene (L) forming along cracks in ilmenite grain. Note the inhomogeneity of the weathered areas.

Alteration of ilmenite starts by the formation of hydrated ilmenite in the form of elongated stringers that develop as irregular patches along cleavage planes, along fractures, from the grain boundary or parallel to the basal plane of ilmenite (0001) (Figure 6.2 A-D and 6.3 A-C). The irregular distribution of the hydrated ilmenite indicates areas of structural weakness within the grain. Hydrated ilmenite has a grey blue colour under reflected light but can be optically very similar to ilmenite which has a dark grey colour under crossed nicols, reflected light with moderate anisotropism and low reflectivity. Figure 6.2 A-D corresponds to the

beginning stages of the Type I ilmenite alteration of Hugo and Cornell (1991) and the first stage of alteration of Grey and Reid (1975).

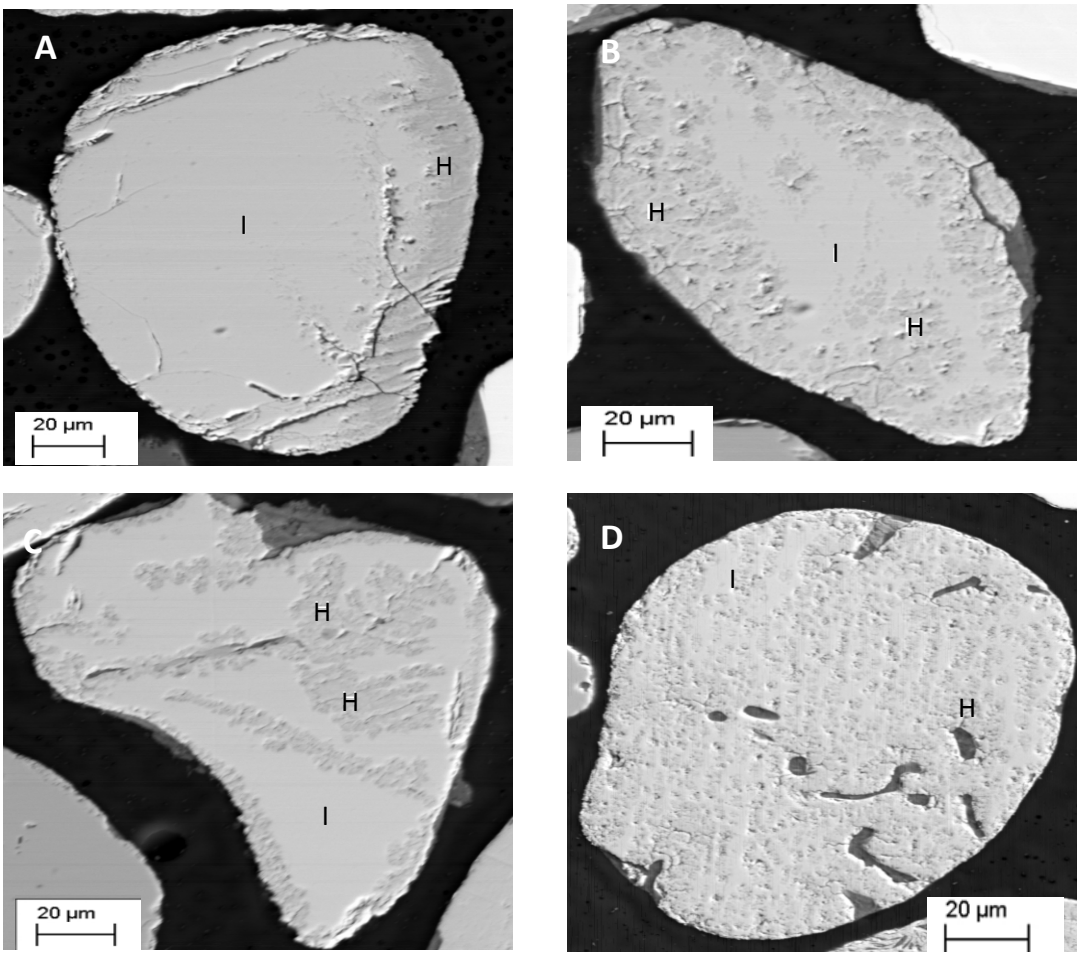

Figure 6.2. Backscatter images of hydrated ilmenite from Graauwduinen and Houtkraal Remainder Portion 2. A) Development of hydrated ilmenite (H) along ilmenite (I) grain edge. B) Irregular patches of hydrated ilmenite (H) along grain edge and cracks in grain. C) Development of hydrated ilmenite (H) along grain edge and fractures and irregularly throughout grain. D) Stringers of hydrated ilmenite (H) parallel to the (0001) crystallographic direction of ilmenite.

Pseudorutile is an intermediate alteration product with a blue grey colour under reflected light. It occurs as patches irregularly distributed throughout the grain, along cracks or fractures, along cleavage planes, along grain boundaries and in areas of hydrated ilmenite (Figure 6.3 A-D) and leucoxenization. It has a porous nature. Figure 6.3 A corresponds to the first stage of Grey and Reid (1975) and the 1st stage of Type I alteration of Hugo and Cornell

(1991). Figure 6.3 B and C corresponds to stage 1 and 2 of Grey and Reid (1975) and stages 1 and 2 of the Type I alteration of Hugo and Cornell (1991). Rutile* is present as prismatic crystals (Figure 6.3 D) and replaces the ilmenite by patches within the grain and corresponds to Type III alteration of Hugo and Cornell (1991). It formed through supergene or hydrothermal alteration of ilmenite.

Leucoxene presents the final stage in the ilmenite alteration process. Leucoxene occurs as monomineralic grains but also as an alteration product of ilmenite. The former is opaque with a brown colour. It has oval to rounded shapes (Figure 6.4 A and C). It has a grey green colour and light grey colour similar to that of rutile* under reflected light and is easily distinguishable from the other alteration products by its bright yellow to white internal reflections. Also characteristic of leucoxene is its sugary texture. Areas of leucoxene formation are also easily identifiable by its luminous nature under crossed nicols (Figure 6.4 C). Characteristic of leucoxene grains is the presence of silica and amorphous material in cracks and cavities. Brown internal reflections in leucoxene are an indication of the presence of iron oxide. In some grains the bright internal reflections of leucoxene can mask the presence of the intermediate alteration phases such as pseudorutile. Leucoxene formation spreads from cracks in the grains, along cleavage planes, at points irregularly distributed through the grain (irregular patches) and along grain edges (Figure 6.4 B and D, Figure 6.3 B-D and Figure 6.5 A). Figure 6.4 B corresponds to stage 1 and 2 of the Type I alteration of Hugo and Cornell (1991) and the 2nd stage of Grey and Reid (1975). Figure 6.4 D corresponds to Type II alteration of Hugo and Cornell (1991).

Rutile* is also present along cracks (Figure 6.5 B) and grain boundaries (Figure 6.5 A). Figure 6.5 A corresponds to stage 1 and 2 of the Type I alteration of Hugo and Cornel (1991) and stage 1 and 2 of Grey and Reid (1975). Figure 6.5 B corresponds to the Type III alteration of Hugo and Cornell (1991).

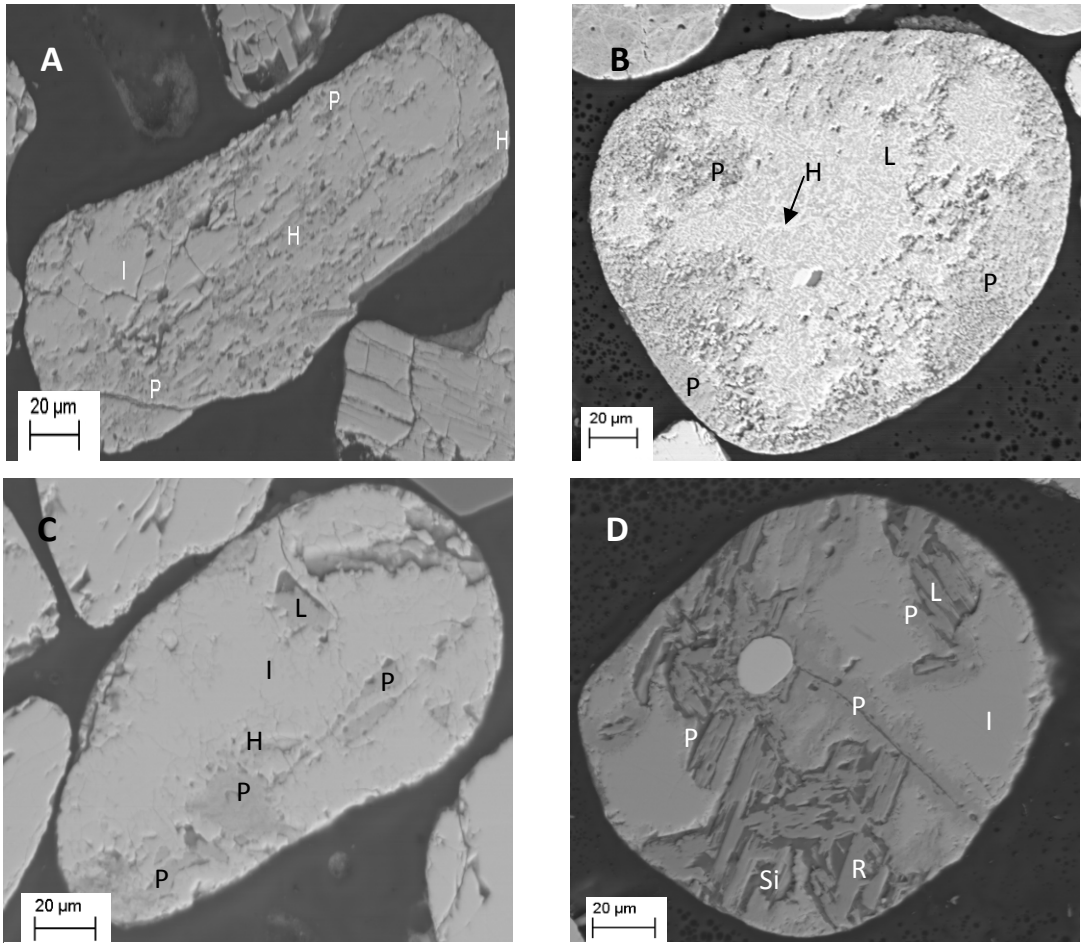

Figure 6.3. Backscatter images of pseudorutile from Graauwduinen, Rietfontein and Houtkraal Remainder.

A) Irregular patches of pseudorutile (P) developed throughout grain and along grain boundaries. Ilmenite (I) is altered to pseudorutile (P) via hydrated ilmenite (H).

B) Pseudorutile (P) present along grain edge. Hydrated ilmenite (H) is altered to leucoxene (L) via pseudorutile (P). Hydrated ilmenite (H) is the white phase and leucoxene (L) the grey phase.

C) Pseudorutile (P) forming irregular patches throughout grain. Pseudorutile (P) occurs in areas of hydrated ilmenite (H). Ilmenite (I) is altered to pseudorutile (P) via hydrated ilmenite (H) and finally to leucoxene (L).

D) Pseudorutile (P) present along fractures and around leucoxene (L). It forms a rim around leucoxene. Ilmenite (I) is altered to leuxocene and rutile* via pseudorutile. Areas of leucoxene and rutile* are enriched in silica. Rutile* (R) is present as prismatic crystals.

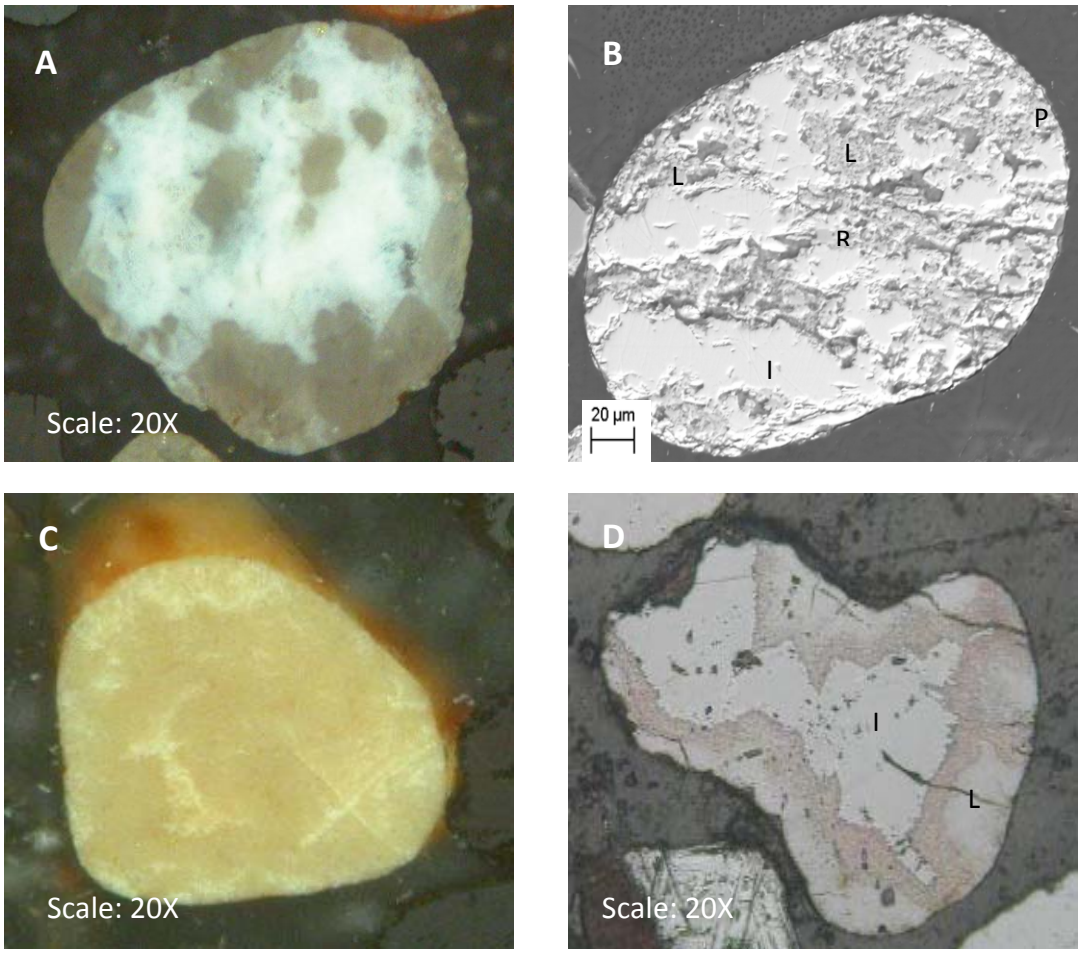

Figure 6.4. Microscope and backscatter electron images of leucoxene from Houtkraal Remainder Portion 2 and Rietfontein. Microscope images were taken under reflected light. A) White and brown internal reflections of leucoxene. B) Leucoxene forming irregular patches throughout grain. Note the porous nature of the leucoxene. Ilmenite (I) is altered to leucoxene (L) via pseudorutile (P). C) Luminous nature of leucoxene. Note the bright yellow to yellow white internal reflections. D) Leucoxene formation along grain boundary. Ilmenite is altered directly to leucoxene without the formation of hydrated ilmenite or pseudorutile.

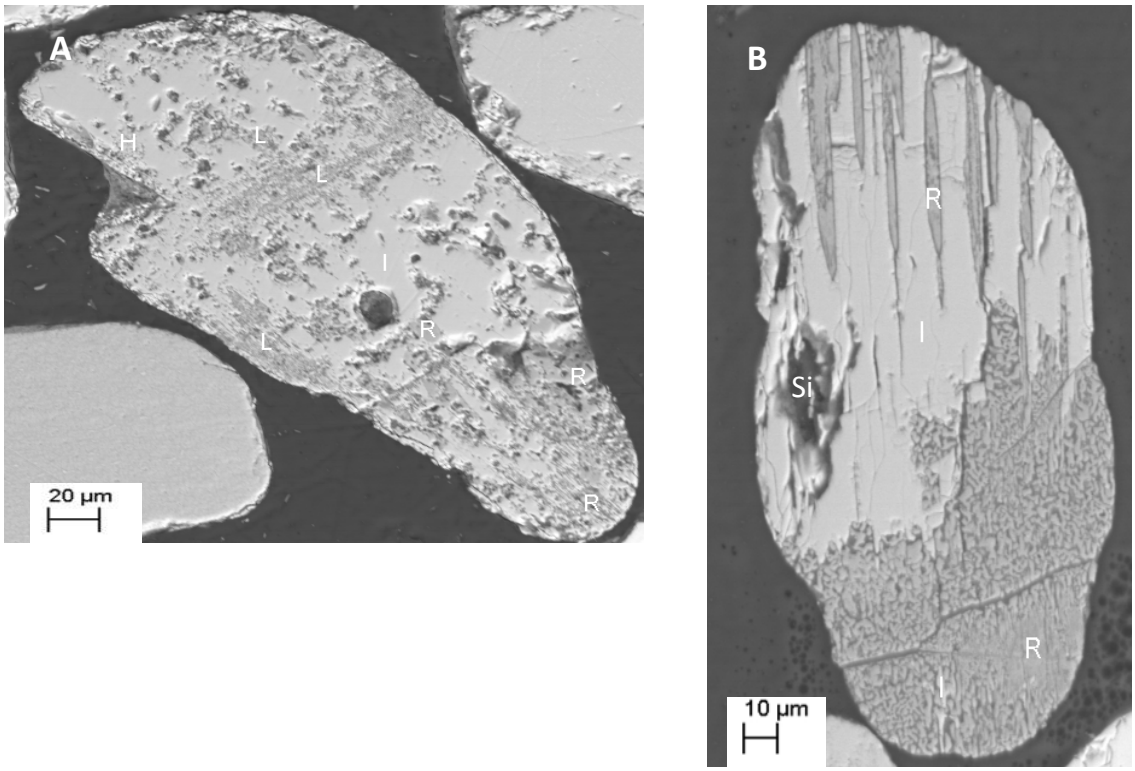

Figure 6.5. Backscatter images of rutile from Rietfontein and Houtkraal Remainder Portion 2. A) Ilmenite is altered to leucoxene and rutile* via hydrated ilmenite. Rutile* replaces ilmenite from the grain edge and as irregular patches throughout the grain. B) The replacement of ilmenite by rutile*. Note the trellis-type structure of rutile*. The cavities are filled by silica.

Below are more descriptions and examples (Figure 6.6) of altered ilmenite grains to illustrate the Type I, II and Type III alteration mechanisms of Hugo and Cornell (1991).

The optical properties of the ilmenite alteration phases reflect the degree of alteration. Bailey et al (1956) stated that ilmenite alteration involves a colour change from dark to light as alteration progresses starting from the dark grey ilmenite to the white leucoxene. Internal reflections become more abundant with increasing alteration. Microscopically altered ilmenite ranges in colour from dark grey, brown grey, brown red, dark grey red, red orange, orange yellow, white grey, yellow red and yellow white. These different colour alteration phases represent the alteration products of ilmenite (hydrated ilmenite, pseudorutile, leucoxene and rutile*).

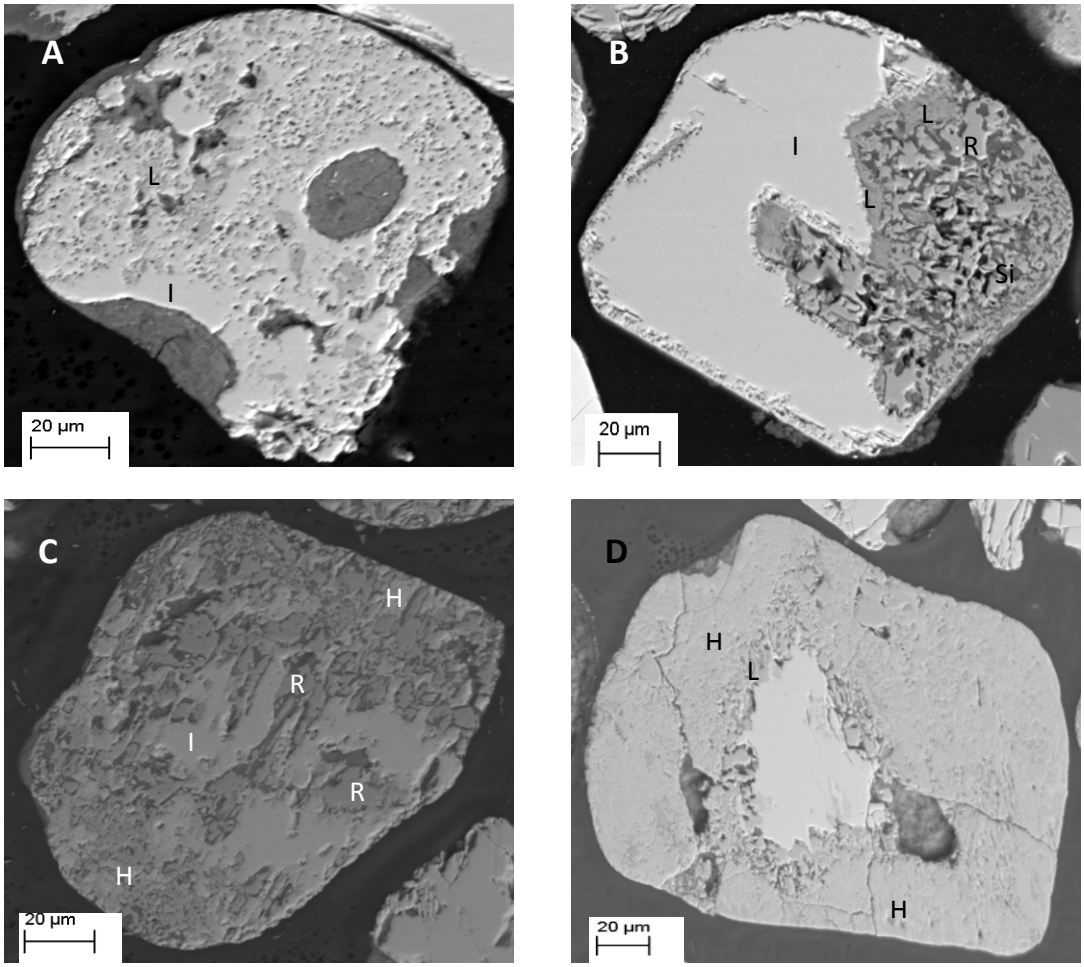

Figure 6.6. Backscatter images from Houtkraal Remainder, Graauwduinen and Rietfontein. A) Ilmenite (I) is altered directly to leucoxene (L) without the formation of any intermediate phases. This type of alteration corresponds to Type II alteration of Hugo and Cornell (1991). B) Replacement of ilmenite by leucoxene and rutile*. The sharp boundary between ilmenite and leucoxene indicates a discontinuous process as stated by Mücke and Chaudhuri (1991). The rutile* forms a symplectite-like structure filled with silica. Such grains formed through alteration in the source rocks (Type III alteration of Hugo and Cornell 1991). C) Replacement of ilmenite by leucoxene and rutile* via hydrated ilmenite. Hydrated ilmenite (H) is restricted to the edges of the ilmenite grain and rutile* occurs as irregular patches throughout the grain. This type of alteration corresponds to the 1st and 2nd stages of Type I alteration of Hugo and Cornell (1991). D) Replacement of ilmenite by leucoxene via hydrated ilmenite. This type of alteration also corresponds to the 1st and 2nd stages of Type I alteration of Hugo and Cornell (1991). Alteration started from grain edge towards the core. Ilmenite relict is unaltered. Note the change in texture from hydrated ilmenite to leucoxene. Leucoxene areas have more cracks.

Hydrated ilmenite has a blue grey colour under reflected light and is dark grey to red under crossed nicols, reflected light (Figure 6.7 A and B). Pseudorutile has a dark grey, brown red and medium grey colour with red orange internal reflections (Figure 6.7 C). Leucoxene has red yellow orange (Figure 6.7 D), yellow orange and yellow white (Figure 6.7 E) internal reflections. Rutile* has white to yellow white internal reflections (Figure 6.7 F).

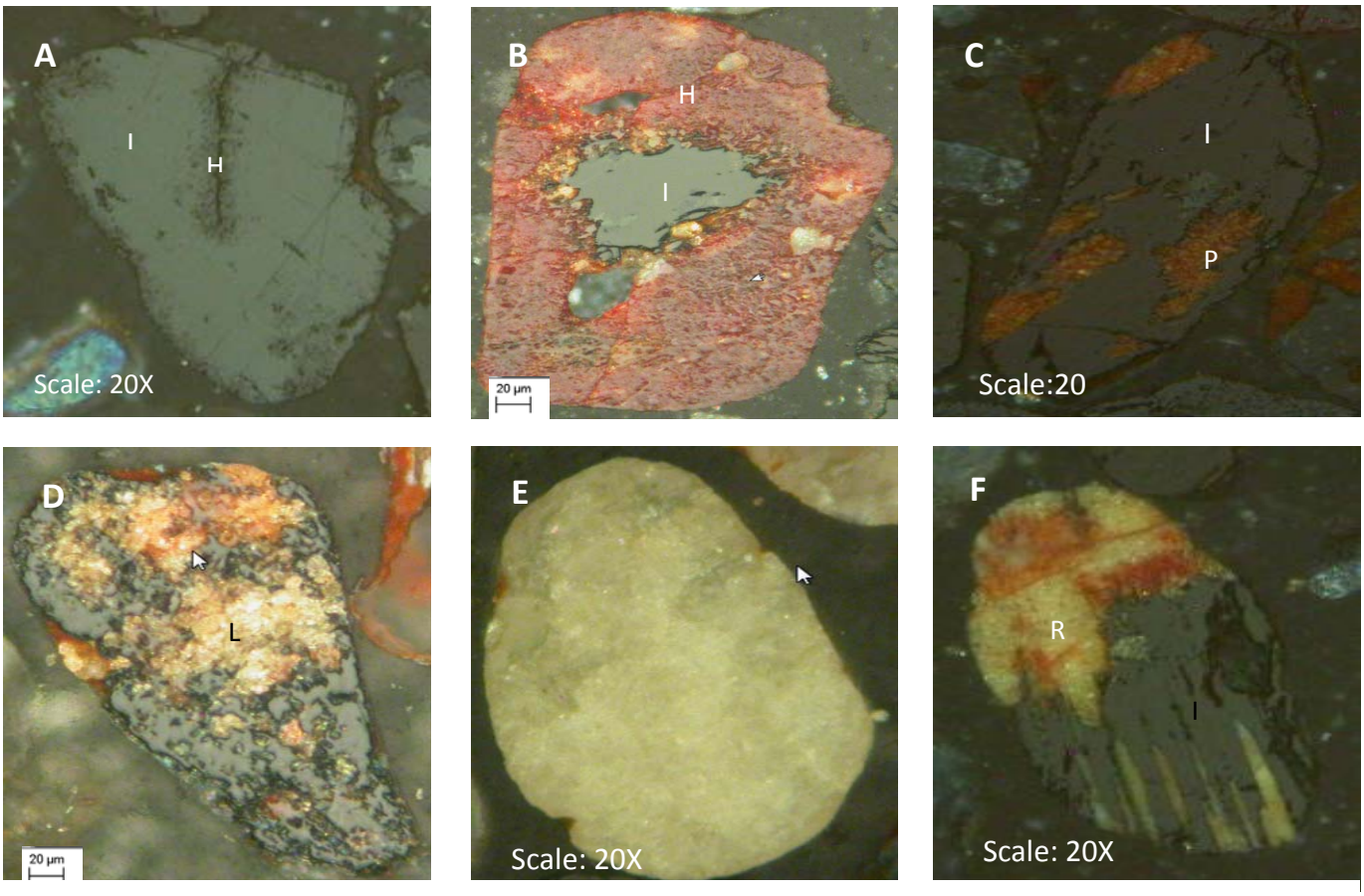

Figure 6.7. Microscope images from all five satellite areas. Pictures were taken under reflected light, crossed nicols. A) Dark grey hydrated ilmenite. B) Red internal reflections of hydrated ilmenite. C) Red orange internal reflections of pseudorutile. D) Yellow orange to white internal reflections of leucoxene. E) Monomineralic yellow white leucoxene grain. F) Yellow white rutile* in cracks and on edge of grain. Red material is the amorphous coating.

Geochemical traverses were done across five altered ilmenite grains; one from each satellite area, to determine the distribution of iron and titanium. The chemical data for each of these grains are listed in Table F18, (Appendix F). These grains are listed in Table F18 with a prefix traverse. Traverses are illustrated graphically in scatter diagrams (Figure 6.8-6.12).

The grain spot number on the y-axis of the scatter diagrams corresponds to the number on the SEM figures.

Figure 6.8 consists of the following phases: (1) unaltered ilmenite, (2) unaltered ilmenite, (3)-(5) leucoxene, (6) pseudorutile, (7) leucoxene and (8) hydrated ilmenite. The whole spectrum of ilmenite alteration products are present and corresponds to the 1st and 2nd stages of Type I alteration of Hugo and Cornell (1991). For all five satellite areas, as the Ti^{4+} content increases, the total Fe content decreases. For Figure 6.8, Al_20_3 increases as alteration increases. MnO and MgO contents decreases with increasing alteration and the highest concentrations thereof are present in unaltered ilmenite with minor amounts in the leucoxene phases. SiO_2 does not show any consistent trend.

Figure 6.9 consists of the following phases: (1) unaltered ilmenite, (2) leucoxene, (3) unaltered ilmenite, (4) hematite (< 40 wt TiO_2), (5) unaltered ilmenite, (6) and (7) hematite, (8) leucoxene, (9) unaltered ilmenite, (10) leucoxene and (11) unaltered ilmenite. This type of alteration corresponds to the Type II alteration of Hugo and Cornell (1991). MgO decreases and is completely removed in the hematite alteration phases. Al_2O_3 and SiO_2 do not show any specific trend and increases and decreases with increasing alteration. MnO decreases with increasing alteration and the highest concentrations thereof are present in unaltered ilmenite with minor amounts in the leucoxene phases. The hematite phases have higher MnO than leucoxene.

Figure 6.10 consist of the following phases. (1) unaltered ilmenite, (2) and (3) pseudorutile, (4) leucoxene, (5) unaltered ilmenite, (6) leucoxene, (7) unaltered ilmenite, (8) leucoxene, (9) hydrated ilmenite and (10) unaltered ilmenite. This type of alteration corresponds to the 1st and 2nd stages of Type I alteration of Hugo and Cornell (1991). MnO decreases with increasing alteration and the highest concentrations thereof are present in unaltered ilmenite with minor amounts in the pseudorutile and leucoxene phases. MgO, Al_2O_3 and SiO_2 do not show any consistent trend with increasing alteration.

Figure 6.11 consist of the following phases: (1) unaltered ilmenite, (2) hydrated ilmenite, (3) leucoxene, (4) and (5) rutile and (6)-(8) leucoxene. This type of alteration corresponds to the Type III alteration of Hugo and Cornell (1991). The latter is due to rutile* being present as prismatic crystals. MgO, MnO, Al_2O_3 and SiO_2 decreases with increasing alteration.

Figure 6.12 consist of the following phases: (1) hydrated ilmenite, (2) leucoxene, (3) hydrated ilmenite, (4) rutile, (5) leucoxene, (6) pseudorutile, and (7) rutile. The primary ilmenite grain was altered completely with no unaltered relict left. This type of alteration corresponds to the 1st and 2nd stages of Type I alteration of Hugo and Cornell (1991). MgO and MnO decreases with increasing alteration. SiO_2 increases up to the leucoxene stage where after its abundance decreases. Al_2O_3 does not show any specific trend.

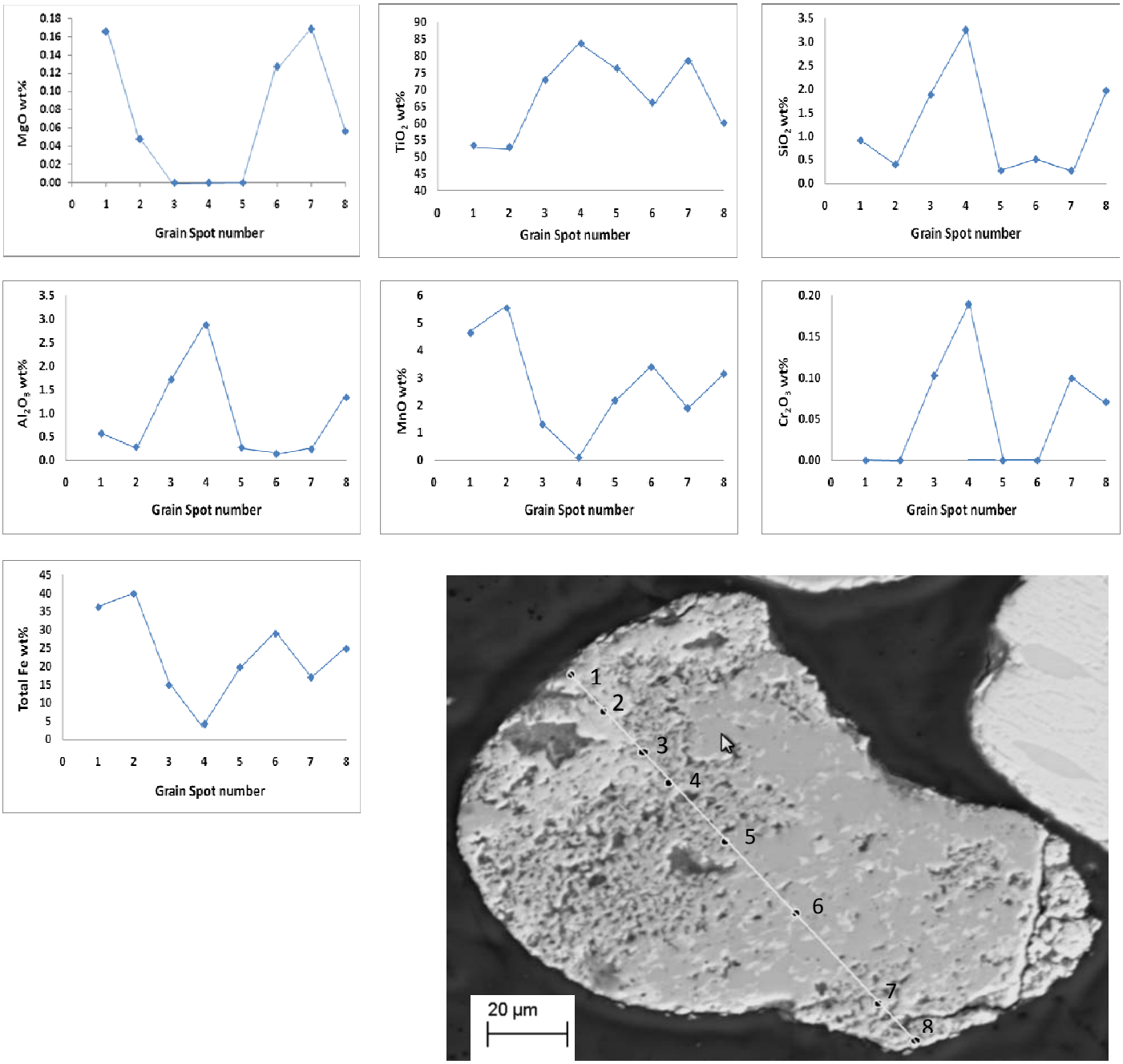

Figure 6.8. Chemical traverse across a Houtkraal Remainder Portion 2 altered ilmenite grain. Ilmenite alteration corresponds to the 1st and 2nd stages of Type I alteration of Hugo and Cornell (1991).

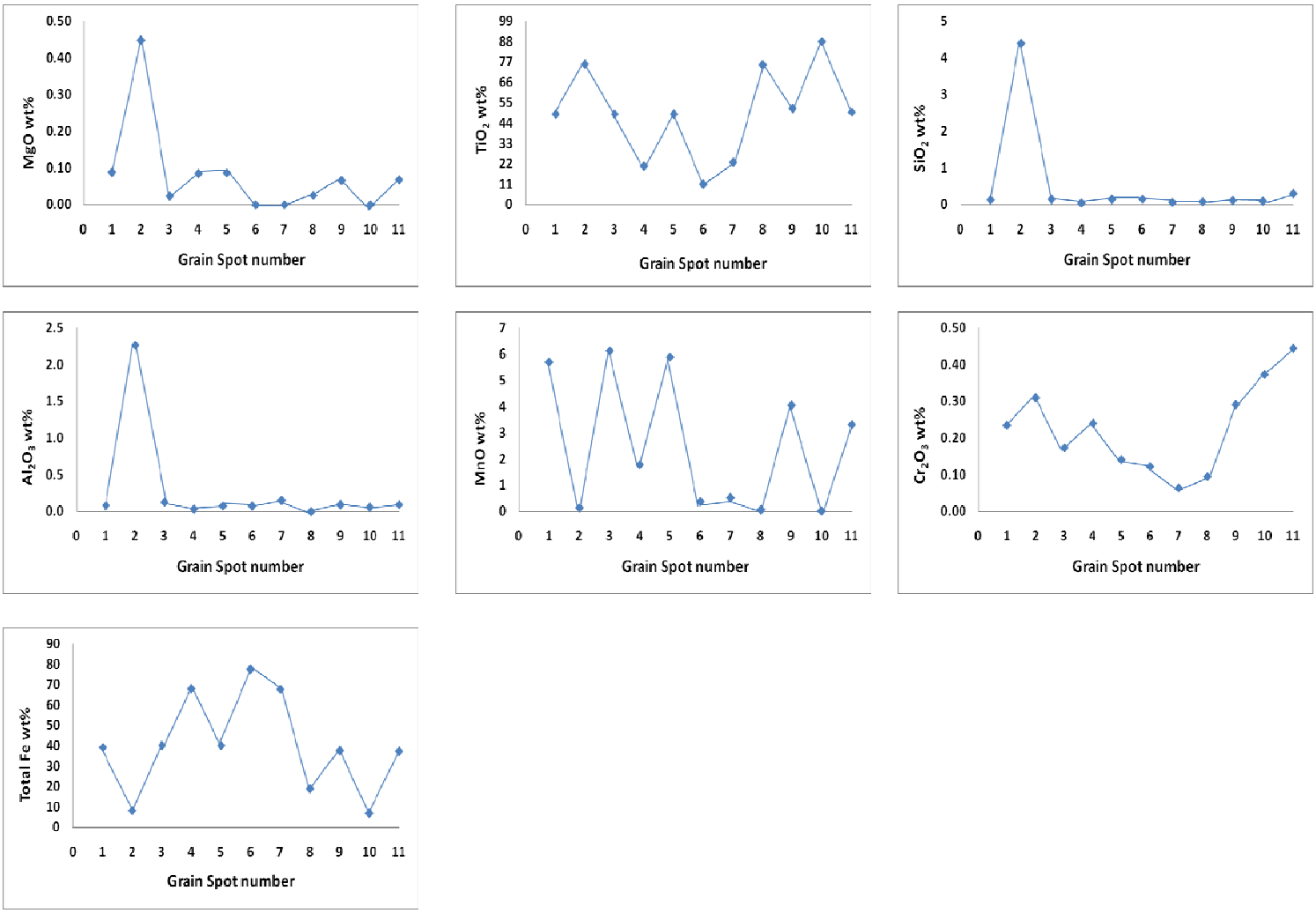

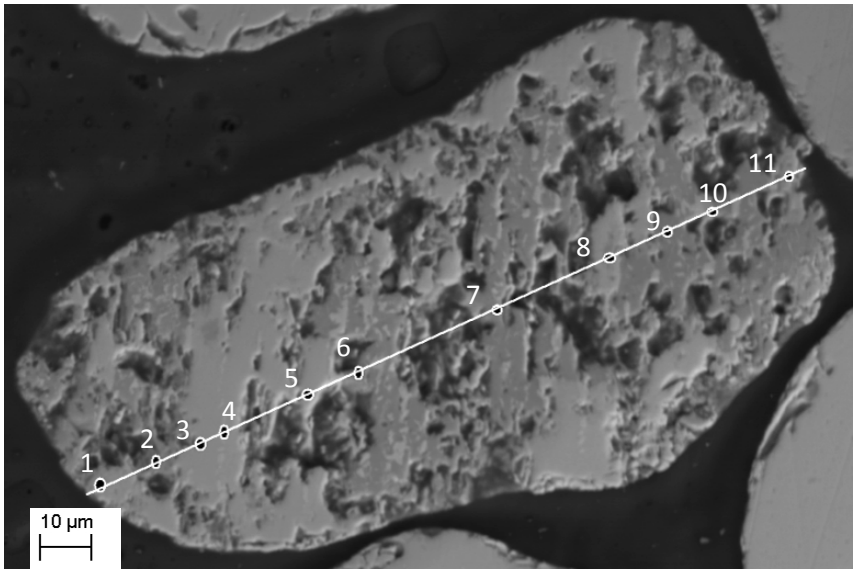

Figure 6.9. Chemical traverse across a Houtkraal Remainder altered ilmenite grain. Ilmenite alteration corresponds to Type II alteration of Hugo and Cornell (1991).

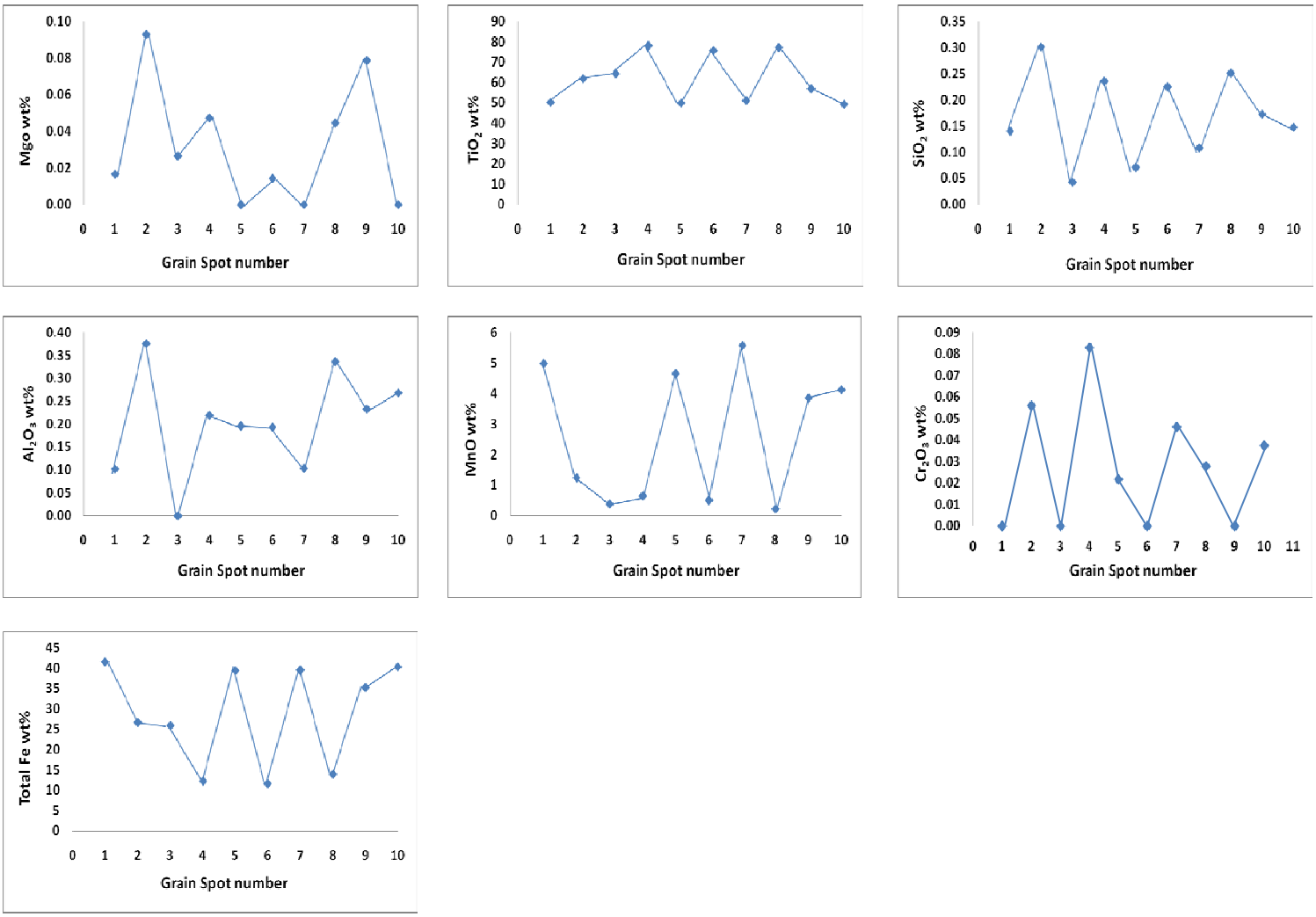

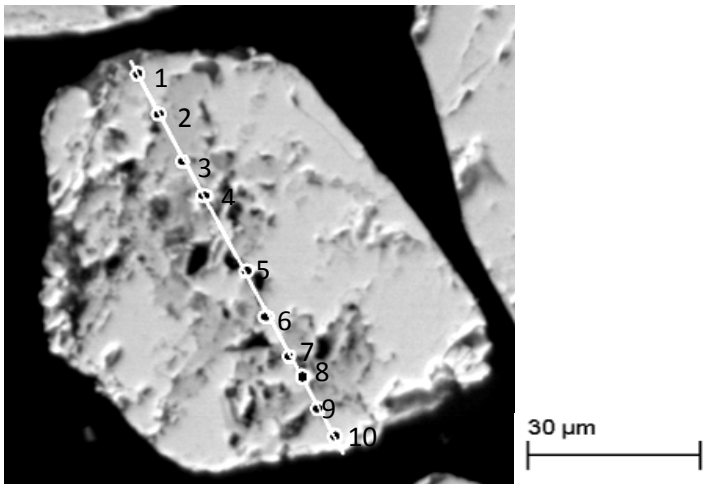

Figure 6.10. Chemical traverse across a Geelwal Karoo altered ilmenite grain. Ilmenite alteration corresponds to the 1st and 2nd stages of Type I alteration of Hugo and Cornell (1991).

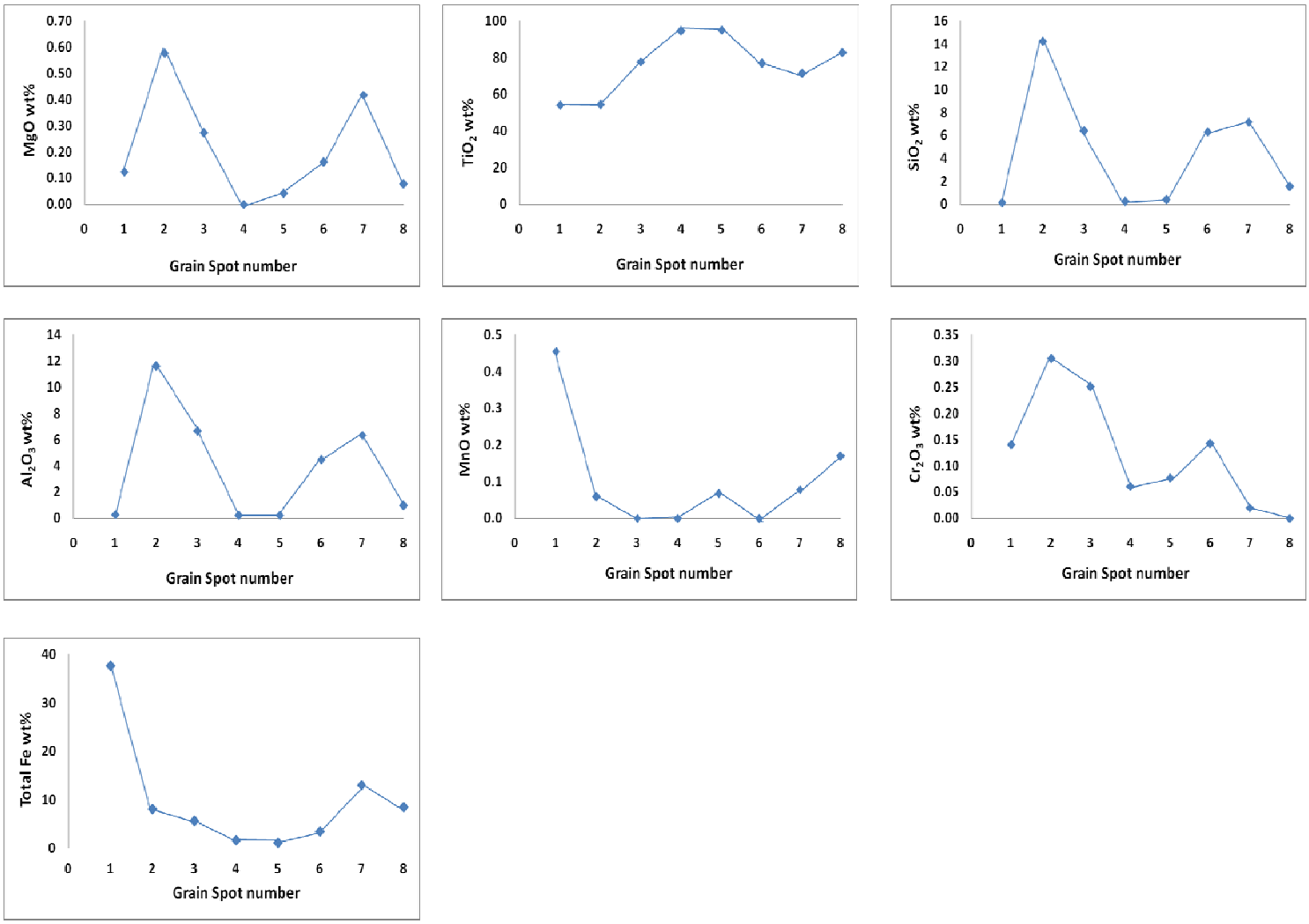

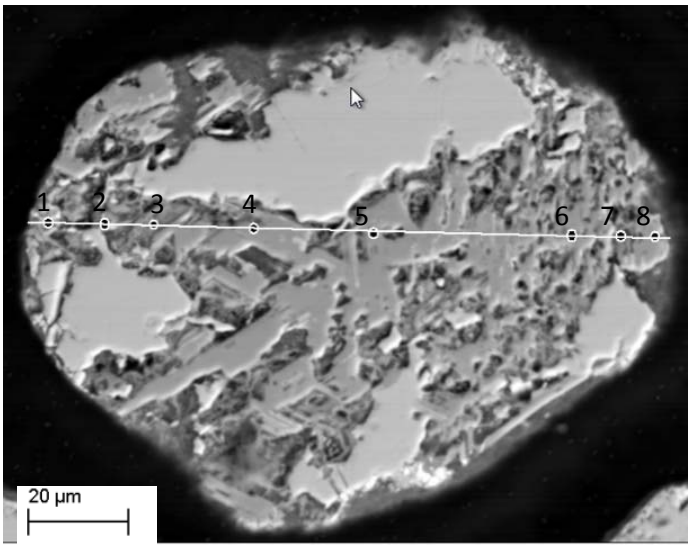

Figure 6.11. Chemical traverse across a Graawduinen altered ilmenite grain. Ilmenite alteration corresponds to Type III alteration of Hugo and Cornell (1991).

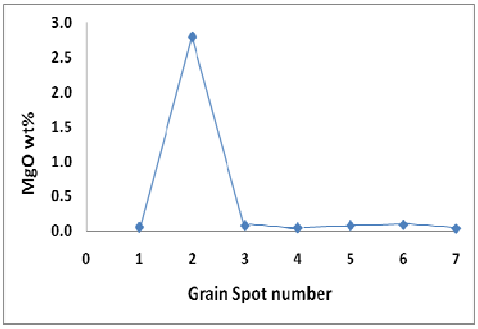

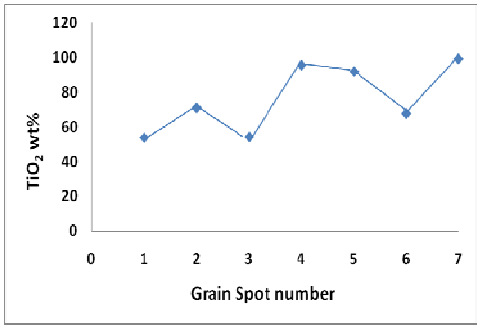

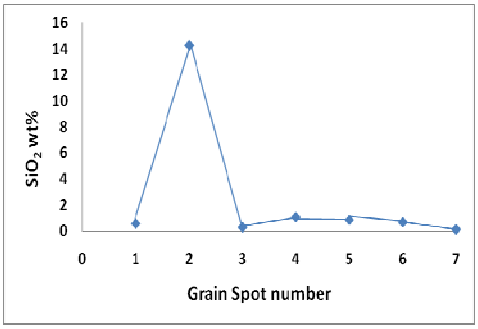

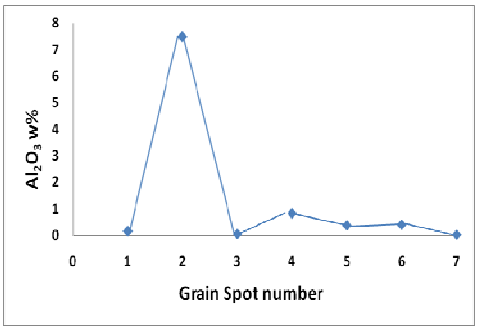

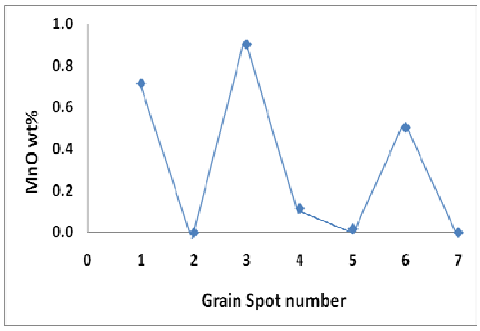

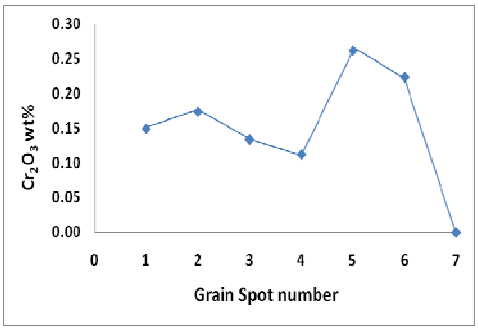

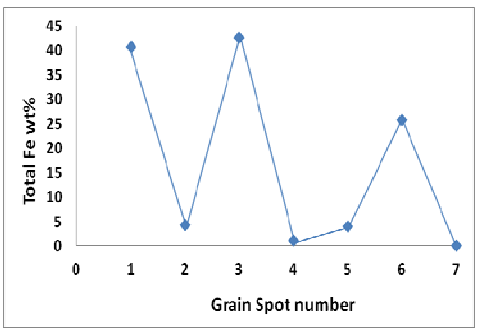

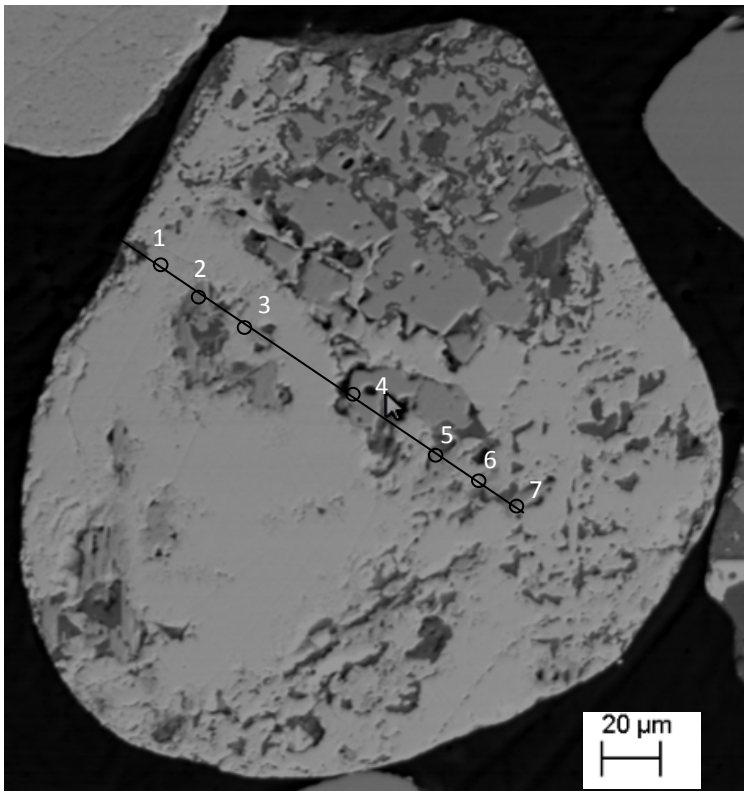

Figure 6.12. Chemical traverse across a Rietfontein altered ilmenite grain. Ilmenite alteration corresponds to the 1st and 2nd stages of Type I alteration of Hugo and Cornell (1991).

6.3 Alteration index

The alteration phases were identified and quantified by QEMSCAN as a percentage of altered ilmenite grains. From this data an alteration index, expressed in percent, was compiled and is expressed by the formula $\frac{Alt-Ilm+Lcx}{\sum Ilm+Lcx}$ where $\sum$ ilm is the sum of the alt-Ilm (altered ilmenite), unalt-Ilm (unaltered ilmenite) and Mn-Ilm (manganese ilmenite). Alt-Ilm indicates percentage altered ilmenite per THM. Leucoxene appears on both sides of the equation to express the equation as a percentage, i.e. to get 100%. The calculation of the alteration index is based on chemistry. QEMSCAN identifies alteration by analyzing 2 μm chosen particles or grains on a specified grid. The beam analyzes the whole particle. Within each grain it then identifies all the alteration phases with > 53 wt % TiO_2 as well as the unaltered ilmenite phases. It then calculates the masses of each of these alteration phases, sums it and divides it by the total mass of the Fe-Ti oxides to give the alteration index. The Fe-Ti oxide minerals include magnetite, titanomagnetite, unaltered ilmenite, hydrated ilmenite, pseudorutile, leucoxene and anatase (> 95% TiO_2)(Philander pers comm).

The proportions of ilmenite and its alteration products as well as the alteration index (percentage of altered grains) calculated by QEMSCAN, are presented in Appendix D. From the data it is clear that most of the ilmenite occur as homogeneous, unaltered grains. This is supported by the petrographic observations under the microscope.

The average alteration indices for each area was calculated in excel and are also presented in Appendix D. The latter represents the average of the alteration indices of all the samples in a specific satellite area. On average 24% of the total ilmenite grains of Houtkraal Remainder Portion 2 are altered, 20% of Houtkraal Remainder, 22% of Geelwal Karoo, 22% of Graauwduinen and 23% of Rietfontein ilmenite are altered (Table D, Appendix D and Table 6.1). All five areas have more or less similar alteration indices. The low percentage of altered ilmenite grains of the five satellite areas is due to the dry to semi-arid conditions that existed during the Pliocene and Pleistocene times along the west coast of South Africa (Hendey, 1981; Tankard et al, 1982). The drier conditions limited the extent and amount of ilmenite alteration that took place. More moist or wetter climatic conditions and thick plant cover would have enhanced alteration as is evidenced in THM concentrations from tropical areas.

Cilliers (1995), Macdonald (1996) and Philander (1999) found the same alteration products (hydrated ilmenite, pseudorutile and leucoxene) in their study areas. Philander (1999) found lower alteration index averages (Table 6.1) for the Kleinzee area's ilmenite. Cilliers (1995) and Macdonald (1996) did not calculate an alteration index for their study areas. The higher percentage of altered ilmenite of the five satellite areas in comparison with Kleinzee can be due to the fact that the satellite samples are surface samples that were leached by a more acidic fluid derived from the upper soil layers. The upper soil layers usually have a higher acidity than the lower layers. The higher leucoxene content can also be verified by the near surface location of the samples since leucoxene formation takes place in the near surface environments/ uppermost soil layers of a deposit.

The alteration index of the five satellite areas are the same as that for the Namakwa Sands deposit indicating that it underwent the same degree of ilmenite alteration because of similar climatic conditions (Table 6.1). Data for the Namakwa Sands deposit (East Mine and West Mine) were obtained from Namakwa Sands mine and were also calculated by means of QEMSCAN (Philander pers comm).

Table 6.1. Alteration index averages of the satellite areas, Namakwa Sands deposit and Kleinzee heavy mineral sands.

Area	**Alteration Index (%)**
Houtkraal Remainder Portion 2	24
Houtkraal Remainder	20
Geelwal Karoo	22
Graauwduinen	22
Rietfontein	23
East Mine	22
West Mine	20
Kleinzee (BMC)	7
Kleinzee (BIC)	8
Kleinzee (KNC)	8
Kleinzee (Palaeochannels)	13
Kleinzee (Rivers)	5

6.4 Discussion

The above observations indicate that that alteration of the five satellite areas occurred via the mechanisms postulated by Grey and Reid (1975) and Hugo and Cornell (1991). Cilliers (1995), Macdonald (1996) and Philander (1999) also stated that the ilmenite of their study areas follow the alteration mechanism of Grey and Reid (1975) and in part that of Hugo and Cornell (1991). The altered areas within the ilmenite grains are porous and consist of mixtures of hydrated ilmenite, pseudorutile, leucoxene, hematite and rutile*. This in turn indicates incomplete alteration. The whole spectrum of ilmenite alteration products is present. This is supported by the chemistry in Table F18, (Appendix F). Grains corresponding to Type I, II and Type III alteration of Hugo and Cornell (1991) were observed.

The geochemical traverses confirm literature data that ilmenite alteration is marked by enrichment in titanium and removal of iron. As titanium increases, iron decreases. MnO and MgO also decrease with increasing alteration. SiO_2 and Al_2O_3 do not follow a particular pattern with increasing alteration.

Some well rounded grains display alteration along grain edges and margins indicating that in-situ (after deposition) alteration took place (Figure 6.4 D). Another example of in-situ alteration is the presence of the needle-like voids in Figure 6.1 A. These dissolution features are not expected to survive transportation and are clearly secondary features.

Ilmenite alteration in the satellite areas was achieved by a multi- stage alteration model. Evidence for this is the presence of ilmenite altered to various stages such as hydrated ilmenite, pseudorutile and leucoxene.

The wide spectrum of ilmenite alteration products conforming to the Type I and Type II alteration models of Hugo and Cornell (1991) indicates that alteration took place before deposition. In-situ alteration products will be restricted to areas that are conducive to produce such in-situ altered grains (Pownceby, 2010). The presence of unaltered and altered ilmenite can also be explained by alteration during transport.

In conclusion the alteration of ilmenite from the five satellite areas was the result of a multi-stage alteration model through the weathering of ilmenite-bearing source rocks before deposition, during the final stages of deposition and transportation as well as after deposition (in-situ). The ilmenite altered after deposition was mixed together, during reworking, with the

ilmenite altered before deposition. Ilmenite alteration per area is not uniform since the extent of alteration varies from grain to grain (Rao et al, 2005).

Ilmenite alteration is important for this study since the degree and type of alteration influences the recoverability of altered ilmenite grains. The magnetic susceptibility of ilmenite decreases with increasing alteration (Grey et al, 1983 and Temple, 1966). Some altered ilmenite may therefore report to the non-magnetic concentrates of the plant. Leucoxene has high or the highest SiO_2 and Al_2O_3 contents and may report to rutile concentrates (Hugo and Cornell, 1991). The latter two elements are considered impurities and negatively affect recovery. Leucoxene also degrades rutile product quality and influences rutile recovery negatively. Leucoxene is therefore an undesirable mineral and is itself difficult to recover.

CHAPTER 7 PROVENANCE INDICATORS OF THE SATELLITE DEPOSITS

7.1 Introduction

The path of heavy minerals from source rocks to deposition region are modified and affected by various controlling factors such as hydrodynamic sorting, chemical and mechanical weathering, diagenesis and transport. These, in turn, are controlled by factors such as time, transport distance, climate, energy and topography. The composition of sediments formed, are controlled by factors such as the mineralogy and composition of the source rocks.

The aim of provenance studies is to determine the nature of these source rocks. Heavy minerals are useful indicators for provenance, petrologic identity and correlation of sands, sandstones and other sedimentary rocks and sediments due to its restricted parageneses and large compositional range. The larger the diversity of a heavy mineral assemblage, the more accurately the provenance of the sediments can be reconstructed (Mange and Wright, 2009). Its usefulness is restricted by its sensitivity to processes such as diagenesis (intrastratal solution) and hydraulic sorting which leads to the formation of a deposit that does not reflect the actual provenance of its source rocks (Rittenhouse, 1943). Intrastratal solution (dissolution process that takes place in deep burial environments under the effects of percolating ground waters, Morton, 1984) is considered the most significant factor affecting the heavy mineral content in sands and sandstones (Krawinkel et al, 1999). It removes diagnostic, but unstable minerals and gives rise to the growth of secondary minerals (clays). In the case of e.g. Fe-Ti oxide minerals (FTM) important provenance indicators such as Mn, Mg and Ti may be leached out. The above processes however do not always obliterate indicators of provenance.

Provenance may influence the petrographic textural relationships of composite grains and chemical composition of economic minerals. Provenance analysis is only regarded as satisfactory if above processes have not occurred and knowledge of the conditions necessary for preservation of the minerals and its chemical stability are available, otherwise the original nature of the heavy mineral suite is difficult to determine. Unstable minerals such as pyroxene, epidote and hornblende are moderately to extremely susceptible to diagenesis and are removed by weathering and can therefore lead to misinterpretation of the source rocks.

To overcome these problems, some authors (Darby and Tsang, 1987; Morton, 1985) proposed the geochemical element analysis of a single mineral species called varietal studies. It involves using micro-analysis equipment (e.g. SEM) to determine the composition of a particular species in a heavy mineral assemblage. In doing so, the effects of secondary modifying processes are minimized.

The varietal study method has since been extended to include heavy minerals such as tourmaline (Krynine, 1946; Henry and Guidotti, 1985; Henry and Dutrow 1992), zircon (Owen, 1987; Hoskin and Ireland, 2000), amphibole (Mange-Rajetzky, 1981; Mange-Rajetzky and Oberhansli, 1982; Ganssloser et al, 1996; Schafer 1997), garnet (Morton, 1984, 1985, 1987; Morton et al, 2002; Copjakova et al, 2005), apatite (Belousova, 2002; Morton and Yaxley, 2007); ilmenite (Basu and Molinaroli, 1991; Grigsby, 1991; Darby, 1994; Bhattacharyya et al, 1997; Hedge 2006) and pyroxene (Cawood, 1991; Morton, 1991; Krawinkel et al, 1999).

Due to the presence of provenance diagnostic minerals such as rutile, zircon, tourmaline, ilmenite and garnet which are stable during diagenesis, erosion and weathering, provenance studies can be applied to the Namakwa Sands heavy mineral satellite deposits and surroundings. Provenance was based on the heavy mineral chemistry. Heavy mineral grains do not show extreme or significant weathering and it is therefore assumed that intrastratal solution did not play a significant role in modifying the chemical composition of the heavy mineral assemblages. The satellite areas occur in arid to semi-arid climatic conditions and the effect of chemical weathering is minor to negligible as was indicated by the alt-index of ilmenite (chapter 6). Garnets for example are more stable than apatite and since apatite is present in the assemblage, garnets can be used for provenance studies. The same applies to tourmaline which is more stable than epidote, pyroxene and amphibole. For this study, only unaltered homogeneous grains have been considered for provenance determination.

7.2 Varietal studies

7.2.1 Ilmenite

Ilmenite can be used as a useful provenance indicator due to its chemical stability, abundance in nature, variation in element content and ease of separation with magnetic techniques. It occurs in a wide range of rock types that includes both extrusive and intrusive igneous rocks, metamorphic rocks such as metapelitic and metabasic rocks, vein rocks and pegmatites (Ramdohr, 1980; Darby and Tsang, 1987). Darby (1984) showed that ilmenite content and the variability in the content are very useful in interpreting provenance. Grigsby (1991) stated that detrital ilmenite grains retain unique chemical signatures (e.g. MnO > 2% is indicative of grains derived from felsic igneous rocks) in felsic and mafic daughter sediments that can be used in provenance studies.

Two approaches in determining ilmenite provenance, in general, have been used so far by workers. Workers (Darby and Tsang, 1987; Grigsby, 1991) used chemical compositions of the ilmenite to identify the sources whereas other studies (Basu and Molinaroli, 1989; Darby and Bischof, 1996; Buddington and Lindsley, 1964) made use of the petrographic characteristics of the Fe-Ti oxide minerals.

Basu and Molinaroli (1989) did a study on Fe-Ti oxide minerals (FTM) from the Rocky Mountain region and from the Appalachian Mountains. For provenance determination they used three criteria (1) presence of exsolution texture (2) the number of crystallographic orientation of the exsolution lamellae and minimum lamellae widths and (3) chemical composition and minor elements of the detrital opaque Fe-Ti oxide minerals (Basu and Molinaroli, 1989). For this study only the chemical composition (major and trace elements) of the ilmenite grains were used as a provenance indicator due to the ease of this method.

Basu and Molinaroli (1989) found that a higher abundance and narrow range of TiO_2 characterize metamorphic source rocks (40% - 55%) with a mode around 52% and a wider range and lower abundance characterizes igneous rocks (30% - 60%) with a mode around 47%. Bivariate plots of TiO_2 vs MgO revealed that > 0.5% MgO is only found in plutonic igneous rocks.

TiO_2 histograms were plotted for the five satellite areas of this study and for the Namakwa Sands deposit. The five satellite areas all show unimodal TiO_2 histograms and similar TiO_2

ranges (Figure 7.1). The similar TiO_2 ranges indicate a similar provenance area for the five satellite areas. Houtkraal Remainder Portion 2, Graauwduinen and Rietfontein have a modal class of 50 wt % TiO_2 and Houtkraal Remainder and Geelwal Karoo a modal class of 49 wt % TiO_2. According to Basu and Molinaroli (1989) these modal class values and wide TiO_2 ranges (45-60 wt %) indicate a mixed source with igneous rocks as the principal source and minor metamorphic rocks as possible source for the ilmenite.

The Namakwa Sands (NS) deposit also shows a unimodal TiO_2 histogram with a modal class of 52 wt % (Figure 7.1). Its TiO_2 range is narrower (50-54 wt %) than that of the satellite areas. This difference in modal classes and TiO_2 ranges between the satellite areas and the Namakwa Sands deposit can be due to a difference in source rock ratios. The narrower TiO_2 range and the 52 wt % modal class value of the Namakwa Sands deposit indicates metamorphic rocks with a subordinate igneous component as the main source for the Namakwa Sands deposit. Cilliers (1995) proposed the metamorphic and igneous rocks of the Namaqualand Metamorphic Complex (NMC) as a probable source for the ilmenite of the Namakwa Sands deposit.

The average MgO content of all five the satellite areas is below 0.5% and according to Basu and Molinaroli (1989) the ilmenite of the satellite areas is therefore derived from both igneous and metamorphic source rocks.

Grigsby (1991) found in his study on Holocene sands that igneous rocks have a wide range in TiO_2 content (40-52%) and that MgO, MnO and V_2O_5 can be used as discriminates to distinguish between igneous rocks. Felsic and intermediate igneous rocks show a wide range in TiO_2 content of (48±2%) and (48±3%) respectively. Mafic igneous rocks however show a more narrow range (50±1%) and a higher TiO_2 content. MgO > 1.5% characterize intermediate and mafic sources, V_2O_3 > 0.5% mafic rocks and MnO > 2% characterizes felsic rocks. These conclusions also correspond to the findings of Mathison (1975); Haggerty (1976a and b) and Whalen and Chappel (1988).

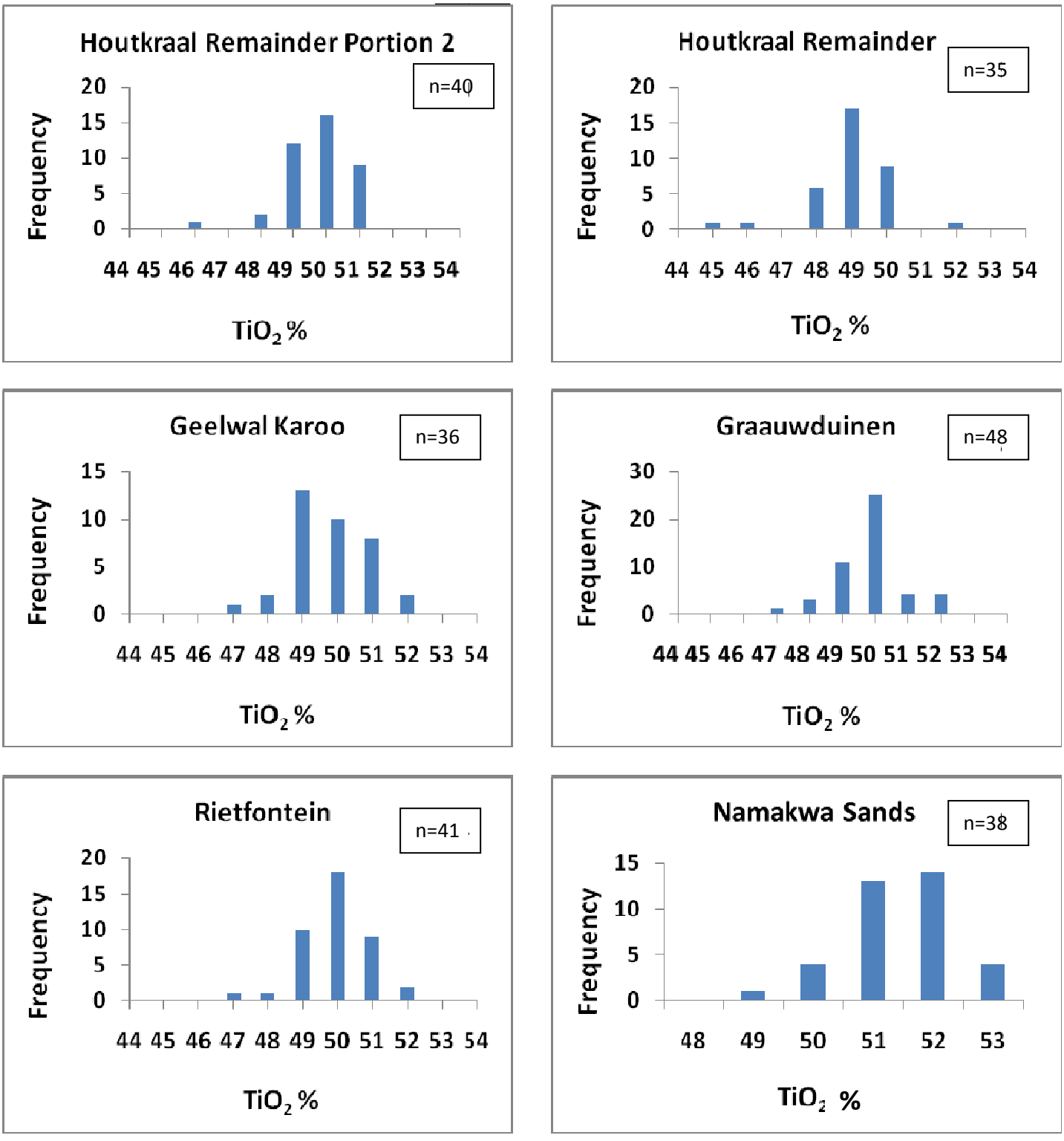

Figure 7.1. Distribution of TiO_2 content of unaltered ilmenite from the five satellite areas. The TiO_2 modal class values and wide TiO_2 ranges indicate that ilmenite from the satellite areas are mainly derived from igneous rocks with a minor contribution from mafic igneous rocks.

Houtkraal Remainder Portion 2 and Houtkraal Remainder have a TiO_2 content range of between 45 and 51 wt %. Geelwal Karoo has a TiO_2 content range of between 47 and 53 wt %, Graauwduinen between 47 and 52 wt % and Rietfontein between 46 and 51 wt % (Table F1 and F2, Appendix F). On the basis of above inference, the TiO_2 content ranges of the satellite areas suggest that the ilmenite grains of the two Houtkraal areas and Rietfontein were mainly derived from felsic and intermediate igneous rocks and Geelwal Karoo and Graauwduinen from mafic igneous rocks. TiO_2 vs MgO and TiO_2 vs MnO binary diagrams (Figure 7.2) of the five satellite areas indicate that most ilmenite have MgO contents less than 1.5 wt % and may suggest metamorphic rocks as a source. Most ilmenite has less than 2 wt % MnO and may also be derived from metamorphic rocks. Ilmenite grains with > 2 wt % MnO are derived from felsic igneous rocks. All the satellite areas except Houtkraal Remainder have > 0.5 wt % V_2O_5 and are derived from mafic rocks.

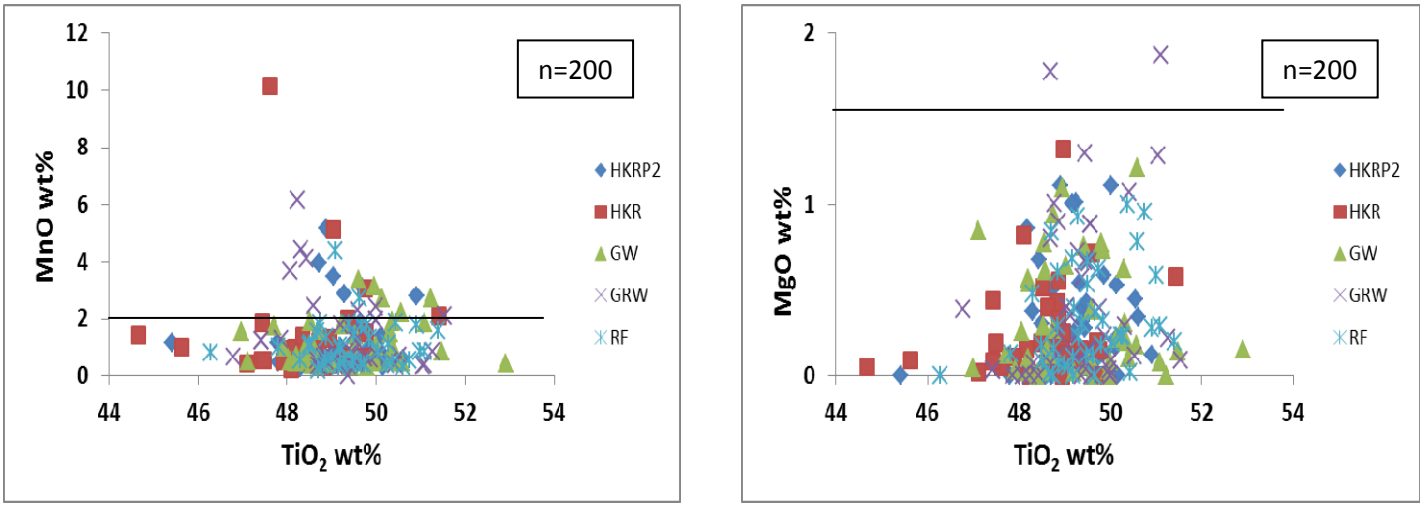

Figure 7.2. Binary diagrams of MgO wt % and MnO wt % versus TiO_2 wt % in unaltered ilmenite from the five satellite areas. Ilmenite with MgO contents < 1.5 wt % is derived from metamorphic rocks. Ilmenite with < 2 wt % MnO is also derived from metamorphic rocks.

Deer et al (1992) mentioned that Mn-rich ilmenite is derived from granitic igneous rocks. The ilmenite of the satellite areas is Mn-poor but also Mg-poor and may indicate metamorphic rocks as a possible source.

Hugo (1993) constructed a MgO-MnO binary diagram for the ilmenite of Richards Bay Minerals and considers it a good provenance indicator. He plotted the MnO and MgO values

of ilmenite from known source rocks (Kaap Igneous Province and the Namaqua-Natal Basement) and in so doing determined the different source rock fields.

Figure 7.3 indicates that ilmenite from the satellite areas and that of the Namakwa Sands deposit mainly occupy the mafic igneous and metamorphic rocks field. Only a few ilmenite grains plot in the felsic igneous and metamorphic rocks field. A few ilmenite grains plot in the transitional field.

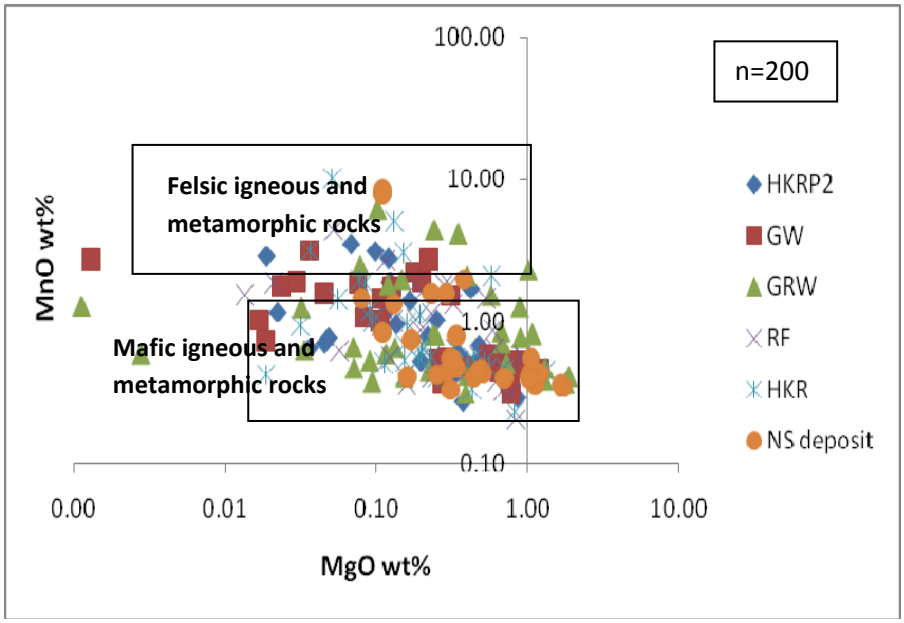

Figure 7.3. MgO-MnO provenance discrimination diagram. The outline boundaries separate ilmenite compositions related to whole rocks from the Namaqua-Natal Basement and Kaap Igneous Province (Hugo, 1993). X and Y scales are plotted as log scales. Ilmenite is derived mainly from mafic igneous and metamorphic rocks with a small contribution from felsic igneous and metamorphic rocks.

Elements like Cr and V indicate basic to gneissic sources (Hedge et al, 2006). These elements are preferentially incorporated in basic rocks during crystallization and hence, ilmenite in these rocks incorporates them more than those in acidic rocks. The titanium content of igneous rocks decreases with silicon content (Sukumaran and Nambiar, 1994). Basic rocks can therefore contain more ilmenite than acidic rocks and ilmenite of basic rocks can incorporate more Cr and V (Sukumaran and Nambiar, 1994).

The V content of all ilmenite grains from the five satellite areas are high and vary between 551 ppm and 13759 ppm (Table F1 and F2, Appendix F). These high V concentrations

indicate that the ilmenite is derived from basic rocks. A few ilmenite grains have no V in its structure and are derived from acidic rocks. Cr content of all five satellite areas are presented as histograms in Figure 7.4. The majority of ilmenite has less than 100 ppm of Cr. Only a few ilmenite grains have high Cr concentrations (> 200 ppm). The low Cr content (< 200 ppm) indicates ilmenite derived from acidic rocks and the high Cr content (> 200 ppm) indicates ilmenite derived from basic rocks.

Igneous and metamorphic rocks containing ilmenite are present in the proximal NMC (Jack, 1980; Kroner, 1973; De Beer et al, 2002). These authors reported on the presence of iron oxides (ilmenite, hematite and magnetite) in aluminous gneisses and schist, mafic granulites, amphibolites and granites in the NMC. The NMC can therefore be considered a provenance area for the ilmenite of the satellite areas.

In conclusion the chemistry of the ilmenite of the five satellite areas indicate a mixed provenance with mainly metamorphic rocks, supported by an igneous (mafic and felsic) suite and intermediate igneous rocks possibly of the NMC.

7.2.2 Zircon

Zircon is a common accessory mineral in igneous rocks such as Na-rich plutonic rocks, granites, pegmatites, metamorphic rocks and in many types of sediment. Hubert (1962) proposed a ZTR (zircon-tourmaline-rutile) index as a measure of mineralogical maturity of a sedimentary deposit (Fedo et al, 2003). Due to its stable nature, detrital zircons can survive multiple sedimentary, transport and weathering cycles, anatexis, high temperature metamorphism and therefore does not reflect its ultimate (rocks in which zircon originally crystallized) source rocks.

Zircon therefore proved to be more useful in determining whether one sand is petrogenetically related to one another. Correlation of sandstone bodies using its heavy mineral content, such as zircon, is also a common technique used in petrology. One feature of zircon that is known to be useful in deciphering ultimate parent rocks is zircon shape. Rounded shapes are characteristic of zircons in sedimentary rocks and euhedral shapes in igneous rocks. Processes such as magmatic resorption may however cause rounding in igneous rocks.

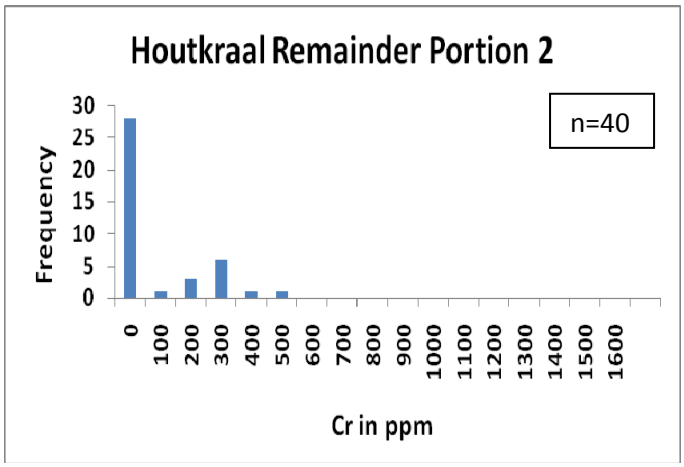

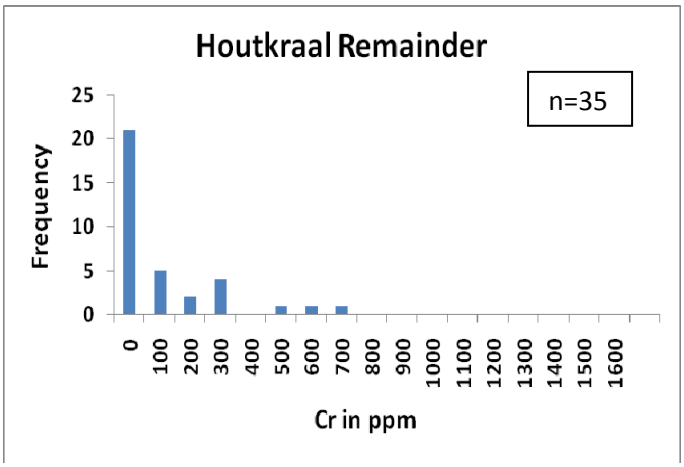

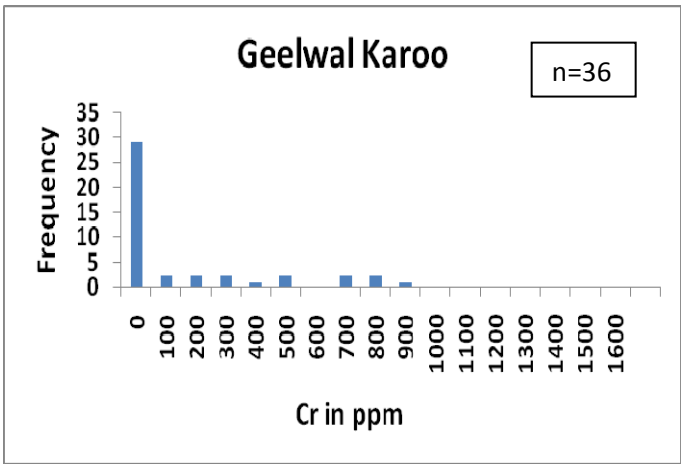

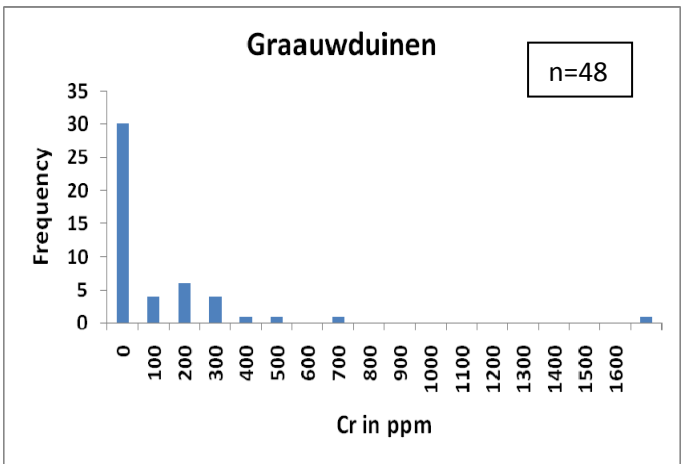

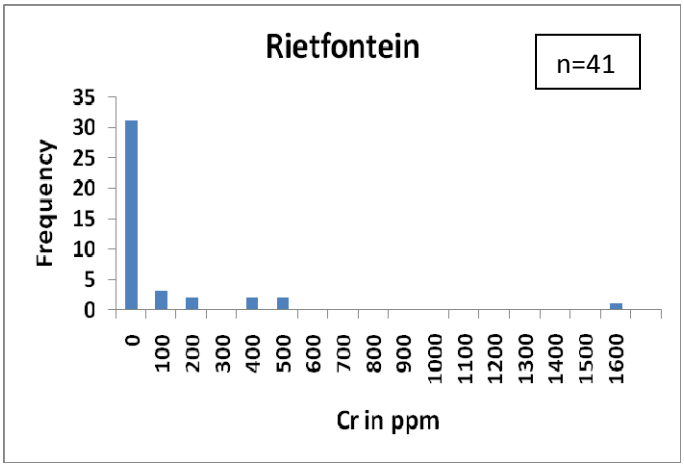

Figure 7.4. Histograms of Cr content in unaltered ilmenite grains from the five satellite areas. Most ilmenite is derived from acidic rocks (Cr contents < 200 ppm).

Generally hafnium is present in variable amounts in zircon with an Hf/Zr ratio around 0.02-0.04 (Deer et al, 1992) with a Hf wt % between 0.6 and 3.0%. Owen (1987) showed that Hf content can be used as a provenance indicator by plotting Hf content as a frequency distribution diagram. The shape of the distribution of values about the mean and the mean itself reflects the variety of zircon populations present. A unimodal Hf distribution indicates a single Zr population or a single source and a bimodal distribution reflects two petrogenetically related zircon populations or two sources. Owen (1987), however, did not propose any source rocks for the zircon populations.

When plotting the Hf data of the five satellite areas as a frequency distribution diagram (Figure 7.5), a unimodal distribution is evident for all five areas indicating a single source. Cilliers (1995), Macdonald (1996) and Philander (1999) also found a single primary source for the zircons in their respective study areas. Philander (1999) showed that the zircons from Graauwduinen, Geelwal Karoo and Kleinzee have identical HfO_2 modal classes (1.2-1.4 wt %) and narrow distributions, indicating a uniform source terrain, namely the NMC. Rietfontein and Graauwduinen have HfO_2 modal classes of between 1.2-1.4 wt %. Geelwal Karoo and Houtkraal Remainder Portion 2 have a modal class of between 1.6-1.8 wt % HfO_2 and Houtkraal Remainder have a HfO_2 modal class of between 1.4-1.6 wt % (Figure 7.5). All five satellite areas have narrow distributions similar to the Namakwa Sands (NS) deposit.

The similar HfO_2 modal classes of Rietfontein and Graauwduinen with the Namakwa Sands deposit indicate that it has the same source terrain. Cilliers (1995) proposed the rocks of the NMC as a likely source for the zircon of the Namakwa Sands deposit. In chapter 5, section 5.4.2 it was shown that the zircon grains of the satellite areas have the same chemistry as the zircon of the Namakwa Sands deposit. The similar chemistry indicates a similar source terrain. Geelwal Karoo, Houtkraal Remainder and Houtkraal Remainder Portion 2 therefore also have the same source terrain as Rietfontein, Graauwduinen and the NS deposit. The higher HfO_2 modal values of the former three satellite areas can possibly be attributed to a difference in source rock ratios or can be due to sorting. Higher Hf values have been reported in pegmatite due to increasing differentiation of the granite. The higher HfO_2 modal classes of Geelwal Karoo, Houtkraal Remainder and Houtkraal Remainder Portion 2 can therefore be due to an input from more pegmatitic rocks. Geelwal Karoo has a wide distribution indicating an input from a wider variety of source rocks than the other areas.

Unaltered igneous zircon has a REE pattern that is characterized by a steeply rising slope from the LREE to the HREE with a negative Eu-anomaly and positive Ce-anomaly (Hoskin and Schaltegger, 2003). The five satellite areas have such REE patterns and are therefore igneous in nature and are derived from igneous rocks.

Belousova et al (2002) studied zircon by means of electron microprobe and LA-ICP-MS in a range of igneous rock types which include kimberlites, lamproites, basalts, carbonatites, dolerite, granitoids, syenitic rocks, syenite pegmatites and nepheline-syenite pegmatites. They found that trace element abundances in zircon are sensitive to source rock types. The zircon grains from the different rock types reveal distinctive elemental abundances for the specific rock types. Trace element abundances increase from ultramafic through mafic to granitic rocks and pegmatites (Belousova et al, 2002). They represented the geochemical signatures, characteristic of the zircon from the different rock types, by means of bivariate discriminant diagrams. They found that Ti concentrations range from a few tens of ppm in kimberlites, dolerite and carbonatites to 500-700 ppm in zircon from granites and syenites (Belousova et al, 2002). Granites are characterized by high concentrations of Mn (10-700 ppm) whereas the other rock types have Mn concentrations below the detection limit (2-5 ppm). Metamict zircon have up to 1000 ppm of Mn. Hf is most enriched in granitoids and pegmatites and least enriched in syenites. Higher Hf values are characteristic of metamict zircon. Y is the least enriched in kimberlites where it rarely exceeds tens of ppm and is the most enriched in granitoids and pegmatites where it occurs in contents of 100 to 1000 ppms and up to the percent level.

Phosphor ranges from 20 to 110 ppm in kimberlites and occurs in concentrations of hundreds to thousands of ppm in zircon from granitoids and may reach percent levels in metamict zircon. Low U (6-60 ppm) and Th (2-15 ppm) contents are characteristic of kimberlites and the highest concentrations (hundreds of ppm to percent level) are present in carbonatites, granitoids and pegmatites. REE concentrations are the highest in granitoids and pegmatites (tens to several tens of thousands of ppm to percent level). Slightly lower REE contents of 100 to 2000 ppm are present in mafic rocks (basalt and dolerites). Carbonitites have < 700 ppm of REE and kimberlites are characterized by less than 50 ppm of REE.

Bivariate discriminant diagrams of Y vs Hf, REE+Y vs P, Th vs Y and U vs Y were plotted for this study to determine the source rock types of the zircon of the five satellite areas.

The Y vs Hf diagram of all five satellite areas indicate that Y ranges from > 100 ppm up to 4600 ppm and the zircon grains are therefore derived from syenites, larvikite, granitoids and pegmatites (Figure 7.6). The > 1.5 wt % Hf indicates granitoids and pegmatites as possible source rocks. For all five satellite areas phosphor occurs in concentrations of 100 to 1000 of ppms and the sum of the REE+Y in concentrations of 1000 ppms (Figure 7.6). These concentrations indicate syenites, granitoids, larvikite and pegmatites as possible sources for the zircon. The U vs Y diagrams indicate that for all five areas, except Houtkraal Remainder, U occurs in concentrations of 10 to 1000 of ppms (Figure 7.6). Houtkraal Remainder has U contents in the order of 10 to 100 of ppms. Y is present in contents of > 100 ppm and possible source rocks are lamproite, dolerite, larvikite and granitoids. The Th vs Y diagram of all five areas indicates that Th is present in the order of 10 to 100 to 1000 of ppms (Figure 7.6). A few zircon grains have less than 10 ppm of Th. Y contents are > 100 ppm and likely source rocks include lamproite, dolerite, larvikite and granitoids and pegmatites. The zircon grains with less than 10 ppm of Th have a kimberlitic source.

Ti histograms of the satellite areas all show peaks at 500 ppm except for Geelwal Karoo that has a peak at 700 ppm. According to Belousova et al (2002), these zircons with Ti contents between 500 and 700 ppm have granites and syenites as source rocks. Zircon with Ti contents > 700 ppm can probably be ascribed to pegmatites.

Mn histograms of the zircon grains from the five satellite areas show peaks at 20 ppm. Mn content ranges between 20 ppm and 260 ppm and therefore indicates granites as source rocks.

From above evidence it can be concluded that the zircon grains from the satellite areas were derived from a single granitic source terrain presumably the NMC.

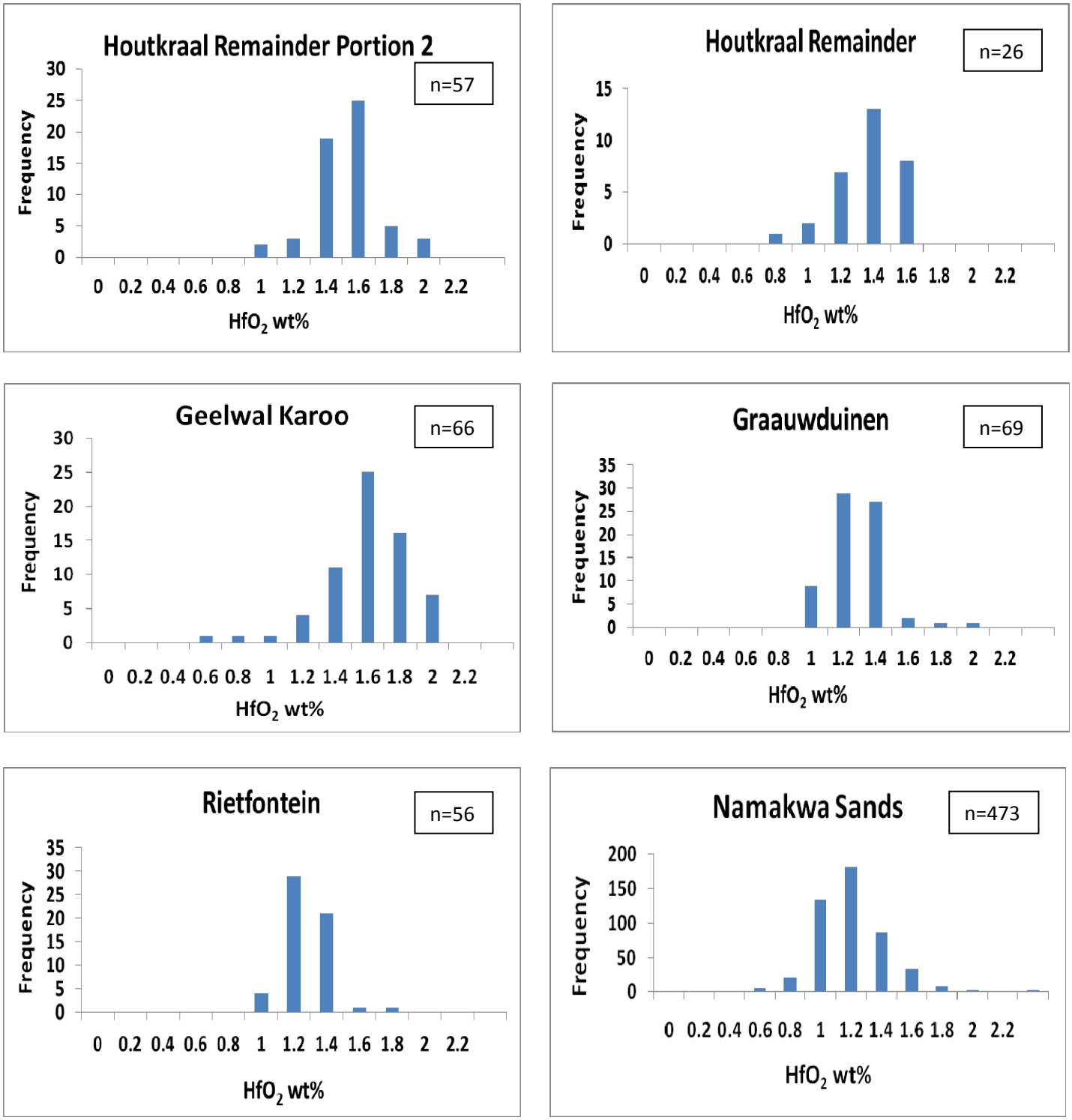

Figure 7.5. Histograms of Hf content in zircon grains from the five satellite areas. All five satellite areas have a unimodal Hf distibution indicating a single source.

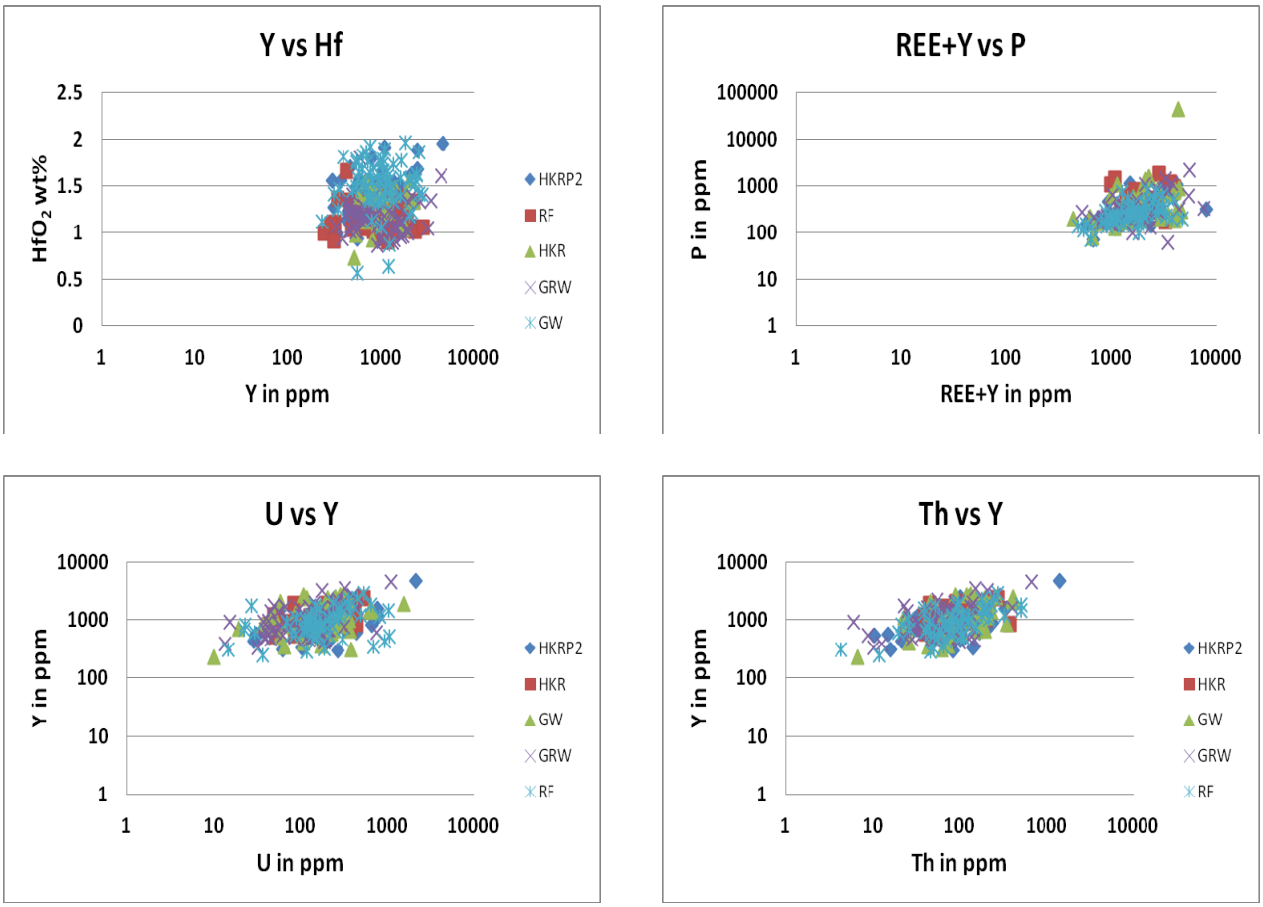

Figure 7.6. Bivariate discriminant diagrams of the trace elements chemistry of zircon for the five satellite areas (diagrams after Belousova et al, 2002). n=267 for all four diagrams. Zircon has a mainly granitic source.

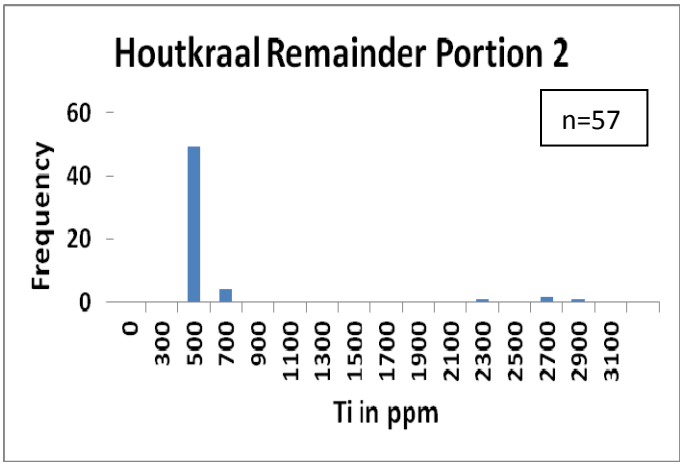

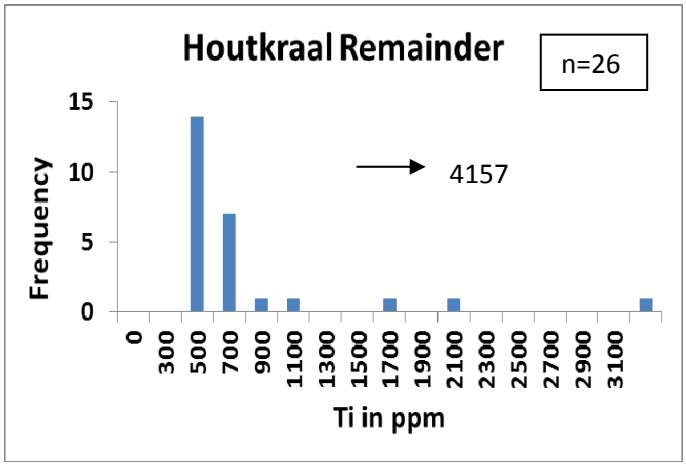

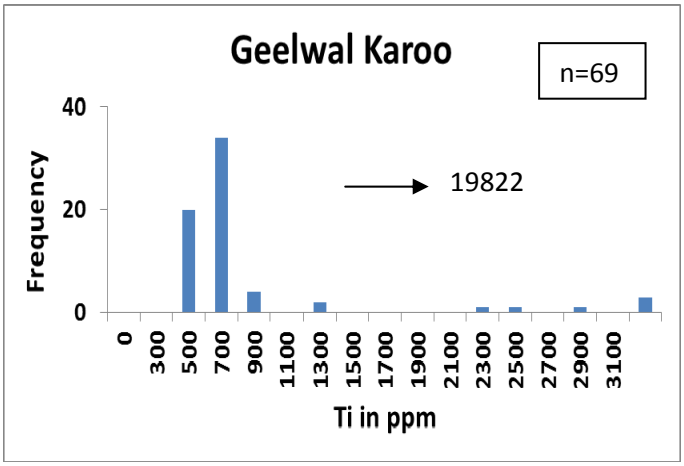

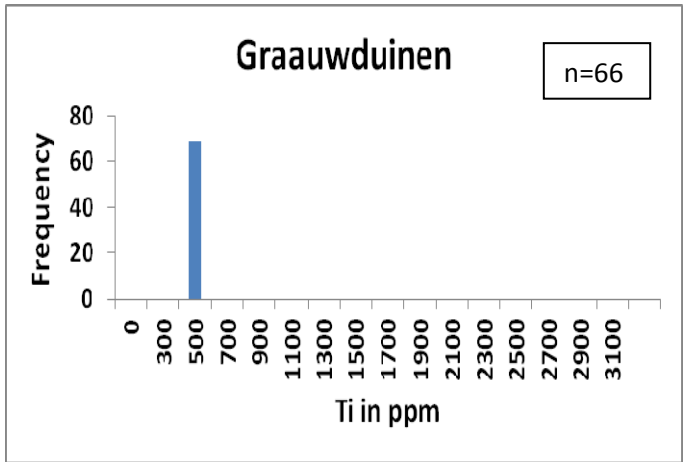

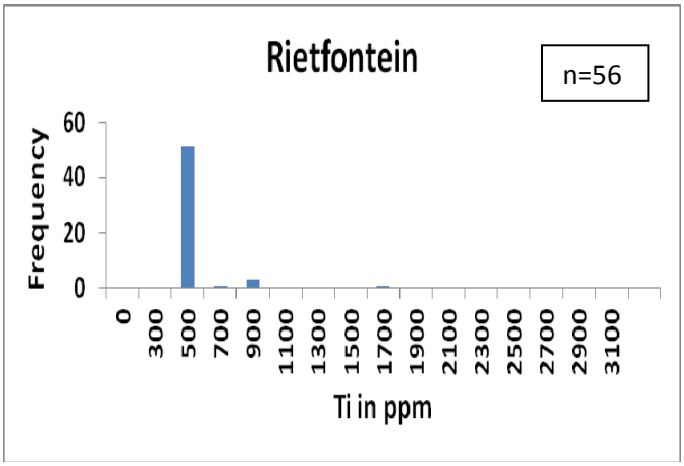

Figure 7.7. Histograms of Ti content in zircon grains from the five satellite areas. Most zircon is derived from granites and syenites (Ti contents between 500 and 700 ppm) with the rest of the zircon being derived from pegmatites (Ti contents > 700 ppm).

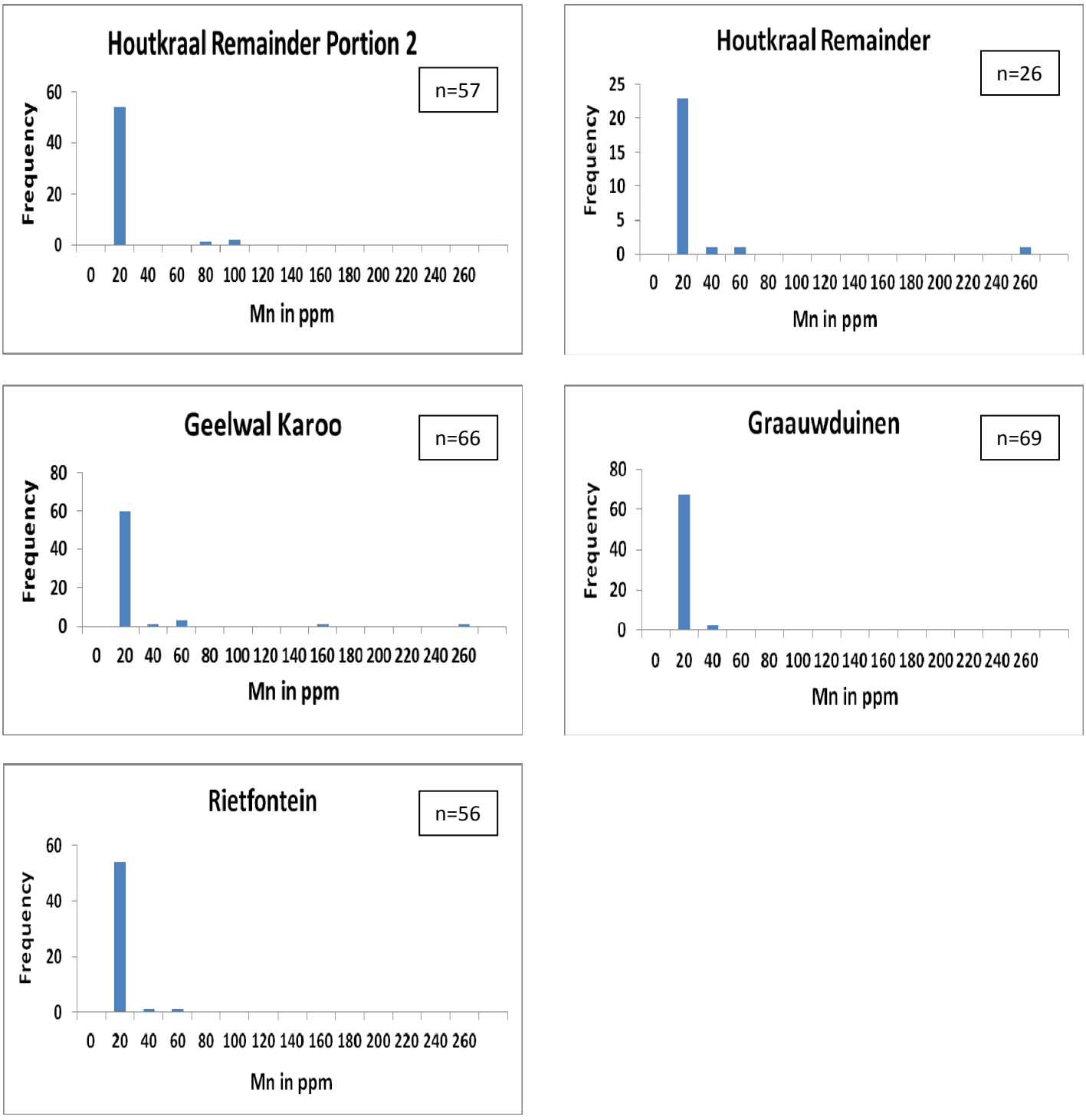

Figure 7.8. Histograms of Mn content in zircon grains from the five satellite areas. Mn content of zircon ranges between 20 and 260 ppm and indicates granites as possible source rocks.

7.2.3 Rutile

Rutile is stable over a wide range of geological conditions and consequently occurs in medium to high-grade metamorphic rocks (eclogites and amphibolites), sediments, hydrothermal ore deposits and metamorphosed limestones and lesser in low-grade metamorphic and igneous rocks (Deer et al, 1992). In low-grade rocks, titanium is present in mineral phases such as hornblende, biotite and sphene. Large rutile grains are restricted to quartz veins and granite pegmatites. Rutile, zircon and tourmaline are among the most stable heavy minerals during diagenetic and sedimentary processes (Hubert, 1962; Morton and Hallsworth, 1999; Zack et al, 2004b). It is chemically and physically stable and therefore contains information about its source rocks even after significant burial to extreme depths and in mature sediments.

Provenance of rutile can be determined by (1) making use of the Zr-in-rutile thermometer (Zack et al, 2002, 2004a, b; Stendal et al, 2006; Watson et al, 2006; Ferry and Watson, 2007; Tomkins et al, 2007; Meinhold et al, 2008; Triebold et al, 2007) to determine source rock temperatures or (2) using the trace element contents of detrital rutile to determine source rock lithology. Nb and Cr contents of rutile grains are used to determine the source rock lithology. Metabasites (mafic) and metapelites (felsic) are the most important source rocks (Frost, 1991) for rutile and imprint a distinct Nb and Cr signature in rutile (Zack et al, 2004b). Rutile derived from mafic rocks has high Cr and low Nb contents (Nb < 900 ppm). Metapelites have low Cr (< 1000 ppm) and high Nb (900-2700 ppm) contents. Nb > 2700 ppm indicates felsic granulites or intrusives (Zack et al, 2004b). Larger than 10000 ppm of Nb and/or Cr indicates rutile derived from kimberlite and > 10000 ppm of Sb, Nb, Sn, W and/or V indicates mineral deposits. Fe indicates a metamorphic origin and metamorphic rutile usually has Fe > 1000 ppm (Zack et al, 2004b; Meinhold et al, 2008).

Cr and Nb contents of the rutile of this study exhibit higher Cr and Nb contents than suggested for classification by Zack et al (2004b) into pelitic and mafic source rocks. Therefore the log (Cr/Nb) vs T (°C) diagram of Triebold et al (2007) was used for source rock classification (Figure 7.9). Temperatures were calculated using the thermometer of Watson et al (2006) and is explained later in the text. Triebold et al (2007) calculated log (Cr/Nb) ratios to differentiate between metapelitic and metamafic source lithologies. They plotted the log ratio against temperature to determine high- and low temperature populations

for the metapelitic and mafic sources. They found that metamafic and metapelitic rocks are perfectly separated by the 0-line in log Cr/Nb.

Nb and Cr systematics of the satellite areas

The Cr and Nb contents of each of the five satellite areas and the Namakwa Sands deposit were plotted on the log (Cr/Nb) vs calculated temperature diagram of Triebold et al (2007) (Figure 7.9). The log (Cr/Nb) vs temperature diagrams indicate metapelitic rocks to be the dominant source rocks for all five the satellite areas. Only a few rutiles are derived from metamafic rocks. Rutile from the Namakwa Sands deposit also indicates metapelitic rocks to be the dominant source. All five area's rutile grains also have > 1000 ppm of iron and indicate a metamorphic origin. No high-or low temperature populations were found for the metapelitic and metamafic rocks.

Rutile thermometry

Rutile is particularly suitable for various thermo- and geochronological applications due to its widespread occurrence, resistance to diffusive re-equilibration and chemical and physical durability (Watson et al, 2006).

Watson et al (2006) and Zack et al (2002, 2004a) both demonstrated that Zr in rutile, co-existing with quartz and zircon, is temperature dependant. The incorporation of Zr into rutile increases with an increase in temperature. The reaction is:

ZrO_2 (Baddeleyite in rutile) + SiO_2 (quartz) = $ZrSiO_4$ (Zircon) equation (1)

Zack et al (2002 2004a, b) presented an empirically calibrated thermometer based on natural samples and expressed the temperature as follows:

T (°C) = 127.8 * ln (Zr ppm) – 10 equation (2)

The estimated accuracy of the rutile thermometer is 50^0C although rocks studied at 500^0C showed that temperature differences can be distinguished with a precision of better than 50^0C (Zack et al, 2004a).

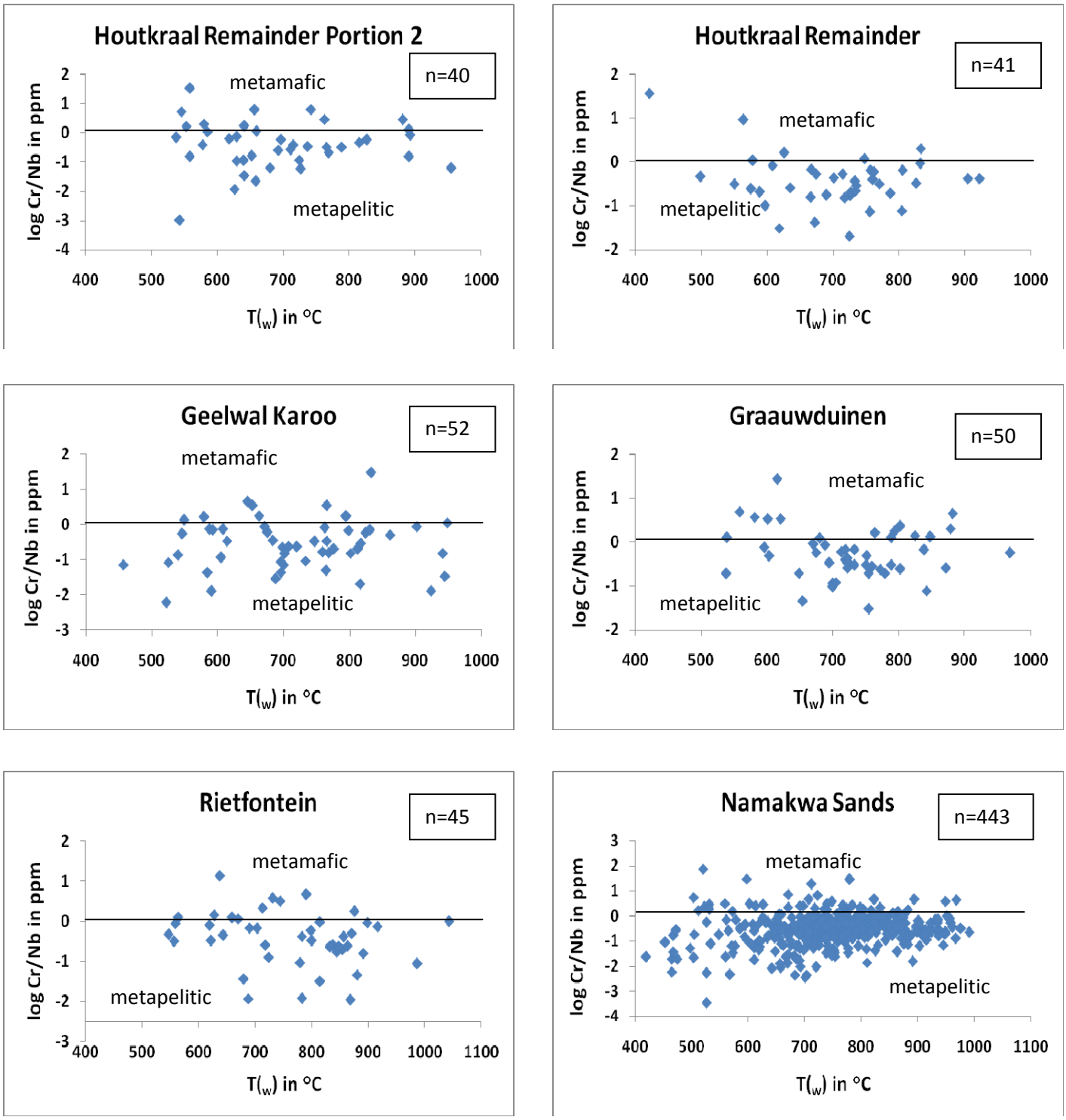

Figure 7.9. Log (Cr/Nb) vs temperature (T_w) diagrams of the five satellite areas. Most of the rutile is derived from metapelitic rocks.

Watson et al (2006) studied the effect of temperature dependence on Zr uptake by making use of experimental and natural samples. Experiments were carried out at 1 GPa. They found that the Zr concentration in rutile varies in a log-linear fashion with T^{-1}. They expressed the dependence of Zr content in rutile upon temperature with a new more improved equation. It has an error of $\pm 20^0$C and is given by the following equation:

$$T(^\circ C) = \left(\frac{4470 \pm 120}{7.36 \pm 0.10 - \log(Zr)} \right) - 273 \qquad \text{equation (3)}$$

Above authors did not study the effects of pressure on the thermometer but Watson et al (2006) stated that pressure must have a minor effect on Zr incorporation in rutile but needs further investigation.

Ferry and Watson (2007) did an experimental study in the ZrO_2-TiO_2-SiO_2 system to improve the thermodynamic constraints on Zr uptake in rutile. They found that Zr in rutile depends on the activity of SiO_2 (αSiO2) in the presence of zircon and either quartz, quartz-and zirconia-undersaturated silicate melt, or zirconia. They also studied the effects of pressure on the thermometer and found that the Zr content in rutile coexisting with zircon and quartz decreases with an increase in pressure at constant temperature and αSiO_2.

They expressed their equation as:

$$\log (\text{ppm Zr-in-rutile}) = (7.420 \pm 0.105) - (4530 \pm 111) / T\,(K) - \log_{\alpha SiO2} \qquad \text{equation (4)}$$

Tomkins et al (2007) did the first comprehensive study on the effect of pressure on the rutile thermometer. They stated that the Zr content in rutile decreases with increasing pressure since there is a volume change due to the larger Zr^{4+}-cation that substitutes for Ti^{4+}. The Zr^{4+}-cation will be less able to substitute for the smaller Ti^{4+} as the rutile structure compresses to higher pressure, therefore introducing pressure dependence (Tomkins et al, 2007). They proposed a new Zr-in-rutile thermometer calibration as follows:

$$T\,(^\circ C) = 83.9 + 0.410\,P / 0.1428 - R \ln \text{ø} - 273 \qquad \text{equation (5)}$$

where ø = Zr in ppm, P is in kbar and R is the universal gas constant, 0.0083144kj K^{-1}.

For this study the source rock temperatures for the rutile of each of the five satellite areas and the Namakwa Sands deposit were calculated using the Zr-in-rutile thermometers of Zack et al

(2004 a, b), which is denoted by (T_z), Watson et al (2006), which is denoted by (T_w), and the pressure dependant thermometer of Tomkins et al (2007) which is expressed as ($T_{5, 6, 7\ kbar}$). For the latter thermometer, temperatures were calculated at 5, 6 and 7kbars. The calculated temperatures, obtained from the Zack et al (2004 a, b), Watson et al (2006) and Tomkins et al (2007) thermometers, for each satellite area and the Namakwa Sands deposit, are presented as histograms in Figures 7.10-7.15. Temperatures were calculated for each satellite area, using all three thermometers, to indicate the different temperature ranges yielded by each of the three thermometers. It was assumed that the source rocks of the rutile had a stable rutile-quartz-zircon assemblage and therefore the Zr-in-rutile thermometer can be applied to the rutile of the satellite areas. The boundaries for the metamorphic facies used, follow that of Zack et al (2004b). Less than 500°C represents greenschist facies, 500-750°C represents amphibolite facies and > 750°C represents granulite facies conditions.

For all five satellite areas and the Namakwa Sands deposit the thermometer of Zack et al (2004a, b) gives higher formation temperatures for the same rutile grain than the thermometers of Watson et al (2006) and Tomkins et al (2007). The thermometer of Zack et al (2004) gives maximum temperatures of up to 1202°C for the satellite areas and up to 1160°C for the Namakwa Sands deposit. These values exceed the limit (< 1100°C) of known granulite facies. The thermometer of Watson et al (2006) and Tomkins et al (2007) are therefore considered more reliable for this study and are used for further description and interpretation.

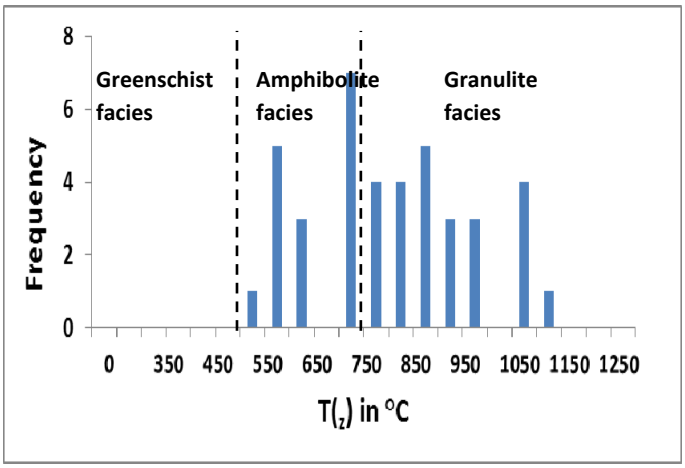

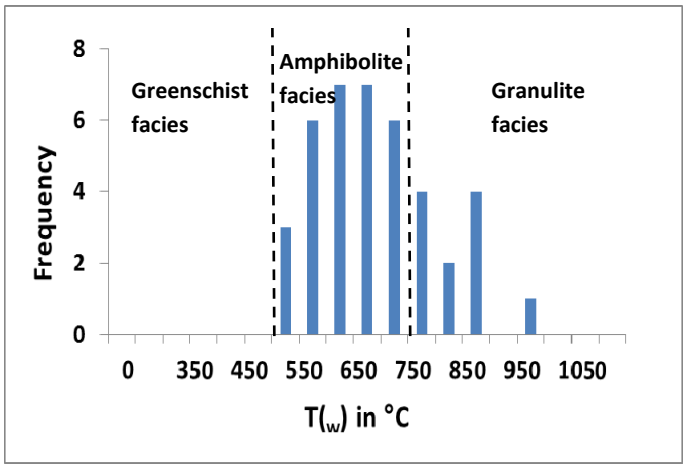

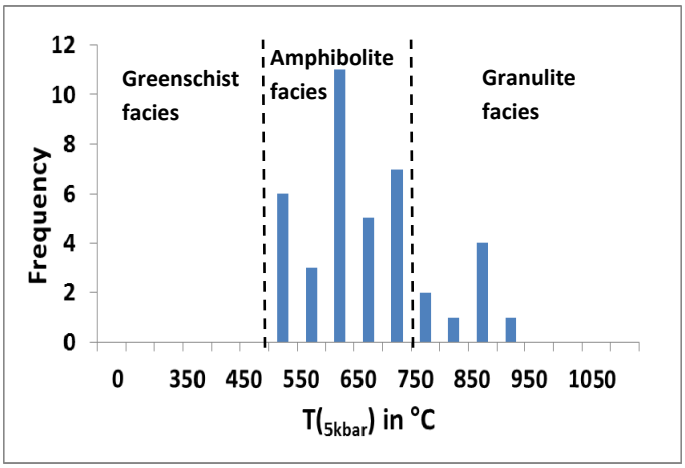

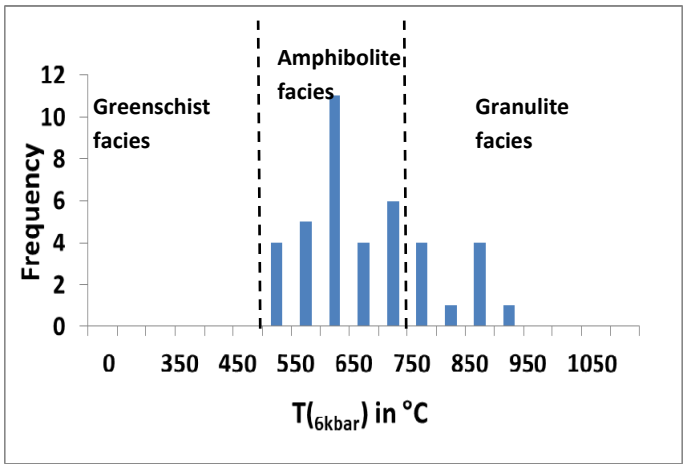

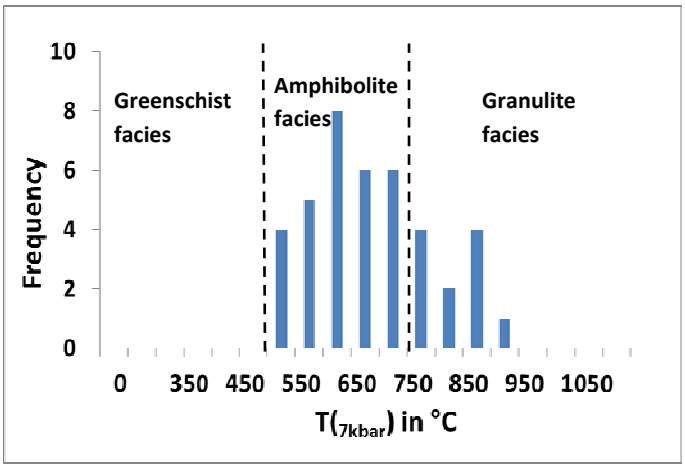

Figure 7.10. Histograms of calculated formation temperatures using the Zack et al (2004) (T_z), Watson et al (2006) (T_w) and pressure dependant Tomkins et al (2007) ($T_{5,\ 6,\ 7\ kbar}$) thermometers for rutile of Houtkraal Remainder Portion 2. n=40 for all five histograms.

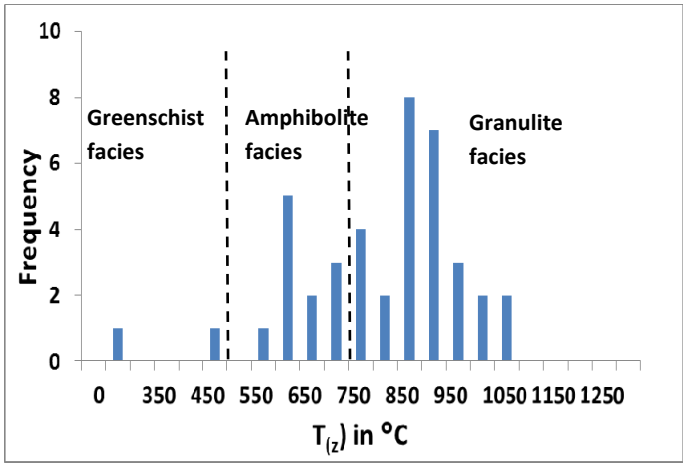

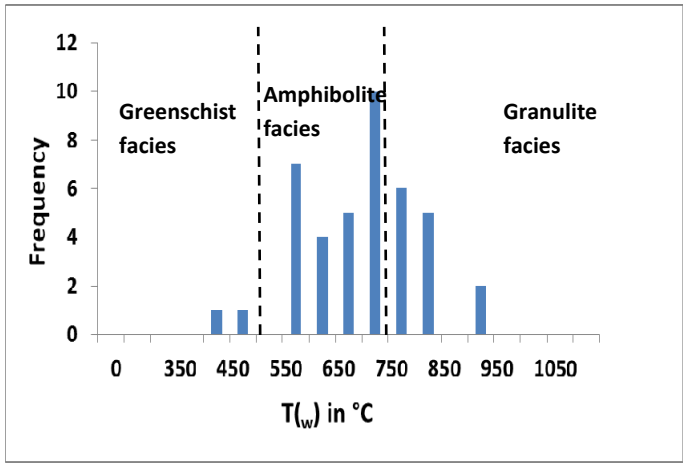

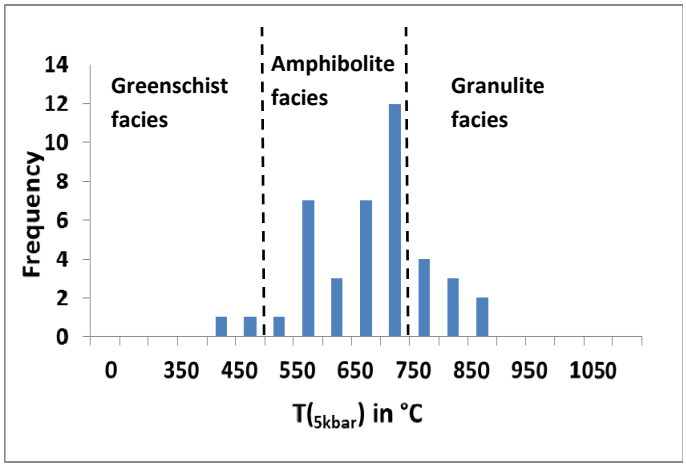

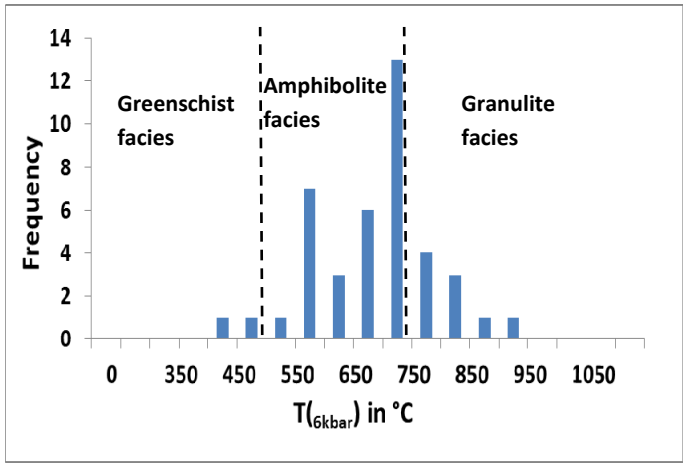

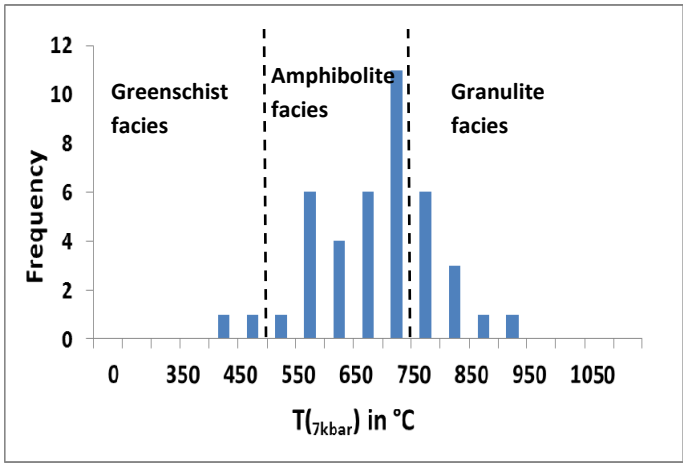

Figure 7.11. Histograms of calculated formation temperatures using the Zack et al (2004) (T_z), Watson et al (2006) (T_w) and pressure dependant Tomkins et al (2007) ($T_{5,\ 6,\ 7\ kbar}$) thermometers for rutile of Houtkraal Remainder. n=41 for all five histograms.

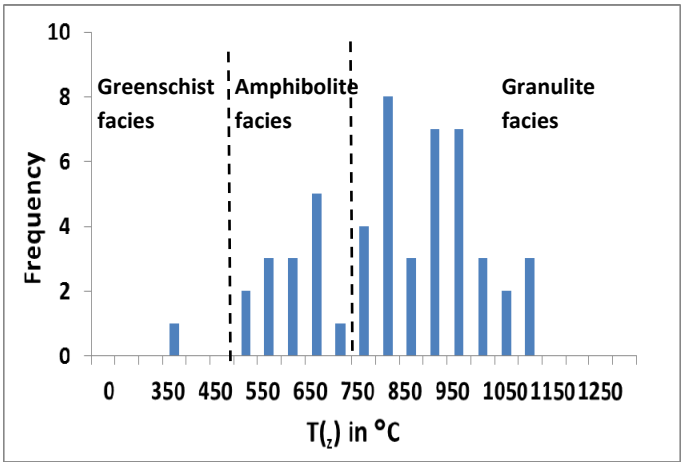

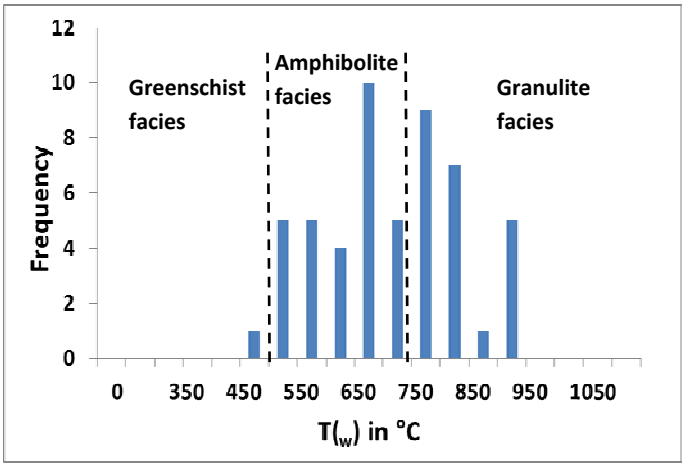

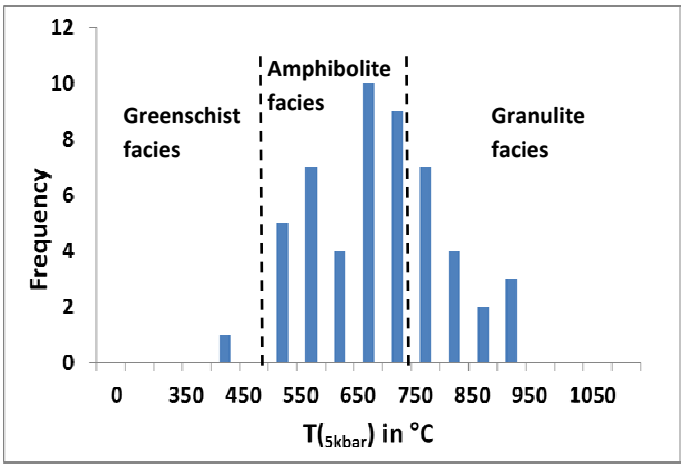

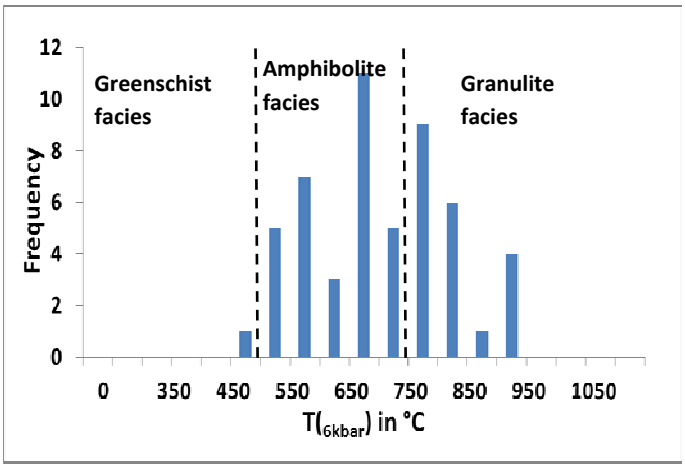

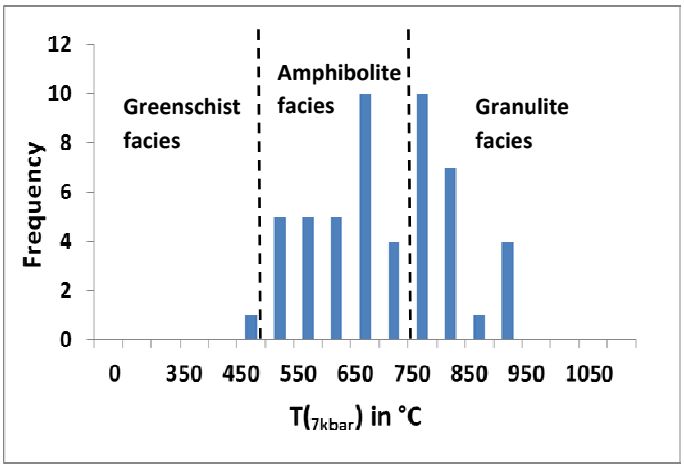

Figure 7.12. Histograms of calculated formation temperatures using the Zack et al (2004) (T_z), Watson et al (2006) (T_w) and pressure dependant Tomkins et al (2007) ($T_{5,\ 6,\ 7\ kbar}$) thermometers for rutile of Geelwal Karoo. n=52 for all five histograms.

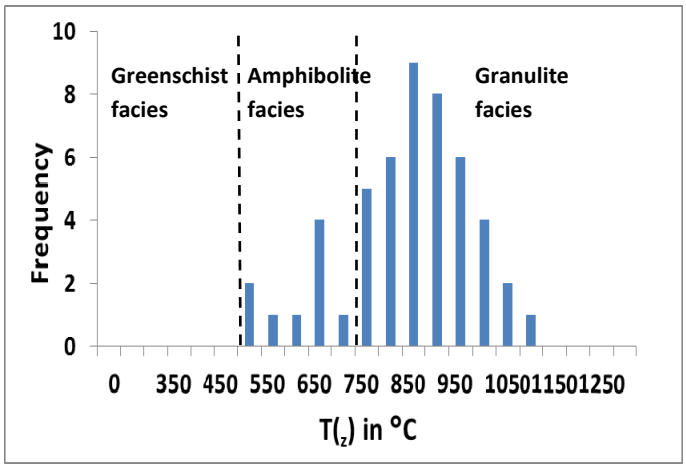

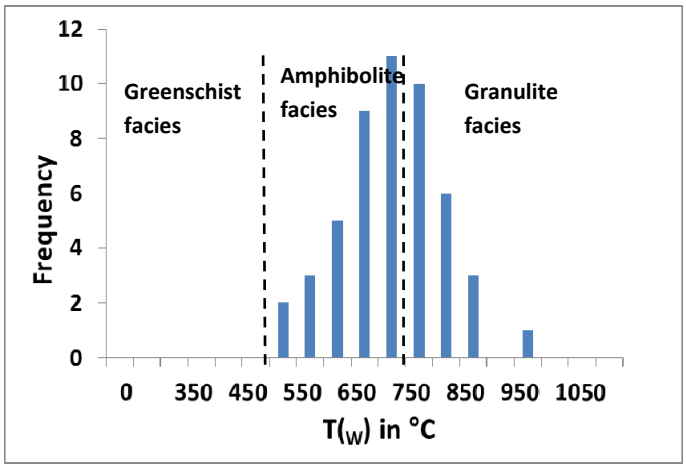

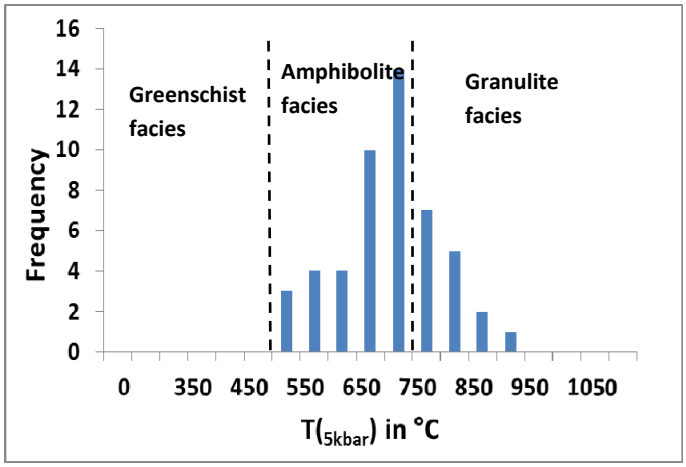

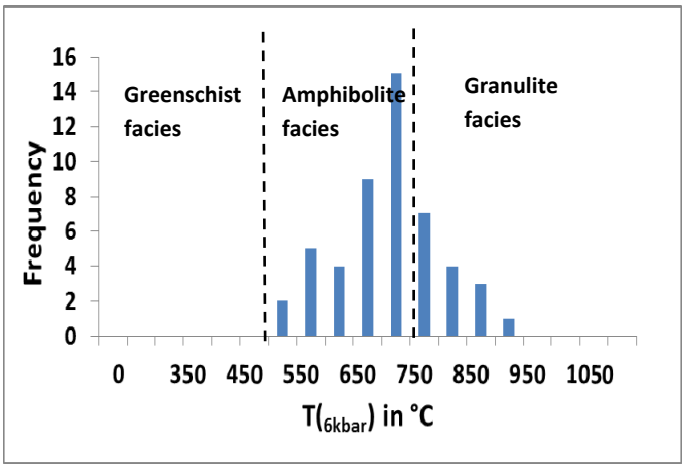

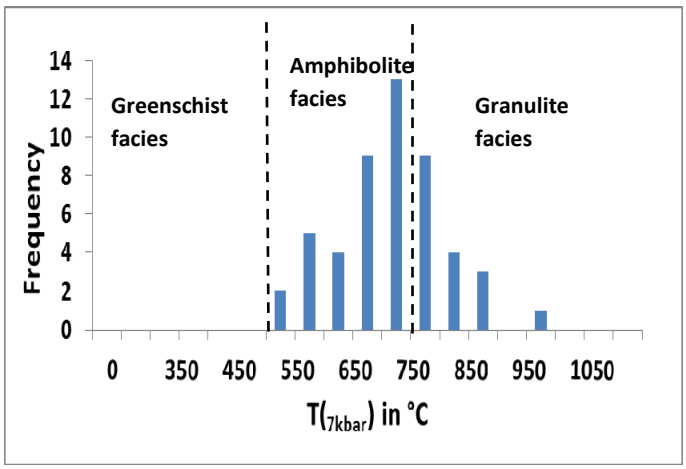

Figure 7.13. Histograms of calculated formation temperatures using the Zack et al (2004) (T_z), Watson et al (2006) (T_w) and pressure dependant Tomkins et al (2007) ($T_{5,\ 6,\ 7\ kbar}$) thermometers for rutile of Graauwduinen. n=50 for all five histograms.

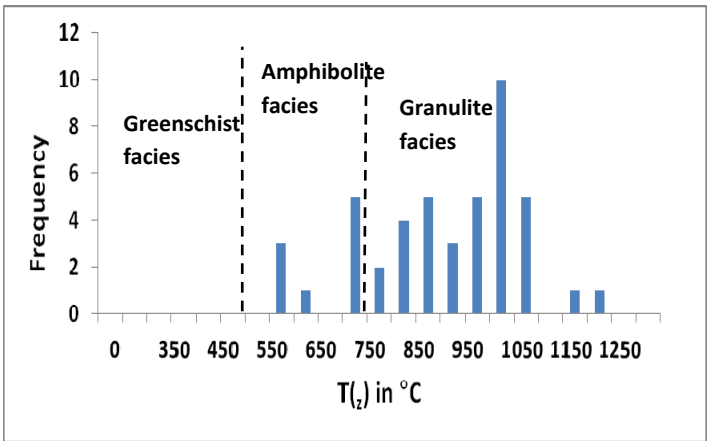

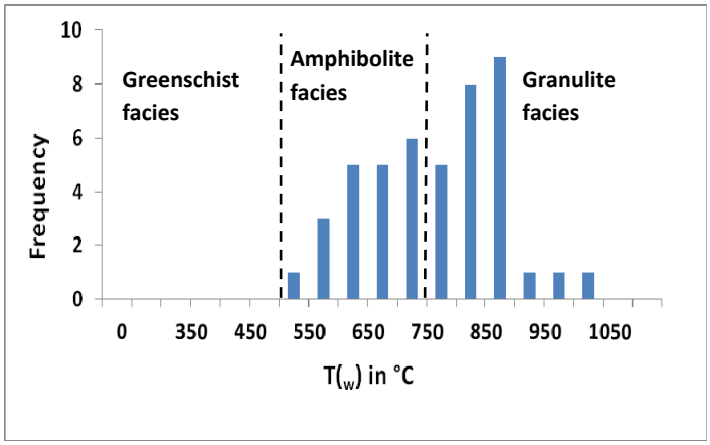

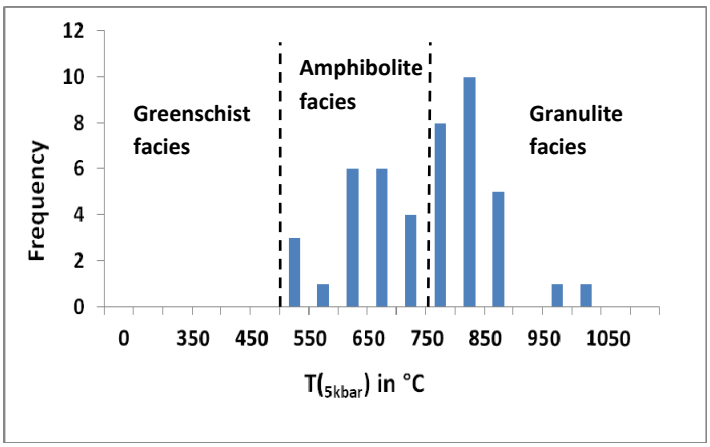

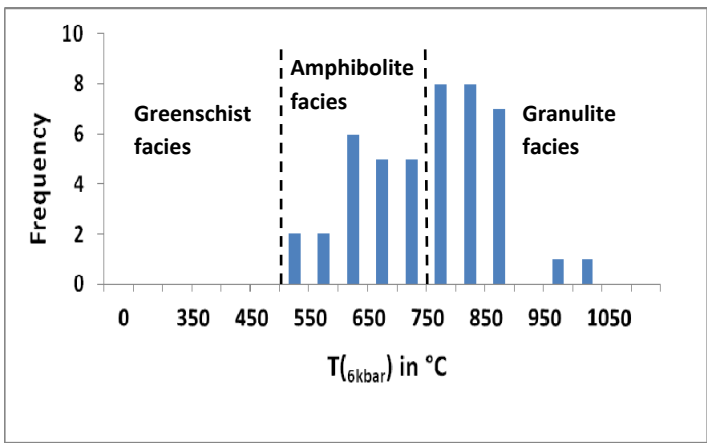

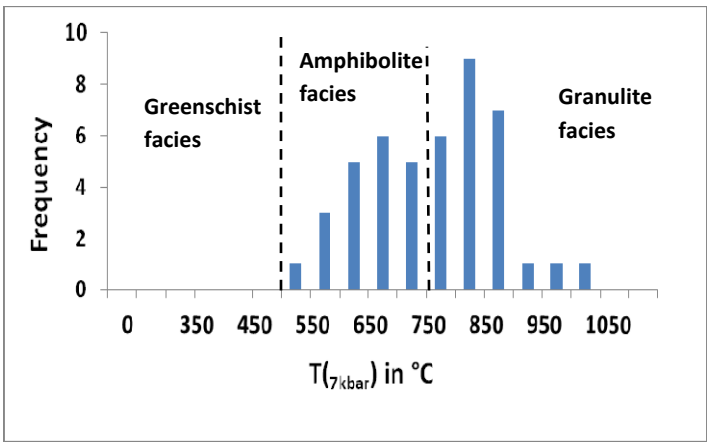

Figure 7.14. Histograms of calculated formation temperatures using the Zack et al (2004) (T_z), Watson et al (2006) (T_w) and pressure dependant Tomkins et al (2007) ($T_{5,\ 6,\ 7\ kbar}$) thermometers for rutile of Rietfontein. n=45 for all five histograms.

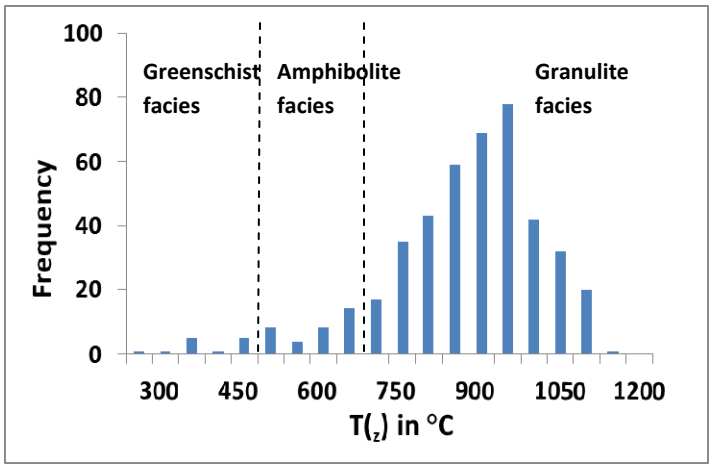

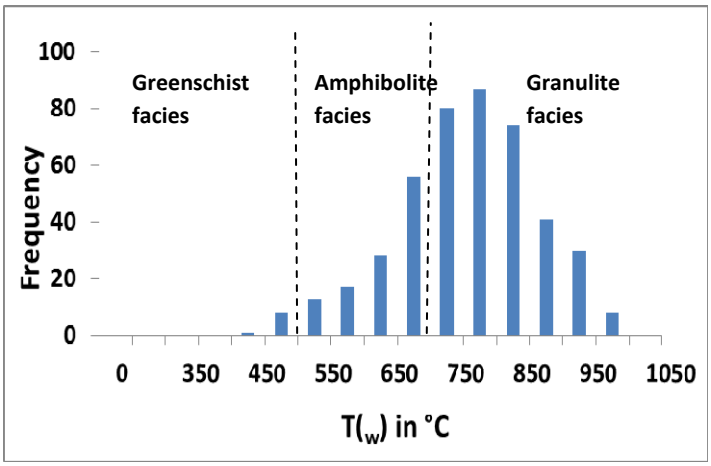

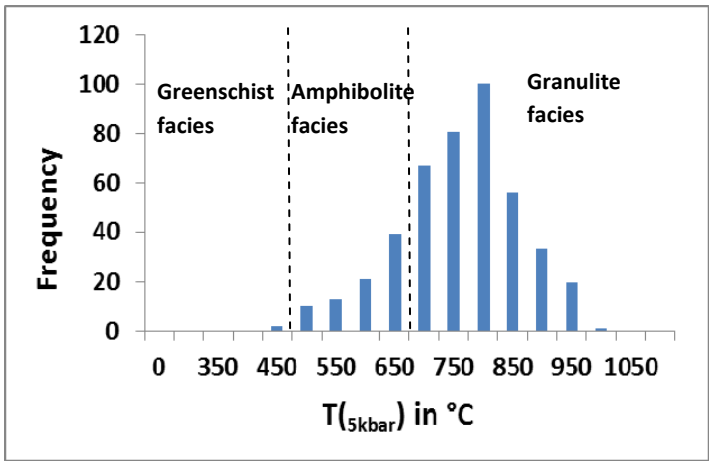

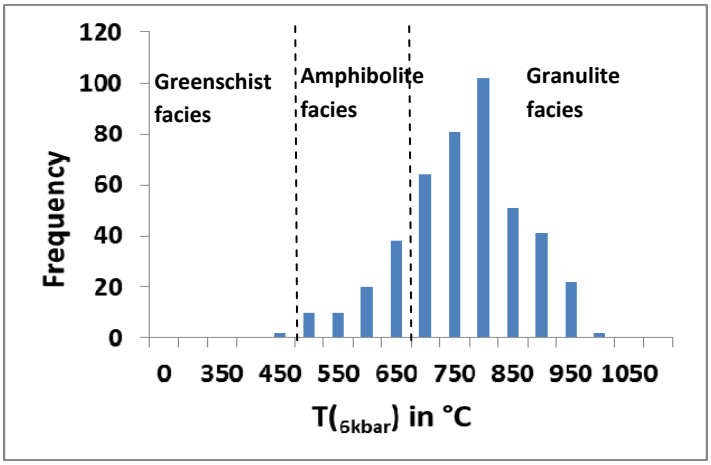

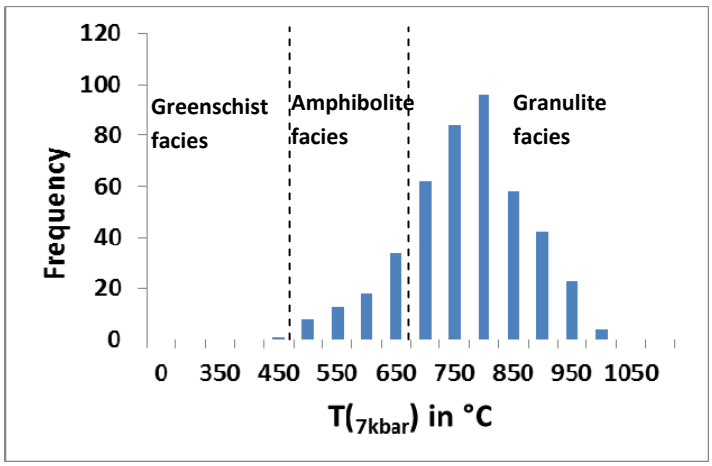

Figure 7.15. Histograms of calculated formation temperatures using the Zack et al (2004) (T_z), Watson et al (2006) (T_w) and pressure dependant Tomkins et al (2007) ($T_{5,\,6,\,7\ kbar}$) thermometers for rutile of the Namakwa Sands deposit. n=443 for all five histograms.

The (T_W) histogram of Houtkraal Remainder Portion 2 indicates that most rutile record amphibolite facies (72%) conditions with the rest of the rutile belonging to the granulite facies (28%) group. No rutile belonging to the greenschist facies group is present. The pressure dependant ($T_{5,\ 6,\ 7\ kbar}$) histograms also indicate that the majority of rutile record amphibolite facies conditions (80%, 75%, and 73% for pressures of 5, 6 and 7 kbars respectively). The rest of the rutile record granulite facies conditions (20%, 25% and 27% respectively). No rutile belonging to the greenschist facies were recorded.

Rutile of Houtkraal Remainder are characterized by a majority of amphibolite facies rutile (63%, 73%, 73% and 68% for the Watson et al (2006) thermometer and 5, 6 and 7 kbar pressure dependant thermometer of Tomkins et al (2006) respectively). The (T_w) histogram indicates that 32% of rutile record granulite facies conditions. The T_{5kbar}, T_{6kbar} and T_{7kbar} histograms indicate that 22%, 22% and 27% of the rutile record granulite facies conditions. All four histograms record 5% of greenschist facies rutile.

Geelwal Karoo is also characterized by a majority of amphibolite facies rutile. The (T_w) histogram and 5, 6 and 7 kbar pressure dependant histograms of Geelwal Karoo show that 56%, 67%, 60% and 56% of the rutile record amphibolite facies respectively and 42%, 31%, 38% and 42% record granulite facies respectively. All four histograms record 2% of greenschist facies rutile.

The Graauwduinen satellite area is also dominated by amphibolite facies rutile and lesser amounts of granulite facies and greenschist facies rutile. The Watson et al (2006) thermometer indicates 60% of amphibolite facies rutile and 40% of granulite facies rutile. The 7 kbar pressure dependant thermometer of Tomkins et al (2007) records 66% amphibolite facies rutile and 34% granulite facies rutile whilst the 5 kbar and 6 kbar thermometers record 70% of amphibolite facies rutile and 30% of granulite facies rutile. All four thermometers record only a small population (4%) of greenschist facies rutile.

Rietfontein is the only satellite area that is dominated by granulite facies rutile. Both thermometers reflect 56% of granulite facies rutile with 44% of amphibolite facies rutile. No greenschist facies rutile was recorded.

Both thermometers, $T_{(w)}$ and $T_{(5,6,7\ kbar)}$, indicate that the Namakwa Sands deposit is dominated by granulite facies rutile.

Above temperature distributions indicate that the rutile of the satellite areas were sourced from rocks that experienced temperatures between 413°C and 1042°C indicating greenschist, amphibolite and granulite facies conditions. Temperatures below 400°C are not reliable because Zr contents are below the detection limit of the LA-ICP-MS.

According to De Beer et al (2002) reported from previous literature, metamorphic conditions in the NMC area ranged from upper amphibolite (in the Koekenaap and Potkley areas) to granulite facies (Garies and Kliprand areas) conditions. De Beer et al (2002) estimated temperature and pressure conditions of 630°C and 6-7 kbars respectively for the Sout River area and 700-850°C and 5-7 kbars for the Potkley and Bitterfontein areas of the NMC. Waters et al (1983) reported on granulite facies conditions north of Bitterfontein and upper amphibolite facies south of Bitterfontein and middle amphibolite facies conditions in the Sout River area.

The calculated temperatures of the satellite areas equate well with the metamorphic temperatures experienced by the medium-grade to high-grade proximal Namaqualand Metamorphic Complex and low-grade Gariep Supergroup (Chapter 3). The Nb and Cr contents indicated metapelitic rocks as the dominant source rocks for the satellite areas with a minor contribution from mafic rocks. The NMC is mainly granitic/felsic in character with mafic rocks such as amphibolites, mafic granulites and mafic gneisses forming only a small component. The dominance of metapelitic rutile in the satellite areas therefore correlate well with the felsic character of the NMC. It can therefore be concluded that the rutile of the five satellite areas were mainly derived from the NMC and the Gariep Supergroup was a minor contributor.

7.2.4 Hematite

Haggerty (1976a) stated that hematite that displays the" blitz" texture of Ramdohr (1980) is common in felsic igneous rocks.

7.2.5 Magnetite-Spinel Series

Magnetite

Magnetite is not abundant in the satellite areas. Due to magnetite's stable nature and occurrence in a wide variety of rocks (igneous and metamorphic) it is one of the most common opaque heavy mineral in sands (Grigsby, 1990; Ramdohr, 1980; Pettijohn et al, 1987). Other factors making it a suitable provenance tool of the Fe-Ti oxides is because it can be easily magnetically separated from the bulk minerals and has a unique mineral chemistry diagnostic of its source rocks (Yang et al, 2009). Magnetite carries a unique chemical and petrographic fingerprint that can be used in provenance studies since the chemical composition of magnetite are inherited from its source rocks and is unlikely to change with transportation and weathering. Grigsby (1990) proposed a discrimination diagram of $TiO_2+V_2O_3$ versus $MgO/(MgO+Al_2O_3)$ based on the chemical composition of magnetite to determine its origin. He also found that homogeneous magnetite grains are common in felsic plutonic and intermediate volcanic parent rocks. TiO_2, $V2O_3$, MgO and Al_2O_3 are < 1% for the former rocks and are enriched in TiO_2, MgO and Al_2O_3 for the latter. On the $TiO_2+V_2O_3$ vs $MgO/MgO+Al_2O_3$ diagram, mafic rocks are characterized by > 5% of $TiO_2+V_2O_3$ and felsic plutonic/volcanic rocks by < 5% of $TiO_2+V_2O_3$. Intermediate volcanic rocks have > 0.1% of $MgO/ (MgO+Al_2O_3)$.

Possible source rocks for the five satellite areas are shown in Figure 7.16 where the magnetite is plotted on the $TiO_2+V_2O_3$ vs $MgO/MgO+Al_2O_3$ discrimination plot of Grigsby (1990).

Figure 7.16 shows that the most likely source rocks for the magnetite of the satellite areas are metamorphic rocks and felsic plutonic or volcanic rocks. One magnetite grain shows a mafic plutonic origin.

Likely source rocks for the magnetite of the satellite areas are therefore metamorphic rocks such as calc-silicate -and pelitic gneisses and granites.

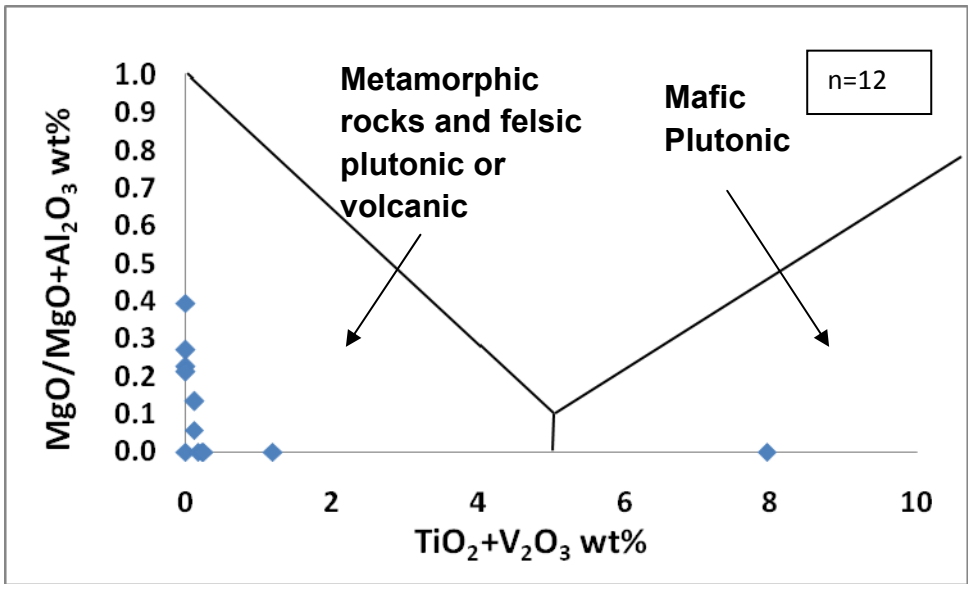

Figure 7.16. Discrimination plot of $TiO_2+V_2O_3$ vs $MgO/MgO+Al_2O_3$ for magnetite grains of the five satellite areas. Magnetite is derived from metamorphic and felsic plutonic rocks with one grain showing a mafic plutonic origin.

Spinel

Hercynite spinel is common in basic- and ultrabasic rocks and metamorphic rocks where it usually occurs with diopside and forsterite and in contact- and regional -metamorphosed limestone and pelites and iron formations (Deer et al, 1992). Albat (1983) studied granulite facies metapelitic gneisses and found the dark green hercynite spinel variety enriched in iron, aluminium and magnesium. Jack (1980) found green hercynite spinel in aluminous gneisses in western Namaqualand, in the Garies area. Moore (1989) found spinel in calc-silicate rocks and metabasic rocks. Joubert (1971) found spinel in pelitic gneisses and schist in the Nababeep area in Namaqualand. Macdonald (1996) also found Mg-rich hercynite spinel in the Geelwal Karoo deposit and some of the Graauwduinen samples that he studied. He, however, did not propose any source rocks for the spinel. De Beer et al (2002) mentioned that dark green hercynite spinel in the Bitterfontein belt is an indication of granulite facies conditions.

Since the spinel of this study also belongs mainly to the hercynite variety, the most probable source lithologies for the spinel of the satellite areas are granulite facies metapelitic schists and gneisses, calc-silicate rocks and metamafic rocks of the NMC.

7.2.6 Garnet

Garnet is relatively stable in deep burial environments and sediments and together with zircon is part of the less sensitive minerals to diagenetic processes and is abundant in sediments and rocks of differing origin (Wach and Kettanah, 2006). It has a wide variety of colours but most importantly, it has a wide compositional range with solid solution between seven garnet end-members (Blatt et al, 1972; Morton et al, 2002; Morton et al, 2004). These end-members (spessartine, almandine, grossular, pyrope, andradite, hydrogrossular and uvarovite) vary greatly in major element composition. Garnet usually shows compositional differences between different garnet-bearing lithologies (Morton et al, 2002; Copjakova et al, 2005).

According to Deer et al (1992) almandine and pyrope are the most widespread species in most metamorphic and igneous rocks. Pyrope for example is characteristic of high-grade ultrabasic and basic rocks such as kimberlites and peridotites and acid igneous rocks. Almandine indicates high-grade rocks (granulite rocks) such as S-type granites and metapelites (garnetiferous and biotite schist). Almandine-spessartine is characteristic of granites and pegmatites (Blatt et al, 1980). Spessartine is present as dominant species in some skarn deposits and usually indicates Mn-rich metasediments or granite pegmatites. Grossular and andradite are common in metamorphosed impure calcareous rocks.

Almandine-spessartine (Alm-Spss) and grossular-andradite (Grss-Andr) are the two dominant garnet types present in the satellite areas with minor pyrope garnets (Figure 7.17). According to Deer et al (1992) the garnets of the satellite areas therefore indicate provenance from mainly metapelites, granites and pegmatites, calc-silicates and partly from ultrabasic, basic and felsic igneous rocks.

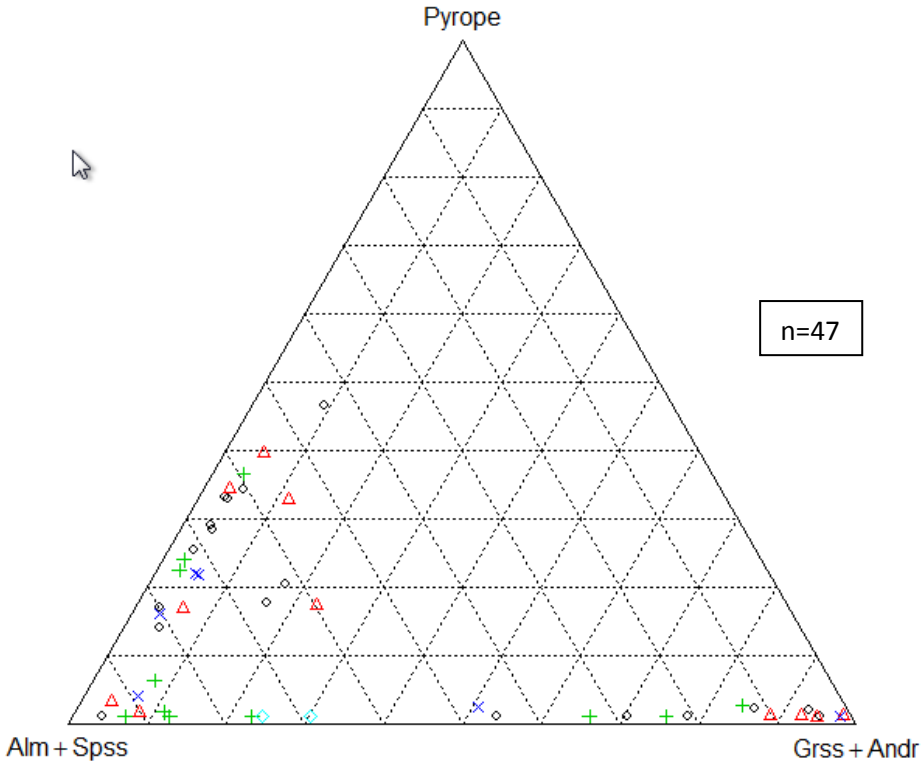

Figure 7.17. Alamandine+Spessartine-Pyrope-Grossular+Andradite ternary diagram showing the composition of garnet of the five satellite areas. The garnet population for the five satellite areas consists of almadine-spessartine and grossular-andradite garnets.

Morton et al (2004) studied the geochemistry of garnet in river sediments sourced by the basement terrains of northern Scotland and Norway. They found that the garnet populations of Scotland and Norway fall into three main groups or fields. Group A includes high Mg and low Ca garnet. Group B includes Fe- and Mn-rich garnets with variable Ca and low Mg. Field C comprises high Ca and high Mg garnet. They found that metasediments (pelitic gneisses and schist), granites, granite pegmatites and intermediate to acidic gneisses contain field B garnets. Basic rocks such as peridotites and pyroxenite contain Field C garnets and basic gneisses contain Field A garnets. High Ca garnet is characteristic of calcareous sediments.

According to above suggestions, the garnet of the five satellite areas are mainly sourced by pelitic gneisses and schist, granite pegmatites, intermediate to acidic gneisses, calcareous sediments and partly from basic rocks.

All the above-mentioned source rocks are consistent with the high-grade rocks of the proximal Namaqualand Metamorphic Complex and the latter are therefore considered the source terrain of the garnet of the satellite areas.

The euhedral nature of the garnet grains indicate that it did not experience long-distance transport which further supports the conclusion that the proximal NMC is the most likely source terrain for the garnet suites. The angular nature can also indicate a first-cycle origin from crystalline rocks.

The chemistry of this study's garnets was compared with the microprobe analysed garnets of Cilliers (1995); Macdonald (1996) and Philander (1999) of the Graauwduinen, Geelwal Karoo and Kleinzee areas respectively. It is illustrated in Figure 7.18.

Philander (1999) reported almandine and pyrope as the main end-members in the Kleinzee sediments and proposed pelitic rocks of the NMC as likely source rocks for the garnets. Macdonald (1999) found mainly almandine with minor grossular and spessartine components and accessory amounts of andradite in the Geelwal Karoo deposit. Cilliers (1995) also reported mainly almandine with a small percentage of the pyrope component in the Graauwduinen deposit. Philander (1999) concluded that these three areas have a uniform source, the NMC, due to the similar chemical composition of the garnets.

The garnets from the four areas all show enrichment in almandine. The garnets of Macdonald (1996) and the satellite areas show enrichment in grossular and a slight enrichment in pyrope. The enrichment of the grossular molecule in the satellite areas and Geelwal Karoo deposit can be attributed to an input from metamorphosed calc-silicate rocks.

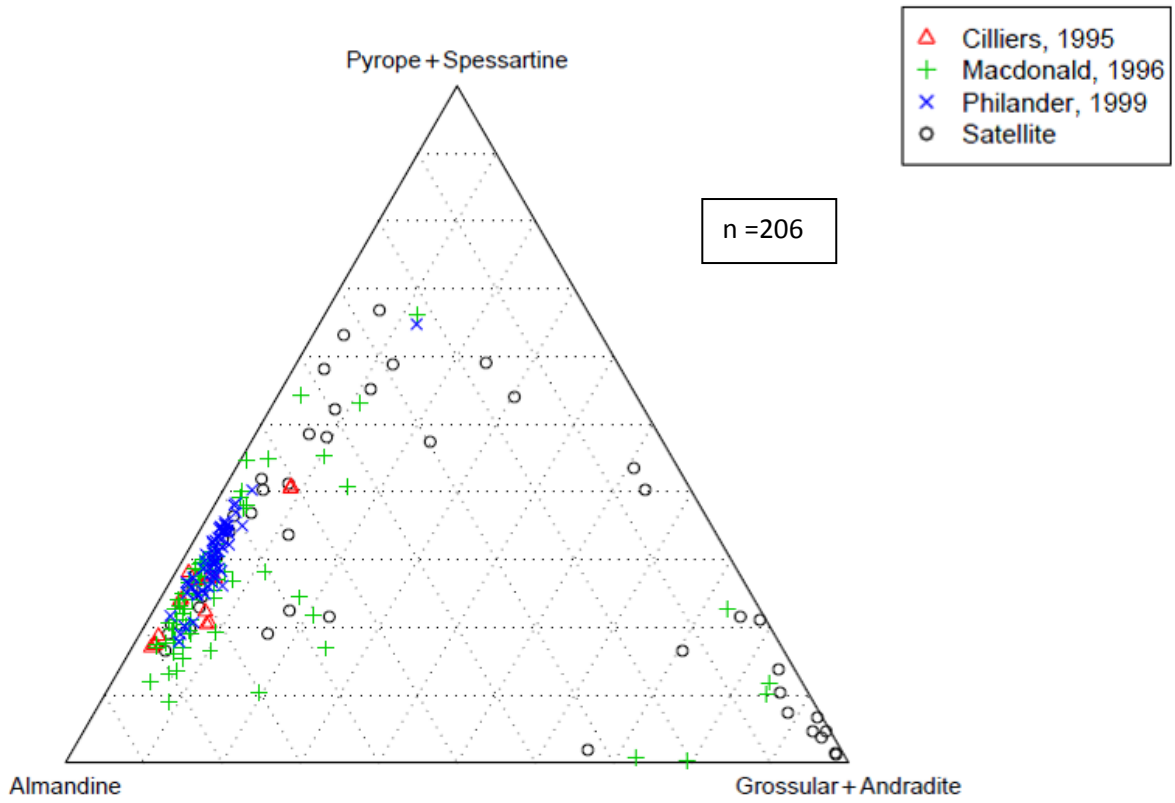

Figure 7.18. Ternary plot illustrating the chemical composition of garnets from the Graauwduinen deposit (Cilliers, 1995), the Geelwal Karoo deposit (Macdonald, 1996), Kleinzee sediments (Philander, 1999) and the five satellite areas. The Geelwal Karoo deposit is enriched in almandine and grossular and Graauwduinen and Kleinzee sediments in almandine and pyrope.

7.2.7 Pyroxene

Pyroxene is unstable and is easily removed by processes such as weathering, transportation and is vulnerable to diagenesis and shows low mechanical stability to abrasion (Pettijohn, 1987; Lenaz, 2008). Pyroxene provenance includes studies by authors such as Cawood. (1991); Nechaev and Isphording (1993); Schweigl and Neubauer (1996) and Krawinkel et al (1999).

The most dominant pyroxene minerals in the satellite areas are the clinopyroxenes, augite and pigeonite, with accessory amounts of orthopyroxene (enstatite) and wollastonite (Figure 7.19). According to Deer et al (1992) augite is characteristic of basic igneous rocks such as gabbros, basalts and dolerites, wollastonite of metamorphosed limestone, pigeonite of

andesites and dacites and magnesium-rich enstatite of ultramafic and ultrabasic rocks. Orthopyroxene and clinopyroxene are index minerals of the granulite facies of metabasites. Orthopyroxene (opx) are present in granulite facies metapelites under specific required conditions (Fe-rich, Al-poor rocks) but clinopyroxene is virtually absent.

Zelt (1980) found augite as the main clinopyroxene (cpx) and lesser pigeonite in mafic granulites in the Namaqualand area. The mafic granulites are believed to have their origin from the metamorphism of mafic (basaltic and tholeiitic) igneous rocks (Zelt, 1980; Moore, 1989). Theart (1980) studied metabasic and metapelitic rocks in northwestern Namaqualand and found opx and cpx (augite) in the metamafic rocks (amphibolites and granulites) from the granulite facies. Albat (1983) found wollastonite in granulite facies calc-silicate gneisses in the NMC and also augite + pigeonite in granulite facies mafic rocks. He also found that for his data orthopyroxene are characteristic of the granulite facies and clinopyroxene of the upper amphibolite facies. Some of the calc-silicates and metacarbonate rocks in western NMC contain clinopyroxene as well (Moore, 1989). Calc-silicate granulites of the Garies wollastonite mine also contain clinopyroxene (Seto et al, 2006). Joubert (1971) found opx and cpx in mafic rocks and pyroxene granulites and wollastonite in calcareous rocks to the south of Nababeep in western Namaqualand.

Considering all above evidence and the suggestions of Deer et al (1992), it can therefore be concluded that the pyroxenes were derived from a variety of source rocks which include granulite facies mafic igneous rocks (amphibolites and granulites), calc-silicates, metabasites and metapelites, ultramafic and ultrabasic rocks.

Cilliers (1995), Macdonald (1996) and Philander (1999) also found mainly augite with subordinate amounts of pigeonite in the Graauwduinen, Geelwal Karoo and Kleinzee areas respectively (Figure 7.20). Pyroxenes range from diopside, augite, pigeonite, ferrosilite and enstatite. This wide range in chemistry of the pyroxenes indicates a wide range of source rocks.

Comparing Figure 7.19 with Figure 7.20 it is evident that the pyroxenes cluster in the same areas on the two graphs indicating a similar chemistry. This in turn may indicate a similar provenance for the satellite areas and the Geelwal Karoo deposit, Kleinzee and Graauwduinen deposits. Macdonald (1996), proposed metabasites of the granulite facies as a probable source for the Geelwal Karoo deposit. Philander (1999) ascribed the pyroxene to a

mafic-rich source that underwent medium-grade (amphibolite facies) conditions. Cilliers (1995) did not propose any source rocks for the Graauwduinen deposit.

The above-mentioned source rocks are all present in the proximal NMC. Albat (1983) reported on metasediments (calc-silicate gneisses and metapelitic gneisses) and mafic rock units, in the Kliprand area of the NMC. Waters et al (1983) also reported on metapelitic (aluminous) gneisses south and west of Bitterfontein and Joubert (1971) on metasediments and mafic gneisses in the Nababeep district and further south. Jack (1980) described aluminous gneisses and schists, amphibolites, and calc-silicate rocks in western (Garies area) Namaqualand.

The NMC also experienced amphibolite to lower granulite facies conditions (Jack, 1980; Waters et al, 1983; De Beer et al, 2002) and are thus a likely source terrain for the pyroxene of the satellite areas.

Since pyroxene is an unstable mineral (two cleavage directions at 90 °) it is likely to be removed or broken down during transport. The high pyroxene content in the Geelwal Karoo and Rietfontein samples is an indication that the grains experience short-distance transport or that weathering and erosion occurred in-situ. Orthopyroxene are less stable than clinopyroxene and usually breaks down first. The presence of orthopyroxene therefore highlights the fact that the minerals experienced short-distance transport and are derived from the proximal NMC.

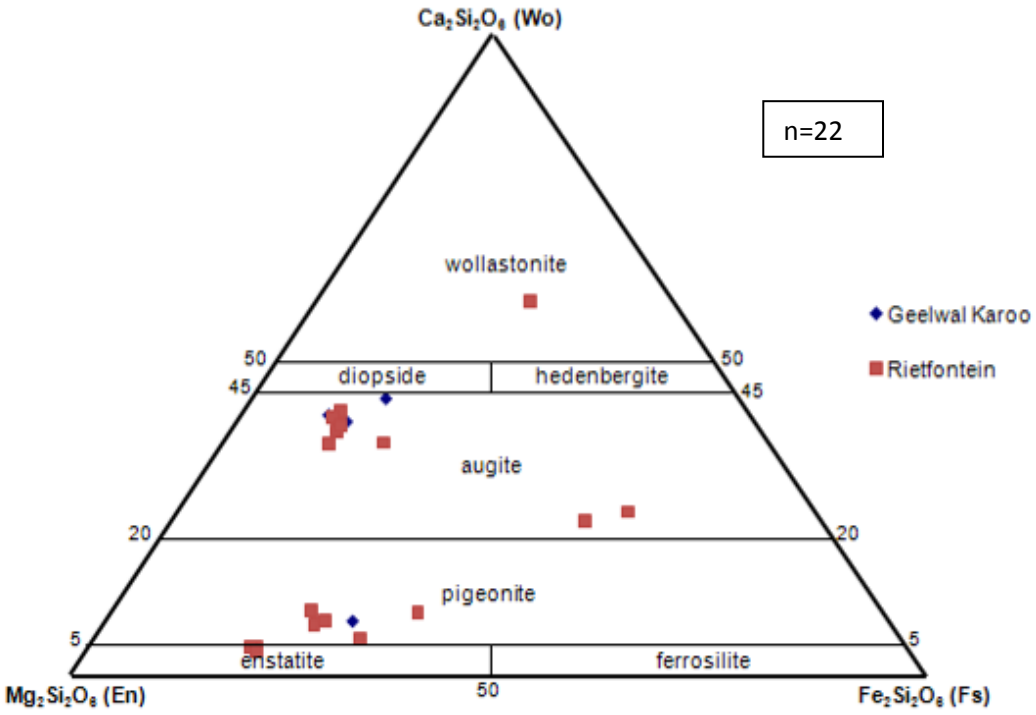

Figure 7.19 Wo-En-Fs graph showing the composition of the Geelwal Karoo and Rietfontein pyroxene (diagram after Morimoto et al, 1988). Dominant pyroxene end-members are augite and pigeonite with trace amounts of wollastanite and enstatite.

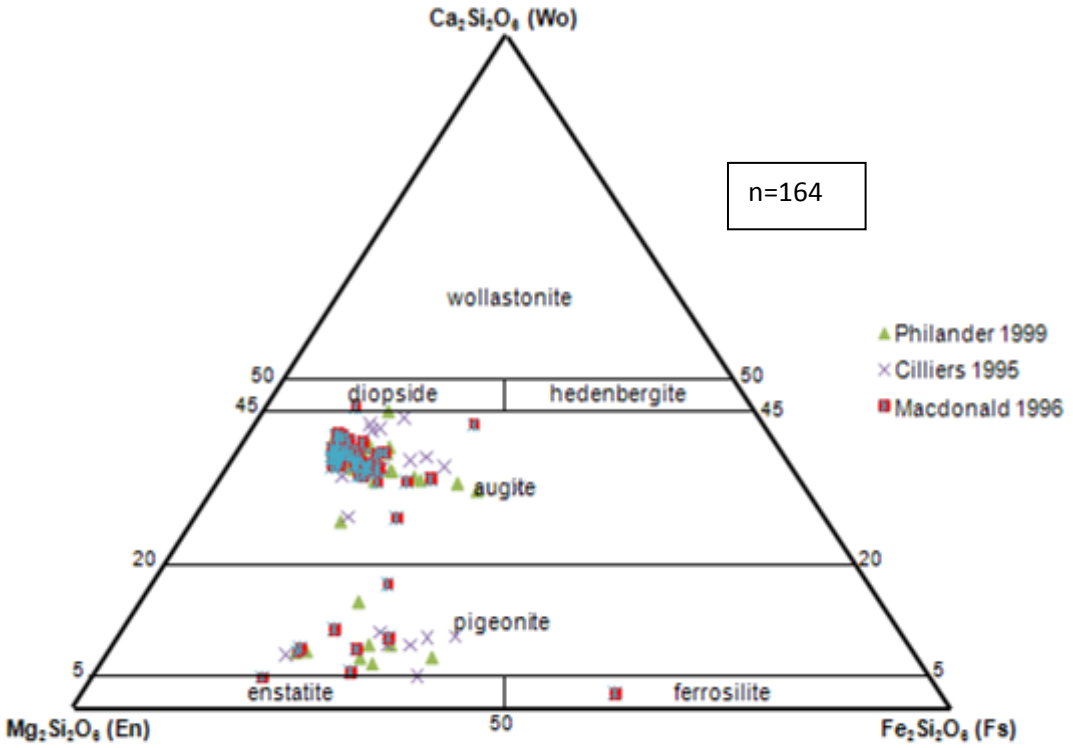

Figure 7.20. Wo-En-Fs graph showing the composition of the Graauwduinen, Geelwal Karoo and Kleinzee sediments. (diagram after Morimoto et al, 1988). Data from Cilliers (1995,) Macdonald (1996) and Philander (1999). Main end-members are augite and pigeonite with trace amounts of diopside, enstatite and ferrosillite.

7.2.8 Tourmaline

Tourmaline occurs in all types and ages of sediments most commonly in granitic to rare earth element enriched pegmatites, granites and in metasedimentary rocks and forms over a wide range of metamorphic grades. It is also present in detrital sediments, calcareous sedimentary rocks, volcanics and in granitoid intrusive rocks with their related pegmatites and aplites and in hydrothermal aureoles. Tourmaline is considered a complex isomorphous aluminosilicate of boron with a rhombohedral cyclosilicate structure.

Theoretically it is the best mineral to use as a provenance indicator due to its ultra stable nature (both mechanically and chemically) and high sensitivity to diverse environments of formation. The latter is due to the chemical complexity which allows a large number of possible elemental substitutions (Hawthorne and Henry, 1999; Viator, 2003).

Since colour is not a reliable provenance indicator for the tourmaline grains of this study (for e.g. two different minerals can have the same colour), possible source rocks for the tourmalines of this study can be explained in terms of its chemical composition. The wide range in chemical composition and colour of the tourmalines from the five areas implies a wide range of source lithologies. Possible source rocks can be delineated on the Al-Fe (tot)-Mg and Ca-Fe (tot)-Mg ternary diagrams of Henry and Guidotti (1985) (Figure 7.21 and 7.22) which utilizes Ca, Fe, Mg and Al as provenance indicators. Figure 7.21 indicates that possible source rocks for the tourmaline (dravite, schorl, buergerite and uvite) of the five heavy mineral satellite areas are fields 2, 4, 5 and 6 which include Li-poor granitoids and pegmatite, Al-rich and Al-poor metapelites and metapsammites and calc-silicate rocks and Fe^{3+}-rich quartz-tourmaline rocks.

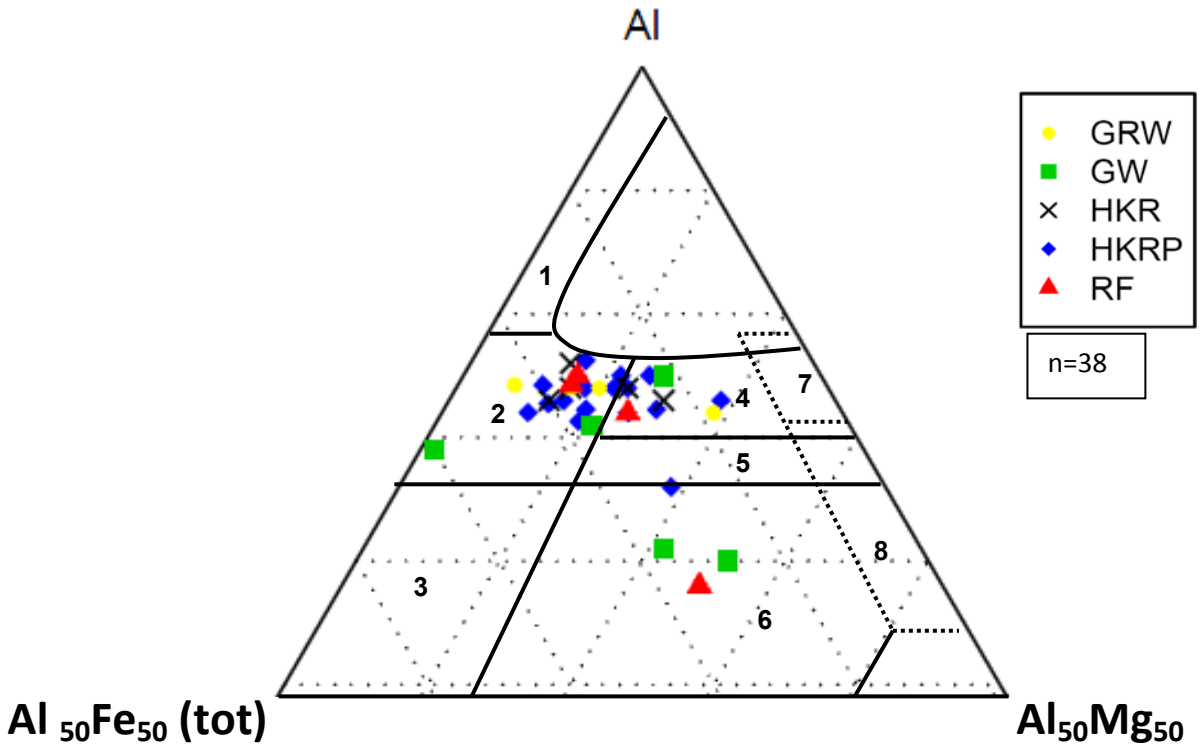

Figure 7.21. Tourmaline of the five satellite areas plotted on Henry and Guidotti's (1985) Al-Fe (tot)-Mg diagram. The numbered fields correspond to the following rock types: (1) Li-rich granitoid pegmatites and aplites (2) Li-poor granitoids and associated pegmatites and aplites (3) Fe^{3+}-rich quartz-tourmaline rocks (hydrothermally altered granites) (4) metapelites coexisting with an Al-saturating phase (5) metapelites without an Al-saturating phase (6) Fe^{3+}-rich quartz-tourmaline rocks, calc-silicate rocks and metapelites (7) low-Ca meta-ultramafics and Cr, V-rich metasediments and (8) metacarbonates and meta-pyroxenites.

On the Ca-Fe(tot)-Mg ternary diagram (Figure 7.22), the tourmaline plot primarily in fields 2, 3 and 4 indicating Li-poor granitoids and associated pegmatites and aplites, Ca-rich metapelites, metapsammites, calc-silicate rocks and Ca-poor metapelites, metapsammites, and quartz-tourmaline rocks as likely source rocks.

Tourmaline with high Fe is indicative of granitic and pegmatitic source rocks, whereas high Mg tourmaline is characteristic of metasediments and metasomatic rocks (Henry and Guidotti, 1985). Schorl, dravite and buergerite are aluminous and Ca-poor and thus indicate an aluminous-rich and Ca-poor source such as metapelites. The uvite component is also aluminous but Ca-rich and indicates a Ca-rich source such as calc-silicate gneisses.

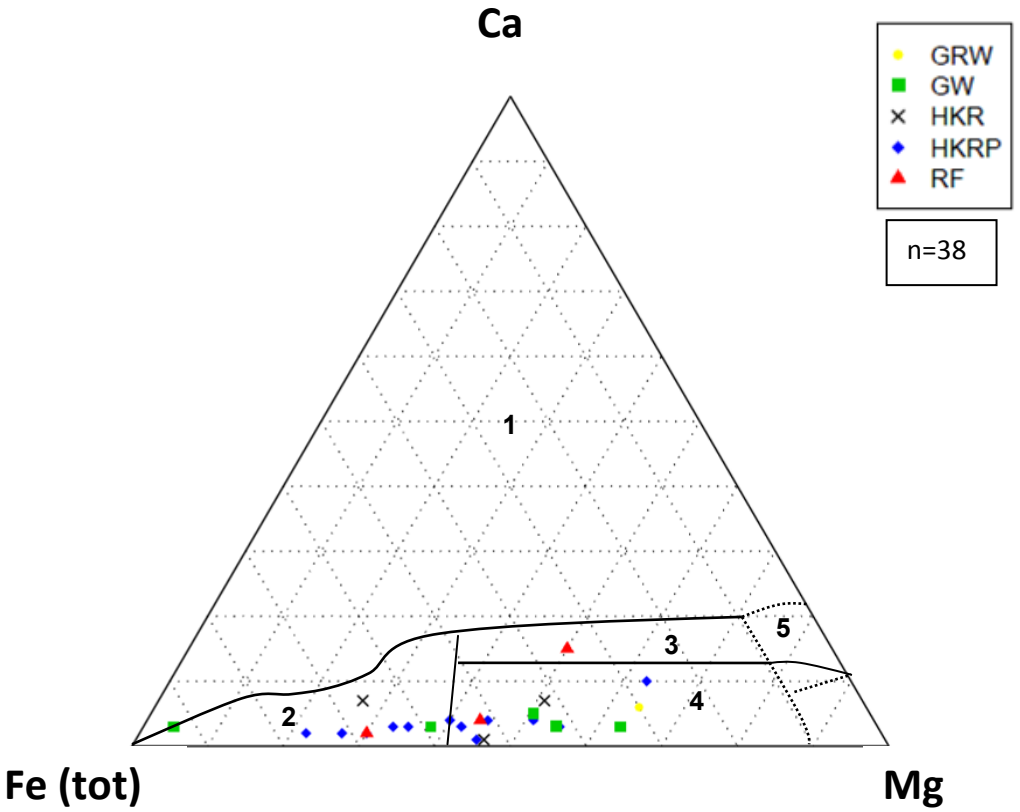

Figure 7.22. Tourmaline of the five satellite areas plotted on Henry and Guidotti's (1985) Ca-Fe (tot)-Mg diagram. The numbered fields correspond to the following rock types: (l) Li-rich granitoid pegmatites and aplites (2) Li-poor granitoids and associated pegmatites and aplites (3) Ca-rich metapelites, metapsammites, and calc-silicate rocks (4) Ca-poor metapelites, metapsammites, and quartz-tourmaline rocks (5) metacarbonates and (6) meta-ultramafics.

Cilliers (1995) and Macdonald (1996) also found tourmaline in their study areas. Philander (1999) did not mention the presence of tourmaline in his samples. Chemical data of Cilliers (1995) was not available and therefore the chemical data of this study was only compared with that of Macdonald (1996) (Figure 7.23). Figures 7.23 and 7.24 show that the tourmaline of the five satellite areas and that of Macdonald (1996) cluster in the same fields indicating a similar chemistry and similar provenance. Macdonald (1996) has more of the schorl molecule than dravite present. The only difference is that Macdonald's (1996) tourmaline does not have any of the buergerite (Fe^{3+}) molecules present. Macdonald (1996) proposed granites and granitic pegmatite as likely sources for his study. Considering above findings and similarities with Macdonald (1996), the primary source of the tourmaline of the satellite areas is Li-poor granitic and pegmatitic sources and metasediments. The contribution from calc-silicates is minor.

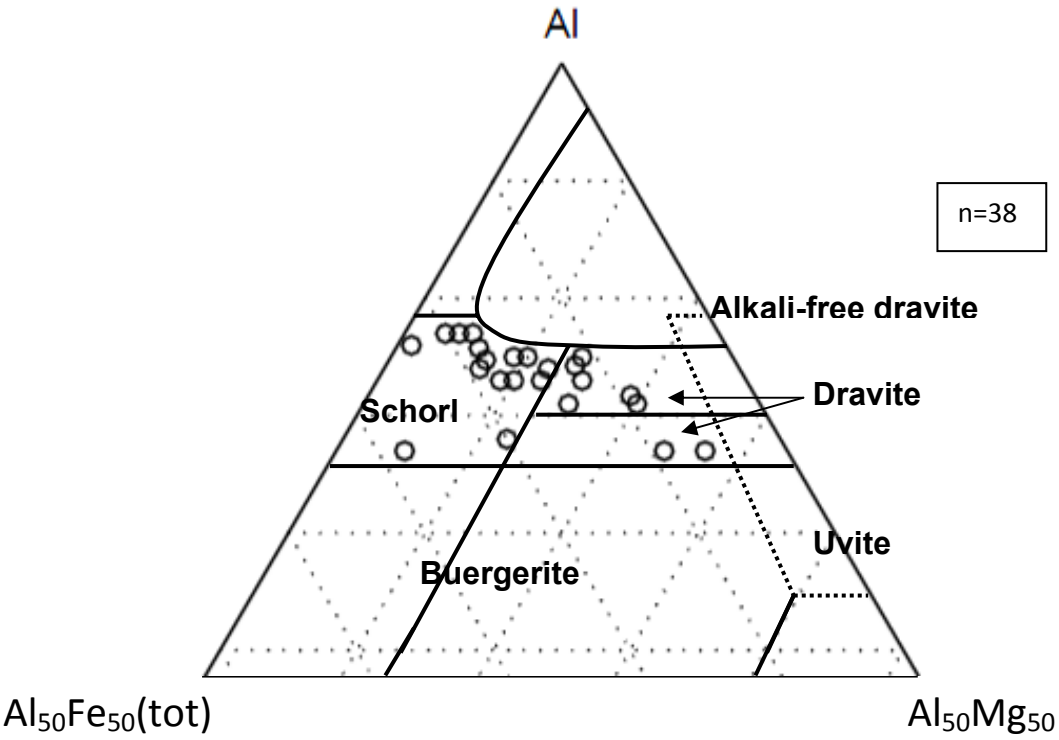

Figure 7.23. Al-Fe (tot)-Mg ternary diagram showing the composition of tourmaline from the Geelwal Karoo modern day beach placer (Macdonald, 1996). Dotted lines indicate field that overlap. Tourmaline consists of dravite and schorl.

Above-mentioned source rocks are present in the proximal NMC. Moore (1989) described tourmaline-bearing rocks such as schists and paragneisses from western Namaqualand Metamorphic Complex (NMC). Moore (1989) mentioned metaquartzites containing accessory tourmaline. Albat (1983) also described metasediments such as aluminous (pelitic) gneisses and schist, granitic gneisses and pegmatites in the Kliprand area in Namaqualand.

The NMC is thus a likely source for the tourmaline of the satellite areas. Elbaite-rich tourmalines are not known in the NMC region and are supported by Figures 7.23 and 7.24.

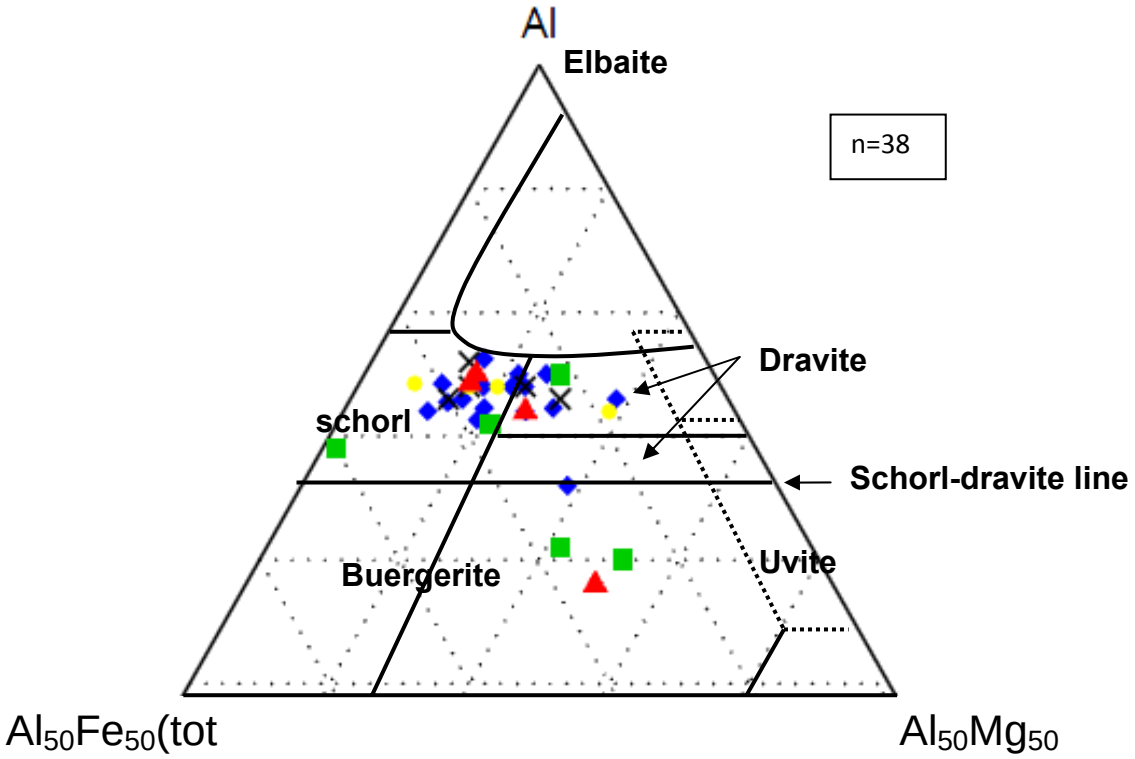

Figure 7.24. Al-Fe (tot)-Mg ternary diagram showing the composition of tourmaline from the five satellite areas. Dotted lines indicate field that overlap. Tourmaline comprises schorl, dravite and buergerite.

7.2.9 Aluminosilicates

The aluminosilicates (kyanite, andalusite, sillimanite) suggest high-grade metamorphic sources. Kyanite generally occurs in regional metamorphosed pelitic rocks, schists and kyanite amphibolites (Deer et al, 1992). Andalusite is characteristic of argillaceous rocks of contact aureoles around igneous intrusions (Deer et al, 1992). Sillimanite is common in metamorphosed sedimentary rocks such as schists and gneisses. The presence of kyanite, andalusite and sillimanite usually indicate that the source rocks experienced different pressures and temperatures ranging from greenschist, through amphibolite to lower granulite facies (Deer et al, 1992). It is also considered as unstable and therefore did not experience long-distance transport.

Zelt (1980) found kyanite in metapelites of the amphibolite facies and the granulite facies in Namaqualand. Jack (1980) found kyanite as an index mineral for aluminous schists and gneisses in western Namaqualand, Garies area. Joubert (1971) mentioned the presence of kyanite-bearing rocks such as metaquartzites and pelitic gneisses and schists in western

Namaqualand in the Nababeep area. Waters et al (1983) described pelitic gneisses and schists in large areas covering the Sout River area and its tributaries and near the confluence of the Sout and Groot Goerap Rivers, southwest of Bittterfontein. The kyanite is believed to have formed from a retrograde reaction. Garnet-staurolite-kyanite-mica schists in the lower Sout River areas experienced pressure and temperature conditions of 6-7 kbars and 630ºC respectively indicating amphibolite facies conditions.

From the evidence above, it can thus be concluded that the aluminosilicates were derived from mainly amphibolite facies pelitic gneisses, schists and amphibolites. These rock types are present in the proximal NMC. The NMC is thus a likely source terrain for the aluminosilicate minerals.

7.2.10 Staurolite

Staurolite is characteristic of medium-grade metamorphosed pelitic gneisses and schists, clastic sediments and heavy mineral assemblages (Deer et al, 1992). Jack (1980) found staurolite in amphibolite facies aluminous schists and gneisses in western Namaqualand, in the Garies area. Albat (1980) also found staurolite occurring together with kyanite and almandine in aluminous gneisses and schists. The latter mineral assemblage indicates amphibolite facies conditions.

Cilliers (1995), Macdonald (1996) and Philander (1999) also found staurolite in their study areas. Macdonald (1996) and Philander (1999) ascribed the origin to pelitic source rocks, in which metamorphism reached the staurolite zone of the amphibolite facies, and to medium-grade (amphibolite) gneisses and schists from the NMC area respectively. Cilliers (1995) did not propose a possible source area for the Graauwduinen's staurolite. Waters et al (1983) mentioned the presence of staurolite in amphibolite facies mica schists in the Sout River area.

From this evidence the most likely source for the staurolite is thus amphibolite facies metapelites and schists of the NMC area.

7.2.11 Epidote Group Minerals

Epidote is indicative of gneissic, granitic and basic sources and calc-silicates as well as epidote-amphibolite facies conditions (Miyashiro, 1973). Zelt (1980) found epidote in mafic rocks from the amphibolite zone in Namaqualand. Albat (1980) also found epidote, zoisite and clinozoisite in calc-silicate gneisses from the amphibolite facies. According to Deer et al (1992) the clinozoisite-epidote series are common in a wide range of metamorphic rocks and greenschist and epidote-amphibolite facies rocks. Epidote-bearing assemblages occur in products of contact metamorphism especially calcareous rocks. Jack (1980) found epidote, zoisite and clinozoisite in calc-silicate rocks, mafic gneisses, mafic granulites and mafic amphibolites. The latter being restricted to near the west coast of his study area in western Namaqualand. Moore (1989) also found epidote in calc-silicate rocks and metabasic rocks. Joubert (1971) found epidote in psammitic and pelitic gneisses and schists and epidote and zoisite in amphibolites in western Namaqualand. De Beer et al (2002) mentioned epidote in granite gneisses of the Little Namaqualand Suite of the NMC.

Philander (1999) ascribed the epidote of the Kleinzee area to a mafic amphibolite source. Cilliers (1995) and Macdonald (1996) did not mention epidote in their study areas. According to Deer et al (1992) and findings of above-mentioned authors, the epidote of this study can be ascribed to mafic rocks, calc-silicate and granite gneisses and pelitic rocks of the amphibolite facies of the NMC.

7.2.12 Sphene

Sphene is found in igneous, acid and intermediate plutonic rocks, sedimentary and metamorphic rocks (Deer et al, 1992). It forms one of the major titanium-bearing minerals together with rutile, anatase, titanomagnetite, titanohematite and perovskite ($CaTiO_3$). In the latter rocks it occurs mainly in schists and gneisses and impure meta calc-silicate rocks (Deer et al, 1992). Albat (1980) studied mafic rocks and concluded that for his study, sphene in mafic rocks (gneisses) are restricted to the upper amphibolite facies but occur in granulite facies calc-silicate gneisses though, where it forms an accessory mineral.

Jack (1980) found sphene in mafic gneisses, mafic granulites, mafic amphibolites, aluminous gneisses and calc-silicate rocks. Moore (1989) described sphene in calc-silicate rocks. Joubert

(1971) found sphene in pelitic gneisses and schists and in the Nababeep augen and streaky gneisses. Philander (1999) ascribed the source of sphene from the Kleinzee area to mafic amphibolites in the near proximity.

Likely sources for the sphene are thus mainly NMC mafic rocks from the amphibolite facies and metapelitic gneisses and schists and calc-silicates.

7.2.13 Corundum

Corundum occurs on a large scale in pegmatites and is a typical detrital mineral in sediments of all ages (Deer et al, 1992). Gem quality corundum is found in placer deposits. Albat (1980) found corundum in pelitic gneisses and semipelitic metamorphites in the Kliprand area. Cilliers (1995), Macdonald (1996) and Philander (1999) did not mention the presence of corundum in their study areas.

Since corundum is an Al-rich mineral, it is likely to be derived from an Al-rich source such as aluminous pelites, gneisses and schists and also pegmatites.

7.2.14 Monazite

Monazite is a common accessory mineral in granitic pegmatites, granitic rocks and syenitic pegmatite (Deer et al, 1992). Albat (1980), Joubert (1971), Jack (1980) and Moore (1989) did not mention the presence of monazite in their study areas.

Cilliers (1995) found one monazite grain in the Graauwduinen deposit but did not propose any source rocks. Macdonald (1996) also did not mention monazite in the Geelwal Karoo beach placer deposits. Philander (1999) found monazite in the Kleinzee area and described its origin to granites and felsic gneisses as well as from the Steenkampskraal deposits due to its high rounded nature.

Steenkampskraal is located within the vicinity of the satellite areas and is situated 350km north of Cape Town and approximately 35km south of Brand-se-Baai. The Steenkampskraal monazite district is located in the southern part of the NMC area. The monazite ore is present as veins within Mesoproterozoic foliated granite and megacrystic granite gneiss (Read et al, 2002). The chemistry of the monazite of the satellite areas were compared to that of

Steenkampskraal (Andreoli et al, 1994; Read et al, 2002). Monazite from the two areas has similar P_2O_5, CaO, FeO and SiO_2 contents. Two monazite grains from the satellite areas have 30 wt % and 31 wt % Al_2O_3 respectively. These high concentrations can be due to aluminosilicate inclusions. There are remarkable differences in the rare earth element concentrations. The Steenkampskraal monazite has three to four times higher La, Ce and Nd contents than the satellite area's monazite. The Th content of the monazite of the satellite areas is up to four times higher than the Steenkamspkraal's monazite. The differences in the REE chemistry exclude Steenkampskraal as a possible source area. Only a few grains were analysed and are probably not representative of the entire suite.

De Beer (2010) reported on the presence of secondary rare earth minerals which include monazite in the Sandkopsdrift Complex. The latter occurs on the farm Zandkopsdrift in the Namaqualand region, about 450km north of Cape Town (Figure 7.25) and far north from the satellite areas. It is one of the largest rare earth deposits in the world and includes explosive breccia, carbonatite, alkaline rocks and glimmerite (intrusive rock) (De Beer, 2010).

Source rocks for the monazite include granitic pegmatites, granitic rocks, syenitic pegmatite and felsic gneisses. The rounded nature of the monazite can indicate monazite derived from the Zandkopsdrift deposit. The fact that there is no correlation with Steenkampskraal's monazite provides further support for a proximal dominated source.

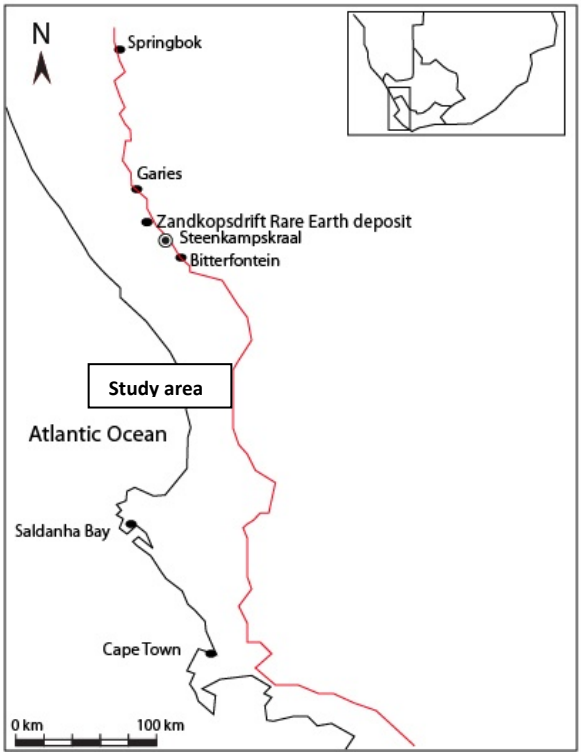

Figure 7.25. Map showing the location of the Zandkopsdrift rare earth deposit.

7.3 Discussion

The wide range in composition of minerals such as garnet, tourmaline and pyroxene and the wide variety of heavy minerals present indicate a wide range in source lithologies. Source lithologies include metamorphic, igneous and sedimentary rocks and pegmatites. Table 7.1 lists the source lithologies as indicated by each mineral in the heavy mineral suite of the satellite areas. The metamorphic rocks range from greenschist facies (epidote) to amphibolite facies (aluminosilicates) and granulite facies (orthopyroxene) rocks. The mineral assemblage of magnetite, green hornblende, ilmenite, zircon, epidote and, sphene in the heavy mineral suite is indicative of granitic, gneissic and basic sources. Rutile, grossular garnet and tourmaline indicate source rocks such as limestone and dolomite and metapelites and aluminosilicates also indicates metapelites.

Table 7.1. Different heavy minerals present in the five satellite areas and the source rocks determined from the chemistry of the heavy minerals.

Mineral	Source rock types
ilmenite	igneous (felsic, mafic and intermediate) rocks and metamorphic rocks
zircon	igneous rocks such as granitoids, pegmatites, syenites and carbonatites
rutile	metamorphic rocks (metapelites and metamafic rocks) that underwent mainly amphibolite and granulite facies metamorphism
hematite	felsic igneous rocks
magnetite-spinel series	metamorphic rocks such as calc-silicate gneisses, metapelites and granites
garnet	Amphibolite and granulite facies mafic igneous rocks and metamorphic rocks (metapelite and metabasites)
pyroxene	metamorphic (metapelites, calc-silicate gneisses and schists) rocks that underwent upper amphibolite to granulite facies metamorphism and igneous (granitoids and pegmatite) rocks
tourmaline	metamorphic rocks (amphibolite facies pelitic gneisses and schist)
aluminosilicates	metamorphic rocks (amphibolite facies metapelites and schist)
staurolite	metamorphic rocks (granite gneisses, metapelites, metabasites and calc-silicates) and igneous (mafic) rocks
epidote group of minerals	amphibolite facies metapelitic schists and gneisses and granulite facies calc-silicate rocks)
sphene	metamorphic rocks (aluminous pelitic gneisses and schist)
corundum	metamorphic rocks (aluminous pelitic gneisses and schist)
monazite	Possibly igneous rocks of Steenkampskraal (granites and granite gneisses) or Sandkopsdrift Complex (carbonatite and alkaline rocks).

The mineralogy of all five satellite areas are the same indicating a common provenance area. Force (1991) stated that high-grade metamorphic terrains are usually the source of such a diversity of heavy minerals.

The temperatures calculated with the thermometers of Watson et al. (2006) and Tomkins et al. (2007) confirms the source area of the satellite areas to be a high-grade metamorphic terrain.

The Namaqualand Metamorphic Complex is one such a terrain where high-grade metamorphic rocks and igneous rocks, amphibolites, pegmatites and metasedimentary rocks are present. It is also proximal to the satellite areas, within a radius of 40km. Authors such as Moore (1989), Albat (1983), Zelt (1980), Theart (1980), De Beer et al (2002) and De Beer

(2010) mentioned the presence of above rocks types in the NMC. It covers a large area that stretches from south and west of Bitterfontein, north of the Orange River and up to Prieska in the west (Figure 7.26). The Bushmanland Subprovince and the central zone of the Gordonia Subprovince experienced granulite facies conditions. Amphibolite facies conditions were recorded along the west coast belt. The Richtersveld Subprovince experienced greenschist facies conditions.

Evidence for amphibolite and granulite facies metamorphism is also present in localities surrounding the satellite areas. The pelitic gneisses of the Sout River area contain the assemblage garnet+cordierite+K-feldspar+liquid. This mineral assemblage is indicative of granulite facies conditions. On Potkley, the pelitic gneisses contain the assemblage garnet+ biotite+sillimanite+quartz which are indicative of amphibolite facies conditions. Metapelitic rocks between Potkley and Bitterfontein show amphibolite facies conditions as well (Waters et al, 1983). The Namaqua basement rocks at Rietfontein contain the assemblage sillimanite-garnet-staurolite-biotite-muscovite-quartz-plagioclase which is indicative of amphibolite facies conditions (De Beer, 2010).

The angular nature of the garnet grains and the idiomorphic zircon grains indicates limited transport and that the source terrain must be proximal. Tourmaline and the Fe-Ti oxides are well rounded and indicate that it is derived from older reworked and eroded source rocks. The rounded grains were then mixed with younger, proximal material resulting in rounded grains occurring together with angular and idiomorphic grains. Unstable minerals such as pyroxene and epidote are also present in the heavy mineral suite indicating further that the source is close since these minerals are easily destroyed during transportation and diagenesis. The proximity of the NMC therefore explains the diverse mineralogy and poor sorting of the heavy mineral suite.

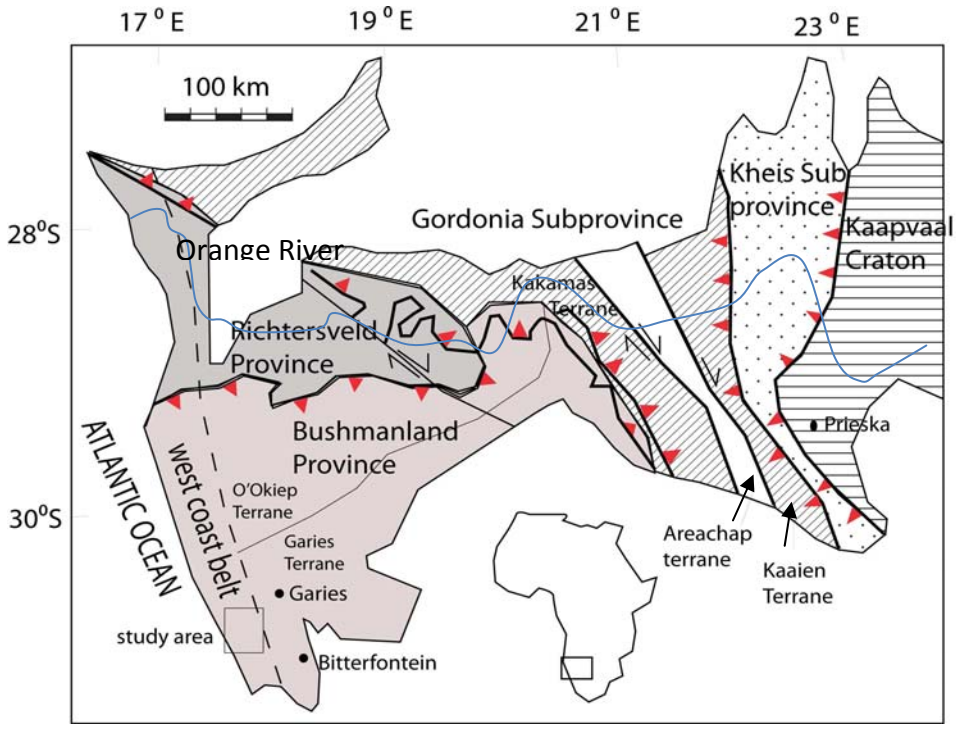

Figure 7.26. Map showing the different tectonic subprovinces and terranes of southern Africa. The study areas are present in the Garies terrain, in particular the West coast belt (modified after Hartnady et al, 1985; Thomas et al, 1993 and Duchesne et al, 2007).

The Gariep Supergroup can also be considered a provenance contributor but has made a minor contribution to the heavy mineral suite. As mentioned in the beginning of the discussion, some of the minerals indicate greenschist facies conditions. The Gariep Supergroup rocks experienced greenschist facies conditions with a temperature and pressure of ~445°C and ~5 kbar.

Grossular garnet is a relatively unstable mineral that is easily destroyed by long distance transport and abrasion (Morton, 1991). The high contents of this mineral in the satellite areas specifically Geelwal Karoo indicates a proximal source.

In addition the Vanrhynsdorp Group rocks cannot be excluded but will be insignificant as a source contributor. These rocks also underwent greenschist facies metamorphism (De Beer et al, 2002).

The three most common minerals in the satellite areas are ilmenite, garnet and zircon indicating that high-grade metamorphic rocks and felsic and mafic igneous rocks are the

dominant source lithologies. The Gariep Supergroup and Vanrhynsdorp Group rocks are therefore minor contributors to the satellite areas.

CHAPTER 8 COMPARISON WITH NAMAKWA SANDS OREBODY AND GENESIS OF THE SATELLITE DEPOSITS

8.1 Introduction

Heavy mineral deposits all over the world are characterized by specific features. It usually forms coast parallel bodies, has a high-grade metamorphic source terrain, occurs at latitudes lower than 35° and is concentrated by sedimentary processes that control particle shape, size and density. These deposits usually contain high concentrations of the ore minerals rutile, ilmenite, zircon and leucoxene. The non-economic fraction consists of minerals such as aluminosilicates, tourmaline, sphene, staurolite, garnet, pyroxene and amphibole.

The five satellite areas have similarities but also differences in its chemistry, mineralogy, maturity and genesis. In this chapter these differences between the five satellite areas are discussed and the satellite areas are then compared to the Namakwa Sands heavy mineral deposit. The Namakwa Sands deposit is divided into the East- and West Mine.

8.2 Comparison of the five satellite areas

Mineral proportions

The five satellite areas contain the same suite of heavy minerals but in different proportions (Table 8.1). Houtkraal Remainder and Houtkraal Remainder Portion 2 have approximately similar mineral proportions. The same is evident for Geelwal Karoo and Graauwduinen which has approximately similar mineral proportions. Rietfontein has different mineral proportions than the other four satellite areas.

Houtkraal Remainder has the highest ilmenite and lowest garnet and pyroxene contents (Table 8.1).

Rietfontein has the lowest ilmenite, zircon and leucoxene contents and the highest garnet content (Table 8.1). In thin-section it was found to have the highest content of epidote as well.

Table 8.1. Averages of mineral proportions and VHM and THM contents of the satellite areas and the Namakwa Sands deposit.

Area	THM	Ilmenite	Leuco-xene	Rutile	Zircon	Garnet	Pyroxene	Other minerals	VHM
HKRP2	3	46	6	6	13	19	3	7	2
HKR	5	61	6	6	13	7	2	6	4
GW	3	43	7	8	11	23	8	1	2
GRW	2	47	7	7	13	14	3	10	2
RF	3	37	5	6	10	32	4	6	2
East Mine	11	61	10	5	16	3	1	3	10
West Mine	10	50	9	6	13	12	5	5	8

Table 8.2. Averages of the whole rock chemistry of the satellite areas and the Namakwa Sands deposit.

Area	Al_2O_3	CaO	Fe_2O_3	MgO	K_2O	MnO	Na_2O	SiO_2	TiO_2	P_2O_5	ZrO_2
HKR	2.09	0.12	2.70	0.09	5.36	0.07	0.18	88.19	2.03	0.04	0.48
HKRP2	2.05	0.11	2.08	0.11	2.52	0.05	0.10	91.60	1.16	0.03	0.28
GW	3.54	0.40	2.32	0.50	7.67	0.04	0.41	84.59	0.94	0.06	0.17
GRW	3.52	0.15	2.06	0.17	0.00	0.04	0.74	85.86	1.00	0.03	0.17
RF	2.61	0.18	2.14	0.18	0.00	0.06	0.91	87.29	1.09	0.02	0.18
East Mine	1.25	0.05	4.31	0.05	0.27	0.13	0.10	92.52	3.81	0.02	1.03
West Mine	2.90	0.04	4.51	0.66	0.04	0.00	0.00	86.60	3.09	0.00	0.62

Geelwal Karoo has the second highest garnet content with the highest pyroxene content. It has the second lowest ilmenite content and the lowest other minerals content of all five the satellite areas.

Graauwduinen is the most enriched in other minerals. The latter includes tourmaline, amphibole, sphene, staurolite, aluminosilicates, monazite, epidote and corundum.

The satellite areas have similar zircon contents except for Rietfontein and Geelwal Karoo that is the least enriched in zircon. Rutile and leucoxene contents are similar for the five areas except for Rietfontein that has a lower leucoxene content (Table 8.1).

The five satellite areas also have different percentages of the garnet end-members with Houtkraal Remainder being the only satellite area that does not have almandine but spessartine as the dominant garnet end-member.

Chemistry

Houtkraal Remainder and Houtkraal Remainder Portion 2 have similar whole rock chemistry. The same is evident for Graauwduinen and Geelwal Karoo which has similar whole rock chemistry (Table 8.2). Rietfontein has its own unique whole rock chemistry and is significantly different from the others.

In chapter 5 it was established that the mineral chemistry of Geelwal Karoo's rutile has higher Pb, Mn and ∑REE average contents than the rest of the satellite areas. Rietfontein's rutile has higher U+Th and Hf average contents than the rest of the satellite areas. Rietfontein is also the only satellite area that is dominated by granulite facies rutile while the other four areas are dominated by amphibolite facies rutile.

THM and VHM

Houtkraal Remainder has the highest VHM and THM contents of the satellite areas (Table 8.1). Due to the highest VHM content, it has the lowest non-economic minerals content. The other four satellite areas have similar VHM and THM contents (Table 8.1).

Maturity

Houtkraal Remainder is the most mature satellite sand followed by Houtkraal Remainder Portion 2 (Figure 4.15). Rietfontein is the least mature. Graauwduinen and Geelwal Karoo have similar maturities (Figure 4.15).

Alteration

In terms of alteration, Rietfontein shows the most alteration of all five satellite areas followed by Houtkraal Remainder Portion 2. These two areas are dominated by leucoxene whereas Houtkraal Remainder, Geelwal Karoo and Graauwduinen are dominated by hydrated ilmenite.

Grain size

The grain sizes for zircon are similar for the five satellite areas. Graauwduinen has the most coarse ilmenite grains and Rietfontein the most coarse rutile grains.

8.3 Discussion

Mineral proportions in a heavy mineral deposit are controlled by parameters such as provenance, mechanism (wind, sea and river), post depositional processes (weathering) and topography. The similar mineral proportions of the two Houtkraal areas and of Geelwal Karoo and Graauwduinen indicate that the same process, wind activity, played a role in the formation of the heavy mineral deposits. A difference in mineral proportions indicates a change in one or more of these parameters.

In-situ weathering can cause depletion in unstable minerals by breaking down these unstable minerals and removing it from the heavy mineral suite. Weathering may also form secondary minerals such as clays from the unstable minerals. Weathering thus modifies relative abundances of the heavy minerals. The five satellite areas probably underwent different degrees of weathering resulting in the different mineral proportions. The provenance of all five the satellite areas are the NMC and the provenance are therefore neglible and not taken into account with respect to the difference in mineral proportions. The topography is discussed in more detail in section 8.6.

The higher U+Th and Hf mean values of Rietfontein's rutile and the higher Pb, Mn and ∑REE mean values of Geelwal Karoo's rutile can probably be ascribed to erosion or weathering. U, Th, Pb and Mn are considered impurities in rutile and negatively affect rutile grade and its recovery. It is possible that in these two areas the U+Th, Pb, Hf, ∑REE and Mn-enriched rutile were not eroded and winnowed, because of higher density, by the wind, whereas in the two Houtkraal areas and Graauwduinen it was. Another explanation is that the areas underwent different degrees of weathering as mentioned above and in the two Houtkraal areas and Graauwduinen these rutile were broken down and removed from the heavy mineral suite.

Rietfontein and Houtkraal Remainder Portion 2 are adjacent to one another. The higher degree of alteration experienced by these two areas can be due to the heavy mineral-bearing sediment being leached by a more acidic fluid derived from the upper soil layers. Leucoxene formation takes place in the uppermost soil layers of a deposit.

In chapter 3 it was stated that pelitic gneisses in the Sout River area contains the assemblage garnet+cordierite+K-feldspar. This assemblage is indicative of granulite facies conditions. Rietfontein is located in the vicinity of the Sout River area and therefore has mostly granulite facies rutile. The Rietfontein assemblage is thus provenance controlled.

Spessartine is the dominant garnet end-member in the East Mine RAS (Philander and Rozendaal, in press). In chapter 4 it was established that the RAS of the East Mine continues into Houtkraal Remainder and the latter is situated along the northern to northeastern boundary of the Namakwa Sands deposit (Figures 1.2 and 8.6). Houtkraal Remainder is therefore a RAS type of sediment and similar in character to the RAS of the East Mine and therefore also has spessartine as its dominant garnet end-member.

The coarser grain sizes of Rietfontein's rutile and Graauwduinen's ilmenite can be due to mechanical abrasion during transport or post depositional weathering. Mechanical abrasion reduces the grain size of minerals by means of fracturing and rounding (Morton and Hallsworth, 1999). Rutile grains of Rietfontein and ilmenite of Graauwduinen underwent less mechanical abrasion and less post depositional weathering resulting in the coarser grain sizes.

From the above discussion it can be concluded that the surficial sands on the five satellite areas are not similar and reflect contrasting morphological, mineralogical and mineral

chemical characteristics. These differences can be explained by distance from the present shoreline, proximity to provenance and sediment transport induced maturity.

8.4 Namakwa Sands deposit

Similar chemistry and mineral correlation diagrams, as used for the satellite areas, were plotted for the East Mine and West Mine of the Namakwa Sands deposit for comparative purposes. XRF data were used to plot the chemistry correlation diagrams and QEMSCAN data were used to plot the mineralogy correlation diagrams. XRF and QEMSCAN data were obtained from Philander (pers comm).

8.4.1 East Mine

The East Mine has the highest correlation coefficients for elements such as Fe and Ti (ρ= 0.95), Mn and Ti (ρ=0.98) and Fe and Mn (ρ=0.96). Houtkraal Remainder shows similar high coefficients (Chapter 4, section 4.4) indicating that for these two areas most of the Fe, Ti and Mn occur in ilmenite and only small amounts are present in rutile, leucoxene and garnet. The satellite areas, unlike Houtkraal Remainder and the East Mine, have a significant amount of Fe, Ti and Mn in rutile, leucoxene and garnet.

The East Mine has a correlation coefficient of ρ=0.87 between Ca and P (Appendix E, Figure E6). The high coefficient indicates that most of the Ca is present in apatite. Al and Al/Al+Fe show a high, positive correlation with a ρ value = 0.85. The satellite areas, except for Rietfontein, do not have this positive correlation. It indicates that as the content of Al-rich minerals increase (staurolite, epidote, aluminosilicates and amphiboles), the content of Al- and Fe-rich minerals (garnet, tourmaline, and pyroxene) also increase. All of these minerals are non-economic. The East Mine has the highest correlation coefficients for Mn and VHM (ρ=0.97), Zr and VHM (ρ=0.95), Fe and VHM (ρ=0.95) and Ti and VHM (ρ=0.99) because of the presence of zircon, rutile and ilmenite.

The East Mine shows no trends for elements such as Ca and Fe, Al and Ca, Ca and Mg, Mg and Fe, Mg and Mn and Al and Mg and is similar to Rietfontein. This is due to the diverse mineralogy of the East Mine. The elements thus occur in various minerals and do not occur in

one specific mineral phase. Another reason is that the East Mine consists solely of RAS. The RAS is a mature sand unit that consists dominantly of valuable heavy minerals such as ilmenite, rutile, zircon and leucoxene.

The mineralogy correlation diagram (Appendix D, Figure D6) indicates that the VHM and THM have a coefficient of 1 for the East Mine indicating that the THM is made up entirely of VHM. Houtkraal Remainder has a similar correlation coefficient of 1 between the VHM and THM.

The high correlation coefficient between the VHM and THM is supported by the absence of any relationships between the elements Ca, Al, Mg and Mn.

8.4.2 West Mine

The West Mine shows the highest, positive correlations for Al and Fe (ρ=0.86), Ca and Mg (ρ=0.87), and Al and Mg (ρ=0.72) compared to the satellite areas. It shows correlations between elements that the other satellite areas and the East Mine do not show (Appendix E, Figure E7). An example is the positive correlation between Ca and Si (ρ=0.74). All of these elements indicate non-economic minerals such as garnet, staurolite, pyroxene, amphibole, epidote and tourmaline. The West Mine consists of orange feldspathic (OFS) -and quartzitic aeolian (QAS) sands. These sands contain Al-, Ca-, Mg- and Mn-bearing minerals such as pyroxene, garnet, amphibole and pyroxene and therefore explain the high, positive correlations between these elements. Zr, Ti, Mn and Fe show poor correlations with VHM unlike the East Mine and satellite areas.

The mineralogy correlation diagram (Appendix D, Figure D7) indicates a positive correlation of ρ=0.95 between the VHM and THM indicating that most of the THM is VHM and only a small amount of non-economic minerals are present.

8.5 Comparison between the Namakwa sands deposit and the satellite areas.

THM-VHM relationship

The THM-VHM relationship (Figure 8.1) of the East- and West Mine of the Namakwa Sands deposit shows that the East Mine has a steep (45°) slope indicating that all the heavy minerals are valuable from an economic point of view and and no non-economic minerals are present. It has the steepest slope of all five the satellite areas and the West Mine (Figure 8.1 B). The steep slope also indicates that the East Mine sediments are very mature. The maturity of the East Mine is due to wind activity. The East Mine consists solely of RAS and the latter is a mature aeolian sand unit. It has high contents of valuable heavy minerals (ilmenite, rutile, leucoxene, and zircon) and was upgraded by wind action over an extensive period of time. The wind winnowed the less stable heavy minerals such as pyroxene and garnet and upgraded the more stable heavy minerals such as ilmenite, rutile, leucoxene and zircon. Table 8.1 indicates that the East Mine has the highest ilmenite, leucoxene and zircon contents and consequently the highest VHM content and has the lowest garnet, pyroxene and other minerals contents. It also has the highest THM content.

The West Mine has a less steep slope than the East Mine indicating it is less mature (Figure 8.1 A). This is due to the presence of more non-economic minerals in the THM fraction. The West Mine consists of orange feldspathic sands (OFS). These sands contain more non-economic minerals than the East Mine's RAS. Table 8.1 indicates that the West Mine contains more garnet, pyroxene and other minerals than the East Mine and has a lower ilmenite and zircon content. The West Mine was also upgraded by wind action but over a shorter period of time and the wind was less effective in removing the unstable, non-economic minerals and upgrading the stable economic minerals, thus resulting in the lower maturity.

Houtkraal Remainder also has a ~45° slope with a high maturity (Chapter 4 and Figure 8.1 B). It has the same ilmenite content as the East Mine and has the second lowest garnet, pyroxene and other minerals contents after the East Mine. The similar slopes of Houtkraal Remainder and the East Mine and the high ilmenite and low non-economic mineral contents, indicates that the same process, wind activity, upgraded the heavy mineral fraction and is responsible for the high and similar maturity of these two areas. Houtkraal Remainder though

has lower VHM and THM contents than the East Mine. This is due to wind activity and topography and is discussed later in the text.

Houtkraal Remainder is more mature than the West Mine since it has a steeper slope (Figure 8.1 B). The higher maturity of Houtkraal Remainder is also illustrated by Table 8.1 where the former area has a higher ilmenite content with lower garnet and pyroxene contents than the West Mine. It borders on the East Mine and seems to be a continuation thereof.

Houtkraal Remainder Portion 2 and the West Mine have similar steep slopes and thus have a similar maturity (Figure 8.1 A). The similar slopes also indicate that the same process, wind activity, upgraded the heavy mineral fraction of the two areas.

Geelwal Karoo, Graauwduinen and Rietfontein are less mature than the East Mine due to the less steep slopes and scattering of data points (Figure 8.1 C-E) and has higher contents of non-economic minerals and lower contents of the ore minerals (ilmenite, zircon and leucoxene, Table 8.1). Geelwal Karoo and Graauwduinen have similar slopes to the West Mine (Figure 8.1). Rietfontein has a less steep slope than the West Mine. These three areas all occur close to the present coastline and their similarities with respect to maturity are therefore expected.

Mineral proportions

Comparing the average values of the mineral proportions of the Namakwa Sands deposit to that of the satellite areas, significant differences are visible between the THM and VHM contents (Table 8.1). The East- and West Mine have two to five times the THM and VHM contents of the satellite areas. Houtkraal Remainder has the highest THM and VHM contents of the five satellite areas. Houtkraal Remainder and the East Mine have the highest and same amount of ilmenite content and have the lowest non-economic mineral content. The West Mine has the 2nd highest ilmenite content but with higher garnet, pyroxene and other minerals contents than the East Mine and Houtkraal Remainder. The West Mine has similar mineral proportions to Geelwal Karoo and Graauwduinen. Rietfontein contains the highest amount of non-economic minerals.

The Namakwa Sands deposit and the satellite areas have similar rutile contents. Houtkraal Remainder and the East Mine as mentioned above have the lowest pyroxene content. Pyroxene is an unstable mineral and is easily removed by sedimentary processes due to its

two cleavage directions. Low pyroxene content therefore is an indication of sediment maturity and indicates that the East Mine and Houtkraal Remainder are the most mature areas. Geelwal Karoo has the highest pyroxene content followed by Rietfontein. The high pyroxene content of these two areas further highlights its immaturity.

Chemistry

The East-and West Mine have higher TiO_2 and FeO(t) (total iron) contents than the satellite areas (Table 8.2). These two elements are a function of the THM (Figure 8.2 and Figure 8.3) indicating the higher the FeO(t) and TiO_2, the higher the THM.

These positive relationships between the THM and FeO(t) and the THM and TiO_2 are a good indication of the amount of Fe and Ti present in the THM for a particular area. For Houtkraal Remainder a THM content of 11% equals 5% of FeO(t) (Figure 8.2). The higher the maturity, the more reliable the prediction based on THM.

The five satellite areas have different whole rock chemistries than the East- and West Mine (Table 8.2). The East Mine has a unique whole rock chemistry. It has the highest MnO, ZrO_2 and TiO_2 contents of them all (Table 8.2). Rietfontein and the West Mine also have its own unique whole rock chemistries. There is a clear association between the East Mine and the two Houtkraal areas and between the West Mine, Geelwal Karoo, Graauwduinen and Rietfontein.

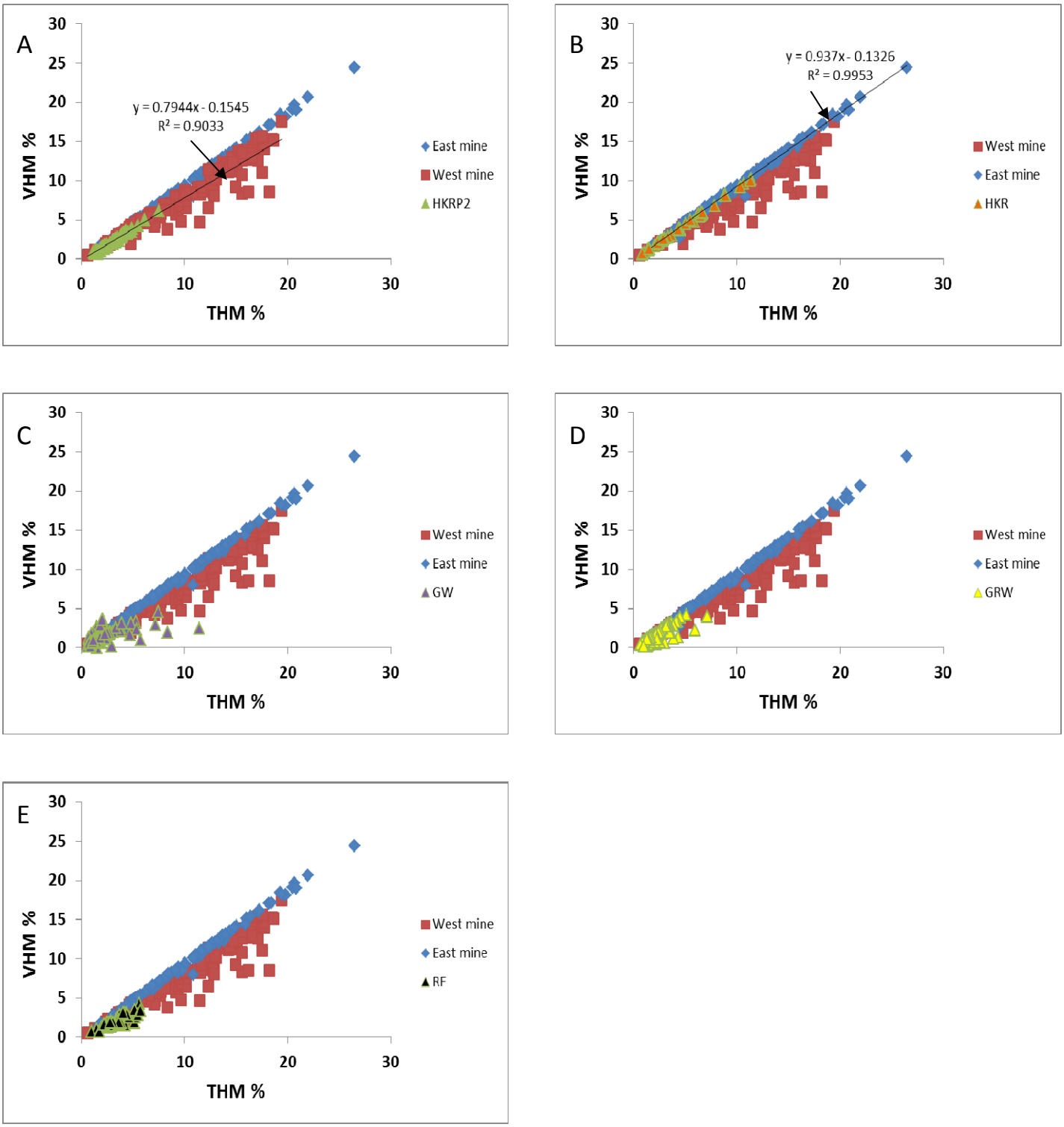

Figure 8.1. THM-VHM binary diagrams of the East –and West mine of the Namakwa Sands deposit and of the five satellite areas. The relationship between the East Mine and the two Houtkraal areas are clearly illustrated. Similarly the West Mine and the other coastal satellite areas have common characteristics.

8.6 Genesis

The satellite areas and the Namakwa Sands deposit contain the same suite of heavy minerals such as ilmenite, rutile, zircon, leucoxene, garnet, pyroxene, amphibole, staurolite, sphene, corundum, aluminosilicates and epidote but in different proportions (Table 8.1). It also has different sediment maturities, indicated by Figure 8.1, and chemistries (Table 8.2).

The different mineral proportions, sediment maturities and chemistries between the satellite areas and the East- and West Mine of the Namakwa Sands deposit indicate that these deposits do not have a common denominator. These differences reflect a different genetic history and factors supporting this are described below.

The lower VHM and THM contents of the satellite areas compared to the East- and West Mine are due to wind activity and topography. Cilliers (1995) showed that the morphology of the coast and topography of the Brand-se-Baai area controlled the formation and extent of the Namakwa Sands deposit. Skimmelkop formed a prominent headland to the south and Grouduin se Kop a headland to the north (Figure 8.5).

Kalkbaken se Kop and Bloukoppies se Knop also controlled the extent of the Namakwa Sands deposit (Figure 8.5). The topography rises in a northeast direction from 0m amsl to 120m amsl. The topography thus forms a depression between adjacent elevated areas. Heavy minerals were transported by the wind and deposited in this depression. Light minerals were winnowed out of the depression and the heavy minerals remained behind. The depression thus acted as a trap for heavy mineral accumulation. Northeastern winds transported the heavy minerals back and forth in the depression upgrading and maturing the sediment. The northeastern winds are responsible for the northeastern trend of the Namakwa Sands deposit (Figure 8.5).

The favourable topography of the Brand-se-Baai area and the RAS of the East Mine that was repeatedly reworked by wind action, upgrading and concentrating the heavy mineral sediment, resulted in the East Mine's high maturity and distinct chemistry.

The lower maturity of the West Mine is due to wind action that operated over a shorter period of time despite the favourable topography. Less stable heavy minerals were not winnowed and the deposit was not upgraded enough. The West Mine is also located closer to the ocean

and its immaturity is also a function of limited transport distance. In addition at least two heavy mineral enriched strandlines mark the West Mine and consist of a poorly sorted THM assemblage. This acted as a source for the aeolian component of the West Mine.

Rietfontein, Houtkraal Remainder Portion 2 and Houtkraal Remainder are located on the northern to northeastern edge of the Namakwa Sands deposit (Figure 8.6) and Graauwduinen and Geelwal Karoo are located south of the Namakwa Sands deposit. The topography surrounding the satellite areas consist of wide, open coastal plains with few bedrock high features (Figure 8.6). Due to the absence of depressions, the wind was unable to concentrate and upgrade the heavy minerals leading to the lower VHM and THM contents of the satellite areas. Houtkraal Remainder is located along the northern to northeastern boundary of the Namakwa Sands deposit (Figure 8.6). THM grades decreases away from the East Mine and topographic depression and therefore Houtkraal Remainder has lower THM and VHM contents.

All five the satellite areas are aeolian in character. The two Houtkraal areas are located east to northeast of Rietfontein (Figures 1.2 and 8.6). Houtkraal Remainder is located further east from Houtkraal Remainder Portion 2. Older sediments of the Cenozoic terraces with THM strandlines (De Beer et al, 2002) were wind eroded and together with the strandlines provided the heavy minerals that formed Rietfontein, Houtkraal Remainder Portion 2 and Houtkraal Remainder (Figure 8.4). The sediment gets more reworked, upgraded and matured, the further it gets transported and deposited from the coast. As a result the proximal sediments (Rietfontein) are less mature than the ones more towards the inland area (Houtkraal Remainder Portion 2 and Houtkraal Remainder). The maturity is thus a function of the distance from the coast. The lower maturity of Houtkraal Remainder Portion 2 is therefore due to its proximity to the coast. The sediments were not reworked and upgraded enough. The higher maturity of Houtkraal Remainder's sediments is due to the longer time spent being reworked and upgraded to a RAS type of sediment by the wind, because it is located further from the coast. There is thus a maturity increase from the immature Rietfontein, to the moderate mature Houtkraal Remainder Portion 2 to the mature Houtkraal Remainder. As a result Houtkraal Remainder has similar characteristics than the RAS as demonstrated previously.

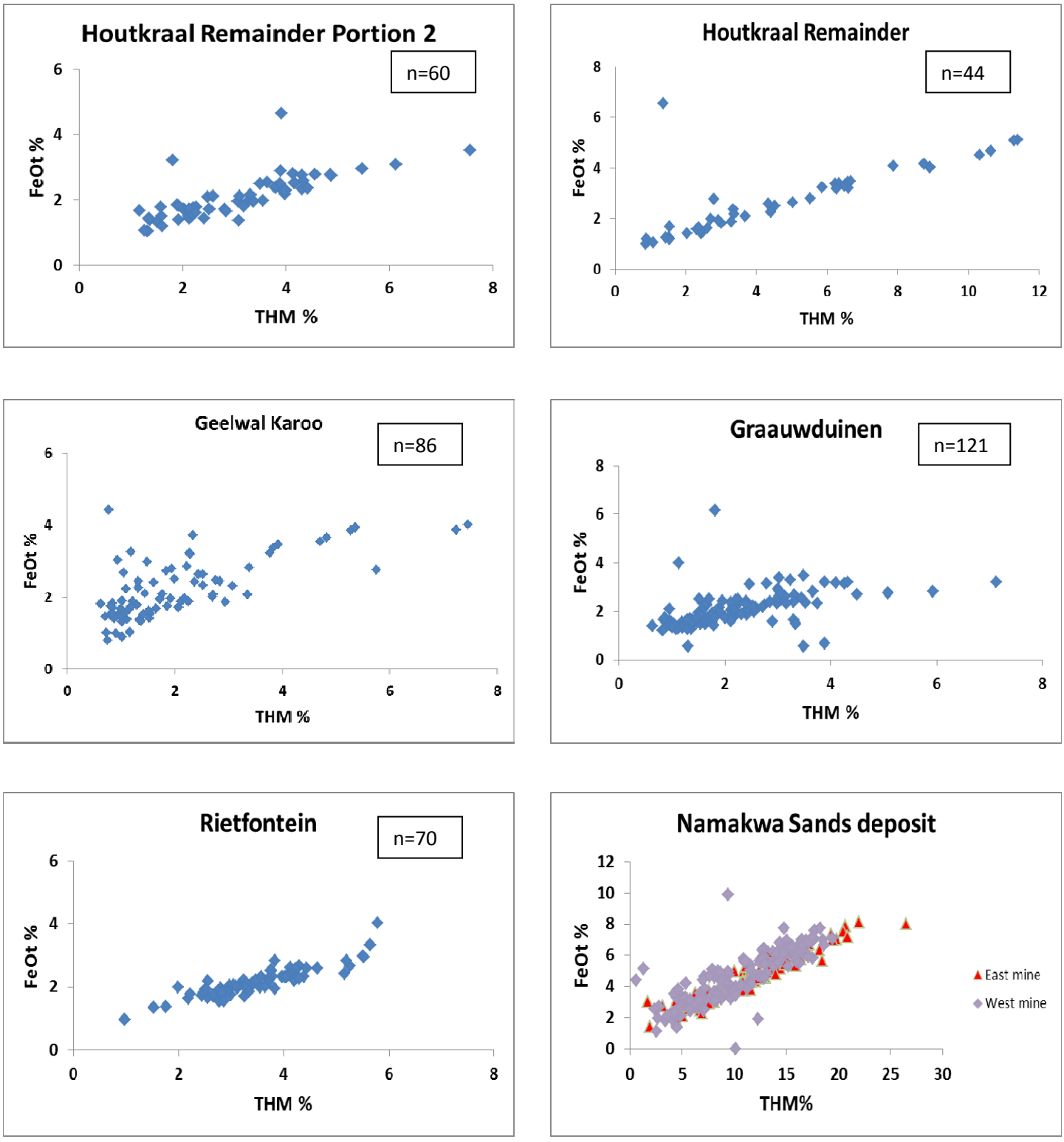

Figure 8.2. THM - FeOt (total iron) binary diagrams of the five satellite areas and the Namakwa Sands deposit. The East-and West Mine have higher FeOt (total iron) contents than the satellite areas.

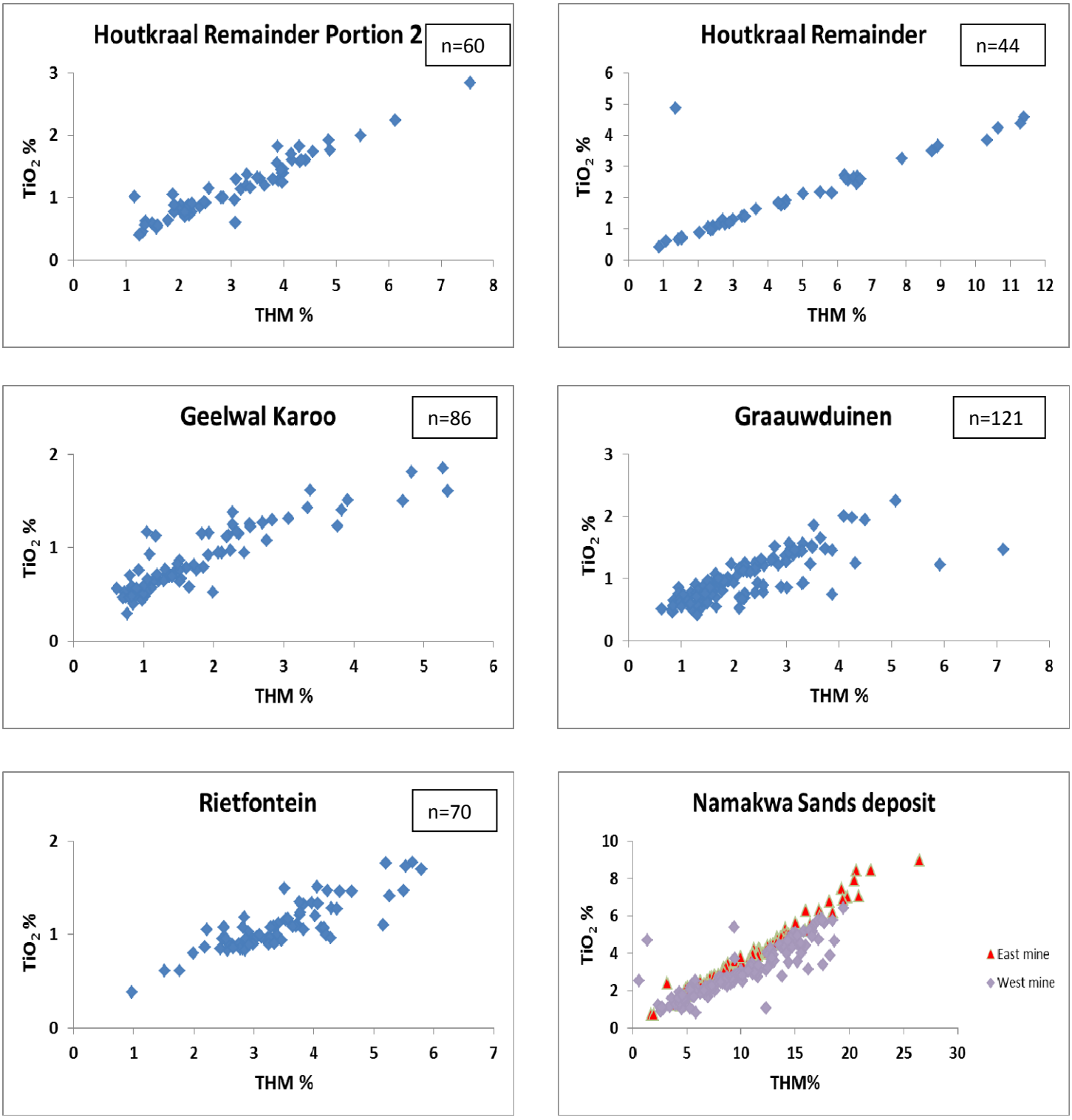

Figure 8.3. THM-TiO_2 binary diagrams of the five satellite areas and the Namakwa Sands deposit. The East-and West Mine have higher TiO_2 contents than the satellite areas.

Figure 4.15 illustrates and supports this increase in maturity. The THM in the Rietfontein area increases from 6% to 8% in the Houtkraal Remainder Portion 2 area and up to 11% in the Houtkraal Remainder area. The wind therefore upgraded and matured the total heavy mineral (THM) suite from Rietfontein to Houtkraal Remainder Portion 2 to Houtkraal Remainder. RAS grades are however not achieved because the area is located on the periphery of the depression that controlled the significant increase in heavy mineral content.

The transition in maturity and increase in THM and VHM contents from the West Mine to the East Mine are therefore reflected in Rietfontein to Houtkraal Remainder Portion 2 to Houtkraal Remainder. The same process, wind activity, created this increase in grade and maturity in the satellite areas and the East- and West Mine but the THM grade is lower in the satellite areas because it is located on the edge and not in a depression as is the Namakwa Sands deposit. The increase in grade and maturity is also controlled by basement geomorphology.

The higher maturity of Houtkraal Remainder compared to the West Mine as well as Houtkraal Remainder Portion 2, Geelwal Karoo, Graauwduinen and Rietfontein is as explained above due to its geomorphological location. Houtkraal Remainder is located on the northeastern edge of the Namakwa Sands deposit (Figure 8.6). The RAS of the East Mine continues into Houtkraal Remainder (Figure 4.5). Houtkraal Remainder therefore forms an extension of the East Mine's RAS and is similar in character to the East Mine. It is therefore regarded as an equivalent to the RAS of the East Mine.

The lower maturity of Houtkraal Remainder Portion 2 indicates that it is not related to the high grade RAS of the East Mine. It is transitional in character between Rietfontein and Houtkraal Remainder.

The similar mineral proportions and chemistry values and maturity of Geelwal Karoo and Graauwduinen indicate that these two areas were formed by the same process (wind) and are of the same character and have the same genesis. Graauwduinen and Geelwal Karoo are located directly along the coast. The immaturity of these areas can be attributed to limited transport and poor sorting and upgrading. Due to the immature nature and low grade of these two areas, their sediment can be regarded as proximal aeolian dune sands and are not related to the high grade RAS of the Namakwa Sands deposit but have West Mine characteristics.

Rietfontein differs significantly from the other four satellite areas in terms of its maturity, mineral proportions and chemistry and therefore has a different genesis and character. Rietfontein is also located along the coast. It is also immature and of low grade like Geelwal Karoo and Graauwduinen. The immature nature of Rietfontein's sediment is also a function of limited transport and the THM were not sufficiently upgraded and matured. Rietfontein can also be classified as a proximal aeolian sand but with a lower maturity than the marine proximal sands of Graauwduinen and Geelwal Karoo. Geelwal Karoo, Graauwduinen and Rietfontein are similar in character in comparison to the West Mine due to the three area's less mature nature and it also being located directly along the coast.

In conclusion the maturity and THM grade decreases northwards and southwards towards the edges of the Namakwa Sands deposit as you move out of the topographic depression. The topography plays a vital role and depressions are important to get a high grade and mature deposit such as the Namakwa Sands deposit. Figure 8.6 summarizes the most important conclusions of the satellite areas.

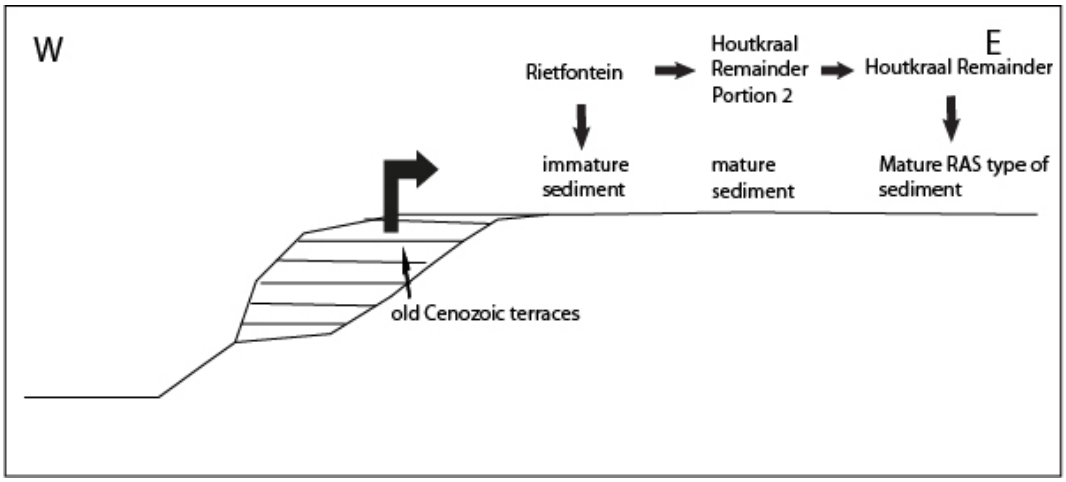

Figure 8.4. Diagram showing the old Cenozoic terraces with THM strandlines acting as the source to form the Rietfontein, Houtkraal Remainder Portion 2 and Houtkraal Remainder satellite areas.

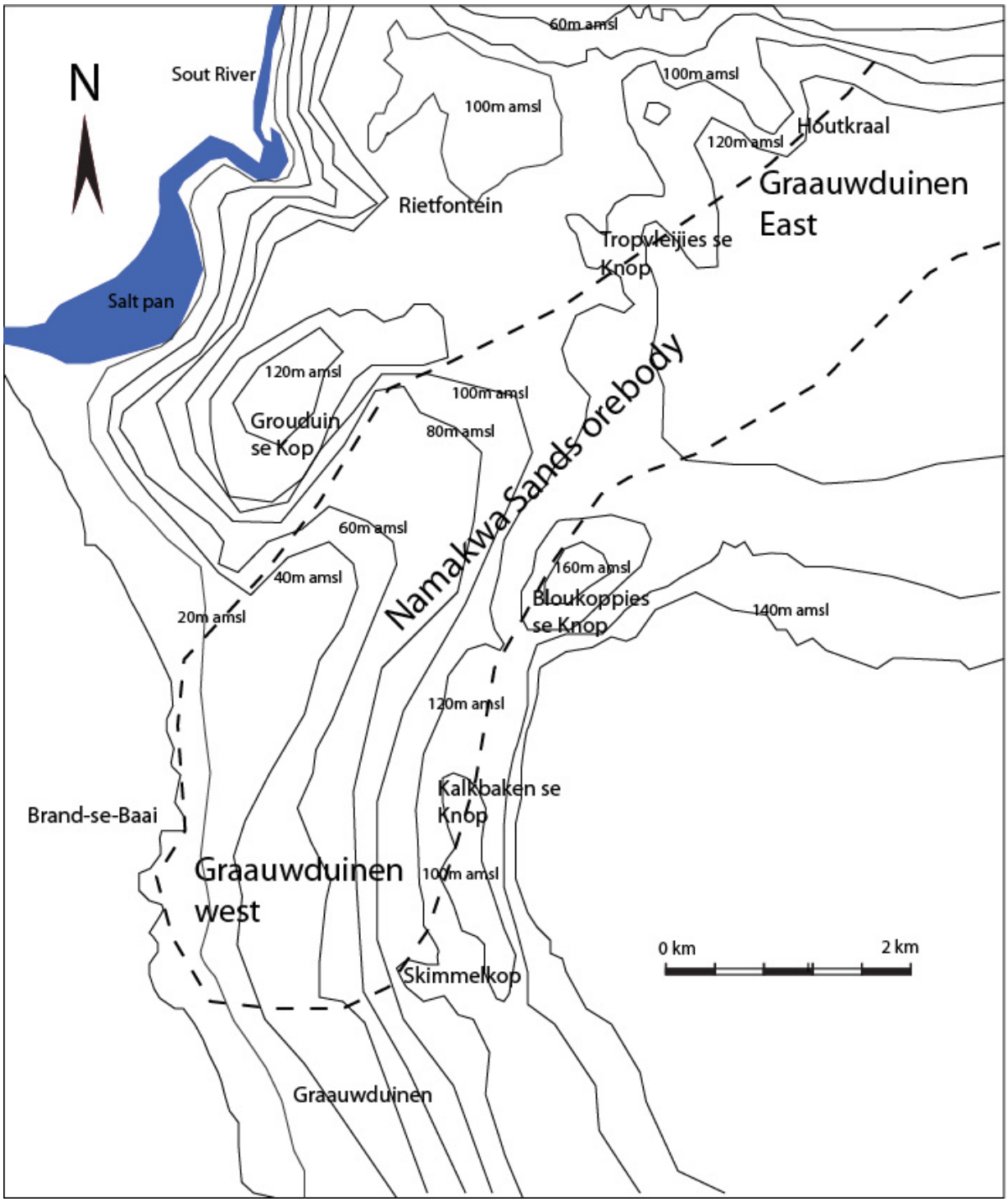

Figure 8.5. Topographic map showing the morphology surrounding the Namakwa Sands deposit and satellite areas.

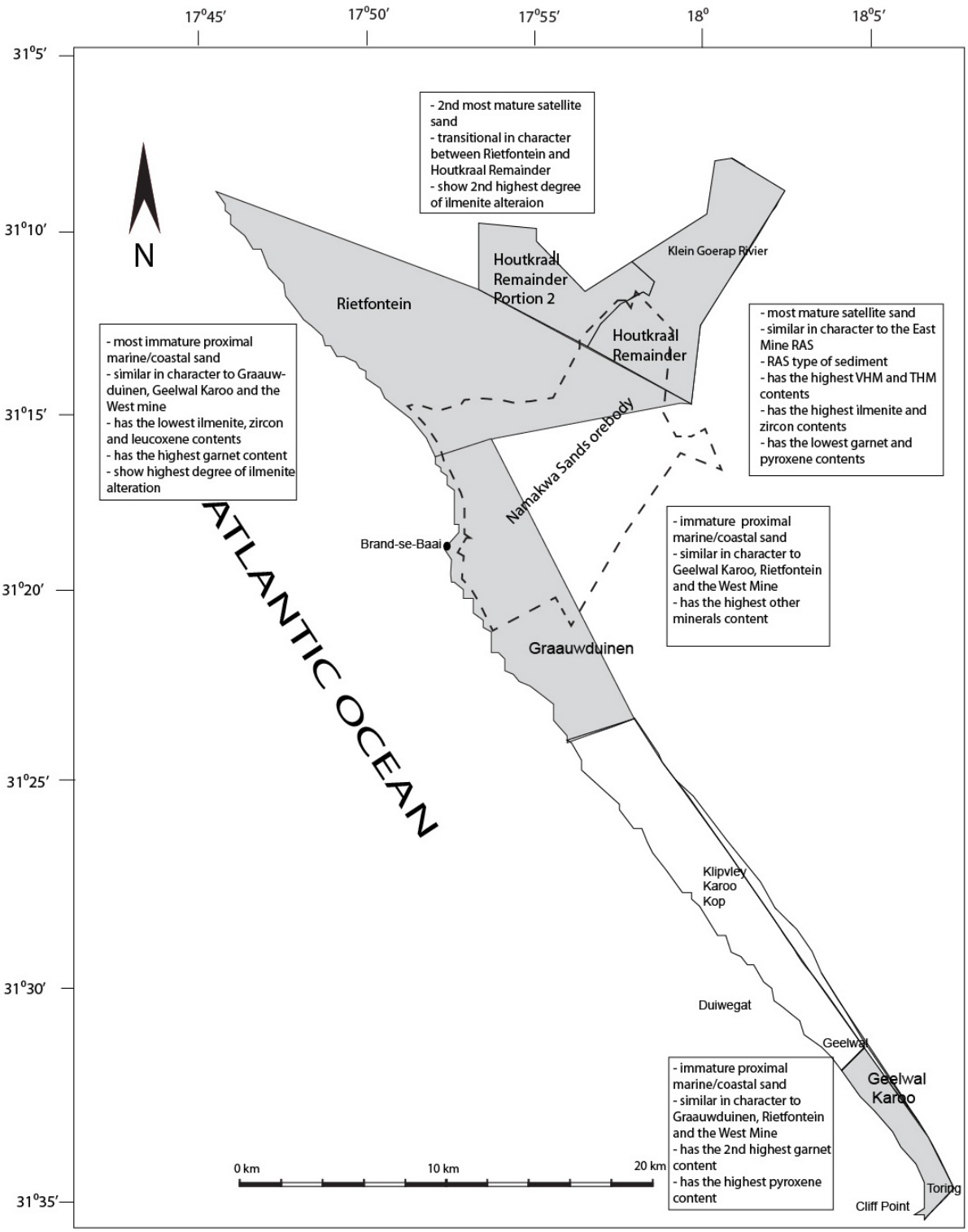

Figure 8.6. Map showing the characteristics and spatial relationship of each satellite area with the Namakwa Sands orebody.

CHAPTER 9 ECONOMIC POTENTIAL OF THE FIVE SATELLITE AREAS

For a heavy mineral deposit to be economic (can be profitably mined) it must have certain properties and includes factors such as a favourable ore mineral or VHM to gangue mineral ratio. Gangue refers to the non-economic fraction (tourmaline, sphene, pyroxene, garnet, corundum, staurolite and amphibole). Economic has to do with profitability. Revenue - costs = profit. The higher the VHM, the greater is the potential of a deposit to be economic. International price plays a major role in determining the profitability of a deposit. The ore minerals must also be low in impurities (Si, Al, Mn, and Cr) since high impurity levels can cause difficulties in the separation processes. It also decreases the grade and quality of the end-products and negatively affects recovery.

In Chapter 8 it was concluded that the East Mine of the Namakwa Sands deposit has a 45° slope indicating that all THM-VHM relationships of the heavy minerals are of economic interest. Houtkraal Remainder has an almost 45° slope and therefore almost all of the THM is VHM. Houtkraal Remainder which shows a similar THM-VHM relationship to the East Mine therefore shows the most economic potential of the satellite areas. Houtkraal Remainder Portion 2, Geelwal Karoo and Graauwduinen have similar THM-VHM slopes but less steep than Houtkraal Remainder. These three areas are therefore of less economic significance than Houtkraal Remainder since it contains less VHM. Rietfontein has the least steep THM-VHM slope and is the least enriched in VHM with a considerable amount of non-economic minerals present. Rietfontein thus shows the least economic potential of all five the satellite areas from a heavy mineral perspective. The slope of the THM-VHM curve is an indication of potential profitability provided that the THM meets certain requirements.

The ore minerals must be low in impurities because these may for example be environmentally detrimental and will incur a penalty if sold. Rutile, ilmenite and zircon must meet specific chemical specifications to be marketable in the heavy mineral industry (Hugo, 1993). For example Si, Cr, Ca, Mg, Mn and V are considered impurities in rutile and ilmenite and Fe, Ti and Al in zircon. Zircon is electrically non-conductive and impurities and inclusions will increase its electromagnetic conductivity and susceptibility which will lead to

recovery losses in the mine. Recovery losses in the mine in turn decrease the economic viability of the deposit.

Namakwa Sands uses the following specifications for its ilmenite, rutile and zircon products. Ilmenite must or may contain a maximum of 1.20% Mn and a maximum of 1.10% SiO_2 but preferably less. The minimum TiO_2 content for ilmenite is 45%.

For rutile the Fe_2O_3, SiO_2, ZrO_2, P_2O_5 and Sn content is important. Fe_2O_3, SiO_2, ZrO_2 and P_2O_5 contents must be less than 1%, 2.5%, 1.2% and 0 09% respectively. Sn contents must be less than 1000 ppm. The total TiO_2 content for a rutile concentrate must be higher than 94%.

The Fe_2O_3, TiO_2 and Al_2O_3 contents in zircon must be less than 0.06%, 0.12% and 0.35% respectively. The ZrO_2+HfO_2 content must be a minimum of 66%.

Ilmenite of all five the satellite areas has > 45% TiO_2 (Table F1 and F2, Appendix F). MnO-SiO_2 binary diagrams were plotted of the SEM data of ilmenite for each satellite area to determine whether ilmenite meets the product specifications outlined above (Figure 9.1). Most ilmenite for all five the satellite areas have < 1.20% Mn and < 1.10% SiO_2 and therefore qualify as ilmenite products (Figure 9.1). Some ilmenite has > 1.20% Mn and > 1.1% SiO_2. These ilmenite grains that do not comply with the set ilmenite specifications will be rejected. Houtkraal Remainder has the best quality ilmenite as expected.

SiO_2 and P_2O_5 contents were not analysed for with the LA-ICP-MS method. TiO_2 was used as a standard and its concentration is therefore also not known. Only Sn, Fe_2O_3 and ZrO_2 were used as specifications for rutile. Most rutile has Sn contents of less than 1000 ppm (Table F4, Appendix F). Only one grain from Graauwduinen and two grains each from Houtkraal Remainder Portion 2, Geelwal Karoo and Rietfontein have > 1000 ppm of Sn. Fe_2O_3-ZrO_2 binary diagrams were plotted of the LA-ICP-MS data of rutile for each satellite area to determine whether rutile meets the set specifications of Namakwa Sands (Figure 9.2). Figure 9.2 indicates that the majority of rutile grains for each satellite area comply with the set specifications of Namakwa Sands and therefore qualify as rutile products. Only a few rutile grains do not comply with the set rutile specifications.

Al_2O_3-TiO_2 and U+Th-Fe_2O_3 binary diagrams were plotted of the LA-ICP-MS data of zircon for the five satellite areas to determine to what extent the zircon of the satellite areas meets the product specifications used by Namakwa Sands (Figures 9.3 and 9.4). Figures 9.3 and 9.4

indicate that most zircon meets the product specifications for zircon and qualify as products. Only a few zircon grains do not comply with the set specifications for prime zircon but effectively all meet the requirements (< 1000ppm U+Th) of the zirkwa product. The zircon grains of Graauwduinen have the lowest TiO_2 content (< 0.05%).

Although the satellite areas have lower VHM and THM contents than the Namakwa Sands deposit, its ore minerals are low in impurities and most ore minerals complies to the set specifications for rutile, zircon and ilmenite products. Houtkraal Remainder has the most ilmenite, zircon and rutile grains that comply to the set specifications of ilmenite, zircon and rutile products respectively. The high VHM and THM contents and purity of Houtkraal Remainder's ore minerals indicates it to be the most economic satellite area. The majority of Houtkraal Remainder Portion 2, Geelwal Karoo, Graauwduinen and Rietfontein's ore minerals also qualifies as products but due to the four area's lower overall VHM and THM contents and higher amount of non-economic minerals present, it is of less economic significance than Houtkraal Remainder.

A large amount of investment is involved in the development of a mineral deposit and due to the lower economic potential of these satellite areas, in comparison with the Namakwa Sands deposit, the most cost effective solution to exploit the deposits would be for the satellite areas to supply heavy minerals to the plants of the Namakwa Sands deposit. Due to the proximity of the Namakwa Sands deposit, the heavy minerals can be easily transported by truck.

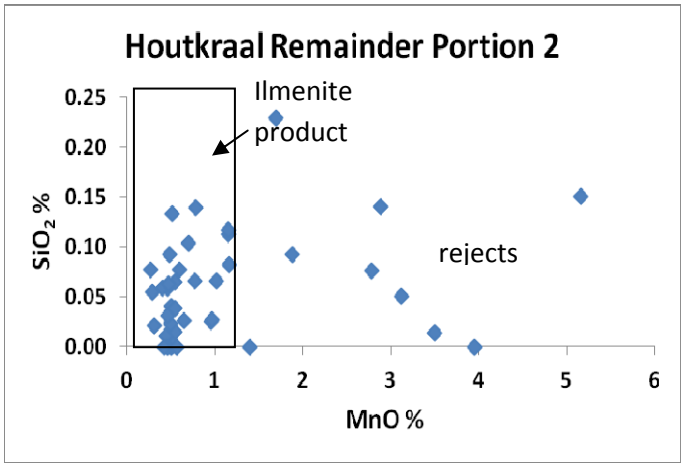

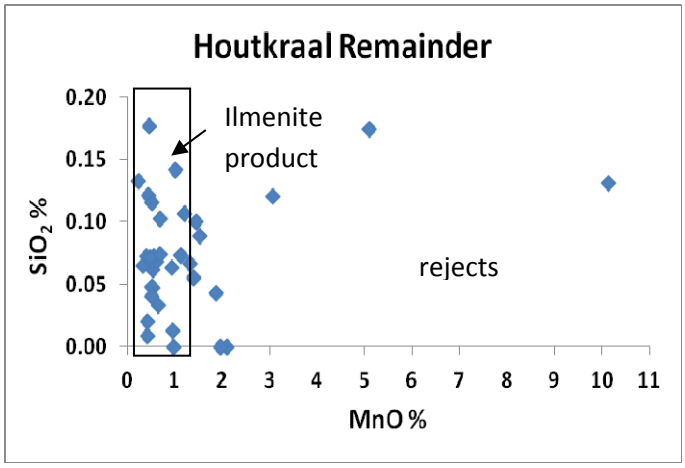

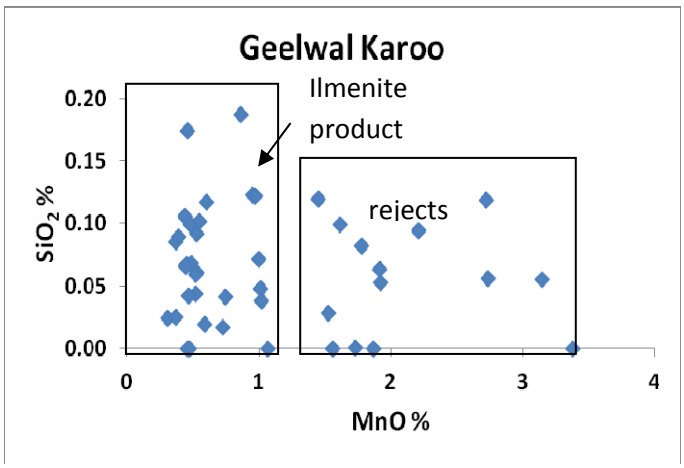

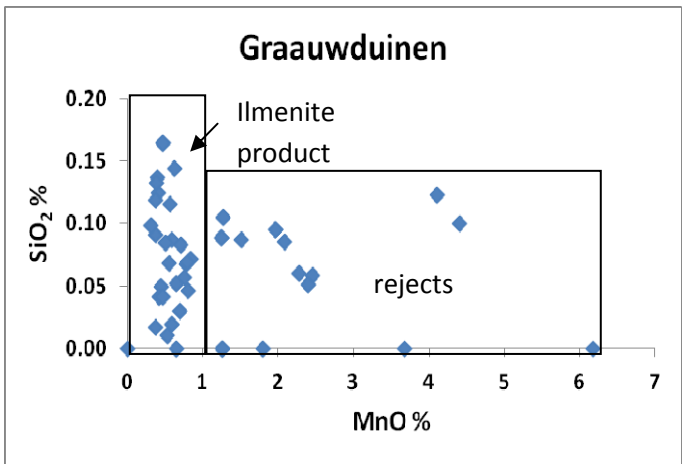

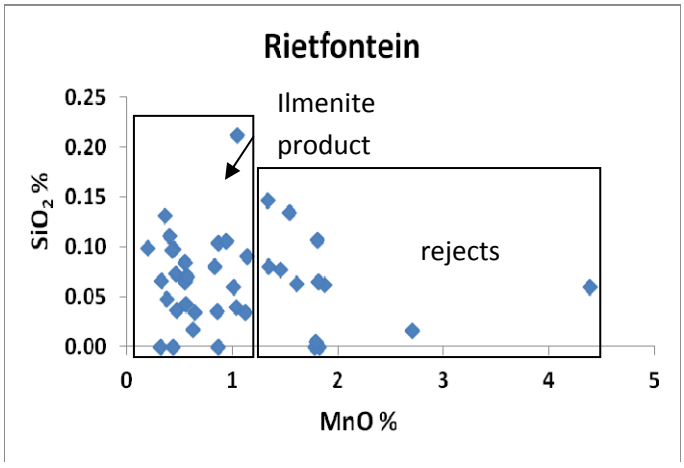

Figure 9.1. MnO-SiO_2 binary diagrams of ilmenite from the five satellite areas. Houtkraal Remainder has the best quality ilmenite.

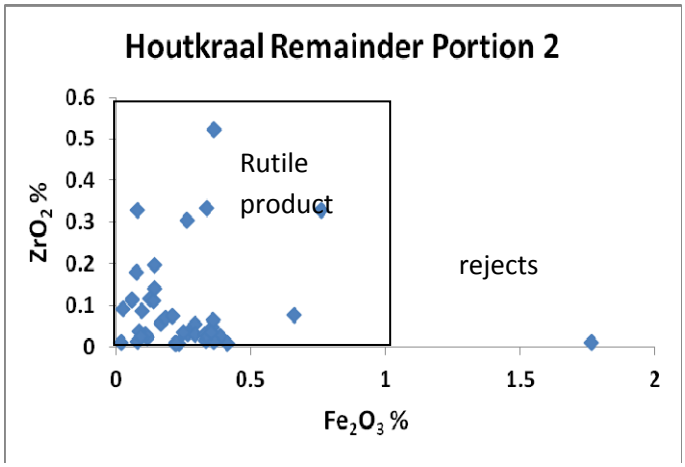

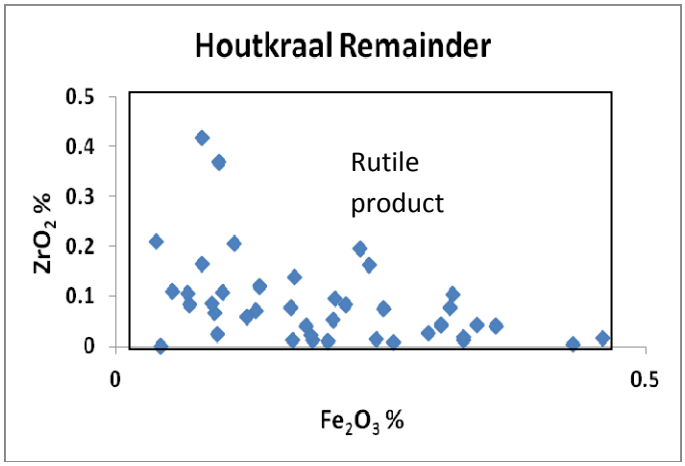

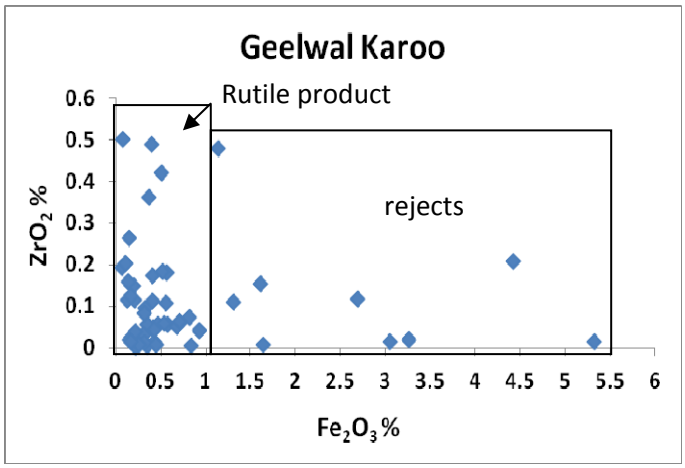

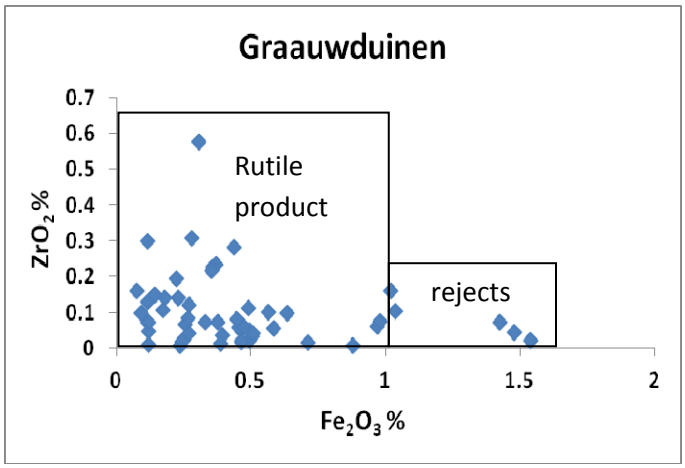

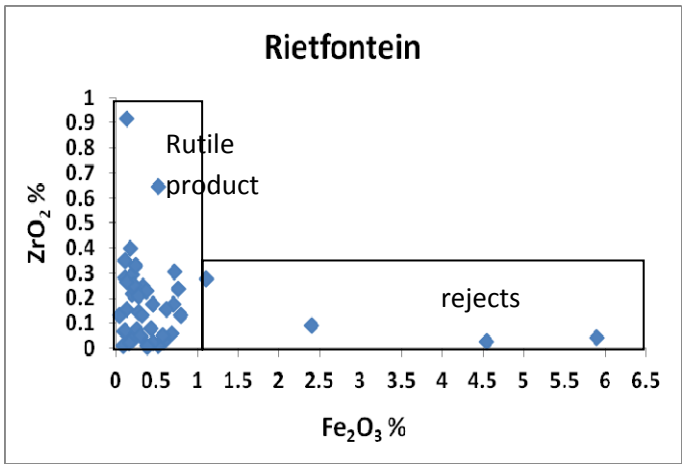

Figure 9.2. Fe_2O_3-ZrO_2 binary diagrams of rutile from the five satellite areas. Houtkraal Remainder has the best quality rutile of the satellite areas however all the satellite areas have good quality rutile.

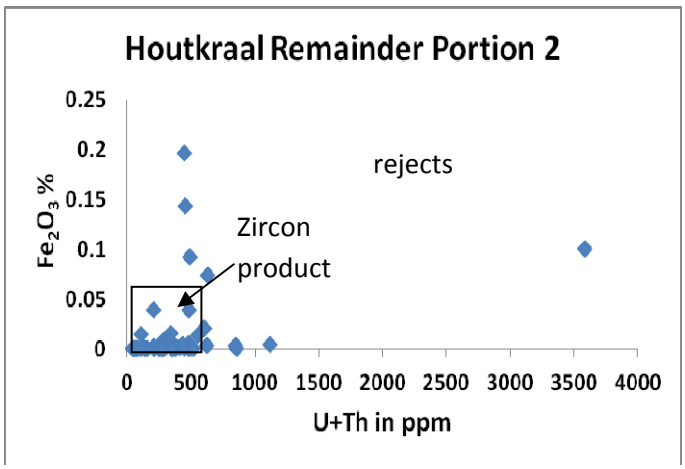

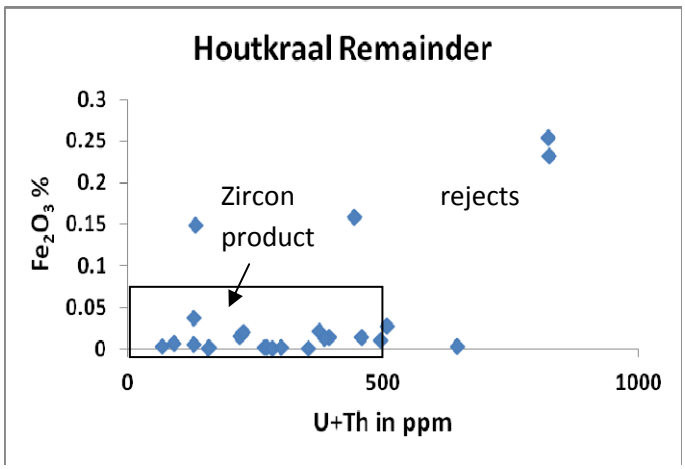

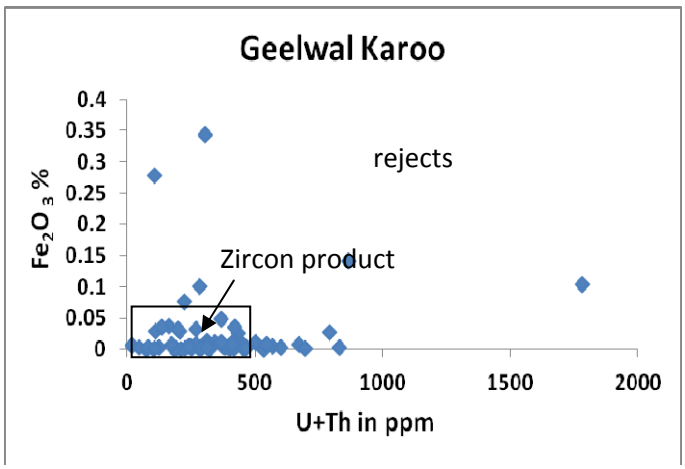

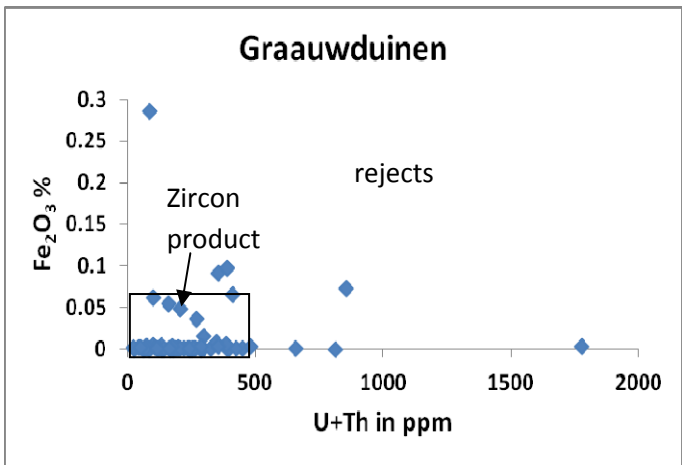

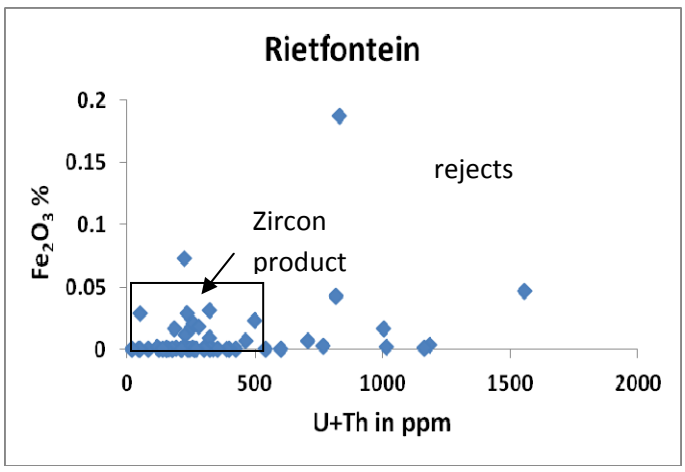

Figure 9.3 U+Th-Fe_2O_3 binary diagrams of zircon from the five satellite areas. It is clear that with increased sediment maturity the quality of zircon increases. In general the satellite areas have good quality zircon.

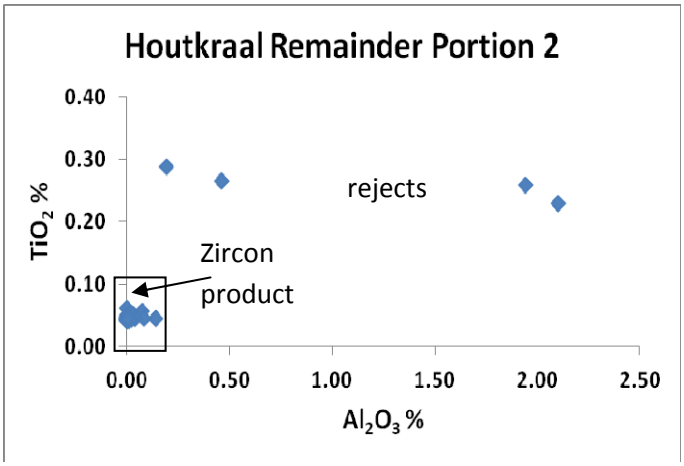

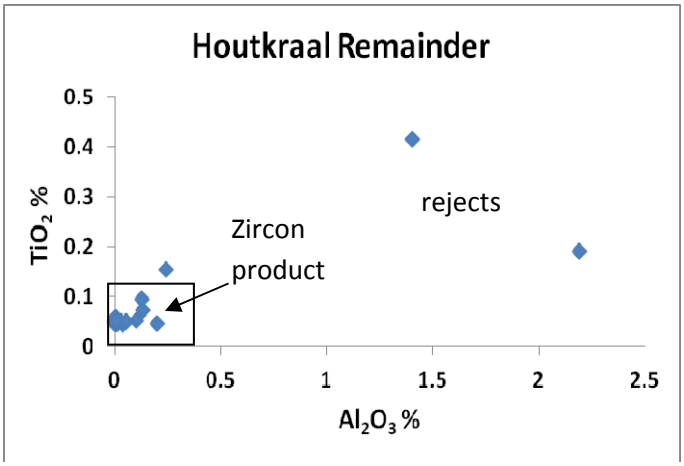

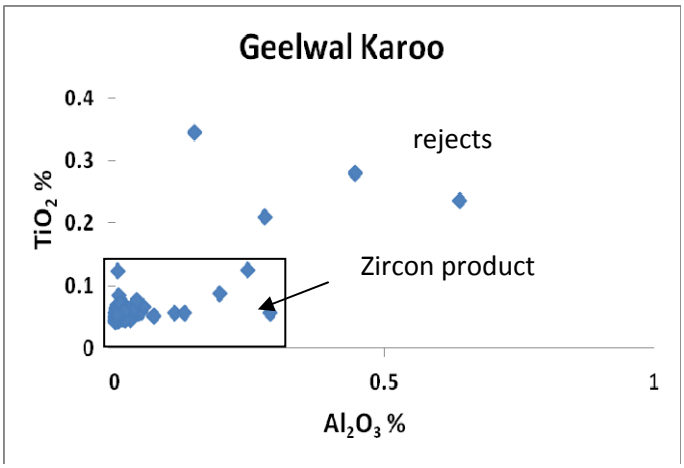

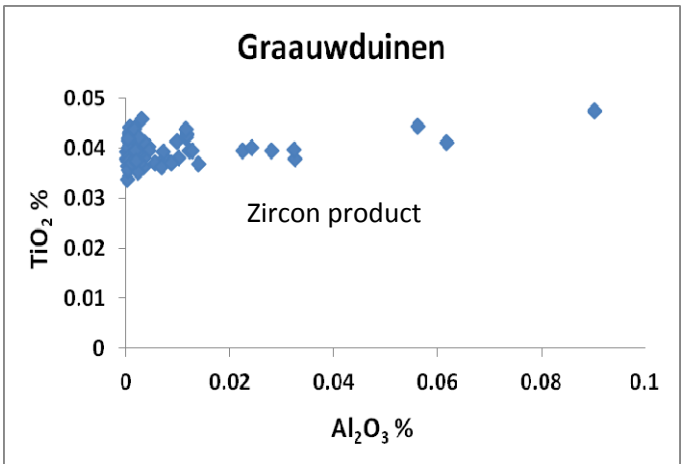

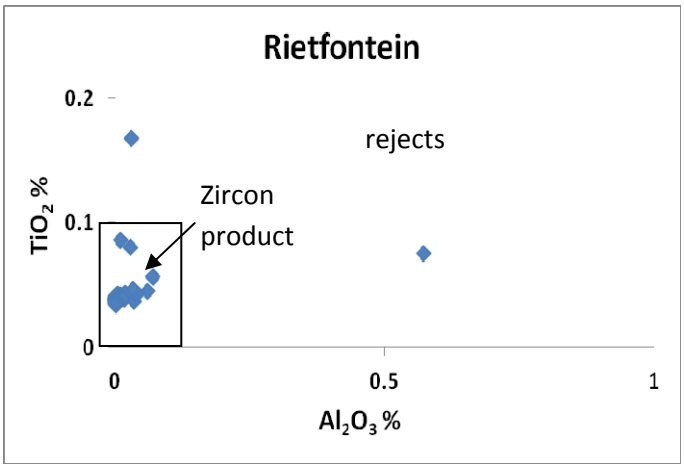

Figure 9.4. Al_2O_3-TiO_2 binary diagrams of zircon from the five satellite areas. Effectively all zircons meet the specifications of the prime product produced by Namakwa Sands. This is to be expected because provenance studies have indicated a common source.

CHAPTER 10 SUMMARY AND CONCLUSIONS

The findings and conclusions of each chapter are summarized below.

Houtkraal Remainder has the highest VHM and THM contents of all five the satellite areas. It is also the most mature satellite sand indicated by its ~45° THM-VHM slope (Figure 4.15). The Namakwa Sands deposit has a northeastern trend and Houtkraal Remainder lies on the northern to northeastern periphery of the Namakwa Sands deposit. The RAS of the East Mine continues into Houtkraal Remainder and explains its higher maturity.

Geelwal Karoo and Graauwduinen display mixed THM-VHM populations. The low THM-VHM populations correspond to immature dune and aeolian sands whereas the high THM-VHM populations correspond to the recently formed red aeolian sand. The high THM-VHM population of Graauwduinen has a similar slope to Houtkraal Remainder and hence a similar maturity. Houtkraal Remainder Portion 2 is the 2nd most mature satellite area. Geelwal Karoo's high THM-VHM population has a similar maturity to Houtkraal Remainder Portion 2 indicated by the similar slopes (Figure 4.15). Rietfontein is the least mature satellite sand indicated by its flat THM-VHM slope and has the most non-economic minerals present.

THM content maps indicate that Houtkraal Remainder has the highest THM grades (up to 11%). These high THM values are regarded as a continuation of the high grade RAS of the East Mine. Rietfontein and Houtkraal Remainder Portion 2's THM does not exceed 6%. Geelwal Karoo has THM grades, in exceptional cases, of up to 17%. These high THM areas correspond to palaeostrandlines. The thickness × THM maps are an indication of heavy mineral content for a specific area. The thickness × THM map of Houtkraal Remainder indicates THM contents of as high as 34%, the most of all the areas studied.

The heavy mineral suite for all five satellite areas is diverse and consists of zircon, magnetite, hematite, spinel, rutile, tourmaline, garnet, pyroxene, amphibole, aluminosilicates, staurolite, corundum, epidote, monazite, sphene and ilmenite and its alteration products. Mineral coatings are present on all minerals and consist of Si-Al-Fe and Ti, Si-Al-Fe and K and Si-Al-Fe and Mg as identified with the SEM. These coatings negatively affect recovery.

Rutile grains of all five the satellite areas consist of a mixed population of yellow and red rutile. Yellow rutile is the dominant rutile variety in all five the satellite areas. Zircons of the

five satellite areas are also represented by a mixed population of brown, yellow and colourless zircon. The latter is most abundant followed by yellow and brown rutile. Ilmenite occurs as homogeneous ilmenite (no exsolution lamellae), heterogeneous ilmenite (exsolution lamellae present) and altered ilmenite. Complex Fe-Ti oxides are also present, although scarce and consist of more than one Fe-Ti oxide phase in one single grain.

The satellite areas contain the same suite of heavy minerals as the Namakwa Sands deposit and the chemistry of the ore minerals (rutile, zircon, ilmenite and leucoxene) are also similar. The similar chemistry indicates a common provenance terrain.

The whole spectrum of ilmenite alteration products (hydrated ilmenite, pseudorutile and leucoxene) are present and indicate an ilmenite alteration index of 22-24% for the five satellite areas. Namakwa Sands has a similar alteration index (20-22%) and indicates relatively dry to semi-arid climatic conditions along the west coast during the Pliocene and Pleistocene. Alteration of ilmenite in the five satellite areas mainly follow the models proposed by Hugo and Cornell (1991) and Type I, II and Type III alterations were observed. With increasing alteration, Ti was found to increase, together with Nb, as iron content decreases. Mn and Mg decreases with increasing alteration and Si and Al do not show any consistent trends with respect to alteration.

Mineral chemistry of the heavy minerals indicates that the satellite areas were sourced from a wide variety of basement rocks which include mainly metamorphic, felsic igneous and sedimentary rocks. The Zr-in-rutile geothermometer indicates that the satellite areas were sourced by a common group of rocks which include amphibolite and granulite facies metamorphites from the Namaqualand Metamorphic Complex. The log Cr/Nb vs calculated temperature diagram of rutile indicates that most of the source rocks are pelitic and felsic in composition with only a few having a mafic character. Grain shape such as the euhedral nature of many garnets indicates a proximal source and is supported by the abundance of pyroxene, epidote and similar unstable minerals. This would suggest that the rounded nature of most of the heavy mineral grains indicates derivation from previously reworked sediments.

Albat (1983), Zelt (1980) and De Beer et al (2002) reported on the presence of above rock types in the Namaqualand Metamorphic Complex (NMC). The latter is proximal to the satellite areas and have a mainly felsic character. The NMC are therefore regarded as the source terrain for the heavy minerals of the satellite areas. The very limited contribution from

the greenschist facies source rocks is equated with the Gariep Supergroup and Vanrhynsdorp Group rocks.

The close proximity of the source area explains the diverse physical and geochemical characteristics of the satellite areas which are a function of limited transport distance and resultant poor sorting.

Of all the satellite deposits Houtkraal Remainder has the highest VHM and THM contents and consequently the highest ilmenite, zircon and leucoxene concentrations. Rietfontien has the lowest zircon, ilmenite and leucoxene contents and the highest garnet content. Geelwal Karoo has the highest pyroxene content. Graauwduinen has the highest other minerals content.

This indicates that the satellite areas have different maturities and is supported by diverse chemistry and mineral proportions. These differences indicate that the satellite area's sediments are different which does not support a common genesis. Houtkraal Remainder and to some extent Houtkraal Remainder Portion 2 is similar in character to the RAS of the East Mine. Graauwduinen, Geelwal Karoo and Rietfontein however are similar in character to the West Mine and represent less mature proximal aeolian sands. It can be concluded that the latter three deposits were formed and sourced close to the older marine and aeolian strandlines and terraces and represent relatively proximal aeolian deposits along the present coastline. The two Houtkraal areas in particular Houtkraal Remainder are peripheral to, and the northeastern extension of the RAS part of the Namakwa Sands orebody, are more distal to the source and consequently more mature and of better heavy mineral grade. It is also concluded that the very high THM concentrations typical of the Namakwa Sands orebody have not been reached in the satellite areas because of the absence of topographical floor rock features such as depressions and highs to channel. Although the source rocks are common to these areas and the mineralogy and mineral chemistry are similar, the THM and VHM concentrations are simply not reached because of these constraints.

This study has also shown that a maturity index can also be derived from the THM and VHM concentrations. Where unity i.e. THM=VHM=1 is reached maximum maturity is indicated. This could be developed as an important exploration tool for heavy mineral deposits with a high index indicating prospective areas.

Houtkraal Remainder shows the most economic potential of all five the satellite areas due to its higher VHM content and low impurity content of its ore minerals. Houtkraal Remainder Portion 2, Geelwal Karoo, Graauwduinen and Rietfontein's ore minerals are also low in impurities but have lower VHM and overall THM content. These areas are therefore of less economic significance.

REFERENCES

Albat, H. (1983). The Proterozoic granulite facies terrane around Kliprand, Namaqualand Metamorphic Complex, P.hD. thesis (unpublished), University of Cape Town, South Africa.

Anand, R.R. and Gikes, R.J. (1985). Some alumina and silica in weathered ilmenite grains is present in clay minerals – a response to Frost et al. (1983). *Mineralogical Magazine.*, **49**,141-145.

Andreoli, M.A.G., Smith, C.B., Watkeys, M., Moore, J.M., Ashwal, L.D. and Hart, R.I. (1994). The Geology of the Steenkampskraal Monazite Deposit, South Africa; Implications for REE-Th-Cu Mineralization in Charnockite-Granulite Terranes. *Economic Geology.*, **89**, 994-1016.

Bailey, S.W., Weege, R.J., Cameron, E.N. and Spedden, H.R. (1956). The alteration of ilmenite in beach sands. *Economic Geology.*, **51**, 263-279.

Basu, A. and Molinaroli, E. (1989). Provenance characteristics of detrital opaque Fe-Ti oxide minerals. *Journal of Sedimentary Petrology*., **59**, 922-934.

Belousova, E. A., Griffin, W.L., O'Reilly, Suzanne. and Fisher, N.I. (2002). Igneous zircon: trace element composition as an indicator of source rock type. *Contributions to Mineralogy and Petrology.*, **143**, 602-622.

Bhattacharyya, S., Sengupta, R. and Chakraborty, M. (1997). Elemental chemistry of Ilmenite - an Indicator of Provenance? *Journal Geological Society of India.*, **50**, 787-789.

Blatt, H., Middleton, G. and Murray, R. (1972). Origin of sedimentary Rocks. Prentice- Hall Inc, Englewood Cliffs, New Jersey, 286-297.

Blatt, H., Middleton, G. and Murray, R. (1980). Origin of sedimentary Rocks, 2nd edition. Prentice -Hall, Englewood Cliffs, New Jersey, 1-782.

Boctor, N.Z. (1966). Ore microscopic studies of the opaque minerals in Rosetta, Damietta black sands, M.Sc. thesis (unpublished), Cairo University, Egypt.

Boynton, W.V. (1984). Cosmochemistry of the rare earth elements: meteorite studies. In: Henderson, P. (Ed.), Rare Earth Element Geochemistry. Elsevier, Amsterdam, pp. 63–114.

Bredell, J. (1987). South African Coal resources explained and analysed. *Open File Report Geological Survey South Africa.*, **1987-0154**, 39pp.

Buddington , A.F., Fahey, J. and Vlisidis, A. (1963). Degree of oxidation of Adirondack Iron oxide and Iron-Titanium Oxide Minerals in Relation to Petrogeny. *Journal Of Petrology.*, **4**, 138-169.

Buddington, A.F. and Lindsley, D.H. (1964). Iron-Titanium Oxide Minerals and Synthetic Equivalents. *Journal of Petrology.*, **5**, 310-357.

Carrington, A J. and Kensley, B.F. (1969). Pleistocene Molluscs from the Namaqualand Coast. *Ann. S. Afr. Mus*., **52**, 189-223.

Cawood, P.A. (1991). Characterisation of intra-oceanic magmatic arc source terranes by provenance studies of derived sediments. *New Zealand Journal of Geology and Geophysics.*, **34**, 347-358.

Cilliers, L. M. (1995). The geology of the Graauwduinen heavy mineral sand deposit, west coast of South Africa, M. Sc. thesis (unpublished), University of Stellenbosch, South Africa.

Cole, D.I. and Roberts, D.L. (1996). Lignite form the western coastal plain of South Africa. *Journal of African Earth Sciences.*, **23**, 95-117.

Copjakova, R., Sulovsky, P. and Paterson, B.A. (2005). Major and trace elements in pyrope-almandine garnets as sediment provenance indicators of the Lower Carboniferous Culm sediments. Drahany Uplands, Bohemian Massif., *Lithos*, **82**, 51-70.

Corbett, I.B. (1996). A review of diamondiferous marine deposits of western southern Africa. *Afr.Geoscience.Rev.*, **3**, 157-174

Corvinus, G. and Hendey, Q. B. (1978). A new Miocene vertebrate locality at Arisdrift in South West Africa (Namibia). *N.Jb.Geol.Palaont.Mh*., **4**, 193-205.

Darby, D.A. (1984). Trace elements in ilmenite; A way to discriminate provenance or age in coastal sands. *Geological Society of America Bulletin.,* **95**, 1208-1218.

Darby, D.A. and Tsang Y.W. (1987). Variation in element composition within and among drainage basins: Implications for provenance. *Journal of Sedimentary Petrology.,* **57**, 831-838.

Darby, D.A. and Bischof, J.F. (1996). A statistical approach to source determination of lithic and Fe oxide grains: An example from the Alpha Ridge, Arctic Ocean. *Journal of Sedimentary Research.,* **66(3**), 599-607.

De Beer, C. H., Gresse, P. G., Theron, J. N. and Almond, J. E. (2002). The Geology of the Calvinia Area. *Council of Geoscience*, 1-55.

De Beer. C.H. (2010). The Geology of the Garies area explanation sheet 3017. *Council of Geoscience*, 1-92.

De Decker, R. H. H. (1986). Surficial sediments on the inner shelf between the Orange River and Wreck point. *Tech. Rept. Geol. Surv. University of Cape Town Mar. Gesci. Unit.*, **15**, 135-156.

De Villiers, J. and Söhnge, P.G. (1959). The Geology of the Richtersveld. *Geol.Surv.S.Afr.Mem.*, **48**, 219-240.

Deer, W. A., Howie, R. A. and Zussman, J. (1992). An Introdution to the Rock-Forming Minerals, 2nd edition. Prentice Hall, Harlow, England, 22-558.

Deysel, K. (2007). Leucoxene study: a mineral liberation analysis (MLA) investigation. *The Journal of the Southern African Institute of Mining and Metallurgy*, 167-172.

Dingle, R.V., Lord, A.R. and Hendey, Q.B. (1979). New sections in the Varswater Formation (Neogene) of Langebaan Road, South-Western Cape South Africa. *Annals of the South African Museum,* **78**, 81-92.

Dingle, R.V., Siesser, W.G. and Newton, A.R. (1983). Mesozoic and Tertiary Geology of Southern Africa. Balkema, Rotterdam, 99-309.

Dobretsov, N.L. (1968). Paragenetic types and compositions of metamorphic pyroxenes. *Journal of Petrology.*, **9**, 358-377.

Droop, G.T.R. (1987). A general equation for estimating Fe^{3+} concentrations in ferromagnesian silicates and oxides from microprobe analyses using stoichiometric criteria. *Mineralogical Magazine.*, **51**, 431-435.

Duchesne, J., Vander Auwera, J., Liegeois, J., Barton, E.S. and Clifford, T.N. (2007). Geochemical constraints of the petrogenesis of the O'okiep Koperberg Suite and granitic

plutons in Namaqualand, South Africa: A crustal source in Namaquan (Grenville) times. *Precambrian Research.*, **153**, 116-142.

Elferink, L. (2005). The Cenozoic stratigraphy and associated heavy mineral palaeo-placer deposit on Geelwal Karoo: west coast, South Africa, M.Sc. thesis (unpublished), University of Stellenbosch, South Africa.

Fedo, C.M., Sircombe, K.N. and Rainbird, R.H. (2003). Detrital zircon analysis of the sedimentary record. *Reviews in Mineralogy and Geochemistry*., **53**, 277-303.

Ferry, J.M. and Watson, E.B. (2007). New thermodynamic models and revised calibrations for the Ti-in-zircon and Zr-in-rutile thermometers. *Contrib. Mineral Petrol.*, **154**, 429-437.

Force, E.R. (1991). Placer Deposits. *Rev. Econ.Geol.*, **5**, 131 – 139.

Frost, B.R. (1991). Stability of oxide minerals in metamorphic rocks. *Reviews in Mineralogy.*, **25**, 469-487.

Ganssloser, M., Theye, T. and Wachendorf, H. (1996). Detrital glaucophane in graywackes of the Rhenohercynian Harz Mountains and the geodynamic implications. *Geologische Rundschau*., **85**, 755-760.

Gous, M. (2006). An overview of the Namakwa Sands Ilmenite smelting operations. *Southern African Pyrometallurgy.*, 189-201.

Green, D.H. and Ringwood, A.E. (1967). The stability fields of aluminous pyroxene peridotite and garnet peridotite and their relevance in upper mantle structure. *Earth planet. Sci. Lett.*, **3**, 151-60.

Gresse, P.G. (1986). The tectono-sedimentary history of the Vanrhynsdorp Group, Ph.D. thesis (unpublished), University of Stellenbosch, South Africa

Gresse, P.G. and Germs, G.J.B. (1993). The Nama Foreland basin: sedimentation, major unconformity bounded sequences and multisided active margin advance. *Precambrian Research.*, **63**, 247-272.

Grey, I. E. and Reid, A. F (1975). The structure of pseudorutile and its role in the natural alteration of ilmenite. *American Mineralogist.*, **60**, 898-906.

Grey, I. E., Frost, M.T., Harrowfield, I.R. and Mason, K. (1983). The dependence of alumina and silica contents on the extent of alteration of weathered ilmenites from Western Australia. *Mineralogical Magazine.*, **47**, 201-208.

Grice, J.D. and Ercit, J.S. (1993). Povondraite, a redefinition of the tourmaline ferridravite. *American Mineralogist*., **78**, 433-436

Grigsby, J.D. (1990). Detrital magnetite as a provenance indicator. *Journal of Sedimentary Petrology.*, **60**, 940-951.

Grigsby, J.D. (1991). Chemical fingerprinting in detrital ilmenite: a viable alternative in provenance research. *Journal of Sedimentary Petrology.*, **62**, 331-337.

Haggerty, S.E. (1976a). Oxidation of opaque mineral oxides in basalts. *Reviews in Mineralogy.*, **3**, Hg1-Hg98.

Haggerty, S.E. (1976b). Opaque mineral oxides in terrestrial igneous rocks. *Reviews in Mineralogy.*, **3**, Hg101-Hg277.

Hallsworth, C.R. and Chisholm, J.I. (2008). Provenance of late Carboniferous sandstones in the Pennine Basin (UK) from combined heavy mineral, garnet geochemistry and palaeocurrents studies. *Sedimentary Geology.*, **203**, 196-212.

Hartnady, C.J.H., Joubert, P. and Stowe, C.W. (1985). Proterozoic crustal evolution in southwestern Africa. *Episodes.*, **8**, 236-244.

Haughton, S H. (1931). The Late Tertiary and Recent deposits of the west coast of South Africa. *Transactions of the Geological .Society of South Africa.*, **31**, 19-57.

Hawthorne, F.C. and Henry, D. J. (1999). Classification of the minerals of the tourmaline group. *Eur.J.Mineral.*, **11**, 201-215.

Hay, D.C., Dempster, T.J., Lee, M.R. and Brown, D.J. (2006). Anatomy of low-temperature zircon overgrowths. *Contributions to Mineralogy and Petrology.*, **159**, 81-92.

Hedge, V.S., Shalini, G. and Gosavi Kanchanagouri, D. (2006). Provenance of heavy minerals with special reference to ilmenite of the Honnavar beach, central west coast of India. *Current Science.*, **91**, 644-648.

Hendey, O.B. (1981). Palaeoecology of the Late Tertiary fossil occurrences in 'E' quarry, Langebaanweg South Africa, and a reinterpretation of their geological context. *Ann.S.Afr.Mus.*, **84**, 1-104.

Henry, D.J. and Dutrow, B.L. (1992). Tourmaline in a low grade clastic sedimentary rock: an example of the petrogenetic potential of tourmaline. *Contributions to Mineralogy and Petrology.,* **112**, 203-218.

Henry, D.J., Dutrow, B.L. and Selverstone, J. (2002). Compositional asymmetry in replacement tourmaline – An example from the Tauern Window, Eastern Alps. *Geological Materials Research.*, **4** ,1-18.

Henry, D.J. and Guidotti, C.V. (1985). Tourmaline as a petrogenetic indicator mineral: an example from the staurolite-grade metapelites of NW Maine. *American Mineralogist.*, **70**, 1-15.

Herzberg, W. (1969). Investigation of Aerial Radiometric Anomalies in Namaqualand, Areas A and B. *Geological Survey of South Africa report* No.G., **196**.

Herzberg, W. (1970). Investigation of aerial radiometric anomalies in Namaqualand, Areas A and B. *Geol.Surv.S.Afr rep* G., **196**, 67pp.

Hickmott, D. and Spear, F.S. (1992). Major and trace element zoning in garnets from calcareous pelites in the NW Shelburne Falls Quadrangle, Massachusetts: Garnet growth histories in retrograded rocks. *Journal of Petrology.*, **33**, 965-1005.

Hoskin, P.W.O. and Ireland , T R. (2000). Rare earth element chemistry of zircon and its use as a provenance indicator. *Geology*., **28**, 627-630.

Hubert, J. F. (1962). A zircon-tourmaline-rutile maturity index and the interdependence of the composition of heavy mineral assemblages with the gross composition and texture of sandstones. *Journal of Sedimentary Research.,* **32**, 440-450.

Hugo, V.E. and Cornell, D.H. (1991). Altered ilmenites in Holocene dunes from Zululand, South Africa: petrographic evidence for multistage alteration. *South African Journal of Geology.*, **94**, 365-378.

Hugo, V.E. (1993). A study of Titanium-Bearing Minerals in Heavy Mineral Deposits along the East Coast of Africa. Ph.D. thesis (unpublished), University of Natal, South Africa.

Jack, A.M. (1980). The Geology of Western Namaqualand. *Bulletin of the Precambrian Research Unit,* University of Cape Town, **29**.

Janse van Vuuren, C.F., Esterhuyse, J.L. and Alchin, D.J. (2008). Namakwa Sands Resources and Reserves Statement, internal and unpublished, Exxaro Report.

Joubert, P. (1971). The Regional tectonism of the gneisses of part of Namaqualand. *Bulletin of the Precambrian Research Unit,* University of Cape Town, **10**.

Krawinkel, H., Wozazek, S., Krawinkel, J. and Hellmann, W. (1999). Heavy-mineral analysis and clinopyroxene geochemistry applied to provenance analysis of lithic sandstones from the Azuero-Sona Complex (NW Panama). *Sedimentary Geology.*, **124**, 149-168.

Kröner, A. (1973). Metasomatism and granitisation in part of the Namaqualand Granite-gneiss complex- a comparison between petrologic evidence geochemical data. *Spec.Publ.Geol.Soc.S.Afr.*, **3**, 411-417.

Krynine, P.D. (1946). The tourmaline group in sediments. *Journal of Geology.*, **54**, 65-87.

Lenaz, D. (2008). Detrital pyroxenes in the Eocene flysch of the Istrian basin (Slovenia, Croatia). *Geologica Acta.*, **6**, 259-266.

Lepp, H. (1957). Stages in the oxidation of magnetite. *American Mineralogist.*, **42**, 679-681.

Locock, A.J. (2008). An excel spreadsheet to recast analysis of garnet into end-member components, and a synopsis of the crystal chemistry of natural silicate garnets. *Computers and Geosciences.*, **34**, 1769-1780.

Macdonald, W. G. and Rozendaal, A. (1995). The Geelwal Karoo heavy mineral placer deposit: a modern day beach placer. *African Journal of Earth Science.*, **21**, 187-200.

Macdonald, W G. (1996). The Geelwal Karoo Heavy Mineral Deposit: a Modern Day Beach Placer, M.Sc. thesis (unpublished), University of Stellenbosch, South Africa.

Macdonald, W. G., Rozendaal, A. and De Meijer, R. J. (1997). Radiometric characteristics of heavy mineral deposits along the west coast of South Africa. *Mineralium Deposita.*, **32,** 371 – 381.

Mange., M.A. and Wright, D.T (2007). Heavy Minerals in use. Developments in Sedimentology, A.J. van loon, Elsevier, 247-263, 277-307.

Mange Rajetsky, M. A. (1981). Detrital blue sodic amphibole in Recent sediments, southern coast, Turkey. *Journal of the Geological Society, London*., **138**, 83-92.

Mange-Rajetzky, M.A. and Oberhansli, R. (1982). Detrital lawsonite and blue sodic amphibole in the molasse of Savoy, France and their significance in assessing Alpine evolution. *Schweizerische mineralogische und petrographische Mitteilungen*., **62**, 425-436.

Mathison, C.E. (1975). Magnetite and ilmenite in the Somerset Dam layered basic intrusion, southeastern Queensland. *Lithos.*, **8**, 93-111.

Meinhold, G., Anders, B., Kostopoulos, D. and Reischmann, T. (2008). Rutile chemistry and thermometry as provenance indicator: an example from Chios Island Greece. *Sedimentary Geology*., **203**, 98-111

Merensky, H. (1927). How I found the richest diamond field in the world. *Min.Ind.Mag.S. Afr*., **4**, 267.

Miyashiro, A. (1973). Metamorphism and metamorphic belts. Allen and Unwin, London, 248-249.

Moore, J.M. (1989). A comparative study of metamorphosed supracrustal rocks from the western Namaqualand Metamorphic Complex. *Bulletin of the Precambrian Research Unit*, University of Cape Town, **37**, 370pp.

Morad, S. and Aldahan, A.A. (1986). Alteration of detrital Fe-Ti oxides in sedimentary rocks. *Geological Society of America Bulletin.*, **97**, 567-578.

Morimoto, N., Fabries, J., Ferguson, A.K., Ginzburg, I.V., Ross, M., Seifert, F.A., Zussman, J., Aoki, K. and Gottardi, G. (1988). Nomenclature of pyroxenes. *Mineralogical Magazine.*, **52**, 535–550.

Morton, A.C. (1984). Stability of detrital heavy minerals in Tertiary sandstones from the North Sea Basin. *Clay Minerals.*, **19**, 287-308.

Morton, A.C. (1985). A new approach to provenance studies: electron microprobe analysis of detrital garnets from Middle Jurassic sandstones of the northern North Sea. *Sedimentology.,* **32**, 553-556.

Morton, A.C. (1987). Influences of Provenance and Diagenesis on detrital garnet suites in the Paleocene Forties sandstone, Central North Sea. *Journal of Sedimentary Petrology.,* **57**, 1027-1032.

Morton, A.C. (1991). Geochemical studies of detrital heavy minerals and their application to provenance research. In: Morton, A.C., Todd, S.P. and Haugton, P.D.W. (eds). Developments in Sedimentary Provenance Studies. *Geology Society Special Publications.,* **47**, 31-45.

Morton, A.C. and Hallsworth, C.R. (1999). Processes controlling the composition of heavy mineral assemblages in sandstones. *Sedimentary Geology*., **124**, 3-29.

Morton, A.C., Sabeen, H.M. and Ranamujan, N. (2002). The provenance of garnet: constraints provided by studies of coastal sediments from Southern India. *Sedimentary Geology.*, **152**, 279-287.

Morton, A., Hallsworth, C. and Chalton, B. (2004). Garnet compositions in Scottish and Norwegain basement terrains: a framework for interpretation of North Sea sandstone Provenance. *Marine and Petroleum Geology.*, **21**, 393-410.

Morton, A.C. and Yaxley, G. (2007). Detrital apatite geochemistry and its application in provenance studies. In: Arribas, J., Critelli, S. and Johnsson, M. (eds). Sediment provenance and petrogenesis: perspectives from petrography and geochemistry. *Geological Society of America, Special Paper.*, **420**, 319-344.

Mücke, A. and Chaudhuri, J.N.B. (1991). The continuous alteration of ilmenite through pseudorutile to leucoxene. *Ore Geology Reviews.*, **6**, 25-44.

Nair, A.G., Suresh Babu, D.S., Vivekanandan, K.L. and Vlach, S.R.F. (2006). Differential alteration of ilmenite in a tropical beach placer, Southern India: Micoscopic and electron probe evidences. *Resource Geology.*, **56**, 75-81.

Nair, A.G., Suresh Babu, D.S., Damodaran, K.T., Shankar, R. and Prabhu, C.N. (2009). Weathering of ilmenite from Chavara deposit and its comparison with Manavalakurichi placer ilmenite, southwestern India. *Journal of Asian Earth Sciences*., **34**, 115-122.

Nechaev, V.P. and Isphording, W.C. (1993). Heavy-mineral assemblages of continental margins as indicators of plate-tectonic environments. *J. Sediment. Petrol*., **63 (6)**, 1110–1117.

Pike, J, E.N. (1976). Pressures and temperatures calculated from chromium-rich pyroxene compositions of megacrysts and peridotite xenoliths, Black Rock Summit, Nevada *American Mineralogist.*, **61**, 725-731.

Owen, M.R (1987). Hafnium content of detrital zircons, a new tool for provenance study. *Journal of Sedimentary Petrology.*, **57**, 824-830.

Palmer, G L. (1994). The Discovery and Delineation of the Heavy Mineral Sand Orebodies at Graauwduinen, Namaqualand, Republic of South Africa. *Exploration Mining Geology.*, **3**, 399-405.

Pether, J. (1986). Late Tertiary and early Quaternary marine deposits of the Namaqualand coast, Cape Province: new perspectives. *South African Journal of Science.*, **82**,464pp

Pether, J. (1994). The Sedimentology, Palaeontology and Stratigraphy of coastal plain deposits at Hondeklip Bay, Namaqualand, South Africa, M.Sc. thesis (unpublished), University of Cape Town, South Africa.

Pether, J., Roberts, D.L. and Ward, J.D. (2000) Deposits of the West Coast. In: Partridge, T.C. and Maud, R.R. (eds). The Cenozoic of Southern Africa. *Oxford Monographs on Geology and Geophysics*., **40**, 406p.

Pettijohn, F.J., Potter, P. and Siever, R. (1987). Sand and sandstone. New York, Springer-Verlag, 1-250p.

Philander, C. (1999). Distribution, mineralogy and provenance of heavy minerals in Cainozoic sediments of the Namaqua mines area, West coast of South Africa, M.Sc. thesis (unpublished), University of Stellenbosch, South Africa.

Philander, C., Rozendaal, A. and de Meijer, R J. (1999). Characteristics of zircon in placer deposits along the west coast of South Africa. South *African Journal of Science.*, **95**, 381-386.

Philander, C. and Rozendaal, A. (2009). Mineral intricacies of the Namakwa Sands mineral resource. HMC 2009 Heavy Minerals Conference, Champagne Sports Resort, Drakensberg, South Africa, *The Southern African Institute of Mining and Metallurgy*, 99-105.

Philander (in press). Geometallurgy of the Namakwa Sands heavy mineral deposit, P.hD. thesis (unpublished), University of Stellenbosch, South Africa.

Philander. C. and Rozendaal, A. (in prep). The geology of the Namakwa Sands heavy mineral deposit.

Pownceby, M.I. (2010). Alteration and associated impurity element enrichment in detrital ilmenites from the Murray Basin, southeast Australia: a product of multistage alteration. *Australian Journal of Earth Sciences.*, **57**,243-258.

Ramdohr, R. (1980). Ore minerals and their intergrowths, 2nd edition. Pergamon Press, New York, 1200p.

Rao, D.S., Vijayakumar, T.V., Prabhakar, S., Bhaskar, Raju, G. and Ghosh, T.K. (2005). Alteration characteristics of ilmenites from South India. *Journal of Minerals & Materials Characterization & Engineering.*, **4**, 47-59.

Read, D., Andreoli, M. A. G., Knoper, M., Williams, C.T. and Jarvis, N. (2002). The degradation of monazite: Implications for the mobility of rare-earth and actinide elements during low-temperature alteration. *Eur. J. Mineral.*, **14**, 487-498.

Riezebos, P.A. (1979). Compositional downstream variation of opaque and translucent heavy residues in some modern Rio Magdalena Sands (Columbia). *Sedimentary Geology.*, **24**, 197-225.

Rittenhouse, G. (1943). Transportation and deposition of heavy minerals. *Geol. Soc. Am. Bull.*, **54**, 1725-1780.

Robb, L.J., Armstrong, R.A. and Waters, D.J. (1999). The history of granulite-facies metamorphism and crustal growth from single-zircon U-Pb geochronology: Namaqualand, South Africa. *Journal of Petrology.*, **40**, (12), 1747-1770.

Roberts, D.L. (2003). Age, genesis and significance of South African coastal belt silcretes. *Memoir 95*, Council for Geoscience, 61 pp.

Roberts, D.L., Botha, G.A., Maud, R.R. and Pether, J. (2006). Coastal Cenozoic deposits. In: (M. R. Johnson, C.R. Anhaeusser and R.J. Thomas, editors). The geology of South Africa. Geological Society of South Africa, Johannesburg, Council for Geoscience, Pretoria, pp 605-608.

Rogers, J. (1980). First report on the Cenozoic sediments between Cape Town and Elands Bay. *Report Geological Survey of South Africa.*, **165**, 1-64

Rogers, J., Pether, J., Molyneux, R., Hill, R.S., Kilham, L.C., Cooper, G. and Corbett, I.B. (1990). Cenozoic geology and mineral deposits along the west coast of South Africa and the Spergebiet: Guidebook of Geocongress `90, *Geological Society of South Africa*., **PR1**, pp.1-11.

Rozendaal, A. and Philander, C (2007). Recovery of duricrust sterilized heavy mineral resources at the Namakwa Sands Mine South Africa: a geometallurgical challenge, The 6th International Heavy Mineral Conference 'Back to Basics', Zulu Nyala Game Lodge, Zululand, Hluhluwe, South Africa, The Southern African Institute of Mining and Metallurgy, Johannesburg, 183-187.

Rozendaal, A., Philander, C. and Carelse, C.B. (2009). Characteristics, recovery and provenance of rutile from the Namakwa Sands heavy mineral deposit. *The Journal of the Southern African Institute of Mining and Metallurgy.*, **110**, 67-74.

Schafer, J. (1997). Electron microprobe study of detrital amphiboles from Famennian synorogenic clastic sediments of the Saxothuringian belt (Erbendorf Paleozoic, NE-Bavaria, Germany): Consequences for provenance and geotectonic development. *Geodinamica Acta.*, **10**, 125-136.

Schweigl, J. and Neubauer, F. (1996). New structural, sedimentological and geochemical data on the Cretaceous geodynamics of the central Northern Calcareous Alps (Eastern Alps). *Zbl. Geologie Paläontologie Teil*., **I H3/4**, 329-343.

Seto, Y., Ohi, S., Shimobayashi, N., Kitamura, M., Miyake, A., Hiroi, Y. and Grantham, G.H. (2006). Clinopyroxene exsolution in wollastonite from Namaqualand granulite, South Africa. *American Mineralogist.*, **91**, 446- 450

Stendal, H., Toteu, S.F., Frei, R., Penaye, J., Njel, U.O., Bassahak, J., Nni, J., Kankeu, B., Ngako, V. and Hell, J.V. (2006). Derivation of detrital rutile in the Yaoundé region from the Neoproterozoic Pan-African belt in southern Cameroon (Central Africa). *Journal of African Earth Sciences.*, **44**, 443-458.

Strum, R. (2002). PX-NOM - an interactive spreadsheet program for the computation of pyroxene analysis derived from the electron microprobe. *Computers and Geosciences.*, **28**, 473-483.

Sukumaran, P.V. and Nambiar, A.R. (1994). Geochemistry of ilmenite from Ratnagiri coast, Maharashtra. *Current Science*., 67, 105-106.

Suresh Babu, S., Thomas, K.A., Mohan Das, P.N. and Damodaran, A.D. (1994). Alteration of ilmenite in the Manavalakurichi deposit, India. C*lays and Clay Minerals*., **42**, 567-571.

Tankard, A.J. (1976). Pleistocene history and coastal morphology of the Ysterfontein-Elands Bay area, Cape Province. *Annals South African Museum.*, **69**,73-119.

Tankard, A.J., Jackson, M.P.A., Eriksson, K.A., Hobday, D.K., Hunter, D.R. and Minter, W.E.L. (1982). Crustal evolution of Southern Africa: 3.8 billion years of Earth history. Springer-Verlag, New York, 1-523.

Temple, A.K. (1966). Alteration of ilmenite. *Economic Geology.*, **61**, 695-714.

Theart, H.F.J. (1980). The geology of the Precambrian terrane in parts of western Namaquland. *Bulletin of the Precambrain Research Unit,* University of Cape Town, **30**.

Theron, J.N., Gresse, P.G., Siegfried, H.P. and Rogers, J. (1980). The Geology of the Cape Town Area: Explanation of Sheet 3318 (Cape Town), Geological Survey of South Africa, 140pp.

Thomas, R.J., Agenbacht, A.L.D., Cornell, D.H. and Moore, J. M. (1993). The Kibaran of southern Africa: tectonic evolution and metallogeny. *Ore. Geol.Rev*., **9**, 131-160.

Toerien, D.K. and Groeneveld, D. (1957). In: Coetzee, C.B. (eds). Ilmenite-houdende sand langs die weskus in die distrik Vanrhynsdorp. *Geol.Surv.S.Afr.Bull*., **25**, 17pp.

Tomkins, H.S., Powell, R. and Ellis, D.J. (2007). The pressure-dependence of the zirconium-in-rutile thermometer. *J. Metamorphic Geol*., **25**, 703-713.

Triebold, S., von Eynatten, H., Luvizotto, G.L. and Zack, T. (2007). Deducing source rock lithology from detrital rutile chemistry: An example from the Erzebirge, Germany. *Chemical Geology*., **244**, 421-426.

Vail, P.R. and Hardenbol, J. (1979). Tertiary sea-level movements around Southern Africa. *Oceanus*., **22**, 71-79

Viator, D. B. (2003). Detrital tourmaline as an indicator of provenance: a chemical and sedimentological study of modern sands from the Black Hills, South Dakota, M.Sc. thesis (unpublished), Louisiana State University, America.

Wach, G.D. and Kettanah, Y.A. (2006). The provenance of heavy minerals in the Mesozoic and Tertiary Formations, Venture B-13 borehole, offshore Nova Scotia, Canada. AAP Annual Convention, Houston, Texas.

Wassef, S.N. (1981). Distribution and Properties of Placer Ilmenite in East Rosetta Beach Sands, Egypt. *Mineral Deposita*., **16**, 259-267.

Waters, D.J., Joubert, P. and Moore, J.M. (1983). A suggested re-interpretation of Namaqua basement and cover rocks south and west of Bitterfontein. *Transactions of the Geological Society of South Africa*., **86**, 293-299.

Watson, E. B., Wark, D. A. and Thomas, J. B. (2006). Crystallisation thermometers for zircon and rutile. *Contributions to Mineralogy and Petrology*., **151**, 413 – 433.

Whalen, J.B. and Chappel, B.W. (1988). Opaque mineralogy and mafic mineral chemistry of I-and S-type granites of the Lachlan fold belt, southeast Australia. *American Mineralogist*., **73**, 281-296.

Wilson, A.F. (1976). Aluminium in coexisting pyroxenes as a sensitive indicator of changes in metamorphic grade within the mafic granulite terrane of the Fraser Range, Western Australia. *Contributions to Mineralogy and Petrology.*, **56**, 255-277.

Woodhead, J.A., Rossman, G.R. and Silver, L.T. (1991). The metamictization of zircon: Radiation dose-dependent structural characteristics. *American Mineralogist.*, **76**, 74-82.

Yang, S., Wang, Z., Guo, Y., Li, C. and Cai, J. (2009). Heavy mineral compositions of the Changjiang (Yangtze River) sediments and their provenance-tracing implication. *Journal of Asian Earth Sciences.*, **35**, 56-65.

Zack, T., Kronz, A., Foley, S. F. and Rivers, T. (2002). Trace element abundances in rutiles from eclogites and associated garnet mica schists. *Chemical Geology.*, **184**, 97 – 122.

Zack, T., Moraes, R. and Kronz, A. (2004a). Temperature dependence of Zr in rutile: empirical calibration of a rutile thermometer. *Contributions to Mineralogy and Petrology.*, **148**, 471-488.

Zack, T., von Eynatten, H. and Kronz, A. (2004b). Rutile geochemistry and its potential use in quantitative provenance studies. *Sedimentary Geology.*, **171**, 37 – 58.

Zelt, G.A.D. (1980). Granultie-facies metamorphism in Namaqualand, South Africa. *Precambrian Research.*, **13**, 253-274.

Titanomagnetite: http://www.encyclopedia.com/doc/1O13-titanomagnetite.html, accessed online 3 December 2011.

QEMSCAN : http://en.wikipedia.org/wiki/QEMSCAN, accessed online 3 December 2011

APPENDIX A:
BOREHOLE COORDINATES AND THM CONTENT AND Al/Al+Fe AND Fe/Fe+Ti RATIOS OF COMPOSITE SAMPLES FROM THE FIVE SATELLITE AREAS

Table A.1 Borehole data of five satellite areas. Data is in the LO17 coordinate system.

Table A.2 THM content, Al/ (Al+Fe) and Fe/ (Fe+Ti) ratios of composite samples. Low and high THM, Al/ (Al+Fe) and Fe/ (Fe+Ti) groups are distinguished by the use of bold digits.

The THM represents all minerals with a specific gravity of > 2.85g/cm^3. THM is usually measured as the float portion of a sample in a heavy liquid such as bromoform or TBE (SG 2.85 to 2.89) (Janse van Vuuren et al, 2006).

The geochemical data of the samples was obtained by means of X-Ray Fluorescence. Analyses were done at the Mineral Separation plant facility at Namakwa sands mine. Pressed pellets of the pulverized sand samples were prepared and used for analysis. The Al/ (Al+Fe) and Fe/ (Fe+Ti) ratios were calculated, for each sample, from the XRF data in Appendix E.

The THM content and Al/ (Al+Fe) and Fe/ (Fe+Ti) ratios were calculated and used to composite the 381 samples into 54 samples. These criteria ensured geochemical and mineralogical homogeneity. The different criteria used to composite the samples are described in more detail in Appendix B.

The THM average in Table A.2 represents the weighted average and was calculated with the formula: $\frac{l \times g}{l}$ where l represents the borehole length and g the grade or THM.

TABLE A.1

BOREHOLE DATA OF FIVE SATELLITE AREAS IN LO17 SYSTEM

HOUTKRAAL REMAINDER PORTION 2

Sample ID	Grid	X (m)	Y (m)	Z (m)	Depth (m)
8A5S001	125x125	3 454 750	-89 750	91	1.75
8A5S002	125x125	3 455 000	-89 750	89	1.63
8A5S003	125x125	3 454 500	-90 000	95	1.58
8A5S004	125x125	3 454 750	-90 000	93	0.87
8A5S005	125x125	3 455 000	-90 000	92	1.50
8A5S006	125x125	3 455 250	-90 000	88	1.40
8A5S007	125x125	3 454 250	-90 250	98	1.24
8A5S008	125x125	3 454 500	-90 250	100	2.08
8A5S009	125x125	3 454 750	-90 250	101	1.70
8A5S010	125x125	3 455 000	-90 250	98	1.50
8A5S011	125x125	3 455 250	-90 250	95	2.54
8A5S012	125x125	3 453 500	-90 500	62	2.55
8A5S013	125x125	3 453 750	-90 500	71	2.14
8A5S014	125x125	3 454 000	-90 500	84	1.56
8A5S015	125x125	3 454 250	-90 500	99	0.76
8A5S016	125x125	3 454 500	-90 500	102	1.13
8A5S017	125x125	3 454 750	-90 500	108	2.44
8A5S018	125x125	3 455 000	-90 500	107	2.00
8A5S019	125x125	3 452 750	-90 750	41	1.40
8A5S020	125x125	3 453 500	-90 750	59	1.07
8A5S021	125x125	3 453 750	-90 750	69	1.64
8A5S022	125x125	3 454 000	-90 750	81	2.30
8A5S023	125x125	3 454 250	-90 750	95	3.20
8A5S024	125x125	3 454 500	-90 750	101	1.44
8A5S025	125x125	3 452 500	-91 000	50	1.07
8A5S026	125x125	3 453 000	-91 000	45	3.00
8A5S027	125x125	3 453 250	-91 000	47	3.00
8A5S028	125x125	3 453 500	-91 000	55	2.50
8A5S029	125x125	3 453 750	-91 000	64	1.60
8A5S030	125x125	3 454 000	-91 000	79	2.26
8A5S031	125x125	3 453 250	-91 750	93	0.65
8A5S032	125x125	3 452 750	-91 125	41	1.97
8A5S033	125x125	3 452 500	-91 250	51	0.84
8A5S034	125x125	3 453 000	-91 250	46	3.00

TABLE A.1 continued

BOREHOLE DATA OF FIVE SATELLITE AREAS IN LO17 SYSTEM

HOUTKRAAL REMAINDER PORTION 2

Sample ID	Grid	X (m)	Y (m)	Z (m)	Depth (m)
8A5S035	125x125	3 453 250	-91 250	50	1.38
8A5S036	125x125	3 453 500	-91 250	60	1.04
8A5S037	125x125	3 453 750	-91 250	72	1.34
8A5S038	125x125	3 454 000	-91 250	86	2.40
8A5S039	125x125	3 452 500	-91 500	46	1.20
8A5S040	125x125	3 453 500	-91 500	49	1.12
8A5S041	125x125	3 453 250	-91 500	58	1.14
8A5S042	125x125	3 453 750	-91 500	97	2.00
8A5S043	125x125	3 452 500	-91 750	46	1.04
8A5S044	125x125	3 453 000	-91 750	57	2.74
8A5S046	125x125	3 453 500	-91 750	91	4.68
8A5S047	125x125	3 453 000	-92 000	58	1.17
8A5S048	125x125	3 453 250	-92 000	70	1.29
8A5S049	125x125	3 452 500	-92 000	51	1.35
8A5S050	125x125	3 452 500	-92 250	52	2.00
8A5S051	125x125	3 453 000	-92 250	51	0.53
8A5S052	125x125	3 453 250	-92 250	68	1.36
8A5S053	125x125	3 452 500	-92 500	60	1.63
8A5S054	125x125	3 453 000	-92 500	52	2.90
8A5S055	125x125	3 452 750	-92 625	51	0.90
8A5S056	125x125	3 452 500	-92 750	73	2.29
8A5S057	125x125	3 452 750	-92 875	55	3.04
8A5S058	125x125	3 452 500	-93 000	78	2.68
8A5S059	125x125	3 452 750	-93 125	59	3.00
8A5S060	125x125	3 453 000	-93 250	54	1.74
8A5S061	125x125	3 452 500	-93 375	97	2.93

BOREHOLE DATA OF FIVE SATELLITE AREAS IN LO17 SYSTEM

HOUTKRAAL REMAINDER

Sample ID	Grid	X (m)	Y (m)	Z (m)	Depth (m)
8A5S062	125x125	3 452 502	-93 752	126	3.29
8A5S063	125x125	3 452 504	-94 000	135	1.88
8A5S064	125x125	3 452 744	-93 985	122	2.48
8A5S065	125x125	3 452 497	-94 251	139	1.40
8A5S066	125x125	3 452 748	-94 250	133	1.23
8A5S067	125x125	3 453 004	-94 373	124	2.55
8A5S068	125x125	3 452 501	-94 498	128	3.00
8A5S069	125x125	3 452 751	-94 495	140	2.18

TABLE A.1 continued

BOREHOLE DATA OF FIVE SATELLITE AREAS IN LO17 SYSTEM

HOUTKRAAL REMAINDER

Sample ID	Grid	X (m)	Y (m)	Z (m)	Depth (m)
8A5S070	125x125	3 453 001	-94 632	135	0.08
8A5S071	125x125	3 453 250	-94 625	121	1.93
8A5S072	125x125	3 452 501	-94 745	115	2.31
8A5S073	125x125	3 452 750	-94 746	141	0.62
8A5S074	125x125	3 453 000	-94 876	139	2.00
8A5S075	125x125	3 453 250	-94 876	133	3.00
8A5S076	125x125	3 453 499	-94 877	112	3.00
8A5S077	125x125	3 452 499	-95 000	108	0.87
8A5S078	125x125	3 452 748	-95 000	131	1.29
8A5S079	125x125	3 453 001	-95 124	134	1.55
8A5S080	125x125	3 453 250	-95 125	134	2.79
8A5S081	125x125	3 453 500	-95 125	122	1.60
8A5S082	125x125	3 452 501	-95 258	92	2.01
8A5S083	125x125	3 452 750	-95 253	114	3,00
8A5S084	125x125	3 453 750	-95 248	107	2.19
8A5S085	125x125	3 453 000	-95 375	118	2.50
8A5S086	125x125	3 453 250	-95 375	122	1.89
8A5S087	125x125	3 453 500	-95 375	128	0.54
8A5S088	125x125	3 452 500	-95 500	77	1.42
8A5S089	125x125	3 452 749	-95 500	102	0.30
8A5S090	125x125	3 453 751	-95 501	112	3.00
8A5S091	125x125	3 454 000	-95 501	94	3.00
8A5S092	125x125	3 453 001	-95 625	103	1.40
8A5S093	125x125	3 453 250	-95 625	115	2.23
8A5S094	125x125	3 453 500	-95 625	127	0.53
8A5S095	125x125	3 452 749	-95 749	88	3.40
8A5S096	125x125	3 453 750	-95 751	112	0.74
8A5S097	125x125	3 454 002	-95 752	101	1.12
8A5S098	125x125	3 453 000	-95 877	94	2.28
8A5S099	125x125	3 453 250	-95 875	108	0.40
8A5S100	125x125	3 453 500	-95 875	123	1.30
8A5S101	125x125	3 453 752	-95 999	114	0.62
8A5S102	125x125	3 454 002	-95 997	110	0.60
8A5S103	125x125	3 453 000	-96 125	95	0.22
8A5S104	125x125	3 453 250	-96 125	102	1.47
8A5S105	125x125	3 453 500	-96 125	116	0.90

TABLE A.1 continued

BOREHOLE DATA OF FIVE SATELLITE AREAS IN LO17 SYSTEM

GEELWAL KAROO

Sample ID	Grid	X (m)	Y (m)	Z (m)	Depth (m)
8A5S106	500x125	3 497 000	-106 948	89	0.28
8A5S107	500x125	3 496 998	-106 697	80	1.22
8A5S108	500x125	3 496 996	-106 447	72	0.24
8A5S109	500x125	3 496 500	-107 450	119	0.60
8A5S110	500x125	3 496 500	-107 200	106	0.57
8A5S111	500x125	3 496 500	-106 950	95	0.50
8A5S112	500x125	3 496 500	-106 699	84	0.55
8A5S113	500x125	3 496 499	-106 453	55	1.69
8A5S114	500x125	3 496 000	-107 076	102	0.82
8A5S115	500x125	3 496 000	-106 950	97	0.40
8A5S116	500x125	3 496 001	-106 700	90	0.15
8A5S117	500x125	3 496 001	-106 325	80	0.31
8A5S118	500x125	3 495 500	-107 075	110	0.70
8A5S119	500x125	3 495 499	-106 825	100	0.80
8A5S120	500x125	3 495 500	-106 575	97	0.23
8A5S121	500x125	3 495 501	-106 325	80	0.32
8A5S122	500x125	3 495 502	-106 073	74	0.54
8A5S123	500x125	3 495 000	-106 702	107	0.37
8A5S124	500x125	3 495 000	-106 575	108	0.26
8A5S125	500x125	3 495 000	-106 200	98	0.50
8A5S126	500x125	3 495 000	-105 950	89	0.36
8A5S127	500x125	3 495 000	-105 702	48	1.00
8A5S128	500x125	3 494 500	-106 450	119	0.62
8A5S129	500x125	3 494 500	-106 325	106	0.80
8A5S130	500x125	3 494 500	-105 949	92	0.45
8A5S131	500x125	3 494 501	-105 701	74	0.37
8A5S132	500x125	3 494 502	-105 452	55	0.82
8A5S133	500x125	3 494 000	-106 325	110	0.30
8A5S134	500x125	3 494 000	-106 075	97	0.68
8A5S135	500x125	3 494 000	-105 950	86	0.83
8A5S136	500x125	3 494 000	-105 575	77	1.20
8A5S137	500x125	3 494 000	-105 325	66	0.80
8A5S138	500x125	3 493 999	-105 076	43	1.02
8A5S139	500x125	3 493 500	-105 950	81	1.15
8A5S140	500x125	3 493 501	-105 701	74	1.10
8A5S141	500x125	3 493 500	-105 575	69	1.30
8A5S142	500x125	3 493 500	-105 200	59	1.54
8A5S143	500x125	3 493 499	-104 950	48	1.16

TABLE A.1 continued

BOREHOLE DATA OF FIVE SATELLITE AREAS IN LO17 SYSTEM

GEELWAL KAROO

Sample ID	Grid	X (m)	Y (m)	Z (m)	Depth (m)
8A5S144	500x125	3 493 495	-104 700	35	1.30
8A5S145	500x125	3 493 000	-105 575	59	0.75
8A5S146	500x125	3 493 000	-105 325	55	0.60
8A5S147	500x125	3 493 000	-105 075	51	1.04
8A5S148	500x125	3 493 000	-104 824	51	2.25
8A5S149	500x125	3 493 000	-104 574	44	2.52
8A5S150	500x125	3 492 500	-105 075	52	2.03
8A5S151	500x125	3 492 500	-104 825	52	1.40
8A5S152	500x125	3 492 500	-104 575	50	1.10
8A5S153	500x125	3 489 000	-102 325	83	0.66
8A5S154	500x125	3 489 000	-101 950	78	0.83
8A5S155	500x125	3 489 000	-101 700	73	0.75
8A5S156	500x125	3 489 001	-101 450	65	0.65
8A5S157	500x125	3 489 001	-101 198	56	0.85
8A5S158	500x125	3 489 001	-101 074	47	0.25
8A5S159	500x125	3 489 000	-100 700	31	0.17
8A5S160	500x125	3 488 501	-102 325	90	0.73
8A5S161	500x125	3 488 500	-102 200	87	0.40
8A5S162	500x125	3 488 500	-101 825	83	0.54
8A5S163	500x125	3 488 500	-101 575	79	0.72
8A5S164	500x125	3 488 500	-101 325	73	0.52
8A5S165	500x125	3 488 500	-101 075	65	0.72
8A5S166	500x125	3 488 500	-100 825	57	0.54
8A5S167	500x125	3 488 500	-100 575	49	0.57
8A5S168	500x125	3 488 500	-100 450	32	0.60
8A5S169	500x125	3 487 999	-101 950	85	0.64
8A5S170	500x125	3 488 001	-101 700	82	0.52
8A5S171	500x125	3 488 000	-101 450	79	0.80
8A5S172	500x125	3 488 000	-101 200	75	0.48
8A5S173	500x125	3 488 000	-101 075	67	1.08
8A5S174	500x125	3 488 000	-100 825	64	0.40
8A5S175	500x125	3 488 002	-100 450	60	0.25
8A5S176	500x125	3 488 001	-100 200	53	0.87
8A5S177	500x125	3 488 000	-99 950	43	0.03
8A5S178	500x125	3 487 500	-101 700	90	0.58
8A5S179	500x125	3 487 501	-101 450	90	0.20
8A5S180	500x125	3 487 500	-101 201	89	0.43

TABLE A.1 continued

BOREHOLE DATA OF FIVE SATELLITE AREAS IN LO17 SYSTEM

GEELWAL KAROO

Sample ID	Grid	X (m)	Y (m)	Z (m)	Depth (m)
8A5S181	500x125	3 487 500	-100 950	87	0.37
8A5S182	500x125	3 487 500	-100 699	84	0.60
8A5S183	500x125	3 487 500	-100 450	75	0.17
8A5S184	500x125	3 487 500	-100 199	65	0.36
8A5S185	500x125	3 487 500	-99 950	57	0.17
8A5S186	500x125	3 487 500	-99 700	48	0.21
8A5S187	500x125	3 487 000	-101 200	107	0.30
8A5S188	500x125	3 486 999	-100 950	103	0.45
8A5S189	500x125	3 487 000	-100 699	97	0.18
8A5S190	500x125	3 487 000	-100 450	88	0.25
8A5S191	500x125	3 486 999	-100 199	79	0.12

BOREHOLE DATA OF FIVE SATELLITE AREAS IN LO17 SYSTEM

GRAAUWDUINEN

Sample ID	Grid	X (m)	Y (m)	Z (m)	Depth (m)
8A5S192	500x125	3 467 998	-88 000	89	2.50
8A5S193	500x125	3 467 999	-88 249	97	1.52
8A5S194	500x125	3 467 999	-88 500	101	0.72
8A5S195	500x125	3 467 999	-88 750	113	0.75
8A5S196	500x125	3 468 001	-88 874	123	1.00
8A5S197	500x125	3 468 001	-89 251	127	0.88
8A5S198	500x125	3 471 502	-87 495	128	0.80
8A5S199	500x125	3 468 503	-86 873	35	0.58
8A5S200	500x125	3 471 500	-88 250	40	0.40
8A5S201	500x125	3 468 501	-87 374	47	0.45
8A5S213	500x125	3 469 000	-86 625	32	0.60
8A5S214	500x125	3 469 000	-86 874	34	0.82
8A5S215	500x125	3 469 000	-87 125	36	0.50
8A5S216	500x125	3 469 000	-87 375	40	0.52
8A5S217	500x125	3 469 000	-87 625	44	0.50
8A5S218	500x125	3 469 000	-87 875	49	0.69
8A5S219	500x125	3 469 000	-88 126	55	0.56
8A5S221	500x125	3 468 999	-88 626	69	0.66
8A5S222	500x125	3 468 999	-88 877	77	0.88
8A5S223	500x125	3 469 002	-89 125	89	1.23
8A5S224	500x125	3 469 000	-89 375	102	1.08
8A5S225	500x125	3 469 000	-89 625	106	1.21

TABLE A.1 continued

BOREHOLE DATA OF FIVE SATELLITE AREAS IN LO17 SYSTEM

GRAAUWDUINEN

Sample ID	Grid	X (m)	Y (m)	Z (m)	Depth (m)
8A5S226	500x125	3 468 502	-86 998	108	1.82
8A5S227	500x125	3 469 500	-85 999	17	0.17
8A5S228	500x125	3 469 501	-86 249	27	0.43
8A5S229	500x125	3 469 500	-86 624	37	0.20
8A5S230	500x125	3 469 500	-86 874	38	0.70
8A5S231	500x125	3 469 001	-89 250	37	0.67
8A5S232	500x125	3 469 500	-87 374	36	0.51
8A5S233	500x125	3 469 500	-87 625	37	0.50
8A5S234	500x125	3 469 500	-87 875	41	0.46
8A5S235	500x125	3 469 500	-88 125	46	0.46
8A5S236	500x125	3 469 500	-88 375	53	0.40
8A5S237	500x125	3 469 500	-88 626	59	0.36
8A5S238	500x125	3 469 000	-89 750	67	1.15
8A5S239	500x125	3 469 503	-86 999	76	1.20
8A5S240	500x125	3 469 501	-89 376	89	1.02
8A5S241	500x125	3 469 500	-89 626	99	1.16
8A5S242	500x125	3 469 500	-89 875	106	0.90
8A5S243	500x125	3 469 500	-90 125	111	1.33
8A5S244	500x125	3 470 000	-86 124	21	0.20
8A5S245	500x125	3 470 000	-86 374	29	0.38
8A5S246	500x125	3 470 000	-86 622	35	0.42
8A5S247	500x125	3 469 501	-89 000	38	0.48
8A5S248	500x125	3 470 000	-87 123	40	0.78
8A5S249	500x125	3 470 001	-87 375	35	0.86
8A5S250	500x125	3 470 001	-86 747	33	0.38
8A5S251	500x125	3 469 999	-87 875	35	0.32
8A5S252	500x125	3 470 000	-88 124	38	0.48
8A5S253	500x125	3 469 998	-88 374	43	0.37
8A5S254	500x125	3 469 999	-88 624	49	0.52
8A5S255	500x125	3 470 002	-86 998	56	0.23
8A5S256	500x125	3 469 999	-89 124	71	0.29
8A5S257	500x125	3 470 000	-89 373	84	0.60
8A5S258	500x125	3 470 000	-89 625	95	0.65
8A5S259	500x125	3 470 000	-89 875	98	0.80
8A5S260	500x125	3 470 000	-90 125	101	0.60

TABLE A.1 continued

BOREHOLE DATA OF FIVE SATELLITE AREAS IN LO17 SYSTEM

GRAAUWDUINEN

Sample ID	Grid	X (m)	Y (m)	Z (m)	Depth (m)
8A5S261	500x125	3 469 999	-90 375	101	0.75
8A5S262	500x125	3 470 498	-86 622	26	0.34
8A5S263	500x125	3 470 498	-86 874	28	0.70
8A5S264	500x125	3 470 498	-87 125	28	0.30
8A5S265	500x125	3 470 499	-87 375	26	0.48
8A5S266	500x125	3 470 499	-87 625	27	0.54
8A5S267	500x125	3 470 500	-87 875	30	0.50
8A5S268	500x125	3 470 500	-88 125	32	0.40
8A5S269	500x125	3 470 501	-88 376	33	0.30
8A5S270	500x125	3 470 501	-88 627	39	0.47
8A5S271	500x125	3 470 502	-88 877	45	0.44
8A5S272	500x125	3 470 500	-89 124	52	0.24
8A5S273	500x125	3 470 499	-89 375	63	0.55
8A5S274	500x125	3 470 500	-89 625	79	0.14
8A5S275	500x125	3 470 500	-89 875	86	0.85
8A5S276	500x125	3 470 500	-90 126	88	0.72
8A5S277	500x125	3 470 500	-90 375	92	0.79
8A5S278	500x125	3 470 500	-90 625	93	0.50
8A5S279	500x125	3 471 000	-87 121	18	0.90
8A5S280	500x125	3 471 000	-87 373	24	0.64
8A5S281	500x125	3 471 000	-87 624	29	0.80
8A5S282	500x125	3 471 000	-87 875	31	0.64
8A5S283	500x125	3 471 000	-88 125	32	0.50
8A5S284	500x125	3 471 000	-88 376	32	0.36
8A5S285	500x125	3 471 000	-88 627	35	0.61
8A5S286	500x125	3 471 000	-88 878	38	0.47
8A5S287	500x125	3 470 996	-89 125	44	0.60
8A5S288	500x125	3 470 997	-89 375	52	0.43
8A5S289	500x125	3 471 000	-89 750	67	0.74
8A5S290	500x125	3 471 000	-89 999	80	0.60
8A5S292	500x125	3 471 000	-89 625	81	0.67
8A5S293	500x125	3 471 000	-90 752	84	0.77
8A5S294	500x125	3 470 999	-91 002	85	0.63
8A5S295	500x125	3 470 999	-90 376	19	0.14

TABLE A.1 continued

BOREHOLE DATA OF FIVE SATELLITE AREAS IN LO17 SYSTEM

GRAAUWDUINEN

Sample ID	Grid	X (m)	Y (m)	Z (m)	Depth (m)
8A5S296	500x125	3 470 999	-90 627	23	0.27
8A5S297	500x125	3 471 500	-87 874	26	0.35
8A5S298	500x125	3 471 500	-88 124	27	0.50
8A5S299	500x125	3 471 500	-88 375	29	0.47
8A5S300	500x125	3 471 500	-88 750	35	0.37
8A5S301	500x125	3 471 499	-88 998	39	0.36
8A5S302	500x125	3 471 500	-89 250	44	0.31
8A5S303	500x125	3 471 501	-89 500	48	0.46
8A5S304	500x125	3 471 500	-89 749	53	0.42
8A5S305	500x125	3 471 500	-89 874	59	0.98
8A5S306	500x125	3 471 501	-90 251	64	0.71
8A5S307	500x125	3 471 500	-90 502	71	0.59
8A5S308	500x125	3 471 500	-90 751	77	0.80
8A5S309	500x125	3 471 499	-91 002	79	1.04
8A5S310	500x125	3 471 500	-91 127	76	0.70
8A5S311	500x125	3 472 000	-88 123	22	0.27
8A5S312	500x125	3 472 001	-88 248	23	0.52
8A5S313	500x125	3 472 000	-88 626	23	0.60
8A5S314	500x125	3 472 000	-88 876	25	0.60
8A5S315	500x125	3 472 001	-89 123	29	0.58
8A5S316	500x125	3 472 000	-89 374	33	0.48
8A5S317	500x125	3 471 999	-89 625	37	0.40
8A5S318	500x125	3 472 000	-89 875	42	0.58
8A5S319	500x125	3 472 000	-90 125	47	0.90
8A5S320	500x125	3 472 000	-90 376	53	0.70
8A5S321	500x125	3 472 000	-90 501	58	0.73
8A5S322	500x125	3 472 000	-90 877	63	0.78
8A5S323	500x125	3 472 000	-91 125	62	1.20
8A5S324	500x125	3 471 998	-91 375	70	0.84
8A5S325	500x125	3 471 998	-91 624	73	0.86

BOREHOLE DATA OF FIVE SATELLITE AREAS IN LO17 SYSTEM

RIETFONTEIN

Sample ID	Grid	X (m)	Y (m)	Z (m)	Depth (m)
8A5S326	500x125	3 455 748	-84 500	30	0.70
8A5S327	500x125	3 455 998	-84 500	42	1.40
8A5S328	500x125	3 455 998	-84 500	43	0.27

TABLE A.1 continued

BOREHOLE DATA OF FIVE SATELLITE AREAS IN LO17 SYSTEM

RIETFONTEIN

Sample ID	Grid	X (m)	Y (m)	Z (m)	Depth (m)
8A5S329	500x125	3 456 249	-84 500	44	0.10
8A5S330	500x125	3 456 369	-84 496	46	0.70
8A5S331	500x125	3 456 626	-84 500	46	0.92
8A5S332	500x125	3 456 876	-84 501	33	3.00
8A5S333	500x125	3 455 999	-84 999	46	0.90
8A5S334	500x125	3 456 123	-84 999	58	0.76
8A5S335	500x125	3 456 500	-85 000	63	1.68
8A5S336	500x125	3 456 751	-85 000	65	1.60
8A5S337	500x125	3 457 002	-85 000	65	0.70
8A5S338	500x125	3 457 253	-85 000	67	0.55
8A5S339	500x125	3 457 504	-85 000	69	1.20
8A5S340	500x125	3 455 999	-85 500	52	2.35
8A5S341	500x125	3 456 249	-85 500	68	1.70
8A5S342	500x125	3 456 500	-85 500	76	0.64
8A5S343	500x125	3 455 998	-86 001	73	0.70
8A5S344	500x125	3 456 249	-86 000	77	2.00
8A5S345	500x125	3 456 500	-86 000	82	1.85
8A5S346	500x125	3 456 751	-86 000	84	0.84
8A5S347	500x125	3 457 002	-85 999	90	2.48
8A5S348	500x125	3 457 254	-86 001	93	2.30
8A5S349	500x125	3 457 504	-86 003	96	2.07
8A5S350	500x125	3 456 500	-86 500	78	1.90
8A5S351	500x125	3 456 751	-86 500	83	1.74
8A5S352	500x125	3 457 002	-86 501	91	2.17
8A5S353	500x125	3 457 252	-86 501	93	0.75
8A5S354	500x125	3 457 502	-86 501	97	0.80
8A5S355	500x125	3 457 750	-86 499	100	0.20
8A5S356	500x125	3 456 002	-87 000	83	2.13
8A5S357	500x125	3 456 251	-87 000	78	1.10
8A5S358	500x125	3 456 501	-86 999	76	1.90
8A5S359	500x125	3 456 751	-87 000	81	2.40

TABLE A.1 continued

BOREHOLE DATA OF FIVE SATELLITE AREAS IN LO17 SYSTEM

RIETFONTEIN

Sample ID	Grid	X (m)	Y (m)	Z (m)	Depth (m)
8A5S360	500x125	3 457 003	-86 999	85	2.13
8A5S361	500x125	3 457 253	-87 001	89	2.60
8A5S362	500x125	3 457 502	-87 001	94	2.20
8A5S363	500x125	3 457 754	-86 999	99	1.66
8A5S364	500x125	3 456 499	-87 500	84	3.00
8A5S365	500x125	3 456 750	-87 500	83	2.10
8A5S366	500x125	3 457 000	-87 500	85	0.80
8A5S367	500x125	3 457 250	-87 499	86	1.12
8A5S368	500x125	3 457 500	-87 499	95	2.20
8A5S369	500x125	3 457 751	-87 498	101	3.00
8A5S370	500x125	3 456 250	-88 000	85	1.20
8A5S371	500x125	3 456 501	-88 000	77	1.06
8A5S372	500x125	3 456 750	-88 000	75	0.95
8A5S373	500x125	3 457 000	-88 000	71	1.52
8A5S374	500x125	3 457 250	-88 000	73	0.88
8A5S375	500x125	3 457 500	-88 000	78	1.04
8A5S376	500x125	3 457 747	-88 000	84	0.60
8A5S377	500x125	3 455 750	-88 500	97	1.43
8A5S378	500x125	3 456 000	-88 499	94	1.40
8A5S379	500x125	3 456 250	-88 500	83	1.80
8A5S380	500x125	3 456 500	-88 499	71	1.40
8A5S381	500x125	3 456 750	-88 499	65	1.40
8A5S382	500x125	3 457 001	-88 501	63	1.03
8A5S383	500x125	3 457 250	-88 499	65	1.30
8A5S384	500x125	3 457 493	-88 499	74	1.68
8A5S385	500x125	3 455 500	-89 000	101	2.55
8A5S386	500x125	3 455 750	-88 999	98	1.60
8A5S387	500x125	3 456 000	-88 998	93	1.80
8A5S388	500x125	3 456 250	-89 000	90	2.42
8A5S389	500x125	3 456 500	-89 000	83	1.20
8A5S390	500x125	3 456 750	-89 000	71	1.80
8A5S391	500x125	3 455 500	-89 500	86	1.40
8A5S392	500x125	3 455 750	-89 500	85	1.20
8A5S393	500x125	3 455 999	-89 500	88	1.83
8A5S394	500x125	3 456 250	-89 500	96	0.25
8A5S395	500x125	3 455 500	-90 000	87	1.03

TABLE A.2				
THM CONTENT, Al(Al+Fe) AND Fe/(Fe+Ti) RATIOS OF COMPOSITE SAMPLES				
HOUTKRAAL REMAINDER OF PORTION 2				
Sample ID	**Sample nrs**	**THM (%)**	**Al/(Al+Fe)%**	**Fe/(Fe+Ti)%**
HKRP001	**8A5S060**	**5**	**0.39**	**0.55**
HKRP002	8A5S017	4	0.32	0.58
	8A5S050	4	0.45	0.59
	8A5S018	4	0.39	0.59
	8A5S011	4	0.36	0.60
	8A5S006	3	0.39	0.60
	8A5S005	5	0.42	0.61
	8A5S024	4	0.43	0.61
average		**4**	**0.40**	**0.59**
HKRP003	**8A5S052**	**3**	**0.42**	**0.61**
	8A5S016	**4**	**0.46**	**0.61**
	8A5S013	**3**	**0.44**	**0.61**
	8A5S059	**4**	**0.44**	**0.61**
	8A5S023	**4**	**0.45**	**0.62**
	8A5S022	**4**	**0.44**	**0.63**
	8A5S010	**5**	**0.44**	**0.65**
	8A5S008	**3**	**0.42**	**0.67**
	8A5S009	**4**	**0.28**	**0.79**
average		**4**	**0.42**	**0.64**
HKRP004	8A5S021	4	0.47	0.60
	8A5S048	4	0.48	0.60
	8A5S025	3	0.52	0.61
	8A5S056	3	0.50	0.61
	8A5S033	3	0.52	0.61
	8A5S058	4	0.49	0.62
	8A5S057	3	0.46	0.62
	8A5S042	3	0.51	0.62
	8A5S039	4	0.53	0.62
	8A5S030	3	0.47	0.62
	8A5S047	3	0.50	0.62
	8A5S019	3	0.55	0.62
	8A5S020	4	0.49	0.63
average		**3**	**1**	**1**
HKRP005	**8A5S043**	**3**	**0.55**	**0.65**
	8A5S053	**3**	**0.49**	**0.65**
	8A5S028	**3**	**0.46**	**0.65**
	8A5S055	**3**	**0.58**	**0.65**
	8A5S015	**4**	**0.51**	**0.68**
	8A5S002	**3**	**0.49**	**0.69**
average		**3**	**0.52**	**0.66**

TABLE A.2 continued				
THM CONTENT, Al(Al+Fe) AND Fe/(Fe+Ti) RATIOS OF COMPOSITE SAMPLES				
HOUTKRAAL REMAINDER OF PORTION 2				
Sample ID	**Sample nrs**	**THM (%)**	**Al/(Al+Fe)%**	**Fe/(Fe+Ti)%**
HKR006	8A5S029	2	0.54	0.63
	8A5S001	2	0.46	0.64
	8A5S041	2	0.55	0.64
	8A5S046	2	0.47	0.64
	8A5S044	2	0.47	0.64
	8A5S038	2	0.46	0.65
	8A5S012	2	0.51	0.65
	8A5S036	2	0.55	0.66
average		**2**	**0.50**	**0.64**
HKR 007	**8A5S037**	**1**	**0.52**	**0.68**
	8A5S014	**2**	**0.49**	**0.68**
	8A5S034	**1**	**0.50**	**0.68**
	8A5S003	**1**	**0.52**	**0.70**
	8A5S004	**2**	**0.54**	**0.71**
	8A5S027	**2**	**0.55**	**0.72**
	8A5S007	**1**	**0.52**	**0.73**
average		**2**	**0.52**	**0.70**
HKR 008	8A5S054	1	0.61	0.62
	8A5S035	1	0.62	0.69
	8A5S049	2	0.56	0.69
	8A5S045	2	0.59	0.69
	8A5S031	8	0.63	0.69
	8A5S026	6	0.56	0.69
	8A5S040	5	0.57	0.72
average		**4**	**0.59**	**0.69**
HKR 009	**8A5S032**	**4**	**0.67**	**0.78**
	8A5S051	**4**	**0.66**	**0.83**
average		**4**	**0.66**	**0.81**
HKR010	8A5S061	2	0.54	0.67
THM, Al(Al+Fe) and Fe/(Fe+Ti) content of composite samples				
HOUTKRAAL REMAINDER				
Sample ID	**Sample nrs**	**THM (%)**	**Al/(Al+Fe)%**	**Fe/(Fe+Ti)%**
HKR 001	8A5S079	2	0.47	0.57
	8A5S078	1	0.54	0.57
	8A5S085	2	0.48	0.60
	8A5S098	2	0.46	0.60
	8A5S089	2	0.52	0.62
	8A5S104	2	0.48	0.63
	8A5S072	2	0.54	0.64
	8A5S077	1	0.51	0.65
average		2	0.50	0.61

TABLE A.2 continued				
THM CONTENT, Al(Al+Fe) AND Fe/(Fe+Ti) RATIOS OF COMPOSITE SAMPLES				
HOUTKRAAL REMAINDER				
Sample ID	**Sample nrs**	**THM (%)**	**Al/(Al+Fe)**	**Fe/(Fe+Ti)**
HKR 002	**8A5S088**	**1**	**0.54**	**0.73**
HKR 003	8A5S083	1	0.58	0.63
	8A5S068	2	0.57	0.64
average		1	0.58	0.64
HKR 004	**8A5S099**	**2**	**0.62**	**0.69**
	8A5S082	**1**	**0.64**	**0.70**
average		**1**	**0.63**	**0.70**
HKR 005	**8A5S093**	**5**	**0.41**	**0.55**
	8A5S065	**4**	**0.47**	**0.56**
	8A5S064	**5**	**0.46**	**0.56**
	8A5S063	**3**	**0.48**	**0.57**
	8A5S073	**4**	**0.42**	**0.57**
average		**4**	**0.45**	**0.56**
HKR 006	8A5S086	3	0.49	0.58
	8A5S092	3	0.46	0.58
	8A5S096	4	0.43	0.59
	8A5S095	3	0.48	0.60
	8A5S105	3	0.43	0.61
average		**3**	**0.46**	**0.59**
HKR 007	**8A5S094**	**4**	**0.51**	**0.56**
	8A5S087	**3**	**0.51**	**0.61**
	8A5S062	**3**	**0.53**	**0.62**
average		**4**	**0.52**	**0.60**
HKR 008	8A5S103	3	0.61	0.71
HKR 009	**8A5S090**	**11**	**0.27**	**0.52**
	8A5S075	**9**	**0.29**	**0.53**
	8A5S084	**11**	**0.30**	**0.53**
	8A5S091	**11**	**0.27**	**0.54**
	8A5S097	**10**	**0.32**	**0.54**
	8A5S074	**9**	**0.33**	**0.54**
average		**10**	**0.30**	**0.53**
HKR 010	8A5S069	7	0.37	0.55
	8A5S076	6	0.35	0.55
	8A5S080	6	0.37	0.55
	8A5S071	8	0.36	0.56
average		**7**	**0.36**	**0.55**
HKR 011	**8A5S081**	**9**	**0.47**	**0.52**
	8A5S066	**6**	**0.39**	**0.55**
	8A5S100	**6**	**0.39**	**0.56**
average		**7**	**0.42**	**0.55**
HKR 012	8A5S067	6	0.40	0.57
	8A5S102	7	0.41	0.57
	8A5S101	7	0.42	0.58
	8A5S070	6	0.43	0.60
average		**6**	**0.42**	**0.58**

TABLE A.2 continued				
THM CONTENT, Al(Al+Fe) AND Fe/(Fe+Ti) RATIOS OF COMPOSITE SAMPLES				
GEELWAL KAROO				
Sample ID	**Sample nrs**	**THM (%)**	**Al/(Al+Fe)**	**Fe/(Fe+Ti)**
GW 001	**8A5S148**	**1**	**0.51**	**0.61**
	8A5S149	**1**	**0.53**	**0.61**
	8A5S150	**1**	**0.55**	**0.63**
	8A5S151	**1**	**0.56**	**0.64**
	8A5S142	**2**	**0.54**	**0.65**
	8A5S136	**1**	**0.60**	**0.66**
	8A5S152	**1**	**0.56**	**0.66**
average		**1**	**0.55**	**0.64**
GW 002	8A5S140	1	0.60	0.69
	8A5S137	1	0.62	0.71
	8A5S139	1	0.61	0.74
average		**1**	**0.61**	**0.71**
GW 003	**8A5S156**	**1**	**0.65**	**0.66**
	8A5S188	**1**	**0.65**	**0.71**
	8A5S171	**1**	**0.64**	**0.71**
	8A5S170	**1**	**0.63**	**0.71**
	8A5S180	**1**	**0.66**	**0.71**
	8A5S118	**1**	**0.69**	**0.72**
	8A5S163	**1**	**0.66**	**0.73**
	8A5S172	**1**	**0.63**	**0.73**
	8A5S133	**1**	**0.67**	**0.74**
	8A5S190	**1**	**0.65**	**0.74**
	8A5S155	**1**	**0.65**	**0.75**
average		**1**	**0.65**	**0.72**
GW 004	8A5S158	1	0.67	0.76
	8A5S157	1	0.64	0.76
	8A5S110	1	0.69	0.76
	8A5S179	1	0.65	0.76
	8A5S114	1	0.67	0.76
	8A5S162	1	0.69	0.76
	8A5S169	1	0.63	0.76
	8A5S109	1	0.70	0.77
	8A5S167	1	0.65	0.77
	8A5S153	1	0.66	0.78
	8A5S166	1	0.65	0.78
	8A5S187	1	0.65	0.78
	8A5S165	1	0.67	0.79
	8A5S178	1	0.67	0.80
	8A5S160	1	0.64	0.80
	8A5S161	1	0.66	0.80
average		**1**	**0.66**	**0.77**
GW 005	**8A5S141**	**2**	**0.53**	**0.61**
	8A5S134	**3**	**0.55**	**0.61**
	8A5S135	**2**	**0.57**	**0.64**
	8A5S147	**2**	**0.51**	**0.65**
average		**2**	**0.54**	**0.63**

TABLE A.2 continued				
THM CONTENT, Al(Al+Fe) AND Fe/(Fe+Ti) RATIOS OF COMPOSITE SAMPLES				
GEELWAL KAROO				
Sample ID	**Sample nrs**	**THM (%)**	**Al/(Al+Fe)**	**Fe/(Fe+Ti)**
GW 006	8A5S130	2	0.59	0.66
	8A5S145	2	0.53	0.66
	8A5S146	2	0.55	0.69
average		**2**	**0.56**	**0.67**
GW 007	**8A5S174**	**2**	**0.67**	**0.63**
	8A5S173	**2**	**0.67**	**0.63**
	8A5S182	**2**	**0.67**	**0.64**
	8A5S129	**2**	**0.62**	**0.65**
	8A5S111	**2**	**0.62**	**0.68**
	8A5S164	**2**	**0.60**	**0.68**
	8A5S185	**3**	**0.61**	**0.68**
	8A5S128	**2**	**0.68**	**0.70**
	8A5S183	**3**	**0.64**	**0.70**
	8A5S191	**2**	**0.64**	**0.70**
	8A5S181	**2**	**0.64**	**0.70**
	8A5S189	**2**	**0.64**	**0.70**
	8A5S184	**2**	**0.63**	**0.71**
	8A5S115	**2**	**0.66**	**0.71**
	8A5S175	**2**	**0.64**	**0.72**
	8A5S176	**2**	**0.63**	**0.72**
	8A5S120	**2**	**0.64**	**0.73**
average		**2**	**0.64**	**0.69**
GW 008	8A5S154	2	0.61	0.75
	8A5S119	2	0.67	0.75
	8A5S186	2	0.64	0.76
	8A5S132	2	0.60	0.83
average		**2**	**0.63**	**0.77**
GW 009	**8A5S143**	**3**	**0.49**	**0.59**
	8A5S144	**16**	**0.36**	**0.62**
	8A5S108	**7**	**0.55**	**0.64**
	8A5S126	**11**	**0.46**	**0.70**
average		**10**	**0.46**	**0.64**
GW 010	8A5S113	7	0.49	0.71
	8A5S122	8	0.50	0.80
	8A5S168	4	0.56	0.83
	8A5S127	17	0.46	0.86
average		**9**	**0.50**	**0.80**
GW 011	**8A5S107**	**3**	**0.60**	**0.64**
	8A5S125	**3**	**0.57**	**0.64**
	8A5S106	**3**	**0.61**	**0.65**
	8A5S124	**4**	**0.58**	**0.67**
	8A5S121	**5**	**0.58**	**0.67**
	8A5S117	**5**	**0.56**	**0.68**
	8A5S177	**4**	**0.62**	**0.70**
	8A5S131	**5**	**0.57**	**0.70**
	8A5S112	**4**	**0.59**	**0.71**
	8A5S123	**5**	**0.58**	**0.71**

TABLE A.2 continued				
THM CONTENT, Al(Al+Fe) AND Fe/(Fe+Ti) RATIOS OF COMPOSITE SAMPLES				
GEELWAL KAROO				
Sample ID	**Sample nrs**	**THM (%)**	**Al/(Al+Fe)**	**Fe/(Fe+Ti)**
GW 012	8A5S159	6	0.58	0.77
	8A5S116	3	0.62	0.80
	8A5S138	3	0.57	0.84
average		**4**	**0.59**	**0.80**
THM CONTENT, Al(Al+Fe) AND Fe/(Fe+Ti) RATIOS OF COMPOSITE SAMPLES				
GRAAUWDUINEN				
Sample ID	**Sample nrs**	**THM (%)**	**Al/(Al+Fe)**	**Fe/(Fe+Ti)**
GRW 001	**8A5S275**	**1**	**0.56**	**0.42**
	8A5S286	**2**	**0.61**	**0.62**
	8A5S259	**2**	**0.65**	**0.63**
	8A5S321	**2**	**0.59**	**0.63**
	8A5S276	**2**	**0.60**	**0.63**
	8A5S221	**2**	**0.60**	**0.63**
	8A5S195	**1**	**0.57**	**0.64**
	8A5S310	**1**	**0.57**	**0.64**
	8A5S261	**2**	**0.61**	**0.64**
	8A5S260	**2**	**0.62**	**0.64**
	8A5S323	**1**	**0.60**	**0.64**
average		**2**	**0.60**	**0.62**
GRW 002	8A5S270	2	0.62	0.65
	8A5S304	2	0.59	0.65
	8A5S293	2	0.63	0.65
	8A5S309	1	0.64	0.65
	8A5S292	2	0.62	0.65
	8A5S240	1	0.61	0.65
	8A5S277	2	0.60	0.65
	8A5S308	1	0.63	0.66
	8A5S285	2	0.65	0.66
	8A5S278	2	0.64	0.66
	8A5S320	1	0.60	0.66
	8A5S224	1	0.57	0.66
	8A5S214	2	0.60	0.66
	8A5S222	2	0.58	0.66
	8A5S238	1	0.62	0.67
	8A5S302	2	0.65	0.67
	8A5S288	2	0.64	0.67
	8A5S226	2	0.61	0.67
	8A5S291	1	0.65	0.67
	8A5S239	1	0.62	0.68
	8A5S204	2	0.56	0.68
	8A5S315	2	0.66	0.68
	8A5S318	2	0.63	0.68
	8A5S205	1	0.61	0.68
	8A5S213	2	0.60	0.69
	8A5S322	1	0.64	0.69

TABLE A.2 continued				
THM CONTENT, Al(Al+Fe) AND Fe/(Fe+Ti) RATIOS OF COMPOSITE SAMPLES				
GRAAUWDUINEN				
Sample ID	**Sample nrs**	**THM (%)**	**Al/(Al+Fe)**	**Fe/(Fe+Ti)**
GRW002	8A5S223	1	0.63	0.69
	8A5S319	1	0.63	0.70
	8A5S290	2	0.62	0.70
	8A5S325	1	0.64	0.71
	8A5S303	1	0.65	0.71
	8A5S317	2	0.66	0.72
	8A5S265	2	0.66	0.72
	8A5S300	2	0.65	0.72
	8A5S307	1	0.64	0.73
	8A5S263	2	0.57	0.75
	8A5S231	1	0.59	0.75
	8A5S249	2	0.66	0.76
	8A5S289	2	0.66	0.76
	8A5S295	2	0.65	0.78
average		**2**	**0.62**	**0.69**
GRW 003	**8A5S284**	**2**	**0.67**	**0.67**
	8A5S268	**2**	**0.67**	**0.67**
	8A5S305	**1**	**0.68**	**0.67**
	8A5S297	**1**	**0.68**	**0.67**
	8A5S258	**2**	**0.71**	**0.68**
	8A5S282	**1**	**0.73**	**0.69**
	8A5S316	**2**	**0.67**	**0.69**
	8A5S314	**1**	**0.70**	**0.69**
	8A5S299	**1**	**0.68**	**0.70**
	8A5S313	**1**	**0.70**	**0.70**
	8A5S306	**1**	**0.68**	**0.70**
	8A5S280	**1**	**0.73**	**0.70**
	8A5S298	**1**	**0.74**	**0.71**
	8A5S283	**2**	**0.67**	**0.71**
	8A5S266	**2**	**0.68**	**0.72**
	8A5S281	**1**	**0.77**	**0.73**
	8A5S246	**2**	**0.70**	**0.73**
	8A5S324	**1**	**0.70**	**0.73**
	8A5S250	**1**	**0.70**	**0.73**
	8A5S247	**2**	**0.74**	**0.74**
	8A5S279	**2**	**0.67**	**0.75**
	8A5S296	**1**	**0.72**	**0.75**
	8A5S312	**2**	**0.68**	**0.76**
average		**1**	**0.70**	**0.71**
GRW 004	8A5S248	1	0.73	0.77

TABLE A.2 continued				
THM CONTENT, Al(Al+Fe) AND Fe/(Fe+Ti) RATIOS OF COMPOSITE SAMPLES				
GRAAUWDUINEN				
Sample ID	**Sample nrs**	**THM (%)**	**Al/(Al+Fe)**	**Fe/(Fe+Ti)**
GRW 005	**8A5S192**	**5**	**0.38**	**0.55**
	8A5S197	**4**	**0.47**	**0.56**
	8A5S193	**4**	**0.45**	**0.58**
	8A5S196	**3**	**0.49**	**0.59**
	8A5S208	**3**	**0.53**	**0.59**
	8A5S200	**4**	**0.50**	**0.60**
	8A5S209	**3**	**0.48**	**0.60**
	8A5S202	**3**	**0.49**	**0.61**
	8A5S198	**3**	**0.46**	**0.61**
	8A5S217	**4**	**0.53**	**0.61**
	8A5S201	**4**	**0.53**	**0.61**
	8A5S194	**4**	**0.51**	**0.61**
average		**4**	**0.49**	**0.59**
GRW 006	8A5S203	2	0.51	0.63
	8A5S199	3	0.53	0.64
	8A5S262	3	0.53	0.67
average		**3**	**0.53**	**0.65**
GRW 007	**8A5S235**	**3**	**0.68**	**0.27**
	8A5S232	**4**	**0.60**	**0.48**
	8A5S255	**5**	**0.56**	**0.60**
average		**4**	**0.61**	**0.45**
GRW 008	8A5S237	3	0.56	0.61
	8A5S274	3	0.68	0.62
	8A5S243	3	0.59	0.62
	8A5S252	3	0.63	0.62
	8A5S271	3	0.65	0.63
	8A5S287	3	0.63	0.63
	8A5S311	2	0.64	0.63
	8A5S218	3	0.56	0.63
	8A5S219	3	0.59	0.63
	8A5S220	3	0.55	0.63
	8A5S241	3	0.64	0.64
	8A5S257	3	0.61	0.64
	8A5S273	2	0.63	0.64
	8A5S251	3	0.66	0.65
	8A5S242	3	0.58	0.65
	8A5S254	3	0.62	0.65
	8A5S253	3	0.64	0.65
	8A5S272	3	0.62	0.66

TABLE A.2 continued				
THM CONTENT, Al(Al+Fe) AND Fe/(Fe+Ti) RATIOS OF COMPOSITE SAMPLES				
GRAAUWDUINEN				
Sample ID	**Sample nrs**	**THM (%)**	**Al/(Al+Fe)**	**Fe/(Fe+Ti)**
GRW008	8A5S215	2	0.60	0.66
	8A5S207	3	0.60	0.66
	8A5S269	3	0.65	0.66
	8A5S301	2	0.65	0.66
	8A5S216	3	0.59	0.67
	8A5S227	7	0.59	0.68
	8A5S228	4	0.60	0.69
	8A5S267	3	0.63	0.69
	8A5S234	3	0.63	0.69
	8A5S211	4	0.58	0.69
	8A5S256	3	0.65	0.70
	8A5S244	6	0.62	0.70
	8A5S236	3	0.65	0.70
	8A5S206	3	0.59	0.71
	8A5S230	2	0.64	0.71
	8A5S233	3	0.62	0.71
	8A5S210	5	0.57	0.72
	8A5S229	4	0.60	0.72
	8A5S212	3	0.60	0.74
	8A5S245	2	0.66	0.77
	8A5S264	3	0.64	0.77
average		**3**	**0.62**	**0.67**
GRW009	**8A5S294**		**0.58**	**0.86**
GRW 010	8A5S225	**1**	0.68	0.85
THM CONTENT, Al(Al+Fe) AND Fe/(Fe+Ti) RATIOS OF COMPOSITE SAMPLES				
RIETFONTEIN				
Sample ID	**Sample nrs**	**THM (%)**	**Al/(Al+Fe)**	**Fe/(Fe+Ti)**
RF 001	**8A5S392**	**3**	**0.45**	**0.63**
	8A5S391	**2**	**0.46**	**0.63**
	8A5S370	**3**	**0.53**	**0.65**
	8A5S377	**2**	**0.54**	**0.66**
	8A5S371	**3**	**0.55**	**0.66**
average		**3**	**0.50**	**0.65**
RF 002	8A5S390	3	0.52	0.67
	8A5S387	3	0.52	0.67
	8A5S389	3	0.49	0.67
	8A5S359	3	0.54	0.67
	8A5S385	3	0.51	0.67
	8A5S386	3	0.51	0.67
	8A5S361	3	0.51	0.70
average		**3**	**0.51**	**0.67**

TABLE A.2 continued				
THM CONTENT, Al(Al+Fe) AND Fe/(Fe+Ti) RATIOS OF COMPOSITE SAMPLES				
RIETFONTEIN				
Sample ID	**Sample nrs**	**THM (%)**	**Al/(Al+Fe)**	**Fe/(Fe+Ti)**
RF 003	**8A5S339**	**3**	**0.61**	**0.61**
	8A5S327	**3**	**0.63**	**0.64**
	8A5S374	**3**	**0.56**	**0.64**
	8A5S356	**3**	**0.63**	**0.64**
	8A5S345	**3**	**0.59**	**0.64**
	8A5S358	**3**	**0.57**	**0.65**
	8A5S350	**2**	**0.62**	**0.65**
	8A5S379	**3**	**0.58**	**0.65**
	8A5S381	**3**	**0.57**	**0.66**
	8A5S344	**3**	**0.61**	**0.66**
	8A5S349	**3**	**0.59**	**0.66**
	8A5S364	**2**	**0.59**	**0.67**
	8A5S353	**3**	**0.58**	**0.67**
	8A5S335	**3**	**0.62**	**0.67**
average		**3**	**0.60**	**0.65**
RF 004	8A5S347	3	0.61	0.68
	8A5S352	3	0.58	0.68
	8A5S354	3	0.59	0.68
	8A5S334	3	0.63	0.68
	8A5S331	3	0.59	0.68
	8A5S343	2	0.65	0.69
	8A5S380	2	0.61	0.69
	8A5S333	3	0.65	0.70
	8A5S337	3	0.61	0.70
	8A5S328	3	0.63	0.70
	8A5S357	2	0.60	0.71
	8A5S373	1	0.58	0.71
	8A5S332	2	0.57	0.71
	8A5S355	3	0.56	0.72
average		**3**	**0.60**	**0.70**
RF 005	**8A5S395**	**4**	**0.44**	**0.61**
	8A5S383	**5**	**0.47**	**0.62**
	8A5S384	**6**	**0.44**	**0.63**
	8A5S382	**5**	**0.45**	**0.64**
	8A5S393	**4**	**0.41**	**0.64**
	8A5S375	**5**	**0.44**	**0.65**
average		**5**	**0.44**	**0.63**
RF 006	8A5S369	5	0.48	0.69
average		**5**	**0.48**	**0.69**
RF 007	**8A5S326**	**4**	**0.58**	**0.59**
	8A5S346	**4**	**0.59**	**0.63**
	8A5S351	**4**	**0.55**	**0.63**
	8A5S338	**4**	**0.53**	**0.64**

TABLE A.2 continued				
THM CONTENT, Al(Al+Fe) AND Fe/(Fe+Ti) RATIOS OF COMPOSITE SAMPLES				
RIETFONTEIN				
Sample ID	**Sample nrs**	**THM (%)**	**Al/(Al+Fe)**	**Fe/(Fe+Ti)**
RF007	**8A5S366**	**4**	**0.50**	**0.64**
	8A5S340	**4**	**0.60**	**0.65**
	8A5S372	**4**	**0.53**	**0.65**
	8A5S388	**4**	**0.50**	**0.65**
	8A5S341	**4**	**0.55**	**0.65**
	8A5S348	**4**	**0.56**	**0.65**
	8A5S342	**6**	**0.50**	**0.65**
average		**4**	**0.54**	**0.64**
RF 008	8A5S367	4	0.50	0.66
	8A5S378	4	0.52	0.66
	8A5S365	4	0.54	0.67
	8A5S360	4	0.52	0.67
	8A5S376	6	0.59	0.67
	8A5S362	4	0.53	0.69
	8A5S363	4	0.53	0.69
	8A5S368	4	0.50	0.70
average		**4**	**0.53**	**0.68**
RF009	**8A5S394**	**6**	**0.36**	**0.70**
RF 010	8A5S330	4	0.57	0.66
	8A5S336	4	0.58	0.67
	8A5S329	4	0.59	0.68
average		**4**	**0.58**	**0.67**

APPENDIX B:
CRITERIA USED TO COMPOSITE BOREHOLE SAMPLES

Samples collected were composited from a total of 381 to 54 using the three criteria listed below. This was done to ensure geochemical and mineralogical homogeneity of the 54 composite samples. The 381 samples were composited to reduce the sample set and to obtain a representative number of samples of the five satellite areas. The THM content of each satellite area was used first to divide the sample suite into a low THM and a high THM fraction. For Houtkraal Remainder, Remainder of Houtkraal Portion 2 and for Geelwal Karoo the low THM fraction represents all samples with a THM content < 3% and the high THM fraction those with a THM content > 3%. For Graauwduinen and Rietfontein the low THM fraction comprise all THM values < 3.5% and the high THM fraction all THM values > 3.5%. These cut-off values are based on a THM population histogram. The THM values of Rietfontein are used as an example (Figure B.1). The bimodality of this histogram indicates that a THM content of 3.5 is a natural subdivision.

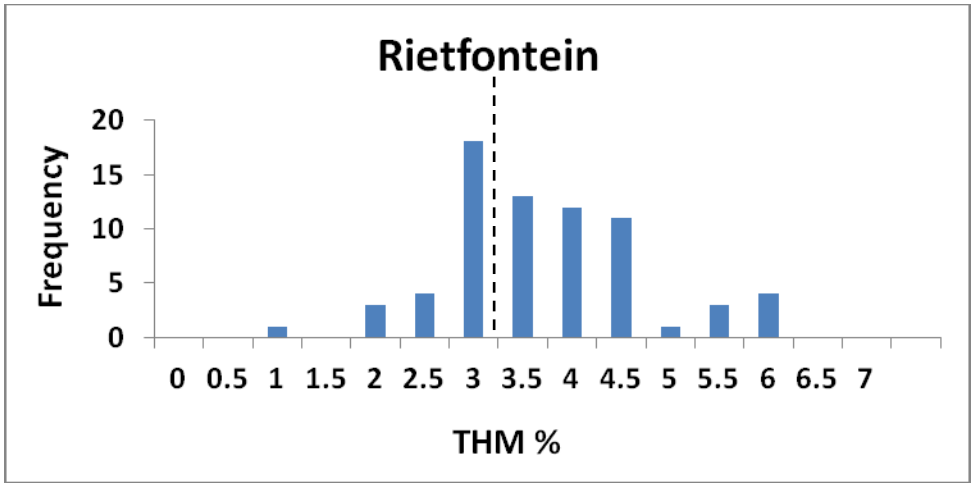

Figure B.1. Frequency distribution of the THM content of Rietfontein farm showing the line of subdivision used to distinguish between the low and high THM group.

The Al/Al+Fe ratio was then calculated for the low and high THM fractions respectively (original chemistr from Appendix E). The low THM fraction was then divided into a low Al/Al+Fe ratio group and a high Al/Al+Fe ratio group (Figure B.2). The same was done for the high THM group. Thirdly the Fe/Fe+Ti ratio was calculated for the four subgroups (low

Al/Al+Fe ratio group and high Al/Al+Fe ratio group of the low THM fraction and the low Al/Al+Fe ratio group and high Al/Al+Fe ratio group of the high THM fraction). The low Al/Al+Fe group of the low THM fraction was divided into a low and high Fe/Fe+Ti ratio group. The high Al/Al+Fe group of the low THM fraction were then also divided into a low and high Fe/Fe+Ti group. The low Al/Al+Fe group of the high THM fraction was then divided into a low and high Fe/Fe+Ti fraction. The same was done for the high Al/Al+Fe group of the high THM fraction. The low and high Al/Al+Fe and Fe/Fe+Ti values were determined in the same manner as the low and high THM fractions (Figure B.2).

This compositing criterion was applied to all five satellite areas. The above two ratios were used due to the fact that ilmenite (Fe+Ti) and garnet (Al+Fe) are the two most dominant heavy minerals present in the heavy mineral fraction. The criteria are shown diagrammatically below:

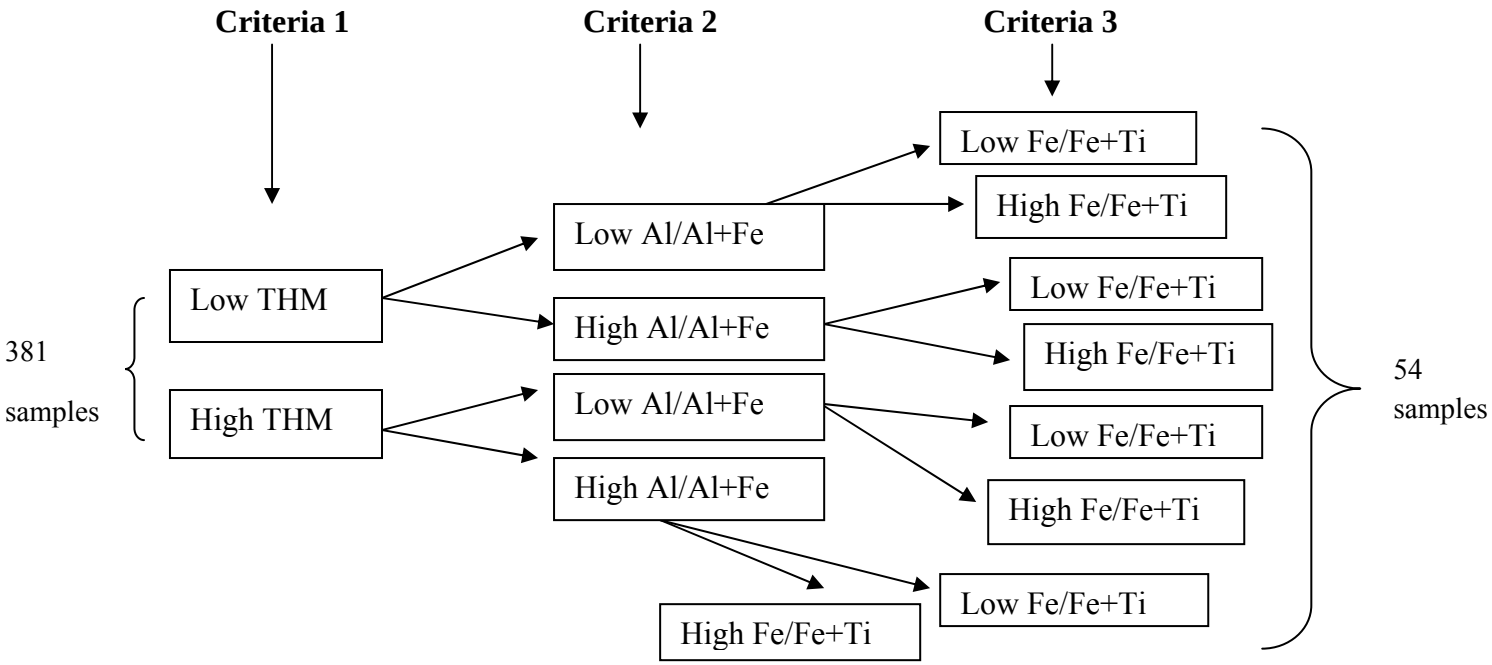

Figure B.2. A flow chart showing the eight groups used for compositing of the 382 samples. This was done for each satellite area

Table B.1. This table illustrates how the X-coordinate was taken into consideration during compositing of the samples to ensure spatial homogeneity.

Rietfontein				
Sample ID	**Sample**	**Grid**	**X (m)**	**Fe/(Fe+Ti)**
8A5S367	RF 008	500x125	37,500	0.66
8A5S378	RF 008	500x125	38,500	0.66
8A5S330	RF 010	500x125	**34,500**	0.66
8A5S365	RF 008	500x125	37,500	0.67
8A5S360	RF 008	500x125	37,000	0.67
8A5S376	RF 008	500x125	38,000	0.67
8A5S336	RF 010	500x125	**35,000**	0.67
8A5S329	RF 010	500x125	**34,500**	0.68
8A5S362	RF 008	500x125	37,000	0.69
8A5S363	RF 008	500x125	37,000	0.69
8A5S368	RF 008	500x125	37,500	0.70

After all the three criteria were applied in the sample selection, the X- coordinates (Table A.1) of the grid system of the different samples were taken into account where necessary. This was only applied to the low and high Fe/Fe+Ti groups. If samples have an X-coordinate that differs from that of the other composite samples in its group by a maximum of 1500 metres and more, it was grouped as a separate composite sample. This was done to overcome possible changes in mineralogy, chemistry and THM content and to ensure spatial homogeneity of the composite samples (Table B.1).

The above composite scheme is a local method used by Namakwa Sands mine for the RAS unit. The RAS is ilmenite-rich (Ti-Fe) and garnet-rich (Al-Fe). This will also allow comparison of the results of the present study with the Namakwa Sands deposit.

APPENDIX C:
DETAILS AND OPERATING CONDITIONS OF ANALYTICAL EQUIPMENT

SEM at University of Stellenbosch

Model:	Leo® 1430VP Scanning Electron Microscope
X-Ray Analyzer:	Oxford Instruments® 133KeV detector
Data Reduction:	Oxford INCA software
Beam Voltage:	20kV
Beam Current:	-3.97nA.
Working Distance:	13mm
Acquire Time:	50
Detection limit:	0.5 wt%

Samples were coated with 15 micrometers of carbon.

QEMSCAN at Anglo American Laboratories, Johannesburg

Beam Voltage:	25kV
Beam Current:	11. 0μA
Working Distance:	23mm
Spot size:	567

XRF at Namakwa Sands

Elements analyzed for:	Mg, Si, Mn, Ti, Ca, Al, Cr, Fe, K, Na, P and Zr.
Counting time:	20s for Mg, Si, Mn, Ti, Ca, Al, P and Zr and 10 s for Cr, K and Na
Method used:	Pressed pellets were used analysing for both majors and traces
Detector:	Gas Flow Proportional counter and for Zr a Scintillation Counter was used
Detection limits:	Mg - 0.295
	Si - 1.923
	Mn - 0.045
	Ti - 0.030

Ca - 0.040

Al - 0.027

Fe - 0.356

P - 0.011

Zr - 0.053

LA-ICP-MS at University of Stellenbsoch

Model:	Agilent 7500ce ICP-MS coupled with a New Wave research UP-213 laser
Spot Size:	55µm
Standards:	NIST SRM 612 for standardization and BVHO-2G for quality control 29Si as internal standard for zircon and 47Ti and 49 Ti as internal standards for rutile
Pulse energy	0.36-0.45mJ
Repition rate spot	10Hz
Wavelength	213nm

APPENDIX D:
1. QUANTITATIVE MINERALOGY OF THE HEAVY MINERAL PHASES AS DETERMINED WITH QEMSCAN.

Table D Mineralogy and alteration of THM as determined by QEMSCAN for total sample population.

Abbreviations

Alt-Ilm	Altered ilmenite per THM
Alt-IDX	Alteration Index
Grt	Garnet
Ilm	Ilmenite
Lcx	Leucoxene
Mn-Ilm	Manganese ilmenite (pyrophanite)
Px	Pyroxene
Rt	Rutile
THM (%)	Total heavy mineral content
Unalt-Ilm	Unaltered ilmenite
Zrn	Zircon
∑-Ilm	sum of altered ilmenite, unaltered ilmenite and Mn-ilmenite

Alteration Index indicates the percentage of altered ilmenite grains being calculated by the equation:

$$\frac{Alt - Ilm + Lcx}{\sum Ilm + Lcx}$$

Other minerals include the rest of the uneconomic fraction such as tourmaline, aluminosilicates, amphibole, sphene, epidote, staurolite, spinel, monazite, corundum

TABLE D														
MINERALOGY AND ALTERATION OF THM AS DETERMINED BY QEMSCAN FOR TOTAL SAMPLE POPULATION														
HOUTKRAAL REMAINDER PORTION 2														
ID	THM (%)	Ilm	Lcx	Rt	Zrn	Grt	Px	Other minerals	Alt-Ilm	Unalt-Ilm	Mn-Ilm	∑-Ilm	Lcx	Alt-IDX
8A5S001	2	30.1	4.1	6.3	9.6	41.0	2.4	6.4	4.2	22.2	0.4	26.9	4.1	27.01
8A5S002	3	40.6	5.0	6.1	12.6	26.3	2.4	7.0	4.6	31.5	0.5	36.7	5.0	23.16
8A5S003	2	37.6	5.1	6.6	11.2	30.3	2.4	6.8	4.2	29.9	0.6	34.7	5.1	23.45
8A5S004	2	36.8	5.2	6.3	11.4	31.1	2.2	7.0	4.5	28.7	0.5	33.7	5.2	24.82
8A5S005	4	46.8	5.3	6.2	15.4	18.3	2.1	5.9	4.9	36.7	0.6	42.2	5.3	21.64
8A5S006	5	51.0	5.1	5.9	16.0	13.1	2.0	7.0	6.0	39.5	0.7	46.3	5.1	21.64
8A5S007	2	31.5	5.0	7.3	10.9	35.8	2.1	7.4	4.6	24.1	0.5	29.1	5.0	28.03
8A5S008	3	43.4	3.5	5.9	14.0	28.4	0.5	4.3	5.2	33.6	0.6	39.4	3.5	20.37
8A5S009	4	43.8	5.1	6.5	14.2	21.2	1.6	7.6	4.5	35.6	0.5	40.6	5.1	20.98
8A5S010	4	45.4	5.1	6.1	15.0	19.8	1.5	7.0	6.2	34.1	0.7	41.0	5.1	24.63
8A5S011	4	51.9	5.3	5.8	15.4	14.1	1.4	6.2	6.3	40.2	0.6	47.1	5.3	22.05
8A5S012	2	39.8	6.0	8.5	11.7	24.9	2.2	6.9	5.3	31.3	0.6	37.2	6.0	26.30
8A5S013	3	47.8	6.0	8.4	14.4	16.2	1.8	5.4	4.6	40.3	0.5	45.4	6.0	20.60
8A5S014	2	38.7	6.0	8.4	12.0	27.4	2.1	5.6	4.3	32.0	0.5	36.8	6.0	24.00
8A5S015	4	41.5	5.0	5.5	13.2	25.7	2.1	6.9	4.5	32.9	0.5	37.9	5.0	22.23
8A5S016	4	49.8	5.7	6.5	15.7	15.5	1.7	5.0	5.3	40.9	0.6	46.7	5.7	20.84
8A5S017	6	53.0	4.9	5.7	16.4	12.3	3.5	4.1	4.2	44.3	0.6	49.1	4.9	16.96
8A5S018	4	47.6	5.1	5.8	14.3	17.6	3.3	6.4	5.7	37.3	0.7	43.7	5.1	22.19
8A5S019	3	49.9	6.2	7.0	12.6	15.3	3.6	5.4	5.8	37.7	1.2	44.7	6.2	23.55
8A5S020	3	45.2	5.7	6.8	14.0	18.3	3.5	6.5	6.1	34.3	0.6	41.0	5.7	25.32
8A5S021	4	47.6	5.6	7.2	15.5	15.2	3.6	5.2	5.0	38.7	0.6	44.4	5.6	21.31
8A5S022	3	41.0	4.8	6.0	13.2	26.0	3.8	5.2	4.8	31.9	0.6	37.4	4.8	22.84
8A5S023	4	47.3	5.0	6.1	15.0	17.5	3.5	5.6	6.1	36.0	0.8	42.9	5.0	23.09
8A5S024	4	47.0	5.6	6.4	14.7	18.2	3.3	4.8	6.8	35.2	0.7	42.8	5.6	25.67
8A5S025	5	57.4	5.3	5.0	11.5	11.7	2.9	6.2	6.4	41.0	1.4	48.8	5.3	21.63
8A5S026	1	28.9	6.6	8.2	10.1	34.1	6.4	5.8	4.7	22.1	0.5	27.3	6.6	33.35
8A5S027	1	34.2	6.7	8.9	9.7	26.8	5.7	7.9	4.9	26.7	0.6	32.2	6.7	29.97
8A5S028	3	45.2	6.5	7.7	14.3	13.9	5.1	7.3	4.8	37.6	0.5	42.9	6.5	22.86

TABLE D continued

MINERALOGY AND ALTERATION OF THM AS DETERMINED BY QEMSCAN FOR TOTAL SAMPLE POPULATION

HOUTKRAAL REMAINDER PORTION 2

ID	THM (%)	Ilm	Lcx	Rt	Zrn	Grt	Px	Other minerals	Alt-Ilm	Unalt-Ilm	Mn-Ilm	∑-Ilm	Lcx	Alt-IDX
8A5S029	2	44.5	5.3	6.4	12.5	20.2	4.1	6.9	6.9	33.4	0.6	40.9	5.3	26.44
8A5S030	3	43.4	5.8	6.5	12.9	20.8	4.2	6.5	5.9	33.0	0.6	39.5	5.8	25.73
8A5S031	1	46.2	6.6	6.0	13.8	15.2	5.4	6.8	7.0	35.1	0.7	42.8	6.6	27.68
8A5S032	2	26.2	4.7	4.6	6.5	46.8	5.4	5.7	4.6	18.5	0.7	23.9	4.7	32.61
8A5S033	4	56.2	6.6	5.6	11.9	8.7	4.9	6.1	5.7	42.0	1.1	48.8	6.6	22.22
8A5S034	2	37.4	6.2	7.7	12.4	23.2	5.4	7.6	4.8	29.5	0.6	34.9	6.2	26.92
8A5S035	1	47.2	6.2	7.9	12.6	12.9	6.4	6.6	3.8	41.0	0.6	45.4	6.2	19.40
8A5S036	2	48.6	6.2	6.3	13.8	13.8	5.1	6.2	4.7	40.4	0.6	45.8	6.2	20.99
8A5S037	2	47.1	6.2	6.8	13.8	13.8	5.2	7.0	5.3	38.2	0.5	44.0	6.2	22.88
8A5S038	2	47.5	5.6	6.9	13.8	15.8	3.9	6.5	7.8	34.8	0.7	43.3	5.6	27.37
8A5S039	3	54.8	6.5	5.2	10.9	11.3	4.1	7.2	6.1	39.7	1.4	47.2	6.5	23.47
8A5S040	1	45.3	6.6	6.4	11.3	17.4	4.5	8.4	4.9	36.8	0.8	42.4	6.6	23.52
8A5S041	2	44.7	6.2	6.1	12.8	17.7	5.2	7.3	5.1	35.4	0.7	41.2	6.2	23.72
8A5S043	4	54.6	8.0	5.7	13.5	7.6	5.3	5.4	5.5	42.3	1.2	48.9	8.0	23.63
8A5S044	2	42.9	5.7	7.0	12.8	20.3	4.1	7.2	6.6	31.7	0.7	39.0	5.7	27.51
8A5S045	2	39.8	5.8	6.0	10.6	25.2	4.9	7.6	5.7	30.3	0.6	36.6	5.8	27.18
8A5S046	2	53.5	6.3	7.3	12.2	10.7	1.0	9.1	11.5	34.5	1.2	47.3	6.3	33.22
8A5S047	4	55.5	6.0	6.8	10.8	9.9	1.5	9.4	6.6	40.3	1.1	48.1	6.0	23.45
8A5S048	4	60.7	5.6	4.3	12.2	8.4	1.3	7.5	6.7	42.2	1.6	50.5	5.6	21.85
8A5S049	2	42.6	5.4	3.8	6.5	27.6	1.2	12.9	5.7	26.9	1.6	34.2	5.4	28.00
8A5S050	5	51.4	4.9	4.6	12.2	17.7	1.4	7.8	5.6	36.3	1.3	43.2	4.9	21.77
8A5S051	2	34.4	4.6	6.1	9.7	18.5	1.4	25.4	5.0	26.8	0.4	32.2	4.6	26.06
8A5S052	4	52.7	5.4	5.8	13.6	14.4	1.1	7.1	7.2	37.3	1.1	45.6	5.4	24.66
8A5S053	3	43.6	4.6	4.3	9.8	26.7	1.3	9.8	6.2	29.0	1.1	36.3	4.6	26.53
8A5S054	1	54.4	5.0	8.9	15.1	12.0	0.5	4.1	4.5	46.5	0.7	51.7	5.0	16.68
8A5S055	3	51.3	5.0	4.5	10.9	16.6	1.4	10.3	7.1	33.5	1.1	41.7	5.0	25.94
8A5S056	3	55.4	4.3	6.0	13.1	15.0	0.4	5.8	6.9	41.1	1.3	49.3	4.3	20.82
8A5S057	4	55.6	5.8	5.2	11.5	11.7	1.4	8.8	6.5	38.3	1.3	46.2	5.8	23.77

TABLE D continued

MINERALOGY AND ALTERATION OF THM AS DETERMINED BY QEMSCAN FOR TOTAL SAMPLE POPULATION

HOUTKRAAL REMAINDER PORTION 2

ID	THM (%)	Ilm	Lcx	Rt	Zrn	Grt	Px	Other minerals	Alt-Ilm	Unalt-Ilm	Mn-Ilm	∑-Ilm	Lcx	Alt-IDX
8A5S058	4	51.7	5.8	5.3	10.7	15.7	1.7	9.1	6.2	36.7	1.4	44.4	5.8	24.01
8A5S059	5	56.5	4.3	4.2	10.6	15.8	0.3	8.3	6.7	39.2	1.1	47.1	4.3	21.42
8A5S060	8	56.3	4.1	5.3	14.6	14.4	0.3	4.9	9.2	38.6	1.1	48.9	4.1	25.12
8A5S061	2	52.0	5.1	5.7	10.9	18.5	0.3	7.5	6.1	38.7	1.2	46.0	5.1	21.93
average	**3**	**46**	**6**	**6**	**13**	**19**	**3**	**7**	**6**	**35**	**1**	**42**	**6**	**24**

MINERALOGY AND ALTERATION OF THM AS DETERMINED BY QEMSCAN FOR TOTAL SAMPLE POPULATION

HOUTKRAAL REMAINDER

ID	THM (%)	Ilm	Lcx	Rt	Zrn	Grt	Px	Other minerals	Alt-Ilm	Unalt-Ilm	Mn-Ilm	∑-Ilm	Lcx	Alt-IDX
8A5S062	3	57.1	7.1	6.8	12.5	7.3	1.6	7.6	5.5	43.4	1.3	50.3	7.1	21.96
8A5S063	3	54.6	7.1	8.3	13.3	8.7	1.7	6.3	4.8	43.1	1.5	49.4	7.1	21.08
8A5S064	5	61.9	4.5	6.0	13.3	8.9	0.2	5.3	4.7	48.4	1.5	54.6	4.5	15.48
8A5S065	4	55.4	7.4	7.3	13.0	9.4	1.8	5.6	5.6	41.6	1.6	48.7	7.4	23.05
8A5S066	6	66.8	4.5	4.4	15.2	5.5	0.2	3.4	3.9	52.6	1.5	58.1	4.5	13.52
8A5S067	6	61.3	6.5	5.8	12.7	5.7	1.6	6.3	5.0	45.4	1.4	51.8	6.5	19.72
8A5S068	2	50.4	7.7	10.1	12.9	10.2	2.3	6.5	4.8	40.9	1.2	46.9	7.7	22.92
8A5S069	7	61.2	5.1	6.5	13.5	8.9	0.3	4.6	4.7	47.8	1.4	53.9	5.1	16.59
8A5S070	6	59.9	4.9	4.9	11.7	13.8	0.9	3.9	3.9	45.5	1.3	50.6	4.9	15.78
8A5S071	8	58.4	6.2	7.2	14.3	5.3	2.0	6.6	4.3	46.6	1.2	52.0	6.2	17.94
8A5S072	2	55.5	5.8	8.9	14.0	10.2	0.2	5.4	5.4	44.4	1.4	51.2	5.8	19.63
8A5S073	4	55.9	6.7	7.2	13.4	8.8	1.6	6.4	5.0	42.1	1.5	48.6	6.7	21.13
8A5S074	9	66.6	4.3	5.6	15.3	4.9	0.2	3.2	4.6	51.1	1.6	57.3	4.3	14.35
8A5S075	9	67.3	4.0	5.3	15.2	4.6	0.1	3.5	5.0	50.6	1.8	57.4	4.0	14.64
8A5S076	6	66.5	4.2	5.4	15.7	3.9	0.1	4.0	5.5	50.5	1.5	57.5	4.2	15.75
8A5S077	1	49.8	7.9	9.4	12.2	10.4	3.3	7.0	5.6	38.6	1.4	45.6	7.9	25.19
8A5S078	1	60.0	5.9	7.1	11.1	9.3	0.2	6.3	6.1	44.9	1.8	52.7	5.9	20.35
8A5S079	2	64.5	4.7	5.8	14.1	6.0	0.2	4.7	6.5	45.4	1.8	53.8	4.7	19.16

TABLE D continued

MINERALOGY AND ALTERATION OF THM AS DETERMINED BY QEMSCAN FOR TOTAL SAMPLE POPULATION

HOUTKRAAL REMAINDER

ID	THM (%)	Ilm	Lcx	Rt	Zrn	Grt	Px	Other minerals	Alt-Ilm	Unalt-Ilm	Mn-Ilm	∑-Ilm	Lcx	Alt-IDX
8A5S080	6	60.9	5.7	5.2	13.8	7.0	1.4	5.8	4.2	45.8	1.6	51.6	5.7	17.35
8A5S081	9	66.3	3.9	5.3	15.2	5.3	0.1	3.8	4.9	50.7	1.7	57.3	3.9	14.45
8A5S082	1	45.5	7.7	6.6	8.6	15.8	4.7	11.1	6.8	31.5	1.2	39.5	7.7	30.56
8A5S083	1	55.4	6.8	8.1	14.0	6.3	1.6	7.9	5.7	42.2	1.5	49.3	6.8	22.14
8A5S084	11	64.3	5.6	5.0	14.6	3.6	2.6	4.3	4.8	47.4	1.5	53.7	5.6	17.62
8A5S085	2	60.6	7.1	5.9	12.5	6.2	1.3	6.4	6.5	41.0	1.7	49.2	7.1	24.18
8A5S086	3	61.8	6.7	6.7	13.7	3.9	1.3	6.1	4.7	48.2	1.6	54.5	6.7	18.65
8A5S087	3	61.7	6.6	4.8	11.5	4.9	3.3	7.1	5.1	45.2	1.9	52.3	6.6	19.98
8A5S088	1	52.6	6.9	6.4	9.4	13.0	1.2	10.6	5.9	37.9	2.0	45.8	6.9	24.24
8A5S089	2	58.3	7.2	6.7	12.0	7.5	1.3	7.0	6.2	42.6	1.8	50.6	7.2	23.19
8A5S090	11	66.1	6.0	4.8	13.1	3.5	1.2	5.3	5.4	46.1	1.6	53.1	6.0	19.25
8A5S091	11	68.9	4.9	3.9	11.1	3.3	2.8	5.1	6.0	46.6	1.7	54.2	4.9	18.41
8A5S092	3	61.3	6.3	6.3	13.3	5.5	1.2	6.0	6.5	42.5	1.7	50.7	6.3	22.50
8A5S093	5	64.9	6.2	5.3	12.8	4.1	1.1	5.5	5.5	46.2	1.9	53.6	6.2	19.60
8A5S094	4	65.0	6.4	4.8	11.6	3.8	3.3	5.1	5.7	46.8	2.3	54.7	6.4	19.74
8A5S095	3	65.9	5.9	4.0	12.3	4.1	2.9	4.9	6.8	45.5	1.9	54.2	5.9	21.22
8A5S096	4	66.2	5.8	3.7	11.9	4.0	3.1	5.2	5.6	45.6	1.7	52.9	5.8	19.44
8A5S097	10	66.3	5.5	3.8	13.8	2.9	1.3	6.4	4.7	48.0	1.6	54.3	5.5	17.00
8A5S098	2	59.3	6.5	7.0	13.2	6.4	1.4	6.1	5.7	43.8	1.5	51.0	6.5	21.29
8A5S099	2	55.4	6.7	8.7	14.4	5.4	2.0	7.5	5.8	43.5	1.4	50.7	6.7	21.80
8A5S100	6	57.5	7.2	8.8	16.9	3.1	1.7	4.8	4.0	48.9	1.2	54.0	7.2	18.17
8A5S101	7	63.5	5.6	5.6	14.8	3.4	1.4	5.7	4.7	48.5	1.4	54.7	5.6	17.17
8A5S102	7	65.0	5.5	4.3	14.7	3.5	1.3	5.7	4.8	47.9	1.8	54.4	5.5	17.12
8A5S103	3	61.4	6.2	5.0	11.6	7.5	1.3	7.0	5.6	46.8	1.6	53.9	6.2	19.59
8A5S104	2	59.2	7.1	6.5	12.1	6.2	1.4	7.3	6.7	42.9	1.7	51.3	7.1	23.73
8A5S105	3	59.8	6.5	7.1	15.1	4.0	1.4	6.2	5.5	45.8	1.6	52.9	6.5	20.12
average	**5**	**61**	**6**	**6**	**13**	**7**	**2**	**6**	**5**	**45**	**2**	**52**	**6**	**20**

TABLE D continued														
MINERALOGY AND ALTERATION OF THM AS DETERMINED BY QEMSCAN FOR TOTAL SAMPLE POPULATION														
GEELWAL KAROO														
ID	THM (%)	Ilm	Lcx	Rt	Zrn	Grt	Px	Other minerals	Alt-Ilm	Unalt-Ilm	Mn-Ilm	∑-Ilm	Lcx	Alt-IDX
8A5S106	3	43.5	8.4	8.3	12.0	11.7	3.9	12.1	2.4	39.2	0.4	42.1	8.4	21.53
8A5S107	3	44.3	7.6	8.1	11.3	12.5	4.4	11.9	2.3	39.7	0.4	42.3	7.6	19.72
8A5S108	7	37.8	7.7	6.4	9.2	17.5	9.3	12.0	1.6	34.1	0.3	35.9	7.7	21.27
8A5S109	1	46.0	7.6	7.8	11.0	16.0	3.2	8.3	2.0	41.1	0.4	43.5	7.6	18.77
8A5S110	1	34.8	5.9	6.3	6.8	20.9	1.9	23.6	1.6	32.1	0.2	33.9	5.9	18.76
8A5S111	2	41.4	7.4	8.6	12.4	11.7	2.7	15.7	2.3	37.6	0.4	40.3	7.4	20.36
8A5S112	4	41.3	7.2	6.8	10.1	19.8	2.7	12.1	2.2	36.5	0.4	39.0	7.2	20.14
8A5S113	7	27.7	5.3	3.4	3.9	18.5	29.3	11.9	0.5	24.5	0.2	25.2	5.3	18.85
8A5S114	1	48.8	7.9	8.9	10.3	11.3	2.4	10.3	2.2	44.8	0.3	47.3	7.9	18.42
8A5S115R	1	48.8	7.0	7.2	9.6	14.6	2.2	10.7	1.9	44.4	0.3	46.5	7.0	16.58
8A5S116R	1	37.6	4.9	4.7	6.8	23.4	1.6	20.9	1.7	34.7	0.2	36.6	4.9	15.91
8A5S117	5	41.2	6.9	5.5	9.2	22.6	5.1	9.4	1.8	36.5	0.3	38.5	6.9	19.04
8A5S118	1	31.1	6.5	4.6	4.7	4.5	3.9	44.8	0.5	22.9	0.4	23.8	6.5	23.09
8A5S119	2	40.4	6.3	6.1	7.0	21.0	2.6	16.6	1.6	37.2	0.2	39.0	6.3	17.48
8A5S120	2	31.1	4.9	4.5	5.9	33.0	3.1	17.5	1.7	27.2	0.3	29.2	4.9	19.32
8A5S121	5	42.4	6.7	5.7	9.1	22.2	3.0	10.9	1.8	37.5	0.3	39.5	6.7	18.35
8A5S122	8	15.6	3.7	1.8	1.9	22.0	44.0	10.8	0.2	13.7	0.1	14.0	3.7	22.45
8A5S123	5	31.5	4.2	3.0	5.3	37.4	4.2	14.3	1.0	27.3	0.2	28.5	4.2	15.86
8A5S124R	4	40.1	5.3	4.6	6.8	25.3	6.3	11.6	1.3	34.5	0.3	36.1	5.3	15.94
8A5S125	3	41.0	7.1	7.2	10.6	20.9	3.3	9.9	2.5	36.7	0.4	39.5	7.1	20.52
8A5S126	11	12.8	3.1	2.0	3.0	29.4	42.1	7.6	1.4	10.5	0.1	12.0	3.1	29.91
8A5S127	17	44.4	6.8	6.0	9.4	19.7	5.1	8.5	1.3	40.7	0.3	42.3	6.8	16.41
8A5S128	2	0.4	0.4	0.1	0.1	4.6	88.5	5.9	0.0	0.3	0.0	0.3	0.4	62.91
8A5S129R	2	40.3	6.8	7.1	8.9	23.7	2.3	10.9	2.1	36.1	0.3	38.5	6.8	19.67
8A5S130	2	42.1	7.2	7.8	11.1	20.4	2.9	8.5	3.1	37.3	0.3	40.7	7.2	21.51
8A5S131	5	22.3	4.0	3.5	4.9	42.4	10.2	12.6	1.6	18.7	0.1	20.5	4.0	22.97
8A5S132	2	19.0	4.5	2.9	2.9	28.6	27.0	15.1	0.7	16.2	0.1	17.0	4.5	24.15
8A5S133	1	37.6	6.1	6.6	7.4	22.4	3.4	16.6	2.6	33.1	0.2	35.9	6.1	20.56

TABLE D continued														
MINERALOGY AND ALTERATION OF THM AS DETERMINED BY QEMSCAN FOR TOTAL SAMPLE POPULATION														
GEELWAL KAROO														
ID	THM (%)	Ilm	Lcx	Rt	Zrn	Grt	Px	Other minerals	Alt-Ilm	Unalt-Ilm	Mn-Ilm	∑-Ilm	Lcx	Alt-IDX
8A5S134	3	39.5	6.2	7.7	11.6	23.3	2.1	9.7	3.9	33.8	0.3	38.1	6.2	22.88
8A5S135R	3	40.7	7.3	8.2	12.7	18.4	1.9	10.8	3.8	35.3	0.5	39.5	7.3	23.68
8A5S136	1	43.9	7.2	8.8	13.3	16.8	2.0	8.0	3.8	38.6	0.4	42.8	7.2	22.05
8A5S137	1	40.5	6.8	8.4	10.6	21.0	1.6	11.0	3.7	35.4	0.4	39.5	6.8	22.75
8A5S138	3	4.4	1.4	0.7	0.8	23.5	56.6	12.7	0.3	3.6	0.0	3.9	1.4	30.97
8A5S139	1	35.6	5.0	6.0	9.0	32.4	2.3	9.6	3.3	30.9	0.3	34.4	5.0	21.03
8A5S140	1	48.6	7.8	10.4	14.1	9.8	1.5	7.8	4.1	43.1	0.4	47.6	7.8	21.62
8A5S141R	2	47.9	7.7	11.8	13.4	11.0	1.4	6.7	4.1	42.6	0.5	47.3	7.7	21.60
8A5S142	2	110.0	9.5	20.6	33.7	22.3	1.1	0.01	9.6	97.5	1.1	108.1	9.5	16.21
8A5S143	3	45.6	7.7	9.0	12.7	15.0	2.4	7.7	3.4	40.0	0.4	43.9	7.7	21.52
8A5S144	16	83.5	9.7	9.1	15.9	33.9	53.9	0.01	3.4	73.8	0.5	77.7	9.7	15.04
8A5S145	2	107.1	11.7	21.0	31.4	38.4	2.9	0.01	10.7	93.3	1.1	105.1	11.7	19.14
8A5S146	2	100.0	10.8	17.8	23.5	53.6	3.3	0.01	9.9	85.8	0.9	96.7	10.8	19.27
8A5S147	2	110.7	11.7	23.4	30.4	26.7	2.7	0.01	10.7	96.2	1.2	108.2	11.7	18.73
8A5S148	1	105.0	11.3	21.4	28.1	31.4	2.4	0.01	11.0	91.0	0.9	102.9	11.3	19.52
8A5S149	1	107.7	10.2	20.2	32.2	21.6	1.9	0.0	12.4	92.5	0.9	105.8	10.2	19.48
8A5S150	1	97.9	10.9	18.3	22.9	46.1	3.5	0.0	8.6	85.4	0.9	94.9	10.9	18.41
8A5S151	1	50.6	7.3	12.3	14.6	7.4	1.6	6.0	5.7	44.1	0.4	50.2	7.3	22.71
8A5S152	1	110.6	10.5	26.2	34.3	18.1	2.1	0.0	10.9	97.3	1.1	109.3	10.5	17.89
8A5S153R	1	40.4	7.4	7.4	7.1	20.9	3.2	13.6	1.6	37.1	0.2	38.9	7.4	19.42
8A5S154	2	25.5	4.3	5.0	5.0	46.0	3.3	10.8	1.1	22.6	0.2	24.0	4.3	19.33
8A5S155	1	18.1	2.8	2.4	2.8	56.9	3.5	13.5	1.0	15.3	0.2	16.5	2.8	19.43
8A5S156	1	43.4	8.9	13.4	14.5	10.8	3.4	5.7	3.4	39.1	0.5	42.9	8.9	23.77
8A5S157	1	24.6	4.1	5.1	5.5	39.7	2.3	18.7	1.8	21.5	0.2	23.6	4.1	21.48
8A5S158R	1	32.0	5.6	7.9	9.1	26.1	2.3	16.9	2.1	28.6	0.3	31.0	5.6	21.06
8A5S159	6	11.1	1.4	1.5	3.3	67.2	11.3	4.3	1.0	9.1	0.1	10.2	1.4	20.39
8A5S160	1	32.4	6.3	6.5	5.0	15.8	11.5	22.5	1.9	28.7	0.1	30.6	6.3	21.99
8A5S161R	1	36.8	6.2	7.0	6.5	19.4	2.7	21.3	2.2	33.2	0.2	35.5	6.2	20.10

TABLE D continued

MINERALOGY AND ALTERATION OF THM AS DETERMINED BY QEMSCAN FOR TOTAL SAMPLE POPULATION

GEELWAL KAROO

ID	THM (%)	Ilm	Lcx	Rt	Zrn	Grt	Px	Other minerals	Alt-Ilm	Unalt-Ilm	Mn-Ilm	∑-Ilm	Lcx	Alt-IDX
8A5S162	1	19.3	4.2	3.8	3.4	36.7	2.9	29.9	1.6	16.3	0.1	18.1	4.2	26.33
8A5S163	1	37.6	6.9	9.3	10.7	22.0	4.1	9.5	2.2	34.2	0.3	36.7	6.9	20.74
8A5S164	2	27.6	4.4	4.3	6.1	41.2	2.0	14.4	1.9	23.7	0.3	25.9	4.4	20.87

MINERALOGY AND ALTERATION OF THM AS DETERMINED BY QEMSCAN FOR TOTAL SAMPLE POPULATION

GRAAUWDUINEN

ID	THM (%)	Ilm	Lcx	Rt	Zrn	Grt	Px	Other minerals	Alt-Ilm	Unalt-Ilm	Mn-Ilm	∑-Ilm	Lcx	Alt-IDX
8A5S165	1	34.1	6.6	8.6	9.0	23.7	3.8	14.2	2.4	30.2	0.4	33.0	6.6	22.77
8A5S166	1	23.8	5.2	5.0	5.3	32.0	11.6	17.0	1.6	21.2	0.3	23.0	5.2	24.09
8A5S167	1	35.7	6.2	7.3	8.5	26.9	2.9	12.7	2.0	32.0	0.4	34.3	6.2	20.19
8A5S168R	2	21.3	4.1	3.7	4.9	49.0	3.2	13.8	2.0	17.3	0.3	19.6	4.1	25.69
8A5S169	1	35.3	6.3	6.6	7.6	4.4	4.0	35.8	0.8	28.7	0.6	30.1	6.3	19.44
8A5S170	1	47.3	7.0	9.3	11.9	8.3	2.0	14.2	3.6	42.4	0.4	46.4	7.0	19.83
8A5S171	1	43.3	7.9	8.0	12.2	11.2	2.4	15.0	2.9	39.0	0.4	42.3	7.9	21.44
8A5S172	1	41.4	6.4	8.0	9.8	18.7	1.9	13.9	3.1	36.6	0.4	40.1	6.4	20.37
8A5S173R	1	41.4	6.5	7.9	11.0	19.0	3.0	11.3	2.6	37.1	0.4	40.1	6.5	19.55
8A5S174R	3	46.3	8.1	10.3	14.0	9.4	2.1	9.9	3.6	40.9	0.5	45.0	8.1	22.00
8A5S175	2	41.5	7.3	9.1	12.1	15.0	1.7	13.3	3.1	36.2	0.4	39.8	7.3	22.01
8A5S176	2	44.1	9.0	10.1	13.2	9.8	2.7	10.9	3.1	39.3	0.5	43.0	9.0	23.39
8A5S177	4	40.9	11.8	10.8	14.9	4.3	11.3	6.0	2.6	37.4	0.5	40.4	11.8	27.54
8A5S178	1	17.6	3.3	3.0	3.8	53.1	5.6	13.6	1.5	13.7	0.3	15.5	3.3	25.66
8A5S179	1	37.0	5.9	6.2	9.1	17.2	1.5	23.0	3.3	31.7	0.4	35.5	5.9	22.37
8A5S180	1	44.5	8.3	9.8	12.4	11.1	2.7	11.2	3.1	39.7	0.4	43.3	8.3	22.22
8A5S181	2	36.6	6.7	6.9	8.9	23.4	5.8	11.6	3.4	30.9	0.5	34.8	6.7	24.32
8A5S182	2	37.5	7.5	7.4	10.1	21.8	5.5	10.2	3.2	32.2	0.4	35.9	7.5	24.75
8A5S183	3	41.1	6.1	8.5	12.3	14.2	9.5	8.2	3.0	36.1	0.5	39.6	6.1	19.99
8A5S184	2	39.3	7.1	7.8	11.3	16.3	5.4	12.7	3.3	34.2	0.4	37.9	7.1	23.07

TABLE D continued

MINERALOGY AND ALTERATION OF THM AS DETERMINED BY QEMSCAN FOR TOTAL SAMPLE POPULATION

GRAAUWDUINEN

ID	THM (%)	Ilm	Lcx	Rt	Zrn	Grt	Px	Other minerals	Alt-Ilm	Unalt-Ilm	Mn-Ilm	∑-Ilm	Lcx	Alt-IDX
8A5S185	3	44.9	7.7	8.8	13.7	11.1	6.0	7.8	3.4	39.9	0.4	43.7	7.7	21.54
8A5S186	2	31.5	5.2	5.0	7.8	33.5	6.6	10.5	3.0	26.2	0.4	29.5	5.2	23.46
8A5S187	1	35.0	6.1	5.6	7.8	29.3	6.3	10.0	2.6	30.9	0.3	33.9	6.1	21.68
8A5S188	1	39.5	6.8	6.7	9.5	16.4	7.2	13.9	5.3	32.2	0.4	37.9	6.8	27.11
8A5S189	2	42.7	7.9	8.6	11.7	10.6	6.4	12.2	4.8	36.2	0.4	41.4	7.9	25.67
8A5S190	1	48.6	7.7	9.3	14.8	4.0	9.2	6.5	3.4	43.7	0.6	47.7	7.7	20.05
8A5S191	2	43.0	7.0	9.1	12.0	23.4	4.1	1.3	3.5	41.8	0.5	45.8	8.4	21.86
8A5S192	5	55.0	7.5	7.3	12.1	5.1	5.8	7.2	4.3	46.5	0.8	51.6	7.5	19.98
8A5S193	4	57.2	7.0	7.6	14.5	5.2	2.2	6.4	3.8	49.9	0.8	54.5	7.0	17.67
8A5S194	4	53.0	7.6	6.9	13.6	5.3	6.6	7.1	4.1	45.4	0.6	50.1	7.6	20.35
8A5S195	1	54.0	7.8	8.0	14.7	4.0	2.6	8.8	5.1	47.0	0.6	52.7	7.8	21.34
8A5S196R	2	55.8	7.0	7.9	14.9	5.0	1.7	7.6	5.8	47.3	0.6	53.6	7.0	21.05
8A5S197	4	53.6	7.4	7.1	14.3	4.4	6.9	6.4	5.1	45.9	0.6	51.5	7.4	21.20
8A5S198R	3	59.2	6.7	7.9	15.8	3.7	1.4	5.2	5.8	51.2	0.6	57.6	6.7	19.40
8A5S199	3	46.4	7.3	7.2	12.5	13.1	7.0	6.4	3.3	40.4	0.6	44.3	7.3	20.61
8A5S200R	1	48.0	6.6	7.9	13.3	14.0	2.0	8.1	3.1	41.1	0.8	45.0	6.6	18.85
8A5S201	4	50.8	8.3	7.1	13.7	6.8	6.9	6.4	3.4	44.1	0.8	48.3	8.3	20.73
8A5S213	2	41.2	6.5	5.9	11.7	17.9	6.7	10.1	2.9	35.7	0.7	39.3	6.5	20.39
8A5S214	2	49.8	7.9	8.6	15.1	5.1	3.3	10.2	3.4	44.3	0.5	48.2	7.9	20.15
8A5S215	2	42.6	7.6	6.9	11.2	15.3	7.7	8.8	3.2	36.6	0.7	40.5	7.6	22.47
8A5S216	3	50.3	8.1	7.2	14.5	5.1	8.1	6.7	3.4	44.5	0.6	48.6	8.1	20.40
8A5S217	4	48.1	7.9	7.1	12.7	7.4	8.0	8.8	3.2	41.4	0.7	45.3	7.9	20.94
8A5S218	3	49.6	8.4	7.5	14.2	5.3	7.2	7.8	3.6	42.7	0.7	47.1	8.4	21.63
8A5S219	3	51.9	7.5	7.7	13.1	6.8	2.6	10.4	3.7	43.5	1.0	48.2	7.5	20.11
8A5S221	2	53.5	7.8	8.9	15.6	4.8	2.6	6.9	4.1	47.1	0.6	51.7	7.8	19.99
8A5S222	2	59.3	5.4	8.9	17.3	5.4	0.3	3.4	5.1	51.9	0.7	57.6	5.4	16.62
8A5S223	1	50.5	7.5	10.9	15.1	4.5	2.9	8.6	4.4	44.7	0.6	49.7	7.5	20.83

TABLE D continued

MINERALOGY AND ALTERATION OF THM AS DETERMINED BY QEMSCAN FOR TOTAL SAMPLE POPULATION

GRAAUWDUINEN

ID	THM (%)	Ilm	Lcx	Rt	Zrn	Grt	Px	Other minerals	Alt-Ilm	Unalt-Ilm	Mn-Ilm	∑-Ilm	Lcx	Alt-IDX
8A5S224	1	56.1	6.9	7.9	12.8	5.8	1.3	9.2	10.9	40.4	0.6	51.9	6.9	30.24
8A5S225	1	51.8	7.6	10.5	15.5	4.4	2.7	7.5	4.5	46.0	0.5	51.0	7.6	20.68
8A5S226R	4	57.0	6.5	9.7	14.3	4.9	1.2	6.4	9.3	44.8	0.6	54.8	6.5	25.82
8A5S227	7	34.8	5.6	5.1	9.8	30.6	5.9	8.2	2.5	29.8	0.5	32.7	5.6	21.18
8A5S228	4	45.5	6.8	7.3	12.7	17.2	2.4	8.1	3.1	39.2	0.7	43.0	6.8	19.87
8A5S229	4	20.5	3.4	2.7	5.2	57.2	2.8	8.2	1.3	17.5	0.4	19.2	3.4	20.84
8A5S230	2	31.0	4.6	4.9	8.3	40.1	2.3	8.7	2.3	26.7	0.4	29.4	4.6	20.38
8A5S231R	1	39.4	4.9	5.4	9.5	30.0	1.6	9.1	3.3	32.7	0.6	36.6	4.9	19.67
8A5S232	4	19.9	3.0	3.2	4.8	59.6	2.3	7.1	1.6	16.8	0.3	18.7	3.0	21.11
8A5S233	3	49.9	7.7	8.9	14.2	10.0	2.3	6.8	3.0	44.7	0.6	48.3	7.7	19.17
8A5S234	3	55.2	7.9	9.0	15.2	4.1	2.2	6.4	3.2	49.5	0.7	53.5	7.9	18.20
8A5S235	3	54.7	8.3	8.6	15.9	3.4	2.3	6.9	3.3	48.8	0.7	52.8	8.3	18.87
8A5S236	3	56.4	7.6	7.7	15.7	4.3	2.3	6.0	3.6	50.1	0.7	54.4	7.6	18.08
8A5S237	3	56.1	8.2	7.3	15.8	4.0	2.5	6.1	4.2	49.0	0.7	53.9	8.2	20.04
8A5S238R	2	56.1	7.0	8.4	15.6	4.6	1.8	6.6	4.5	48.3	0.7	53.5	7.0	19.01
8A5S239R	2	56.8	6.6	8.6	14.9	5.0	1.5	6.6	5.5	48.3	0.7	54.4	6.6	19.73
8A5S240	1	50.7	7.9	10.3	16.2	3.8	2.9	8.2	3.7	45.5	0.7	49.9	7.9	20.15
8A5S241	3	56.5	8.0	8.8	16.8	2.3	2.3	5.2	3.9	50.9	0.6	55.4	8.0	18.85
8A5S242	3	55.5	8.2	8.1	14.6	5.3	1.3	7.0	7.9	44.4	0.6	53.0	8.2	26.28
8A5S243	3	55.5	7.8	10.6	16.2	2.6	2.4	4.9	4.1	50.1	0.6	54.7	7.8	19.01
8A5S244	6	24.8	4.3	3.2	6.0	45.2	3.6	13.0	2.1	19.2	0.4	21.7	4.3	24.67
8A5S245	2	24.6	4.1	3.5	5.6	46.9	2.1	13.2	2.0	19.2	0.4	21.7	4.1	23.81
8A5S246	2	44.3	8.4	9.7	15.0	7.5	4.0	11.1	2.5	40.4	0.6	43.4	8.4	21.04
8A5S247R	1	24.3	3.9	4.0	5.7	47.2	2.2	12.6	1.9	20.2	0.4	22.5	3.9	21.99
8A5S248	1	10.7	2.2	1.9	2.2	67.3	2.9	12.8	1.1	8.5	0.2	9.7	2.2	27.44
8A5S249	2	40.9	6.3	7.3	10.6	23.6	2.7	8.6	2.0	37.2	0.6	39.7	6.3	18.00
8A5S250R	2	41.3	5.4	5.1	10.1	25.2	1.9	11.0	2.5	34.8	0.6	37.9	5.4	18.15

TABLE D continued

MINERALOGY AND ALTERATION OF THM AS DETERMINED BY QEMSCAN FOR TOTAL SAMPLE POPULATION

GRAAUWDUINEN

ID	THM (%)	Ilm	Lcx	Rt	Zrn	Grt	Px	Other minerals	Alt-Ilm	Unalt-Ilm	Mn-Ilm	∑-Ilm	Lcx	Alt-IDX
8A5S251	3	53.3	8.0	8.7	16.0	6.3	2.3	5.5	3.3	47.4	0.8	51.4	8.0	19.02
8A5S252	3	55.2	8.3	8.7	15.5	3.5	2.3	6.6	3.3	49.4	0.8	53.5	8.3	18.72
8A5S253	3	51.1	9.7	10.1	16.2	2.8	3.2	6.9	3.2	46.3	0.7	50.2	9.7	21.52
8A5S254	3	54.6	8.8	7.8	16.1	3.3	2.8	6.6	3.3	49.0	0.7	53.0	8.8	19.59
8A5S255R	1	56.0	6.8	8.2	15.1	4.4	1.7	7.8	4.5	47.9	0.6	53.0	6.8	18.86
8A5S256	3	53.7	7.2	7.1	15.1	5.1	2.0	9.9	5.0	44.9	0.8	50.6	7.2	20.96
8A5S257	3	53.7	7.7	8.4	15.1	4.1	2.1	8.9	4.0	47.5	0.6	52.0	7.7	19.50
8A5S258	2	54.1	7.5	8.7	16.5	3.9	1.9	7.5	5.5	46.4	0.6	52.4	7.5	21.61
8A5S259	2	52.6	6.7	7.3	14.9	4.7	1.7	12.1	8.0	41.2	0.6	49.7	6.7	25.97
8A5S260	2	55.7	7.0	7.9	15.0	5.3	1.5	7.7	7.6	44.1	0.7	52.5	7.0	24.65
8A5S261	2	56.7	6.9	8.1	16.0	4.0	1.7	6.5	6.9	46.8	0.7	54.4	6.9	22.59
8A5S262	3	35.9	5.1	4.9	9.4	33.4	2.0	9.4	2.3	30.3	0.6	33.2	5.1	19.36
8A5S263	2	19.1	3.9	2.4	4.3	55.0	2.1	13.2	1.5	15.7	0.3	17.5	3.9	24.99
8A5S264	3	12.7	2.0	1.5	2.9	66.9	1.4	12.6	0.8	10.8	0.2	11.8	2.0	20.06
8A5S265	2	40.2	6.8	6.0	10.7	26.5	2.0	7.8	2.3	36.4	0.4	39.1	6.8	19.73
8A5S266	2	15.3	2.3	2.1	3.4	66.5	1.0	9.4	1.2	12.9	0.2	14.3	2.3	20.80
8A5S267	3	18.4	3.1	2.9	4.2	62.6	1.2	7.7	1.4	15.4	0.2	17.1	3.1	22.36
8A5S268	2	49.1	8.2	9.4	14.9	8.5	2.4	7.4	2.9	44.7	0.6	48.2	8.2	19.70
8A5S269	3	53.7	7.8	8.3	15.8	6.3	1.7	6.4	3.9	47.1	0.6	51.6	7.8	19.67
8A5S270	2	54.5	7.4	8.1	15.8	5.4	1.7	7.1	3.7	48.2	0.7	52.6	7.4	18.59
8A5S271	3	56.2	7.8	8.6	16.2	3.9	1.7	5.5	3.6	50.1	0.7	54.4	7.8	18.29
8A5S272	3	55.5	8.2	8.0	16.5	3.3	1.8	6.7	4.6	48.6	0.7	53.9	8.2	20.56
8A5S273	2	50.8	6.9	8.4	14.8	5.0	2.0	12.0	8.7	39.2	0.7	48.6	6.9	28.19
8A5S274	3	53.7	7.3	7.5	17.6	3.5	2.7	7.7	5.8	45.4	0.7	51.9	7.3	22.08
8A5S275	1	52.5	7.8	9.7	17.2	3.8	2.5	6.4	4.8	45.7	0.6	51.2	7.8	21.40
8A5S276	2	52.7	7.8	10.0	17.2	3.4	2.5	6.4	4.6	46.2	0.6	51.4	7.8	20.94
8A5S277	2	53.6	7.5	9.3	17.3	3.8	2.0	6.5	7.7	43.1	0.7	51.5	7.5	25.78

TABLE D continued														
MINERALOGY AND ALTERATION OF THM AS DETERMINED BY QEMSCAN FOR TOTAL SAMPLE POPULATION														
GRAAUWDUINEN														
ID	THM (%)	Ilm	Lcx	Rt	Zrn	Grt	Px	Other minerals	Alt-Ilm	Unalt-Ilm	Mn-Ilm	∑-Ilm	Lcx	Alt-IDX
8A5S278	2	53.0	8.0	9.6	17.2	3.3	2.3	6.6	6.1	45.0	0.6	51.7	8.0	23.61
8A5S279	2	21.3	3.5	3.1	5.0	51.8	1.7	13.6	2.3	16.9	0.4	19.6	3.5	25.02
8A5S280	1	36.9	5.2	6.4	10.3	22.3	2.1	16.8	2.8	32.1	0.5	35.4	5.2	19.88
8A5S281	1	51.9	7.5	8.9	15.5	4.4	2.7	9.2	3.9	45.7	0.7	50.3	7.5	19.71
8A5S282	1	45.0	7.0	7.8	12.1	16.7	2.4	9.0	3.1	39.6	0.6	43.3	7.0	19.97
8A5S283	2	45.7	6.4	6.3	11.8	18.0	2.8	9.0	2.8	40.4	0.6	43.8	6.4	18.37
8A5S284	2	52.7	7.6	9.3	15.0	5.9	2.7	6.7	3.2	47.4	0.7	51.3	7.6	18.40
8A5S285	2	54.9	7.3	8.4	15.1	5.1	2.2	7.0	3.8	48.2	0.7	52.7	7.3	18.57
8A5S286	2	52.8	7.3	7.9	15.2	5.1	2.1	9.6	4.5	44.9	0.7	50.1	7.3	20.50
8A5S287	3	53.9	7.7	8.9	15.6	3.1	2.2	8.6	4.5	46.8	0.7	52.0	7.7	20.37
8A5S288	2	54.5	7.8	8.3	16.4	3.2	2.3	7.5	4.5	47.4	0.7	52.7	7.8	20.34
8A5S289	2	53.6	6.7	8.2	16.0	4.3	1.6	9.4	5.7	45.0	0.6	51.2	6.7	21.34
8A5S290	2	44.7	6.6	7.7	12.5	7.4	2.3	18.8	5.6	36.5	0.6	42.7	6.6	24.76
8A5S292R	2	52.6	6.3	8.2	13.3	9.2	1.4	9.0	9.9	36.9	0.7	47.5	6.3	30.18
8A5S293	2	53.4	7.5	8.7	15.3	5.5	1.6	7.9	7.9	41.5	0.7	50.1	7.5	26.80
8A5S294	2	56.3	6.9	8.3	16.8	4.4	1.4	5.9	7.7	44.7	0.7	53.0	6.9	24.29
8A5S295R	1	55.6	7.8	6.7	15.1	2.5	3.1	9.2	1.0	50.6	0.7	52.3	7.8	14.65
8A5S296R	1	16.2	2.8	2.1	4.1	53.6	1.6	19.7	1.0	12.8	0.4	14.3	2.8	22.24
8A5S297	1	41.4	6.5	5.9	11.7	21.8	2.0	10.7	2.9	35.3	0.7	38.9	6.5	20.74
8A5S298X	1	43.9	9.5	8.9	13.8	9.1	2.6	12.3	1.9	40.4	0.3	42.7	9.5	21.84
8A5S299	1	30.3	4.5	4.4	6.1	40.2	1.3	13.2	3.1	23.1	0.5	26.7	4.5	24.38
8A5S300	2	51.9	7.2	8.2	15.2	8.2	2.1	7.3	3.7	45.6	0.6	50.0	7.2	19.11
8A5S301	2	51.4	7.7	8.3	15.0	8.2	2.3	7.2	4.4	44.3	0.5	49.2	7.7	21.19
8A5S302	2	55.4	7.3	10.0	16.4	3.6	1.7	5.7	5.0	47.7	0.7	53.3	7.3	20.38
8A5S303	1	50.8	6.6	8.3	14.1	6.8	1.5	11.9	8.2	39.4	0.6	48.2	6.6	27.08
8A5S304	2	52.5	7.4	8.1	14.6	6.1	2.0	9.2	8.9	40.5	0.7	50.0	7.4	28.41
8A5S305R	2	54.0	7.2	8.4	15.0	5.7	1.6	8.2	6.1	44.7	0.7	51.5	7.2	22.75
8A5S306	1	51.3	7.3	8.4	14.3	6.5	2.2	9.9	6.2	42.1	0.6	48.9	7.3	23.90

TABLE D continued														
MINERALOGY AND ALTERATION OF THM AS DETERMINED BY QEMSCAN FOR TOTAL SAMPLE POPULATION														
GRAAUWDUINEN														
ID	**THM (%)**	**Ilm**	**Lcx**	**Rt**	**Zrn**	**Grt**	**Px**	**Other minerals**	**Alt-Ilm**	**Unalt-Ilm**	**Mn-Ilm**	**∑-Ilm**	**Lcx**	**Alt-IDX**
8A5S307	1	54.4	7.0	8.8	16.1	5.4	1.9	6.5	7.0	43.9	0.6	51.5	7.0	23.85
8A5S308	1	51.8	7.1	8.8	15.7	4.1	1.8	10.6	8.9	40.6	0.4	49.8	7.1	28.08
8A5S309	1	52.2	8.0	8.4	15.3	5.2	1.4	9.5	8.0	41.0	0.6	49.6	8.0	27.77
8A5S310R	1	55.6	6.3	8.0	13.8	5.6	1.2	9.5	8.6	41.8	0.7	51.2	6.3	25.95
8A5S311	2	29.8	4.6	5.5	8.2	30.0	2.1	19.9	2.3	25.4	0.4	28.0	4.6	21.03
8A5S312R	2	26.3	3.5	4.6	7.3	37.5	1.1	19.8	2.1	21.8	0.4	24.2	3.5	20.17
8A5S313	1	50.4	5.8	7.6	13.3	13.2	1.8	7.9	4.3	42.6	0.7	47.6	5.8	18.90
8A5S314	1	37.3	4.7	5.0	9.0	27.3	1.2	15.5	4.2	27.8	0.5	32.5	4.7	23.84
8A5S315R	2	40.6	7.1	3.4	9.7	4.1	4.2	30.8	0.7	33.8	0.7	35.2	7.1	18.50
8A5S316	2	39.8	5.5	6.3	9.9	24.9	1.7	12.0	3.1	34.1	0.4	37.6	5.5	19.98
8A5S317	2	52.8	7.0	8.1	14.7	7.9	2.2	7.4	4.4	45.8	0.7	50.9	7.0	19.63
8A5S318	2	52.8	7.1	8.7	13.2	7.2	1.7	9.3	5.7	43.5	0.9	50.0	7.1	22.41
8A5S319	1	49.0	6.7	7.8	12.9	7.0	1.5	15.1	6.4	38.7	0.6	45.7	6.7	25.03
8A5S320X	1	52.6	5.7	6.5	15.2	5.6	2.2	12.2	6.6	42.5	0.7	49.8	5.7	22.10
8A5S321R	1	45.2	7.1	7.1	12.1	8.8	3.0	16.8	6.3	35.2	0.6	42.1	7.1	27.29
8A5S322	1	51.7	7.1	7.8	13.6	6.8	1.2	11.8	7.2	39.1	0.6	47.0	7.1	26.53
8A5S323	1	52.9	7.2	7.8	15.4	4.8	6.2	5.7	7.8	41.7	0.6	50.2	7.2	26.22
8A5S324	1	44.1	5.9	9.7	10.0	10.4	1.0	18.9	9.7	30.1	0.6	40.4	5.9	33.67
8A5S325	1	12.4	5.0	0.3	1.2	8.3	6.2	66.6	0.1	10.5	0.2	10.8	5.0	32.48
average	**2**	**47**	**7**	**7**	**13**	**14**	**3**	**10**	**4**	**40**	**1**	**45**	**7**	**22**

TABLE D continued														
MINERALOGY AND ALTERATION OF THM AS DETERMINED BY QEMSCAN FOR TOTAL SAMPLE POPULATION														
RIETFONTEIN														
ID	THM (%)	Ilm	Lcx	Rt	Zrn	Grt	Px	Other minerals	Alt-Ilm	Unalt-Ilm	Mn-Ilm	∑-Ilm	Lcx	Alt-IDX
8A5S326	4	49.2	5.5	5.6	9.2	23.1	1.2	6.2	4.9	35.4	1.1	41.3	5.5	22.19
8A5S327	3	48.4	6.2	8.4	10.6	18.7	1.4	6.4	4.6	38.3	1.0	43.8	6.2	21.43
8A5S328R	3	32.7	4.7	5.9	8.0	40.6	2.1	6.0	2.9	26.3	0.5	29.7	4.7	22.09
8A5S329R	4	34.7	5.7	2.0	5.3	7.6	4.3	40.4	0.6	25.5	0.6	26.6	5.7	19.49
8A5S330R	4	40.3	4.8	5.5	8.8	31.8	1.8	7.0	3.6	29.8	0.8	34.2	4.8	21.49
8A5S331R	3	38.3	4.3	5.5	10.1	34.1	1.6	6.2	3.7	28.1	0.6	32.5	4.3	21.81
8A5S332R	3	36.5	4.0	4.8	8.0	39.2	1.4	6.1	3.2	26.4	0.7	30.2	4.0	20.89
8A5S333	3	33.2	4.8	5.0	7.9	36.4	7.1	5.6	2.7	26.8	0.6	30.0	4.8	21.45
8A5S334R	4	27.3	4.0	3.1	5.1	51.6	2.2	6.7	2.3	20.3	0.7	23.3	4.0	23.24
8A5S335	3	37.1	4.6	5.6	8.4	35.7	1.6	7.0	3.7	27.3	0.8	31.8	4.6	22.63
8A5S336	4	37.0	4.6	6.2	9.2	34.7	1.8	6.4	3.8	27.2	0.8	31.8	4.6	23.20
8A5S337	3	38.7	4.2	5.3	8.8	35.2	1.5	6.3	3.4	26.6	0.7	30.7	4.2	21.60
8A5S338	4	39.9	5.3	7.2	10.6	27.5	2.5	7.1	3.4	33.0	0.5	36.9	5.3	20.72
8A5S339	3	35.8	4.6	5.9	9.5	35.8	1.8	6.6	3.7	27.9	0.4	32.0	4.6	22.76
8A5S340	4	45.9	7.1	7.9	9.8	16.5	7.2	5.7	4.5	35.1	1.0	40.5	7.1	24.30
8A5S341	4	47.0	7.0	9.6	11.3	16.2	2.4	6.5	4.7	37.5	0.9	43.0	7.0	23.40
8A5S342X	6	47.5	6.8	10.4	10.2	15.5	1.7	7.9	6.6	35.1	0.8	42.5	6.8	27.18
8A5S343	2	42.7	5.5	7.6	10.1	24.8	1.6	7.6	4.7	31.7	0.7	37.1	5.5	24.05
8A5S344	3	45.5	6.1	7.7	11.6	19.9	2.1	7.0	4.6	37.0	0.7	42.3	6.1	22.09
8A5S345	3	41.5	6.2	8.0	9.1	24.5	2.6	8.1	3.7	34.4	0.7	38.8	6.2	21.91
8A5S346	4	44.8	5.9	7.1	11.9	21.4	2.5	6.4	3.0	37.9	0.6	41.6	5.9	18.67
8A5S347X	3	38.9	5.5	5.8	8.5	32.7	1.8	6.8	3.1	31.2	0.7	35.0	5.5	21.03
8A5S348	4	37.4	5.6	6.3	9.3	30.6	3.9	6.8	2.9	31.8	0.4	35.1	5.6	21.01
8A5S349	3	32.5	5.6	7.7	7.8	35.1	4.6	6.6	3.4	27.4	0.4	31.2	5.6	24.54
8A5S350	2	45.4	7.0	9.5	10.7	19.2	2.3	5.9	3.4	39.6	0.5	43.5	7.0	20.55
8A5S351	4	38.9	5.8	7.0	9.4	28.3	6.0	4.5	3.4	32.8	0.4	36.6	5.8	21.82
8A5S352	3	30.3	5.2	6.0	7.4	38.6	7.4	5.0	2.9	25.4	0.4	28.7	5.2	23.78
8A5S353	3	32.8	5.0	5.4	7.4	38.3	6.1	4.9	3.0	27.4	0.4	30.8	5.0	22.33
8A5S354	3	31.4	6.2	5.6	7.2	38.6	6.5	4.5	2.7	26.7	0.3	29.7	6.2	24.88

TABLE D continued

MINERALOGY AND ALTERATION OF THM AS DETERMINED BY QEMSCAN FOR TOTAL SAMPLE POPULATION

RIETFONTEIN

ID	THM (%)	Ilm	Lcx	Rt	Zrn	Grt	Px	Other minerals	Alt-Ilm	Unalt-Ilm	Mn-Ilm	∑-Ilm	Lcx	Alt-IDX
8A5S355	3	31.4	5.5	5.0	7.2	40.4	6.3	4.2	2.7	26.5	0.4	29.5	5.5	23.47
8A5S356	3	45.1	8.3	8.3	11.0	17.1	5.5	4.7	4.2	37.3	0.7	42.2	8.3	24.75
8A5S357	2	38.5	7.1	7.9	9.9	26.6	5.6	4.4	4.1	31.2	0.5	35.8	7.1	26.11
8A5S358	3	44.4	6.3	7.7	10.8	22.6	2.5	5.7	4.0	36.4	0.7	41.1	6.3	21.56
8A5S359	3	33.6	5.6	5.9	7.8	36.2	6.6	4.2	3.1	27.8	0.5	31.4	5.6	23.65
8A5S360	4	34.3	6.3	7.0	8.4	32.4	7.2	4.4	2.7	29.5	0.4	32.6	6.3	23.10
8A5S361	3	33.5	6.2	6.5	8.8	31.9	9.3	3.7	2.1	29.4	0.4	31.9	6.2	21.90
8A5S362	4	27.8	4.4	5.2	7.4	46.3	4.4	4.5	2.4	23.4	0.3	26.1	4.4	22.43
8A5S363	4	46.4	7.7	7.9	11.4	12.3	7.9	6.4	4.1	38.7	0.5	43.3	7.7	23.09
8A5S364	2	37.1	5.2	7.3	9.3	34.4	2.6	4.0	3.2	31.2	0.3	34.7	5.2	20.98
8A5S365	4	35.5	5.4	6.6	9.3	35.3	2.9	5.0	3.0	29.7	0.4	33.1	5.4	21.75
8A5S366	4	38.0	5.1	6.4	10.0	30.9	2.6	7.0	3.1	32.0	0.4	35.5	5.1	20.14
8A5S367	4	31.6	3.6	5.0	8.8	42.7	1.9	6.3	2.9	25.7	0.3	28.9	3.6	19.99
8A5S368	4	22.6	3.5	4.6	5.8	51.8	5.4	6.3	2.9	17.2	0.3	20.4	3.5	26.77
8A5S369	5	22.1	3.4	3.9	6.3	49.5	10.3	4.4	2.5	17.3	0.3	20.1	3.4	25.24
8A5S370	3	34.6	4.4	6.5	8.9	36.6	1.9	7.3	3.3	28.6	0.4	32.3	4.4	20.89
8A5S371	3	32.4	4.8	6.1	8.8	40.5	2.4	5.1	3.1	26.7	0.3	30.2	4.8	22.74
8A5S372	4	31.9	4.0	5.3	8.5	42.8	1.9	5.6	3.1	26.2	0.3	29.6	4.0	21.20
8A5S373	1	46.3	3.8	7.2	12.6	23.0	2.9	4.3	4.6	38.5	0.1	43.2	3.8	17.80
8A5S374	3	39.1	4.5	5.3	11.6	32.9	1.8	4.9	3.1	32.7	0.3	36.1	4.5	18.69
8A5S375	5	29.8	3.9	4.5	9.3	42.9	4.8	4.8	3.1	23.4	0.4	26.9	3.9	22.53
8A5S376	6	33.9	5.0	6.1	8.6	35.5	5.1	5.8	3.5	27.8	0.4	31.7	5.0	22.98
8A5S377	2	34.8	5.0	7.8	9.1	34.9	2.4	6.0	3.8	28.4	0.5	32.7	5.0	23.45
8A5S378	4	28.2	3.3	6.1	7.9	45.8	2.2	6.6	3.2	22.8	0.4	26.5	3.3	21.84
8A5S379	3	28.9	3.7	7.1	8.6	43.5	2.2	6.0	3.2	24.6	0.3	28.1	3.7	21.73
8A5S380	2	22.4	3.4	6.6	7.0	52.5	2.0	6.0	3.1	17.7	0.3	21.1	3.4	26.73

TABLE D continued														
MINERALOGY AND ALTERATION OF THM AS DETERMINED BY QEMSCAN FOR TOTAL SAMPLE POPULATION														
RIETFONTEIN														
ID	**THM (%)**	**Ilm**	**Lcx**	**Rt**	**Zrn**	**Grt**	**Px**	**Other minerals**	**Alt-Ilm**	**Unalt-Ilm**	**Mn-Ilm**	**∑-Ilm**	**Lcx**	**Alt-IDX**
8A5S381	3	26.6	3.0	8.0	9.6	45.5	1.5	5.8	3.5	21.8	0.4	25.8	3.0	22.75
8A5S382	5	33.1	3.5	7.2	10.4	37.6	1.7	6.5	4.1	26.4	0.5	31.0	3.5	21.88
8A5S383	5	42.4	4.2	7.0	12.9	24.9	1.6	6.9	4.6	33.3	0.5	38.4	4.2	20.70
8A5S384	6	32.5	3.9	4.5	10.3	38.2	5.4	5.2	3.6	24.7	0.4	28.7	3.9	23.02
8A5S385	3	31.1	4.8	5.6	9.1	37.2	5.3	6.8	3.7	24.4	0.5	28.6	4.8	25.42
8A5S386	3	30.7	4.5	4.7	9.2	39.3	5.2	6.4	3.7	23.7	0.4	27.8	4.5	25.42
8A5S387	3	32.4	3.7	8.2	11.4	36.5	1.9	5.9	3.5	25.4	0.4	29.3	3.7	21.95
8A5S388	4	32.8	4.3	5.0	10.0	37.2	4.5	6.2	4.4	24.6	0.5	29.5	4.3	25.78
8A5S389	3	38.3	4.1	5.4	11.0	33.2	1.5	6.4	4.3	29.7	0.5	34.4	4.1	21.72
8A5S390	3	37.7	4.7	5.3	11.3	30.5	4.6	6.1	5.0	28.0	0.5	33.6	4.7	25.33
8A5S391	2	49.7	5.2	5.9	15.2	14.5	4.0	5.5	4.9	40.3	0.5	45.7	5.2	19.72
8A5S392	3	42.8	5.3	5.6	13.8	20.8	4.4	7.2	5.5	32.9	0.5	38.9	5.3	24.35
8A5S393	4	42.8	4.9	4.9	13.1	24.4	3.9	6.0	5.6	31.4	0.6	37.6	4.9	24.68
8A5S394	6	38.5	4.2	4.3	11.4	29.1	4.0	8.4	6.1	26.3	0.6	32.9	4.2	27.55
8A5S395	4	51.1	5.6	5.4	15.9	11.8	4.1	6.1	6.8	37.9	0.7	45.4	5.6	24.21
average	**3**	**37**	**5**	**6**	**10**	**32**	**4**	**6**	**4**	**29**	**1**	**33**	**5**	**23**

APPENDIX D: 2. CORRELATION COEFFICIENT DIAGRAMS OF THE MINERALOGY OF THE FIVE SATELLITE AREAS.

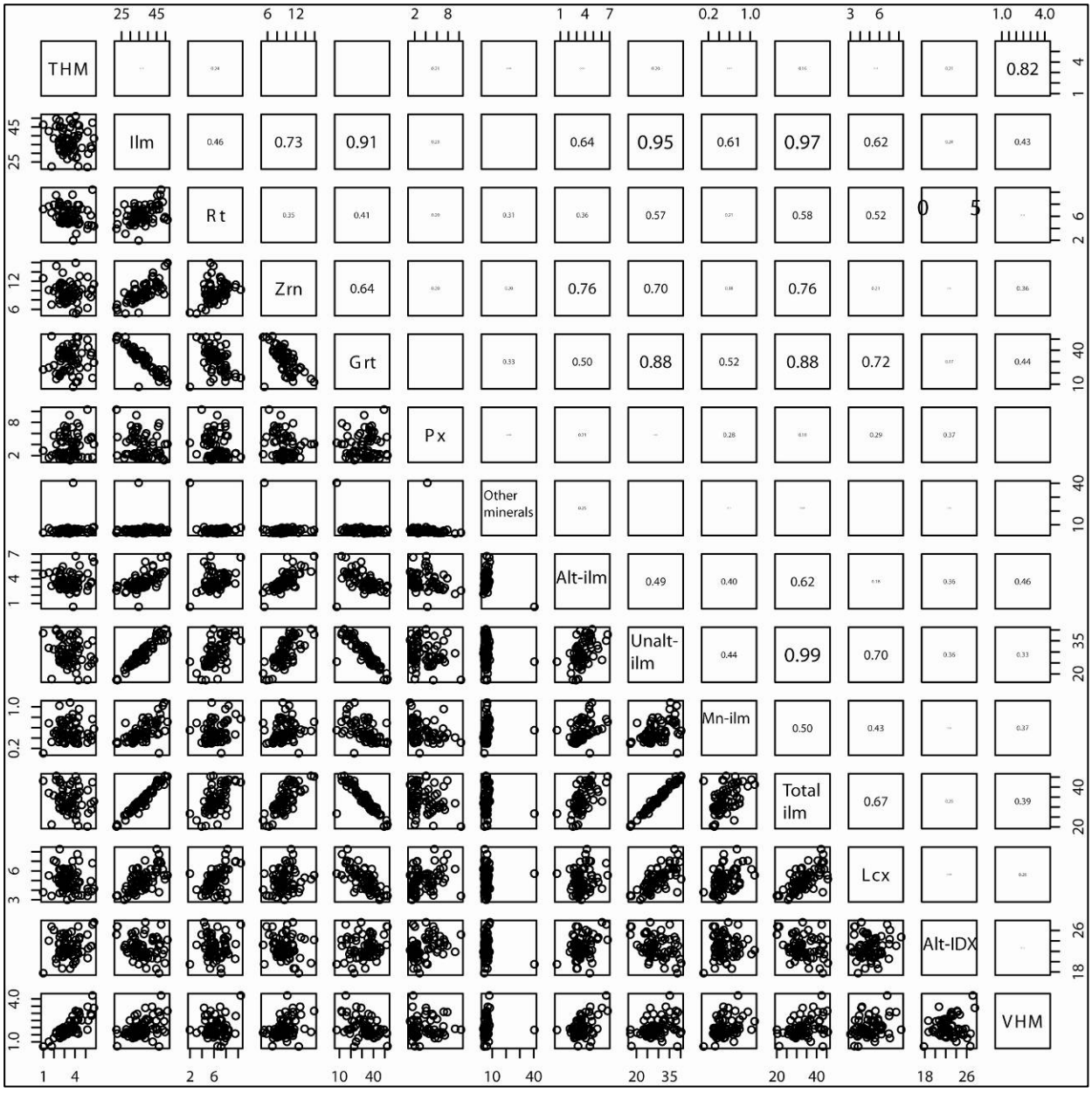

Figure D1. Correlation coefficient diagram of the mineralogy of Rietfontein as determined with QEMSCAN. n=70

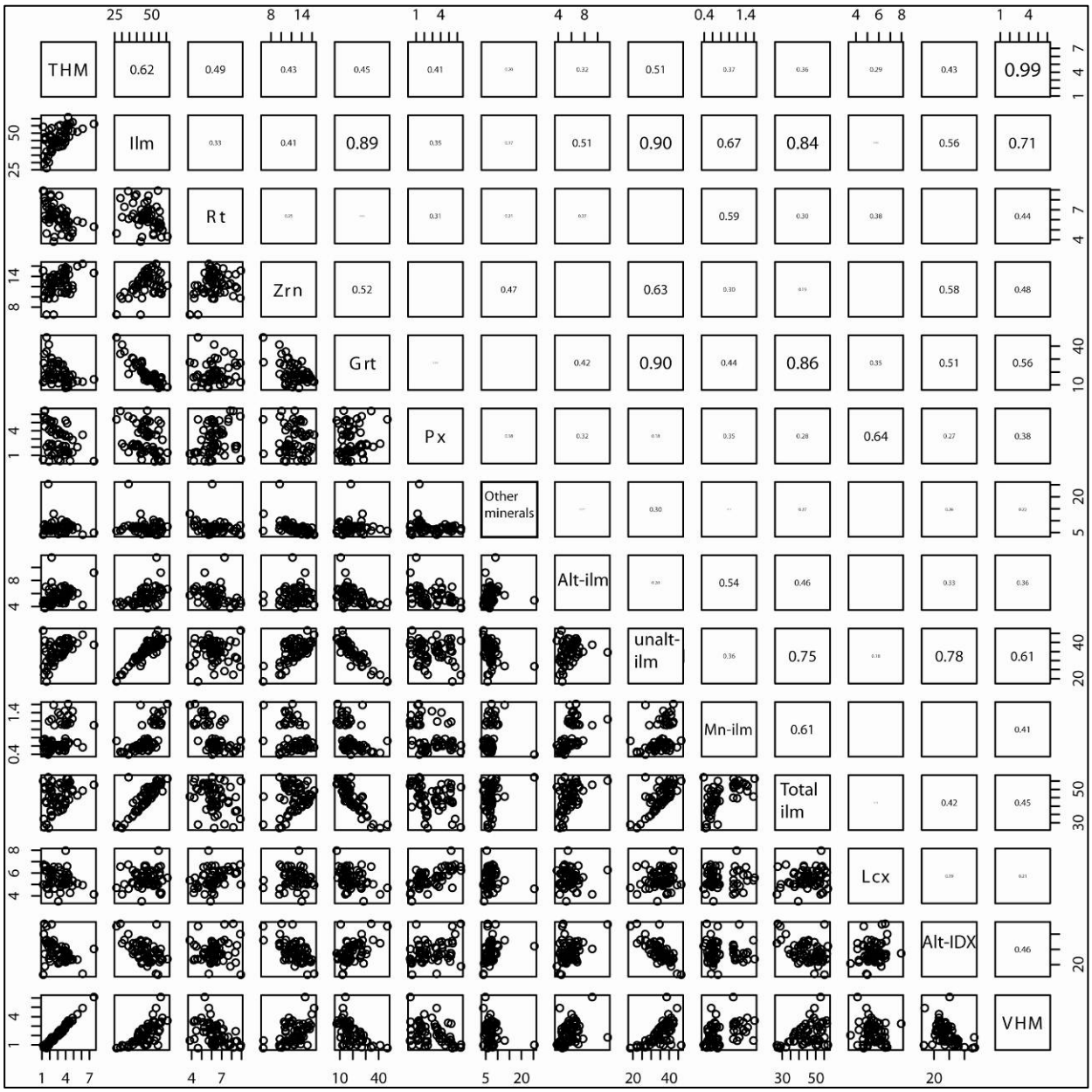

Figure D2. Correlation coefficient diagram of the mineralogy of Houtkraal Remainder Portion 2 as determined with QEMSCAN. n=60

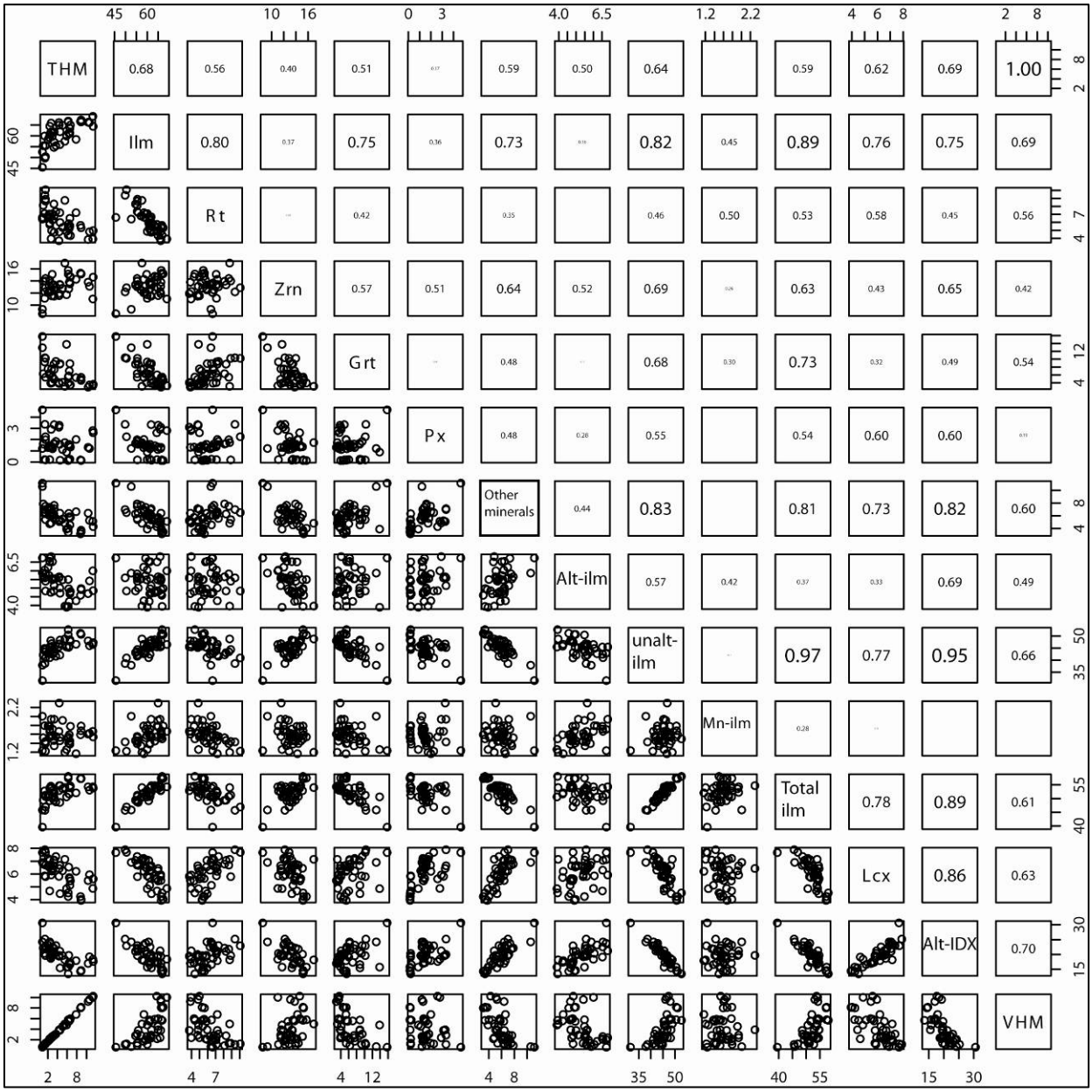

Figure D3. Correlation coefficient diagram of the mineralogy of Houtkraal Remainder as determined with QEMSCAN. n=44

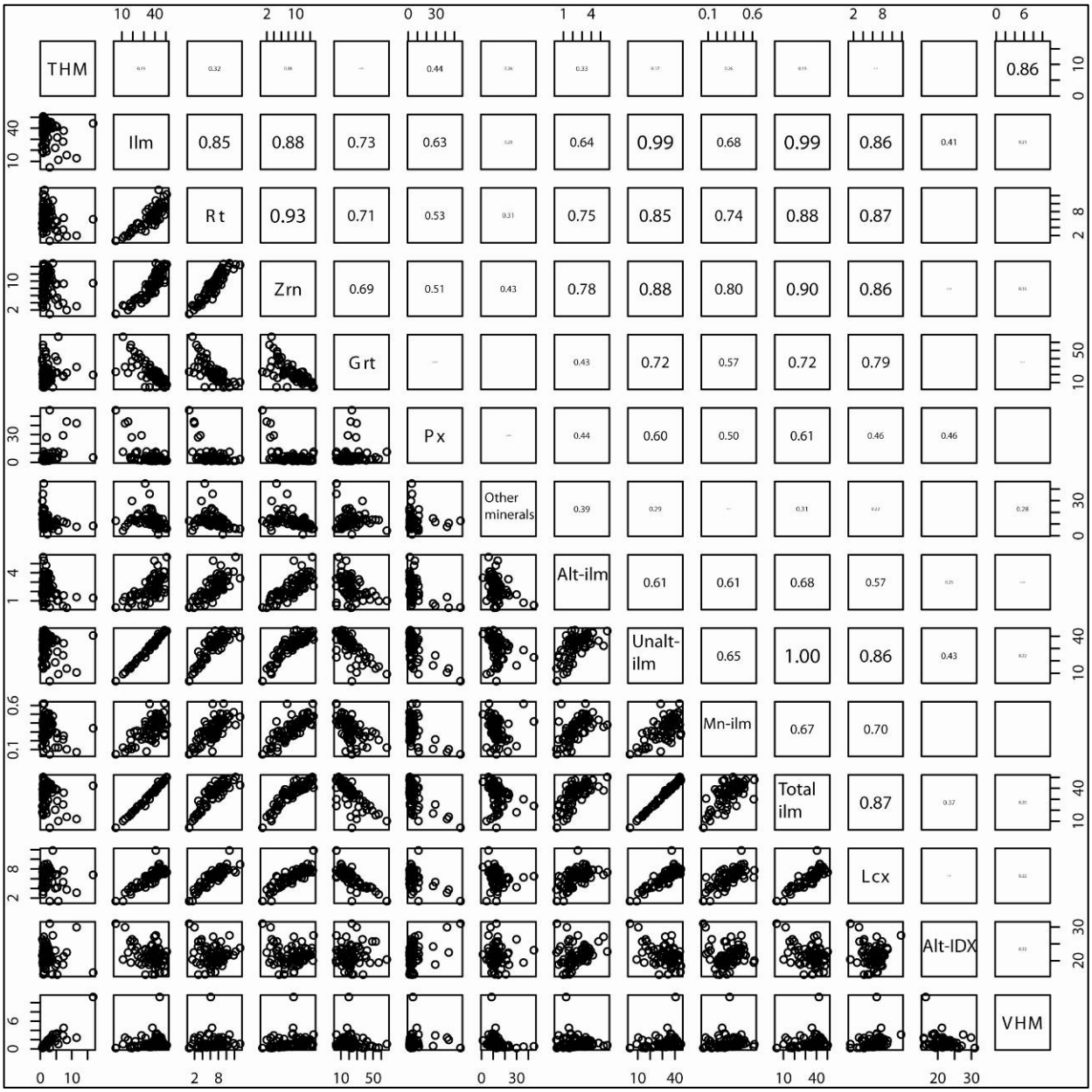

Figure D4. Correlation coefficient diagram of the mineralogy of Geelwal Karoo as determined with QEMSCAN. n=86

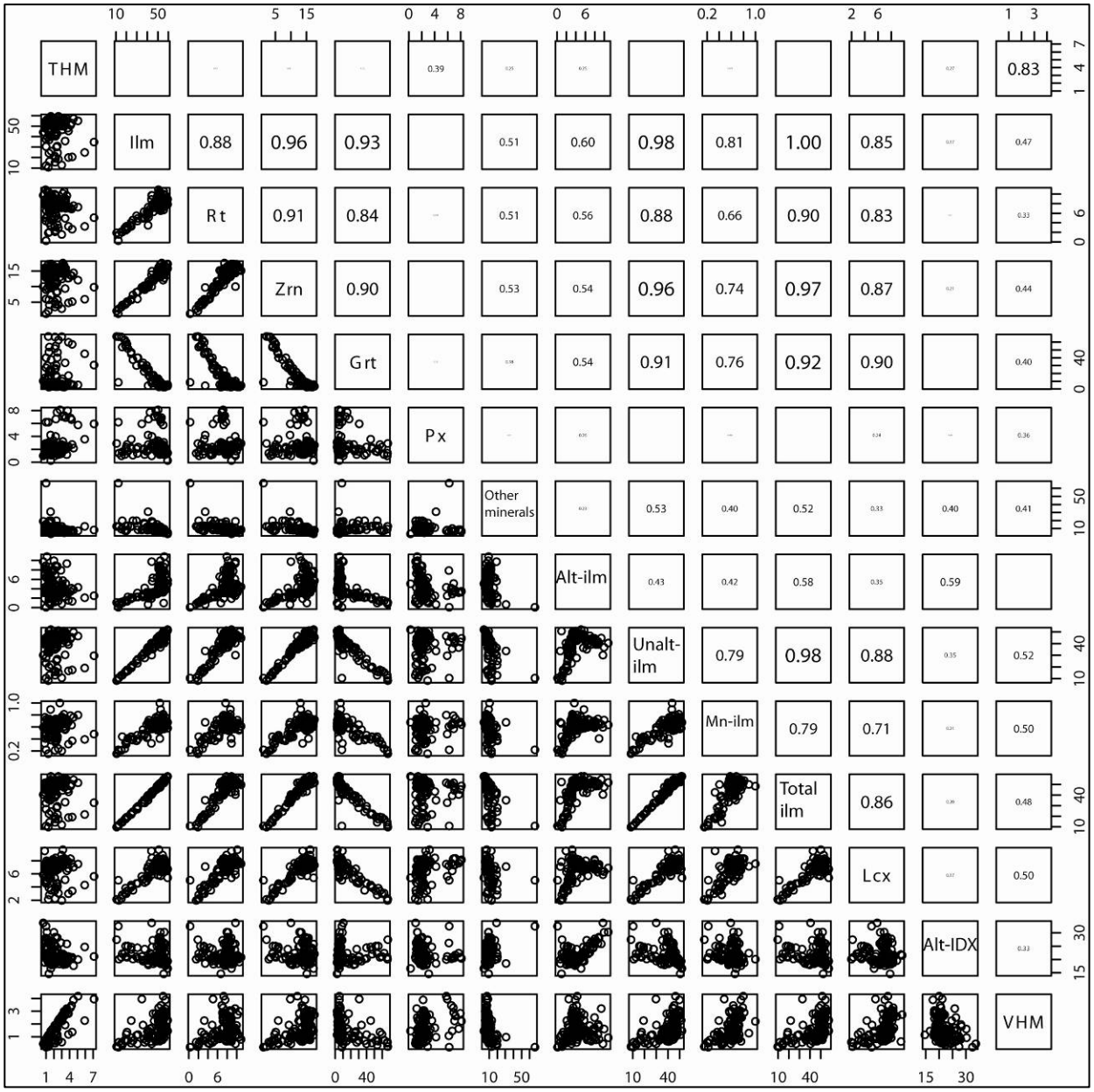

Figure D5. Correlation coefficient diagram of the mineralogy of Graauwduinen as determined with QEMSCAN. n= 121

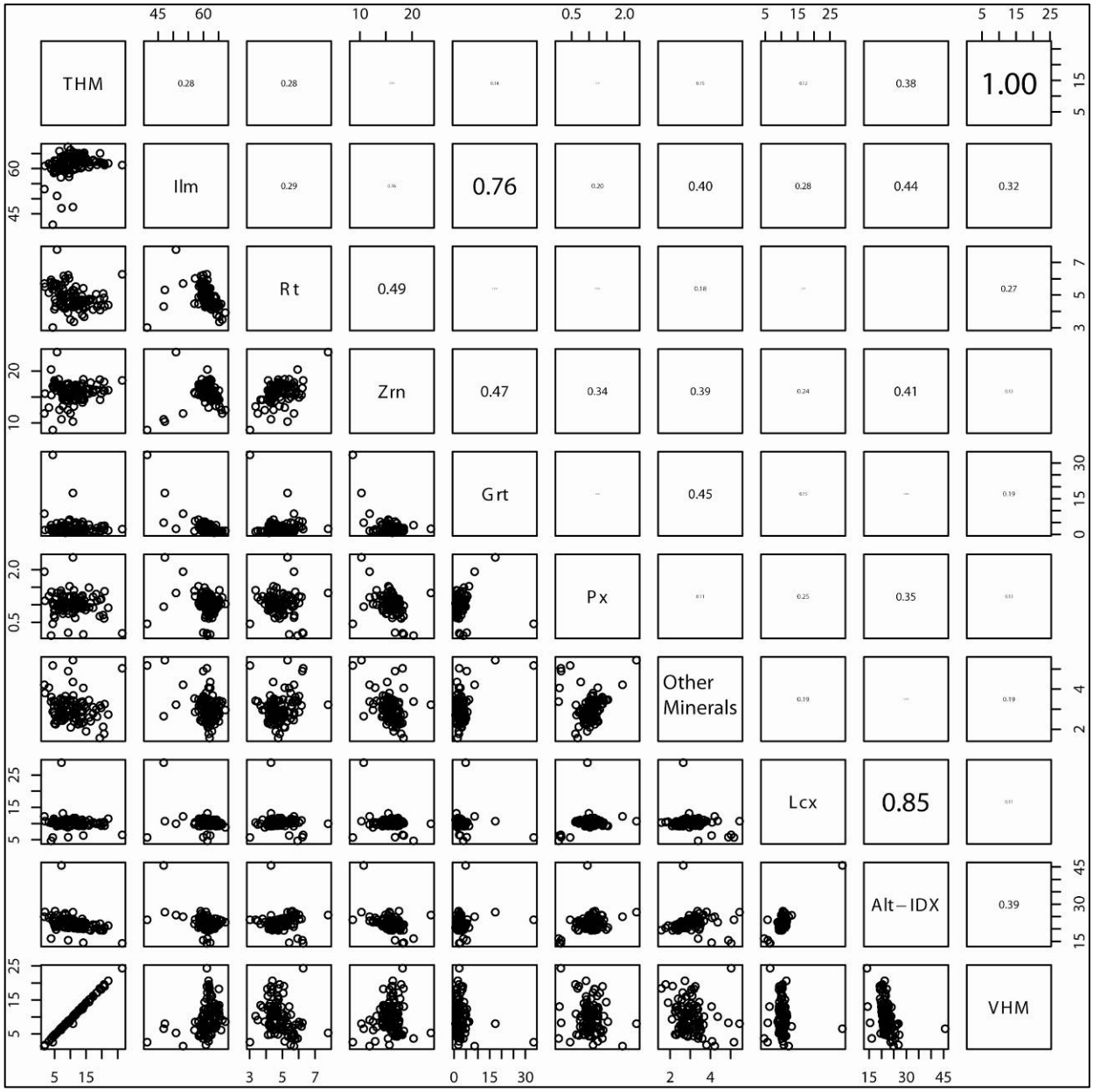

Figure D6. Correlation coefficient diagram of the mineralogy of the East mine as determined with QEMSCAN. n=103

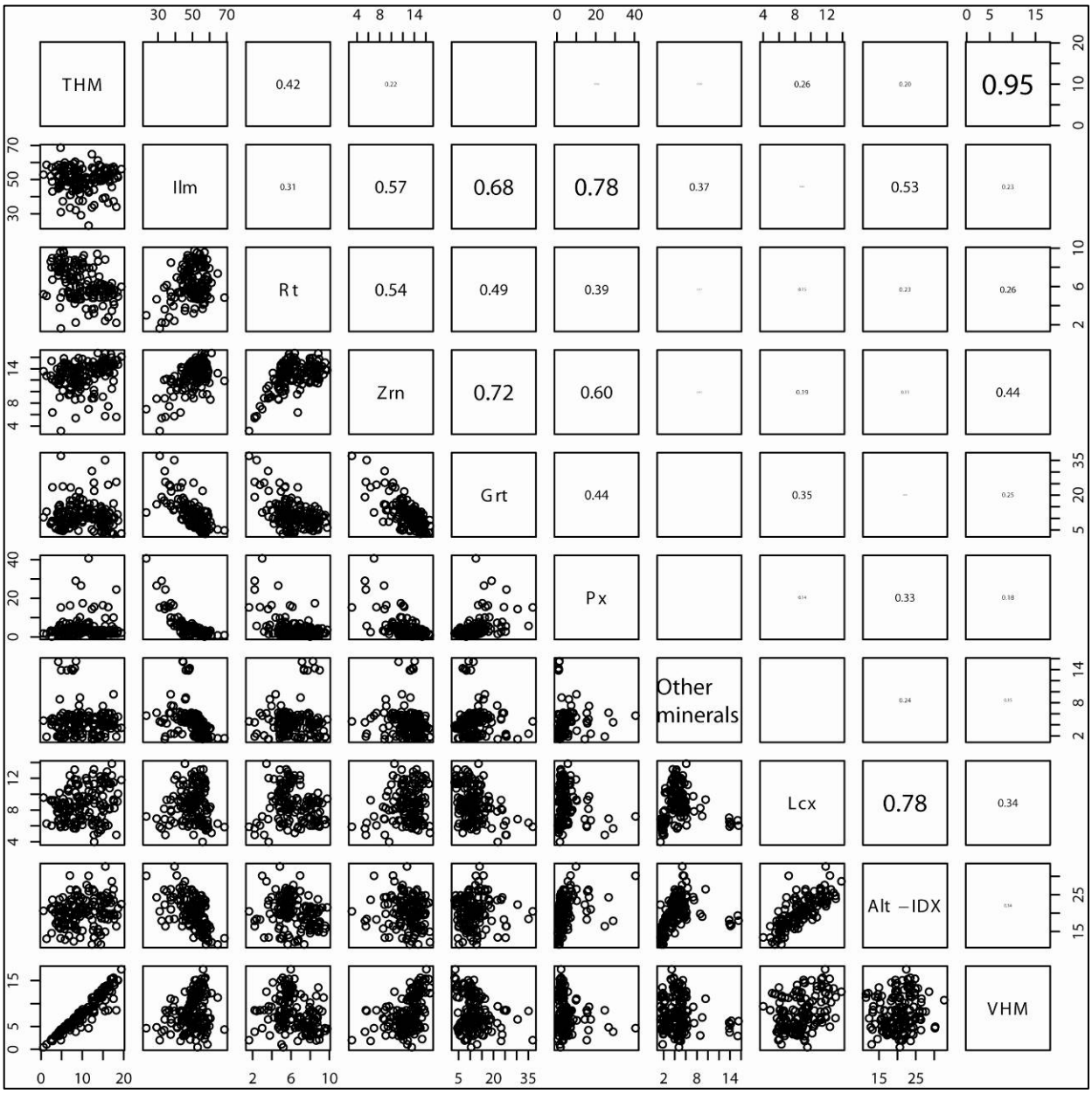

Figure D7. Correlation coefficient diagram of the mineralogy of the West mine as determined with QEMSCAN. n= 152

APPENDIX E:
1. GEOCHEMISTRY OF SAMPLES AS DETERMINED BY XRF.

Table E Geochemistry of individual samples grouped according to composites as obtained by XRF.

Low totals could be ascribed to the quantitative XRF method. Pressed pellets were used and not fusion discs. The latter is more accurate. Pressed pellets were used by Namakwa Sands since it is cheap and fast to prepare.

TABLE E														
XRF GEOCHEMISTRY OF INDIVIDUAL SAMPLES GROUPED INTO COMPOSITES BASED ON THE THM CONTENT, Al/Al+Fe AND Fe/Fe+Ti RATIOS														
HOUTKRAAL REMAINDER PORTION 2														
Sample	**Sample ID**	**Al_2O_3**	**CaO**	**Cr_2O_3**	**Fe_2O_3**	**P_2O_5**	**TiO_2**	**ZrO_2**	**SiO_2**	**MgO**	**MnO**	**K_2O**	**Na_2O**	**Total**
HKRP001	8A5S060	2	0	0	4	0	3	0.8	87	0	0	2	0	101
	8A5S017	1	0	0	3	0	2	0.6	91	0	0	2	0	101
	8A5S050	2	0	0	3	0	2	0.5	89	0	0	3	0	101
	8A5S018	2	0	0	2	0	2	0.5	92	0	0	2	0	101
HKRP002	8A5S011	1	0	0	2	0	2	0.4	92	0	0	2	0	101
	8A5S006	2	0	0	3	0	2	0.6	90	0	0	2	0	101
	8A5S005	2	0	0	2	0	1	0.4	92	0	0	2	0	101
	8A5S024	2	0	0	2	0	1	0.4	92	0	0	2	0	101
	8A5S052	2	0	0	3	0	2	0.5	90	0	0	2	0	101
	8A5S016	2	0	0	2	0	1	0.4	92	0	0	2	0	102
	8A5S013	1	0	0	2	0	1	0.3	93	0	0	2	0	101
	8A5S059	2	0	0	3	0	2	0.4	90	0	0	2	0	100
HKRP003	8A5S023	2	0	0	2	0	1	0.4	92	0	0	2	0	101
	8A5S022	2	0	0	2	0	1	0.3	93	0	0	2	0	101
	8A5S010	2	0	0	2	0	1	0.3	92	0	0	2	0	101
	8A5S008	1	0	0	2	0	1	0.3	93	0	0	2	0	100
	8A5S009	2	0	0	5	0	1	0.3	89	0	0	2	0	101
	8A5S021	2	0	0	2	0	1	0.3	92	0	0	3	0	101
	8A5S048	3	0	0	3	0	2	0.4	89	0	0	3	0	101
	8A5S025	3	0	0	3	0	2	0.4	88	0	0	3	0	101
HKRP004	8A5S056	2	0	0	2	0	1	0.3	92	0	0	2	0	102
	8A5S033	3	0	0	3	0	2	0.4	89	0	0	3	0	101
	8A5S058	2	0	0	2	0	2	0.3	90	0	0	3	0	100
	8A5S057	2	0	0	3	0	2	0.4	90	0	0	3	0	100

TABLE E continued														
XRF GEOCHEMISTRY OF INDIVIDUAL SAMPLES GROUPED INTO COMPOSITES BASED ON THE THM CONTENT, Al/Al+Fe AND Fe/Fe+Ti RATIOS														
HOUTKRAAL REMAINDER PORTION 2														
Sample	**Sample ID**	**Al_2O_3**	**CaO**	**Cr_2O_3**	**Fe_2O_3**	**P_2O_5**	**TiO_2**	**ZrO_2**	**SiO_2**	**MgO**	**MnO**	**K_2O**	**Na_2O**	**Total**
HKRP 004	8A5S042	2	0	0	2	0	1	0.2	92	0	0	3	0	101
	8A5S039	2	0	0	2	0	1	0.3	90	0	0	3	0	101
	8A5S030	1	0	0	2	0	1	0.3	93	0	0	2	0	101
	8A5S047	3	0	0	3	0	2	0.4	88	0	0	4	0	102
	8A5S019	2	0	0	2	0	1	0.3	91	0	0	3	0	101
	8A5S020	2	0	0	2	0	1	0.2	93	0	0	2	0	101
HKRP 005	8A5S043	3	0	0	2	0	1	0.3	89	0	0	3	0	101
	8A5S053	2	0	0	2	0	1	0.3	91	0	0	2	0	100
	8A5S028	1	0	0	2	0	1	0.2	93	0	0	2	0	101
	8A5S055	4	0	0	2	0	1	0.3	87	0	0	3	0	100
	8A5S015	3	0	0	3	0	1	0.3	89	0	0	2	0	101
	8A5S002	1	0	0	1	0	1	0.1	95	0	0	2	0	102
HKRP 006	8A5S029	2	0	0	1	0	1	0.2	94	0	0	2	0	101
	8A5S001	2	0	0	2	0	1	0.3	93	0	0	2	0	101
	8A5S041	2	0	0	2	0	1	0.2	95	0	0	2	0	103
	8A5S046	1	0	0	2	0	1	0.2	93	0	0	3	1	102
	8A5S044	1	0	0	1	0	1	0.2	95	0	0	2	0	101
	8A5S038	1	0	0	2	0	1	0.2	94	0	0	2	0	101
	8A5S012	1	0	0	1	0	1	0.1	94	0	0	2	0	101
	8A5S036	2	0	0	2	0	1	0.2	93	0	0	2	0	101

TABLE E continued														
XRF GEOCHEMISTRY OF INDIVIDUAL SAMPLES GROUPED INTO COMPOSITES BASED ON THE THM CONTENT, Al/Al+Fe AND Fe/Fe+Ti RATIOS														
HOUTKRAAL REMAINDER PORTION 2														
Sample	**Sample ID**	**Al_2O_3**	**CaO**	**Cr_2O_3**	**Fe_2O_3**	**P_2O_5**	**TiO_2**	**ZrO_2**	**SiO_2**	**MgO**	**MnO**	**K_2O**	**Na_2O**	**Total**
HKRP 007	8A5S037	2	0	0	2	0	1	0.2	94	0	0	2	0	102
	8A5S014	1	0	0	1	0	1	0.2	95	0	0	2	0	102
	8A5S034	1	0	0	1	0	1	0.1	95	0	0	3	0	102
	8A5S003	2	0	0	2	0	1	0.2	92	0	0	3	0	101
	8A5S004	2	0	0	2	0	1	0.2	93	0	0	2	0	102
	8A5S027	1	0	0	1	0	0	0.1	95	0	0	2	0	101
	8A5S007	2	0	0	1	0	1	0.1	94	0	0	2	0	101
HKRP 008	8A5S054	3	0	0	2	0	1	0.3	91	0	0	3	0	101
	8A5S035	2	0	0	1	0	1	0.1	93	0	0	5	0	103
	8A5S049	3	0	0	2	0	1	0.2	91	0	0	3	0	101
	8A5S031	2	0	0	1	0	1	0.1	92	0	0	3	0	101
	8A5S026	1	0	0	1	0	0	0.1	95	0	0	3	0	101
	8A5S040	2	0	0	1	0	1	0.1	93	0	0	3	0	101
HKRP 009	8A5S032	4	0	0	2	0	1	0.1	88	1	0	3	0	101
	8A5S051	6	0	0	3	0	1	0.1	84	0	0	2	0	100
HKRP 010	8A5S061	2	0	0	2	0	1	0.2	92	0	0	3	0	101

TABLE E continued														
XRF GEOCHEMISTRY OF INDIVIDUAL SAMPLES GROUPED INTO COMPOSITES BASED ON THE THM CONTENT, Al/Al+Fe AND Fe/Fe+Ti RATIOS														
HOUTKRAAL REMAINDER														
Sample	**Sample ID**	**Al_2O_3**	**CaO**	**Cr_2O_3**	**Fe_2O_3**	**P_2O_5**	**TiO_2**	**ZrO_2**	**SiO_2**	**MgO**	**MnO**	**K_2O**	**Na_2O**	**Total**
HKR 001	8A5S079	1	0	0	1	0	1	0.2	92	0	0	5	0	102
	8A5S078	8	2	0	7	0	5	1.1	69	1	0	8	2	103
	8A5S085	1	0	0	1	0	1	0.2	94	0	0	4	0	102
	8A5S098	1	0	0	2	0	1	0.2	92	0	0	7	0	103
	8A5S089	2	0	0	1	0	1	0.2	92	0	0	5	0	101
	8A5S104	1	0	0	2	0	1	0.2	91	0	0	6	0	102
	8A5S072	1	0	0	1	0	1	0.1	93	0	0	4	0	101
	8A5S077	1	0	0	1	0	1	0.1	92	0	0	5	0	100
HKR 002	8A5S088	1	0	0	1	0	0	0.1	89	0	0	8	0	101
HKR 003	8A5S083	1	0	0	1	0	1	0.1	93	0	0	4	0	101
	8A5S068	2	0	0	1	0	1	0.1	93	0	0	3	0	101
HKR 004	8A5S099	3	0	0	2	0	1	0.1	89	0	0	7	0	103
	8A5S082	2	0	0	1	0	0	0.1	93	0	0	4	0	101
HKR 005	8A5S093	2	0	0	3	0	2	0.5	89	0	0	7	0	103
	8A5S065	2	0	0	2	0	2	0.3	91	0	0	4	0	102
	8A5S064	2	0	0	2	0	2	0.4	90	0	0	3	0	101
	8A5S063	2	0	0	2	0	1	0.3	92	0	0	4	0	101
	8A5S073	2	0	0	2	0	2	0.4	89	0	0	5	0	101
HKR 006	8A5S086	2	0	0	2	0	1	0.3	92	0	0	5	0	102
	8A5S092	2	0	0	2	0	1	0.3	90	0	0	8	0	104
	8A5S096	2	0	0	3	0	2	0.5	88	0	0	6	0	102
	8A5S095	2	0	0	2	0	1	0.3	90	0	0	6	0	103
	8A5S105	1	0	0	2	0	1	0.2	91	0	0	5	0	102
HKR 007	8A5S094	2	0	0	2	0	2	0.4	88	0	0	9	0	105
	8A5S087	2	0	0	2	0	1	0.3	89	0	0	6	0	103
	8A5S062	3	0	0	2	0	1	0.3	90	0	0	4	0	102

TABLE E continued														
XRF GEOCHEMISTRY OF INDIVIDUAL SAMPLES GROUPED INTO COMPOSITES BASED ON THE THM CONTENT, Al/Al+Fe AND Fe/Fe+Ti RATIOS														
HOUTKRAAL REMAINDER														
Sample	**Sample ID**	**Al_2O_3**	**CaO**	**Cr_2O_3**	**Fe_2O_3**	**P_2O_5**	**TiO_2**	**ZrO_2**	**SiO_2**	**MgO**	**MnO**	**K_2O**	**Na_2O**	**Total**
HKR 008	8A5S103	4	0	0	3	0	1	0.2	84	0	0	8	0	104
HKR 009	8A5S090	2	0	0	5	0	4	1.1	83	0	0	7	0	104
	8A5S075	2	0	0	4	0	4	0.9	86	0	0	4	0	101
	8A5S084	2	0	0	5	0	5	1.2	83	0	0	5	0	102
	8A5S091	2	0	0	5	0	4	1.2	84	0	0	5	0	103
	8A5S097	2	0	0	5	0	4	1.0	83	0	0	8	0	104
	8A5S074	2	0	0	4	0	4	0.9	85	0	0	4	0	100
HKR 010	8A5S069	2	0	0	3	0	3	0.6	89	0	0	0	0	97
	8A5S076	2	0	0	3	0	3	0.7	87	0	0	4	0	100
	8A5S080	2	0	0	3	0	3	0.7	87	0	0	5	0	101
	8A5S071	2	0	0	4	0	3	0.8	85	0	0	4	0	101
HKR 011	8A5S081	4	0	0	4	0	4	0.9	86	0	0	5	0	104
	8A5S066	2	0	0	3	0	3	0.7	86	0	0	3	0	99
	8A5S100	2	0	0	3	0	2	0.5	89	0	0	6	0	102
HKR 012	8A5S067	2	0	0	3	0	3	0.6	85	0	0	4	0	100
	8A5S102	2	0	0	3	0	3	0.7	86	0	0	6	0	102
	8A5S101	3	0	0	3	0	2	0.6	85	0	0	6	0	101
	8A5S070	2	0	0	3	0	2	0.5	87	0	0	0	0	96
XRF GEOCHEMISTRY OF INDIVIDUAL SAMPLES GROUPED INTO COMPOSITES BASED ON THE THM CONTENT, Al/Al+Fe AND Fe/Fe+Ti RATIOS														
GEELWAL KAROO														
Sample	**Sample ID**	**Al_2O_3**	**CaO**	**Cr_2O_3**	**Fe_2O_3**	**P_2O_5**	**TiO_2**	**ZrO_2**	**SiO_2**	**MgO**	**MnO**	**K_2O**	**Na_2O**	**Total**
GW 001	8A5S148	1	0	0	1	0	1	0.2	89	0	0	7	0	99
	8A5S149	1	0	0	1	0	1	0.1	90	0	0	9	0	102
	8A5S150	1	0	0	1	0	0	0.1	90	0	0	11	0	104
	8A5S151	1	0	0	1	0	1	0.1	87	0	0	21	0	112
	8A5S142	2	0	0	2	0	1	0.2	90	0	0	5	0	101
	8A5S136	2	0	0	1	0	1	0.2	89	0	0	6	0	101
	8A5S152	1	0	0	1	0	1	0.1	91	0	0	14	0	109

TABLE E continued														
XRF GEOCHEMISTRY OF INDIVIDUAL SAMPLES GROUPED INTO COMPOSITES BASED ON THE THM CONTENT, Al/Al+Fe AND Fe/Fe+Ti RATIOS														
GEELWAL KAROO														
Sample	**Sample ID**	**Al_2O_3**	**CaO**	**Cr_2O_3**	**Fe_2O_3**	**P_2O_5**	**TiO_2**	**ZrO_2**	**SiO_2**	**MgO**	**MnO**	**K_2O**	**Na_2O**	**Total**
GW 002	8A5S140	2	0	0	1	0	1	0.1	89	0	0	16	0	111
	8A5S137	2	0	0	1	0	1	0.1	89	0	0	11	0	106
	8A5S139	3	0	0	2	0	1	0.1	86	0	0	9	0	102
GW 003	8A5S156	2	0	0	1	0	1	0.1	89	0	0	0	0	95
	8A5S188	4	0	0	2	0	1	0.2	85	0	0	0	1	96
	8A5S171	3	0	0	1	0	1	0.1	89	0	0	0	0	96
	8A5S170	3	0	0	2	0	1	0.1	88	0	0	0	0	96
	8A5S180	3	0	0	2	0	1	0.1	88	0	0	0	0	96
	8A5S118	4	0	0	2	0	1	0.1	86	0	0	12	0	106
	8A5S163	3	0	0	1	0	1	0.1	88	0	0	0	0	95
	8A5S172	3	0	0	2	0	1	0.1	89	0	0	0	0	97
	8A5S133	4	0	0	2	0	1	0.1	83	1	0	7	1	104
	8A5S190	6	0	0	3	0	1	0.2	79	1	0	0	1	96
	8A5S155	3	0	0	1	0	0	0.1	89	0	0	0	0	95
GW 004	8A5S158	4	0	0	2	0	1	0.1	85	0	0	0	0	96
	8A5S157	3	0	0	1	0	0	0.1	89	0	0	0	0	95
	8A5S110	4	0	0	2	0	1	0.1	87	0	0	7	0	103
	8A5S179	4	0	0	2	0	1	0.1	83	1	0	0	0	96
	8A5S114	5	0	0	2	0	1	0.1	84	1	0	6	0	102
	8A5S162	4	0	0	2	0	1	0.1	85	0	0	0	0	94
	8A5S169	3	0	0	2	0	0	0.1	89	0	0	0	0	96
	8A5S109	4	0	0	2	0	1	0.1	86	0	0	8	1	104

TABLE E continued														
XRF GEOCHEMISTRY OF INDIVIDUAL SAMPLES GROUPED INTO COMPOSITES BASED ON THE THM CONTENT, Al/Al+Fe AND Fe/Fe+Ti RATIOS														
GEELWAL KAROO														
Sample	**Sample ID**	**Al_2O_3**	**CaO**	**Cr_2O_3**	**Fe_2O_3**	**P_2O_5**	**TiO_2**	**ZrO_2**	**SiO_2**	**MgO**	**MnO**	**K_2O**	**Na_2O**	**Total**
GW 004	8A5S167	3	0	0	2	0	1	0.1	88	0	0	0	0	96
	8A5S153	3	0	0	1	0	0	0.1	88	0	0	0	0	95
	8A5S166	3	0	0	2	0	0	0.0	86	0	0	0	0	94
	8A5S187	6	0	0	3	0	1	0.1	81	1	0	0	0	96
	8A5S165	3	0	0	2	0	0	0.1	89	0	0	0	0	97
	8A5S178	6	0	0	3	0	1	0.2	78	1	0	0	1	92
	8A5S160	3	0	0	2	0	0	0.1	86	0	0	0	0	95
	8A5S161	4	0	0	2	0	0	0.1	86	0	0	0	0	95
GW 005	8A5S141	1	0	0	1	0	1	0.2	89	0	0	11	0	105
	8A5S134	2	0	0	2	0	1	0.3	87	0	0	7	0	102
	8A5S135	2	0	0	2	0	1	0.2	87	0	0	7	0	101
	8A5S147	2	0	0	2	0	1	0.2	88	0	0	9	0	103
GW 006	8A5S130	3	0	0	2	0	1	0.2	87	0	0	7	0	102
	8A5S145	2	0	0	2	0	1	0.2	88	0	0	13	0	109
	8A5S146	2	0	0	2	0	1	0.2	89	0	0	6	0	102
GW 007	8A5S174	4	0	0	2	0	1	0.3	87	0	0	0	0	97
	8A5S173	3	0	0	2	0	1	0.2	90	0	0	0	0	97
	8A5S182	4	0	0	2	0	1	0.2	85	0	0	0	0	93
	8A5S129	2	0	0	2	0	1	0.2	88	0	0	8	0	103
	8A5S111	4	0	0	2	0	1	0.2	84	0	0	7	1	102
	8A5S164	3	0	0	2	0	1	0.2	88	0	0	0	0	96
	8A5S185	4	0	0	3	0	1	0.3	83	1	0	0	0	96
	8A5S128	3	0	0	2	0	1	0.1	87	0	0	9	0	104
	8A5S183	4	0	0	2	0	1	0.2	84	0	0	0	0	96

TABLE E continued														
XRF GEOCHEMISTRY OF INDIVIDUAL SAMPLES GROUPED INTO COMPOSITES BASED ON THE THM CONTENT, Al/Al+Fe AND Fe/Fe+Ti RATIOS														
GEELWAL KAROO														
Sample	**Sample ID**	**Al_2O_3**	**CaO**	**Cr_2O_3**	**Fe_2O_3**	**P_2O_5**	**TiO_2**	**ZrO_2**	**SiO_2**	**MgO**	**MnO**	**K_2O**	**Na_2O**	**Total**
GW 007	8A5S191	6	0	0	3	0	1	0.3	81	1	0	0	1	96
	8A5S181	3	0	0	2	0	1	0.2	79	0	0	0	0	95
	8A5S189	5	0	0	3	0	1	0.2	81	0	0	0	1	96
	8A5S184	5	0	0	3	0	1	0.2	83	0	0	0	0	95
	8A5S115	4	0	0	2	0	1	0.1	85	0	0	7	0	102
	8A5S175	5	1	0	3	0	1	0.2	78	1	0	0	1	95
	8A5S176	5	0	0	3	0	1	0.3	79	1	0	0	1	94
	8A5S120	5	0	0	3	0	1	0.1	83	1	0	9	1	105
GW 008	8A5S154	3	0	0	2	0	1	0.1	88	0	0	0	0	95
	8A5S119	5	0	0	2	0	1	0.1	83	1	0	9	1	105
	8A5S186	7	0	0	4	0	1	0.2	78	1	0	0	0	96
	8A5S132	4	1	0	3	0	1	0.1	86	0	0	6	1	103
GW 009	8A5S143	2	0	0	2	0	1	0.3	87	0	0	6	0	101
	8A5S144	3	1	0	6	0	4	0.7	75	2	0	9	1	105
	8A5S108	5	1	0	4	0	2	0.5	78	1	0	9	1	103
	8A5S126	4	1	0	5	0	2	0.4	76	3	0	8	0	104
GW 010	8A5S113	4	1	0	4	0	2	0.2	80	1	0	7	0	102
	8A5S122	4	4	0	4	0	1	0.1	75	3	0	7	1	103
	8A5S168	4	1	0	3	0	1	0.1	83	1	0	0	1	96
	8A5S127	4	3	0	4	0	1	0.1	79	3	0	9	1	105

TABLE E continued														
XRF GEOCHEMISTRY OF INDIVIDUAL SAMPLES GROUPED INTO COMPOSITES BASED ON THE THM CONTENT, Al/Al+Fe AND Fe/Fe+Ti RATIOS														
GEELWAL KAROO														
Sample	**Sample ID**	**Al_2O_3**	**CaO**	**Cr_2O_3**	**Fe_2O_3**	**P_2O_5**	**TiO_2**	**ZrO_2**	**SiO_2**	**MgO**	**MnO**	**K_2O**	**Na_2O**	**Total**
GW 011	8A5S107	4	0	0	3	0	2	0.3	82	1	0	7	0	102
	8A5S125	3	0	0	2	0	1	0.3	85	0	0	9	0	104
	8A5S106	4	0	0	2	0	1	0.3	84	0	0	7	1	102
	8A5S124	4	0	0	3	0	2	0.3	81	0	0	8	1	103
	8A5S121	5	0	0	4	0	2	0.3	79	0	0	7	1	103
	8A5S117	5	1	0	4	0	2	0.4	78	1	0	7	1	103
	8A5S177	6	0	0	3	0	2	0.3	79	1	0	0	0	96
	8A5S131	5	1	0	4	0	1	0.3	80	1	0	7	1	103
	8A5S112	5	1	0	3	0	1	0.3	78	1	0	7	0	102
	8A5S123	6	0	0	4	0	2	0.2	77	2	0	9	1	105
GW 012	8A5S159	4	1	0	3	0	1	0.2	81	1	0		0	94
	8A5S116	7	1	0	4	0	1	0.2	76	2	0	8	1	103
	8A5S138	2	1	0	2	0	0	0.0	86	1	0	10	0	104
XRF GEOCHEMISTRY OF INDIVIDUAL SAMPLES GROUPED INTO COMPOSITES BASED ON THE THM CONTENT, Al/Al+Fe AND Fe/Fe+Ti RATIOS														
GRAAUWDUINEN														
Sample	**Sample ID**	**Al_2O_3**	**CaO**	**Cr_2O_3**	**Fe_2O_3**	**P_2O_5**	**TiO_2**	**ZrO_2**	**SiO_2**	**MgO**	**MnO**	**K_2O**	**Na_2O**	**Total**
GRW 001	8A5S275	1	0	0	1	0	1	0.2	88	0	0	0	0	96
	8A5S286	3	0	0	2	0	1	0.2	87	0	0	0	0	95
	8A5S259	3	0	0	2	0	1	0.2	86	0	0	0	0	92
	8A5S321	2	0	0	2	0	1	0.2	89	0	0	0	0	95
	8A5S276	2	0	0	1	0	1	0.2	90	0	0	0	0	95
	8A5S221	2	0	0	1	0	1	0.1	91	0	0	0	0	96
	8A5S195	2	0	0	2	0	1	0.2	93	0	0	0	0	98
	8A5S310	2	0	0	2	0	1	0.2	89	0	0	0	0	95
	8A5S261	3	0	0	2	0	1	0.2	93	0	0	0	0	98
	8A5S260	3	0	0	2	0	1	0.1	87	0	0	0	0	93
	8A5S323	2	0	0	1	0	1	0.1	91	0	0	0	0	95

TABLE E continued

XRF GEOCHEMISTRY OF INDIVIDUAL SAMPLES GROUPED INTO COMPOSITES BASED ON THE THM CONTENT, Al/Al+Fe AND Fe/Fe+Ti RATIOS

GRAAUWDUINEN

Sample	Sample ID	Al_2O_3	CaO	Cr_2O_3	Fe_2O_3	P_2O_5	TiO_2	ZrO_2	SiO_2	MgO	MnO	K_2O	Na_2O	Total
	8A5S270	3	0	0	2	0	1	0.2	85	0	0	0	0	93
	8A5S304	3	0	0	2	0	1	0.2	88	0	0	0	0	95
	8A5S293	3	0	0	2	0	1	0.2	88	0	0	0	0	93
	8A5S309	2	0	0	1	0	1	0.1	89	0	0	0	0	93
	8A5S292	2	0	0	1	0	1	0.1	89	0	0	0	0	95
	8A5S240	2	0	0	1	0	1	0.1	82	0	0	0	0	86
	8A5S277	3	0	0	2	0	1	0.2	84	0	0	0	0	93
	8A5S308	2	0	0	1	0	1	0.2	90	0	0	0	0	95
	8A5S285	3	0	0	2	0	1	0.2	85	0	0	0	0	93
	8A5S278	3	0	0	2	0	1	0.2	87	0	0	0	0	94
	8A5S320	2	0	0	1	0	1	0.1	91	0	0	0	0	95
	8A5S224	2	0	0	1	0	1	0.1	93	0	0	0	0	97
	8A5S214	4	0	0	2	0	1	0.3	86	0	0	0	0	95
GRW002	8A5S222	2	0	0	2	0	1	0.2	89	0	0	0	0	95
	8A5S238	2	0	0	1	0	1	0.1	89	0	0	0	0	93
	8A5S302	4	0	0	2	0	1	0.2	83	0	0	0	0	93
	8A5S288	4	0	0	2	0	1	0.2	84	0	0	0	0	93
	8A5S226	3	0	0	2	0	1	0.1	92	0	0	0	0	97
	8A5S239	2	0	0	1	0	1	0.1	90	0	0	0	0	94
	8A5S315	3	0	0	2	0	1	0.1	87	0	0	0	0	95
	8A5S318	3	0	0	2	0	1	0.1	87	0	0	0	0	94
	8A5S213	4	0	0	2	0	1	0.2	86	0	0	0	0	96
	8A5S322	2	0	0	1	0	1	0.1	91	0	0	0	0	94
	8A5S223	3	0	0	2	0	1	0.1	91	0	0	0	0	96
	8A5S319	2	0	0	1	0	1	0.1	90	0	0	0	0	95
	8A5S290	3	0	0	2	0	1	0.1	88	0	0	0	0	94
	8A5S325	2	0	0	1	0	1	0.1	90	0	0	0	0	94

TABLE E continued														
XRF GEOCHEMISTRY OF INDIVIDUAL SAMPLES GROUPED INTO COMPOSITES BASED ON THE THM CONTENT, Al/Al+Fe AND Fe/Fe+Ti RATIOS														
GRAAUWDUINEN														
Sample	**Sample ID**	**Al_2O_3**	**CaO**	**Cr_2O_3**	**Fe_2O_3**	**P_2O_5**	**TiO_2**	**ZrO_2**	**SiO_2**	**MgO**	**MnO**	**K_2O**	**Na_2O**	**Total**
GRW 002	8A5S303	4	0	0	2	0	1	0.1	86	0	0	0	0	94
	8A5S317	5	0	0	3	0	1	0.2	83	0	0	0	0	94
	8A5S265	4	0	0	2	0	1	0.1	86	0	0	0	0	92
	8A5S300	5	0	0	3	0	1	0.2	84	0	0	0	0	95
	8A5S307	3	0	0	2	0	1	0.1	88	0	0	0	0	94
	8A5S263	3	0	0	2	0	1	0.2	85	0	0	0	0	93
	8A5S231	4	0	0	3	0	1	0.2	85	0	0	0	0	95
	8A5S249	3	0	0	2	0	1	0.1	86	0	0	0	0	92
	8A5S289	4	0	0	2	0	1	0.1	86	0	0	0	0	93
	8A5S295	5	0	0	2	0	1	0.1	78	0	0	0	0	91
GRW 003	8A5S294	9	2	0	6	0	1	0.2	67	0	0	0	1	91
GRW 004	8A5S284	4	0	0	2	0	1	0.1	85	0	0	0	0	94
	8A5S268	4	0	0	2	0	1	0.1	86	0	0	0	0	93
	8A5S305	3	0	0	1	0	1	0.1	86	0	0	0	0	91
	8A5S297	3	0	0	2	0	1	0.1	88	0	0	0	0	95
	8A5S258	5	0	0	2	0	1	0.1	80	0	0	0	0	90
	8A5S282	4	0	0	1	0	1	0.1	85	0	0	0	0	91
	8A5S316	3	0	0	2	0	1	0.1	86	0	0	0	0	94
	8A5S314	4	0	0	2	0	1	0.1	87	0	0	0	0	94
	8A5S299	3	0	0	2	0	1	0.1	88	0	0	0	0	95
	8A5S313	4	0	0	2	0	1	0.1	86	0	0	0	0	94
	8A5S306	3	0	0	1	0	1	0.1	86	-1	0	0	0	91
	8A5S280	4	0	0	2	0	1	0.1	85	0	0	0	0	93
	8A5S298	4	0	0	1	0	0	0.1	86	0	0	0	0	92
	8A5S283	5	0	0	2	0	1	0.1	85	0	0	0	0	95
	8A5S266	4	0	0	2	0	1	0.1	67	0	0	0	0	91

TABLE E continued														
XRF GEOCHEMISTRY OF INDIVIDUAL SAMPLES GROUPED INTO COMPOSITES BASED ON THE THM CONTENT, Al/Al+Fe AND Fe/Fe+Ti RATIOS														
GRAAUWDUINEN														
Sample	**Sample ID**	**Al_2O_3**	**CaO**	**Cr_2O_3**	**Fe_2O_3**	**P_2O_5**	**TiO_2**	**ZrO_2**	**SiO_2**	**MgO**	**MnO**	**K_2O**	**Na_2O**	**Total**
GRW 004	8A5S281	5	0	0	1	0	1	0.1	84	0	0	0	0	91
	8A5S246	4	0	0	2	0	1	0.1	81	0	0	0	0	88
	8A5S324	3	0	0	1	0	1	0.1	88	0	0	0	0	94
	8A5S250	4	0	0	2	0	1	0.1	84	0	0	0	0	92
	8A5S247	4	0	0	1	0	1	0.0	82	0	0	0	0	89
	8A5S279	3	0	0	2	0	1	0.1	85	0	0	0	0	92
	8A5S296	4	0	0	2	0	1	0.1	82	0	0	0	0	91
	8A5S312	6	0	0	3	0	1	0.1	80	1	0	0	0	94
GW 005	8A5S248	4	0	0	1	0	0	0.0	75	0	0	0	0	81
GRW 006	8A5S225	9	2	0	4	0	1	0.1	77	1	0	0	0	95
GRW 007	8A5S192	2	0	0	3	0	2	0.5	91	0	0	0	0	98
	8A5S197	2	0	0	2	0	2	0.5	91	0	0	0	0	98
	8A5S193	2	0	0	3	0	2	0.5	89	0	0	0	0	97
	8A5S196	2	0	0	2	0	1	0.3	93	0	0	0	0	99
	8A5S200	3	0	0	3	0	2	0.5	89	0	0	0	0	98
	8A5S198	2	0	0	2	0	2	0.4	91	0	0	0	0	97
	8A5S217	3	0	0	2	0	1	0.3	89	0	0	0	0	96
	8A5S201	4	0	0	3	0	2	0.5	87	0	0	0	0	98
	8A5S194	3	0	0	3	0	2	0.5	88	0	0	0	0	98
GRW008	8A5S199	3	0	0	3	0	1	0.3	90	0	0	0	0	98
	8A5S262	3	0	0	3	0	1	0.3	90	0	0	0	0	98
GRW 009	8A5S235	1	0	0	1	0	2	0.2	93	0	0	0	0	95
	8A5S232	1	0	0	1	0	1	0.1	92	0	0	0	0	96
	8A5S255	4	0	0	3	0	2	0.4	82	0	0	0	0	93

TABLE E continued														
XRF GEOCHEMISTRY OF INDIVIDUAL SAMPLES GROUPED INTO COMPOSITES BASED ON THE THM CONTENT, Al/Al+Fe AND Fe/Fe+Ti RATIOS														
GRAAUWDUINEN														
Sample	**Sample ID**	**Al_2O_3**	**CaO**	**Cr_2O_3**	**Fe_2O_3**	**P_2O_5**	**TiO_2**	**ZrO_2**	**SiO_2**	**MgO**	**MnO**	**K_2O**	**Na_2O**	**Total**
	8A5S237	3	0	0	2	0	2	0.3	86	0	0	0	0	94
	8A5S274	5	0	0	2	0	1	0.2	93	0	0	0	0	98
	8A5S243	2	0	0	1	0	1	0.2	90	0	0	0	0	94
	8A5S252	4	0	0	2	0	1	0.2	83	0	0	0	0	93
	8A5S271	4	0	0	2	0	1	0.2	80	0	0	0	0	92
	8A5S287	4	0	0	2	0	1	0.2	84	0	0	0	0	92
	8A5S311	3	0	0	2	0	1	0.2	86	0	0	0	0	94
	8A5S218	3	0	0	3	0	2	0.3	85	0	0	0	0	93
	8A5S219	3	0	0	2	0	1	0.2	86	0	0	0	0	94
	8A5S241	3	0	0	2	0	1	0.1	88	0	0	0	0	93
	8A5S257	3	0	0	2	0	1	0.2	85	0	0	0	0	93
	8A5S273	4	0	0	2	0	1	0.2	83	0	0	0	0	93
	8A5S251	5	0	0	2	0	1	0.2	80	0	0	0	0	91
GRW 010	8A5S242	2	0	0	2	0	1	0.2	91	0	0	0	0	95
	8A5S254	4	0	0	3	0	1	0.2	84	0	0	0	0	94
	8A5S253	5	0	0	3	0	1	0.2	81	0	0	0	0	92
	8A5S272	4	0	0	3	0	1	0.2	87	0	0	0	0	93
	8A5S215	4	0	0	2	0	1	0.2	86	0	0	0	0	95
	8A5S269	4	0	0	2	0	1	0.2	85	0	0	0	0	94
	8A5S301	4	0	0	2	0	1	0.2	85	0	0	0	0	96
	8A5S216	4	0	0	3	0	2	0.3	85	0	0	0	0	96
	8A5S227	5	1	0	3	0	1	0.3	81	0	0	0	0	95
	8A5S228	5	0	0	3	0	1	0.3	83	0	0	0	0	95
	8A5S267	4	0	0	2	0	1	0.1	85	0	0	0	0	93
	8A5S234	6	0	0	3	0	2	0.3	82	0	0	0	0	95
	8A5S256	5	0	0	3	0	1	0.2	82	0	0	0	0	94
	8A5S244	5	0	0	3	0	1	0.2	82	0	0	0	0	93

TABLE E continued

XRF GEOCHEMISTRY OF INDIVIDUAL SAMPLES GROUPED INTO COMPOSITES BASED ON THE THM CONTENT, Al/Al+Fe AND Fe/Fe+Ti RATIOS

GRAAUWDUINEN

Sample	Sample ID	Al_2O_3	CaO	Cr_2O_3	Fe_2O_3	P_2O_5	TiO_2	ZrO_2	SiO_2	MgO	MnO	K_2O	Na_2O	Total
GRW 010	8A5S236	6	0	0	3	0	1	0.2	77	0	0	0	0	91
	8A5S230	3	0	0	2	0	1	0.1	88	0	0	0	0	95
	8A5S233	6	0	0	3	0	1	0.3	80	0	0	0	0	95
	8A5S229	5	0	0	3	0	1	0.2	84	0	0	0	0	95
	8A5S245	6	0	0	3	0	1	0.1	78	0	0	0	0	91
	8A5S264	5	0	0	3	0	1	0.1	84	0	0	0	0	92

XRF GEOCHEMISTRY OF INDIVIDUAL SAMPLES GROUPED INTO COMPOSITES BASED ON THE THM CONTENT, Al/Al+Fe AND Fe/Fe+Ti RATIOS

RIETFONTEIN

Sample	Sample ID	Al_2O_3	CaO	Cr_2O_3	Fe_2O_3	P_2O_5	TiO_2	ZrO_2	SiO_2	MgO	MnO	K_2O	Na_2O	Total
RF 001	8A5S392	1	0	0	2	0	1	0.3	93	0	0	0	0	98
	8A5S391	2	0	0	2	0	1	0.2	91	0	0	0	0	96
	8A5S370	2	0	0	2	0	1	0.1	90	0	0	0	0	94
	8A5S377	2	0	0	2	0	1	0.1	88	0	0	0	0	94
	8A5S371	2	0	0	2	0	1	0.2	91	0	0	0	0	96
RF 002	8A5S390	2	0	0	2	0	1	0.2	89	0	0	0	0	93
	8A5S387	2	0	0	2	0	1	0.2	88	0	0	0	0	93
	8A5S389	2	0	0	2	0	1	0.2	90	0	0	0	0	94
	8A5S359	2	0	0	2	0	1	0.1	85	0	0	0	0	94
	8A5S385	2	0	0	2	0	1	0.2	90	0	0	0	0	95
	8A5S386	2	0	0	2	0	1	0.2	85	0	0	0	0	93
	8A5S361	2	0	0	2	0	1	0.2	89	0	0	0	0	95
RF 003	8A5S339	3	0	0	2	0	1	0.2	87	0	0	0	0	94
	8A5S327	3	0	0	2	0	1	0.1	86	0	0	0	0	92
	8A5S374	2	0	0	2	0	1	0.1	88	0	0	0	0	92
	8A5S356	3	0	0	2	0	1	0.1	86	0	0	0	0	91
	8A5S345	3	0	0	2	0	1	0.1	83	0	0	0	0	91
	8A5S358	3	0	0	2	0	1	0.2	87	0	0	0	0	93
	8A5S350	3	0	0	2	0	1	0.1	89	0	0	0	0	94

TABLE E continued														
XRF GEOCHEMISTRY OF INDIVIDUAL SAMPLES GROUPED INTO COMPOSITES BASED ON THE THM CONTENT, Al/Al+Fe AND Fe/Fe+Ti RATIOS														
RIETFONTEIN														
Sample	**Sample ID**	**Al_2O_3**	**CaO**	**Cr_2O_3**	**Fe_2O_3**	**P_2O_5**	**TiO_2**	**ZrO_2**	**SiO_2**	**MgO**	**MnO**	**K_2O**	**Na_2O**	**Total**
RF 003	8A5S379	2	0	0	2	0	1	0.1	89	0	0	0	0	93
	8A5S381	2	0	0	2	0	1	0.2	89	0	0	0	0	93
	8A5S344	3	0	0	2	0	1	0.1	81	0	0	0	0	92
	8A5S349	3	0	0	2	0	1	0.1	90	0	0	0	0	97
	8A5S364	2	0	0	2	0	1	0.1	88	0	0	0	0	93
	8A5S353	3	0	0	2	0	1	0.1	87	0	0	0	0	93
	8A5S335	3	0	0	2	0	1	0.1	85	0	0	0	0	91
RF 004	8A5S347	3	0	0	2	0	1	0.1	86	0	0	0	0	92
	8A5S352	3	0	0	2	0	1	0.1	90	0	0	0	0	96
	8A5S354	3	0	0	2	0	1	0.1	86	0	0	0	0	93
	8A5S334	3	0	0	2	0	1	0.1	85	0	0	0	0	91
	8A5S331	3	0	0	2	0	1	0.1	86	0	0	0	0	92
	8A5S343	3	0	0	1	0	1	0.1	89	0	0	0	0	94
	8A5S380	2	0	0	1	0	1	0.1	88	0	0	0	0	94
	8A5S333	4	0	0	2	0	1	0.1	82	0	0	0	0	90
	8A5S337	3	0	0	2	0	1	0.1	83	0	0	0	0	91
	8A5S328	4	0	0	2	0	1	0.1	83	0	0	0	0	92
	8A5S357	3	0	0	2	0	1	0.1	86	0	0	0	0	93
	8A5S373	1	0	0	1	0	0	0.1	93	0	0	0	0	95
	8A5S332	3	0	0	2	0	1	0.1	90	0	0	0	0	95
	8A5S355	3	0	0	2	0	1	0.1	87	0	0	0	0	95
RF 005	8A5S395	2	0	0	2	0	2	0.4	91	0	0	0	0	97
	8A5S383	2	0	0	3	0	2	0.3	85	0	0	0	0	92
	8A5S384	2	0	0	3	0	2	0.4	87	0	0	0	0	95
	8A5S382	2	0	0	3	0	1	0.3	88	0	0	0	0	94
	8A5S393	2	0	0	3	0	1	0.4	90	0	0	0	0	96
	8A5S375	2	0	0	3	0	1	0.3	88	0	0	0	0	95

TABLE E continued														
XRF GEOCHEMISTRY OF INDIVIDUAL SAMPLES GROUPED INTO COMPOSITES BASED ON THE THM CONTENT, Al/Al+Fe AND Fe/Fe+Ti RATIOS														
RIETFONTEIN														
Sample	**Sample ID**	**Al_2O_3**	**CaO**	**Cr_2O_3**	**Fe_2O_3**	**P_2O_5**	**TiO_2**	**ZrO_2**	**SiO_2**	**MgO**	**MnO**	**K_2O**	**Na_2O**	**Total**
RF 006	8A5S369	2	0	0	2	0	1	0.2	88	0	0	0	0	94
RF 007	8A5S326	3	0	0	2	0	1	0.2	86	0	0	0	0	93
	8A5S346	3	0	0	2	0	1	0.2	80	0	0	0	0	93
	8A5S351	3	0	0	3	0	1	0.2	96	0	0	0	0	104
	8A5S338	3	0	0	2	0	1	0.2	88	0	0	0	0	95
	8A5S366	2	0	0	2	0	1	0.2	90	0	0	0	0	96
	8A5S340	3	0	0	2	0	1	0.2	84	0	0	0	0	92
	8A5S372	2	0	0	2	0	1	0.2	89	0	0	0	0	95
	8A5S388	2	0	0	2	0	1	0.2	89	0	0	0	0	94
	8A5S341	3	0	0	3	0	1	0.2	88	0	0	0	0	96
	8A5S348	3	0	0	2	0	1	0.2	87	0	0	0	0	94
	8A5S342	3	0	0	3	0	2	0.3	83	0	0	0	0	92
RF 008	8A5S367	2	0	0	2	0	1	0.2	89	0	0	0	0	95
	8A5S378	2	0	0	2	0	1	0.2	87	0	0	0	0	93
	8A5S365	3	0	0	2	0	1	0.2	86	0	0	0	0	92
	8A5S360	2	0	0	2	0	1	0.2	89	0	0	0	0	95
	8A5S376	4	1	0	3	0	1	0.3	81	0	0	0	0	94
	8A5S362	3	0	0	2	0	1	0.2	87	0	0	0	0	93
	8A5S363	3	0	0	2	0	1	0.2	87	0	0	0	0	93
	8A5S368	2	0	0	2	0	1	0.2	89	0	0	0	0	95
RF 009	8A5S394	2	0	0	4	0	2	0.5	88	0	0	0	0	97
RF 010	8A5S330	3	0	0	3	0	1	0.2	86	0	0	0	0	94
	8A5S336	3	0	0	3	0	1	0.2	85	0	0	0	0	93
	8A5S329	4	0	0	3	0	1	0.2	82	0	0	0	0	93

APPENDIX E: 2. CORRELATION COEFFICIENT DIAGRAMS OF THE CHEMISTRY OF THE FIVE SATELLITE AREAS.

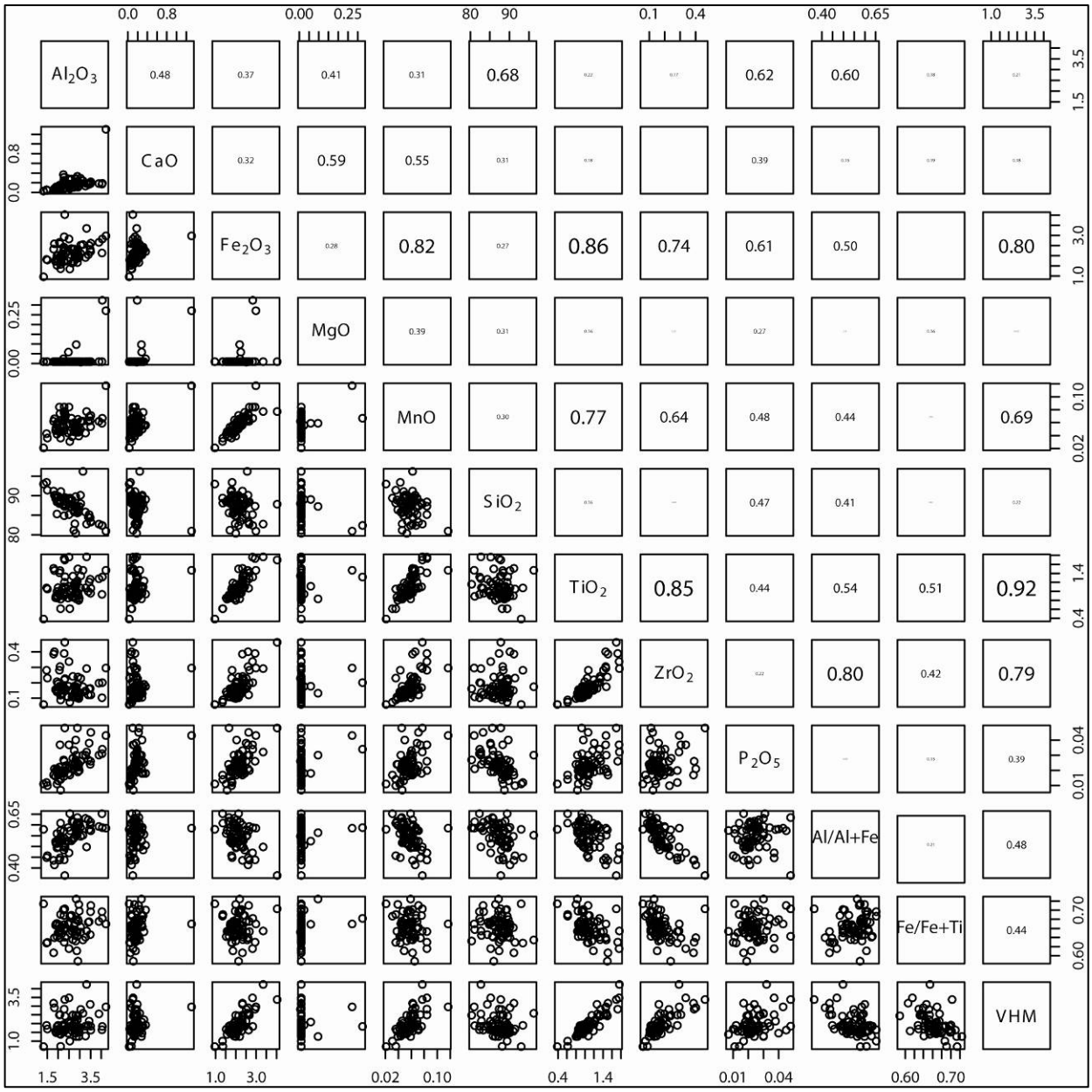

Figure E1. Correlation coefficient diagram of the major element chemistry of Rietfontein as determined with XRF. n=70

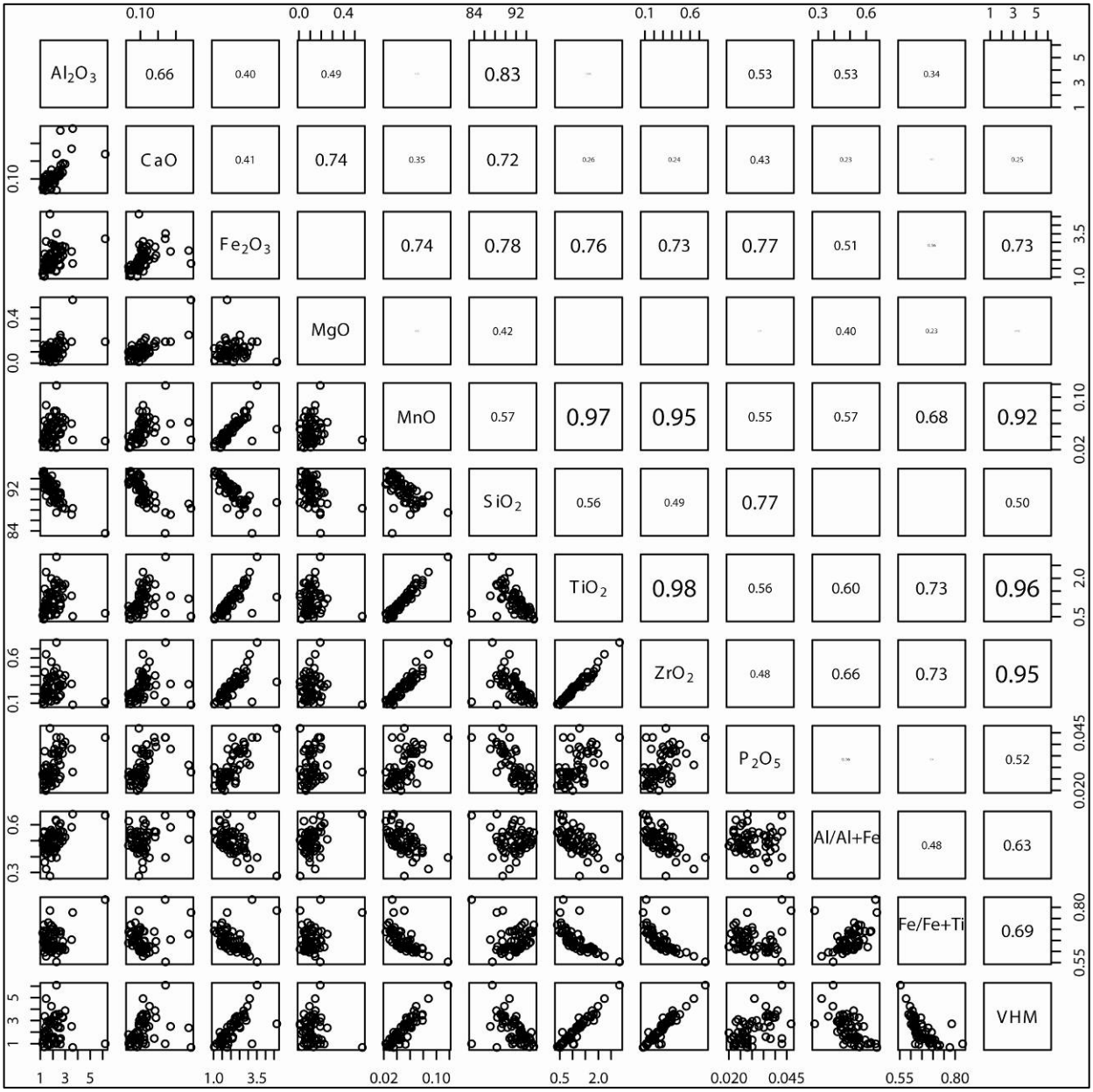

Figure E2. Correlation coefficient diagram of the major element chemistry of Houtkraal Remainder Portion 2 as determined with XRF. n=60

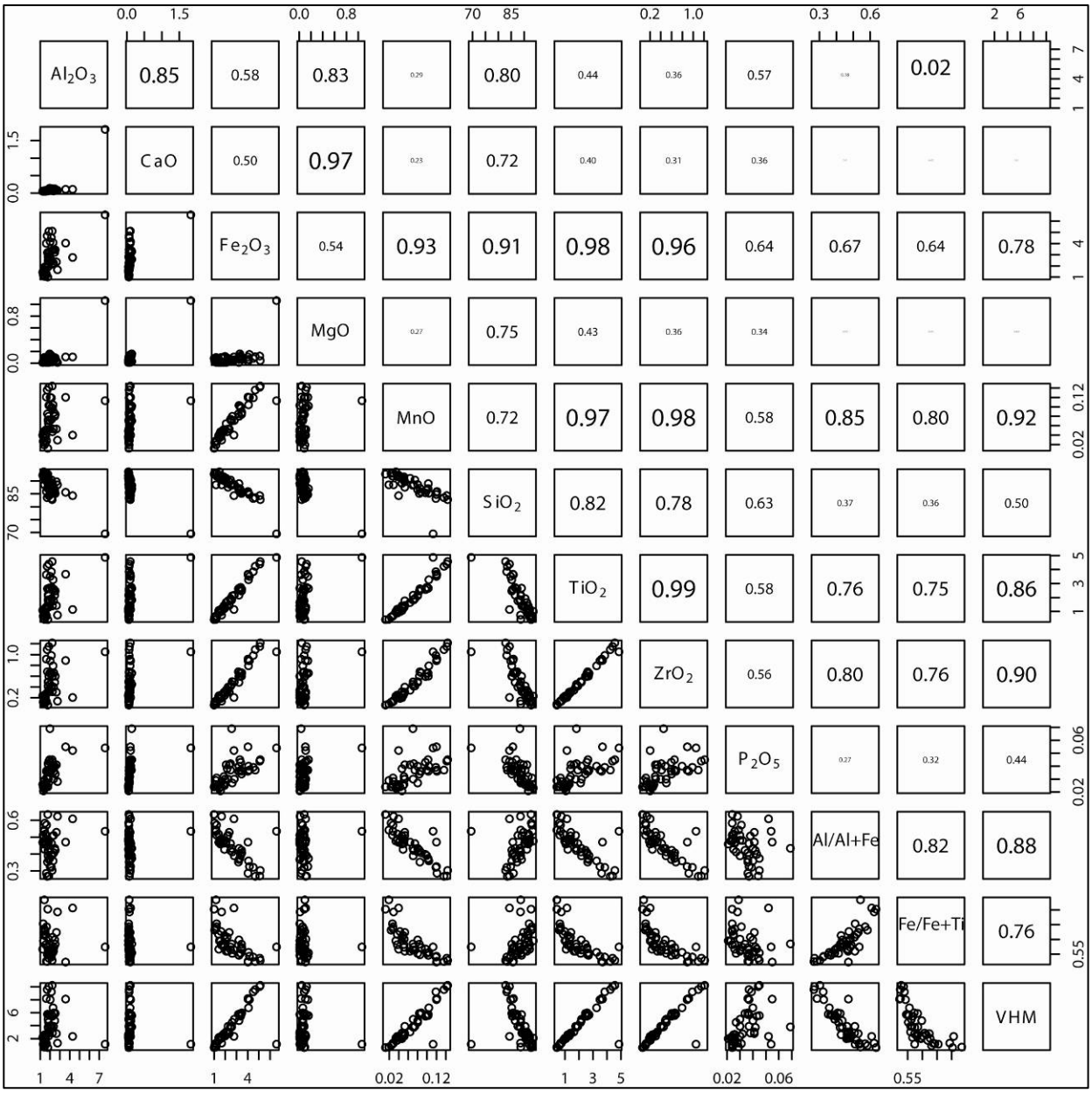

Figure E3. Correlation coefficient diagram of the major element chemistry of Houtkraal Remainder as determined with XRF. n= 44

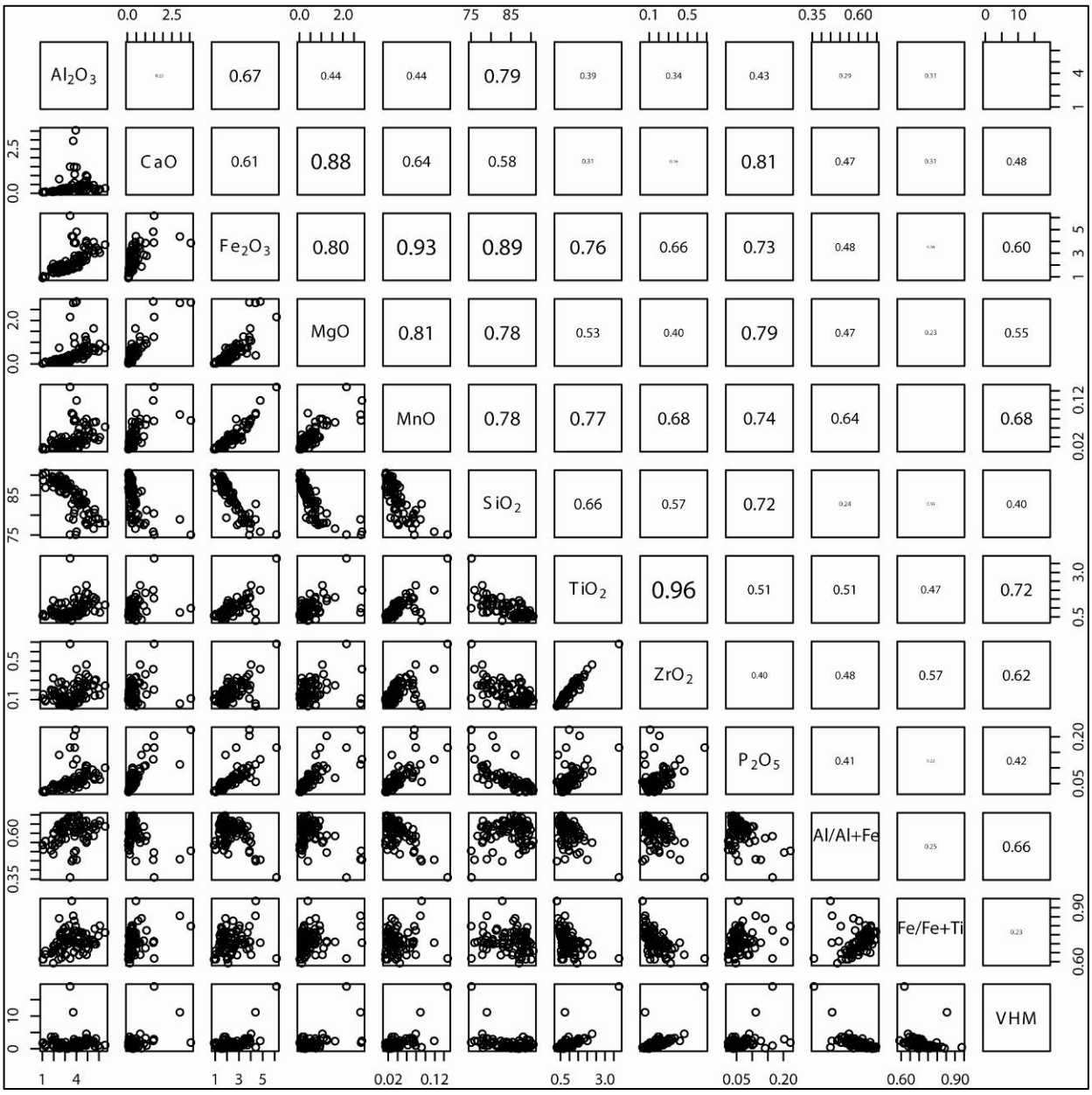

Figure E4. Correlation coefficient diagram of the major element chemistry of Geelwal Karoo as determined with XRF. n=86

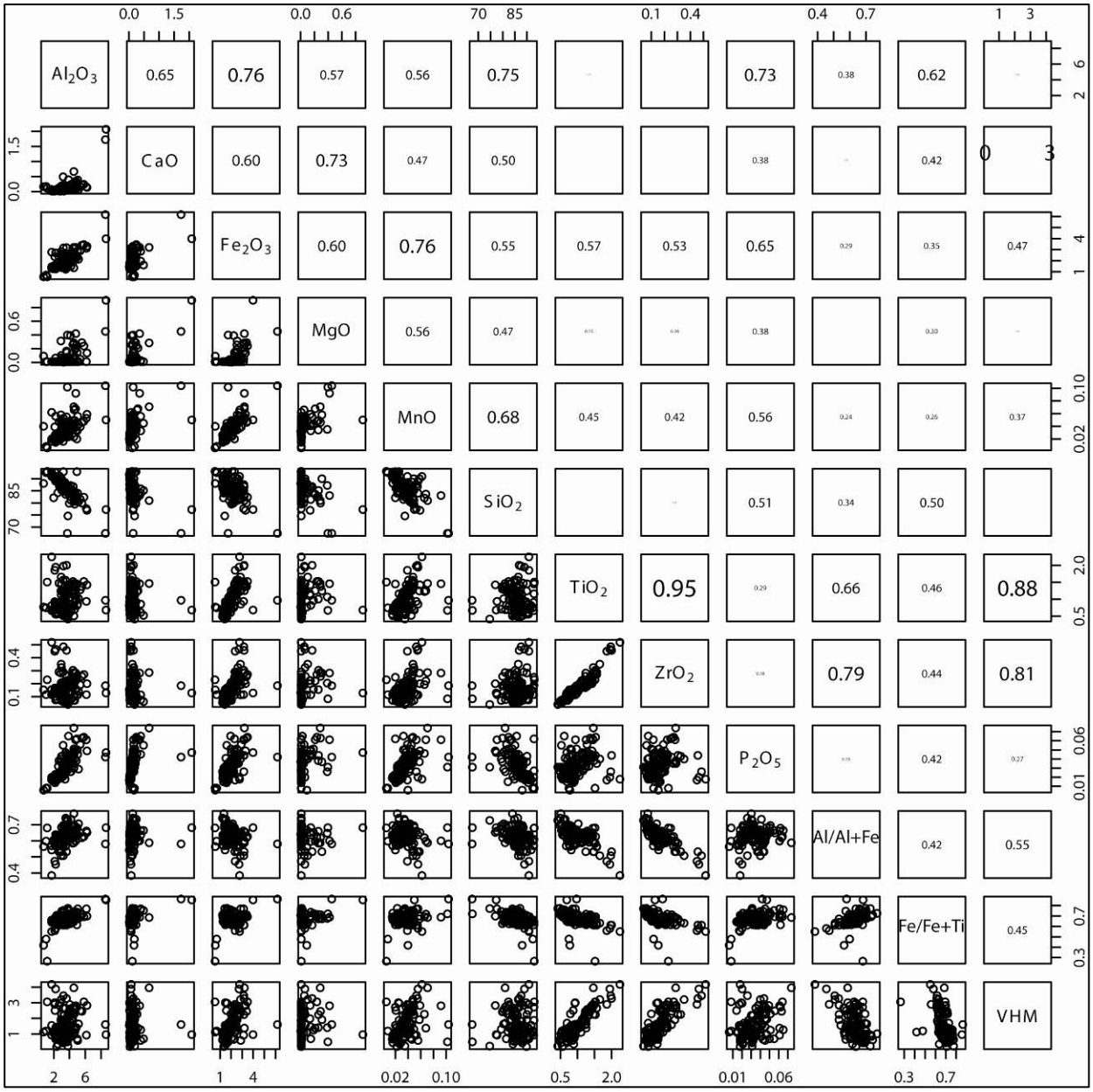

Figure E5. Correlation coefficient diagram of the major element chemistry of Graauwduinen as determined with XRF. n=121

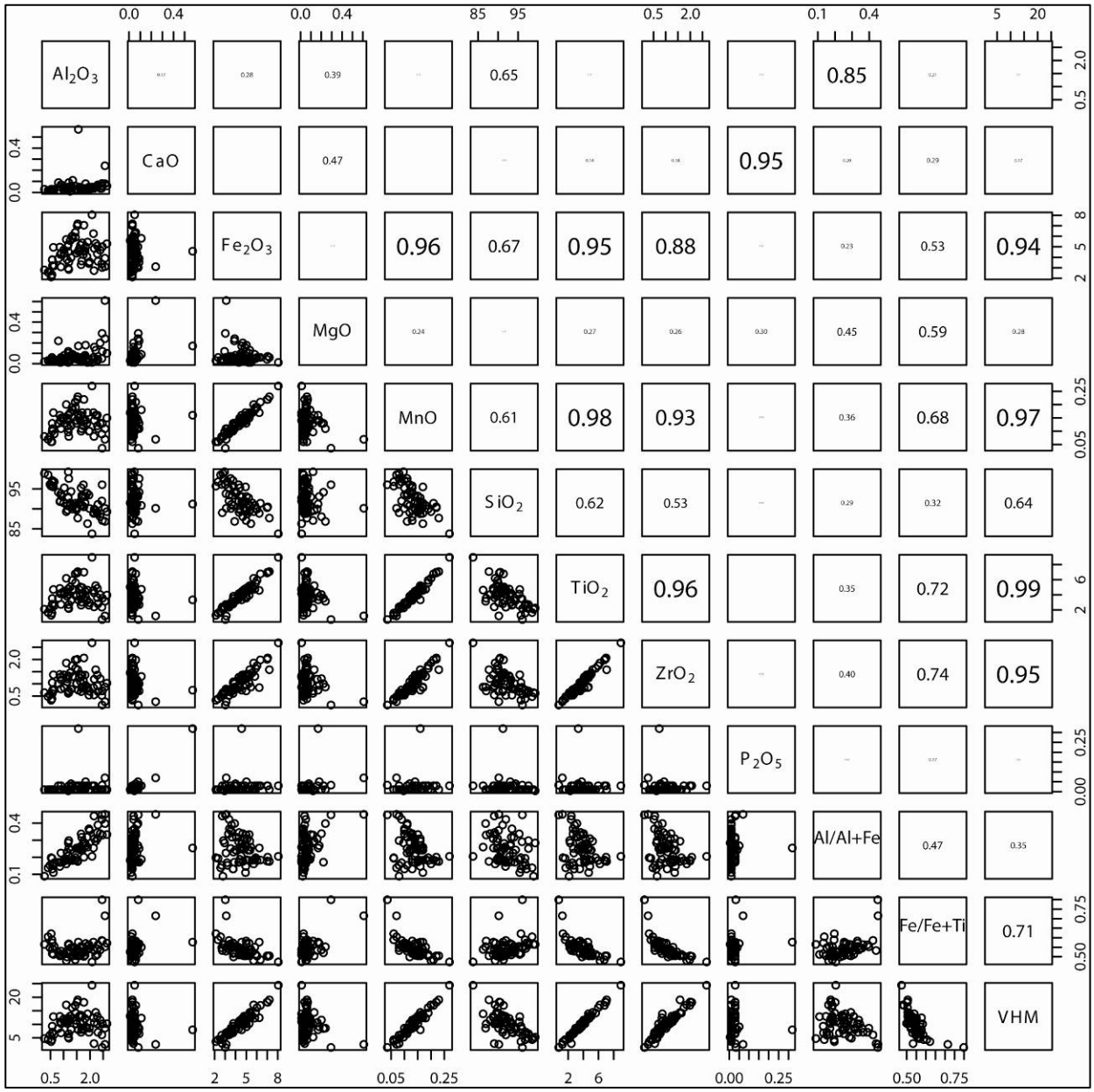

Figure E6: Correlation coefficient diagram of the major element chemistry of the East mine as determined with XRF. n=103

Figure E7. Correlation coefficient diagram of the major element chemistry of the West Mine as determined with XRF. n=152

APPENDIX F:
HEAVY MINERAL CHEMISTRY DETERMINED WITH SEM AND LA-ICP-MS ANALYSES

Table F1. Unaltered ilmenite

Table F2. Ferrian Ilmenite

Table F3A and F3B. Zircon

Table F4A and F4B. Rutile

Table F5. Titanohematite

Table F6. Hematite

Table F7. Magnetite

Table F8. Spinel

Table F9. Garnet

Table F10. Pyroxene

Table F11. Tourmaline

Table F12. Aluminosilicates

Table F13. Staurolite

Table F14. Epidote

Table F15. Sphene

Table F16. Corundum

Table F17. Monazite

Table F18. Altered Ilmenite

Table F19. Amorphous coating of heavy minerals

Table F20. Amorphous coating of ilmenite

Iron is presented as FeO and represents the total iron ($FeO + Fe_2O_3$). Fe_2O_3 was calculated making use of the Method of Droop (1987). The equation used for this purpose is: $F= 2X (1-T/S)$ where T indicates the ideal number of cations per formula unit and S is the observed cation total per X oxygens calculated assuming all iron to be Fe^{2+} (Droop, 1987). This

equation can be used for any silicate mineral or ferromagnesian oxide with all iron initially as Fe^{2+}. The new FeO wt% and Fe_2O_3 wt% are calculated by the following formulas, wt% FeO= old wt% FeO * Fe^{2+}/ (Fe^{2+} +Fe^{3+}) and for Fe^{3+}: wt% Fe_2O_3 = 1.1113 * old wt% FeO *Fe^{3+}/ (Fe^{2+}+Fe^{3+}).

TABLE F1

SEM ANALYSIS OF ILMENITE (in wt %)

HOUTKRAAL REMAINDER PORTION 2

Sample	SiO_2	TiO_2	Al_2O_3	Cr_2O_3	Fe_2O_3	FeO	MgO	CaO	V_2O_5	MnO	ZnO	Total
1	0.00	49.38	0.00	0.00	5.70	41.27	0.39	0.00	1.41	0.51	0.00	98.66
2	0.00	48.72	0.00	0.00	4.66	39.22	0.00	0.00	0.47	3.95	0.00	97.01
3	0.23	49.48	0.00	0.00	4.37	39.77	0.42	0.00	1.80	1.69	0.00	97.77
4	0.14	49.29	0.05	0.00	5.32	40.91	0.02	0.00	0.42	2.88	0.11	99.15
5	0.15	48.88	0.12	0.00	5.23	38.05	0.00	0.03	0.46	5.16	1.69	99.76
6	0.02	49.65	0.02	0.00	4.37	43.38	0.00	0.01	0.53	0.55	0.00	98.51
7	0.02	50.15	0.11	0.00	2.76	44.14	0.00	0.02	0.31	0.31	0.27	98.10
8	0.01	49.86	0.03	0.03	5.31	42.86	0.59	0.03	0.30	0.44	0.07	99.53
9	0.00	50.26	0.00	0.02	4.41	43.98	0.20	0.00	0.27	0.52	0.00	99.65
10	0.06	50.01	0.20	0.00	5.74	41.20	1.11	0.00	0.75	0.46	0.10	99.63
11	0.00	50.12	0.00	0.03	4.99	42.10	0.17	0.00	0.91	1.40	0.09	99.80
12	0.02	49.86	0.06	0.02	4.44	42.40	0.14	0.02	0.79	0.96	0.09	98.81
13	0.05	49.70	0.00	0.00	5.13	40.61	0.10	0.01	0.62	3.12	0.00	99.33
14	0.14	50.14	0.01	0.02	5.48	42.37	0.22	0.01	1.22	0.79	0.06	100.45
15	0.08	50.90	0.06	0.00	2.74	41.83	0.12	0.02	0.61	2.78	0.12	99.27
16	0.08	50.61	0.06	0.01	2.37	43.27	0.35	0.05	0.65	0.60	0.07	98.11
17	0.02	50.56	0.05	0.05	3.94	43.52	0.45	0.03	0.36	0.49	0.13	99.59
18	0.09	50.14	0.15	0.03	4.78	42.58	0.53	0.02	0.61	0.49	0.10	99.51
19	0.09	49.65	0.01	0.00	5.06	41.45	0.12	0.00	0.87	1.88	0.09	99.22
average	**0.06**	**49.86**	**0.05**	**0.01**	**4.57**	**41.84**	**0.26**	**0.01**	**0.70**	**1.52**	**0.16**	

SEM ANALYSIS OF ILMENITE (in wt %)

HOUTKRAAL REMAINDER

Sample	SiO_2	TiO_2	Al_2O_3	Cr_2O_3	Fe_2O_3	FeO	MgO	CaO	V_2O_5	MnO	ZnO	Total
1	0.00	51.42	0.00	0.00	0.00	42.71	0.58	0.00	0.00	2.10	0.00	96.81
average	**0.00**	**51.42**	**0.00**	**0.00**	**0.00**	**42.71**	**0.58**	**0.00**	**0.00**	**2.10**	**0.00**	

SEM ANALYSIS OF ILMENITE (in wt %)

GEELWAL KAROO

Sample	SiO_2	TiO_2	Al_2O_3	Cr_2O_3	Fe_2O_3	FeO	MgO	CaO	V_2O_5	MnO	ZnO	Total
1	0.00	49.99	0.00	0.00	3.57	44.54	0.00	0.00	0.00	0.46	0.00	98.56
2	0.03	50.31	0.04	0.02	3.71	42.86	0.31	0.00	0.19	1.52	0.12	99.10
3	0.05	50.39	0.14	0.02	4.11	42.73	0.11	0.02	0.78	1.01	0.00	99.36
4	0.09	50.57	0.05	0.01	3.80	42.10	0.18	0.02	0.57	2.21	0.16	99.78
5	0.06	49.96	0.10	0.00	4.15	40.73	0.04	0.00	0.59	3.15	0.03	98.80
6	0.06	51.22	0.03	0.00	1.44	42.69	0.00	0.03	0.41	2.74	0.17	98.78
7	0.10	49.58	0.07	0.00	5.55	42.57	0.38	0.04	0.61	0.48	0.00	99.37
8	0.00	50.00	0.00	0.02	4.19	42.66	0.08	0.00	0.77	1.06	0.10	98.89
9	0.00	49.84	0.03	0.00	5.14	42.53	0.74	0.01	0.35	0.47	0.00	99.11
10	0.12	50.14	0.00	0.06	4.58	41.09	0.22	0.00	0.67	2.72	0.02	99.63
11	0.09	49.42	0.07	0.00	5.77	41.52	0.76	0.00	0.87	0.37	0.00	98.87
12	0.02	49.79	0.11	0.00	5.48	41.88	0.78	0.02	0.75	0.31	0.05	99.18
13	0.00	51.09	0.03	0.00	0.94	43.45	0.08	0.04	0.25	1.87	0.24	97.99

TABLE F1 continued

SEM ANALYSIS OF ILMENITE (in wt %)

GEELWAL KAROO

Sample	SiO_2	TiO_2	Al_2O_3	Cr_2O_3	Fe_2O_3	FeO	MgO	CaO	V_2O_5	MnO	ZnO	Total
14	0.17	50.59	0.00	0.04	3.89	41.95	1.22	0.00	0.78	0.46	0.00	99.10
15	0.09	50.30	0.11	0.00	4.12	42.75	0.63	0.01	0.62	0.53	0.13	99.29
16	0.06	50.36	0.05	0.00	3.82	42.27	0.20	0.00	0.52	1.91	0.06	99.26
17	0.08	49.22	0.00	0.00	5.68	41.82	0.02	0.03	0.53	1.78	0.11	99.28
18	0.00	49.61	0.04	0.00	4.54	40.58	0.00	0.00	0.42	3.38	0.03	98.59
19	0.12	49.54	0.01	0.01	3.80	42.23	0.11	0.00	0.57	1.45	0.04	97.88
20	0.04	48.40	0.02	0.00	5.33	42.79	0.00	0.06	0.00	0.74	0.00	97.39
20	0.07	47.93	0.00	0.00	6.50	42.16	0.03	0.08	0.00	1.00	0.00	97.76
20	0.12	48.62	0.02	0.08	3.64	42.52	0.16	0.00	0.00	0.95	0.00	96.11
20	0.12	49.48	0.06	0.04	1.29	43.39	0.06	0.00	0.00	0.97	0.00	95.42
21	0.12	48.20	0.04	0.07	4.92	42.53	0.10	0.05	0.00	0.60	0.00	96.63
21	0.11	52.91	0.14	0.07	0.00	38.52	0.15	0.04	0.00	0.44	0.00	92.38
21	0.19	51.48	0.15	0.08	0.00	39.98	0.14	0.12	0.00	0.86	0.00	93.02
average	**0.06**	**50.10**	**0.05**	**0.01**	**4.12**	**42.26**	**0.31**	**0.01**	**0.54**	**1.47**	**0.07**	**98.99**

SEM ANALYSIS OF ILMENITE (in wt %)

GRAAUWDUINEN

Sample	SiO_2	TiO_2	Al_2O_3	Cr_2O_3	Fe_2O_3	FeO	MgO	CaO	V_2O_5	MnO	ZnO	Total
1	0.00	49.38	0.00	0.00	2.94	44.44	0.00	0.00	0.00	0.00	0.00	96.76
2	0.00	48.08	0.00	0.00	5.40	39.61	0.00	0.00	0.00	3.68	0.00	96.77
3	0.00	48.24	0.00	0.00	4.64	37.21	0.00	0.00	0.00	6.17	0.00	96.26
4	0.07	51.27	0.09	0.27	4.46	42.79	0.22	0.05	1.11	0.84	0.18	101.35
5	0.04	49.52	0.12	0.00	8.52	41.96	0.67	0.02	0.67	0.42	0.06	102.00
6	0.02	49.05	0.09	0.00	9.60	42.21	0.40	0.00	0.49	0.59	0.00	102.45
7	0.10	50.00	0.00	0.02	7.14	42.51	0.00	0.01	0.48	1.96	0.27	102.49
8	0.09	49.55	0.05	0.00	8.34	42.71	0.15	0.00	0.37	1.24	0.00	102.51
9	0.00	47.43	0.07	0.00	12.34	40.60	0.03	0.00	0.71	1.26	0.01	102.46
10	0.16	49.56	0.03	0.02	8.78	41.89	0.89	0.00	0.67	0.47	0.04	102.51
11	0.09	51.54	0.10	0.06	2.56	43.38	0.09	0.00	0.37	2.08	1.77	102.03
average	**0.05**	**49.42**	**0.05**	**0.03**	**6.79**	**41.76**	**0.22**	**0.01**	**0.44**	**1.70**	**0.21**	

SEM ANALYSIS OF ILMENITE (in wt %)

RIETFONTEIN

Sample	SiO_2	TiO_2	Al_2O_3	Cr_2O_3	Fe_2O_3	FeO	MgO	CaO	V_2O_5	MnO	ZnO	Total
1	0.00	48.75	0.00	0.00	5.07	42.08	0.00	0.00	0.00	1.82	0.00	97.72
2	0.21	49.18	0.00	0.00	3.62	42.50	0.00	0.12	0.57	1.05	0.00	97.25
3	0.00	49.67	0.00	0.00	3.10	41.92	0.00	0.00	0.69	1.78	0.00	97.15
4	0.06	50.44	0.09	0.00	4.12	44.41	0.02	0.06	0.46	1.88	0.11	101.64
5	0.10	51.00	0.06	0.00	5.01	43.48	0.59	0.03	0.88	0.87	0.11	102.13
6	0.06	51.40	0.07	0.15	2.97	44.75	0.20	0.01	0.53	1.61	0.10	101.85
7	0.11	49.79	0.07	0.00	5.72	43.67	0.18	0.05	0.48	1.81	0.11	101.99
8	0.15	49.85	0.02	0.01	5.97	43.83	0.32	0.00	0.45	1.34	0.00	101.94
9	0.09	50.28	0.05	0.00	5.69	43.04	0.23	0.00	1.15	1.14	0.20	101.88
10	0.00	50.60	0.08	0.00	4.36	43.17	0.78	0.00	0.53	0.32	0.07	99.90
11	0.11	50.23	0.08	0.00	4.64	43.76	0.23	0.00	0.44	0.41	0.00	99.90
12	0.00	50.90	0.07	0.05	4.86	42.48	0.28	0.00	0.59	1.78	0.00	101.02
13	0.04	51.09	0.13	0.00	5.13	43.64	0.29	0.00	0.54	0.86	0.00	101.71
average	**0.07**	**50.24**	**0.06**	**0.02**	**4.64**	**43.29**	**0.24**	**0.02**	**0.56**	**1.28**	**0.05**	

TABLE F2

SEM ANALYSIS OF FERRIAN ILMENITE (in wt %)

HOUTKRAAL REMAINDER PORTION2

Sample	SiO_2	TiO_2	Al_2O_3	Cr_2O_3	Fe_2O_3	FeO	MgO	CaO	V_2O_5	MnO	ZnO	Total
1	0.00	47.81	0.00	0.00	6.20	41.31	0.00	0.00	0.93	0.46	0.00	97.77
2	0.08	47.79	0.07	0.00	7.68	41.07	0.12	0.00	0.55	1.17	0.04	98.40
3	0.00	48.43	0.11	0.00	7.17	40.78	0.68	0.03	0.61	0.56	0.02	99.15
4	0.06	49.45	0.14	0.00	6.07	42.74	0.28	0.00	0.41	0.55	0.00	99.76
5	0.07	49.21	0.04	0.00	6.04	41.56	0.25	0.04	0.89	1.02	0.00	98.51
6	0.03	48.47	0.02	0.00	6.92	42.43	0.04	0.00	0.41	0.65	0.18	99.53
7	0.04	48.51	0.02	0.00	7.44	41.98	0.31	0.00	0.53	0.50	0.00	99.65
8	0.11	48.65	0.02	0.00	6.02	42.20	0.02	0.00	0.38	1.15	0.00	100.13
9	0.06	49.40	0.08	0.00	6.62	42.64	0.32	0.00	0.59	0.40	0.02	99.25
10	0.00	48.91	0.11	0.00	7.33	41.00	1.11	0.00	0.36	0.42	0.00	99.74
11	0.01	49.05	0.00	0.00	6.62	39.89	0.07	0.04	0.46	3.50	0.10	99.92
12	0.03	49.26	0.08	0.00	7.19	41.16	1.01	0.00	0.62	0.46	0.11	98.81
13	0.12	45.42	0.07	0.02	12.33	39.49	0.00	0.03	0.42	1.15	0.01	98.92
14	0.10	48.59	0.01	0.02	6.42	42.73	0.05	0.00	0.26	0.70	0.03	99.38
15	0.05	48.17	0.11	0.03	8.74	40.21	0.86	0.00	0.91	0.29	0.00	99.81
16	0.06	49.32	0.05	0.00	6.45	42.30	0.54	0.00	0.60	0.48	0.01	99.76
17	0.04	48.71	0.06	0.00	7.62	41.66	0.49	0.00	0.56	0.55	0.06	98.82
18	0.03	48.58	0.07	0.00	6.57	42.20	0.00	0.05	0.32	0.96	0.03	99.27
19	0.08	48.30	0.18	0.00	8.05	41.16	0.38	0.00	0.86	0.27	0.04	98.11
20	0.07	49.02	0.08	0.00	6.13	42.73	0.05	0.01	0.36	0.77	0.03	99.59
21	0.13	49.18	0.01	0.00	6.25	41.41	1.01	0.00	0.53	0.52	0.01	99.00
average	**0.06**	**48.58**	**0.06**	**0.00**	**7.14**	**41.56**	**0.36**	**0.01**	**0.55**	**0.79**	**0.03**	

SEM ANALYSIS OF FERRIAN ILMENITE (in wt %)

HOUTKRAAL REMAINDER

Sample	SiO_2	TiO_2	Al_2O_3	Cr_2O_3	Fe_2O_3	FeO	MgO	CaO	V_2O_5	MnO	ZnO	Total
1	0.06	48.10	0.13	0.04	9.96	41.48	0.03	0.01	0.69	0.93	0.00	101.44
2	0.06	49.31	0.08	0.00	7.91	43.29	0.15	0.00	0.24	0.53	0.13	101.69
3	0.07	47.43	0.09	0.00	11.34	40.49	0.44	0.00	0.78	0.55	0.01	101.19
4	0.07	48.48	0.08	0.00	9.28	41.58	0.20	0.01	0.85	0.61	0.00	101.15
5	0.05	47.49	0.12	0.02	11.14	41.35	0.19	0.03	0.42	0.54	0.01	101.36
6	0.07	48.95	0.07	0.06	8.52	42.28	0.23	0.01	0.57	0.56	0.03	101.36
7	0.06	48.85	0.05	0.00	8.75	42.27	0.43	0.02	0.52	0.33	0.00	101.28
8	0.05	48.52	0.05	0.00	8.84	41.54	0.52	0.01	0.57	0.52	0.05	100.66
9	0.10	44.68	0.00	0.03	12.69	38.70	0.06	0.00	0.36	1.45	2.00	100.06
10	0.13	47.63	0.08	0.00	7.42	32.23	0.05	0.03	0.26	10.14	1.25	99.22
11	0.17	49.05	0.03	0.00	7.75	38.35	0.13	0.04	0.44	5.10	0.11	101.19
12	0.01	48.24	0.00	0.00	8.81	42.09	0.00	0.00	0.40	0.96	0.12	100.64
13	0.11	48.71	0.02	0.01	7.37	42.21	0.09	0.00	0.31	1.21	0.26	100.30
14	0.10	49.70	0.04	0.00	7.30	42.09	0.20	0.02	1.20	0.68	0.07	101.42
15	0.00	48.17	0.16	0.01	9.46	41.35	0.16	0.00	0.43	0.98	0.03	100.75
16	0.01	49.34	0.07	0.01	7.35	43.29	0.15	0.00	0.27	0.42	0.06	100.97
17	0.18	49.60	0.02	0.01	6.76	42.48	0.72	0.00	0.47	0.46	0.00	100.70
18	0.07	48.96	0.00	0.00	8.01	42.22	0.00	0.00	0.52	1.32	0.00	101.09
19	0.13	48.09	0.08	0.00	10.34	40.89	0.82	0.00	0.69	0.23	0.00	101.28
20	0.12	49.75	0.08	0.00	6.33	40.89	0.15	0.00	0.40	3.07	0.31	101.10
21	0.04	48.64	0.05	0.00	8.17	41.66	0.40	0.01	0.69	0.53	0.00	100.18

TABLE F2 continued

SEM ANALYSIS OF FERRIAN ILMENITE (in wt %)

HOUTKRAAL REMAINDER

Sample	SiO_2	TiO_2	Al_2O_3	Cr_2O_3	Fe_2O_3	FeO	MgO	CaO	V_2O_5	MnO	ZnO	Total
22	0.03	48.88	0.08	0.00	8.50	41.88	0.33	0.02	0.63	0.64	0.08	101.07
23	0.12	48.97	0.03	0.00	8.87	40.67	1.32	0.00	0.61	0.45	0.05	101.09
24	0.12	47.91	0.12	0.00	9.52	41.86	0.11	0.00	0.47	0.51	0.41	101.03
25	0.00	49.37	0.11	0.00	6.99	41.53	0.08	0.08	0.47	1.97	0.06	100.64
26	0.07	49.37	0.10	0.00	7.90	41.61	0.15	0.05	1.27	0.68	0.00	101.21
27	0.07	48.97	0.05	0.01	8.44	41.61	0.25	0.00	1.21	0.41	0.00	101.04
28	0.09	49.78	0.04	0.01	6.64	42.65	0.00	0.03	0.47	1.53	0.04	101.27
29	0.07	48.72	0.07	0.02	8.43	41.75	0.20	0.02	0.47	1.12	0.00	100.88
30	0.02	47.11	0.04	0.03	10.58	41.55	0.02	0.03	0.40	0.42	0.45	100.65
31	0.07	48.87	0.00	0.01	8.72	41.72	0.56	0.03	0.71	0.48	0.00	101.16
32	0.14	45.63	0.05	0.05	13.45	39.92	0.09	0.01	0.34	1.01	0.00	100.69
33	0.06	48.35	0.03	0.00	9.47	41.44	0.00	0.00	0.64	1.40	0.09	101.47
34	0.04	47.44	0.00	0.00	10.73	40.31	0.08	0.00	0.49	1.88	0.03	101.01
average	**0.08**	**48.44**	**0.06**	**0.01**	**8.87**	**41.21**	**0.24**	**0.01**	**0.57**	**1.28**	**0.17**	

SEM ANALYSIS OF FERRIAN ILMENITE (in wt %)

GEELWAL KAROO

Sample	SiO_2	TiO_2	Al_2O_3	Cr_2O_3	Fe_2O_3	FeO	MgO	CaO	V_2O_5	MnO	ZnO	Total
1	0.10	48.71	0.15	0.00	6.43	41.36	0.13	0.03	0.41	1.61	0.03	98.96
2	0.09	48.56	0.05	0.00	7.59	41.55	0.77	0.00	0.37	0.39	0.00	99.37
3	0.02	48.21	0.14	0.00	7.59	42.11	0.02	0.01	0.25	0.72	0.27	99.35
4	0.07	48.96	0.17	0.04	7.29	40.60	1.10	0.04	0.55	0.46	0.11	99.39
5	0.00	47.72	0.04	0.00	8.02	40.37	0.13	0.00	0.48	1.73	0.13	98.62
6	0.07	48.20	0.06	0.00	7.37	41.38	0.57	0.00	0.40	0.49	0.06	98.61
7	0.04	47.11	0.02	0.00	10.12	39.37	0.84	0.00	0.90	0.52	0.00	98.93
8	0.04	48.75	0.10	0.00	6.98	40.93	0.94	0.01	0.52	0.47	0.00	98.74
9	0.02	48.22	0.18	0.00	8.61	40.05	0.55	0.00	1.12	0.59	0.13	99.47
10	0.04	48.41	0.05	0.00	7.44	41.88	0.02	0.00	0.49	1.02	0.15	99.50
11	0.03	48.76	0.17	0.00	7.17	42.02	0.27	0.01	0.55	0.37	0.00	99.35
12	0.07	49.03	0.13	0.00	6.43	41.51	0.65	0.02	0.62	0.45	0.06	98.95
13	0.06	48.07	0.09	0.00	7.64	41.67	0.26	0.05	0.39	0.53	0.00	98.76
14	0.06	48.58	0.08	0.00	6.95	41.47	0.61	0.00	0.46	0.52	0.08	98.81
15	0.00	46.99	0.05	0.00	9.05	40.06	0.04	0.00	0.47	1.56	0.08	98.31
16	0.05	48.51	0.07	0.00	6.61	41.60	0.03	0.00	0.06	1.92	0.05	98.89
17	0.10	48.53	0.15	0.00	6.42	41.73	0.29	0.00	0.55	0.55	0.00	98.31
average	**0.05**	**48.31**	**0.10**	**0.00**	**7.51**	**41.16**	**0.42**	**0.01**	**0.51**	**0.82**	**0.07**	

SEM ANALYSIS OF FERRIAN ILMENITE (in wt %)

GRAAUWDUINEN

Sample	SiO_2	TiO_2	Al_2O_3	Cr_2O_3	Fe_2O_3	FeO	MgO	CaO	V_2O_5	MnO	ZnO	Total
1	0.06	48.60	0.00	0.00	8.87	41.08	0.10	0.00	0.23	2.45	0.16	101.55
2	0.07	49.49	0.08	0.01	7.40	43.46	0.08	0.00	0.12	0.78	0.00	101.49
3	0.07	48.86	0.00	0.00	9.32	42.36	0.25	0.01	0.46	0.80	0.00	102.14
4	0.09	49.87	0.05	0.01	8.33	42.02	0.24	0.02	1.38	0.59	0.00	102.60
5	0.05	48.83	0.08	0.00	9.58	42.16	0.12	0.04	0.70	0.65	0.02	102.23
6	0.10	48.33	0.01	0.00	9.14	38.68	0.07	0.04	0.34	4.41	0.07	101.20
7	0.05	49.26	0.08	0.03	8.51	42.74	0.24	0.00	0.53	0.44	0.02	101.90
8	0.04	49.52	0.12	0.00	8.52	41.96	0.67	0.02	0.67	0.42	0.06	102.00
9	0.02	49.05	0.09	0.00	9.60	42.21	0.40	0.00	0.49	0.59	0.00	102.45
10	0.10	50.00	0.00	0.02	7.14	42.51	0.00	0.01	0.48	1.96	0.27	102.49

Table F2 continued

SEM ANALYSIS OF FERRIAN ILMENITE (in wt %)

GRAAUWDUINEN

Sample	SiO_2	TiO_2	Al_2O_3	Cr_2O_3	Fe_2O_3	FeO	MgO	CaO	V_2O_5	MnO	ZnO	Total
11	0.09	49.55	0.05	0.00	8.34	42.71	0.15	0.00	0.37	1.24	0.00	102.51
12	0.00	47.43	0.07	0.00	12.34	40.60	0.03	0.00	0.71	1.26	0.01	102.46
13	0.16	49.56	0.03	0.02	8.78	41.89	0.89	0.00	0.67	0.47	0.04	102.51
14	0.05	49.45	0.00	0.00	8.01	43.03	0.07	0.00	0.52	0.81	0.30	102.24
15	0.14	50.42	0.05	0.00	7.64	42.41	1.07	0.07	0.52	0.40	0.00	102.72
16	0.09	49.51	0.03	0.00	8.32	41.41	0.15	0.00	1.09	1.51	0.04	102.15
17	0.09	49.39	0.05	0.00	9.28	42.68	0.57	0.00	0.42	0.37	0.05	102.90
18	0.02	48.69	0.13	0.02	10.99	39.16	1.77	0.05	0.77	0.38	0.23	102.21
19	0.06	50.01	0.02	0.00	6.95	43.47	0.09	0.06	0.45	0.76	0.01	101.89
20	0.08	48.87	0.16	0.00	10.77	40.63	0.89	0.02	0.91	0.50	0.06	102.91
21	0.12	49.29	0.07	0.00	8.94	41.98	0.72	0.00	0.62	0.41	0.08	102.24
22	0.13	51.10	0.11	0.01	6.68	41.09	1.87	0.00	0.83	0.38	0.00	102.21
23	0.12	51.05	0.11	0.00	6.21	42.44	1.29	0.01	0.57	0.37	0.00	102.16
24	0.10	47.87	0.09	0.00	11.48	40.99	0.00	0.00	0.77	1.27	0.03	102.61
25	0.12	48.44	0.12	0.02	8.06	39.06	0.00	0.04	0.29	4.11	0.10	100.36
26	0.03	49.14	0.05	0.02	9.32	42.15	0.35	0.00	0.62	0.70	0.10	102.46
27	0.04	49.44	0.04	0.00	9.17	42.19	0.67	0.00	0.57	0.47	0.00	102.60
28	0.01	49.45	0.10	0.00	9.35	40.80	1.30	0.01	0.61	0.53	0.00	102.16
29	0.14	49.76	0.00	0.03	7.00	43.28	0.40	0.00	0.28	0.62	0.14	101.66
30	0.05	49.99	0.10	0.00	7.50	42.09	0.03	0.00	0.28	2.39	0.00	102.44
31	0.06	49.59	0.07	0.00	7.94	42.06	0.00	0.05	0.20	2.28	0.10	102.34
32	0.10	48.77	0.10	0.00	8.47	40.87	1.01	0.01	0.68	0.31	0.00	100.32
33	0.00	46.79	0.02	0.00	12.31	40.50	0.39	0.00	0.45	0.65	0.06	101.17
34	0.00	49.21	0.03	0.00	9.07	40.98	0.13	0.05	0.94	1.80	0.00	102.21
35	0.08	50.53	0.17	0.00	6.41	43.31	0.12	0.00	0.74	0.70	0.02	102.08
36	0.07	48.69	0.09	0.00	9.95	40.93	0.80	0.03	0.71	0.56	0.10	101.93
37	0.12	50.32	0.03	0.05	6.24	43.56	0.29	0.04	0.48	0.56	0.00	101.69
average	**0.07**	**49.30**	**0.06**	**0.01**	**8.70**	**41.77**	**0.47**	**0.02**	**0.58**	**1.05**	**0.06**	

SEM ANALYSIS OF FERRAIN ILMENITE (in wt %)

RIETFONTEIN

Sample	SiO_2	TiO_2	Al_2O_3	Cr_2O_3	Fe_2O_3	FeO	MgO	CaO	V_2O_5	MnO	ZnO	Total
1	0.05	49.73	0.11	0.00	7.13	42.81	0.63	0.02	0.56	0.38	0.07	101.51
2	0.04	50.37	0.11	0.00	6.75	42.63	1.00	0.00	0.47	0.48	0.16	102.00
3	0.03	48.52	0.08	0.04	9.09	42.57	0.08	0.00	0.56	1.12	0.18	102.27
4	0.08	50.74	0.18	0.00	6.33	42.67	0.96	0.03	0.63	0.55	0.16	102.33
5	0.00	49.66	0.05	0.00	7.72	43.39	0.37	0.00	0.41	0.43	0.11	102.14
6	0.07	49.39	0.04	0.00	6.82	43.16	0.31	0.00	0.60	1.82	0.00	102.19
7	0.03	48.86	0.01	0.00	8.84	42.09	0.61	0.00	0.66	0.64	0.06	101.82
8	0.04	48.49	0.15	0.00	8.40	41.96	0.18	0.08	0.75	1.04	0.08	101.18
9	0.07	49.32	0.17	0.03	8.32	42.94	0.23	0.00	0.53	0.55	0.13	102.29
10	0.07	49.51	0.02	0.00	7.76	43.09	0.68	0.00	0.31	0.46	0.00	101.90
11	0.10	48.71	0.13	0.02	10.74	41.35	0.84	0.02	0.77	0.20	0.00	102.87
12	0.13	48.78	0.07	0.04	8.81	42.56	0.16	0.00	0.71	0.36	0.20	101.81
13	0.02	49.01	0.07	0.00	8.25	43.36	0.06	0.03	0.46	0.62	0.00	101.88
14	0.08	46.29	0.08	0.00	12.31	41.03	0.00	0.00	0.64	0.83	0.08	101.35

TABLE F2 continued

SEM ANALYSIS OF FERRIAN ILMENITE (in wt %)

RIETFONTEIN

Sample	SiO_2	TiO_2	Al_2O_3	Cr_2O_3	Fe_2O_3	FeO	MgO	CaO	V_2O_5	MnO	ZnO	Total
15	0.04	49.48	0.05	0.00	8.27	42.79	0.12	0.00	1.09	0.56	0.06	102.46
16	0.10	49.20	0.08	0.00	8.50	42.90	0.39	0.00	0.56	0.45	0.00	102.18
17	0.06	48.30	0.09	0.00	9.70	41.93	0.48	0.01	0.58	0.55	0.00	101.71
18	0.13	48.68	0.00	0.00	7.51	43.27	0.01	0.01	0.56	1.54	0.00	101.71
19	0.11	49.20	0.11	0.00	8.23	42.66	0.11	0.02	0.43	0.94	0.00	101.80
20	0.07	49.28	0.11	0.00	8.68	41.47	0.93	0.02	0.46	0.57	0.19	101.79
21	0.07	49.18	0.14	0.00	8.67	41.90	0.68	0.05	0.51	0.33	0.02	101.54
22	0.00	50.05	0.05	0.00	6.12	43.06	0.20	0.00	0.50	0.87	0.00	100.85
23	0.06	49.08	0.07	0.00	7.27	39.20	0.05	0.00	0.35	4.39	0.00	100.47
24	0.06	47.82	0.10	0.00	10.57	41.45	0.13	0.02	0.34	1.01	0.00	101.49
25	0.10	48.85	0.12	0.00	8.12	41.89	0.29	0.00	0.81	0.43	0.00	100.60
26	0.02	49.63	0.07	0.00	6.27	41.33	0.12	0.00	0.24	2.71	0.27	100.65
27	0.08	49.51	0.09	0.00	6.77	41.45	0.53	0.00	0.47	1.46	0.07	100.43
28	0.08	48.88	0.03	0.00	8.16	42.11	0.07	0.05	0.37	1.34	0.00	101.10
average	**0.06**	**49.09**	**0.08**	**0.00**	**8.22**	**42.25**	**0.36**	**0.01**	**0.55**	**0.95**	**0.07**	

TABLE F3A

LA-ICP-MS ANALYSIS OF ZIRCON (in ppm)

HOUTKRAAL REMAINDER PORTION 2

Sample	Mg	Al	P	K	Ca	Sc	Ti	Mn	Fe	Y	Hf	Pb	Th	U	U+Th
1	14	168	206	1090	296	116	466	2	13	1196	11053	6	95	207	302
2	1	76	240	22	171	103	440	1	42	811	15226	11	175	674	849
3	1	3	270	4	153	106	620	3	151	1098	10842	1	48	60	108
4	0	14	157	4	153	111	489	0	4	313	10811	1	16	63	79
5	0	15	478	4	153	141	432	0	3	1149	12040	4	77	128	205
6	0	29	280	28	153	125	458	2	6240	789	11162	4	36	94	130
7	0	158	256	166	153	112	454	1	3	692	11358	1	27	42	68
8	39	1960	792	241	340	186	2878	5	920	2073	11100	12	106	381	487
9	6	5	171	10	153	128	424	0	4	473	14381	5	52	160	211
10	0	1	145	4	153	77	419	0	3	1408	12990	6	101	272	373
11	24	746	311	189	153	110	573	3	398	1040	11717	6	82	124	206
12	1	11	202	4	153	106	439	0	11	691	12696	11	107	175	282
13	8	25	207	31	372	126	446	1	740	746	13199	11	174	454	628
14	1	3	71	11	153	95	412	0	3	300	13186	5	85	271	357
15	4	105	881	4	153	277	478	0	14	1735	11742	14	162	250	412
16	2	3	203	9	153	92	443	1	6	714	11922	7	93	387	480
17	45	70	496	46	153	235	442	1	84	1026	12591	31	120	161	281
18	90	1420	309	288	218	125	459	2	1001	4650	16521	18	1439	2145	3583
19	18	152	1091	23	153	334	528	1	209	2470	15907	9	131	470	601
20	2	21	209	6	153	93	433	1	29	1103	16191	11	97	346	443
21	1	38	222	4	153	121	467	0	24	1059	12774	5	88	117	205
22	154	865	839	273	153	162	452	6	1961	2449	14191	12	104	346	450
23	3	23	275	5	153	117	412	0	16	702	13152	5	68	323	391
24	3	4	281	10	153	115	422	0	8	675	12819	15	207	240	447
25	37	381	226	95	153	92	471	1	394	856	12148	8	96	386	482
26	2	6	125	6	153	89	448	0	8	649	11035	4	40	238	278
27	1	29	208	4	153	124	484	0	7	430	9672	1	22	30	51
28	0	9	303	4	153	130	496	0	6	1114	12244	9	86	170	256
29	3	94	265	5	153	99	423	1	59	811	10319	4	83	400	483
30	1	35	199	4	153	107	481	0	9	336	8330	8	143	105	248
31	1	120	208	61	153	156	460	0	4	672	10728	3	35	120	155
32	2	1	202	4	153	86	456	0	3	833	11083	4	38	99	137
33	0	2	356	4	153	162	457	0	3	1333	12200	12	211	139	350

TABLE 3A continued

LA-ICP-MS ANALYSIS OF ZIRCON (in ppm)

HOUTKRAAL REMAINDER PORTION 2

Sample	Mg	Al	P	K	Ca	Sc	Ti	Mn	Fe	Y	Hf	Pb	Th	U	U+Th
34	0	97	141	63	153	104	425	0	3	370	13155	7	80	188	267
35	55	250	243	128	153	115	431	3	137	891	10819	12	241	309	550
36	7	12	234	16	153	114	470	1	61	1048	12869	13	116	225	341
37	2348	4604	317	4509	156	122	2651	63	9606	809	10420	10	115	158	274
38	1	7	252	4	153	97	440	0	9	1162	12421	8	61	793	853
39	1	9	253	5	153	118	447	0	5	542	12578	1	10	31	41
40	4	1	125	4	146	90	451	0	3	569	7881	1	15	32	47
41	1	3	252	4	153	112	447	0	3	645	11195	1	25	38	62
42	7	316	486	55	471	129	524	1	160	1040	14091	9	69	275	344
43	3	11	353	5	153	187	429	0	14	1153	12113	4	33	96	129
44	0	1	237	4	153	144	439	0	3	867	11947	2	27	115	142
45	7	421	552	55	157	99	445	4	1429	2348	9034	10	203	250	453
46	2	4	177	6	153	118	442	0	7	613	11886	9	95	185	280
47	0	2	421	4	182	180	475	0	6	1528	11397	5	49	60	109
48	1	3	267	4	153	149	468	0	3	1084	11756	23	226	258	483
49	3	246	216	405	153	116	449	2	51	772	11817	11	189	241	429
50	2135	21011	459	3481	1456	95	2297	80	14419	446	10433	59	102	221	323
51	848	19444	1115	4358	4732	114	2587	99	26346	828	9153	92	48	172	220
52	3	3	710	6	153	109	459	0	8	2162	13821	14	134	384	518
53	2	6	145	7	216	117	447	0	38	602	13230	17	170	452	622
54	8	149	347	154	153	127	445	2	78	1004	12884	7	106	235	341
55	7	10	327	896	209	113	459	0	20	882	12954	12	134	224	358
56	3	9	268	41	153	104	443	1	10	1570	12853	16	67	291	358
57	4	33	332	10	544	243	452	1	50	1544	12485	17	337	781	1118
average	**109**	**985**	**333**	**295**	**282**	**128**	**617**	**5**	**1199**	**1053**	**12078**	**11**	**121**	**265**	**398**

LA-ICP-MS ANALYSIS OF ZIRCON (in ppm)

HOUTKRAAL REMAINDER

Sample	Mg	Al	P	K	Ca	Sc	Ti	Mn	Fe	Y	Hf	Pb	Th	U	U+Th
1	25	1019	1824	914	1097	177	522	8	101	1682	9213	5	67	428	495
2	7	49	575	28	1049	249	510	1	31	817	7796	2	24	43	67
3	16	142	767	105	1049	283	456	1	36	1038	11414	10	203	442	645
4	678	1330	923	943	548	131	733	31	2538	2302	11251	27	276	548	824
5	16	112	492	33	233	136	516	1	69	1174	10405	1	40	50	90
6	7	82	804	37	702	158	463	3	2318	845	12249	10	378	448	826
7	11	63	691	37	191	141	471	1	139	1876	12107	16	188	207	395
8	12	27	337	22	1049	147	466	4	26	658	9905	4	64	203	267
9	1	13	560	29	1049	175	507	4	23	1015	11774	11	104	55	159
10	3272	21894	1049	8934	1049	95	1912	246	12515	521	6227	48	75	54	129
11	13	276	1094	64	226	119	499	1	275	2010	11272	20	204	303	507
12	21	89	457	63	1049	129	508	2	157	1135	10283	8	90	130	220
13	1295	2407	578	1260	6676	111	1533	16	1584	702	13119	28	67	376	444
14	3	11	456	29	1049	141	458	4	23	1257	10369	8	98	175	273
15	3	38	550	22	266	128	584	3	218	1126	10829	9	168	207	375
16	1	374	530	322	1049	200	452	1	4	1366	11901	16	119	235	354

TABLE 3A continued

LA-ICP-MS ANALYSIS OF ZIRCON (in ppm)

HOUTKRAAL REMAINDER

Sample	Mg	Al	P	K	Ca	Sc	Ti	Mn	Fe	Y	Hf	Pb	Th	U	U+Th
17	9	125	1180	29	1049	217	473	2	136	2034	13147	5	92	293	385
18	1	10	326	29	1049	154	477	4	12	920	12261	4	82	201	283
19	12	1991	291	2524	1049	160	472	9	208	894	11138	12	108	118	226
20	24	28	298	20	1049	122	456	1	23	710	9490	5	83	219	302
21	1	24	336	29	1049	131	478	4	10	705	11454	5	55	103	158
22	232	1275	440	1095	3026	118	947	10	1486	917	9232	12	56	78	134
23	1320	14033	1435	9453	6978	106	4158	45	11388	538	8249	21	48	86	134
24	20	318	170	43	1049	89	479	4	52	1850	8819	5	45	85	129
25	119	554	197	271	333	116	508	2	373	589	11729	5	40	89	130
26	9	48	330	20	1049	293	493	1	138	1409	12502	21	221	237	458
average	**16**	**222**	**335**	**89**	**175**	**133**	**545**	**1**	**426**	**1146**	**12586**	**8**	**139**	**314**	**354**

LA-ICP-MS ANALYSIS OF ZIRCON (in ppm)

GEELWAL KAROO

Sample	Mg	Al	P	K	Ca	Sc	Ti	Mn	Fe	Y	Hf	Pb	Th	U	U+Th
1	28	289	706	79	153	255	458	1	280	2021	13178	47	415	376	791
2	11	87	1488	55	2942	136	462	6	117	1298	12555	20	194	308	502
3	6	140	401	17	153	176	472	1	37	1164	14055	9	76	171	247
4	1	5	170	4	153	114	415	0	3	640	14189	10	159	377	536
5	4	17	220	14	153	116	471	0	18	572	13321	7	52	229	281
6	213	1941	591	669	3519	140	883	10	1003	945	11204	34	96	188	283
7	2	13	412	7	456	316	462	1	36	1378	11277	10	145	688	832
8	3	6	79	12	153	81	455	0	15	312	12021	4	63	389	452
9	119	363	258	262	4587	142	598	5	259	649	12861	21	196	239	435
10	56	435	493	281	153	184	572	3	363	1282	11913	5	75	88	163
11	9	44	209	20	369	146	499	1	22	780	13879	7	188	280	467
12	5	71	327	23	226	141	429	0	48	1157	13048	13	208	360	568
13	17	50	906	43	1549	144	488	4	101	1619	11832	22	177	165	342
14	1	9	220	4	153	113	491	0	14	747	11675	6	73	118	192
15	25	18	339	5	153	117	649	0	8	1275	12382	6	56	169	225
16	2	67	729	18	677	110	490	2	3	1111	11778	3	23	51	74
17	1	9	261	4	153	99	432	0	3	943	11566	5	45	164	209
18	0	16	326	4	153	126	438	0	3	958	13309	8	109	214	323
19	119	2451	229	375	217	81	1256	11	3812	984	13036	16	138	370	508
20	1	3	204	7	153	125	496	0	3	797	9591	2	25	79	103
21	1461	6962	763	2392	20241	112	8906	42	2785	1238	7391	135	59	48	107
22	3	6	212	4	153	110	459	0	3	550	12578	7	58	126	185
23	178	2878	645	411	820	165	568	55	1041	1845	16653	28	223	1557	1780
24	6	43	122	19	153	144	464	1	80	548	14855	8	69	106	176
25	5	29	220	4	180	104	442	3	45	790	11628	8	158	219	376
26	1	25	155	4	153	113	501	1	9	358	12448	8	76	175	250
27	97	1105	393	312	1347	113	568	6	763	1018	8992	21	85	140	225
28	46	184	198	39	153	132	450	3	128	1027	11366	15	123	190	313
29	5	74	194	13	242	125	520	0	54	231	9443	2	7	10	17
30	234	1291	308	246	830	100	569	18	3429	592	13932	10	107	198	306

TABLE 3A continued

LA-ICP-MS ANALYSIS OF ZIRCON (in ppm)

GEELWAL KAROO

Sample	Mg	Al	P	K	Ca	Sc	Ti	Mn	Fe	Y	Hf	Pb	Th	U	U+Th
31	4	18	745	29	1049	153	497	4	10	2370	13205	13	196	206	403
32	59	487	217	212	1049	132	577	2	293	345	10590	3	43	66	109
33	11	49	409	13	1049	174	566	4	23	707	12633	3	26	19	45
34	0	26	794	25	1049	139	501	4	23	2400	13790	15	264	337	601
35	13	32	296	30	235	124	506	1	33	1116	12281	11	185	196	381
36	18	726	44202	110	104826	160	512	255	70	2314	12826	15	152	118	270
37	19	531	282	38	1049	99	665	2	115	2761	11894	12	135	312	447
38	1867	17457	1049	8882	18217	115	19822	152	12552	567	4835	98	86	116	202
39	12	65	602	18	1315	195	515	2	27	504	12359	6	66	58	124
40	77	252	1533	156	2021	126	627	8	489	1250	13302	11	123	246	369
41	5	348	252	8	1049	124	637	4	38	2011	13323	8	181	197	378
42	3	23	168	29	1049	119	534	4	23	823	13074	8	169	229	398
43	15	150	226	74	1049	179	592	1	128	842	14382	18	347	72	419
44	648	6389	929	2700	3887	61	2357	48	3951	1226	5406	32	75	324	399
45	14	41	160	25	1049	220	1227	36	359	395	15332	3	26	109	135
46	**3**	10	186	29	1049	154	613	2	23	759	11338	2	40	43	83
47	112	183	193	147	447	141	675	3	282	557	15073	5	64	144	208
48	312	4448	538	1235	931	138	2802	14	6178	1043	14653	15	120	224	344
49	59	1478	321	96	1049	176	3442	3	1414	1376	14682	19	235	633	867
50	54	397	231	211	277	122	759	10	321	2592	12002	8	91	109	200
51	2	10	359	29	1049	177	527	1	52	1627	13460	8	101	139	241
52	**3**	16	198	6	1049	166	559	4	5	1657	15029	11	220	243	463
53	10	27	231	50	372	161	698	4	72	1094	16079	17	204	341	545
54	17	72	1375	32	10777	125	849	10	69	1170	13496	7	113	199	312
55	5	76	303	26	1049	153	528	1	70	2434	13676	36	415	256	671
56	6	48	181	9	1049	124	532	4	30	1061	14078	4	95	190	286
57	22	96	176	74	1049	117	580	5	314	649	15414	8	73	195	268
58	**3**	10	226	29	1049	107	541	4	10	2045	9955	3	46	59	105
59	3	12	177	29	1049	133	583	4	12	767	16258	8	97	192	289
60	51	2779	188	106	443	135	2104	2	358	702	15774	16	186	237	423
61	1	12	161	29	1049	118	557	4	23	733	14887	4	74	237	311
62	5	5	207	29	1049	131	559	1	7	1065	15128	6	125	294	419
63	11	91	866	19	432	277	714	1	77	2592	15777	5	120	290	410
64	7	104	232	49	1049	139	527	1	104	991	14980	10	108	260	368
65	1	172	212	107	1049	135	590	6	5074	801	13189	1	28	37	65
66	1	26	181	11	1049	176	532	1	7	2170	10308	29	407	290	697
average	**99**	**909**	**367**	**299**	**321**	**135**	**603**	**5**	**1086**	**1073**	12764	15	129	227	356

TABLE 3A continued

LA-ICP-MS ANALYSIS OF ZIRCON (in ppm)

GRAAUWDUINEN

Sample	Mg	Al	P	K	Ca	Sc	Ti	Mn	Fe	Y	Hf	Pb	Th	U	U+Th
1	2	19	245	18	65	104	415	0	5	953	9362	1	33	43	76
2	2	6	148	7	65	116	430	0	4	566	10192	9	84	152	236
3	1	44	734	11	65	185	403	0	5	1632	11741	4	42	177	219
4	2	115	627	81	1066	98	421	4	619	534	9046	2	37	63	100
5	0	7	300	1	65	143	441	0	1	703	9565	2	34	97	131
6	0	6	223	3	65	98	422	0	1	566	10511	4	58	181	240
7	0	11	598	1	65	97	387	1	8	3159	8893	21	211	178	389
8	3	16	273	23	65	105	439	0	9	680	9812	1	28	40	68
9	5	13	280	10	65	94	395	0	28	1745	8215	3	23	50	73
10	1	9	312	1	400	138	416	0	5	1531	10973	20	204	247	450
11	1	35	217	22	65	95	411	0	8	642	10275	6	66	133	199
12	3	8	158	7	65	105	401	0	5	517	10067	11	99	153	252
13	0	1	62	1	65	76	393	0	11	1966	8424	11	144	252	396
14	3	10	329	5	429	96	394	0	32	4469	13656	8	664	1115	1780
15	0	1	205	1	65	94	378	0	1	664	9736	5	57	112	168
16	0	74	758	9	151	290	380	1	9	1939	9955	9	89	146	235
17	2	122	410	1	65	117	394	0	4	982	12372	11	110	188	298
18	0	31	203	1	65	118	458	0	1	387	7891	1	13	14	26
19	1	101	340	1	137	134	381	0	1	595	15269	3	51	764	815
20	0	14	277	1	65	101	416	0	41	1668	9441	1	64	67	130
21	32	618	861	135	335	322	411	5	975	1577	12131	8	72	319	391
22	1	6	163	6	65	94	398	0	1	415	11371	5	100	188	287
23	1	44	289	41	65	98	395	0	3	787	10520	1	48	71	119
24	0	9	516	1	65	165	383	0	1	1315	10296	4	60	192	251
25	1	33	1108	1	65	306	380	0	6	2151	11780	11	56	272	328
26	4	98	419	47	718	88	412	5	9047	666	10868	9	102	215	316
27	0	5	167	1	105	103	417	0	1	456	10648	4	50	127	177
28	1	1	208	6	136	107	374	0	3	759	10357	11	105	319	424
29	4	19	356	7	65	144	396	0	4	882	10863	10	88	175	263
30	1	11	230	5	65	94	406	0	10	941	10530	1	49	70	119
31	2	7	268	7	65	124	395	0	52	1585	9417	12	148	237	385
32	0	11	198	1	65	108	372	0	11	472	10453	14	128	138	267
33	1	4	216	1	65	96	415	0	5	1131	9287	8	141	111	252
34	4	116	276	5	65	131	427	0	19	332	9048	1	10	33	43
35	202	563	1081	285	2223	87	444	25	547	1197	9121	8	59	102	160
36	8	225	897	133	1601	135	395	5	732	1579	9859	45	401	456	857
37	1	4	197	1	65	94	387	0	12	647	10128	1	30	47	77
38	2	127	493	59	552	94	395	2	24	984	10491	5	47	152	199
39	13	27	187	26	65	154	389	0	488	501	11855	8	54	151	205
40	0	6	314	1	134	164	366	0	1	695	9839	3	46	95	141
41	0	17	279	7	65	111	438	0	3	993	7986	5	90	74	164
42	0	25	232	6	65	101	422	0	1	488	9102	3	48	39	87
43	8	56	258	11	158	119	370	1	13	665	10875	7	63	127	190
44	47	903	239	184	65	122	474	3	365	681	10054	12	67	203	270
45	0	5	207	6	65	92	400	0	1	530	10045	0	22	38	61

TABLE 3A continued

LA-ICP-MS ANALYSIS OF ZIRCON (in ppm)

GRAAUWDUINEN

Sample	Mg	Al	P	K	Ca	Sc	Ti	Mn	Fe	Y	Hf	Pb	Th	U	U+Th
46	3	326	150	241	131	77	378	1	11	574	9792	6	48	137	185
47	4	115	170	17	65	96	437	0	79	452	11003	15	150	197	348
48	4	88	2171	33	1631	255	369	5	34	3420	11339	13	154	325	480
49	112	14	244	5	196	120	391	27	908	686	10277	12	148	205	352
50	13	71	782	59	65	209	392	3	656	2006	11221	9	98	312	410
51	1	140	1415	81	3289	72	368	17	38	1904	8727	9	90	263	353
52	6	33	98	14	304	72	363	1	25	923	7285	1	6	15	21
53	7	22	131	12	65	85	374	1	31	1400	7824	3	25	46	71
54	6	26	212	21	65	91	369	0	51	819	9910	1	40	58	98
55	0	4	202	1	65	111	418	0	5	502	10340	6	57	87	144
56	2	21	316	14	65	104	391	0	15	1391	8914	1	52	56	108
57	1	2	221	3	65	150	364	0	6	909	10177	8	66	139	206
58	8	280	193	38	65	101	395	1	160	1077	8636	8	124	174	298
59	6	324	182	187	65	92	396	2	37	473	8571	2	29	46	74
60	4	7	360	8	65	125	384	0	9	1634	8069		134	127	261
61	3	68	447	13	65	113	362	0	29	1213	10450	6	88	200	288
62	1	18	316	4	65	89	395	0	6	2607	11259	3	255	403	658
63	1	5	234	1	65	99	374	0	4	918	9031	1	29	38	67
64	0	2	240	1	65	66	337	0	5	1056	7637	3	26	89	115
65	1	4	212	1	153	73	356	0	8	1352	7592	7	81	160	241
66	3	23	178	16	65	74	352	0	21	547	8519	1	9	43	52
67	3	241	385	158	151	105	400	1	35	1519	8903	1	76	98	174
68	0	11	239	10	118	88	370	0	2855	616	9538	2	33	53	86
69	0	20	205	1	65	97	373	0	6	457	10373	5	47	117	164
average	**107**	**903**	**378**	**305**	**323**	**135**	**603**	**5**	**1092**	**1094**	9967	7	88	167	255

LA-ICP-MS ANALYSIS OF ZIRCON (in ppm)

RIETFONTEIN

Sample	Mg	Al	P	K	Ca	Sc	Ti	Mn	Fe	Y	Hf	Pb	Th	U	U+Th
1	22	54	189	60	102	100	429	2	123	568	10688	8	86	142	228
2	0	4	72	3	120	95	393	0	2	319	9380	3	50	187	237
3	1	56	330	14	102	100	382	1	4	726	8928	3	43	134	178
4	0	97	544	3	102	288	422	0	4	829	8619	2	21	23	45
5	0	1	138	3	102	101	406	0	3	474	11363	11	115	309	424
6	1	11	162	3	102	81	389	1	22	431	14064	4	70	945	1015
7	12	159	142	77	102	90	388	0	98	719	9377	7	155	166	321
8	3	9	181	3	102	90	393	0	22	752	10344	5	98	120	218
9	0	1	157	3	102	101	412	0	2	570	9359	4	63	89	152
10	122	703	815	63	192	217	571	60	1872	1173	10028	14	328	501	830
11	18	275	237	24	102	116	804	2	289	574	10183	8	76	157	233
12	0	2	179	3	102	106	396	0	5	488	8749	4	56	155	210
13	14	98	233	22	102	99	407	1	180	811	10610	5	80	170	250
14	2	17	289	3	102	219	389	0	37	512	11107	5	109	1074	1183
15	1	1	154	3	102	71	375	0	14	1059	9358	7	87	214	301
16	9	92	390	5	102	120	859	5	173	1136	12262	16	182	821	1003
17	68	174	747	85	1103	105	441	8	288	673	9115	3	27	23	50

TABLE 3A continued

LA-ICP-MS ANALYSIS OF ZIRCON (in ppm)

RIETFONTEIN

Sample	Mg	Al	P	K	Ca	Sc	Ti	Mn	Fe	Y	Hf	Pb	Th	U	U+Th
18	1	1	223	4	102	126	382	0	4	1924	9570	9	98	239	337
19	2	27	187	20	251	98	391	4	13	654	8896	4	41	112	153
20	1	9	636	3	263	126	378	1	2	1760	8735	5	53	28	81
21	1	13	192	3	102	100	390	0	6	549	11479	11	104	157	261
22	0	8	441	3	102	143	393	0	4	1203	11237	11	108	292	400
23	0	3	208	19	102	103	392	0	10	828	11296	4	68	187	256
24	18	102	262	33	155	105	419	2	208	945	8638	9	126	134	260
25	0	19	303	7	102	105	373	0	3	1718	9815	9	94	149	243
26	0	4	115	3	102	101	388	0	2	291	9241	2	46	118	164
27	1	19	195	3	102	73	367	0	6	2224	11263	15	182	361	542
28	1	30	774	3	102	173	371	1	8	1541	11603	2	39	283	322
29	0	1	246	3	102	75	377	0	16	1276	11641	4	39	153	192
30	6	54	497	20	102	104	375	23	69	2324	8629	26	251	457	707
31	1	53	218	7	102	102	375	0	4	658	9963	5	58	118	176
32	0	5	229	3	102	95	398	0	2	614	9008	0	20	30	50
33	232	607	305	376	102	112	455	20	730	885	9726	10	104	121	225
34	1	3	162	3	102	88	381	1	2	1042	8010	5	63	91	153
35	0	7	137	3	102	99	381	0	2	245	8454	1	12	38	49
36	0	2	175	3	102	77	370	0	2	1108	10244	7	112	278	390
37	0	1	245	3	102	114	393	0	2	1198	7636	8	130	133	263
38	11	292	214	56	102	102	1674	3	167	636	9680	4	40	144	184
39	38	131	348	78	163	88	400	5	235	1602	10230	17	199	302	501
40	5	17	129	8	102	119	363	0	29	342	11518	5	66	703	769
41	1	3	364	3	102	119	363	0	3	833	11282	8	77	224	302
42	0	1	220	3	102	112	367	0	2	538	10527	6	51	217	268
43	41	356	538	78	181	147	374	8	473	1455	11158	31	506	1050	1556
44	1	1	193	3	102	95	389	0	3	553	8968	2	46	79	125
45	35	392	227	151	102	110	431	2	314	1172	10150	11	84	238	322
46	3	18	277	4	102	112	357	1	68	1005	10749	40	220	245	465
47	0	11	392	3	102	110	369	0	2	936	9778	5	85	126	211
48	435	5728	439	1284	415	88	751	16	6321	1378	8535	21	208	389	597
49	22	327	195	57	102	93	466	6	431	2852	8955	16	275	542	817
50	0	7	147	6	102	76	385	0	2	313	7787	0	4	15	19
51	0	7	318	3	155	109	340	1	17	1788	9116	52	510	653	1163
52	1	15	252	3	102	112	373	0	20	908	9353	5	45	71	116
53	1	7	244	3	102	147	348	0	2	1562	9352	18	187	167	355
54	6	37	232	4	102	98	369	1	184	922	10489	13	126	154	280
55	0	4	361	3	102	89	349	0	3	1808	10969	3	236	366	602
56	1	3	99	3	102	76	354	0	2	1039	9369	2	26	113	139
average	**20**	**180**	**284**	**47**	**137**	**111**	**436**	**3**	**223**	**1008**	**9939**	**9**	**114**	**259**	**373**

TABLE F3B

REE CHEMISTRY OF ZIRCON DETERMINED WITH LA-ICP-MS (in ppm)

HOUTKRAAL REMAINDER PORTION 2

Sample	La	Ce	Pr	Nd	Sm	Eu	Gd	Tb	Dy	Ho	Er	Tm	Yb	Lu	TREE
1	0.14	20.64	0.53	6.46	10.38	2.01	43.53	12.35	127.32	41.81	166.84	32.82	347.18	53.91	865.92
2	0.02	10.85	0.04	0.80	2.08	0.08	13.58	5.36	70.96	27.65	129.09	28.37	345.02	50.26	684.17
3	0.02	6.70	0.14	1.67	4.72	0.44	24.85	8.24	101.20	37.90	162.34	32.84	349.46	57.88	788.39
4	0.01	5.67	0.04	0.91	1.65	0.52	8.97	2.60	30.03	10.54	45.11	9.54	143.63	17.61	276.83
5	0.01	31.58	0.11	2.09	4.58	0.82	22.88	7.95	99.97	38.33	176.86	37.72	424.46	72.23	919.58
6	0.03	8.68	0.08	1.46	3.47	0.72	18.79	6.31	74.57	27.34	120.14	24.65	286.25	44.93	617.41
7	0.01	5.58	0.03	1.23	2.03	0.23	13.26	4.95	60.84	23.62	107.40	22.47	268.58	41.45	551.68
8	2.22	10.34	0.98	7.13	9.75	0.44	51.79	17.53	200.81	73.19	307.61	60.57	588.48	101.02	1431.86
9	0.02	8.98	0.03	0.65	1.31	0.41	8.37	2.73	34.92	14.64	71.69	17.11	259.08	42.34	462.27
10	0.01	21.21	0.12	2.35	5.79	0.11	32.54	11.23	135.69	49.66	215.27	43.10	435.24	66.92	1019.24
11	0.11	28.84	0.10	1.91	3.82	0.84	22.51	8.05	94.49	35.44	155.88	32.70	366.40	61.47	812.56
12	0.25	15.58	0.11	0.98	1.96	0.15	12.55	4.54	58.68	23.30	111.31	24.20	300.82	47.67	602.10
13	3.48	23.54	1.04	6.86	4.85	0.54	20.88	6.67	71.09	26.62	109.86	22.75	273.38	40.58	612.14
14	0.01	23.45	0.04	0.54	1.03	0.41	6.22	1.55	20.00	8.18	48.24	12.66	214.81	35.92	373.06
15	0.11	4.66	0.31	6.25	12.94	1.07	62.97	18.05	183.02	60.42	242.12	47.64	479.56	79.68	1198.80
16	0.01	9.24	0.08	0.89	2.42	0.10	14.06	4.89	59.88	23.46	108.20	23.46	283.20	43.37	573.25
17	0.02	8.71	0.10	2.10	5.64	0.27	27.51	8.73	100.34	35.69	154.00	31.56	348.20	53.93	776.80
18	0.23	74.77	0.44	4.31	10.26	0.28	60.09	26.99	369.28	153.87	731.94	161.45	1555.11	267.72	3416.74
19	0.18	14.91	0.11	1.74	5.72	0.31	38.58	16.03	212.41	80.85	376.17	81.07	820.86	139.63	1788.57
20	0.03	14.75	0.06	1.12	2.84	0.12	18.78	7.31	94.30	37.35	172.50	36.21	413.82	61.65	860.84
21	0.02	17.20	0.12	2.26	4.87	1.04	27.63	8.61	97.74	34.84	152.84	31.65	360.86	58.34	798.01
22	0.50	10.16	0.42	4.40	7.01	0.54	44.03	16.52	220.11	85.37	392.56	81.46	821.73	146.54	1831.35
23	0.04	12.38	0.14	1.58	2.93	0.36	14.92	5.34	63.29	23.68	108.09	22.83	279.58	40.86	576.02
24	0.18	14.59	0.10	1.02	1.70	0.13	12.33	4.52	58.12	21.67	93.04	18.69	227.77	31.13	484.98
25	2.08	11.70	0.48	1.97	3.04	0.18	15.55	5.85	70.87	28.61	131.90	28.16	329.59	52.14	682.12
26	1.29	6.61	0.07	0.86	2.59	0.15	15.53	5.33	61.08	22.57	97.77	20.24	244.46	36.87	515.42
27	0.10	5.11	0.09	1.34	2.87	0.51	12.68	3.92	42.43	14.76	60.38	11.94	158.72	21.52	336.37
28	0.11	11.02	0.14	2.49	6.10	1.03	29.77	9.10	104.22	36.95	159.78	32.09	351.89	55.15	799.84
29	0.07	3.97	0.11	1.38	2.61	0.38	15.44	5.37	68.33	28.07	129.92	27.40	310.36	53.86	647.27
30	0.03	15.52	0.19	2.85	3.27	1.55	11.09	2.99	31.91	10.74	45.72	9.62	139.77	19.95	295.20

TABLE 3B continued															
REE CHEMISTRY OF ZIRCON DETERMINED WITH LA-ICP-MS (in ppm)															
HOUTKRAAL REMAINDER PORTION 2															
Sample	**La**	**Ce**	**Pr**	**Nd**	**Sm**	**Eu**	**Gd**	**Tb**	**Dy**	**Ho**	**Er**	**Tm**	**Yb**	**Lu**	**TREE**
31	0.07	6.23	0.05	0.91	2.28	0.74	12.63	4.48	54.26	21.51	101.59	22.08	268.45	44.03	539.31
32	0.01	8.92	0.06	1.22	3.19	0.24	19.93	6.59	78.56	28.82	126.71	25.29	279.95	42.57	622.07
33	0.01	22.60	0.09	2.59	5.49	0.50	31.92	10.71	127.10	46.34	200.61	41.31	439.43	72.62	1001.33
34	0.07	9.37	0.05	0.73	1.19	0.10	6.79	2.29	28.16	11.43	56.25	12.48	192.35	25.78	347.04
35	0.21	70.40	0.25	4.32	6.48	1.42	27.39	8.07	87.11	29.55	125.10	25.42	285.06	44.24	715.02
36	0.06	12.16	0.21	3.34	5.85	0.44	26.11	8.03	93.97	34.00	149.44	30.82	348.17	54.38	766.98
37	0.07	9.17	0.15	2.00	3.69	0.25	19.23	6.53	75.73	27.69	117.14	23.23	258.16	38.99	582.03
38	0.01	7.18	0.05	1.31	3.71	0.22	22.23	7.83	98.34	38.01	176.40	38.24	430.51	75.45	899.49
39	0.01	10.73	0.05	0.84	1.94	0.30	11.33	3.87	46.58	17.43	79.18	16.09	214.37	30.52	433.23
40	0.02	40.18	0.07	0.82	1.90	0.79	11.13	3.89	49.66	19.44	91.28	19.86	233.87	39.32	512.23
41	0.01	5.26	0.05	0.88	1.99	0.25	12.88	4.40	55.49	21.93	98.76	20.56	250.16	38.03	510.66
42	0.17	7.39	0.24	1.99	3.35	0.21	19.42	7.32	91.70	35.10	157.45	33.04	380.21	60.14	797.73
43	0.06	5.05	0.07	1.28	3.30	0.57	23.26	8.28	101.60	38.49	172.16	35.25	384.97	65.33	839.67
44	0.01	7.48	0.03	0.61	1.78	0.56	13.31	5.00	66.47	26.70	130.25	29.47	354.94	62.61	699.21
45	13.59	35.46	2.34	15.46	30.35	7.78	139.52	32.42	290.57	84.99	319.53	56.26	489.71	76.68	1594.66
46	0.12	10.53	0.09	1.39	2.51	0.35	13.68	4.52	52.57	19.98	88.88	18.20	230.16	33.33	476.32
47	0.13	10.05	0.61	9.66	14.44	2.56	56.23	15.75	162.31	52.88	210.67	39.67	399.55	64.71	1039.22
48	0.14	10.85	0.78	10.78	13.50	1.02	47.84	12.27	119.68	37.86	146.77	26.69	285.19	41.82	755.19
49	0.11	61.97	0.12	2.16	3.75	0.75	17.71	5.83	68.33	24.98	113.08	24.07	287.48	44.73	655.06
50	5.66	36.44	1.15	7.89	2.44	0.75	8.30	2.92	40.43	15.79	84.65	19.30	243.04	35.46	504.22
51	4.83	19.72	1.66	6.74	7.31	0.92	20.45	7.01	76.99	29.32	131.85	26.24	292.51	47.53	673.08
52	0.01	54.79	0.08	1.44	3.94	0.46	30.44	12.06	165.53	69.24	338.27	73.82	780.77	146.21	1677.06
53	0.02	19.83	0.05	0.89	2.59	0.31	13.02	4.45	51.89	19.34	89.70	18.81	244.56	35.99	501.45
54	3.13	15.18	1.24	7.49	5.84	0.33	25.94	8.05	95.78	33.48	146.28	28.77	322.48	51.38	745.37
55	0.05	13.27	0.16	2.27	3.76	0.29	18.26	6.39	76.94	29.11	134.76	28.74	335.09	53.50	702.59
56	0.06	6.49	0.08	1.55	3.71	0.57	28.30	10.13	131.25	53.00	245.40	51.26	538.01	95.39	1165.20
57	0.05	28.26	0.17	3.18	5.25	1.30	27.92	9.37	117.97	48.08	233.76	51.53	567.62	109.73	1204.19
average	**0.70**	**17.58**	**0.29**	**2.90**	**4.91**	**0.70**	**25.03**	**8.21**	**96.89**	**35.99**	**160.53**	**33.39**	**369.56**	**60.12**	**816.81**

TABLE 3B continued															
REE CHEMISTRY OF ZIRCON DETERMINED WITH LA-ICP-MS (in ppm)															
HOUTKRAAL REMAINDER															
Sample	**La**	**Ce**	**Pr**	**Nd**	**Sm**	**Eu**	**Gd**	**Tb**	**Dy**	**Ho**	**Er**	**Tm**	**Yb**	**Lu**	**TREE**
1	6.64	19.47	2.93	17.68	11.96	0.67	48.54	14.57	163.81	59.14	254.82	49.21	486.60	82.07	1218.11
2	0.05	1.33	0.13	2.23	4.20	1.88	23.15	7.26	82.38	29.14	130.06	25.25	274.16	44.69	625.91
3	0.05	26.18	0.15	3.00	7.40	1.59	37.09	10.46	107.99	35.71	155.53	30.61	347.41	53.86	817.03
4	1.82	21.34	1.15	9.49	10.48	0.43	55.08	18.80	224.26	83.64	369.61	72.17	702.60	118.18	1689.05
5	0.26	6.15	0.15	2.09	4.78	0.54	28.25	9.21	109.07	41.86	188.55	37.10	404.06	63.93	896.00
6	3.79	51.99	1.54	7.44	4.51	1.47	18.18	5.89	71.17	28.06	139.29	31.77	392.22	63.21	820.53
7	2.18	39.15	0.59	6.03	8.85	1.02	45.94	15.22	177.18	66.56	304.90	61.54	637.49	109.86	1476.51
8	0.02	5.79	0.08	1.15	2.25	0.51	12.00	4.09	50.54	20.80	108.18	26.27	339.77	57.30	628.75
9	0.07	16.80	0.27	4.99	7.84	1.16	34.50	9.99	108.09	37.34	153.99	29.53	326.97	46.53	778.07
10	5.40	47.05	1.16	11.06	1.96	0.61	20.08	4.95	58.34	18.75	77.32	15.36	179.75	25.14	466.93
11	0.26	36.09	0.30	3.65	5.86	0.26	39.14	14.85	192.63	73.29	341.60	71.91	711.66	113.54	1605.04
12	0.11	9.62	0.25	3.80	6.76	1.31	33.51	10.48	115.08	40.44	176.17	35.24	371.72	55.61	860.10
13	5.24	24.31	2.54	12.64	4.37	0.90	23.83	6.51	71.85	27.93	114.97	25.01	309.40	41.66	671.16
14	0.62	11.79	0.44	6.07	8.75	2.16	39.55	11.80	134.34	46.06	198.15	38.55	404.51	61.85	964.64
15	0.65	9.68	0.39	2.28	3.97	0.33	22.24	7.68	99.64	39.32	181.92	37.78	402.35	63.64	871.88
16	0.07	17.67	0.11	2.57	4.68	0.92	28.16	9.83	124.11	47.05	228.95	50.64	558.44	94.04	1167.24
17	0.64	14.84	0.84	5.57	7.31	1.03	38.99	14.43	187.37	72.74	344.34	73.11	754.57	122.23	1638.00
18	0.04	11.57	0.08	1.68	2.43	0.37	17.78	6.47	84.42	32.58	155.61	33.48	382.14	57.62	786.27
19	0.23	9.67	0.31	5.17	5.96	1.16	28.42	8.35	92.76	32.73	146.18	29.38	335.58	50.37	746.28
20	0.03	4.06	0.06	1.21	2.73	0.61	16.87	5.54	66.10	24.24	111.04	22.56	265.64	39.45	560.14
21	0.02	8.52	0.15	1.16	2.53	0.30	14.29	5.15	62.21	24.24	115.18	25.08	300.52	45.00	604.35
22	2.67	13.82	0.55	7.03	8.16	0.93	31.50	9.53	103.73	34.91	144.72	28.27	299.45	44.08	729.35
23	3.75	22.50	3.19	7.10	3.01	0.39	12.61	3.64	45.53	16.21	87.22	20.26	278.69	46.56	550.66
24	0.18	16.09	1.27	18.52	24.09	1.98	85.04	22.80	229.69	72.85	297.77	56.45	532.33	84.77	1443.83
25	0.49	7.61	0.23	1.65	3.06	0.25	17.01	5.23	59.74	21.12	92.93	17.95	235.26	30.39	492.92
26	0.50	47.23	0.44	4.31	6.08	2.03	32.34	10.73	130.20	49.11	233.82	49.15	551.89	94.03	1211.85
average	**1.38**	**19.24**	**0.74**	**5.75**	**6.31**	**0.95**	**30.93**	**9.75**	**113.55**	**41.38**	**186.65**	**38.22**	**414.81**	**65.75**	**935.41**

TABLE 3B continued															
REE CHEMISTRY OF ZIRCON DETERMINED WITH LA-ICP-MS (in ppm)															
GEELWAL KAROO															
Sample	**La**	**Ce**	**Pr**	**Nd**	**Sm**	**Eu**	**Gd**	**Tb**	**Dy**	**Ho**	**Er**	**Tm**	**Yb**	**Lu**	**TREE**
1	0.19	25.27	0.97	16.91	27.82	1.09	99.38	24.93	234.17	69.93	256.30	48.01	458.72	69.73	1333.42
2	0.12	28.48	0.20	2.94	5.30	0.89	27.92	9.66	114.94	44.28	195.28	41.28	447.36	75.91	994.56
3	0.08	11.28	0.09	1.12	3.92	0.65	22.63	8.05	102.78	40.78	183.23	38.90	432.87	71.80	918.18
4	0.01	24.96	0.01	0.40	1.58	0.39	9.78	3.72	49.41	20.30	101.35	23.23	310.03	49.29	594.46
5	0.05	3.93	0.04	0.62	1.79	0.05	10.85	4.05	48.80	19.24	87.65	18.34	237.92	32.41	465.73
6	1.01	11.66	0.74	3.55	8.27	0.45	21.96	7.07	82.33	32.12	137.41	27.40	296.79	46.85	677.61
7	0.07	15.41	0.09	1.83	4.35	1.37	27.73	9.13	113.17	45.05	215.39	48.13	538.73	101.24	1121.69
8	0.01	3.77	0.05	0.38	0.82	0.18	4.91	1.85	24.46	9.88	52.61	12.75	209.91	32.96	354.53
9	0.30	26.06	0.08	2.13	2.80	0.48	13.04	4.66	53.54	20.00	89.93	20.44	255.63	35.82	524.91
10	0.24	6.31	0.33	5.05	8.96	0.66	38.07	11.32	126.18	43.03	178.49	35.08	366.62	56.67	877.01
11	0.14	26.83	0.21	4.77	6.08	1.84	26.82	6.83	76.10	26.29	111.36	23.48	288.49	41.22	640.46
12	0.08	14.36	0.14	1.95	4.50	0.25	25.26	8.56	102.57	38.13	167.14	34.96	390.02	60.53	848.45
13	1.36	36.18	1.24	0.03	9.20	1.56	40.53	12.88	148.00	54.09	243.98	49.38	513.25	87.85	1199.53
14	0.02	11.07	0.06	1.18	2.66	0.39	16.67	5.60	68.14	25.36	112.03	23.45	272.97	40.73	580.33
15	0.10	11.00	0.09	2.02	3.98	1.29	22.34	8.04	101.08	41.72	202.31	46.21	559.29	101.84	1101.31
16	0.26	6.76	0.44	5.76	8.61	0.70	37.67	11.23	117.63	39.88	157.64	30.55	318.26	47.63	783.02
17	0.02	13.20	0.07	1.53	3.49	0.40	21.01	6.93	86.63	32.58	145.22	31.32	344.22	55.35	741.97
18	0.06	6.79	0.12	1.92	4.25	0.29	21.94	7.63	89.76	33.13	144.29	30.34	342.73	51.55	734.80
19	0.52	17.33	0.20	1.54	3.46	0.11	19.47	7.16	91.40	34.00	148.33	30.21	336.05	48.38	738.17
20	0.01	3.14	0.07	1.46	3.68	0.70	21.76	7.09	76.88	27.26	113.07	22.82	254.48	40.43	572.85
21	3.02	22.48	2.18	14.77	12.01	3.88	37.00	12.64	119.63	40.72	165.49	33.87	303.69	55.59	826.97
22	0.03	9.53	0.03	0.71	1.56	0.24	9.93	3.60	46.51	18.37	84.86	18.92	248.79	36.16	479.23
23	1.06	14.06	0.63	4.76	6.47	0.39	38.04	13.20	164.39	61.39	289.45	64.55	707.64	126.03	1492.06
24	0.13	20.56	0.14	1.44	2.62	1.03	13.78	3.99	47.62	17.40	82.48	18.70	281.79	47.98	539.66
25	0.02	83.89	0.14	2.63	4.49	1.16	21.23	6.87	74.42	26.04	112.53	24.30	289.35	43.47	690.54
26	0.01	24.99	0.06	0.93	2.18	0.41	10.15	2.96	31.60	11.23	50.52	11.11	174.36	22.25	342.76
27	0.44	32.70	0.19	1.54	3.78	0.74	20.93	6.62	82.98	32.32	148.78	32.28	345.42	58.90	767.62
28	0.45	36.77	0.45	5.20	8.66	3.09	35.52	10.09	105.20	34.67	142.52	29.23	327.18	52.08	791.10
29	0.03	3.29	0.08	1.36	1.53	0.61	7.86	2.18	22.95	7.76	32.28	6.25	107.68	11.40	205.25
30	10.97	34.46	2.09	9.04	4.68	0.23	16.34	5.27	59.77	20.71	87.36	17.52	228.95	29.52	526.91

TABLE 3B continued

REE CHEMISTRY OF ZIRCON DETERMINED WITH LA-ICP-MS (in ppm)

GEELWAL KAROO

Sample	La	Ce	Pr	Nd	Sm	Eu	Gd	Tb	Dy	Ho	Er	Tm	Yb	Lu	TREE
31	0.10	5.49	0.18	4.41	11.57	0.40	64.98	20.92	240.90	85.47	370.18	70.21	677.98	112.86	1665.65
32	0.19	12.81	0.31	4.18	5.64	2.48	17.70	4.58	40.63	11.27	43.06	7.61	124.48	10.86	285.80
33	0.10	6.80	0.09	1.36	3.43	0.70	17.41	5.50	68.58	25.16	113.57	22.87	276.13	39.86	581.57
34	0.04	6.44	0.30	4.29	10.07	0.30	60.65	19.87	235.87	84.77	379.86	73.09	706.86	118.85	1701.26
35	0.14	70.44	0.45	5.95	8.31	1.73	32.82	9.60	110.15	37.78	171.46	34.78	381.78	60.63	926.02
36	48.95	197.05	21.95	111.67	42.68	12.39	95.62	23.64	243.02	81.15	353.53	68.83	664.78	116.70	2081.96
37	0.20	19.91	0.41	6.21	13.21	0.49	78.01	24.95	295.09	104.86	450.45	83.28	753.42	123.57	1954.07
38	10.24	47.30	6.53	19.41	19.80	2.09	34.23	6.14	81.42	23.52	77.79	16.18	197.00	25.82	567.47
39	0.11	19.88	0.18	2.15	2.72	1.13	11.97	3.50	42.30	16.47	80.73	17.94	250.23	41.47	490.78
40	12.92	47.33	5.23	26.56	10.22	0.47	34.91	10.11	121.49	43.78	195.48	38.75	419.10	65.77	1032.12
41	0.12	22.70	0.83	12.58	18.84	0.85	77.26	21.65	228.46	73.88	307.18	55.88	542.38	87.15	1449.75
42	0.01	64.44	0.09	1.56	3.70	0.91	16.86	5.92	71.15	26.63	128.43	28.52	340.06	52.94	741.22
43	0.06	15.49	0.18	3.75	6.77	0.76	27.29	7.82	83.94	27.87	115.87	21.92	264.21	34.80	610.73
44	10.33	38.78	1.58	13.10	5.34	1.55	26.25	11.40	115.26	38.59	187.65	35.07	331.83	53.73	870.46
45	0.04	5.73	0.06	0.76	1.46	0.58	8.81	2.67	31.63	12.61	63.24	14.26	233.40	35.28	410.53
46	0.07	6.01	0.29	4.50	6.25	1.03	26.78	7.56	82.80	26.95	113.23	20.95	244.10	34.63	575.15
47	0.02	7.90	0.07	0.86	1.75	0.24	9.99	3.78	45.96	17.98	89.59	19.32	270.18	38.46	506.10
48	2.64	17.23	1.57	8.49	7.92	2.08	28.64	9.68	109.36	37.81	174.88	35.13	401.01	60.56	897.00
49	1.64	28.03	0.85	7.65	10.51	2.27	41.23	13.30	144.66	49.78	218.38	45.40	517.28	87.37	1168.35
50	1.38	13.64	1.09	14.63	21.89	4.01	97.66	27.72	303.90	99.08	404.69	72.80	672.17	112.12	1846.78
51	0.03	9.25	0.19	3.75	8.70	0.88	45.70	14.29	169.08	58.23	252.19	48.86	488.66	79.03	1178.84
52	0.05	18.19	0.77	13.86	20.83	2.59	77.32	20.10	201.77	60.18	243.29	44.04	441.60	66.46	1211.06
53	0.10	18.97	0.17	1.63	4.23	1.10	25.07	8.60	103.13	38.23	179.97	37.81	427.54	68.26	914.81
54	5.68	30.30	3.58	25.27	11.58	0.94	35.59	10.62	123.00	42.54	183.52	35.31	371.84	56.25	936.02
55	0.17	34.94	1.01	14.78	20.77	3.77	94.36	26.09	280.08	90.42	377.46	69.98	647.49	108.70	1770.02
56	0.04	20.72	0.11	2.41	4.41	0.28	27.46	9.11	105.89	37.42	169.74	34.06	374.49	56.09	842.23
57	0.09	7.69	0.06	0.78	2.19	0.09	12.69	4.70	59.71	21.62	105.56	21.93	283.32	39.61	560.04
58	0.21	12.27	0.89	14.50	20.18	1.95	84.80	22.67	245.42	78.58	314.46	55.86	502.10	86.45	1440.34
59	0.25	12.63	0.08	0.85	1.89	0.14	12.11	4.56	60.96	24.59	129.51	28.35	358.12	55.23	689.27
60	0.07	15.26	0.07	0.95	2.26	0.21	11.27	4.35	60.01	23.56	121.21	26.50	333.47	51.93	651.12

TABLE 3B continued

REE CHEMISTRY OF ZIRCON DETERMINED WITH LA-ICP-MS (in ppm)

GEELWAL KAROO

Sample	La	Ce	Pr	Nd	Sm	Eu	Gd	Tb	Dy	Ho	Er	Tm	Yb	Lu	TREE
61	0.10	10.43	0.07	1.27	2.75	0.15	16.40	5.61	69.58	25.76	121.90	25.10	303.02	45.09	627.23
62	0.02	11.43	0.07	1.56	3.87	0.23	22.25	7.88	100.85	37.09	173.70	35.12	391.33	59.85	845.25
63	0.04	4.15	0.26	4.02	9.14	0.50	56.95	19.70	250.08	88.64	410.96	84.09	814.78	140.03	1883.34
64	0.28	14.75	0.35	2.84	4.74	0.43	21.82	7.56	94.19	34.35	161.24	33.10	377.90	59.04	812.59
65	0.22	5.91	0.12	1.57	2.61	0.31	16.77	5.66	74.86	27.61	131.90	27.26	316.37	47.97	659.14
66	0.08	23.43	0.41	6.24	9.60	4.97	46.52	14.80	183.25	69.34	360.34	82.94	918.72	193.32	1913.96
average	**1.78**	**22.58**	**0.93**	**6.82**	**7.66**	**1.22**	**32.68**	**10.01**	**114.26**	**40.17**	**177.51**	**35.85**	**391.04**	**63.00**	**905.50**

REE CHEMISTRY OF ZIRCON DETERMINED WITH LA-ICP-MS (in ppm)

GRAAUWDUINEN

Sample	La	Ce	Pr	Nd	Sm	Eu	Gd	Tb	Dy	Ho	Er	Tm	Yb	Lu	TREE
1	0.08	5.07	0.10	1.76	3.93	0.38	22.13	7.15	87.14	32.60	142.98	28.64	307.00	50.24	689.20
2	0.04	18.28	0.21	3.59	4.94	1.54	21.22	5.62	57.38	19.23	79.97	15.72	198.68	28.78	455.20
3	0.32	1.81	0.16	1.35	3.61	0.07	26.10	11.04	142.59	54.85	244.45	49.51	503.42	84.64	1123.92
4	12.77	40.40	3.75	17.28	5.49	0.64	17.07	4.79	52.85	18.80	79.11	15.72	190.94	27.97	487.58
5	0.02	9.23	0.10	1.92	4.06	0.58	20.54	6.37	69.20	23.54	94.67	18.39	212.86	30.70	492.18
6	0.04	8.16	0.06	0.97	1.90	0.19	11.21	3.99	48.27	18.96	88.63	19.66	249.90	39.34	491.28
7	0.27	90.96	0.18	2.22	5.95	1.89	48.21	19.32	265.82	110.38	505.18	103.35	967.94	175.57	2297.25
8	0.18	6.46	0.14	1.10	2.51	0.16	14.61	4.61	60.55	23.50	105.00	21.29	255.09	40.01	535.21
9	0.13	4.35	0.58	8.07	13.37	1.22	57.48	17.27	183.32	62.59	249.92	47.26	446.75	74.98	1167.29
10	0.05	15.35	0.58	7.28	10.50	1.07	45.37	13.89	152.13	52.74	218.35	41.96	421.42	69.22	1049.91
11	0.02	18.25	0.06	1.15	2.56	0.40	13.61	4.84	57.53	22.44	99.59	20.95	250.75	38.92	531.07
12	0.01	13.44	0.05	0.82	1.93	0.37	11.15	3.93	44.48	16.57	77.93	17.27	223.71	36.18	447.83
13	0.09	7.96	0.58	8.82	14.30	1.11	60.05	19.24	216.40	75.99	325.96	66.01	624.85	106.68	1528.03
14	0.05	28.27	0.40	5.40	12.82	0.21	74.76	29.70	385.37	154.40	712.63	147.78	1382.23	239.11	3173.12
15	0.09	9.14	0.17	1.38	3.17	0.46	17.02	5.37	62.93	23.09	100.47	20.80	235.53	35.70	515.33
16	0.01	13.25	0.05	1.18	3.58	1.07	27.86	11.25	154.17	66.17	327.07	73.79	783.72	158.76	1621.93
17	0.00	6.59	0.04	1.00	2.86	0.12	18.90	7.45	91.55	33.67	148.91	29.74	324.96	49.86	715.66
18	0.03	4.06	0.18	2.53	3.61	1.23	15.19	4.20	41.61	13.57	53.88	10.13	133.61	17.85	301.68

TABLE 3B continued															
REE CHEMISTRY OF ZIRCON DETERMINED WITH LA-ICP-MS (in ppm)															
GRAAUWDUINEN															
Sample	**La**	**Ce**	**Pr**	**Nd**	**Sm**	**Eu**	**Gd**	**Tb**	**Dy**	**Ho**	**Er**	**Tm**	**Yb**	**Lu**	**TREE**
19	0.00	0.78	0.07	1.42	7.03	0.11	44.80	12.75	94.75	19.60	49.42	6.64	125.57	6.08	369.02
20	0.02	7.92	0.33	5.69	9.96	0.79	47.98	14.62	164.45	58.52	245.92	47.63	460.84	78.03	1142.70
21	26.08	115.99	9.88	50.76	20.39	5.49	39.08	12.21	140.37	51.68	251.71	60.13	685.21	129.45	1598.43
22	0.01	19.34	0.08	1.39	2.54	0.34	10.01	3.06	35.40	13.19	60.38	13.70	196.60	28.44	384.47
23	2.01	13.78	0.83	4.91	3.05	0.19	15.43	5.50	68.80	26.85	122.19	25.29	285.81	45.66	620.30
24	0.02	33.00	0.12	2.18	4.97	1.35	27.32	9.38	116.16	43.88	200.84	43.28	472.13	86.31	1040.94
25	0.00	2.98	0.04	1.16	3.40	0.39	30.15	12.98	182.16	75.59	358.36	76.23	772.73	141.09	1657.26
26	7.69	35.29	2.54	13.66	5.31	0.42	15.86	5.18	60.45	22.80	102.39	21.69	259.32	39.43	592.03
27	0.01	5.98	0.03	0.60	1.46	0.16	8.87	3.15	39.62	15.11	68.93	14.31	189.55	26.54	374.32
28	0.01	8.20	0.03	0.79	2.33	0.27	14.98	5.33	65.11	25.26	114.99	24.25	282.14	45.19	588.87
29	0.01	9.85	0.08	1.33	2.70	0.27	16.80	6.13	77.57	29.62	132.79	28.12	314.97	50.38	670.62
30	0.04	7.43	0.11	1.12	3.53	0.23	18.37	6.55	80.35	31.20	142.46	29.18	323.69	52.85	697.11
31	0.07	10.15	0.47	6.31	9.75	1.55	44.56	13.82	154.64	55.23	229.08	43.89	424.10	72.08	1065.71
32	0.02	16.08	0.10	1.65	3.11	0.29	13.68	4.25	47.01	16.33	67.95	14.20	183.80	25.04	393.50
33	0.04	39.01	0.38	6.50	10.34	0.92	41.49	11.60	121.33	39.60	161.98	31.44	326.30	53.34	844.28
34	0.02	4.74	0.10	1.81	2.49	0.26	10.96	3.62	37.18	10.88	35.56	5.21	85.21	4.81	202.86
35	7.36	26.87	2.80	15.11	9.44	1.11	36.42	10.75	120.50	42.14	177.54	35.47	359.31	60.80	905.62
36	10.16	47.25	3.98	21.93	14.70	1.08	51.59	14.99	161.39	54.38	225.37	43.59	421.80	68.74	1140.95
37	0.02	6.00	0.05	0.97	2.04	0.22	13.09	4.46	56.05	21.94	99.57	20.59	244.80	37.78	507.57
38	5.19	20.80	2.23	13.06	7.89	0.57	28.17	8.73	94.95	33.38	142.07	28.33	308.57	48.90	742.84
39	0.10	14.48	0.08	0.72	1.57	0.47	9.57	3.32	40.44	16.08	77.37	17.55	240.90	38.52	461.17
40	0.00	9.76	0.03	0.73	2.30	1.14	16.58	5.49	62.52	22.99	100.51	20.95	252.29	41.56	536.85
41	0.19	35.26	0.65	10.09	12.10	3.63	43.00	11.16	109.75	34.50	136.25	25.85	266.39	43.17	731.99
42	0.15	24.64	0.14	2.02	3.61	1.13	14.82	4.45	48.40	16.64	71.69	15.00	187.69	28.04	418.42
43	0.48	16.13	0.11	1.08	1.82	0.45	10.41	3.83	48.43	20.63	103.40	24.44	309.18	56.01	596.40
44	0.39	11.77	0.10	1.38	3.45	0.28	16.24	5.13	60.76	22.90	101.84	21.76	256.68	40.45	543.13
45	0.01	5.36	0.04	0.69	1.49	0.16	9.89	3.55	45.80	17.81	81.92	17.19	214.19	32.40	430.50

TABLE 3B continued															
REE CHEMISTRY OF ZIRCON DETERMINED WITH LA-ICP-MS (in ppm)															
GRAAUWDUINEN															
Sample	**La**	**Ce**	**Pr**	**Nd**	**Sm**	**Eu**	**Gd**	**Tb**	**Dy**	**Ho**	**Er**	**Tm**	**Yb**	**Lu**	**TREE**
46	0.17	6.16	0.10	1.08	2.30	0.08	14.39	4.51	52.74	19.39	83.85	16.93	203.06	29.34	434.11
47	0.26	13.36	0.05	0.94	1.24	0.11	6.69	2.56	32.82	13.47	71.08	19.86	279.48	50.69	492.60
48	15.30	37.34	5.10	29.25	20.08	0.28	91.40	31.21	355.45	118.85	462.72	84.24	749.03	120.88	2121.13
49	0.10	5.33	0.13	2.09	3.56	0.37	19.06	6.18	66.82	23.51	97.31	19.22	221.37	31.43	496.48
50	0.76	9.60	1.13	6.13	7.99	0.93	43.53	15.35	186.55	70.76	315.09	64.63	637.20	112.18	1471.83
51	5.14	47.04	5.63	42.85	21.92	1.50	58.72	17.45	196.67	69.08	285.28	53.74	497.03	80.13	1382.18
52	0.14	3.83	0.14	2.71	5.50	1.16	30.49	9.10	99.60	34.25	138.66	26.77	279.57	49.46	681.38
53	0.10	5.79	0.54	7.86	12.66	1.36	53.40	15.18	157.56	51.52	204.87	38.63	372.22	63.26	984.96
54	0.02	6.86	0.06	1.01	2.43	0.19	16.04	5.83	70.74	27.77	125.76	25.89	289.81	46.68	619.09
55	0.04	12.29	0.05	0.94	1.89	0.22	9.96	3.54	43.51	16.87	77.59	16.61	212.18	31.37	427.06
56	0.14	6.82	0.29	4.55	7.71	0.67	38.15	11.89	132.17	47.96	202.12	39.76	394.53	66.07	952.83
57	0.03	14.40	0.03	0.75	1.90	0.58	11.84	4.44	61.87	27.80	145.84	35.33	438.29	91.69	834.78
58	0.15	56.07	0.54	8.42	11.16	2.70	40.11	10.64	108.35	35.63	145.53	28.35	300.18	49.22	797.05
59	0.20	10.28	0.12	1.49	2.81	0.39	13.02	4.01	45.46	16.13	69.00	13.89	173.91	25.34	376.04
60	0.12	21.09	0.48	7.32	10.75	3.53	50.06	14.63	160.10	55.61	229.56	43.67	421.84	73.61	1092.36
61	0.06	5.56	0.08	1.34	3.52	0.32	25.29	8.65	107.48	40.45	178.05	36.83	386.01	64.04	857.68
62	0.15	19.24	0.22	3.93	9.11	0.21	53.26	18.80	237.11	90.50	404.82	81.37	763.28	130.69	1812.69
63	0.02	4.74	0.10	1.87	4.39	0.48	21.26	7.03	83.55	31.22	134.70	27.22	293.70	47.57	657.85
64	0.06	20.37	0.09	1.67	3.68	1.09	22.69	7.66	96.02	36.62	159.25	31.74	316.62	51.82	749.38
65	0.11	16.60	0.30	5.06	8.64	0.44	38.73	11.95	136.45	48.41	202.84	39.35	381.71	64.38	954.97
66	0.02	2.49	0.04	0.85	2.63	0.26	12.53	4.08	48.98	18.59	82.09	16.91	201.27	31.35	422.09
67	0.53	9.85	0.45	5.98	8.32	0.59	39.37	12.40	142.29	51.80	218.51	43.08	421.89	71.93	1026.99
68	0.00	6.81	0.04	0.82	1.84	0.14	11.36	4.14	51.53	20.16	92.21	19.43	231.63	35.58	475.68
69	0.01	6.73	0.04	0.77	1.49	0.19	9.02	3.08	37.13	14.54	67.64	14.65	197.11	29.03	381.43
average	**1.42**	**17.37**	**0.70**	**5.46**	**5.96**	**0.78**	**27.58**	**8.99**	**104.62**	**38.30**	**166.83**	**33.94**	**359.80**	**59.90**	**831.65**

TABLE 3B continued															
REE CHEMISTRY OF ZIRCON DETERMINED WITH LA-ICP-MS (in ppm)															
RIETFONTEIN															
Sample	**La**	**Ce**	**Pr**	**Nd**	**Sm**	**Eu**	**Gd**	**Tb**	**Dy**	**Ho**	**Er**	**Tm**	**Yb**	**Lu**	**TREE**
1	0.00	11.88	0.07	0.65	1.70	0.13	9.77	3.73	48.10	19.37	91.30	20.48	255.27	40.78	503.23
2	0.05	11.24	0.06	0.70	1.00	0.36	5.34	1.70	22.35	9.43	49.04	11.99	181.81	31.07	326.14
3	0.10	5.11	0.22	2.67	4.22	0.57	20.92	6.15	70.48	25.17	107.33	21.41	238.20	37.02	539.57
4	0.05	2.53	0.15	2.77	5.51	0.15	23.93	8.53	94.81	30.74	120.10	23.55	248.45	36.85	598.13
5	0.01	11.19	0.04	0.70	1.78	0.16	9.25	3.30	41.51	16.15	76.04	17.35	232.63	35.39	445.49
6	0.16	9.38	0.13	1.03	1.41	0.21	7.78	2.98	36.72	14.00	63.05	13.34	197.77	22.95	370.91
7	0.04	70.67	0.20	3.52	6.74	2.01	27.69	7.29	73.58	24.16	99.73	19.86	234.62	36.16	606.27
8	0.04	30.85	0.06	1.50	3.43	0.45	17.89	5.98	70.08	25.74	113.31	23.98	278.04	44.08	615.43
9	0.01	24.48	0.11	2.38	4.07	1.33	17.84	5.15	56.10	19.69	82.67	16.99	206.98	31.28	469.08
10	3.46	61.55	3.10	19.80	13.36	4.79	35.84	11.08	118.01	38.51	169.68	38.13	436.91	79.97	1034.19
11	0.52	11.20	0.14	1.21	2.00	0.46	12.32	4.09	49.20	18.41	84.31	17.85	223.44	33.59	458.74
12	0.00	7.12	0.07	1.22	2.39	0.25	14.48	4.17	47.41	17.10	74.92	14.69	183.38	26.92	394.12
13	0.03	9.95	0.07	1.53	3.32	0.13	19.26	6.64	76.44	28.34	123.12	24.35	272.58	41.81	607.56
14	0.04	2.76	0.14	2.00	5.99	0.55	31.85	8.22	65.64	16.87	59.15	10.80	151.34	17.14	372.49
15	0.05	17.06	0.08	1.60	4.75	0.27	26.36	9.30	109.90	39.42	161.11	30.25	299.42	43.25	742.82
16	1.35	20.38	0.87	5.11	5.43	1.06	22.03	7.65	94.03	37.23	176.73	40.60	472.38	87.39	972.23
17	5.23	32.40	2.03	8.99	4.05	1.00	16.24	5.19	62.49	23.49	105.75	22.53	265.13	43.63	598.16
18	0.02	10.43	0.26	4.63	9.01	1.58	51.01	15.96	184.52	69.67	302.71	60.85	602.63	109.32	1422.59
19	0.08	6.98	0.16	2.26	4.05	0.58	18.57	5.84	65.35	23.50	98.72	19.67	225.23	34.79	505.77
20	0.53	50.26	0.56	7.12	10.39	3.39	45.87	15.17	172.54	63.15	274.93	55.02	546.35	98.93	1344.21
21	0.00	10.46	0.03	0.61	1.73	0.15	10.98	3.78	48.79	18.49	84.63	17.74	223.24	31.05	451.68
22	0.00	7.27	0.09	1.36	4.27	0.09	24.34	8.95	111.13	41.80	187.02	38.41	409.38	67.02	901.13
23	0.00	5.42	0.04	1.16	2.74	0.22	16.54	5.74	72.76	27.77	123.51	25.78	292.73	44.96	619.37
24	0.50	9.44	0.37	3.81	6.40	0.70	26.68	8.32	92.67	33.17	137.76	26.99	281.31	44.39	672.51
25	0.18	12.37	0.78	11.77	17.53	1.25	73.46	20.06	200.09	63.37	239.37	42.91	403.59	63.46	1150.18
26	0.01	14.92	0.13	1.77	3.19	1.17	11.12	2.93	29.04	9.30	39.28	7.95	126.62	15.53	262.95
27	2.45	36.84	1.28	7.91	11.56	0.66	55.38	18.66	223.03	81.96	346.69	67.80	630.51	101.87	1586.60
28	0.29	2.32	0.09	1.14	3.07	0.10	20.23	9.34	125.68	51.06	241.21	51.78	546.26	93.43	1146.01
29	0.53	17.16	0.18	1.85	4.57	0.18	28.25	9.92	122.61	45.61	200.28	39.49	409.16	63.86	943.66
30	1.12	16.66	0.55	5.68	10.87	1.32	57.98	19.62	221.75	81.90	350.88	68.57	652.76	115.53	1605.19

TABLE 3B continued															
REE CHEMISTRY OF ZIRCON DETERMINED WITH LA-ICP-MS (in ppm)															
RIETFONTEIN															
Sample	**La**	**Ce**	**Pr**	**Nd**	**Sm**	**Eu**	**Gd**	**Tb**	**Dy**	**Ho**	**Er**	**Tm**	**Yb**	**Lu**	**TREE**
31	0.30	7.75	0.13	1.52	2.67	0.34	14.48	4.95	57.62	21.62	98.24	20.50	242.13	37.22	509.47
32	0.25	4.42	0.11	0.88	2.02	0.23	12.06	4.30	54.91	21.27	92.99	19.93	226.79	34.73	474.89
33	0.35	50.69	0.17	2.87	3.91	0.74	19.54	6.60	79.14	30.18	136.72	29.39	331.92	55.65	747.87
34	0.38	58.57	0.26	1.73	2.54	1.02	15.54	6.02	79.93	33.55	167.76	37.78	409.07	73.29	887.44
35	1.29	11.57	0.38	0.86	1.05	0.42	5.35	1.70	20.07	8.01	36.93	8.28	126.16	16.99	239.06
36	0.35	18.59	0.10	1.52	3.99	0.30	23.76	8.60	106.85	39.36	170.47	33.20	338.83	51.48	797.41
37	0.31	9.59	0.61	8.19	8.90	3.10	35.25	10.33	112.88	40.79	171.89	32.63	324.12	55.42	814.01
38	0.36	7.91	0.20	1.61	2.26	0.32	12.96	4.31	52.93	20.69	94.34	20.74	251.33	40.41	510.38
39	1.28	24.19	0.54	4.99	9.13	0.89	41.48	13.60	155.68	56.44	244.27	48.25	485.43	81.13	1167.29
40	0.19	9.26	0.07	0.49	1.10	0.25	6.33	2.56	29.91	11.03	50.85	10.88	168.26	20.05	311.22
41	0.17	4.92	0.08	1.32	2.77	0.07	16.64	6.02	75.68	28.69	127.49	26.31	299.99	45.22	635.37
42	0.17	3.37	0.06	0.59	1.45	0.07	8.37	3.28	43.28	17.62	83.55	18.01	226.17	34.36	440.35
43	1.59	55.57	2.10	13.82	13.08	1.58	37.37	12.76	144.27	50.50	218.34	43.78	452.75	73.50	1121.01
44	0.05	9.11	0.10	1.37	3.01	0.23	15.17	4.67	53.73	19.33	83.04	16.72	203.58	30.65	440.75
45	0.10	6.27	0.22	2.91	5.84	0.55	32.83	10.12	115.65	41.11	172.68	34.35	351.18	56.61	830.41
46	0.18	50.43	0.12	1.45	3.27	0.41	16.62	6.28	80.69	32.83	160.02	35.21	407.79	71.07	866.37
47	0.16	11.73	0.18	3.89	6.85	0.67	26.30	8.08	88.29	31.19	133.55	27.04	290.58	45.01	673.52
48	10.71	113.68	5.29	27.13	14.75	2.28	44.56	13.40	143.12	49.58	205.75	39.81	390.51	64.12	1124.69
49	0.66	25.01	0.82	7.87	13.59	3.61	79.16	27.88	314.52	110.29	442.81	82.12	707.11	109.19	1924.64
50	0.04	1.12	0.05	0.56	1.40	0.21	7.81	2.64	30.12	10.85	48.44	10.09	136.21	19.90	269.45
51	0.07	33.55	0.55	7.31	10.46	2.07	41.49	13.30	152.10	56.27	263.11	59.44	635.73	120.75	1396.20
52	0.02	7.51	0.11	1.74	4.37	0.65	24.21	7.77	89.38	31.89	131.69	25.41	274.74	41.91	641.40
53	0.14	16.18	0.28	3.96	7.17	1.14	33.05	10.50	128.89	51.68	239.55	49.45	507.45	93.33	1142.76
54	0.15	23.70	0.13	1.56	3.16	0.40	16.99	6.28	77.36	30.57	145.94	31.88	366.39	62.28	766.78
55	0.14	21.51	0.14	2.29	5.15	0.10	31.74	12.01	156.01	62.91	287.46	59.22	595.75	99.80	1334.23
56	0.06	3.72	0.06	1.15	3.79	0.67	22.32	7.80	97.23	37.10	164.92	33.21	349.99	55.91	777.93
average	**0.65**	**20.18**	**0.44**	**3.79**	**5.33**	**0.85**	**25.01**	**8.24**	**95.48**	**35.00**	**152.81**	**31.16**	**336.22**	**54.70**	**769.84**

TABLE F4A																			
LA-IC-MS ANALYSIS OF RUTILE (in ppm)																			
HOUTKRAAL REMAINDER PORTION 2																			
Sample	**Mg**	**Sc**	**V**	**Cr**	**Mn**	**Fe**	**Y**	**Zr**	**Nb**	**Mo**	**Sn**	**Ba**	**Hf**	**Ta**	**W**	**Pb**	**Th**	**U**	**U+Th**
1	60	5	1682	312	0	1182	0	221	493	15	1565	0	9	2	0	1	3	1	5550
2	55	16	2343	983	0	1430	0	1967	1743	32	14	0	92	117	48	0	0	4	8845
3	55	19	1317	372	1	1271	1	1165	1829	21	65	0	63	139	28	0	0	10	6357
4	328	1	1601	217	7	192	2	95	6	2	4	6	6	0	0	1	0	2	2472
5	57	7	985	339	23	2352	0	88	208	6	10	0	3	8	1212	0	1	2	5302
6	51	41	2233	1194	1	2681	0	336	7523	4	157	0	16	846	308	0	0	6	15397
7	58	50	1439	685	1	2204	1	79	133	3	354	0	3	3	437	0	1	25	5478
8	2492	26	628	500	240	17635	93	95	3314	6	147	501	5	258	278	119	655	150	27140
9	52	6	1464	3413	0	257	0	904	545	6	10	0	20	66	16	0	0	4	6762
10	54	3	1178	185	0	2938	1	536	725	6	12	0	21	25	132	2	0	0	5819
11	110	10	1228	1375	2	3340	1	141	1285	1	114	1	8	47	77	1	2	5	7747
12	52	29	1855	41	1	2926	0	293	1203	50	148	0	14	116	103	0	0	93	6927
13	191	35	306	177	29	3318	23	289	1575	3	90	68	8	42	23	84	18	6	6285
14	54	7	1324	136	2	801	0	127	349	11	17	0	3	1	0	1	0	4	2838
15	629	559	2061	613	68	7614	58	3295	4089	2	468	1086	184	324	133	39	54	29	21307
16	53	5	3000	499	0	606	0	1132	1548	25	20	0	79	96	37	0	0	20	7121
17	85	14	1294	769	19	3379	34	3343	934	1	77	3369	78	40	84	23	35	5	13582
18	53	12	1130	1282	0	1671	2	560	2214	1	113	3	21	190	904	0	2	2	8160
19	92	111	2253	59	9	3560	4	465	963	11	57	1	23	35	34	2	5	31	7713
20	61	218	1141	232	2	3415	11	252	2190	3	604	1	17	56	75	1	7	19	8303
21	51	11	1803	359	0	1092	0	295	215	7	12	0	10	18	0	0	0	1	3874
22	53	3	2376	103	3	1842	0	687	273	40	45	1	30	9	45	1	2	4	5517
23	56	3	2580	621	0	765	0	1788	1357	14	20	0	101	51	33	0	0	24	7414
24	65	2	1172	1087	1	2624	1	3055	396	1	109	0	111	115	19	0	5	144	8906
25	52	23	1595	508	1	2096	0	752	4403	19	48	0	41	313	318	0	0	12	10182
26	54	9	2044	2783	1	865	2	365	2493	5	206	1	18	416	518	1	6	9	9794
27	52	2	2597	790	0	1410	0	1106	281	3	16	1	32	20	0	0	1	1	6314
28	57	2	968	4	4	3857	0	243	309	8	35	0	9	10	52	0	0	1	5560
29	52	6	2180	488	0	1418	0	1409	1498	38	59	0	69	99	216	0	0	4	7536

TABLE 4A continued																			
LA-ICP-MS ANALYSIS OF RUTILE (in ppm)																			
HOUTKRAAL REMAINDER PORTION 2																			
Sample	**Mg**	**Sc**	**V**	**Cr**	**Mn**	**Fe**	**Y**	**Zr**	**Nb**	**Mo**	**Sn**	**Ba**	**Hf**	**Ta**	**W**	**Pb**	**Th**	**U**	**U+Th**
30	52	20	1891	1313	9	928	1	255	1774	3	128	1	14	107	166	0	2	7	6670
31	68	33	805	1055	2	3636	1	131	534	3	207	2	5	22	91	2	11	20	6629
32	52	51	491	1571	4	2249	0	69	2273	2	44	0	2	268	131	0	0	6	7214
33	56	2	911	66	17	3618	1	652	250	20	11	0	22	15	5	0	4	2	5651
34	51	64	1264	119	1	3548	0	360	5449	10	326	0	28	680	1766	0	0	86	13752
35	52	7	3228	1290	0	789	0	3295	1012	35	17	0	132	62	38	0	0	4	9960
36	99	524	1450	242	25	3632	462	5211	3876	1	533	502	261	114	76	15	92	23	17138
37	50	61	2316	1152	0	968	0	855	3332	7	102	0	53	129	278	0	1	4	9309
38	71	30	596	849	2	6612	0	773	14703	164	830	1	50	880	369	1	0	28	25959
39	50	65	508	8	1	4155	8	75	7388	0	1092	0	12	83	5	1	15	17	13484
40	52	1	1585	1291	20	2516	0	355	217	8	7	4	7	3	14	1	2	0	6084
average	**145**	**52**	**1571**	**727**	**12**	**2785**	**18**	**928**	**2122**	**15**	**197**	**139**	**42**	**146**	**202**	**7**	**23**	**20**	9151
LA-ICP-MS ANALYSIS OF RUTILE (in ppm)																			
HOUTKRAAL REMAINDER																			
Sample	**Mg**	**Sc**	**V**	**Cr**	**Mn**	**Fe**	**Y**	**Zr**	**Nb**	**Mo**	**Sn**	**Ba**	**Hf**	**Ta**	**W**	**Pb**	**Th**	**U**	**U+Th**
1	74	144	670	377	1	2950	0	274	1494	9	116	0	19	105	171	1	0	19	6423
2	64	2	1120	35	6	1856	1	124	144	3	3	6	5	14	7	1	5	1	3398
3	51	2	1658	493	0	2458	0	150	2406	7	188	0	5	77	17	0	0	5	7519
4	566	28	1097	388	35	4590	1	166	3897	2	214	5	9	246	352	2	0	11	11609
5	57	2	1300	1987	0	380	0	2088	987	56	34	0	62	61	59	0	0	28	7102
6	59	10	2379	1375	0	815	0	1641	2163	10	63	0	80	144	373	0	0	36	9149
7	57	3	604	18	1	3064	2	431	432	26	26	8	18	13	21	1	7	1	4735
8	332	5	2111	3914	22	960	0	244	2441	22	312	7	10	65	3	0	0	1	10449
9	58	8	2769	434	1	691	0	833	1183	4	28	0	42	98	121	0	0	56	6325
10	64	5	465	190	1	3283	0	126	172	187	17	0	4	0	2	3	0	29	4548
11	59	9	1623	1695	0	2070	0	962	1426	8	207	0	35	45	690	0	0	22	8853
12	57	7	1776	415	0	1235	0	590	963	15	5	0	30	22	3	0	0	0	5119
13	58	6	601	65	2	2617	1	85	212	1	32	5	2	27	516	0	2	0	4232

TABLE 4A continued																			
LA-ICP-MS ANALYSIS OF RUTILE (in ppm)																			
HOUTKRAAL REMAINDER																			
Sample	**Mg**	**Sc**	**V**	**Cr**	**Mn**	**Fe**	**Y**	**Zr**	**Nb**	**Mo**	**Sn**	**Ba**	**Hf**	**Ta**	**W**	**Pb**	**Th**	**U**	**U+Th**
14	59	8	1316	345	4	1792	0	406	524	10	46	0	18	46	145	0	0	15	4736
15	58	11	3074	452	2	973	0	3679	1073	22	17	0	160	60	42	0	0	32	9656
16	55	6	3320	656	0	1008	0	1082	1624	30	38	0	66	86	43	0	0	4	8019
17	62	9	2734	848	0	809	0	4173	2029	32	21	0	175	129	325	0	5	95	11447
18	67	1	633	268	1	3409	5	438	510	133	36	6	21	48	465	2	9	11	6064
19	58	7	2194	779	0	928	0	682	1491	9	65	0	37	95	17	0	0	14	6376
20	69	4	584	1334	14	3277	0	194	1607	9	44	0	7	121	39	0	0	23	7327
21	61	8	1482	464	0	2302	0	1959	1418	102	249	0	93	95	67	0	4	229	8532
22	61	4	1811	955	0	1121	0	2064	1040	18	23	0	58	53	57	0	0	4	7268
23	57	2	761	1153	9	423	1	8	32	2	6	6	3	2	0	0	3	1	2470
24	74	50	1818	217	2	3581	1	399	1385	30	89	1	18	20	3548	1	4	80	11315
25	58	16	1672	772	0	2049	0	525	4364	3	262	0	26	288	75	0	0	9	10121
26	57	2	944	43	44	2522	119	759	2087	40	64	0	33	35	133	29	523	69	7504
27	99	12	846	107	62	3155	3	766	617	34	32	2	23	24	356	5	10	10	6165
28	60	19	1021	288	1	1654	0	778	1455	23	25	0	37	20	17	0	0	8	5409
29	102	7	2858	684	11	680	1	1049	1053	13	15	0	54	38	43	0	1	13	6621
30	59	5	3319	1247	0	530	0	1098	2081	25	54	0	53	67	12	0	0	16	8567
31	66	31	2004	603	5	1686	0	1392	3154	120	19	0	72	217	352	1	0	13	9736
32	70	19	1526	2253	1	1670	0	128	2107	3	107	2	7	96	505	0	0	3	8498
33	60	58	1928	1011	2	2170	1	841	4603	3	243	0	42	413	242	1	3	16	11639
34	130	29	86	33	3	1835	3	222	1080	0	153	7	8	198	16	3	2	4	3812
35	60	4	651	113	1	3173	0	1042	1567	92	16	0	33	78	296	0	0	11	7138
36	65	6	1765	1019	10	1998	0	105	112	14	15	5	6	7	24	3	0	26	5182
37	64	20	3018	189	2	906	0	846	645	6	100	0	42	37	14	1	1	26	5917
38	62	11	1868	102	4	1325	2	710	689	21	176	1	43	52	120	1	4	29	5220
39	60	1	837	98	0	2392	0	1635	1268	11	16	0	49	87	25	0	0	64	6544
40	61	19	2084	735	0	1358	0	1195	2340	22	51	0	66	79	28	0	0	10	8051
41	61	18	548	1010	0	4310	0	37	2184	0	177	0	2	91	450	0	1	4	8894
average	**84**	**15**	**1582**	**711**	**6**	**1951**	**4**	**876**	**1514**	**29**	**83**	**2**	**38**	**85**	**239**	**1**	**14**	**26**	7261

TABLE 4A continued

LA-ICP-MS ANALYSIS OF RUTILE (in ppm)

GEELWAL KAROO

Sample	Mg	Sc	V	Cr	Mn	Fe	Y	Zr	Nb	Mo	Sn	Ba	Hf	Ta	W	Pb	Th	U	U+Th
1	76	67	560	40	228	8392	4	54	6715	3	182	3	6	489	925	2	2	24	17771
2	1613	90	1627	11906	239	44249	20	2079	392	16	145	537	62	19	31	1309	290	69	64693
3	597	53	1608	2243	66	32571	130	194	3048	10	991	196	9	247	660	196	341	95	43257
4	253	298	366	534	5	2028	14	1488	313	0	14	137	64	10	15	10	1	0	5552
5	81	3	722	38	15	1511	4	187	334	16	18	22	12	19	19	12	11	10	3033
6	67	2	692	3	4	2194	0	17	38	1	2	1	0	12	4	0	1	1	3038
7	570	78	883	171	57	26950	82	1174	1101	1	39	289	41	64	209	326	24	30	32090
8	463	78	330	257	214	5618	7	1074	1535	2	21	262	39	98	234	111	30	25	10400
9	178	463	451	456	88	11419	42	4784	3064	1	366	1069	220	196	174	81	70	27	23151
10	1378	216	596	1109	43	16109	21	1549	1632	4	63	268	56	85	104	59	56	33	23383
11	140	107	690	565	25	4167	33	488	1645	5	159	332	20	93	87	171	189	95	9009
12	129	43	1623	34	10	4019	32	4881	1020	4	69	2	138	67	162	2	5	45	12283
13	336	34	825	729	10	7107	20	582	10466	6	543	37	26	1355	1006	10	33	23	23148
14	102	143	611	536	22	4138	24	1742	2687	0	135	3493	79	262	44	11	32	22	14083
15	93	2	872	41	56	3482	1	568	187	27	30	10	23	5	13	2	2	10	5424
16	223	7	1559	912	7	2192	2	340	269	5	5	5	15	9	61	3	6	0	5620
17	171	167	854	363	60	8170	23	724	1563	1	74	1011	27	68	28	32	29	25	13388
18	68	31	1423	817	1	2103	0	209	2439	2	116	1	11	234	614	2	0	6	8078
19	62	1	752	283	4	5819	0	559	3347	4	66	0	19	71	25	0	0	29	11043
20	71	5	3546	892	1	715	0	1938	1554	21	17	1	81	58	10	3	0	31	8948
21	828	95	1521	732	193	13052	110	1100	921	14	60	433	26	46	230	245	258	34	19898
22	63	33	873	241	4	4709	0	558	5523	11	179	0	19	29	2215	1	0	27	14485
23	85	2	763	107	2	3319	1	951	327	7	20	1	28	21	48	1	2	1	5685
24	66	65	1576	1516	5	2059	10	1138	441	12	128	0	41	23	47	1	3	15	7146
25	64	186	515	48	1	4279	1	140	1111	0	2525	0	15	51	722	0	0	1	9661
26	66	4	2467	413	2	1274	6	1140	1227	20	9	15	54	126	24	1	14	6	6869
27	62	96	771	103	2	5730	5	1808	5013	2	2575	0	153	123	5	0	2	32	16484
28	158	41	592	578	7	30510	1	152	44882	10	901	63	11	4348	1548	3	5	26	83838
29	142	30	416	325	10	3690	14	3605	376	2	23	205	69	28	93	4	14	10	9057
30	66	11	203	15	4	5054	18	4202	1225	81	99	165	110	100	154	1	3	16	11529

TABLE 4A continued																			
LA-ICP-MS ANALYSIS OF RUTILE (in ppm)																			
GEELWAL KAROO																			
Sample	**Mg**	**Sc**	**V**	**Cr**	**Mn**	**Fe**	**Y**	**Zr**	**Nb**	**Mo**	**Sn**	**Ba**	**Hf**	**Ta**	**W**	**Pb**	**Th**	**U**	**U+Th**
31	64	17	2657	2816	4	1455	5	2628	5659	26	53	1	104	560	1192	0	0	20	17261
32	86	4	1980	694	3	1126	5	2038	992	47	7	3	56	37	26	2	1	6	7115
33	96	3	1157	412	2	5412	1	590	2841	97	80	1	29	625	385	1	0	69	11802
34	372	2	694	257	19	4248	6	443	437	8	11	126	20	28	43	6	35	3	6759
35	65	10	1371	230	4	1651	0	1257	1149	10	33	0	72	21	50	0	1	24	5948
36	276	15	531	108	7	3534	3	57	1295	0	32	12	2	109	33	4	8	2	6029
37	64	3	1282	681	4	3046	1	311	155	8	23	4	9	8	36	1	1	20	5655
38	74	24	6000	1357	1	743	41	5015	1212	34	7	1	177	74	35	1	5	18	14817
39	604	23	426	417	109	5187	51	1822	1492	7	95	64	63	114	183	59	22	70	10808
40	131	20	652	109	4	3151	14	824	1200	37	165	23	34	58	299	5	11	30	6768
41	58	5	1488	170	1	1422	14	1582	1134	60	18	0	61	74	19	1	1	15	6123
42	76	13	440	244	2	4057	10	1124	4939	4	114	3	37	115	343	1	6	40	11568
43	119	39	1617	224	7	6843	1	511	7770	119	230	2	22	586	125	1	1	136	18352
44	86	501	1654	422	95	7112	44	634	1769	2	150	1325	26	70	56	25	39	37	14049
45	257	4	661	418	8	3227	11	130	257	7	11	78	3	17	104	11	31	4	5239
46	418	12	995	541	20	9250	42	421	632	17	27	38	19	19	41	43	8	10	12552
47	441	13	218	277	57	4500	52	73	2058	13	29	1271	3	141	329	105	167	239	9987
48	63	9	1730	2814	4	2559	1	83	2114	0	93	2	4	170	4353	0	1	5	14004
49	114	2	678	396	7	2188	7	383	232	26	30	30	14	7	15	10	16	8	4161
50	126	8	1994	4227	2	1715	1	145	5830	2	108	1	9	406	142	2	2	8	14727
51	4447	94	1374	1221	394	53224	120	157	1747	4	75	1923	6	138	188	236	847	316	66509
52	1348	15	1205	1085	56	16423	82	80	1983	6	86	268	3	120	384	42	416	34	23636
average	**340**	**63**	**1175**	**868**	**42**	**7860**	**22**	**1149**	**2909**	**16**	**213**	**264**	**43**	**228**	**344**	**61**	**59**	**36**	15691

TABLE 4A continued

LA-ICP-MS ANALYSIS OF RUTILE (in ppm)

GRAAUWDUINEN

Sample	Mg	Sc	V	Cr	Mn	Fe	Y	Zr	Nb	Mo	Sn	Ba	Hf	Ta	W	Pb	Th	U	U+Th
1	162	2	695	23	11	3956	1	346	506	4	12	4	12	18	18	3	1	1	5774
2	319	6	392	1312	17	4950	6	227	384	1	43	1985	7	21	2211	5	5	12	11902
3	62	5	524	258	1	1200	1	467	207	19	21	0	15	10	48	0	3	62	2904
4	73	2	829	456	2	2562	1	671	755	63	37	4	34	58	21	5	2	27	5602
5	66	75	1416	1504	1	2383	2	71	1180	2	308	1	5	58	202	1	1	10	7287
6	61	39	2354	843	2	1166	0	717	1235	5	124	0	36	71	598	0	0	29	7279
7	57	11	1071	3902	2	2423	0	176	1172	20	116	0	11	51	375	0	0	50	9439
8	71	14	2017	627	2	1196	2	728	1824	24	31	3	34	140	36	1	0	11	6762
9	56	125	1908	4471	2	1217	0	96	916	5	93	1	2	82	35	0	1	28	9037
10	429	5	940	194	21	5861	5	547	572	11	43	17	17	32	40	25	11	2	8770
11	93	2	120	399	3	5043	7	323	2044	0	25	597	15	62	17	12	42	8	8811
12	120	3	1380	1157	26	4904	4	1114	697	2	4	16	34	59	4	3	2	12	9542
13	76	7	1881	1319	1	1818	1	1412	1044	6	128	3	61	54	57	1	2	24	7898
14	113	15	1294	27	5	2251	51	1933	19	5	6	3	68	1	1	2	6	14	5813
15	63	8	2699	479	1	950	8	976	1593	37	24	1	46	54	24	1	1	20	6986
16	102	3	773	232	4	4531	4	577	2026	21	32	2	33	75	186	2	1	12	8617
17	162	2	600	3282	4	3694	9	2346	2499	99	208	2	109	136	321	1	1	4	13478
18	126	1	1143	61	18	2718	7	417	69	10	23	8	14	2	26	2	5	45	4696
19	1276	25	463	889	57	14798	96	437	1530	3	66	3561	26	84	327	85	122	145	23991
20	501	14	1791	408	24	5653	14	1018	2137	6	28	32	41	104	175	15	2	10	11974
21	109	36	2950	6553	4	772	4	1588	2852	1	143	4	69	139	564	1	1	227	16018
22	56	7	833	140	2	3569	4	2240	1812	33	57	1	68	157	98	2	1	49	9128
23	81	2	1378	1800	1	4939	2	511	2138	18	127	1	20	251	9	1	3	20	11303
24	56	11	2007	630	2	2695	0	1202	2692	99	537	0	67	221	245	0	4	95	10564
25	114	23	976	1305	5	3551	7	2179	1950	7	154	11	64	87	211	2	4	12	10660
26	916	29	838	3486	38	15388	5	212	130	7	153	29	7	9	192	9	13	22	21481
27	2311	127	466	464	55	14251	152	738	1825	5	160	532	27	120	584	110	105	40	22072
28	171	111	2319	960	25	6360	17	985	2013	1	1114	45	44	80	440	11	7	17	14718
29	566	97	590	796	31	7108	7	163	1061	31	283	11	7	118	17	14	11	2	10912

TABLE 4A continued																			
LA-ICP-MS ANALYSIS OF RUTILE (in ppm)																			
GRAAUWDUINEN																			
Sample	**Mg**	**Sc**	**V**	**Cr**	**Mn**	**Fe**	**Y**	**Zr**	**Nb**	**Mo**	**Sn**	**Ba**	**Hf**	**Ta**	**W**	**Pb**	**Th**	**U**	**U+Th**
30	346	5	658	96	26	10358	11	1024	3205	25	77	222	29	167	617	9	8	12	16895
31	257	30	542	157	19	4750	12	580	1607	1	230	98	18	62	99	30	34	15	8540
32	53	4	859	325	50	5079	0	412	356	13	40	0	16	16	31	1	0	26	7281
33	95	6	1110	341	38	4632	2	181	708	2	25	4	9	45	157	3	2	1	7358
34	125	6	1459	145	4	4391	15	2830	576	153	23	2	75	15	225	1	2	58	10105
35	63	93	3210	4057	3	1428	12	1477	2327	7	164	0	60	64	828	1	1	57	13851
36	281	7	2340	629	5	3321	5	717	1604	19	44	37	26	70	284	37	2	8	9436
37	156	2	632	1071	6	3892	2	133	292	2	26	4	6	15	46	2	1	1	6288
38	103	66	2780	986	3	1160	2	2995	500	14	17	3	121	22	16	2	1	6	8797
39	315	5	723	233	21	8811	4	70	1215	0	453	12688	2	98	586	5	6	1	25236
40	75	3	1798	319	2	1735	1	1072	1157	25	14	2	47	68	5	1	0	7	6329
41	760	21	734	764	145	9704	142	614	6319	42	343	9056	12	294	199	144	539	102	29933
42	85	2	623	283	1	3791	16	734	649	6	36	14	32	32	58	1	3	12	6380
43	88	15	1691	354	3	2318	1	1413	1198	35	25	6	66	56	46	3	4	19	7341
44	58	12	2666	448	2	1169	1	1287	2296	38	8	4	67	71	54	1	1	11	8193
45	560	5	999	271	38	9785	1	743	754	36	25	17	43	36	32	54	6	8	13414
46	159	7	1253	404	16	4472	1	816	1356	7	35	3	22	127	17	1	0	8	8703
47	67	2	486	1991	2	2805	10	3075	446	30	16	0	83	39	3023	1	1	3	12080
48	101	12	1026	4116	6	3079	23	5752	7291	33	312	65	155	278	253	3	5	78	22587
49	162	526	1385	388	74	10203	42	1593	1586	1	182	1545	62	35	55	35	21	80	17975
50	234	69	1819	1753	8	2681	10	824	2566	1	117	12	40	114	639	2	3	10	10904
average	**250**	**34**	**1309**	**1142**	**17**	**4629**	**15**	**1055**	**1538**	**21**	**126**	**613**	**40**	**81**	**287**	**13**	**20**	**31**	11221
LA-ICP-MS ANALYSIS OF RUTILE (in ppm)																			
RIETFONTEIN																			
Sample	**Mg**	**Sc**	**V**	**Cr**	**Mn**	**Fe**	**Y**	**Zr**	**Nb**	**Mo**	**Sn**	**Ba**	**Hf**	**Ta**	**W**	**Pb**	**Th**	**U**	**U+Th**
1	125	41	7118	1031	1	3260	1	2478	5298	25	365	3	176	356	561	1	2	34	20874
2	159	8	3305	630	1	7059	1	1781	661	80	75	2	73	23	129	1	1	1	13991
3	143	100	3935	1018	1	7151	0	3066	22523	100	244	1	243	1292	1733	0	1	66	41616
4	119	33	2817	1562	49	6857	1	601	2372	16	169	0	28	225	135	0	0	131	15116

TABLE 4A continued																			
LA-ICP-MS ANALYSIS OF RUTILE (in ppm)																			
RIETFONTEIN																			
Sample	**Mg**	**Sc**	**V**	**Cr**	**Mn**	**Fe**	**Y**	**Zr**	**Nb**	**Mo**	**Sn**	**Ba**	**Hf**	**Ta**	**W**	**Pb**	**Th**	**U**	**U+Th**
5	139	466	2689	7330	13	6167	3	1545	12363	7	940	8	116	560	459	2	26	63	32897
6	114	30	7637	1980	1	1810	0	3997	2776	122	49	0	249	39	23	0	0	43	18870
7	112	101	2610	2662	1	7597	0	2362	11518	103	1866	0	129	718	3118	0	0	249	33147
8	120	13	4193	451	1	11012	4	2775	42402	60	435	4	118	1411	385	0	1	201	63586
9	109	12	6905	729	1	5229	0	6470	8422	56	808	0	281	805	467	0	0	224	30519
10	106	186	4797	4752	1	5867	0	281	354	11	470	0	9	30	1237	0	0	41	18142
11	107	42	4249	1816	2	1113	6	2826	3655	55	73	12	119	291	23	2	25	8	14426
12	99	25	4750	995	1	1927	0	2153	3988	69	176	0	153	350	513	0	0	15	15214
13	1226	76	2138	4562	214	45473	282	249	3274	3	123	1940	7	270	651	324	1160	202	62174
14	91	11	3896	728	4	3769	0	2286	4349	38	205	0	190	349	691	1	0	95	16703
15	91	23	3446	813	1	2158	0	2351	3517	30	33	1	157	276	537	0	0	64	13498
16	158	67	5037	111	3	2553	0	755	885	10	205	2509	32	20	111	2	0	29	12487
17	7789	38	4932	6024	183	24032	35	931	1966	22	486	71	35	84	97	27	0	112	46865
18	541	12	3558	180	49	7989	2	1301	1965	45	74	12	59	107	9	6	2	7	15917
19	121	15	2190	1819	3	1984	0	2938	1040	15	40	1	65	125	52	2	1	71	10482
20	81	2	1284	698	1	5756	0	523	1028	88	19	0	18	135	242	2	0	1	9879
21	74	4	2690	1578	13	1968	0	364	1304	17	25	1	13	82	978	1	1	8	9119
22	171	22	2069	891	21	3735	2	104	709	1	522	3	11	29	1019	5	7	3	9324
23	236	147	1408	399	70	5178	10	93	1296	3	2273	19	7	124	187	11	9	26	11497
24	5291	158	4696	6793	244	58889	100	417	5872	16	155	1732	16	444	392	552	1363	273	87403
25	69	11	2746	313	1	2468	0	3312	1987	224	47	2	83	62	335	1	2	3	11666
26	79	5	932	2149	3	934	7	668	1011	44	24	4	28	56	46	5	22	18	6034
27	65	17	2823	2350	1	1057	0	3493	2545	37	98	0	185	138	328	0	0	46	13184
28	92	5	1632	29	2	3137	1	467	795	10	20	1	16	45	210	1	2	2	6467
29	70	8	3552	1783	1	2220	0	2521	4352	93	198	0	160	328	501	2	1	110	15900
30	63	2	930	425	1	4558	1	222	547	7	8	2	9	42	15	1	2	0	6835
31	64	19	2788	1098	2	4291	0	809	290	8	36	1	31	14	2	1	0	1	9456

TABLE 4A continued																			
LA-ICP-MS ANALYSIS OF RUTILE (in ppm)																			
RIETFONTEIN																			
Sample	**Mg**	**Sc**	**V**	**Cr**	**Mn**	**Fe**	**Y**	**Zr**	**Nb**	**Mo**	**Sn**	**Ba**	**Hf**	**Ta**	**W**	**Pb**	**Th**	**U**	**U+Th**
32	68	43	2673	3149	1	874	1	97	3592	0	147	0	6	264	97	0	1	1	11014
33	68	231	4696	1644	1	436	0	1331	3990	1	202	0	58	162	430	0	0	27	13277
34	63	4	3255	188	1	4572	0	1775	5890	80	292	0	117	332	32	1	0	134	16735
35	59	38	2715	822	16	1365	0	1568	2550	37	69	0	68	182	51	0	0	8	9549
36	139	2	936	282	10	2807	0	2072	1225	11	57	2	70	69	36	0	1	51	7768
37	68	15	3046	498	3	1339	0	2662	2106	131	226	0	129	110	501	0	0	50	10884
38	60	80	3199	1186	3	1147	0	703	4637	2	166	0	32	385	276	4	0	12	11892
39	69	3	387	1434	1	2732	0	1430	313	61	10	0	46	29	52	0	0	9	6577
40	140	19	176	1896	3	3821	12	80	4069	1	33	3	6	1157	33	4	8	26	11486
41	58	1	933	52	2	3244	0	1335	4448	4	36	0	48	218	21	2	0	72	10473
42	72	17	1993	1023	2	1299	12	9166	1050	22	35	0	310	45	16	1	1	35	15098
43	58	7	450	553	14	1977	1	305	1247	44	19	3	8	30	27	2	2	31	4776
44	180	1	771	67	4	1605	2	229	208	20	3	10	5	10	12	1	9	1	3138
45	289	14	655	30	5	2923	2	511	2632	30	157	2	19	25	274	1	5	42	7616
average	**427**	**48**	**2970**	**1567**	**21**	**6163**	**11**	**1720**	**4289**	**41**	**260**	**141**	**83**	**263**	**379**	**22**	**59**	**59**	18524

TABLE F4B

REE CHEMISTRY OF RUTILE DETERMINED WITH LA-ICP-MS (in ppm)

HOUTKRAAL REMAINDER PORTION 2

Sample	La	Ce	Pr	Nd	Sm	Eu	Gd	Tb	Dy	Ho	Er	Tm	Yb	Lu	TREE
1	0.11	0.19	0.02	0.03	0.05	0.02	0.09	0.02	0.11	0.03	0.06	0.01	0.09	0.01	0.83
2	0.00	0.00	0.00	0.02	0.02	0.01	0.01	0.00	0.01	0.00	0.00	0.00	0.51	0.00	0.59
3	0.01	0.12	0.01	0.07	0.14	0.00	0.12	0.02	0.16	0.02	0.18	0.01	0.57	0.04	1.47
4	0.90	0.61	0.21	0.93	0.18	0.03	0.21	0.03	0.26	0.07	0.21	0.04	0.28	0.04	3.99
5	0.05	0.14	0.04	0.28	0.14	0.04	0.07	0.02	0.23	0.06	0.16	0.01	0.23	0.04	1.49
6	0.01	0.02	0.00	0.02	0.02	0.01	0.02	0.00	0.01	0.00	0.01	0.00	0.06	0.00	0.17
7	0.06	0.23	0.04	0.34	0.21	0.03	0.28	0.07	0.22	0.05	0.07	0.02	0.15	0.02	1.78
8	51.02	117.72	17.85	86.31	49.65	11.40	55.95	7.21	38.57	6.50	16.63	2.08	13.72	1.72	476.33
9	0.24	0.42	0.04	0.19	0.08	0.01	0.02	0.00	0.01	0.00	0.00	0.00	0.13	0.00	1.14
10	0.00	0.00	0.00	0.02	0.02	0.01	0.02	0.00	0.01	0.02	0.11	0.03	0.50	0.10	0.84
11	0.87	1.81	0.43	1.75	0.33	0.05	0.20	0.02	0.16	0.03	0.11	0.01	0.11	0.02	5.88
12	0.04	0.04	0.00	0.02	0.01	0.00	0.01	0.01	0.04	0.02	0.04	0.01	0.19	0.03	0.45
13	31.15	37.78	8.95	34.41	6.04	0.97	6.27	0.89	4.86	0.87	1.80	0.23	1.31	0.20	135.74
14	0.38	1.01	0.16	0.76	0.13	0.04	0.08	0.01	0.05	0.01	0.03	0.00	0.03	0.00	2.70
15	18.43	43.30	5.00	20.92	8.03	2.73	10.74	2.32	16.93	3.73	10.16	1.42	9.62	1.14	154.47
16	0.00	0.01	0.00	0.02	0.02	0.01	0.02	0.00	0.01	0.00	0.01	0.00	0.41	0.00	0.50
17	43.10	59.44	9.32	33.55	8.25	3.22	14.78	2.12	10.53	1.67	4.74	0.70	6.29	1.18	198.89
18	0.20	0.66	0.09	0.35	0.30	0.04	0.18	0.11	0.43	0.11	0.50	0.23	1.13	0.13	4.44
19	0.67	3.02	0.42	1.75	0.51	0.14	0.73	0.16	0.70	0.26	0.53	0.13	1.22	0.15	10.39
20	11.16	43.37	8.76	47.62	16.05	3.10	11.17	1.37	5.55	0.72	1.39	0.14	1.12	0.11	151.63
21	0.00	0.02	0.01	0.02	0.02	0.01	0.02	0.00	0.01	0.00	0.03	0.00	0.07	0.00	0.20
22	0.47	1.01	0.23	0.64	0.12	0.02	0.10	0.01	0.10	0.02	0.04	0.00	0.17	0.01	2.94
23	0.03	0.04	0.01	0.01	0.02	0.01	0.02	0.00	0.01	0.00	0.01	0.00	0.55	0.00	0.70
24	0.51	0.82	0.09	0.36	0.08	0.02	0.11	0.02	0.15	0.04	0.12	0.02	0.80	0.04	3.17
25	0.11	0.13	0.02	0.16	0.01	0.01	0.01	0.00	0.01	0.00	0.01	0.00	0.23	0.00	0.69
26	0.44	1.23	0.25	1.43	0.92	0.07	0.97	0.11	0.67	0.15	0.32	0.05	0.34	0.03	6.98
27	0.05	0.19	0.02	0.07	0.02	0.01	0.03	0.01	0.06	0.01	0.02	0.00	0.21	0.01	0.71
28	0.00	0.01	0.00	0.01	0.02	0.01	0.02	0.00	0.01	0.00	0.01	0.00	0.05	0.00	0.14
29	0.00	0.00	0.00	0.02	0.02	0.01	0.02	0.00	0.01	0.00	0.01	0.00	0.41	0.00	0.50
30	0.13	0.27	0.05	0.12	0.07	0.02	0.06	0.02	0.18	0.03	0.08	0.01	0.17	0.01	1.22

TABLE F4B continued															
REE CHEMISTRY OF RUTILE DETERMINED WITH LA-ICP-MS (in ppm)															
HOUTKRAAL REMAINDER PORTION 2															
Sample	**La**	**Ce**	**Pr**	**Nd**	**Sm**	**Eu**	**Gd**	**Tb**	**Dy**	**Ho**	**Er**	**Tm**	**Yb**	**Lu**	**TREE**
31	2.93	4.21	0.49	1.85	0.26	0.06	0.15	0.03	0.19	0.04	0.10	0.02	0.18	0.02	10.52
32	0.16	0.26	0.08	0.20	0.03	0.01	0.03	0.00	0.03	0.00	0.02	0.00	0.01	0.00	0.84
33	0.25	0.65	0.13	0.47	0.05	0.01	0.02	0.01	0.08	0.02	0.06	0.01	0.36	0.02	2.13
34	0.00	0.00	0.00	0.02	0.02	0.01	0.02	0.00	0.01	0.00	0.02	0.00	0.20	0.00	0.30
35	0.00	0.00	0.00	0.01	0.02	0.01	0.02	0.00	0.01	0.00	0.01	0.00	0.78	0.00	0.86
36	44.62	58.65	13.25	58.22	18.66	5.63	31.94	7.24	54.89	13.64	43.21	6.31	42.60	6.39	405.25
37	0.00	0.04	0.00	0.02	0.02	0.01	0.02	0.00	0.02	0.00	0.03	0.00	0.26	0.01	0.42
38	0.19	0.25	0.04	0.11	0.01	0.01	0.02	0.01	0.07	0.00	0.01	0.00	0.24	0.01	0.95
39	2.95	14.79	3.53	18.95	6.27	2.29	5.42	0.71	3.18	0.45	1.06	0.13	0.98	0.16	60.87
40	0.80	0.96	0.17	0.49	0.17	0.04	0.27	0.04	0.11	0.03	0.10	0.01	0.10	0.01	3.30
average	**5.30**	**9.84**	**1.74**	**7.81**	**2.92**	**0.75**	**3.51**	**0.56**	**3.47**	**0.71**	**2.05**	**0.29**	**2.16**	**0.30**	**41.41**
REE CHEMISTRY OF RUTILE DETERMINED WITH LA-ICP-MS (in ppm)															
HOUTKRAAL REMAINDER															
Sample	**La**	**Ce**	**Pr**	**Nd**	**Sm**	**Eu**	**Gd**	**Tb**	**Dy**	**Ho**	**Er**	**Tm**	**Yb**	**Lu**	**TREE**
1	0.12	0.17	0.15	0.40	0.19	0.02	0.27	0.02	0.09	0.02	0.05	0.01	0.24	0.01	1.76
2	0.57	1.68	0.27	1.17	0.49	0.11	0.35	0.08	0.38	0.05	0.14	0.02	0.17	0.04	5.52
3	0.19	0.41	0.05	0.19	0.09	0.00	0.03	0.02	0.02	0.02	0.03	0.01	0.04	0.00	1.11
4	0.74	1.58	0.19	1.02	0.22	0.04	0.19	0.05	0.40	0.08	0.18	0.04	0.20	0.03	4.95
5	0.02	0.13	0.07	0.01	0.01	0.01	0.27	0.02	0.09	0.02	0.05	0.01	0.35	0.00	1.07
6	0.60	0.41	0.09	0.40	0.06	0.02	0.07	0.00	0.06	0.01	0.02	0.00	0.45	0.01	2.19
7	0.15	0.69	0.09	0.49	0.23	0.12	0.57	0.14	1.03	0.18	0.50	0.07	0.41	0.05	4.73
8	0.24	0.51	0.04	0.23	0.19	0.02	0.04	0.02	0.03	0.00	0.05	0.01	0.04	0.01	1.42
9	0.03	0.12	0.01	0.05	0.01	0.01	0.02	0.02	0.09	0.01	0.05	0.00	0.25	0.00	0.68
10	0.04	0.02	0.00	0.01	0.19	0.02	0.27	0.00	0.01	0.02	0.00	0.01	0.03	0.01	0.64
11	0.12	0.02	0.07	0.03	0.02	0.00	0.01	0.02	0.01	0.02	0.05	0.01	0.18	0.00	0.55
12	0.05	0.06	0.07	0.01	0.19	0.00	0.27	0.00	0.01	0.02	0.05	0.01	0.14	0.01	0.89
13	0.22	0.78	0.11	0.73	0.21	0.04	0.31	0.08	0.45	0.10	0.23	0.01	0.17	0.00	3.45
14	0.01	0.02	0.07	0.01	0.01	0.02	0.27	0.02	0.01	0.02	0.05	0.01	0.15	0.01	0.67
15	0.00	0.01	0.07	0.70	0.19	0.00	0.27	0.02	0.01	0.00	0.00	0.01	0.85	0.00	2.14

TABLE F4B continued															
REE CHEMISTRY OF RUTILE DETERMINED WITH LA-ICP-MS (in ppm)															
HOUTKRAAL REMAINDER															
Sample	**La**	**Ce**	**Pr**	**Nd**	**Sm**	**Eu**	**Gd**	**Tb**	**Dy**	**Ho**	**Er**	**Tm**	**Yb**	**Lu**	**TREE**
16	0.01	0.03	0.07	0.05	0.19	0.02	0.27	0.02	0.09	0.02	0.05	0.01	0.35	0.01	1.19
17	0.00	0.13	0.07	0.70	0.01	0.02	0.27	0.02	0.01	0.02	0.05	0.00	0.91	0.01	2.23
18	1.84	4.25	0.67	2.75	1.18	0.31	1.21	0.29	1.99	0.38	1.11	0.17	1.25	0.16	17.55
19	0.12	0.13	0.07	0.03	0.19	0.00	0.27	0.02	0.02	0.02	0.05	0.01	0.17	0.00	1.11
20	0.00	0.00	0.07	0.01	0.01	0.02	0.27	0.02	0.01	0.02	0.05	0.01	0.04	0.01	0.55
21	0.00	0.01	0.00	0.01	0.19	0.02	0.27	0.02	0.09	0.02	0.01	0.00	0.42	0.01	1.07
22	0.01	0.07	0.01	0.03	0.19	0.02	0.27	0.02	0.01	0.00	0.05	0.01	0.32	0.01	1.03
23	0.14	0.16	0.03	0.10	0.08	0.04	0.17	0.04	0.19	0.03	0.12	0.02	0.08	0.01	1.22
24	0.89	0.08	0.43	0.04	0.13	0.01	0.15	0.01	17.59	19.50	3548.04	0.96	3.99	80.17	3671.99
25	0.11	0.13	0.07	0.11	0.19	0.02	0.01	0.02	0.01	0.00	0.05	0.01	0.17	0.01	0.90
26	46.29	7.53	27.54	4.23	9.40	2.17	2.90	0.20	33.19	35.13	133.27	28.88	523.19	68.78	922.70
27	0.97	2.76	0.39	0.98	0.68	0.10	0.91	0.16	0.87	0.15	0.49	0.12	1.16	0.22	9.96
28	0.12	4.97	0.01	0.02	0.19	0.00	0.27	0.02	0.09	0.01	0.05	0.00	0.18	0.01	5.94
29	0.53	0.98	0.11	0.57	0.16	0.03	0.17	0.03	0.21	0.05	0.13	0.03	0.44	0.03	3.48
30	0.12	0.03	0.00	0.07	0.19	0.02	0.05	0.01	0.09	0.02	0.05	0.00	0.29	0.00	0.94
31	0.10	0.13	0.03	0.70	0.19	0.02	0.27	0.01	0.01	0.02	0.05	0.01	0.51	0.01	2.06
32	0.09	0.20	0.03	0.12	0.08	0.00	0.03	0.01	0.06	0.01	0.01	0.00	0.06	0.01	0.72
33	2.02	5.52	0.77	3.92	1.01	0.06	0.42	0.06	0.19	0.07	0.17	0.03	0.18	0.01	14.42
34	2.51	1.53	0.43	2.86	0.43	0.08	0.42	0.09	0.91	0.17	0.48	0.08	1.05	0.17	11.21
35	0.18	0.13	0.04	0.14	0.19	0.01	0.27	0.02	0.13	0.02	0.07	0.01	0.18	0.00	1.39
36	0.12	0.14	0.04	0.19	0.10	0.02	0.07	0.01	0.06	0.01	0.06	0.01	0.07	0.00	0.89
37	0.02	0.12	0.01	0.02	0.19	0.01	0.02	0.02	0.01	0.02	0.00	0.01	0.25	0.01	0.70
38	0.31	1.77	0.44	2.89	1.50	0.07	1.25	0.15	0.84	0.14	0.30	0.05	0.50	0.04	10.25
39	0.12	0.13	0.00	0.70	0.19	0.02	0.02	0.00	0.01	0.01	0.00	0.00	0.29	0.00	1.49
40	0.01	0.04	0.00	0.02	0.19	0.02	0.27	0.02	0.09	0.00	0.00	0.01	0.38	0.01	1.06
41	0.52	0.94	0.17	0.72	0.20	0.02	0.17	0.03	0.11	0.03	0.06	0.01	0.04	0.00	3.01
average	**1.47**	**0.94**	**0.80**	**0.67**	**0.48**	**0.09**	**0.34**	**0.04**	**1.45**	**1.38**	**89.91**	**0.75**	**13.17**	**3.66**	**115.14**

TABLE F4B continued															
REE CHEMISTRY OF RUTILE DETERMINED WITH LA-ICP-MS (in ppm)															
GEELWAL KAROO															
Sample	**La**	**Ce**	**Pr**	**Nd**	**Sm**	**Eu**	**Gd**	**Tb**	**Dy**	**Ho**	**Er**	**Tm**	**Yb**	**Lu**	**TREE**
1	0.72	1.12	0.14	0.73	0.36	0.24	0.80	0.19	1.11	0.24	0.57	0.10	0.76	0.09	7.16
2	238.25	300.54	40.92	124.56	17.00	2.68	9.94	1.31	6.67	1.16	2.68	0.42	3.13	0.44	749.70
3	99.07	134.99	16.38	65.67	29.45	10.13	53.79	8.48	46.81	9.34	26.17	4.30	32.45	5.06	542.09
4	10.87	20.70	2.61	12.11	3.25	2.68	3.88	0.55	3.23	0.59	1.34	0.17	1.12	0.09	63.19
5	1.51	4.09	0.54	2.42	1.00	0.33	1.24	0.25	1.37	0.28	0.88	0.14	0.95	0.13	15.13
6	0.95	2.09	0.21	0.74	0.17	0.03	0.10	0.02	0.10	0.03	0.06	0.01	0.05	0.01	4.55
7	29.92	63.01	7.65	31.61	8.77	1.80	10.57	2.83	25.11	4.96	16.20	2.73	19.82	2.60	227.58
8	7.22	20.13	1.66	6.38	1.96	0.45	1.62	0.35	2.19	0.54	1.58	0.21	1.91	0.29	46.49
9	25.22	60.86	7.86	38.70	16.79	3.77	18.98	2.94	14.85	2.39	5.61	0.72	5.61	0.62	204.92
10	91.31	93.14	14.03	61.20	21.76	3.18	12.77	1.83	8.64	1.60	3.80	0.45	3.86	0.44	318.01
11	204.63	145.09	14.97	49.98	10.23	2.64	18.01	2.82	14.37	2.39	5.43	0.76	5.28	0.70	477.30
12	1.65	4.17	0.40	1.79	0.80	0.22	0.90	0.26	2.83	1.00	5.56	1.51	17.09	4.10	42.28
13	13.23	26.76	3.88	16.01	4.42	1.24	5.21	1.00	6.41	1.39	3.95	0.65	4.44	0.74	89.32
14	10.06	18.34	2.29	8.86	3.10	1.04	4.05	0.89	6.32	1.41	3.93	0.64	5.67	0.79	67.39
15	0.83	1.38	0.23	1.53	0.10	0.03	0.15	0.05	0.38	0.05	0.13	0.03	0.34	0.01	5.23
16	3.70	2.77	0.48	2.57	1.08	0.15	1.24	0.18	0.99	0.18	0.31	0.06	0.41	0.04	14.17
17	16.63	42.80	4.67	19.64	6.38	1.58	8.11	1.64	8.88	1.48	3.31	0.37	2.53	0.28	118.30
18	0.17	0.37	0.05	0.08	0.07	0.01	0.05	0.01	0.03	0.01	0.01	0.01	0.07	0.06	0.93
19	0.02	0.04	0.03	0.01	0.1	0.01	0.01	0.06	0.01	0.00	0.00	0.00	0.13	0.06	0.33
20	0.07	0.18	0.02	0.10	0.02	0.01	0.1	0.01	0.02	0.01	0.06	0.02	0.57	0.03	1.12
21	127.16	237.04	30.85	119.26	32.84	8.33	34.97	6.60	39.07	6.82	16.10	1.91	11.52	1.44	673.91
22	0.17	0.41	0.04	0.18	0.04	0.02	0.03	0.01	0.04	0.01	0.03	0.00	0.12	0.01	1.11
23	0.41	0.69	0.10	0.49	0.25	0.02	0.28	0.06	0.17	0.04	0.16	0.04	0.43	0.06	3.19
24	0.22	3.49	0.18	1.13	0.59	0.19	1.45	0.22	1.73	0.37	1.35	0.24	2.38	0.31	13.85
25	0.02	0.19	0.10	0.14	0.1	0.01	0.06	0.02	0.15	0.03	0.07	0.02	0.24	0.04	1.09
26	0.74	4.18	0.37	2.23	1.71	0.44	2.09	0.27	2.09	0.41	1.18	0.16	1.74	0.14	17.75
27	0.18	1.55	0.16	1.03	0.41	0.12	0.70	0.14	1.28	0.15	0.35	0.08	1.51	0.10	7.74

TABLE F4B continued															
REE CHEMISTRY OF RUTILE DETERMINED WITH LA-ICP-MS (in ppm)															
GEELWAL KAROO															
Sample	**La**	**Ce**	**Pr**	**Nd**	**Sm**	**Eu**	**Gd**	**Tb**	**Dy**	**Ho**	**Er**	**Tm**	**Yb**	**Lu**	**TREE**
28	1.05	1.80	0.21	0.74	0.29	0.09	0.39	0.09	0.35	0.07	0.16	0.03	0.31	0.03	5.60
29	1.59	3.65	0.36	1.72	0.64	0.20	1.31	0.29	1.93	0.57	1.80	0.38	3.20	0.41	18.03
30	0.30	2.31	0.15	0.80	0.61	0.20	1.12	0.28	2.44	0.58	2.34	0.46	4.43	0.55	16.56
31	0.02	0.27	0.02	0.08	0.06	0.00	0.16	0.06	0.59	0.15	0.66	0.16	1.72	0.16	4.11
32	0.21	0.67	0.12	0.38	0.15	0.03	0.23	0.07	0.81	0.22	0.76	0.18	1.99	0.20	6.03
33	0.39	0.58	0.11	0.41	0.06	0.01	0.08	0.02	0.13	0.06	0.13	0.02	0.49	0.03	2.52
34	32.03	59.05	6.06	22.69	3.63	0.72	2.44	0.36	1.97	0.36	0.93	0.15	0.88	0.10	131.36
35	0.25	0.43	0.11	0.52	0.04	0.01	0.03	0.01	0.04	0.01	0.01	0.00	0.41	0.01	1.87
36	1.80	5.16	0.65	2.80	1.30	0.26	1.47	0.18	1.16	0.18	0.65	0.10	0.77	0.08	16.57
37	0.38	0.99	0.17	0.71	0.26	0.09	0.36	0.03	0.21	0.04	0.06	0.02	0.14	0.01	3.45
38	0.16	1.78	0.18	1.26	1.24	0.48	2.90	0.73	6.19	1.41	4.69	1.16	10.80	1.17	34.15
39	32.43	38.71	5.68	22.70	5.95	1.36	7.14	1.64	11.41	2.21	5.80	1.15	11.21	1.19	148.58
40	3.22	4.40	0.46	1.97	1.10	0.32	1.64	0.38	2.89	0.65	2.22	0.36	3.14	0.43	23.18
41	0.19	0.62	0.08	0.45	0.34	0.15	0.92	0.25	1.79	0.42	1.92	0.35	3.81	0.42	11.71
42	0.37	1.27	0.13	0.67	0.42	0.16	1.24	0.26	1.93	0.51	1.64	0.35	3.26	0.34	12.55
43	0.62	1.01	0.16	0.80	0.19	0.06	0.22	0.03	0.25	0.07	0.13	0.04	0.36	0.03	3.96
44	25.51	46.66	4.57	17.18	5.24	1.52	6.07	1.64	12.86	2.73	7.60	1.09	7.35	0.85	140.87
45	5.31	10.50	1.83	9.39	3.44	1.20	3.58	0.55	3.52	0.75	2.16	0.25	1.83	0.25	44.57
46	45.94	85.58	10.22	44.99	11.53	2.10	12.26	1.97	11.44	2.28	6.45	0.96	7.02	1.17	243.91
47	173.74	272.63	27.57	129.37	30.50	7.27	28.39	3.09	13.85	2.29	4.82	0.56	3.30	0.38	697.76
48	0.39	0.69	0.07	0.29	0.05	0.03	0.07	0.03	0.10	0.02	0.05	0.02	0.46	0.00	2.27
49	6.05	9.86	1.16	4.69	1.85	0.63	2.65	0.43	2.12	0.42	1.06	0.12	0.77	0.10	31.92
50	0.42	0.85	0.09	0.31	0.06	0.02	0.10	0.03	0.12	0.03	0.06	0.02	0.07	0.00	2.18
51	109.97	274.93	34.79	160.95	71.22	15.74	67.66	9.61	50.42	8.78	21.41	2.95	19.07	2.60	850.10
52	27.31	74.82	11.46	62.81	30.63	6.72	44.07	6.29	31.93	5.48	13.06	1.67	10.09	1.36	327.70
average	**26.05**	**40.18**	**4.95**	**20.34**	**6.67**	**1.55**	**7.40**	**1.18**	**6.83**	**1.29**	**3.49**	**0.54**	**4.25**	**0.61**	**124.91**

TABLE F4B continued															
REE CHEMISTRY OF RUTILE DETERMINED WITH LA-ICP-MS (in ppm)															
GRAAUWDUINEN															
Sample	**La**	**Ce**	**Pr**	**Nd**	**Sm**	**Eu**	**Gd**	**Tb**	**Dy**	**Ho**	**Er**	**Tm**	**Yb**	**Lu**	**TREE**
1	0.41	0.86	0.20	0.42	0.14	0.08	0.15	0.06	0.20	0.14	0.21	0.04	0.30	0.02	3.24
2	6.15	13.49	1.29	4.42	1.26	0.44	1.60	0.25	1.65	0.21	0.55	0.11	0.99	0.08	32.48
3	0.08	0.30	0.03	0.14	0.10	0.03	0.21	0.02	0.12	0.02	0.07	0.00	0.18	0.03	1.33
4	0.72	0.74	0.12	0.52	0.23	0.10	0.39	0.06	0.32	0.07	0.19	0.02	0.33	0.02	3.82
5	0.32	0.69	0.07	0.40	0.09	0.04	0.26	0.05	0.28	0.07	0.23	0.04	0.33	0.04	2.88
6	0.11	0.32	0.04	0.23	0.13	0.02	0.07	0.02	0.18	0.02	0.06	0.02	0.26	0.01	1.48
7	0.03	0.16	0.01	0.04	0.04	0.00	0.03	0.01	0.03	0.02	0.11	0.01	0.15	0.02	0.65
8	0.05	0.24	0.02	0.05	0.07	0.02	0.05	0.01	0.14	0.07	0.30	0.02	0.43	0.05	1.52
9	0.18	0.35	0.04	0.15	0.06	0.01	0.08	0.01	0.09	0.02	0.12	0.00	0.06	0.02	1.19
10	15.34	28.71	3.84	15.00	4.08	0.50	3.98	0.42	1.94	0.27	0.69	0.10	0.69	0.11	75.65
11	23.20	63.42	8.71	35.99	6.95	2.14	4.27	0.57	2.59	0.32	0.57	0.06	0.42	0.05	149.26
12	0.47	1.84	0.14	0.75	0.17	0.08	0.37	0.08	0.51	0.12	0.28	0.06	0.60	0.05	5.51
13	0.23	0.73	0.09	0.47	0.16	0.04	0.15	0.05	0.26	0.04	0.23	0.02	0.52	0.04	3.05
14	0.49	2.87	0.32	1.98	1.64	0.84	4.36	0.84	7.43	1.41	4.92	0.98	8.93	1.26	38.28
15	0.11	0.87	0.07	0.61	0.27	0.14	0.62	0.22	1.81	0.36	1.11	0.25	2.32	0.26	9.02
16	0.37	1.25	0.11	0.36	0.10	0.06	0.13	0.13	0.85	0.16	0.23	0.11	1.09	0.11	5.07
17	0.45	1.23	0.40	0.88	0.31	0.05	0.45	0.12	1.24	0.28	1.24	0.29	2.56	0.32	9.82
18	0.74	1.82	0.23	1.28	0.37	0.14	0.67	0.16	1.49	0.32	1.16	0.25	1.59	0.21	10.42
19	48.46	74.56	8.74	43.61	12.58	2.92	16.06	2.49	16.09	4.24	13.86	1.91	14.71	2.56	262.79
20	1.27	2.86	0.26	2.17	0.66	0.09	0.34	0.25	1.00	0.65	1.50	0.22	1.68	0.44	13.39
21	0.56	1.25	0.17	0.79	0.21	0.04	0.25	0.05	0.56	0.13	0.44	0.11	1.64	0.15	6.35
22	0.22	0.42	0.04	0.19	0.02	0.02	0.11	0.07	0.33	0.12	0.43	0.10	1.03	0.13	3.22
23	0.89	2.09	0.49	1.45	0.61	0.05	0.59	0.08	0.44	0.07	0.21	0.03	0.30	0.04	7.33
24	0.01	0.04	0.00	0.02	0.01	0.01	0.02	0.00	0.06	0.01	0.02	0.00	0.37	0.00	0.58
25	0.37	0.82	0.09	0.35	0.08	0.03	0.51	0.05	0.57	0.22	1.64	0.50	7.42	1.87	14.52
26	5.33	5.70	0.57	3.41	1.67	0.19	1.42	0.22	1.31	0.22	0.61	0.34	1.06	0.12	22.16
27	99.23	193.99	21.72	101.36	29.33	6.73	33.62	5.13	31.66	6.87	21.04	3.18	24.23	3.74	581.83

TABLE F4B continued															
REE CHEMISTRY OF RUTILE DETERMINED WITH LA-ICP-MS (in ppm)															
GRAAUWDUINEN															
Sample	**La**	**Ce**	**Pr**	**Nd**	**Sm**	**Eu**	**Gd**	**Tb**	**Dy**	**Ho**	**Er**	**Tm**	**Yb**	**Lu**	**TREE**
28	10.86	23.75	2.67	10.89	2.32	0.51	2.37	0.43	2.64	0.66	2.56	0.43	3.28	0.48	63.84
29	3.41	6.51	0.79	3.47	1.05	0.25	1.67	0.35	1.80	0.35	0.60	0.09	0.71	0.05	21.09
30	4.78	5.09	0.90	3.65	0.83	0.30	1.04	0.26	1.65	0.39	1.28	0.30	2.87	0.63	23.96
31	4.67	7.33	0.89	4.84	4.44	1.53	7.26	1.12	4.90	0.68	1.75	0.33	2.27	0.32	42.33
32	0.43	0.68	0.08	0.22	0.02	0.01	0.06	0.01	0.03	0.00	0.02	0.00	0.10	0.00	1.65
33	0.39	0.76	0.14	0.59	0.16	0.09	0.17	0.09	0.58	0.18	0.35	0.04	0.40	0.05	3.98
34	0.67	2.01	0.31	1.66	1.12	0.18	1.25	0.40	2.68	0.71	2.89	0.51	6.15	0.45	20.98
35	0.38	1.06	0.16	0.79	0.39	0.26	0.67	0.19	1.61	0.48	1.72	0.21	2.05	0.25	10.23
36	7.58	10.41	1.63	3.41	0.64	0.19	0.87	0.14	0.98	0.20	0.51	0.03	0.93	0.13	27.65
37	0.40	1.04	0.12	0.75	0.24	0.08	0.49	0.04	0.52	0.10	0.21	0.08	0.38	0.06	4.49
38	0.94	1.75	0.23	1.42	0.33	0.08	0.32	0.07	0.63	0.14	0.40	0.06	1.17	0.08	7.63
39	2.04	3.18	0.33	1.58	0.69	0.37	0.96	0.16	0.89	0.16	0.51	0.08	0.61	0.10	11.67
40	0.22	0.40	0.03	0.18	0.03	0.01	0.01	0.00	0.14	0.01	0.03	0.01	0.27	0.00	1.34
41	31.76	91.48	13.18	78.26	64.00	19.05	97.52	11.65	52.63	9.72	26.39	4.23	29.26	4.48	533.61
42	0.21	1.66	0.17	0.80	0.58	0.17	1.35	0.30	2.55	0.76	2.20	0.39	3.08	0.37	14.58
43	0.45	0.90	0.14	0.50	0.25	0.08	0.51	0.08	0.39	0.13	0.26	0.07	0.72	0.04	4.51
44	0.09	0.16	0.02	0.11	0.07	0.01	0.07	0.01	0.06	0.04	0.10	0.02	0.46	0.02	1.24
45	4.75	6.48	0.97	3.82	0.67	0.13	1.02	0.08	0.38	0.06	0.53	0.07	0.27	0.05	19.27
46	0.22	0.44	0.05	0.13	0.11	0.03	0.08	0.01	0.22	0.01	0.10	0.02	0.37	0.02	1.78
47	0.29	0.73	0.12	0.45	0.30	0.04	0.38	0.11	1.18	0.37	1.40	0.29	3.18	0.40	9.23
48	1.18	2.73	0.26	1.51	0.75	0.16	1.12	0.31	3.09	0.98	3.29	0.68	7.00	0.84	23.91
49	42.66	56.84	6.71	24.08	5.89	1.50	6.72	1.57	10.09	2.03	5.48	0.81	5.21	0.63	170.22
50	1.06	3.03	0.22	2.13	0.76	0.10	0.82	0.40	1.94	0.65	1.61	0.36	2.18	0.24	15.51
average	**6.50**	**12.60**	**1.56**	**7.25**	**2.94**	**0.80**	**3.95**	**0.58**	**3.29**	**0.71**	**2.12**	**0.36**	**2.94**	**0.43**	**46.03**

TABLE F4B continued															
REE CHEMISTRY OF RUTILE DETERMINED WITH LA-ICP-MS (in ppm)															
RIETFONTEIN															
Sample	**La**	**Ce**	**Pr**	**Nd**	**Sm**	**Eu**	**Gd**	**Tb**	**Dy**	**Ho**	**Er**	**Tm**	**Yb**	**Lu**	**TREE**
1	0.29	0.68	0.14	0.59	0.07	0.01	0.04	0.01	0.05	0.05	0.16	0.03	0.67	0.06	2.84
2	0.28	0.29	0.09	0.16	0.03	0.01	0.04	0.01	0.03	0.01	0.03	0.01	1.23	0.01	2.22
3	0.01	0.05	0.00	0.03	0.04	0.01	0.03	0.00	0.05	0.01	0.08	0.02	0.32	0.03	0.68
4	11.29	12.94	2.00	7.39	1.31	0.13	0.72	0.16	0.63	0.10	0.35	0.07	0.77	0.07	37.94
5	0.01	0.02	0.01	0.05	0.03	0.01	0.05	0.01	0.11	0.01	0.01	0.01	1.47	0.01	1.80
6	0.01	0.01	0.01	0.10	0.04	0.01	0.04	0.00	0.03	0.01	0.03	0.01	0.70	0.00	1.00
7	3.66	6.34	0.65	1.67	0.24	0.06	0.62	0.07	0.57	0.21	0.62	0.13	2.12	0.32	17.28
8	0.03	0.01	0.01	0.05	0.04	0.01	0.04	0.01	0.03	0.01	0.03	0.01	1.49	0.01	1.78
9	0.07	0.12	0.04	0.05	0.11	0.01	0.03	0.00	0.03	0.01	0.03	0.01	0.07	0.01	0.57
10	2.54	4.93	0.75	4.00	2.56	0.50	2.56	0.40	2.48	0.48	0.91	0.20	1.71	0.20	24.23
11	0.05	0.10	0.01	0.05	0.04	0.01	0.04	0.01	0.01	0.00	0.03	0.01	0.78	0.01	1.16
12	208.39	279.60	70.83	326.76	132.11	30.40	118.94	16.60	95.68	18.25	52.16	7.04	42.26	5.58	1404.60
13	0.01	0.02	0.01	0.05	0.04	0.01	0.04	0.01	0.03	0.01	0.03	0.01	0.97	0.01	1.25
14	0.10	0.14	0.01	0.05	0.05	0.01	0.11	0.01	0.03	0.01	0.03	0.01	0.84	0.01	1.40
15	1.09	1.42	0.39	1.27	0.08	0.09	0.30	0.02	0.12	0.01	0.03	0.01	0.23	0.01	5.07
16	16.85	27.89	3.67	16.76	3.59	0.90	5.21	1.05	6.53	1.64	4.32	0.83	4.50	0.59	94.33
17	2.68	5.19	0.74	2.60	0.57	0.14	0.46	0.07	0.43	0.10	0.28	0.04	0.51	0.04	13.85
18	0.35	0.38	0.12	0.30	0.04	0.02	0.17	0.03	0.14	0.01	0.02	0.01	0.33	0.01	1.93
19	0.01	0.04	0.01	0.05	0.04	0.01	0.04	0.01	0.03	0.01	0.03	0.01	0.11	0.00	0.39
20	0.25	0.47	0.05	0.37	0.05	0.03	0.04	0.01	0.05	0.05	0.16	0.01	0.20	0.01	1.75
21	1.72	2.63	0.43	1.80	0.66	0.20	0.47	0.13	0.47	0.06	0.16	0.02	0.25	0.02	9.02
22	6.52	15.03	2.30	8.90	2.43	0.84	2.50	0.54	3.14	0.74	1.94	0.25	1.70	0.26	47.09
23	143.30	263.02	56.27	249.39	70.69	16.59	64.82	9.35	47.78	7.80	19.42	2.74	17.40	2.33	970.90
24	0.34	0.64	0.09	0.38	0.12	0.10	0.17	0.03	0.14	0.03	0.10	0.01	0.47	0.00	2.63

TABLE F4B continued															
REE CHEMISTRY OF RUTILE DETERMINED WITH LA-ICP-MS (in ppm)															
RIETFONTEIN															
Sample	**La**	**Ce**	**Pr**	**Nd**	**Sm**	**Eu**	**Gd**	**Tb**	**Dy**	**Ho**	**Er**	**Tm**	**Yb**	**Lu**	**TREE**
25	1.27	3.78	0.97	5.63	3.86	0.60	4.09	0.58	3.07	0.53	1.11	0.21	1.34	0.13	27.17
26	0.09	0.15	0.04	0.14	0.02	0.01	0.03	0.00	0.03	0.01	0.02	0.01	1.21	0.01	1.76
27	0.69	1.06	0.27	0.99	0.27	0.05	0.36	0.04	0.25	0.07	0.16	0.02	0.30	0.04	4.57
28	0.39	0.45	0.12	0.35	0.14	0.03	0.10	0.02	0.10	0.02	0.02	0.01	0.99	0.01	2.73
29	0.16	0.37	0.10	0.54	0.17	0.06	0.23	0.03	0.18	0.04	0.06	0.01	0.18	0.01	2.13
30	0.09	0.22	0.06	0.19	0.04	0.03	0.06	0.01	0.07	0.00	0.05	0.00	0.18	0.01	1.00
31	1.56	2.19	0.25	0.81	0.11	0.04	0.03	0.03	0.18	0.05	0.05	0.01	0.15	0.01	5.45
32	0.11	0.25	0.07	0.18	0.03	0.01	0.04	0.01	0.03	0.00	0.01	0.01	0.33	0.01	1.10
33	0.08	0.16	0.02	0.16	0.04	0.01	0.02	0.00	0.02	0.01	0.03	0.01	0.50	0.01	1.06
34	0.06	0.05	0.01	0.03	0.02	0.00	0.04	0.01	0.03	0.00	0.03	0.01	0.35	0.00	0.64
35	0.64	0.59	0.10	0.37	0.18	0.03	0.17	0.03	0.13	0.04	0.05	0.03	0.31	0.13	2.78
36	0.27	0.30	0.10	0.19	0.04	0.01	0.01	0.01	0.01	0.01	0.03	0.00	0.66	0.00	1.64
37	0.05	0.01	0.01	0.16	0.04	0.00	0.04	0.01	0.03	0.01	0.03	0.01	0.18	0.00	0.57
38	0.26	0.45	0.15	0.56	0.04	0.01	0.08	0.01	0.06	0.00	0.01	0.01	0.24	0.00	1.89
39	1.76	3.01	0.37	1.70	0.73	0.47	1.39	0.40	2.82	0.51	1.41	0.19	1.12	0.09	15.97
40	0.01	0.03	0.01	0.05	0.04	0.01	0.04	0.01	0.03	0.01	0.03	0.01	0.36	0.01	0.66
41	0.88	1.68	0.21	1.13	0.69	0.06	1.18	0.33	2.30	0.48	1.30	0.13	2.35	0.14	12.85
42	0.26	0.38	0.08	0.57	0.35	0.09	0.36	0.05	0.23	0.03	0.05	0.01	0.09	0.01	2.56
43	0.52	1.30	0.29	1.13	0.70	0.34	1.07	0.21	0.86	0.19	0.57	0.08	0.38	0.05	7.69
44	0.96	1.39	0.42	1.39	0.70	0.10	0.63	0.33	0.82	0.28	0.28	0.10	0.48	0.12	7.99
average	**9.32**	**14.54**	**3.23**	**14.52**	**5.07**	**1.18**	**4.71**	**0.70**	**3.86**	**0.74**	**1.96**	**0.28**	**2.11**	**0.24**	**62.45**

TABLE F5

SEM ANALYSIS OF TINANOHEMATITE

HOUTKRAAL REMAINDER PORTION 2

Sample	SiO_2	TiO_2	Al_2O_3	Cr_2O_3	Fe_2O_3	FeO	MgO	CaO	Na_2O	K_2O	P_2O_5	V_2O_5	MnO	Total
1	0.00	8.97	0.41	0.16	61.06	27.60	0.00	0.00	0.00	0.00	0.00	0.32	0.00	98.50
2	0.00	17.85	0.27	0.00	50.39	26.48	0.00	0.00	0.00	0.00	0.00	0.46	0.86	96.32
3	0.00	12.25	0.29	0.00	51.07	24.82	0.00	0.00	0.00	0.00	0.49	0.00	0.53	89.44
4	0.00	11.26	0.28	0.00	55.82	26.31	0.00	0.00	0.00	0.00	0.00	0.33	0.24	94.25
5	0.00	8.14	0.25	0.00	58.54	26.90	0.00	0.00	0.00	0.00	0.00	0.00	0.20	94.02
6	0.00	11.44	0.00	0.18	55.30	26.13	0.00	0.00	0.00	0.00	0.00	0.53	0.38	93.95
7	0.00	8.16	0.00	0.00	57.75	26.43	0.00	0.00	0.00	0.00	0.00	0.48	0.29	93.11
8	0.22	8.66	0.33	0.00	58.12	26.59	0.00	0.00	0.00	0.00	0.00	0.00	0.41	94.31
9	0.00	11.49	0.00	0.00	55.45	27.39	0.00	0.00	0.00	0.00	0.00	0.00	0.00	94.33
10	0.00	9.57	0.24	0.00	57.10	26.37	0.00	0.00	0.00	0.00	0.00	0.52	0.00	93.80
11	0.29	16.37	1.82	0.00	51.86	22.78	0.00	0.00	0.00	0.00	0.00	1.41	0.46	94.98
12	0.45	17.72	0.97	0.08	51.45	26.25	0.22	0.02	0.00	0.00	0.00	0.00	0.37	92.39
average	**0.05**	**11.28**	**0.35**	**0.03**	**55.68**	**26.16**	**0.00**	**0.00**	**0.00**	**0.00**	**0.04**	**0.37**	**0.31**	

SEM ANALYSIS OF TINANOHEMATITE

HOUTKRAAL REMAINDER

Sample	SiO_2	TiO_2	Al_2O_3	Cr_2O_3	Fe_2O_3	FeO	MgO	CaO	Na_2O	K_2O	P_2O_5	V_2O_5	MnO	Total
1	0.00	7.26	0.00	0.00	55.81	25.68	0.00	0.00	0.00	0.00	0.00	0.44	0.00	89.19
2	0.00	14.12	0.00	0.00	47.76	24.78	0.00	0.00	0.00	0.00	0.00	0.62	0.00	87.29
3	0.00	11.65	0.00	0.42	52.63	23.78	0.00	0.00	0.00	0.00	0.00	1.20	0.66	90.35
4	0.00	15.64	0.00	0.00	48.07	25.06	0.00	0.00	0.00	0.00	0.00	0.00	1.28	90.04
5	0.00	8.26	0.00	0.18	56.42	25.96	0.00	0.00	0.00	0.00	0.00	0.47	0.00	91.28
average	0.00	9.89	0.00	0.00	55.93	27.00	0.00	0.00	0.00	0.00	0.00	0.00	0.00	92.83

TABLE F5 continued														
SEM ANALYSIS OF TINANOHEMATITE														
GRAAUWDUINEN														
Sample	**SiO_2**	**TiO_2**	**Al_2O_3**	**Cr_2O_3**	**Fe_2O_3**	**FeO**	**MgO**	**CaO**	**Na_2O**	**K_2O**	**P_2O_5**	**V_2O_5**	**MnO**	**Total**
1	0.00	13.99	0.00	0.00	52.46	26.01	0.00	0.00	0.00	0.00	0.00	0.39	0.79	93.65
2	0.00	15.05	0.00	0.00	51.93	26.94	0.00	0.00	0.00	0.00	0.00	0.00	0.59	94.51
3	0.00	8.25	0.00	0.00	59.00	27.79	0.00	0.00	0.00	0.00	0.00	0.00	0.00	95.05
4	0.00	8.92	3.29	0.00	63.87	21.70	0.00	0.00	0.00	0.00	0.00	2.15	0.00	99.94
5	0.00	23.57	1.84	0.00	45.88	24.77	0.00	0.00	0.00	0.00	0.00	1.63	0.00	97.68
6	0.00	8.36	0.00	0.00	59.27	27.94	0.00	0.00	0.00	0.00	0.00	0.00	0.00	95.58
7	0.00	11.86	0.00	0.00	55.30	27.04	0.00	0.00	0.00	0.00	0.00	0.00	0.42	94.62
8	1.31	9.64	2.01	0.00	59.40	21.11	0.00	1.06	0.00	0.00	0.00	2.53	0.00	97.06
9	0.00	12.88	0.00	0.00	54.87	27.04	0.00	0.00	0.00	0.00	0.00	0.00	0.67	95.46
10	0.00	11.88	3.52	0.00	59.20	20.74	0.00	0.00	0.00	0.00	0.00	1.54	0.00	96.89
average	**0.13**	**12.44**	**1.07**	**0.00**	**56.12**	**25.11**	**0.00**	**0.11**	**0.00**	**0.00**	**0.00**	**0.82**	**0.25**	
SEM ANALYSIS OF TINANOHEMATITE														
RIETFONTEIN														
Sample	**SiO_2**	**TiO_2**	**Al_2O_3**	**Cr_2O_3**	**Fe_2O_3**	**FeO**	**MgO**	**CaO**	**Na_2O**	**K_2O**	**P_2O_5**	**V_2O_5**	**MnO**	**Total**
1	0.00	11.04	0.35	0.00	58.33	26.77	0.00	0.00	0.00	0.00	0.00	0.39	0.56	97.44

TABLE F6														
SEM ANALYSIS OF HEMATITE														
HOUTKRAAL REMAINDER PORTION 2														
Sample	**SiO_2**	**TiO_2**	**Al_2O_3**	**Cr_2O_3**	**Fe_2O_3**	**FeO**	**MgO**	**CaO**	**Na_2O**	**K_2O**	**P_2O_5**	**V_2O_5**	**MnO**	**Total**
1	0.00	2.59	0.38	0.00	70.39	31.10	0.00	0.00	0.00	0.00	0.00	0.00	0.00	104.46
2	0.00	2.29	0.44	0.00	62.42	26.48	0.00	0.00	0.00	0.00	0.00	0.00	0.91	92.53
average	**0.00**	**2.59**	**0.38**	**0.00**	**70.39**	**31.10**	**0.00**	**0.00**	**0.00**	**0.00**	**0.00**	**0.00**	**0.00**	
SEM ANALYSIS OF HEMATITE														
HOUTKRAAL REMAINDER														
Sample	SiO2	**TiO_2**	**Al_2O_3**	**Cr_2O_3**	**Fe_2O_3**	**FeO**	**MgO**	**CaO**	**Na_2O**	**K_2O**	**P_2O_5**	**V_2O_5**	**MnO**	**Total**
1	0.00	4.71	0.37	0.00	62.69	27.94	0.00	0.00	0.00	0.00	0.00	0.00	0.00	95.71

TABLE F7													
SEM ANALYSIS OF MAGNETITE													
HOUTKRAAL REMAINDER PORTION 2													
Sample	**SiO_2**	**TiO_2**	**Al_2O_3**	**Cr_2O_3**	**Fe_2O_3**	**FeO**	**MgO**	**CaO**	**Nb_2O_5**	**P_2O_5**	**V_2O_5**	**MnO**	**Total**
1	7.82	0.77	5.92	0.00	38.67	33.94	0.00	0.15	0.00	0.59	0.43	0.00	88.28
2	0.08	0.00	0.10	0.00	52.17	46.65	0.04	0.03	0.00	0.00	0.00	0.15	99.21
3	0.26	0.12	0.37	0.02	48.22	42.79	0.06	0.07	0.05	0.00	0.00	0.23	92.19
average	**2.72**	**0.30**	**2.13**	**0.01**	**46.35**	**41.13**	**0.03**	**0.08**	**0.02**	**0.20**	**0.14**	**0.13**	
SEM ANALYSIS OF MAGNETITE													
HOUTKRAAL REMAINDER													
Sample	**SiO_2**	**TiO_2**	**Al_2O_3**	**Cr_2O_3**	**Fe_2O_3**	**FeO**	**MgO**	**CaO**	**Nb_2O_5**	**P_2O_5**	**V_2O_5**	**MnO**	**Total**
1	3.03	0.11	3.20	0.02	44.29	36.56	0.20	0.00	0.00	0.00	0.00	0.11	87.52
2	0.15	0.22	0.00	0.04	49.48	44.86	0.00	0.00	0.05	0.00	0.00	0.00	94.81
3	0.10	7.95	0.13	0.00	40.85	45.00	0.00	0.00	0.00	0.00	0.00	0.50	94.54
average	**1.10**	**2.76**	**1.11**	**0.02**	**44.88**	**42.14**	**0.07**	**0.00**	**0.02**	**0.00**	**0.00**	**0.20**	

TABLE F7 continued													
SEM ANALYSIS OF MAGNETITE													
GEELWAL KAROO													
Sample	**SiO_2**	**TiO_2**	**Al_2O_3**	**Cr_2O_3**	**Fe_2O_3**	**FeO**	**MgO**	**CaO**	**Nb_2O_5**	**P_2O_5**	**V_2O_5**	**MnO**	**Total**
1	4.01	0.00	0.75	0.00	38.44	37.73	0.49	0.60	0.00	0.57	0.00	0.00	82.59
SEM ANALYSIS OF MAGNETITE													
GRAAUWDUINEN													
Sample	**SiO_2**	**TiO_2**	**Al_2O_3**	**Cr_2O_3**	**Fe_2O_3**	**FeO**	**MgO**	**CaO**	**Nb_2O_5**	**P_2O_5**	**V_2O_5**	**MnO**	**Total**
1	3.75	0.00	1.18	0.00	42.60	40.29	0.35	0.00	0.00	0.00	0.00	0.00	88.17
SEM ANALYSIS OF MAGNETITE													
RIETFONTEIN													
Sample	**SiO_2**	**TiO_2**	**Al_2O_3**	**Cr_2O_3**	**Fe_2O_3**	**FeO**	**MgO**	**CaO**	**Nb_2O_5**	**P_2O_5**	**V_2O_5**	**MnO**	**Total**
1	4.99	0.00	1.88	0.00	39.91	37.70	0.51	0.00	0.00	1.52	0.00	0.31	86.82
2	2.72	0.00	2.80	0.15	43.20	36.19	0.00	0.00	0.00	1.00	0.00	0.00	86.06
3	0.00	0.16	0.17	0.08	51.96	46.15	0.00	0.02	0.00	0.00	0.00	0.05	98.60
4	0.25	0.24	0.31	0.03	47.12	42.14	0.00	0.00	0.00	0.00	0.00	0.00	90.08
average	**1.99**	**0.10**	**1.29**	**0.07**	**45.55**	**40.54**	**0.13**	**0.01**	**0.00**	**0.63**	**0.00**	**0.09**	

TABLE F8									
SEM ANALYSIS OF SPINEL									
HOUTKRAAL REMAINDER PORTION 2									
Sample	**SiO_2**	**TiO_2**	**Al_2O_3**	**Cr_2O_3**	**FeO**	**MgO**	**CaO**	**Na_2O**	**K_2O**	**Total**
1	0.00	0.00	58.80	2.14	24.52	12.52	0.00	0.00	0.00	97.98

TABLE F9

SEM ANALYSIS OF GARNETS AND CALCULATED END-MEMBERS (calculated after method by Locock, 2008)

HOUTKRAAL REMAINDER PORTION 2

Sample	SiO_2	TiO_2	Al_2O_3	Cr_2O_3	FeO	MnO	MgO	CaO	Na_2O	Total	Spessartine	Pyrope	Almandine	Grossular	Andradite
1	38.82	0.00	22.29	0.00	30.25	0.53	8.62	1.20	0.00	101.70	1.15	33.12	62.44	2.70	0.60
2	38.59	b.d	22.18	0.00	30.82	1.81	7.52	1.27	0.00	102.19	3.97	29.05	63.43	2.64	0.89
3	36.40	0.00	21.06	0.00	35.73	0.98	3.45	1.55	0.00	99.16	2.28	14.11	79.06	4.27	0.27
4	36.89	0.00	21.22	0.00	34.60	1.56	4.18	1.12	0.00	99.57	3.59	16.89	76.27	3.10	0.15
5	37.06	0.00	21.16	0.00	27.78	1.14	8.52	1.82	0.00	97.47	2.60	34.26	57.87	3.14	2.12
6	35.11	0.00	20.22	0.00	29.25	0.77	6.67	1.38	0.00	93.41	1.87	28.34	65.60	3.05	1.15
7	35.85	0.00	20.20	0.00	27.22	0.51	7.90	1.30	0.00	92.98	1.21	32.85	62.07	2.82	1.04
8	38.18	0.58	16.69	0.00	7.62	1.16	0.50	33.34	0.00	98.06	2.64	1.99	2.27	72.07	21.04
9	36.59	0.41	18.42	0.00	9.24	6.75	0.00	24.65	0.00	96.06	15.54	1.00	12.94	58.61	11.90
10	36.73	0.00	18.15	0.00	5.25	1.58	0.00	32.85	0.00	94.55	3.59	1.00	0.54	80.71	14.16
11	36.58	0.00	19.57	0.00	3.48	8.71	0.00	26.96	0.00	95.30	19.97	1.00	0.82	70.91	7.29
12	34.53	0.00	20.19	0.00	18.58	23.55	0.00	1.27	0.00	98.11	57.18	1.02	37.91	2.23	1.66
13	36.54	0.00	21.16	0.00	32.43	0.17	6.27	0.81	0.00	97.37	0.38	25.32	70.95	2.34	1.01
14	36.33	0.00	20.77	0.00	29.83	0.54	4.27	5.51	0.07	97.31	1.27	17.64	64.72	15.48	0.89
15	36.04	0.18	20.23	0.00	27.97	0.87	4.91	6.03	0.00	96.24	2.05	20.35	60.21	13.97	3.42
16	38.25	0.00	21.87	0.00	20.43	0.73	11.92	3.33	0.00	96.52	1.61	46.47	42.59	8.83	0.50
17	37.14	0.33	20.05	0.00	2.96	3.52	0.52	30.05	0.00	94.57	8.10	2.12	3.62	81.88	4.28
18	35.14	0.60	19.70	0.00	4.53	16.32	0.00	18.38	0.00	94.67	39.19	1.02	5.88	49.82	4.09
average	**36.71**	**0.12**	**20.28**	**0.00**	**21.00**	**3.96**	**4.18**	**10.71**	**0.00**		**9.34**	**17.09**	**42.73**	**26.59**	**4.25**

SEM ANALYSIS OF GARNETS AND CALCULATED END-MEMBERS (calculated after method by Locock, 2008)

HOUTKRAAL REMAINDER

Sample	SiO_2	TiO_2	Al_2O_3	Cr_2O_3	FeO	MnO	MgO	CaO	Na_2O	Total	Spessartine	Pyrope	Almandine	Grossular	Andradite
1	36.52	0.50	20.56	0.00	8.47	25.18	0.00	8.80	0.00	100.02	58.10	1.01	16.74	21.79	2.36
2	36.62	0.00	20.56	0.00	6.96	23.22	0.00	10.16	0.00	97.53	53.04	0.98	15.70	29.29	0.98
average	**36.57**	**0.25**	**20.56**	**0.00**	**7.71**	**24.20**	**0.00**	**9.48**	**0.00**	**98.77**	**55.57**	**1.00**	**16.22**	**25.54**	**1.67**

TABLE F9 continued

SEM ANALYSIS OF GARNETS AND CALCULATED END-MEMBERS (calculated after method by Locock, 2008)

GEELWAL KAROO

Sample	SiO_2	TiO_2	Al_2O_3	Cr_2O_3	FeO	MnO	MgO	CaO	Na_2O	Total	Spessartine	Pyrope	Almandine	Grossular	Andradite
1	34.65	0.82	19.50	0.00	14.79	24.07	0.73	2.45	0.00	97.01	59.98	3.22	32.85	1.14	2.81
2	37.81	0.00	21.82	0.00	28.54	0.83	8.73	1.18	0.00	98.90	1.85	34.43	60.38	3.06	0.28
3	37.84	0.00	21.83	0.00	25.90	0.30	10.04	1.80	0.00	97.71	0.68	39.54	54.67	4.92	0.19
4	38.56	0.00	20.63	0.00	4.47	2.80	0.31	31.87	0.00	98.64	6.15	1.18	4.12	82.02	6.53
5	36.83	0.00	20.92	0.00	25.56	1.84	4.27	7.88	0.00	97.30	4.22	17.28	55.56	21.81	1.12
6	36.95	0.00	21.31	0.00	25.68	0.42	8.11	4.00	0.00	96.48	0.97	32.70	54.73	10.91	0.69
7	35.91	0.00	20.46	0.00	33.02	1.14	4.07	2.05	0.00	96.66	2.69	16.88	74.30	5.12	1.01
8	37.98	0.36	21.09	0.00	1.95	2.56	0.00	33.43	0.00	97.37	5.67	1.01	0.68	89.05	3.60
9	35.09	0.00	20.07	0.00	18.39	21.00	0.36	2.72	0.00	97.63	50.70	1.53	39.48	6.54	1.75
10	37.75	0.45	18.59	0.00	4.70	0.66	0.00	35.21	0.00	97.36	0.17	1.01	1.01	83.92	13.89
11	38.16	0.00	19.13	0.00	5.58	1.29	0.23	33.72	0.00	98.10	2.86	0.89	1.57	81.57	13.11
average	**37.05**	**0.15**	**20.49**	**0.00**	**17.14**	**5.17**	**3.35**	**14.21**	**0.00**	**97.56**	**12.36**	**13.61**	**34.49**	**35.46**	**4.09**

SEM ANALYSIS OF GARNETS AND CALCULATED END-MEMBERS (calculated after method by Locock, 2008)

GRAAUWDUINEN

Sample	SiO_2	TiO_2	Al_2O_3	Cr_2O_3	FeO	MnO	MgO	CaO	Na_2O	Total	Spessartine	Pyrope	Almandine	Grossular	Andradite
1	34.96	0.00	19.86	0.00	23.45	14.41	1.46	2.57	0.00	96.70	34.92	6.23	50.98	5.24	2.62
2	35.36	0.44	19.47	0.00	13.93	19.45	0.00	8.05	0.00	96.69	46.33	1.01	29.80	18.97	3.89
3	34.88	0.45	19.81	0.00	15.60	21.96	0.38	4.15	0.00	97.23	53.60	1.65	33.42	8.64	2.70
4	36.21	0.00	20.86	0.00	31.80	1.61	5.82	0.93	0.00	97.22	0.98	0.98	32.34	64.73	0.98
5	35.25	0.00	20.12	0.00	14.38	24.26	0.00	4.13	0.00	98.14	57.71	1.01	28.86	10.23	2.19
6	37.80	0.00	21.83	0.00	25.90	2.37	9.28	1.43	0.00	98.60	5.31	36.60	54.04	3.52	0.52
7	36.54	0.00	21.03	0.00	33.61	0.00	5.57	1.00	0.00	97.74	1.00	22.47	73.63	2.55	0.35
8	37.52	1.15	18.75	0.00	4.37	4.71	0.64	30.16	0.00	97.29	11.01	2.64	2.12	73.76	10.47
9	34.97	0.00	19.81	0.00	13.27	27.39	0.00	2.23	0.00	97.67	65.69	1.01	26.55	4.13	2.63
10	36.69	0.00	18.16	0.00	6.28	8.99	0.00	26.08	0.00	96.19	20.53	1.00	3.08	61.40	13.99
average	**36.02**	**0.20**	**19.97**	**0.00**	**18.26**	**12.51**	**2.31**	**8.07**	**0.00**	**97.35**	**29.71**	**7.46**	**33.48**	**25.32**	**4.03**

TABLE F9 continued

SEM ANALYSIS OF GARNETS AND CALCULATED END-MEMBERS (calculated after method by Locock, 2008)

RIETFONTEIN

Sample	SiO_2	TiO_2	Al_2O_3	Cr_2O_3	FeO	MnO	MgO	CaO	Na_2O	Total	Spessartine	Pyrope	Almandine	Grossular	Andradite
1	35.91	0.00	20.81	0.00	35.05	1.20	3.89	1.21	0.00	98.08	2.83	16.12	77.42	2.79	0.84
2	36.97	0.00	19.21	0.00	5.72	17.84	0.62	17.55	0.00	97.91	40.88	2.50	5.77	41.75	9.11
3	37.37	0.00	21.46	0.00	32.78	1.11	5.48	1.83	0.00	100.03	2.52	21.86	70.36	4.52	0.74
4	36.15	0.35	20.41	0.00	21.38	18.93	0.99	2.66	0.00	100.88	44.52	4.09	44.58	3.37	3.43
5	37.03	0.00	21.17	0.00	32.53	0.24	5.48	1.98	0.00	98.17	1.00	21.82	71.50	5.64	0.04
6	36.96	0.00	20.63	0.00	31.23	0.00	1.55	8.96	0.00	0.00	0.00	6.24	67.77	23.52	2.47
average	36.43	0.14	17.35	0.00	25.76	7.86	8.18	4.21	0.00	98.63	15.29	12.11	56.23	13.6	2.77

Table 10.1					
SEM ANALYSIS OF PYROXENE, END-MEMBERS AND CATION PROPORTIONS					
GEELWAL KAROO					
Sample	**1**	**2**	**3**	**4**	**5**
SiO_2	50.61	51.44	51.393	51.407	52.093
TiO_2	0.25	0.39	0.377	0.34	0.224
Al_2O_3	2.08	1.11	2.603	1.896	1.025
FeO	6.69	9.29	6.104	7.546	17.574
MnO	0.20	0.28	0	0.205	0.399
MgO	16.15	14.07	16.454	16.014	21.564
CaO	18.74	20.79	19.137	18.757	4.196
K_2O	0.00	0.00	0	0	0
Na_2O	0.00	0.00	0	0	0
Li_2O	0.00	0.00	0.00	0.00	0.00
ZnO	0.00	0.00	0.00	0.00	0.00
NiO	0.00	0.00	0.00	0.00	0.00
Cr_2O_3	0.78	0.00	1.09	0.38	0.00
Sc_2O_3	0.00	0.00	0.00	0.00	0.00
Total	**95.492**	**97.355**	**97.157**	**96.548**	**97.075**
Number of ions on the basis of 6O (Deer et al, 1992, pg 151-153)					
Si	1.951	1.973	1.944	1.965	1.982
Ti	0.007	0.011	0.011	0.010	0.006
Al (T)	0.049	0.027	0.056	0.035	0.018
Al (M1)	0.045	0.023	0.060	0.050	0.028
Fe^{3+} (T)	0.000	0.000	0.000	0.000	0.000
Fe^{3+} (M1)	0.000	0.000	0.000	0.000	0.000
Fe^{2+}	0.216	0.298	0.193	0.241	0.559
Mn	0.006	0.009	0.000	0.007	0.013
Mg	0.928	0.804	0.928	0.912	1.223
Ca	0.774	0.854	0.776	0.768	0.171
K	0.000	0.000	0.000	0.000	0.000
Na	0.000	0.000	0.000	0.000	0.000
Li	0.000	0.000	0.000	0.000	0.000
Zn	0.000	0.000	0.000	0.000	0.000
Ni	0.000	0.000	0.000	0.000	0.000
Cr	0.024	0.000	0.033	0.012	0.000
Sc	0.000	0.000	0.000	0.000	0.000
Total	**4.000**	**4.000**	**4.000**	**4.000**	**4.000**
pyroxene	**augite**	**augite**	**augite**	**augite**	**pigeonite**
End-members (calculated after Strum, 2002)					
enstatite	48.23	40.92	48.92	47.32	62.21
ferrosillite	11.54	15.62	10.18	12.85	29.09
wollastonite	40.23	43.46	40.89	39.83	8.70

TABLE F10.2								
SEM ANALYSIS OF PYROXENE, END-MEMBERS AND CATION PROPORTIONS								
RIETFONTEIN								
Sample	**1**	**2**	**3**	**4**	**5**	**6**	**7**	**8**
SiO_2	49.70	44.61	42.46	51.58	52.09	50.52	50.91	51.71
TiO_2	0.40	1.40	1.73	0.00	0.00	0.60	0.00	0.00
Al_2O_3	2.55	5.67	6.81	1.96	2.03	2.12	1.94	2.07
FeO	6.40	24.32	26.37	7.64	7.49	11.12	6.46	7.60
MnO	0.28	0.31	0.00	0.00	0.00	0.21	0.00	0.00
MgO	15.58	7.76	6.02	16.70	16.93	15.11	16.26	16.55
CaO	18.98	9.67	10.04	18.03	18.32	17.20	18.84	18.64
K_2O	0.00	0.76	0.99	0.00	0.00	0.00	0.00	0.00
Na_2O	0.00	1.98	2.10	0.00	0.00	0.00	0.00	0.00
Li_2O	0.00	0.00	0.00	0.00	0.00	0.00	0.00	0.00
ZnO	0.00	0.00	0.00	0.00	0.00	0.00	0.00	0.00
NiO	0.00	0.00	0.00	0.00	0.00	0.00	0.00	0.00
Cr_2O_3	0.86	0.00	0.00	0.00	0.00	0.20	0.76	0.00
Sc_2O_3	0.00	0.00	0.00	0.00	0.00	0.00	0.00	0.00
Total	**94.738**	**96.477**	**96.525**	**95.902**	**96.856**	**97.075**	**95.166**	**96.569**
Number of ions on the basis of 6O (Deer et al, 1992)								
Si	1.933	1.790	1.717	1.975	1.973	1.942	1.965	1.967
Ti	0.012	0.042	0.053	0.000	0.000	0.017	0.000	0.000
Al (T)	0.067	0.210	0.283	0.025	0.027	0.058	0.035	0.033
Al (M1)	0.050	0.058	0.042	0.063	0.064	0.038	0.053	0.060
Fe^{3+} (T)	0.000	0.000	0.000	0.000	0.000	0.000	0.000	0.000
Fe^{3+} (M1)	0.000	0.260	0.352	0.000	0.000	0.000	0.000	0.000
Fe^{2+}	0.208	0.556	0.540	0.244	0.237	0.357	0.209	0.242
Mn	0.009	0.010	0.000	0.000	0.000	0.007	0.000	0.000
Mg	0.903	0.464	0.363	0.953	0.956	0.866	0.936	0.938
Ca	0.791	0.416	0.435	0.740	0.743	0.708	0.779	0.760
K	0.000	0.039	0.051	0.000	0.000	0.000	0.000	0.000
Na	0.000	0.154	0.165	0.000	0.000	0.000	0.000	0.000
Li	0.000	0.000	0.000	0.000	0.000	0.000	0.000	0.000
Zn	0.000	0.000	0.000	0.000	0.000	0.000	0.000	0.000
Ni	0.000	0.000	0.000	0.000	0.000	0.000	0.000	0.000
Cr	0.026	0.000	0.000	0.000	0.000	0.006	0.023	0.000
Sc	0.000	0.000	0.000	0.000	0.000	0.000	0.000	0.000
Total	**4.000**	**4.000**	**4.000**	**4.000**	**4.000**	**4.000**	**4.000**	**4.000**
pyroxene	**augite**	**augite**	**augite**	**augite**	**augite**	**augite**	**augite**	**augite**
End-members (calculated after Strum, 2002)								
enstatite	47.26	27.22	21.47	49.19	49.36	44.67	48.65	48.37
ferrosillite	11.37	48.43	52.78	12.62	12.25	18.80	10.84	12.46
wollastonite	41.37	24.36	25.74	38.19	38.39	36.53	40.51	39.16

TABLE F10.2 continued									
SEM ANALYSIS OF PYROXENE, END-MEMBERS AND CATION PROPORTIONS									
RIETFONTEIN									
Sample	**9**	**10**	**11**	**12**	**13**	**14**	**15**	**16**	**17**
SiO_2	52.48	51.99	53.39	51.35	47.57	52.67	52.59	52.62	45.85
TiO_2	0.00	0.00	0.00	0.00	0.00	0.18	0.00	0.00	0.53
Al_2O_3	1.94	0.83	0.88	0.94	1.15	0.88	0.91	0.96	6.90
FeO	7.66	14.79	16.12	21.82	12.08	19.04	12.02	11.64	9.78
MnO	0.00	0.43	0.00	0.00	0.00	0.43	0.26	0.28	3.99
MgO	17.51	22.95	22.91	18.34	19.19	21.86	26.15	26.55	5.13
CaO	17.33	3.91	4.25	4.77	4.14	2.86	2.26	2.22	25.36
K_2O	0.00	0.00	0.00	0.00	0.00	0.00	0.00	0.00	0.00
Na_2O	0.00	0.00	0.00	0.00	0.00	0.00	0.00	0.00	0.34
Li_2O	0.00	0.00	0.00	0.00	0.00	0.00	0.00	0.00	0.00
ZnO	0.00	0.00	0.00	0.00	0.00	0.00	0.00	0.00	0.00
NiO	0.00	0.00	0.00	0.00	0.00	0.00	0.00	0.00	0.00
Cr_2O_3	0.00	0.00	0.00	0.00	0.00	0.00	0.28	0.32	0.00
Sc_2O_3	0.00	0.00	0.00	0.00	0.00	0.00	0.00	0.00	0.00
Total	**96.909**	**94.904**	**97.554**	**97.226**	**84.116**	**97.913**	**94.458**	**94.579**	**97.882**
Number of ions on the basis of 6O (Deer et al, 1992)									
Si	1.984	1.997	2.003	1.991	2.067	1.992	1.993	1.987	1.808
Ti	0.000	0.000	0.000	0.000	0.000	0.005	0.000	0.000	0.016
Al (T)	0.016	0.003	0.000	0.009	0.000	0.008	0.007	0.013	0.192
Al (M1)	0.070	0.035	0.039	0.034	0.059	0.031	0.033	0.030	0.129
Fe^{3+} (T)	0.000	0.000	0.000	0.000	0.000	0.000	0.000	0.000	0.000
Fe^{3+} (M1)	0.000	0.000	0.000	0.000	0.000	0.000	0.000	0.000	0.058
Fe^{2+}	0.242	0.475	0.506	0.708	0.439	0.602	0.381	0.368	0.265
Mn	0.000	0.014	0.000	0.000	0.000	0.014	0.008	0.009	0.133
Mg	0.986	1.315	1.281	1.060	1.243	1.232	1.477	1.495	0.302
Ca	0.702	0.161	0.171	0.198	0.193	0.116	0.092	0.090	1.071
K	0.000	0.000	0.000	0.000	0.000	0.000	0.000	0.000	0.000
Na	0.000	0.000	0.000	0.000	0.000	0.000	0.000	0.000	0.026
Li	0.000	0.000	0.000	0.000	0.000	0.000	0.000	0.000	0.000
Zn	0.000	0.000	0.000	0.000	0.000	0.000	0.000	0.000	0.000
Ni	0.000	0.000	0.000	0.000	0.000	0.000	0.000	0.000	0.000
Cr	0.000	0.000	0.000	0.000	0.000	0.000	0.008	0.009	0.000
Sc	0.000	0.000	0.000	0.000	0.000	0.000	0.000	0.000	0.000
Total	**4.000**	**4.000**	**4.000**	**4.000**	**4.000**	**4.000**	**4.000**	**4.000**	**4.000**
pyroxene	**augite**	**pigeonite**	**pigeonite**	**pigeonite**	**pigeonite**	**pigeonite**	**enstatite**	**enstatite**	**wollastonite**
End-members (calculated after Strum, 2002)									
enstatite	51.11	66.91	65.43	53.93	66.31	62.74	75.44	76.23	16.49
ferrosillite	12.54	24.90	25.84	36.00	23.41	31.37	19.89	19.20	24.93
wollastonite	36.35	8.20	8.73	10.07	10.28	5.89	4.68	4.57	58.58

TABLE F11

SEM ANALYSIS OF TOURMALINE (in wt %)

HOUTKRAAL REMAINDER PORTION 2

Sample	SiO_2	TiO_2	Al_2O_3	FeO*	MnO	MgO	CaO	Na_2O	K_2O	B_2O_3	Total	Mg/(Mg+Fe)
1	32.57	0.82	30.97	11.41	0.15	2.83	0.28	2.01	0.00	10.50	81.03	0.31
2	34.43	0.65	32.55	11.07	0.19	3.45	0.39	2.14	0.00	10.50	84.87	0.36
3	35.42	0.59	33.18	8.90	0.00	4.19	0.17	2.04	0.00	10.50	84.48	0.46
4	31.56	0.00	28.96	12.30	0.00	2.01	0.00	1.83	0.00	10.50	76.66	0.23
5	32.30	0.94	29.80	8.84	0.00	4.39	0.56	1.80	0.00	10.50	78.63	0.47
6	37.67	0.61	35.60	5.44	0.00	7.20	1.56	1.85	0.00	10.50	89.92	0.70
7	32.85	0.00	31.68	14.62	0.00	0.00	0.00	1.49	0.00	10.50	80.64	0.00
8	35.39	0.00	34.50	10.00	0.00	2.75	0.00	1.70	0.00	10.50	94.85	0.33
9	33.60	0.77	31.20	12.22	0.00	2.54	0.26	2.12	0.00	10.50	93.19	0.27
10	34.65	1.07	32.29	11.94	0.00	3.41	0.50	2.25	0.00	10.50	96.60	0.34
11	34.28	0.00	33.37	10.71	0.00	3.03	0.00	2.17	0.00	10.50	94.06	0.34
12	34.30	0.91	32.85	9.52	0.00	3.85	0.60	1.99	0.00	10.50	94.51	0.42
13	34.84	0.00	33.59	7.31	0.00	4.58	0.00	1.84	0.00	10.50	92.66	0.53
14	34.43	0.88	31.82	7.97	0.00	5.03	0.53	2.18	0.00	10.50	93.35	0.53
15	34.82	0.69	33.46	9.15	0.00	3.91	0.40	2.14	0.00	10.50	95.07	0.43
16	33.42	0.31	32.63	12.03	0.00	1.94	0.20	2.02	0.00	10.50	93.05	0.22
17	34.62	0.69	28.68	8.93	0.00	6.64	0.52	2.64	0.00	10.50	93.22	0.57
18	33.25	0.39	32.97	14.02	0.36	0.00	0.00	1.78	0.00	10.50	93.26	0.00
average	**34.13**	**0.52**	**32.23**	**10.35**	**0.04**	**3.43**	**0.33**	**2.00**	**0.00**	**10.50**	**93.59**	

SEM ANALYSIS OF TOURMALINE (in wt %)

HOUTKRAAL REMAINDER

Sample	SiO_2	TiO_2	Al_2O_3	FeO*	MnO	MgO	CaO	Na_2O	K_2O	B_2O_3	Total	Mg/(Mg+Fe)
1	34.67	0.55	32.67	8.39	0.00	4.14	0.16	2.05	0.00	10.50	93.12	0.47
2	33.45	0.73	32.11	11.14	0.00	2.59	0.87	1.91	0.00	10.50	93.29	0.29
3	35.86	0.00	34.86	10.96	0.00	2.38	0.00	2.08	0.00	10.50	96.64	0.28
4	35.69	0.90	32.89	12.64	0.00	2.52	0.00	2.49	0.00	10.50	97.63	0.26
5	36.37	0.00	33.75	7.96	0.00	5.37	1.00	1.91	0.00	10.50	96.86	0.55
average	**35.21**	**0.44**	**33.26**	**10.22**	**0.00**	**3.40**	**0.41**	**2.09**	**0.00**	**10.50**	**95.51**	

TABLE F11 continued

SEM ANALYSIS OF TOURMALINE (in wt %)

GEELWAL KAROO

Sample	SiO_2	TiO_2	Al_2O_3	FeO*	MnO	MgO	CaO	Na_2O	K_2O	B_2O_3	Total	Mg/(Mg+Fe)
1	35.74	0.74	26.36	8.60	0.00	9.09	0.68	2.62	0.00	10.50	94.33	0.65
2	34.14	0.63	32.04	11.35	0.00	4.12	0.41	2.39	0.00	10.50	95.58	0.39
3	35.01	1.12	26.51	11.03	0.00	7.06	1.02	2.42	0.00	10.50	94.66	0.53
4	33.56	0.33	29.54	18.12	0.00	0.43	0.45	2.31	0.00	10.50	95.23	0.04
5	35.38	0.81	34.14	6.96	0.00	4.97	0.45	2.00	0.00	10.50	95.20	0.56
average	**34.77**	**0.73**	**29.72**	**11.21**	**0.00**	**5.13**	**0.60**	**2.35**	**0.00**		**95.00**	

SEM ANALYSIS OF TOURMALINE (in wt %)

GRAAUWDUINEN

Sample	SiO_2	TiO_2	Al_2O_3	FeO*	MnO	MgO	CaO	Na_2O	K_2O	B_2O_3	Total	Mg/(Mg+Fe)
1	35.16	0.00	33.05	9.90	0.00	3.68	0.00	1.98	0.00	10.50	94.25	0.40
2	35.51	0.00	33.53	11.38	0.00	2.85	0.00	2.11	0.00	10.50	95.87	0.31
3	36.19	0.00	33.02	5.72	0.00	6.91	0.86	1.97	0.00	10.50	95.16	0.68
4	34.12	0.00	33.00	13.42	0.00	1.38	0.00	1.97	0.00	10.50	94.38	0.15
zoned tourmaline												
darkgrey	36.50	0.00	32.65	2.91	0.00	8.56	0.67	1.30	0.00	10.50	93.08	0.84
lightgrey	33.98	0.00	31.29	13.86	0.00	2.24	0.00	2.15	0.00	10.50	94.01	0.22
Darkgrey zonedlines	34.30	0.00	30.31	10.18	0.00	4.75	0.00	2.26	0.00	10.50	92.31	0.45
average	**35.11**	**0.00**	**32.41**	**9.62**	**0.00**	**4.34**	**0.22**	**1.96**	**0.00**	**10.50**	**94.15**	

SEM ANALYSIS OF TOURMALINE (in wt %)

RIETFONTEIN

Sample	SiO_2	TiO_2	Al_2O_3	FeO*	MnO	MgO	CaO	Na_2O	K_2O	B_2O_3	Total	Mg/(Mg+Fe)
1	36.28	0.87	26.78	11.14	0.00	9.02	3.64	1.04	0.00	10.50	99.26	0.59
2	36.93	0.44	34.77	10.17	0.00	4.75	0.57	2.00	0.00	10.50	100.14	0.45
3	35.22	0.62	34.26	11.15	0.00	2.79	0.23	1.79	0.00	10.50	96.55	0.31
4	35.37	0.00	34.03	10.85	0.00	2.86	0.00	1.87	0.00	10.50	95.47	0.32
5	35.27	0.53	33.75	11.24	0.00	2.72	0.00	1.94	0.00	10.50	95.94	0.30
average	**35.81**	**0.49**	**32.72**	**10.91**	**0.00**	**4.43**	**0.89**	**1.73**	**0.00**		**97.47**	

FeO*=total iron

B assumed to be stiochiometric =10.5wt% (Deer et al, 1992)

TABLE F12

SEM ANALYSIS OF ALUMINOSILICATES (in wt %)

HOUTKRAAL REMAINDER PORTION 2

Sample	SiO_2	TiO_2	Al_2O_3	Cr_2O_3	FeO	MnO	MgO	CaO	Na_2O	K_2O	V_2O_3	Total
1	35.51	0.00	62.91	0.00	0.00	0.00	0.00	0.00	0.00	0.00	0.00	98.42
2	36.08	0.00	63.92	0.00	0.00	0.00	0.00	0.00	0.00	0.00	0.00	100.00
3	35.97	0.00	64.31	0.00	0.17	0.00	0.00	0.00	0.00	0.00	0.38	100.82
4	36.31	0.00	63.44	0.00	0.26	0.00	0.00	0.00	0.00	0.00	0.00	100.00
5	36.05	0.00	63.72	0.00	0.23	0.00	0.00	0.00	0.00	0.00	0.00	100.00
6	38.61	0.00	61.39	0.00	0.00	0.00	0.00	0.00	0.00	0.00	0.00	100.00
7	36.00	0.00	63.72	0.00	0.28	0.00	0.00	0.00	0.00	0.00	0.00	100.00
8	36.21	0.00	63.79	0.00	0.00	0.00	0.00	0.00	0.00	0.00	0.00	100.00
9	35.72	0.00	62.57	0.00	0.00	0.00	0.00	0.00	0.00	0.00	0.00	98.29
average	**36.27**	**0.00**	**63.31**	**0.00**	**0.10**	**0.00**	**0.00**	**0.00**	**0.00**	**0.00**	**0.04**	

SEM ANALYSIS OF ALUMINOSILICATES (in wt %)

HOUTKRAAL REMAINDER

Sample	SiO_2	TiO_2	Al_2O_3	Cr_2O_3	FeO	MnO	MgO	CaO	Na_2O	K_2O	V_2O_3	Total
1	36.48	0.00	63.31	0.00	0.21	0.00	0.00	0.00	0.00	0.00	0.00	100.00
2	36.13	0.00	61.63	0.00	0.00	0.00	0.00	0.00	0.00	0.00	0.00	97.76
3	36.95	0.00	63.05	0.00	0.00	0.00	0.00	0.00	0.00	0.00	0.00	100.00
4	36.81	0.00	64.68	0.00	0.43	0.00	0.00	0.00	0.00	0.00	0.32	102.23
5	36.00	0.00	63.74	0.00	0.26	0.00	0.00	0.00	0.00	0.00	0.00	100.00
6	36.01	0.00	63.27	0.23	0.49	0.00	0.00	0.00	0.00	0.00	0.00	100.00
average	**36.40**	**0.00**	**63.28**	**0.04**	**0.23**	**0.00**	**0.00**	**0.00**	**0.00**	**0.00**	**0.05**	

SEM ANALYSIS OF ALUMINOSILICATES (in wt %)

GEELWAL KAROO

Sample	SiO_2	TiO_2	Al_2O_3	Cr_2O_3	FeO	MnO	MgO	CaO	Na_2O	K_2O	V_2O_3	Total
1	34.79	0.00	61.46	0.00	0.86	0.00	0.00	0.00	0.00	0.00	0.00	97.11
2	35.91	0.00	63.82	0.00	0.27	0.00	0.00	0.00	0.00	0.00	0.00	100.00
average	**35.35**	**0.00**	**62.64**	**0.00**	**0.56**	**0.00**	**0.00**	**0.00**	**0.00**	**0.00**	**0.00**	

SEM ANALYSIS OF ALUMINOSILICATES (in wt %)

GRAAUWDUINEN

Sample	SiO_2	TiO_2	Al_2O_3	Cr_2O_3	FeO	MnO	MgO	CaO	Na_2O	K_2O	V_2O_3	Total
1	36.10	0.00	63.90	0.00	0.00	0.00	0.00	0.00	0.00	0.00	0.00	100.00
2	34.86	0.00	61.92	0.00	0.27	0.00	0.00	0.00	0.00	0.00	0.00	97.05
3	35.41	0.00	61.46	0.00	0.00	0.00	0.00	0.00	0.00	0.00	0.00	96.87
average	**35.46**	**0.00**	**62.43**	**0.00**	**0.09**	**0.00**	**0.00**	**0.00**	**0.00**	**0.00**	**0.00**	

SEM ANALYSIS OF ALUMINOSILICATES (in wt %)

RIETFONTEIN

Sample	SiO_2	TiO_2	Al_2O_3	Cr_2O_3	FeO	MnO	MgO	CaO	Na_2O	K_2O	V_2O_3	Total
1	34.82	0.00	61.15	0.00	0.27	0.00	0.00	0.00	0.00	0.00	0.00	96.24
2	35.83	0.00	62.91	0.00	0.25	0.00	0.00	0.00	0.00	0.00	0.00	98.99
average	**35.33**	**0.00**	**62.03**	**0.00**	**0.26**	**0.00**	**0.00**	**0.00**	**0.00**	**0.00**	**0.00**	

TABLE F13												
SEM ANALYSIS OF STAUROLITE (in wt %)												
HOUTKRAAL REMAINDER PORTION 2												
Sample	**SiO_2**	**TiO_2**	**Al_2O_3**	**Cr_2O_3**	**FeO**	**MnO**	**MgO**	**CaO**	**Na_2O**	**K_2O**	**V_2O_3**	**Total**
1	27.28	0.70	54.24	0.00	13.31	0.48	1.99	0.00	0.00	0.00	0.00	98.00
2	28.15	0.67	54.91	0.00	13.54	0.00	1.45	0.00	0.00	0.00	0.00	98.72
3	27.58	0.50	55.17	0.00	12.27	0.20	2.28	0.00	0.00	0.00	0.00	98.00
4	27.83	0.64	54.26	0.00	12.85	0.53	1.89	0.00	0.00	0.00	0.00	98.00
5	27.45	0.64	54.01	0.00	14.23	0.19	1.47	0.00	0.00	0.00	0.00	98.00
6	27.93	0.70	54.14	0.00	12.86	0.31	2.07	0.00	0.00	0.00	0.00	98.00
7	27.58	0.50	54.80	0.16	13.25	0.00	1.72	0.00	0.00	0.00	0.00	98.00
8	27.43	0.54	54.53	0.00	13.29	0.26	1.94	0.00	0.00	0.00	0.00	98.00
9	26.43	0.55	52.96	0.00	13.59	0.00	1.64	0.00	0.00	0.00	0.00	95.17
10	27.18	0.57	54.31	0.00	13.82	0.17	1.95	0.00	0.00	0.00	0.00	98.00
average	**27.48**	**0.60**	**54.33**	**0.02**	**13.30**	**0.21**	**1.84**	**0.00**	**0.00**	**0.00**	**0.00**	
SEM ANALYSIS OF STAUROLITE (in wt %)												
HOUTKRAAL REMAINDER												
Sample	**SiO_2**	**TiO_2**	**Al_2O_3**	**Cr_2O_3**	**FeO**	**MnO**	**MgO**	**CaO**	**Na_2O**	**K_2O**	**V_2O_3**	**Total**
1	27.61	0.68	54.32	0.00	13.73	0.16	1.50	0.00	0.00	0.00	0.00	98.00
2	27.62	0.00	54.39	0.00	13.34	0.00	1.47	0.00	0.00	0.00	0.00	96.83
average	**27.61**	**0.34**	**54.36**	**0.00**	**13.53**	**0.08**	**1.48**	**0.00**	**0.00**	**0.00**	**0.00**	

TABLE F13 continued												
SEM ANALYSIS OF STAUROLITE (in wt %)												
GEELWAL KAROO												
Sample	**SiO_2**	**TiO_2**	**Al_2O_3**	**Cr_2O_3**	**FeO**	**MnO**	**MgO**	**CaO**	**Na_2O**	**K_2O**	**V_2O_3**	**Total**
1	27.56	0.32	54.36	0.00	13.79	0.00	1.74	0.00	0.24	0.00	0.00	98.00
2	26.93	0.67	53.65	0.00	13.42	0.00	1.94	0.00	0.00	0.00	0.00	96.61
3	26.25	0.49	52.85	0.00	14.20	0.31	1.57	0.00	0.00	0.00	0.00	95.67
4	26.70	0.55	52.85	0.00	12.75	0.59	1.77	0.00	0.00	0.00	0.00	95.20
5	25.99	0.47	51.57	0.00	12.93	0.53	1.91	0.00	0.00	0.00	0.00	93.39
average	**26.68**	**0.50**	**53.05**	**0.00**	**13.42**	**0.29**	**1.79**	**0.00**	**0.05**	**0.00**	**0.00**	
SEM ANALYSIS OF STAUROLITE (in wt %)												
GRAAUWDUINEN												
Sample	**SiO_2**	**TiO_2**	**Al_2O_3**	**Cr_2O_3**	**FeO**	**MnO**	**MgO**	**CaO**	**Na_2O**	**K_2O**	**V_2O_3**	**Total**
1	28.15	0.00	56.79	0.00	11.16	0.00	1.90	0.00	0.00	0.00	0.00	98.00
2	27.36	0.00	53.61	0.00	13.24	0.00	1.60	0.00	0.00	0.00	0.00	95.81
3	26.63	0.00	52.69	0.00	13.05	0.00	1.69	0.00	0.00	0.00	0.00	94.06
average	**27.38**	**0.00**	**54.36**	**0.00**	**12.48**	**0.00**	**1.73**	**0.00**	**0.00**	**0.00**	**0.00**	
SEM ANALYSIS OF STAUROLITE (in wt %)												
RIETFONTEIN												
Sample	**SiO_2**	**TiO_2**	**Al_2O_3**	**Cr_2O_3**	**FeO**	**MnO**	**MgO**	**CaO**	**Na_2O**	**K_2O**	**V_2O_3**	**Total**
1	27.443	0	52.943	0	13.314	0	1.775	0	0	0	0	95.475
2	26.565	0	52.715	0	14.476	0	1.583	0	0	0	0	95.339
average	**27.00**	**0.00**	**52.83**	**0.00**	**13.90**	**0.00**	**1.68**	**0.00**	**0.00**	**0.00**	**0.00**	

TABLE F14											
SEM ANALYSIS OF EPIDOTE GROUP MINERALS (in wt %)											
HOUTKRAAL REMAINDER PORTION 2											
Sample	**SiO_2**	**TiO_2**	**Al_2O_3**	**Cr_2O_3**	**FeO**	**MnO**	**MgO**	**CaO**	**Na_2O**	**K_2O**	**Total**
1	38.18	0.00	18.46	0.00	6.31	3.66	0.24	31.92	0.00	0.00	98.77
2	37.74	0.00	23.03	0.00	13.54	0.18	0.00	23.50	0.00	0.00	98.00
average	**37.96**	**0.00**	**20.75**	**0.00**	**9.93**	**1.92**	**0.12**	**27.71**	**0.00**	**0.00**	
SEM ANALYSIS OF EPIDOTE GROUP MINERALS (in wt %)											
GEELWAL KAROO											
Sample	**SiO_2**	**TiO_2**	**Al_2O_3**	**Cr_2O_3**	**FeO**	**MnO**	**MgO**	**CaO**	**Na_2O**	**K_2O**	**Total**
1	36.93	0.00	22.18	0.00	13.60	0.21	0.00	22.94	0.00	0.00	95.86
SEM ANALYSIS OF EPIDOTE GROUP MINERALS (in wt %)											
GRAAUWDUINEN											
Sample	**SiO_2**	**TiO_2**	**Al_2O_3**	**Cr_2O_3**	**FeO**	**MnO**	**MgO**	**CaO**	**Na_2O**	**K_2O**	**Total**
1	37.68	0.00	21.85	0.00	15.02	0.00	0.00	23.45	0.00	0.00	98.00
SEM ANALYSIS OF EPIDOTE GROUP MINERALS (in wt %)											
RIETFONTEIN											
Sample	**SiO_2**	**TiO_2**	**Al_2O_3**	**Cr_2O_3**	**FeO**	**MnO**	**MgO**	**CaO**	**Na_2O**	**K_2O**	**Total**
1	37.13	0.00	21.50	0.00	14.55	0.27	0.00	22.82	0.00	0.00	96.27
2	36.98	0.62	14.33	0.00	5.66	0.97	3.60	35.84	0.00	0.00	98.00
3	37.82	0.00	23.67	0.00	12.67	0.48	0.00	23.37	0.00	0.00	98.00
4	37.99	0.00	23.52	0.00	12.95	0.00	0.00	23.54	0.00	0.00	98.00
5	38.64	0.00	25.93	0.00	9.40	0.00	0.00	24.04	0.00	0.00	98.00
6	37.53	0.32	19.11	0.00	4.95	4.85	1.04	29.76	0.00	0.48	98.03
7	36.05	0.47	19.26	0.00	8.40	18.19	0.63	14.44	0.00	0.12	97.55
8	35.92	0.00	15.26	0.00	9.76	3.14	0.00	31.40	0.00	0.00	95.49
average	**37.26**	**0.18**	**20.32**	**0.00**	**9.79**	**3.49**	**0.66**	**25.65**	**0.00**	**0.07**	

TABLE F15											
SEM ANALYSIS OF SPHENE (in wt %)											
GEELWAL KAROO											
Sample	**SiO_2**	**TiO_2**	**Al_2O_3**	**Cr_2O_3**	**FeO**	**MnO**	**MgO**	**CaO**	**K_2O**	**V_2O_3**	**Total**
1	29.53	36.72	1.04	0.00	0.68	0.00	0.00	27.38	0.00	0.49	95.83
SEM ANALYSIS OF SPHENE (in wt %)											
RIETFONTEIN											
Sample	**SiO_2**	**TiO_2**	**Al_2O_3**	**Cr_2O_3**	**FeO**	**MnO**	**MgO**	**CaO**	**K_2O**	**V_2O_3**	**Total**
1	30.73	34.38	2.00	0.00	1.57	0.00	0.30	26.73	0.35	1.70	97.76
2	30.03	37.75	1.18	0.00	0.00	0.00	0.00	28.16	0.00	0.00	97.13
3	30.27	38.24	1.06	0.00	0.00	0.00	0.00	28.33	0.00	0.00	97.90
4	30.02	36.77	1.26	0.00	0.58	0.00	0.06	27.59	0.07	0.54	
average	**30.26**	**36.79**	**1.38**	**0.00**	**0.54**	**0.00**	**0.09**	**27.70**	**0.11**	**0.56**	

TABLE F16									
SEM ANALYSIS OF CORUNDUM (in wt %)									
RIETFONTEIN									
Sample	**SiO_2**	**TiO_2**	**Al_2O_3**	**Cr_2O_3**	**FeO**	**MnO**	**MgO**	**CaO**	**Total**
1	0.00	0.00	99.47	0.00	0.64	0.00	0.00	0.00	100.11

TABLE F17												
SEM ANALYSIS OF MONAZITE (in wt %)												
HOUTKRAAL												
Sample	**SiO_2**	**Al_2O_3**	**P_2O_5**	**S_2O_3**	**CaO**	**FeO**	**La**	**Ce**	**Nd**	**Th**	**Sr**	**Total**
1	0.00	29.51	23.04	0.45	1.02	0.41	5.43	11.00	3.64	0.00	0.00	74.49
SEM ANALYSIS OF MONAZITE (in wt %)												
GRAAUWDUINEN												
Sample	**SiO_2**	**Al_2O_3**	**P_2O_5**	**S_2O_3**	**CaO**	**FeO**	**La**	**Ce**	**Nd**	**Th**	**Sr**	**Total**
1	1.31	0.00	27.08	0.00	1.84	0.00	9.15	24.74	9.04	16.53	0.00	89.69
2	0.00	30.46	27.10	1.53	1.18	0.51	4.88	10.45	3.99	0.00	4.81	84.91
average	**0.66**	**15.23**	**27.09**	**0.77**	**1.51**	**0.25**	**7.02**	**17.60**	**6.51**	**8.26**	**2.40**	

Table F18

SEM ANALYSIS OF ALTERED ILMENITE IN THE FIVE SATELLITE AREAS (in wt %)

HOUTKRAAL REMAINDER PORTION 2

Sample	MgO	Al_2O_3	SiO_2	CaO	TiO_2	Cr_2O_3	MnO	FeO	Nb_2O_5	Total
4085ilm	0.02	0.02	0.02	0.00	50.84	0.00	7.83	40.40	0.22	99.35
4085lx	0.04	0.00	0.17	0.09	93.29	0.03	0.08	4.60	0.33	98.62
4085ilm2	0.07	0.30	0.30	0.12	52.51	0.00	5.28	38.45	0.00	97.03
4085lx2	0.04	0.10	0.23	0.12	88.86	0.10	0.02	7.65	0.26	97.39
4085lx3	0.10	1.24	1.82	0.10	85.88	0.00	0.17	5.47	0.12	94.89
9206ilm	0.02	0.04	0.21	0.00	48.64	0.06	7.76	40.55	0.11	97.39
9206lx	0.13	2.43	2.82	0.11	75.12	0.11	0.39	10.81	0.00	91.92
9206lx2	0.08	0.40	0.53	0.01	90.30	0.00	0.25	4.50	0.05	96.12
9206rt	0.00	0.04	0.16	0.01	95.41	0.02	0.20	1.62	0.15	97.62
9206lx3	0.00	0.09	0.19	0.03	88.74	0.02	0.04	6.91	0.21	96.23
9206ps	0.36	3.68	7.03	0.35	67.10	0.21	0.46	9.15	0.00	88.35
4817ilm	0.15	0.05	0.13	0.00	49.45	0.05	3.14	46.26	0.22	99.44
4817lx	0.06	0.74	1.08	0.03	90.97	0.06	0.00	3.89	0.41	97.25
4817ilm2	0.34	5.29	8.04	0.35	51.24	0.51	0.72	20.28	0.00	86.76
4817lx2	0.00	0.25	0.43	0.00	92.19	0.00	0.12	3.70	0.83	97.52
4817ilm3	0.00	0.10	0.12	0.00	48.98	0.00	4.20	44.27	0.30	97.97
4817lx3	0.36	2.60	4.81	0.02	82.93	0.00	0.31	5.75	0.30	97.08
4817ilm4	0.08	0.13	0.30	0.08	48.22	0.00	3.31	44.21	0.26	96.58
4819ps	0.02	1.27	1.80	0.13	61.49	0.12	0.04	27.95	0.12	92.94
4819hydrilm	0.00	0.94	1.28	0.14	58.82	0.11	0.03	30.90	0.00	92.22
4819lx	0.10	1.77	3.07	0.08	75.17	0.16	0.00	14.02	0.34	94.72
4819lx2	0.16	0.69	0.73	0.02	83.09	0.00	0.11	10.85	0.40	96.04
4819lx3	0.05	1.10	1.78	0.02	80.38	0.08	0.12	10.50	0.40	94.44
4819hydrilm2	0.25	1.58	2.30	0.12	60.52	0.09	0.08	28.55	0.21	93.71
9209ilm	0.81	0.06	0.07	0.00	51.76	0.02	1.21	45.04	0.14	99.12
9209rt	0.00	0.09	0.09	0.00	96.40	0.17	0.00	0.67	0.13	97.55
9209rt2	0.03	0.21	0.34	0.10	93.93	0.14	0.03	1.21	0.06	96.04
9209lx	0.10	1.47	1.12	0.12	77.10	0.18	0.14	8.79	0.00	89.02
9209rt	0.00	0.12	0.12	0.04	96.44	0.08	0.00	0.62	0.16	97.58
9209lx2	0.08	1.06	1.02	0.14	77.89	0.14	0.34	14.20	0.00	94.87
9209hydrilm	0.44	1.72	0.66	0.10	55.50	0.10	1.32	37.39	0.00	97.24
9209lx3	0.02	0.98	0.83	0.06	88.87	0.13	0.03	3.59	0.00	94.50
4841(2)ilm	0.00	0.04	0.14	0.04	50.84	0.06	2.46	46.25	0.09	99.93
4841(2)lx	0.02	0.66	1.48	0.09	92.11	0.07	0.00	2.29	0.14	96.87
4841(2)hydrilm	0.06	0.36	0.51	0.03	57.16	0.00	1.67	34.40	0.15	94.34
4841(2)lx2	0.52	3.64	7.98	0.08	75.91	0.00	0.06	4.12	0.19	92.49
4841(2)hydrilm2	0.00	0.50	1.02	0.05	60.30	0.05	1.86	29.78	0.15	93.72
4841(2)ps	0.10	2.65	5.11	0.02	61.80	0.00	1.04	19.97	0.00	90.68
4841(2)ilm2	0.00	0.40	0.55	0.04	53.74	0.00	2.22	40.53	0.22	97.70
4841(2)lx3	0.07	0.80	1.32	0.05	73.95	0.00	1.07	20.07	0.11	97.43

All Fe is reported as FeO

Table F18 continued

SEM ANALYSIS OF ALTERED ILMENITE IN THE FIVE SATELLITE AREAS (in wt %)

HOUTKRAAL REMAINDER PORTION 2

Sample	MgO	Al_2O_3	SiO_2	CaO	TiO_2	Cr_2O_3	MnO	FeO	Nb_2O_5	Total
4844ilm	0.12	0.10	0.11	0.00	47.95	0.00	2.84	48.60	0.33	100.04
4844hem	0.05	0.15	0.02	0.00	26.39	0.00	0.53	69.04	0.26	96.43
4844lx	0.06	0.15	0.19	0.00	83.58	0.00	0.17	12.81	0.15	97.12
444lx2	0.00	0.61	0.27	0.00	80.84	0.08	0.13	14.87	0.25	97.06
4844ilm2	0.04	0.09	0.18	0.03	48.30	0.03	3.30	47.74	0.24	99.95
4835lx	0.00	0.00	0.12	0.00	75.32	0.00	0.47	19.61	1.02	96.54
4835rt	0.00	0.05	0.27	0.08	94.73	0.07	0.10	3.32	0.83	99.44
4835hem	0.00	0.18	0.11	0.03	7.97	0.00	0.58	84.81	0.00	93.68
4835lx2	0.00	0.14	0.15	0.00	83.85	0.02	0.23	12.75	1.13	98.26
4835lx3	0.07	0.95	1.58	0.12	86.21	0.00	0.13	6.11	0.71	95.88
4838ilm	0.17	0.57	0.91	0.15	53.36	0.00	4.62	36.15	0.08	96.01
4838ilm2	0.05	0.28	0.40	0.07	52.88	0.00	5.54	39.85	0.00	99.07
4838lx	0.00	1.71	1.88	0.11	72.74	0.10	1.30	14.87	0.00	92.71
4838lx2	0.00	2.87	3.25	0.12	83.68	0.19	0.10	4.22	0.00	94.42
4838lx3	0.00	0.27	0.27	0.16	76.28	0.00	2.17	19.66	0.17	98.97
4838ps	0.13	0.14	0.51	0.09	66.20	0.00	3.38	28.99	0.00	99.43
traverse4838ilm	0.17	0.57	0.91	0.15	53.36	0.00	4.62	36.15	0.08	96.01
traverse4838ilm2	0.05	0.28	0.40	0.07	52.88	0.00	5.54	39.85	0.00	99.07
traverse4838lx	0.00	1.71	1.88	0.11	72.74	0.10	1.30	14.87	0.00	92.71
traverse4838lx2	0.00	2.87	3.25	0.12	83.68	0.19	0.10	4.22	0.00	94.42
traverse4838lx3	0.00	0.27	0.27	0.16	76.28	0.00	2.17	19.66	0.17	98.97
traverse4838ps	0.13	0.14	0.51	0.09	66.20	0.00	3.38	28.99	0.00	99.43
traverse4838lx4	0.17	0.23	0.27	0.07	78.58	0.10	1.88	16.95	0.00	98.25
traverse4838hydrilm	0.06	1.34	1.96	0.09	60.19	0.07	3.14	24.79	0.00	91.62
4838hydrilmspots	0.06	0.12	0.16	0.03	58.99	0.00	4.32	36.34	0.00	100.02

SEM ANALYSIS OF ALTERED ILMENITE IN THE FIVE SATELLITE AREAS (in wt %)

HOUTKRAAL REMAINDER

Sample	MgO	Al_2O_3	SiO_2	CaO	TiO_2	Cr_2O_3	MnO	FeO	Nb_2O_5	Total
hydrated ilmenite	1.12	0.43	0.21	0.00	56.45	0.12	0.26	35.27	0.00	93.87
hydrated ilm2	0.80	0.44	0.43	0.06	61.45	0.04	0.31	29.49	0.05	93.07
hydrated ilm3	0.98	0.94	0.26	0.08	57.15	0.06	0.41	33.99	0.00	93.86
4886ilm	0.09	0.00	0.12	0.06	46.51	0.00	7.96	44.32	0.34	99.41
4886ps	0.06	3.46	3.02	0.08	70.42	0.11	0.27	13.41	0.38	91.21
4886lx	0.04	1.82	1.85	0.02	78.42	0.04	1.20	11.74	0.26	95.39
4886ilmrelict	0.07	1.07	1.23	0.02	52.35	0.00	7.25	35.13	0.09	97.21
4886lx2	0.04	3.78	4.69	0.06	79.19	0.06	0.32	7.12	0.13	95.39
4886lx3	0.07	0.84	0.50	0.03	90.42	0.08	0.22	6.29	0.33	98.78
4886lx4	0.00	1.79	1.32	0.06	79.95	0.06	0.27	10.97	0.51	94.94
4886lx5	0.00	2.46	2.94	0.09	79.35	0.02	0.58	8.80	0.48	94.72
4886lx6	0.36	6.38	9.18	0.06	71.82	0.06	0.14	8.97	0.00	96.97
4886ps2	0.17	5.46	6.55	0.16	69.87	0.05	0.57	14.34	0.15	97.32

Table F18 continued

SEM ANALYSIS OF ALTERED ILMENITE IN THE FIVE SATELLITE AREAS (in wt %)

HOUTKRAAL REMAINDER

Sample	MgO	Al_2O_3	SiO_2	CaO	TiO_2	Cr_2O_3	MnO	FeO	Nb_2O_5	Total
hydratedilmenite2	0.13	0.31	0.15	0.03	60.08	0.00	1.50	31.31	0.18	93.68
hydrilm2lx	0.00	0.07	7.71	0.02	89.76	0.16	0.04	1.60	0.24	99.61
hydrilm2lx2	0.04	0.85	1.24	0.08	81.42	0.14	0.00	10.71	0.51	94.98
hydrilmps	0.07	1.16	0.74	0.07	65.23	0.12	0.10	24.18	0.00	91.66
hydrilmps2	0.05	1.02	0.63	0.15	65.30	0.06	0.06	25.08	0.00	92.35
hydrilm2(2)on edge	0.06	0.37	0.25	0.03	59.61	0.00	0.68	32.66	0.05	93.72
4888lx	0.08	0.62	0.28	0.01	83.71	0.09	0.00	1.10	0.31	86.20
4888lx2	0.03	0.46	0.38	0.00	83.72	0.35	0.03	0.72	0.34	86.04
4888lx3	0.00	0.34	0.16	0.03	83.94	0.08	0.02	1.40	0.10	86.07
traverseilm	0.09	0.08	0.14	0.04	48.76	0.23	5.70	39.25	0.16	94.44
traverseilmlx	0.45	2.27	4.38	0.18	75.70	0.31	0.14	8.17	0.00	91.60
traverseilm(2)	0.02	0.13	0.14	0.01	48.85	0.17	6.13	39.98	0.33	95.76
traverseilmmagn	0.08	0.03	0.04	0.00	20.66	0.24	1.78	67.89	0.09	90.81
traverseilm(3)	0.09	0.07	0.14	0.00	48.80	0.14	5.89	40.15	0.06	95.33
traverseilmmagn2	0.00	0.07	0.15	0.00	10.81	0.12	0.36	77.50	0.06	89.06
traverseilmmagn3	0.00	0.15	0.07	0.01	22.66	0.06	0.50	67.72	0.00	91.17
traverseilmlx2	0.03	0.00	0.07	0.00	75.37	0.09	0.06	18.95	0.36	94.93
traverseilm4	0.07	0.09	0.11	0.00	51.67	0.29	4.04	37.59	0.00	93.86
traverseilmlx3	0.00	0.05	0.10	0.04	87.99	0.37	0.02	6.89	0.49	95.96
traverseilm5	0.07	0.09	0.30	0.03	49.90	0.44	3.30	37.26	0.24	91.63
ilm	0.38	0.08	0.15	0.00	51.90	0.06	0.47	45.25	0.12	98.42
ilmhydrilm	0.27	0.12	0.11	0.01	55.29	0.06	1.25	37.11	0.00	94.22
ilmhydrilm2	0.57	0.28	0.19	0.04	55.09	0.06	0.55	36.57	0.00	93.36
ilmhydrilm3	0.54	0.20	0.22	0.02	54.31	0.00	0.59	38.96	0.00	94.83
ilm3	0.20	0.03	0.18	0.00	49.54	0.07	0.91	47.57	0.00	98.50
ilm3hydrilm	0.15	0.53	0.73	0.04	54.94	0.10	0.59	38.09	0.00	95.15
ilm3hydrilm2	0.24	0.22	0.32	0.02	55.83	0.06	0.78	35.84	0.00	93.32
4891ilm	0.13	0.08	0.00	0.00	52.10	0.01	0.93	42.69	0.17	96.11
4891rt	0.00	0.00	0.10	0.02	97.93	0.27	0.00	0.44	0.30	99.05
4891rt2	0.04	0.20	0.77	0.13	96.39	0.00	0.07	0.96	0.38	98.92
4891lx	0.07	1.11	1.85	0.02	92.84	0.23	0.00	1.36	0.76	98.23
4891hydrilm	0.17	0.12	0.17	0.02	55.40	0.00	0.86	33.27	0.14	90.15
4891hydrilm2	0.04	0.43	0.74	0.10	57.99	0.00	0.68	34.67	0.12	94.77
4891hydrilm3	0.08	0.85	1.11	0.00	54.52	0.07	0.79	36.80	0.19	94.42
4898ilm	0.07	0.07	0.12	0.00	52.96	0.00	1.15	44.98	0.16	99.52
4898ps	0.00	1.39	0.89	0.17	67.55	0.09	0.30	22.32	0.00	92.71
488ps2	0.14	1.49	4.84	0.18	60.30	0.12	0.23	24.65	0.00	91.97
4898lx	0.00	0.39	7.32	0.35	92.01	0.21	0.02	0.75	0.25	101.31
4898rt	0.00	0.14	0.74	0.06	97.80	0.21	0.10	0.34	0.35	99.74
4898ilm2	0.08	0.08	0.07	0.02	53.19	0.07	1.38	44.27	0.09	99.24
4898ps3	0.32	2.90	2.83	0.19	63.86	0.15	0.26	23.89	0.00	94.41

Table F18 continued

SEM ANALYSIS OF ALTERED ILMENITE IN THE FIVE SATELLITE AREAS (in wt %)

HOUTKRAAL REMAINDER

Sample	MgO	Al_2O_3	SiO_2	CaO	TiO_2	Cr_2O_3	MnO	FeO	Nb_2O_5	Total
4894ilm	0.17	0.02	0.06	0.03	53.12	0.05	0.95	44.90	0.09	99.38
4894hydrilm	0.11	0.58	0.49	0.02	61.02	0.12	0.22	32.00	0.19	94.74
4894ps	0.08	0.36	0.34	0.00	61.26	0.05	0.42	32.01	0.27	94.78
4894hydrilm2	0.07	0.34	0.30	0.02	60.19	0.14	0.31	32.53	0.07	93.97
4894rt	0.02	0.05	0.31	0.10	98.05	0.39	0.00	0.61	0.78	100.30
4894klx	0.00	0.29	0.44	0.05	92.17	0.35	0.08	3.77	0.56	97.70
4894hydrilm3	0.12	0.51	0.62	0.03	59.07	0.00	0.30	33.28	0.15	94.09
4894hydrilm	0.10	0.39	0.28	0.00	60.89	0.08	0.31	31.85	0.11	94.01
4894lx2	0.00	0.24	0.33	0.00	92.90	0.37	0.02	4.46	0.54	98.87

SEM ANALYSIS OF ALTERED ILMENITE IN THE FIVE SATELLITE AREAS (in wt %)

GEELWAL KAROO

Sample	MgO	Al_2O_3	SiO_2	CaO	TiO_2	Cr_2O_3	MnO	FeO	Nb_2O_5	Total
4935ilm	0.30	0.05	0.15	0.04	48.03	0.00	0.59	47.10	0.00	96.26
4935ilm2	0.26	0.24	0.47	0.04	51.74	0.00	0.55	38.25	0.00	91.55
4938ilm	0.07	0.06	0.05	0.02	45.53	0.00	3.22	46.56	0.00	95.50
4938ilm2	0.06	0.04	0.05	0.03	47.19	0.05	2.66	45.24	0.00	95.32
4938hydrilm	0.21	2.97	4.89	0.08	57.48	0.03	0.80	22.88	0.07	89.43
4938ps	0.27	2.35	4.62	0.11	61.12	0.00	0.23	20.40	0.08	89.19
4938hydrilm2	0.03	0.49	0.89	0.07	59.63	0.00	0.40	27.97	0.00	89.48
4938ps2	0.24	1.50	2.96	0.28	61.65	0.11	0.94	22.73	0.00	90.41
4938ps3	0.31	3.65	6.19	0.39	67.23	0.13	0.19	11.34	0.00	89.43
4938ps4	0.30	3.00	4.63	0.22	67.44	0.00	0.31	14.93	0.00	90.82
9334 ilm	0.13	0.08	0.06	0.06	51.15	0.04	0.37	46.56	0.17	98.61
9334 lx	0.00	1.14	1.99	0.30	87.93	0.21	0.07	2.88	0.08	94.61
9334 lx2	0.22	2.42	4.42	0.09	86.30	0.13	0.00	1.59	0.47	95.63
9334lx3	0.49	3.72	7.40	0.31	79.28	0.20	0.05	2.30	0.00	93.76
9334 ilmrelict	0.07	2.20	4.12	0.08	53.20	0.02	0.48	35.66	0.23	96.07
4903ilm	0.24	0.07	0.04	0.05	47.65	0.03	0.32	48.87	0.14	97.41
4903hydrlm	0.51	2.58	2.46	0.60	54.76	0.07	0.09	28.45	0.00	89.53
4903lx	0.04	0.08	0.27	0.02	90.45	0.11	0.03	4.20	0.50	95.69
4903lx2	0.07	0.44	0.50	0.17	90.18	0.07	0.00	4.60	0.32	96.35
4903lx3	0.02	0.34	0.90	0.22	92.61	0.00	0.00	1.58	0.49	96.16
4903hydrilm2	0.15	1.78	1.58	0.39	59.22	0.14	0.03	26.42	0.00	89.72
4903hem	0.10	0.05	0.11	0.06	39.25	0.03	0.00	45.70	0.10	85.38
4904lx	0.02	0.16	0.31	0.16	92.42	0.00	0.00	2.46	0.26	95.81
4904lx2	0.10	1.60	1.91	0.08	79.10	0.16	0.02	10.00	0.25	93.22
4904ps	0.14	0.81	0.53	0.08	63.30	0.06	0.13	27.50	0.31	92.86
4904ps2	0.21	5.17	6.83	0.18	67.46	0.11	0.05	12.50	0.25	92.78
4904lx2	0.00	0.16	0.30	0.12	91.52	0.00	0.09	3.03	0.30	95.52
4904lx3	0.10	0.85	0.89	0.11	80.48	0.03	0.00	12.14	0.31	94.90
4904ps3	0.15	1.99	1.75	0.14	64.16	0.00	0.02	26.19	0.32	94.73

Table F18 continued

SEM ANALYSIS OF ALTERED ILMENITE IN THE FIVE SATELLITE AREAS (in wt %)

GEELWAL KAROO

Sample	MgO	Al_2O_3	SiO_2	CaO	TiO_2	Cr_2O_3	MnO	FeO	Nb_2O_5	Total
4908lx	0.05	0.00	0.06	0.06	95.84	0.09	0.00	0.17	0.13	96.41
4908lx2	0.01	1.40	1.57	0.22	85.90	0.21	0.00	1.63	0.12	91.06
4908lx3	0.00	1.13	1.10	0.16	86.50	0.14	0.04	1.49	0.28	90.85
4911ilm	0.00	0.02	0.04	0.06	48.40	0.00	0.74	47.58	0.13	96.98
4911ilm2	0.03	0.00	0.07	0.08	47.93	0.00	1.00	48.00	0.06	97.18
4911ilm3	0.16	0.02	0.12	0.00	48.62	0.08	0.95	45.80	0.25	96.00
4911ilm4	0.06	0.06	0.12	0.00	49.48	0.04	0.97	44.55	0.11	95.40
4920lx	0.07	0.18	0.51	0.17	93.74	0.05	0.00	0.35	0.00	95.08
4920lx2	0.00	0.17	0.16	0.10	94.96	0.00	0.02	0.32	0.04	95.77
4919 (1) ilm	0.00	0.00	0.13	0.06	46.49	0.03	2.52	46.26	0.05	95.54
4919 (1)ps	0.26	2.21	4.49	0.33	65.75	0.05	0.34	16.11	0.00	89.54
4919 (1)ps2	0.09	1.18	1.82	0.13	65.97	0.15	0.16	21.01	0.00	90.49
4919 (1)lx	0.06	1.02	1.69	0.11	75.27	0.00	0.06	13.45	0.00	91.66
4919 (1)hydrilm	0.12	2.09	3.22	0.11	54.37	0.08	0.89	26.68	0.07	87.63
4919 (1) ilm2	0.00	0.14	0.19	0.00	47.52	0.07	2.24	44.85	0.00	95.01
4919 (1) ps3	0.16	1.12	2.19	0.13	64.92	0.08	0.13	21.50	0.11	90.35
traverse4919(2)ilm	0.02	0.10	0.14	0.04	50.25	0.00	4.97	41.57	0.00	97.10
traverse4919 (2)ps	0.09	0.38	0.30	0.12	61.79	0.06	1.23	26.56	0.00	90.53
traverse4919 (2)ps2	0.03	0.00	0.04	0.07	64.23	0.00	0.37	25.79	0.00	90.53
traverse4919 (2)lx	0.05	0.22	0.24	0.13	78.10	0.08	0.64	12.13	0.05	91.64
traverse4919 (2) ilm2	0.00	0.20	0.07	0.05	49.95	0.02	4.65	39.36	0.10	94.40
traverse4919 (2) lx2	0.01	0.19	0.22	0.14	75.70	0.00	0.50	11.65	0.00	88.42
traverse4919(2)ilm3	0.00	0.10	0.11	0.07	50.99	0.05	5.57	39.46	0.00	96.34
traverse4919 (2) lx3	0.04	0.34	0.25	0.10	77.06	0.03	0.22	13.90	0.00	91.95
traverse4919 (2) hydrilm	0.08	0.23	0.17	0.12	56.86	0.00	3.86	35.19	0.17	96.68
traverse4919 (2)ilm4	0.00	0.27	0.15	0.06	49.12	0.04	4.11	40.31	0.00	94.06
4923 ilm	0.10	0.04	0.12	0.05	48.20	0.07	0.60	46.95	0.00	96.14
4923ilm2	0.15	0.14	0.11	0.04	52.91	0.07	0.44	38.52	0.00	92.38
4923ilm3	0.14	0.15	0.19	0.12	51.48	0.08	0.86	39.98	0.08	93.09
4926ilm	0.13	0.00	0.14	0.02	50.59	0.19	0.59	42.20	0.11	93.96
4926lx	0.03	0.30	1.58	0.65	91.14	0.16	0.00	1.10	0.32	95.28
4926hydrilm	0.14	0.49	0.95	0.14	58.17	0.16	0.25	27.98	0.12	88.40
4926hydrilm2	0.25	0.27	0.38	0.05	56.21	0.13	0.29	32.74	0.15	90.49
4926hydrilm3	0.09	0.43	0.64	0.09	57.90	0.06	0.27	29.81	0.12	89.42
4926hydrilm4	0.12	0.22	0.49	0.09	54.82	0.11	0.44	34.63	0.19	91.12
4926lx2	0.05	0.73	1.70	0.14	72.29	0.18	0.20	14.92	0.24	90.46

Table F18 continued

SEM ANALYSIS OF ALTERED ILMENITE IN THE FIVE SATELLITE AREAS (in wt %)

GEELWAL KAROO

Sample	MgO	Al_2O_3	SiO_2	CaO	TiO_2	Cr_2O_3	MnO	FeO	Nb_2O_5	Total
4929ilm	0.09	0.02	0.17	0.02	49.20	0.00	3.43	41.12	0.00	94.05
4929ps	0.02	0.00	0.12	0.08	64.14	0.00	0.40	24.91	0.00	89.68
4929ps2	0.12	0.10	0.10	0.07	64.23	0.10	0.27	24.52	0.00	89.51
4929ps3	0.00	0.27	0.13	0.17	65.45	0.05	0.32	23.10	0.09	89.57
4929hydrilm	0.12	1.24	1.97	0.16	55.48	0.02	1.64	28.71	0.00	89.33

SEM ANALYSIS OF ALTERED ILMENITE IN THE FIVE SATELLITE AREAS (in wt %)

GRAAUWDUINEN

Sample	MgO	Al_2O_3	SiO_2	CaO	TiO_2	Cr_2O_3	MnO	FeO	Nb_2O_5	Total
4975ilm	0.00	0.06	0.08	0.00	48.52	0.02	0.72	48.56	0.10	98.06
4975ilm	0.06	0.04	0.13	0.00	49.29	0.02	0.50	48.15	0.33	98.52
4975rt	0.00	0.03	0.03	0.07	94.94	0.13	0.07	1.75	0.95	97.97
4975lx	0.12	1.21	1.50	0.08	90.57	0.00	0.02	2.51	0.87	96.89
4975lx2	0.07	0.58	1.06	0.08	90.01	0.07	0.10	4.23	0.82	97.01
4975rt2	0.03	0.08	0.15	0.04	95.28	0.03	0.00	1.49	0.67	97.78
4975ps	0.36	10.73	11.72	0.25	67.92	0.32	0.04	6.06	0.07	97.46
4975lx3	0.30	6.89	7.18	0.24	76.24	0.39	0.00	5.59	0.36	97.19
4975ps2	0.23	7.67	8.96	0.31	61.15	0.32	0.10	9.36	0.00	88.10
4975hydrilm	0.39	11.09	13.19	0.34	57.67	0.35	0.08	8.22	0.09	91.42
4978ilm	0.09	0.08	0.09	0.01	49.94	0.00	0.89	47.14	0.14	98.39
4978hydrilm	0.16	1.73	3.24	0.12	59.54	0.08	0.30	25.16	0.13	90.45
4978hydrilm2	0.19	1.95	3.43	0.15	60.79	0.08	0.30	25.25	0.00	92.14
4978ilm2	0.06	0.25	0.52	0.02	52.03	0.06	0.75	40.34	0.00	94.02
4978hydrilm3	0.14	1.49	2.55	0.11	58.78	0.03	0.36	27.25	0.15	90.86
ilm2	0.00	0.03	0.00	0.00	49.51	0.00	1.61	46.18	0.28	97.61
ilm2hydrilm	0.13	1.77	2.24	0.01	57.49	0.00	0.80	31.00	0.12	93.57
ilmhydrilm2	0.10	1.56	1.58	0.09	62.07	0.12	0.27	26.90	0.00	92.71
ilm2ilm2	0.09	0.29	0.30	0.00	53.49	0.02	0.91	39.36	0.38	94.84
4965lx	0.32	1.16	3.72	0.08	85.80	0.21	0.03	3.73	0.20	95.25
4965ps	1.18	3.22	12.87	0.08	67.54	0.26	0.02	9.11	0.00	94.29
4965ilm2	2.12	5.93	23.91	0.07	46.25	0.29	0.02	14.47	0.00	93.07
4965lx2	0.48	1.40	4.82	0.10	83.17	0.29	0.00	5.15	0.13	95.54
4962ilm	0.04	0.04	0.08	0.09	51.53	0.03	1.03	46.01	0.23	99.09
4962hydrilm	0.12	0.41	0.44	0.12	57.31	0.16	0.87	34.23	0.06	93.73
4962hydrilm2	0.24	0.76	0.37	0.14	56.88	0.14	0.82	33.61	0.00	92.96
4962hydrilm3	0.30	0.55	1.13	0.02	55.78	0.11	0.98	32.55	0.00	91.43
4970rt	0.02	0.11	0.13	0.08	96.33	0.06	0.11	0.45	0.64	97.95
4969rt2	0.07	0.06	0.12	0.00	94.50	0.00	0.08	0.66	0.24	95.73

Table F18 continued

SEM ANALYSIS OF ALTERED ILMENITE IN THE FIVE SATELLITE AREAS (in wt %)

GRAAUWDUINEN

Sample	MgO	Al_2O_3	SiO_2	CaO	TiO_2	Cr_2O_3	MnO	FeO	Nb_2O_5	Total
ilm3	0.15	0.10	0.05	0.08	50.89	0.02	6.03	40.31	0.23	97.85
ilm3lx	0.06	0.57	1.10	0.04	78.97	0.06	0.83	13.39	0.54	95.55
ilm3ilm2	0.25	1.47	3.58	0.07	52.27	0.18	3.74	33.84	0.17	95.56
ilm3lx2	0.14	0.25	0.86	0.03	87.04	0.04	0.06	5.85	0.44	94.71
4973ilm	0.28	0.18	0.07	0.01	49.24	0.02	4.04	44.90	0.00	98.74
4973ilm2	0.20	0.28	0.09	0.01	53.14	0.10	2.01	38.96	0.00	94.79
4973hydrilm	0.12	0.28	0.13	0.03	54.10	0.14	0.45	37.68	0.00	92.94
4973ilm2	0.24	0.63	1.37	0.01	52.20	0.09	0.75	36.99	0.00	92.27
traverse4975ilm	0.80	14.49	20.10	0.26	52.52	0.17	0.00	6.13	0.00	94.47
traverse4975hydrilm	0.58	11.61	14.23	0.38	54.34	0.30	0.06	8.15	0.00	89.65
traverse4975lx	0.27	6.64	6.39	0.22	77.66	0.25	0.00	5.62	0.35	97.40
traverse4975rt	0.00	0.21	0.25	0.00	94.54	0.06	0.00	1.60	1.36	98.02
traverse4975rt	0.04	0.20	0.40	0.03	95.00	0.08	0.07	1.14	0.98	97.93
traverse4975lx2	0.16	4.47	6.32	0.11	76.80	0.14	0.00	3.47	0.50	91.97
traverse4975lx3	0.42	6.34	7.18	0.16	71.38	0.02	0.08	13.05	0.39	99.02
traverse4975lx4	0.08	0.98	1.54	0.13	82.84	0.00	0.17	8.51	0.88	95.13
4981ilm	0.26	0.04	0.08	0.01	43.97	0.09	0.28	51.60	0.24	96.57
4981ps	0.17	2.39	3.17	0.13	63.25	0.05	0.16	23.99	0.00	93.31
4981hydrilm	0.10	1.36	1.97	0.12	58.06	0.00	0.09	30.57	0.00	92.27
4981hydrilm2	0.13	2.15	2.60	0.07	56.44	0.00	0.05	29.46	0.07	90.98
4981ilm2	0.18	3.15	4.27	0.12	53.06	0.04	0.09	30.49	0.00	91.39
4981ilm3	0.23	2.90	4.24	0.06	46.72	0.11	0.09	37.67	0.08	92.11
4981hydrilm3	0.20	2.19	2.99	0.05	54.52	0.05	0.20	33.86	0.00	94.06
4991ilm	0.22	0.12	0.03	0.01	51.60	0.11	0.50	47.24	0.14	99.98
4991lx	0.11	1.64	8.95	0.23	80.65	0.13	0.07	3.23	0.00	95.01
4991lx2	0.11	1.37	16.47	0.31	72.16	0.21	0.10	3.16	0.00	93.88
4991rt	0.03	0.10	0.20	0.06	96.74	0.29	0.05	0.37	0.00	97.84
4991lx3	0.20	1.10	10.92	0.33	84.87	0.12	0.00	0.65	0.11	98.28
4991lx4	0.87	2.96	5.95	0.09	78.39	0.22	0.07	6.38	0.04	94.98
4991ilm2	0.08	0.18	0.19	0.00	53.58	0.16	0.39	39.33	0.10	94.01
4991ilm3	0.13	0.10	0.21	0.00	52.25	0.13	0.44	41.71	0.00	94.99
4984ilm	0.20	0.05	0.13	0.05	49.64	0.06	0.66	48.37	0.00	99.18
4984hydrilm	0.08	0.62	0.45	0.06	54.91	0.15	0.36	35.55	0.00	92.17
4984hydrilm2	0.09	0.21	0.14	0.06	54.52	0.11	0.78	37.94	0.00	93.85
4984hydrilm3	0.21	0.19	0.23	0.02	55.18	0.10	0.69	36.41	0.00	93.02

Table F18 continued

SEM ANALYSIS OF ALTERED ILMENITE IN THE FIVE SATELLITE AREAS (in wt %)

GRAAUWDUINEN

Sample	MgO	Al_2O_3	SiO_2	CaO	TiO_2	Cr_2O_3	MnO	FeO	Nb_2O_5	Total
4987hydrilm	0.45	0.02	0.07	0.00	54.16	0.05	0.46	40.34	0.00	95.55
4987hydrilm2	0.11	0.15	0.15	0.00	55.48	0.05	0.33	37.92	0.00	94.18
4987hydrilm3	0.42	0.08	0.09	0.00	54.61	0.00	0.46	40.04	0.00	95.70
4987hydrilm4	0.24	0.12	0.05	0.00	56.29	0.00	0.48	36.86	0.00	94.03
4987hydrilm5	0.29	0.10	0.09	0.05	54.16	0.09	0.55	39.83	0.11	95.26
4950lx	0.03	0.41	1.12	0.05	92.48	0.13	0.02	0.95	0.86	96.04
4950lx2	0.42	2.48	8.77	0.00	73.38	0.17	0.00	5.82	0.56	91.61
4970lx3	0.46	2.47	7.23	0.00	78.18	0.11	0.15	4.58	0.45	93.64
4950lx4	0.37	2.02	6.67	0.06	79.89	0.11	0.01	4.00	0.58	93.72
4950lx5	0.00	0.52	1.34	0.11	91.90	0.09	0.00	0.88	0.61	95.45
4952rt	0.00	0.10	0.19	0.01	96.46	0.09	0.00	0.37	0.24	97.46
4952lx	0.08	5.47	7.65	0.09	80.89	0.08	0.10	1.13	0.00	95.51
4952lx2	0.13	4.47	6.28	0.06	82.28	0.09	0.08	1.09	0.00	94.48
4952lx3	0.06	6.61	9.06	0.02	74.78	0.08	0.03	1.14	0.00	91.77
4952ps	0.19	8.18	13.25	0.04	68.36	0.12	0.00	1.93	0.08	92.15
4952lx4	0.05	3.10	5.53	0.01	79.72	0.07	0.00	1.03	0.00	89.51
4952lx5	0.11	7.35	10.19	0.09	76.35	0.17	0.00	1.21	0.21	95.68
4952lx6	0.13	6.23	8.19	0.05	79.66	0.17	0.00	1.20	0.38	96.03
4955hem	0.00	0.13	0.09	0.00	33.24	0.00	1.61	58.28	0.09	93.43
4955ps	0.17	2.27	2.85	0.05	64.99	0.14	0.38	23.68	0.19	94.72
4955ps2	0.20	3.63	4.67	0.11	62.26	0.13	0.62	22.24	0.14	94.01
4955ps3	0.25	4.59	5.92	0.09	62.27	0.08	0.38	19.03	0.06	92.66
4955ps4	0.27	4.82	6.23	0.15	67.01	0.27	0.16	15.15	0.09	94.14
4955ps5	0.22	4.94	6.47	0.11	67.73	0.08	0.23	14.72	0.29	94.80
4955lx	0.00	0.04	0.04	0.01	77.25	0.00	0.46	16.88	0.57	95.26
4955ilm2	0.09	0.04	0.04	0.00	31.23	0.00	0.84	61.23	0.05	93.52
4955hem3	0.06	0.08	0.07	0.02	38.65	0.08	1.80	51.40	0.10	92.26
4955ps6	0.00	0.01	0.16	0.00	67.22	0.00	1.01	26.42	0.38	95.20
4955ps7	0.04	0.10	0.10	0.01	67.61	0.03	0.42	26.65	0.31	95.27
4943ilm	0.03	0.12	0.10	0.00	50.21	0.00	1.02	45.70	0.20	97.39
4943ilm2	0.09	0.74	0.92	0.08	53.00	0.00	0.80	37.18	0.21	93.01
4943hydrilm	0.05	0.31	0.39	0.04	55.02	0.05	0.82	35.99	0.10	92.77
4943hydrilm2	0.08	0.08	0.18	0.07	54.04	0.06	0.88	39.28	0.18	94.84
4943hydrilm3	0.03	0.29	0.38	0.00	54.69	0.03	0.84	35.82	0.20	92.27
4943hydrilm4	0.06	0.18	0.19	0.00	54.35	0.02	0.66	38.17	0.23	93.87

Table F18 continued

SEM ANALYSIS OF ALTERED ILMENITE IN THE FIVE SATELLITE AREAS (in wt %)

GRAAUWDUINEN

Sample	MgO	Al_2O_3	SiO_2	CaO	TiO_2	Cr_2O_3	MnO	FeO	Nb_2O_5	Total
4947(1)ilm	0.00	0.00	0.00	0.00	49.47	0.07	3.19	45.85	0.30	98.87
4947(1)ps	0.02	1.45	2.21	0.07	64.49	0.00	0.21	23.53	0.21	92.18
4947(1)lx	0.02	0.15	0.19	0.00	82.82	0.07	0.25	9.96	0.40	93.86
4947(1)rt	0.00	0.07	0.34	0.05	94.41	0.00	0.04	1.53	0.30	96.73
4947(1)rt2	0.00	0.14	0.26	0.05	94.83	0.00	0.00	1.71	0.51	97.50
4947(1)lx2	0.09	4.13	5.09	0.13	73.10	0.06	0.45	10.79	0.15	93.99
4947(1)rt3	0.00	0.05	0.28	0.03	95.37	0.00	0.09	1.23	0.47	97.53
4947(1)ps2	0.05	0.74	0.75	0.08	64.46	0.00	1.37	26.50	0.30	94.24
4947(1)ps3	0.05	0.85	0.79	0.10	67.27	0.06	0.86	22.49	0.29	92.75
4947(1)lx3	0.00	3.41	4.27	0.05	74.69	0.00	0.16	12.28	0.38	95.24
4947(2)ilm	0.49	0.03	0.12	0.00	50.60	0.21	0.58	45.95	0.09	98.07
4947(2)ydrilm	0.48	0.13	0.12	0.06	55.89	0.13	0.53	36.59	0.00	93.93
4947(2)ilm2	0.43	0.19	0.14	0.02	53.26	0.28	0.69	39.90	0.00	94.91
4947(2)ilm3	0.37	0.33	0.05	0.01	53.61	0.19	0.64	38.70	0.00	93.89
4947(2)hydrilm2	0.39	0.14	0.13	0.04	54.52	0.03	0.41	38.09	0.03	93.77
4947(2)hydrilm3	0.56	0.30	0.09	0.02	55.09	0.13	0.39	37.62	0.00	94.18
ilmhydrilm	0.05	0.56	0.70	0.00	57.05	0.16	0.04	34.27	0.00	92.84
ilmlx	0.02	1.52	2.41	0.00	87.56	0.16	0.10	4.11	0.00	95.89
ilmlx2	0.00	0.88	1.34	0.00	90.94	0.11	0.18	2.98	0.00	96.44
ilmlx3	0.00	0.48	0.65	0.04	87.08	0.00	0.24	9.23	0.00	97.73
ilmhydrilm2	0.00	0.62	0.88	0.00	56.32	0.05	0.16	35.03	0.00	93.05

SEM ANALYSIS OF ALTERED ILMENITE IN THE FIVE SATELLITE AREAS (in wt %)

RIETFONTEIN

Sample	MgO	Al_2O_3	SiO_2	CaO	TiO_2	Cr_2O_3	MnO	FeO	Nb_2O_5	Total
5004rt	0.00	0.11	0.37	0.06	94.38	0.02	0.00	0.51	0.50	95.95
5004lx	0.55	5.11	10.36	0.02	71.94	0.00	0.00	4.48	0.24	92.71
5004unknown	0.88	11.37	20.90	0.55	7.10	0.63	0.04	45.81	0.00	87.29
5004lx2	0.29	4.03	7.49	0.06	79.38	0.10	0.00	2.14	0.35	93.86
5004lx3	0.05	0.53	1.22	0.28	91.40	0.02	0.09	0.63	0.37	94.58
5004lx4	0.02	0.40	0.81	0.17	91.26	0.16	0.00	1.85	0.40	95.07
5000hydrilm	0.18	0.25	0.33	0.03	56.29	0.02	1.81	32.45	0.00	91.36
5000hydrilm2	0.20	0.47	0.31	0.06	57.92	0.14	1.77	29.89	0.00	90.76
5000lx	0.08	0.22	0.27	0.03	92.63	0.11	0.22	4.55	0.34	98.46
5000ps	0.13	0.31	0.45	0.13	61.61	0.12	1.52	29.52	0.00	93.78
5000lx2	0.08	0.64	1.04	0.10	90.12	0.06	0.08	5.61	0.36	98.09
5000hydrilm3	0.18	1.10	1.93	0.10	59.31	0.20	1.39	29.90	0.08	94.19
5000lx3	0.22	1.82	3.31	0.05	81.03	0.12	0.08	7.59	0.10	94.34
5000hydrilm4	0.17	0.71	1.34	0.12	60.28	0.10	1.46	28.75	0.00	92.94
5000lx4	0.16	0.39	0.68	0.01	74.04	0.08	0.49	18.53	0.18	94.56

Table F18 continued

SEM ANALYSIS OF ALTERED ILMENITE IN THE FIVE SATELLITE AREAS (in wt %)

RIETFONTEIN

Sample	MgO	Al_2O_3	SiO_2	CaO	TiO_2	Cr_2O_3	MnO	FeO	Nb_2O_5	Total
5006rt	0.05	0.04	0.26	0.10	96.45	0.06	0.00	0.31	0.26	97.53
5006lx	0.00	0.09	0.08	0.08	87.91	0.02	0.00	7.79	0.11	96.07
5006hem	0.00	0.21	0.59	0.10	32.97	0.06	0.87	57.11	0.03	91.95
5006ps	0.07	0.22	0.35	0.00	62.85	0.04	0.27	30.30	0.20	94.30
5006hem2	0.07	0.20	0.23	0.06	47.40	0.08	0.30	45.43	0.16	93.94
5006lx2	0.03	0.00	0.18	0.03	76.93	0.03	0.27	16.75	0.43	94.64
5006rt2	0.03	0.78	1.40	0.06	93.64	0.04	0.09	1.44	0.41	97.88
5006lx3	0.08	1.37	2.37	0.08	86.15	0.09	0.09	2.26	0.12	92.62
5006hem3	0.05	0.13	0.42	0.09	40.48	0.15	0.28	53.35	0.15	95.11
5006hem4	0.06	0.11	0.31	0.08	40.69	0.07	0.47	51.63	0.14	93.57
5012ilm	0.00	0.03	0.10	0.04	50.19	0.08	9.07	40.36	0.10	99.97
5012lx	0.09	0.16	0.47	0.03	91.52	0.10	0.08	4.56	0.00	97.00
5012ilm2	0.18	0.02	0.09	0.04	49.74	0.00	10.13	39.06	0.00	99.27
5012lx2	0.04	0.13	0.46	0.03	92.30	0.07	0.17	3.80	0.00	97.00
5012lx3	0.11	0.22	0.62	0.01	85.64	0.06	0.31	8.44	0.08	95.50
5012ilm3	0.00	0.07	0.08	0.04	48.06	0.00	9.49	37.44	0.00	95.18
5009ilm	0.02	0.06	0.13	0.00	51.95	0.00	2.60	44.84	0.00	99.60
5009ps	0.11	0.71	0.85	0.21	67.11	0.15	1.14	22.41	0.00	92.70
5009ps2	0.16	0.69	0.86	0.12	64.02	0.06	1.33	23.10	0.00	90.35
5009ps3	0.03	0.69	0.87	0.12	61.71	0.18	1.03	26.30	0.00	90.93
5009ps4	0.11	0.52	0.62	0.09	61.79	0.13	1.52	25.87	0.00	90.65
5009hydrilm	0.06	0.18	0.21	0.01	58.31	0.10	1.55	32.07	0.00	92.49
5015ilm	0.18	0.04	0.08	0.00	51.20	0.06	0.67	46.26	0.00	98.49
5015rt	0.00	0.39	0.55	0.00	94.81	0.02	0.03	0.64	0.46	96.90
5015rt2	0.04	0.08	0.10	0.00	95.70	0.00	0.13	0.71	0.40	97.16
5015rt	0.02	0.34	0.73	0.08	93.91	0.17	0.00	1.67	0.30	97.23
5015lx	0.19	1.06	2.16	0.30	88.75	0.09	0.00	1.93	0.33	94.81
5015lx2	0.03	0.92	2.01	0.34	87.08	0.09	0.06	3.95	0.30	94.77
5015lx3	0.20	1.55	2.07	0.08	91.41	0.14	0.00	1.24	0.43	97.13
4995hydrilm	0.09	0.52	0.37	0.08	60.17	0.12	1.56	30.60	0.00	93.50
4995hydrilm2	0.16	0.59	0.37	0.12	58.10	0.10	1.97	29.44	0.00	90.85
4995lx	0.00	0.40	0.64	0.06	88.30	0.00	0.12	3.79	0.14	93.45
4995lx2	0.00	0.13	0.12	0.00	92.51	0.02	0.00	3.10	0.00	95.87
4995lx3	0.04	0.40	0.54	0.06	92.24	0.04	0.00	2.53	0.05	95.89
4995lx4	0.21	1.83	0.54	0.21	85.50	0.44	0.08	4.14	0.00	92.93
4995hydrilm2	0.21	0.63	0.38	0.16	57.62	0.24	1.75	29.49	0.00	90.47

Table F18 continued

SEM ANALYSIS OF ALTERED ILMENITE IN THE FIVE SATELLITE AREAS (in wt %)

RIETFONTEIN

Sample	MgO	Al_2O_3	SiO_2	CaO	TiO_2	Cr_2O_3	MnO	FeO	Nb_2O_5	Total
5022ilm	0.05	0.03	0.02	0.00	46.08	1.11	2.75	29.74	0.00	79.77
5022ilm2	0.16	0.08	0.04	0.00	48.91	0.36	7.59	35.23	0.15	92.51
5022lx	0.00	0.12	0.29	0.08	79.41	1.27	0.03	0.72	0.97	82.87
5022lx2	0.00	0.09	0.13	0.00	81.15	1.24	0.05	0.58	0.53	83.76
5022lx3	0.04	0.14	0.72	0.06	82.99	0.91	0.08	0.91	0.18	86.03
5022lx	0.00	0.09	0.16	0.06	91.06	0.48	0.03	0.73	0.43	93.04
5022lx4	0.05	0.45	0.67	0.18	77.11	1.07	0.05	2.82	0.07	82.47
5025ilm	0.06	0.00	0.16	0.01	46.84	0.00	5.16	44.40	0.03	96.66
5025lx	0.00	0.08	0.16	0.04	90.81	0.09	0.00	4.45	0.00	95.63
5022lx2	0.00	0.10	0.16	0.00	80.54	0.11	0.13	13.40	0.00	94.43
5025ilm2	0.07	0.03	0.07	0.00	47.33	0.02	4.67	44.50	0.03	96.72
5025lx4	0.03	0.48	0.70	0.05	87.30	0.02	0.00	7.29	0.21	96.09
5028ilm	0.03	0.02	0.10	0.00	49.33	0.02	5.33	39.73	0.08	94.65
5028lx	0.02	0.54	0.86	0.00	82.47	0.09	0.12	7.91	0.34	92.34
5028lx2	0.03	0.96	1.01	0.05	85.41	0.08	0.05	6.78	0.00	94.37
5028lx3	0.00	1.33	2.06	0.02	78.36	0.06	0.08	10.27	0.47	92.65
5028hydrilm	0.36	3.20	5.38	0.14	58.67	0.09	0.27	20.99	0.00	89.11
5028hydrilm	0.05	0.80	1.41	0.07	56.13	0.00	0.77	30.99	0.00	90.22
traversehydrilm	0.05	0.15	0.57	0.06	53.99	0.15	0.71	40.70	0.21	96.59
traversehydrilmlcx	2.80	7.48	14.25	0.18	70.83	0.17	0.00	4.36	0.17	100.24
traversehydrilm2	0.07	0.06	0.29	0.00	54.36	0.13	0.90	42.67	0.12	98.61
traversehydrilmrt	0.04	0.82	1.07	0.03	95.55	0.11	0.11	1.08	0.32	99.14
traversehydrilm2lx	0.07	0.38	0.87	0.10	91.93	0.26	0.02	3.96	0.19	97.78
traversehydrilmps	0.09	0.41	0.71	0.07	67.60	0.22	0.50	25.83	0.21	95.65
traversehydrilmrt2	0.04	0.04	0.12	0.00	99.13	0.00	0.00	0.16	0.23	99.73

TABLE F19

CHEMISTRY OF AMORPHOUS COATING AS DETERMINED WITH THE SEM

HOUTKRAAL REMAINDER PORTION 2

Sample	SiO_2	TiO_2	Al_2O_3	Cr_2O_3	FeO	MgO	CaO	K_2O	MnO	Na_2O	V_2O_5
1	0.00	2.71	31.23	0.23	20.51	16.46	0.26	1.48	0.00	0.74	0.24
2	39.21	3.56	35.20	0.00	4.46	1.12	0.16	2.41	0.00	0.26	0.00
3	32.96	1.60	25.05	0.00	14.23	0.66	0.22	0.75	0.00	0.41	0.57
4	29.40	0.54	16.34	0.00	6.92	0.58	0.22	2.04	0.00	0.00	0.00
5	49.47	3.25	29.96	0.00	30.62	9.32	0.96	0.00	0.79	0.00	0.00
6	49.61	1.58	28.36	0.00	10.65	1.04	0.25	1.44	0.15	0.60	0.00
7	21.39	0.41	15.33	0.72	21.67	0.42	0.00	0.44	0.00	0.29	0.00
8	35.59	0.00	27.96	0.28	4.37	0.31	0.11	0.26	0.00	0.16	0.00
9	44.64	2.87	31.87	0.00	6.95	1.35	0.00	9.48	0.00	0.00	0.00
10	40.72	1.17	20.95	0.00	22.80	1.81	0.00	1.84	0.00	0.41	0.00

CHEMISTRY OF AMORPHOUS COATING AS DETERMINED WITH THE SEM

HOUTKRAAL REMAINDER

Sample	SiO_2	TiO_2	Al_2O_3	Cr_2O_3	FeO	MgO	CaO	K_2O	MnO	Na_2O	V_2O_5
11	41.92	1.97	33.66	0.00	12.04	0.46	0.22	0.18	0.00	0.29	0.00
12	26.30	0.44	52.32	0.00	11.79	1.42	0.00	0.00	0.52	0.00	0.00
13	21.32	0.90	15.39	0.00	10.90	0.53	0.31	1.00	0.59	0.00	0.00
14	33.46	0.22	19.67	0.52	13.97	2.23	0.23	3.69	0.84	0.00	0.00
15	45.62	0.96	19.89	0.00	17.06	2.03	0.53	4.02	0.00	0.33	0.00
16	35.55	1.06	18.62	0.72	24.47	1.08	0.58	1.54	0.00	0.45	0.00
17	63.16	0.30	20.49	0.00	0.17	0.00	1.78	0.46	0.00	9.47	0.00
18	31.12	3.29	14.43	0.85	32.08	1.84	0.37	2.30	0.00	0.46	0.00
19	31.87	3.85	11.28	0.00	27.04	4.45	0.00	8.31	0.51	0.53	0.00
20	48.30	2.82	35.91	0.00	3.71	0.48	0.00	7.52	0.00	0.00	0.00
21	45.09	1.27	31.86	0.00	4.07	1.22	0.00	9.18	0.00	0.30	0.00

CHEMISTRY OF AMORPHOUS COATING AS DETERMINED WITH THE SEM

GEELWAL KAROO

Sample	SiO_2	TiO_2	Al_2O_3	Cr_2O_3	FeO	MgO	CaO	K_2O	MnO	Na_2O	V_2O_5
22	44.13	3.69	29.01	0.00	3.89	1.64	0.00	9.55	0.00	0.00	0.00
23	29.61	35.02	2.68	0.00	0.00	0.00	27.75	0.00	0.00	0.00	0.00
24	42.90	1.48	31.55	0.00	4.41	0.48	0.00	0.00	0.00	0.00	0.00
25	17.79	0.00	51.13	0.00	1.86	0.98	4.91	0.00	0.00	0.64	0.00
26	46.91	0.00	2.00	0.00	16.41	13.26	3.74	0.00	0.00	0.00	0.00
27	29.29	0.99	11.05	0.00	31.90	1.67	0.91	1.01	0.00	0.39	0.00
28	44.05	2.33	31.23	0.00	1.95	0.00	0.00	7.92	0.00	0.00	0.00

CHEMISTRY OF AMORPHOUS COATING AS DETERMINED WITH THE SEM

GRAAUWDUINEN

Sample	SiO_2	TiO_2	Al_2O_3	Cr_2O_3	FeO	MgO	CaO	K_2O	MnO	Na_2O	V_2O_5
29	34.58	1.03	20.78	0.00	27.58	0.96	0.00	1.57	0.00	0.00	0.00
30	1.27	0.14	48.40	0.00	1.08	0.00	0.74	0.00	0.00	0.14	0.00
31	51.11	0.00	37.26	0.00	4.37	0.99	0.00	1.61	0.00	0.26	0.00
32	6.88	0.00	37.71	0.00	1.37	0.00	0.49	0.00	0.00	0.16	0.00
33	39.61	3.04	27.50	0.00	2.60	0.44	0.00	7.64	0.00	0.21	0.00
34	46.31	1.68	17.84	0.49	18.61	1.15	0.27	2.06	0.00	0.40	0.00

TABLE F19 continued

CHEMISTRY OF AMORPHOUS COATING AS DETERMINED WITH THE SEM

RIETFONTEIN

Sample	SiO_2	TiO_2	Al_2O_3	Cr_2O_3	FeO	MgO	CaO	K_2O	MnO	Na_2O	V_2O_5
35	36.08	1.66	32.72	0.00	14.49	0.77	0.27	1.07	0.00	0.47	0.00
36	0.77	6.57	31.72	0.00	5.53	0.00	0.30	0.00	0.00	0.13	0.24
37	45.26	0.00	19.34	0.00	18.76	6.18	0.00	3.13	0.00	0.57	0.00
38	0.50	11.03	36.27	0.00	7.61	0.00	0.20	0.00	0.28	0.00	0.57
39	2.90	0.67	21.05	0.16	6.60	0.00	2.44	0.68	0.00	0.00	0.00
40	43.05	0.53	28.67	0.00	5.08	1.00	0.00	4.72	0.00	0.20	0.00

TABLE F20

AMORPHOUS COATING OF ILMENITE AS DETERMINED WITH THE SEM

HOUTKRAAL REMAINDER PORTION 2

Sample	SiO_2	TiO_2	Al_2O_3	Cr_2O_3	FeO	MgO	CaO	MnO	Nb_2O_5
1	26.00	29.45	11.30	0.11	22.03	6.22	0.15	1.30	0.00
2	37.03	20.77	29.05	0.00	4.09	0.48	0.10	0.14	0.00
3	36.26	18.56	16.77	0.13	9.76	1.76	0.19	0.00	0.07

AMORPHOUS COATING OF ILMENITE AS DETERMINED WITH THE SEM

HOUTKRAAL REMAINDER

Sample	SiO_2	TiO_2	Al_2O_3	Cr_2O_3	FeO	MgO	CaO	MnO	Nb_2O_5
4	9.48	21.98	47.26	0.20	7.23	0.21	0.25	0.34	0.00
5	37.47	12.23	19.84	0.50	19.69	1.76	0.13	0.00	0.00
6	36.76	3.79	13.21	0.67	30.94	2.08	0.14	0.20	0.00
7	32.91	8.22	17.12	0.20	23.68	4.54	0.00	0.16	0.00

AMORPHOUS COATING OF ILMENITE AS DETERMINED WITH THE SEM

GEELWAL KAROO

Sample	SiO_2	TiO_2	Al_2O_3	Cr_2O_3	FeO	MgO	CaO	MnO	Nb_2O_5
8	35.86	0.79	17.67	0.29	24.09	3.89	0.00	0.00	0.00
9	60.33	0.25	17.33	0.04	0.29	0.40	0.60	0.02	0.00
10	28.65	9.81	15.20	0.08	17.76	2.69	0.00	0.15	0.00

AMORPHOUS COATING OF ILMENITE AS DETERMINED WITH THE SEM

GRAAUWDUINEN

Sample	SiO_2	TiO_2	Al_2O_3	Cr_2O_3	FeO	MgO	CaO	MnO	Nb_2O_5
11	27.70	16.19	14.00	0.22	23.38	3.65	0.00	0.05	0.00
12	38.23	13.78	26.79	0.04	9.41	0.96	0.13	0.00	0.00
13	30.76	31.84	7.82	0.31	20.63	3.06	0.03	0.08	0.07
14	85.98	5.26	2.48	0.00	5.74	0.45	0.01	0.00	0.21

AMORPHOUS COATING OF ILMENITE AS DETERMINED WITH THE SEM

RIETFONTEIN

Sample	SiO_2	TiO_2	Al_2O_3	Cr_2O_3	FeO	MgO	CaO	MnO	Nb_2O_5
15	101.00	0.63	0.10	0.00	0.05	0.02	0.00	0.06	0.29
16	33.89	19.98	13.51	0.10	14.61	1.72	0.00	0.00	0.22
17	37.24	12.86	15.52	0.01	15.75	4.98	0.00	0.13	0.11
18	36.39	8.54	23.53	0.05	5.97	1.37	0.03	0.00	0.06

APPENDIX G:
END-MEMBER CLASSIFICATION

Garnet

Garnet end-member calculations were performed using a Microsoft Excel spreadsheet designed by Locock (2008). He made use of chemical compositional data of garnet to calculate the molar proportions of the different garnet end-members. Some 29 Possible end-members were evaluated for each analysis, which include 15 natural mineral species and 14 hypothetical end-members. (Locock, 2008). The Method of Droop (1987) was used to calculate the FeO and Fe_2O_3 proportions.

Pyroxene

PX-NOM is a Microsoft Excel spreadsheet program that enables the user to calculate structural formulae of pyroxene analyses obtained from analytical techniques such as the electron microprobe and SEM. It is also used to determine respective pyroxene names according to the classification scheme of the International Mineralogical Association as determined by Morimoto et al (1988). The Fe^{3+} was calculated, where needed, using the method of Droop (1987). Pyroxene end-member classification is based on 4 cations and 6 oxygens (Deer et al, 1992). "Other minerals" refers to the minerals tabulated below.

Mineral Name	Structural Formula
Esseneite	$CaFe_{3+}AlSiO_6$
Kanoite	$MnMgSi_2O_6$
Donpeacorite	$(Mn,Mg)MgSi_2O_6$
Spodumene	$LiAlSi_2O_6$
Johannsenite	$CaMnSi_2O_6$
Petedunnite	$CaZnSi_2O_6$

Tourmaline

The chemical formula of tourmaline may be written as XY_3Z_6 $[T_6O_{18}]$ $[BO_3]_3V_3W$ (Hawthorne and Henry, 1999).

Tourmalines were classified using the classification scheme proposed by Hawthorne and Henry (1999). First the dominant X-site occupant is established to determine the principal

tourmaline group which can be Alkali, Calcic or Vacancy tourmalines. Second the dominant anion (F^-, OH^- or O^{2-}) at the W-site is determined. Thirdly the dominant anion (O^{2-} or OH^-) at the V-site is determined. It is believed that most tourmalines are dominated by OH^- at the V-site. Next the dominant Y-cation is determined and lastly the dominant Z-cation. Al is the most common cation in the Z-site.

All of the tourmalines of the five areas can be classified as mainly alkali tourmalines with a minor amount of calcic tourmalines due to the X-site that is primary filled by Na and minor Ca. From the chemical data (Table F11, Appendix F) it is evident that the major elements in the Y-site are trivalent cations. As stated by Grice and Ercit (1993) the dominant specie in the W-site is generally O^{2-} except for tourmalines with trivalent cations at the Y-site as is the case with this study's tourmaline. According to Hawthorne and Henry (1999) F^- occupies the W-site as is the case for Buergerite.

The V-site is also assumed to be occupied by the anion OH^- due to the fact that OH^- is usually the most dominant V-site occupant in most tourmalines. For Buergerite it is dominated by O^{2-} .The dominant Y-cation are Mg and Fe^{2+} and Fe^{3+} for Buergerite. The Z-site is occupied by Al.

Boron and OH^- are not measured by the SEM. The stoichiometric B_2O_3 value in Deer et al (1992) was used which equals 10.5wt%. The amount of OH^- molecules can in some cases be determined by electro neutrality requirements (Henry and Dutrow, 1996, Henry et al, 1999, Henry and Hawthorne, 1999) but was not determined for this study.